Progress Report 24

for the Period March 1984 to October 1984

and Proceedings of the
24th Project Integration Meeting

Progress Report 24

for the Period March 1984 to October 1984

and Proceedings of the 24th Project Integration Meeting

ABSTRACT

This report describes progress made by the Flat-Plate Solar Array
Project during the period March 1984 to October 1984. It includes reports on
silicon sheet growth and characterization, silicon material, process
development, high-efficiency cells, environmental isolation, engineering
sciences, and reliability physics. It includes a report on, and copies of
visual presentations made at, the 24th Project Integration Meeting held at
Pasadena, California, on October 2 and 3, 1984.

NOMENCLATURE

A	Ampere(s); Angstrom(s)
ac	Alternating current
AM	Air mass (e.g., AM1 = unit air mass)
AR	Antireflective
a-Si	Amorphous silicon
ASME	American Society of Mechanical Engineers
ASTM	American Society for Testing and Materials
BA	Butyl acrylate
BOS	Balance of System (non-array elements of a PV system)
BSF	Back-surface field
BSR	Back-surface reflection
C	Celsius (temperature scale)
Caltech	California Institute of Technology
CEC	Commission of European Communities
CER	Controlled-environment reactor
COSMIC	Computer Software Management Information Center
CPVC	Chlorinated polyvinyl chloride
c-Si	Single-crystal silicon
C-V	Capacitance-voltage
CVD	Chemical vapor deposition
CVT	Chemical vapor transport
Cz	Czochralski (classical silicon crystal growth method)
dc	Direct current
DCS	Dichlorosilane
DI	De-ionized
DLTS	Deep-level transient spectroscopy

DOE	U.S. Department of Energy
EBIC	Electron-beam-induced current
EDAX, EDX	Electron-dispersive analysis of X-rays
EDS	Electron-dispersion spectroscopy
EFG	Edge-defined film-fed growth (silicon-ribbon growth method)
EMA	Ethylene methyl acrylate
EPDM	Ethylene-propylene-diene monomer
EPRI	Electric Power Research Institute
EPSDU	Experimental process system development unit
ESP	Edge-supported pulling (silicon-sheet production process)
EVA	Ethylene vinyl acetate
FBR	Fluidized-bed reactor
FF	Fill factor
FSA	Flat-Plate Solar Array Project
FSR	Free-space reactor
FTIR	Fourier transform infrared
FY	Fiscal year
FZ	Float-zone (silicon sheet growth method)
GC	Gas chromatography
GFCI	Ground-fault circuit interruptor
h	Heat transfer coefficient; hour(s)
HEM	Heat-exchange method (silicon-crystal ingot-growth method)
ICB	Ion cluster beam
I_{sc}	Short-circuit current
I-V	Current-voltage
ID	Inside diameter
IEEE	Institute of Electrical and Electronics Engineers, Inc.

IIT	Illinois Institute of Technology
IITRI	IIT Research Institute
IPEG	Improved Price Estimation Guidelines
IR	Infrared
ITO	Indium-tin oxide
J_{sc}	Short-circuit current density
JPL	Jet Propulsion Laboratory
K	Degree(s) Kelvin
k	Equilibrium constant
LAPSS	Large-area pulsed solar simulator
LASS	Low-angle silicon sheet growth method
LBIC	Light-beam-induced current
L_D	Minority carrier diffusion length
LPE	Liquid-phase epitaxy
MBE	Molecular-beam epitaxy
MEPSDU	Module experimental process system development unit
mgSi	Metallurgical-grade silicon
MINP	Metal insulator, n-p
MIS	Metal-insulator-semiconductor (cell configuration)
MOD	Metallo-organic deposition
MSEC	Mobil Solar Energy Corp.
m-Si	Microcrystalline silicon
MT	Metric ton(s)
NASA	National Aeronautics and Space Administration
NEC	National Electrical Code
NMA	Non-mass-analyzed
NOC	Nominal operating conditions

NOCT	Nominal operating cell temperature
OFHC	Oxygen-free hard copper
O&M	Operation and maintenance
P	Power
P_{max}	Maximum power
PA&I	Project Analysis and Integration Area (of FSA)
P/FR	Problem/failure report
PC	Power conditioner
PCS	Power-conditioning system
PC/TS	Performance Criteria/Test Standards (SERI)
PDU	Process development unit
PE	Polyethylene
PEBA	Pulsed electron beam annealing
PIM	Project Integration Meeting
PMMA	Polymethyl methacrylate
PnBA	Poly-n-butyl acrylate
ppba	Parts per billion, atomic
ppm	Parts per million
ppma	Parts per million, atomic
ppmw	Parts per million, weight
PU	Polyurethane
PV	Photovoltaic(s)
PVB	Polyvinyl butyral
PVC	Polyvinyl chloride
PVD	Physical vapor deposition
R&D	Research and development
RES	Residential Experiment Station

RF	Radio frequency
RH	Relative humidity
RTV	Room-temperature vulcanized
S	Incident solar energy density
s	Second(s)
SAMICS	Solar Array Manufacturing Industry Costing Standards
SAMIS	Standard Assembly-Line Manufacturing Industry Simulation
SCAP1D	Solar-Cell Analysis Program in One Dimension
SCLS	Solar-cell laser scanner
SEEMA	Solar-Cell Efficiency Estimation Methodology and Analysis
SEM	Scanning electron microscope
SERI	Solar Energy Research Institute
SIMRAND	SIMulation of Research ANd Development Projects
SIMS	Secondary ion mass spectroscopy
SMUD	Sacramento (California) Municipal Utility District
SOA	State of the art
SOC	Standard operating conditions (module performance)
SOLMET	Solar radiation surface meteorological observations
STC	Silicon tetrachloride
STC	Standard test conditions
T	Temperature
TCM	Transparent conducting material
TCO	Transparent conducting oxide
TCS	Trichlorosilane
TEM	Transmission electron microscope
TMY	Typical meteorological year
TREI	Texas Research and Engineering Institute

TTU	Texas Tech University
U	Superficial velocity
U_{mf}	Minimum fluidization velocity
UCP	Ubiquitous crystallization process
UL	Underwriters Laboratories, Inc.
UV	Ultraviolet
V_{oc}	Open-circuit voltage
W_p	Peak watt(s)
y	Mol % silane
	Greek letter eta: efficiency
σ_{xx}	Greek letter sigma: lateral stress
σ_{yy}	Greek letter sigma: longitudinal stress
Ω	Greek letter omega: resistance in ohms

METRIC CONVERSION FACTORS

Approximate Conversions to Metric Measures

Symbol	When You Know	Multiply by	To Find	Symbol
		LENGTH		
in	inches	*2.5	centimeters	cm
ft	feet	30	centimeters	cm
yd	yards	0.9	meters	m
mi	miles	1.6	kilometers	km
		AREA		
in²	square inches	6.5	square centimeters	cm²
ft²	square feet	0.09	square meters	m²
yd²	square yards	0.8	square meters	m²
mi²	square miles	2.6	square kilometers	km²
	acres	0.4	hectares	ha
		MASS (weight)		
oz	ounces	28	grams	g
lb	pounds	0.45	kilograms	kg
	short tons (2000 lb)	0.9	tonnes	t
		VOLUME		
tsp	teaspoons	5	milliliters	ml
Tbsp	tablespoons	15	milliliters	ml
fl oz	fluid ounces	30	milliliters	ml
c	cups	0.24	liters	l
pt	pints	0.47	liters	l
qt	quarts	0.95	liters	l
gal	gallons	3.8	liters	l
ft³	cubic feet	0.03	cubic meters	m³
yd³	cubic yards	0.76	cubic meters	m³
		TEMPERATURE (exact)		
°F	Fahrenheit temperature	5/9 (after subtracting 32)	Celsius temperature	°C

Approximate Conversions from Metric Measures

Symbol	When You Know	Multiply by	To Find	Symbol
		LENGTH		
mm	millimeters	0.04	inches	in
cm	centimeters	0.4	inches	in
m	meters	3.3	feet	ft
m	meters	1.1	yards	yd
km	kilometers	0.6	miles	mi
		AREA		
cm²	square centimeters	0.16	square inches	in²
m²	square meters	1.2	square yards	yd²
km²	square kilometers	0.4	square miles	mi²
ha	hectares (10,000 m²)	2.5	acres	
		MASS (weight)		
g	grams	0.035	ounces	oz
kg	kilograms	2.2	pounds	lb
t	tonnes (1000 kg)	1.1	short tons	
		VOLUME		
ml	milliliters	0.03	fluid ounces	fl oz
l	liters	2.1	pints	pt
l	liters	1.06	quarts	qt
l	liters	0.26	gallons	gal
m³	cubic meters	35	cubic feet	ft³
m³	cubic meters	1.3	cubic yards	yd³
		TEMPERATURE (exact)		
°C	Celsius temperature	9/5 (then add 32)	Fahrenheit temperature	°F

°F −40   0   32   98.6   212
°C −40 −20   0   20   40   60   80   100   37

xi
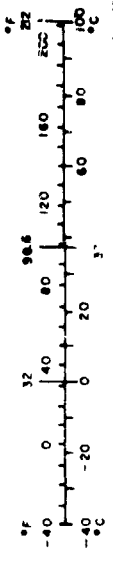
CONTENTS

PROGRESS REPORT

PRECEDING PAGE BLANK NOT FILMED

CONTENTS

PROCEEDINGS OF THE PROJECT INTEGRATION MEETING

PROGRESS REPORT

Project Summary

INTRODUCTION

This report describes the activities of the Flat-Plate Solar Array Project (FSA) from April 1984 through September 1984, including the 24th FSA Project Integration Meeting (PIM), held on October 2 and 3, 1984.

The Flat-Plate Solar Array Project at the Jet Propulusion Laboratory (JPL), sponsored by the U.S. Department of Energy (DOE), has the responsibility for advancing solar array technology while encouraging industry to reduce the price of arrays to a level at which photovoltaic (PV) electric power systems will be competitive with more conventional power sources. This responsibility has included developing the technology for producing low-cost, long-life photovoltaic modules and arrays. More than 100 organizations have participated in FSA-sponsored research and development of low-cost solar module manufacturing and mass-production technology, the transfer of this technology to industry for commercialization, and the development and testing of advanced prototype modules and arrays. Economic analyses were used to select, for sponsorship, those research and development efforts most likely to result in significant cost reductions. Set forth here is an account of the progress that has been made during the reporting period.

SUMMARY OF PROGRESS

Experimental test runs of a fluidized-bed reactor (FBR) at the Union Carbide Corp. (UCC) experimental process system development unit (EPSDU) at Washougal, Washington, continue to demonstrate the practicality of converting silane to silicon. The 6-inch-dia. FBR was equipped with a high-purity polysilicon liner to prevent metallic impurity contamination of the silicon product from the FBR walls during operation. During a successful 66-hour test (50% longer than any previous test) the seed particles (280 micrometer average diameter) were grown to about 480 micrometers. Initial neutron activation analysis results showed that there was no gross contamination introduced in the FBR.

The 6-in.-dia. research FBR at JPL, which was also equipped with a quartz liner, has been operated successfully. A 4-hour run at 30 mole % silane in hydrogen (twice the UCC FBR concentration) and 3-hour 50% concentration run demonstrated the integrity of the liner and the absence of metallic impurities in the silicon. A fluid-jet mill specifically designed for making FBR silicon-seed material has been fabricated and used successfully.

Theoretical analyses of silicon particle growth at the California Institute of Technology provided valuable information regarding the narrow dividing line between the conditions for the formation of new particles and

1

PROJECT SUMMARY

conditions for growth on seed particles. Seed particle size is an important parameter for the control of nucleation and the prevention of excessive fines production during the pyrolysis or conversion of silane to silicon.

The feasibility of microwave heating of a fluidized bed of silicon particles, about 300 μm in diameter, under nonreactive steady-state conditions was demonstrated successfully by Superwave Technology, Inc. The properties of silane should preclude the likelihood of excessive silicon fines formation or other problems if microwave heating were used in a reactive FBR.

A computer model of silane pyrolysis in an FBR that can be used for designing scaled-up reactors for pilot plants has been completed for some operational conditions by Washington University at St. Louis. The effort is continuing to model more FBR operational conditions.

A well-planned, comprehensive, multiorganization research effort on defining growth-induced stresses in silicon ribbons and evaluating the quality of the resultant ribbon, initiated early in 1983, is making good progress. Mathematical models have been created that predict more accurately stress and strain history during the silicon growth process and the residual stresses in the silicon ribbons. These models are an advance over previous ones because they take into account the growth history of the ribbon and the material's non-linearity and creep behavior. Relevant ribbon-temperature data and boundary conditions are obtained experimentally from various growth equipment and are used to refine and confirm the theoretical analyses. Thus, researchers are evaluating various grower geometric configurations and ribbon temperature distributions, allowing them to identify critical tradeoffs in ribbon-growth equipment.

During this reporting period a number of dendritic-web silicon ribbons, ranging from 5 to 9.6 meters in length, have been grown at Westinghouse Electric Corp. with growers of various designs, some with silicon melt replenishment. Some ribbons had no residual stress. The ribbon growth and grower knowledge required to increase growth speeds and retain good quality ribbon is gradually being acquired.

Creep studies in float-zone (FZ) and Czochralski (Cz) silicon at high temperatures being done at Mobil Solar Energy Corp. have established that silicon sheet above 1200°C responds as an essentially plastic material at the stresses and strains expected during silicon ribbon growth. This creep information is being incorporated into stress analyses to obtain new predictions for residual stress buildup in edge-defined film-fed growth (EFG) ribbons. The temperature gradient at the EFG ribbon-growth interface was clearly identified as a major control parameter needed to achieve reduced ribbon stress. Further studies will continue to evaluate the role and sensitivity of other parameters and the effects of high and low temperatures on stress.

A new low-angle silicon sheet (LASS) unit for growing a higher-quality horizontal silicon ribbon was put into operation at Energy Materials Corp.

A report titled "Viscoplastic Stress/Strain Model," written by the University of Kentucky, described an analytical model that handles plasticity, creep, and dislocation generation in silicon ribbons as a function of strain

rate, initial dislocation density, and oxygen concentration. Elastic stress and buckling analytical results are reasonably consistent with experimental observations.

Evaluation of fracture properties and crack propagation in single-crystal silicon was demonstrated at JPL by use of an acoustic emission technique that has the capability to locate a crack and to monitor crack growth speed in silicon sheet.

Maximum residual stress measurements in silicon sheet by the use of laser interferometry, at the University of Illinois at Chicago, showed that EFG nonagon silicon ribbon had stresses about 4 to 10 times greater than that measured for silicon web ribbon.

A number of supportive analytical and experimental techniques are under development at numerous organizations to supplement the silicon-sheet studies described above.

Steady progress has been made on gaining a basic understanding of possible carbon gettering mechanisms in EFG silicon ribbons at Cornell University.

A preliminary study of oxygen effects on the structural defects in EFG silicon ribbons has been completed. Results indicate that oxygen content influences the formation of planar defects, e.g. twins, probably due to oxygen hardening of the ribbons. This is consistent with previous data that indicate that EFG ribbons with high oxygen content are often better electrically.

A new technique, developed at the University of Florida, for measuring minority carrier lifetimes and surface recombination velocities in bulk silicon has been described in its annual report.

Westinghouse has shown that lasers can be used effectively as a patterning device in metallizing cells. In one of its experiments, silver neodecanoate dissolved in xylene was spun onto diffused silicon wafers coated with evaporated titanium-palladium. The cells were then exposed to a laser beam that scanned (wrote) a fixed metallization pattern on the cells. These cells were then plated in a silver cyanide bath; selective plating occurred only on those areas exposed to the laser beam. The unexposed metal areas were easily etched away. Cell efficiencies were good. This technique shows promise in eliminating expensive masking steps.

ARCO Solar, Inc., and Spire Corp. are showing promising results in laser-annealing ion-implanted solar cells. Likewise, laser drive-in of liquid dopants has, thus far, shown the most promise in the simultaneous front-and-back junction formation effort.

A test program is under way at Clemson University to investigate first-order failure mechanisms on thin-film cells. initial tests are identical with those developed by Clemson for use with crystalline-silicon cells.

Measurements of electrochemical degradation of crystalline silicon solar cells at JPL has related leakage current levels, integrated over exposure times, with cell power output reduction when polymer-encapsulated

PROJECT SUMMARY

two-electrode cell-frame samples were exposed to temperature-humidity environments. The degradation mechanisms differ for positive and negative cell polarities.

Dow Corning observed that EVA bonds strongly to aluminized back surfaces of solar cells, but bonds weakly to aluminum foil or sheet when the same primer is used. Initial observations indicate that the cell back surface is a mixture of aluminum and silicon.

The overall rate of photothermal yellowing of pottants is governed by three mechanisms. The rate of thermal yellowing is found to be faster than that of photothermal yellowing, however; photo-induced bleaching is significant. The individual rates of these reactions are being determined for inclusion in a quantitative model.

The overall status of module reliability from mechanism and circuit-redundancy perspectives has been emphasized in a number of recent JPL papers. The reliability goals for 13 principal failure mechanisms have been updated and the research status of each has been defined.

Guidelines for future testing of modules for susceptibility to hot-spot problems if the modules are to be used in central-station applications, and the guidelines for circuit design strategies, were developed by JPL in conjunction with ARCO Solar, Inc., and Acurex Corp.

The General Electric Co. final report on the integration of bypass diodes in PV modules and arrays was distributed.

A series of tests were completed at Underwriters Laboratories, Inc., in conjunction with ARCO Solar, Inc., to characterize various module back-cover-material temperatures during fire testing.

Environmental test activity has continued on Block V modules, commerciahouseules procured under Block V type contracts and commercial mo'ules procured to investigate module developments. Module deficiencies, in both design and fabrication as in earlier modules, have been uncovered by use of the more stringent Block V test conditions.

JPL is participating in a series of comparative silicon reference-cell performance measurements with the Commission of European Communities, the British Petroleum Co. Ltd. and the Solar Energy Research Institute (SERI). The series of measurements by JPL and SERI has ultimately resulted in data showing that the SERI calibration values now match the JPL values very closely.

To prepare for failure-analysis evaluation of thin-film amorphous silicon solar cells, an argon laser was integrated into the existing JPL solar-cell laser scanner (SCLS). The laser's six selectable spectral lines significantly expand the capability of the SCLS and also provide the means for depth-profiling cell performance properties.

Work is continuing at Spire Corp. on the development of a high-efficiency crystalline silicon cell module. A batch of solar cells, manufactured using ion-implanted FZ silicon wafers with back-surface reflector, averaged 15.5% efficiency.

Area Reports

MATERIALS AND DEVICES RESEARCH AREA

Silicon Materials Research Task and Advanced Silicon Sheet Task

INTRODUCTION

The objectives of the Silicon Materials Research Task and the Advanced Silicon Sheet Task are to identify the critical technical barriers to low-cost silicon (Si) purification and sheet growth that must be overcome to produce a photovoltaic (PV) cell substrate material at a price consistent with Flat-Plate Solar Array Project (FSA) objectives, and then to overcome those barriers by performing and supporting appropriate research and development.

Present solar-cell technology is based mainly on the use of Si wafers obtained by inner-diameter slicing of Czochralski (Cz)-grown ingots from Siemens-reactor-produced semiconductor-grade Si. This method of obtaining single-crystal Si wafers is tailored to the needs of semiconductor-device production (e.g., integrated circuits and discrete power and control devices other than solar cells). The small market offered by present solar-cell users does not justify industry's development of the high-volume Si production techniques that would result in low-cost PV electrical energy.

It is important to develop alternative low-cost processes for producing refined Si and sheet material suitable for long-life, high-efficiency solar PV energy conversion. To meet FSA objectives, research must be performed to overcome the barriers to the success of the most promising processes for producing large quantities of pure Si and large areas of crystallized Si at a low, competitive cost. The form of the refined Si must be suitable for use in the sheet-growth processes. The sheet, in turn, must be suitable for direct incorporation into automated solar-array industry schemes.

Silicon purification involving deposition of the material from silane is being pursued because this substance can be purified relatively easily and, because of its high reactivity, it can be more readily decomposed or reduced to form Si than can trichlorosilane (TCS), which is used today in the conventional process. Research on two other processes that offer promise for making less-pure, solar-cell-grade Si by refinement of metallurgical-grade Si (mgSi) is also being conducted because of the potential for further reduction of product cost.

Growth of crystalline Si material in a geometry that does not require cutting to achieve proper thickness is an obvious way to eliminate costly processing and material waste. Growth techniques such as edge-defined film-fed growth (EFG), dendritic-web growth (web), low-angle Si sheet (LASS), and edge-supported pulling (ESP) are candidates for such solar-cell material.

MATERIALS AND DEVICES RESEARCH AREA

In addition to research on processes for Si refinement and sheet growth, various supporting studies are under way to investigate key problems in both of these categories.

SUMMARY OF PROGRESS
Silicon Material Research Task

Semiconductor-Grade Silicon Refinement Process

Silicon Refinement Using Silane (Union Carbide Corp.)

The objective of the Union Carbide Corp. (UCC) program is to solve the critical problem of silane pyrolysis in fluidized-bed reactors (FBRs) for producing semiconductor-grade Si for PV applications. The principal activities during the current period were the implementation of a high-purity liner in the six-inch-diameter FBR to prevent contamination of the Si product by the metal reactor wall. Tests were made using liners made of quartz and of polysilicon to obtain operational data and to produce samples for purity analysis. With quartz liners, breakage occurred near the start of one test before silane was introduced and in other tests during cool-down. Additional information on tests with silicon liners is presented below, in the report titled "Research on Silane Pyrolysis in Fluidized-Bed Reactors" (JPL). The first test with a polysilicon liner was conducted, using 10 to 15 mole % silane in hydrogen. It was run for 66 hours (the planned duration); the longest previous test in this size FBR was 44 hours. The average Si production rate for the entire test was about 0.9 kg/h. Although operation was otherwise successful, the liner broke during cool-down after the test. The breakage was attributed to compression by the FBR wall due to differential contraction; the annular space between the wall and the liner had filled with Si powder during the test because of failure of a seal. Redesign is under way to correct the liner seal and support system.

In the 66-hour test, the seed particles, which had an average diameter of 280 micrometers, were grown to about 480 micrometers.

Initial results from neutron activation analysis showed that the initial seed material was not clean to the semiconductor purity level and that there was no gross contamination introduced in the FBR processing step. However, the question of purity of FBR product grown from clean seed remains to be answered.

Silicon Refinement Using Dichlorosilane (Hemlock Semiconductor Corp.)

In the study of the critical portions of a process for making Si approaching semiconductor-grade in purity, the final report on the cold-wall Si deposition reactor program was issued. Highlights of the effort were presented in Progress Report 22.

Solar-Cell-Grade Silicon Refinement Processes

Electrochemical Refining of Metallurgical-Grade Silicon (Energy Materials Corp.)

The objective of this contract is to demonstrate the technical feasibility of producing high-purity Si from metallurgical-grade Si in a process using a $Cu_3Si:Si$ anode in a fused-salt electrochemical cell.

A considerable purification of the metallurgical-grade Si in the anode was found to occur during the formation of the anode. The extent of purification was determined using mass spectroscopy measurements. For example, the Fe concentration was reduced from about 3400 ppm to 100 ppm, Cr from about 300 to 2, Ti from about 400 to 2, and Al from about 2100 to 5. The mechanism of purification for the volatile elements was probably primarily vaporization. The non-volatile elements were apparently incorporated in a slag that formed on top of the melt during the anode preparation.

Attempts to operate the electrolysis cell were unsuccessful due to experimental problems. The contract ends on October 23, 1984.

Chemical Vapor Transport Process for Purifying Metallurgical-Grade Silicon (Solar Energy Research Institute)

This research investigates a chemical vapor transport process in which HCl is reacted with a $Cu_3Si:Si$ material (the Si being metallurgical-grade Si) at about 700°C to generate (predominantly) trichlorosilane, and then Si is deposited by chemical vapor deposition from the trichlorosilane on a filament kept at 1050°C. The Cu-Si alloy is employed because it acts as a filter for impurities, the diffusion rates for impurities being much lower than that for Si. The characterization of the operating conditions for a larger reactor with a deposition rate capability of about 10 g/h is nearly complete, and a method was developed to fabricate the larger alloy plates. The refined Si product was shown to yield solar cells with near-state-of-the-art conversion efficiencies.

Silicon Refinement Process Supporting Studies

Silicon Particle Growth Research (California Institute of Technology)

The objective of this research is to describe theoretically the growth of Si particles from silane in a free-space reactor and to develop experimentally the conditions for maximum particle growth. The initial experiments in the new reactor system, which was constructed to allow extension of the operating range and a more thorough study of aerosol phenomena in the silane system, were designed to replicate the results obtained in the original apparatus; similar number concentrations and seed aerosol characteristics were used. Nucleation control was a more difficult problem in the new reactor than it was in the smaller reactor. A systematic analysis of the conditions under which nucleation could be quenched provided an explanation for the difficulty. The important feature obtained from plots

of the particle size and number concentration is the presence of an extremely narrow dividing line between the formation of new particles and the growth of the seed aerosol. The experimental difficulty in reproducing earlier results was caused by the use of seed particles that were too small. Runaway nucleation was avoided and the earlier results were duplicated by increasing the seed particle size by 50%.

Theoretical calculations of the effectiveness factor for nucleation quenching yielded a range for this factor for the prevention of runaway nucleation; it is considerably larger than had been expected. Nevertheless, nucleation can be quenched at much lower number concentrations than the traditional theoretical treatment of simultaneous nucleation and particle growth indicates.

Since seed particle size is a very important parameter for the control of nucleation, a two-stage seed generator was constructed to gain additional control on nucleation. This modification enables a variation from 0.2 to 1.5 micrometers in the diameter of the seed particles entering the primary reactor stage and allows number concentrations ranging from 10^3 to 10^6 particles per cm^3 to be achieved. The grown particles were found by X-ray diffraction to be amorphous and rapidly to become crystalline when heated.

Aerodynamic particle traps were developed for the separation of large particles from a gas stream with a minimum of contamination. High particle-separation efficiencies were attained with a simple design. Collection efficiencies exceeded 80% for particles with Stokes numbers greater than about 0.5.

The program will be extended through June 1985 to enable a more extensive theoretical effort to describe the aerosol growth phenomena for this chemical system and additional experimental efforts to increase particle growth.

Microwave Heating of Fluidized-Bed-Reactor Bed (Superwave Technology Inc.)

A three-month study to investigate the feasibility of microwave heating of a fluidized bed of Si particles about 300 m in diameter under nonreactive steady-state conditions was completed by Superwave Technology Inc. and the Final Technical Report was issued. The study was conducted to improve further the JPL and UCC designs for fluidized-bed reactors by providing direct heating of Si particles, and the feasibility of the scheme was shown. The following conclusions were reached: The fluidized bed of Si particles (about 300 m dia) can be easily heated to 800°C under a non-reactive environment. Under steady state, the axial temperature variation is approximately +5°C. The maintainability of the bed temperature was demonstrated for a duration of 30 minutes after steady state was achieved. At 800°C bed temperature and 60 standard liters per minute of nitrogen flow, the power consumption is 2 kW.

As far as applicability of the scheme to a reactive system is concerned, the only concern is whether the microwave energy would couple with silane and

cause formation of excessive amounts of Si fines. The properties of silane preclude the likelihood of such fines formation.

Research on Silane Pyrolysis in Fluidized-Bed Reactors (JPL)

JPL is conducting FBR research with the objective of characterizing the deposition of Si from silane and providing information upon which significant improvements in this process can be based. Work continued to establish the process and basic mechanism for Si deposition in an FBR during silane pyrolysis.

The work concentrated on achieving a major advance in product purity by incorporating a quartz liner in the FBR, thereby preventing contamination by the metal wall material that has been found to occur. Fabrication of the support and seal for the liner was completed, and the liner system was installed and successfully tested. First, a preliminary purity run of 4-h duration with 30 mole % silane in hydrogen was conducted. Initial results of analysis of product samples by emission spectroscopy indicated that metal impurity levels were below detection limits (e.g., iron below 20 ppmw, chromium below 10 ppmw, and nickel below 8 ppmw). A high-silane-concentration run with 50 mole % silane was successfully made for 3 h, proving the mechanical integrity of the quartz-liner approach. Future emphasis will be placed on determination of product purity by neutron activation analysis and other sensitive elemental determinations.

Fabrication of a prototype polyethylene-lined fluid jet mill for making FBR Si seed material was completed. Initial data were obtained on operating parameters such as jet velocity, particle feed rate, and length of the impact chamber. Purchased Si particles of 4- to 12-mm-diameter range were used to feed the jet mill, and product was used as seed material for the FBR.

A paper titled "Fluidized-Bed Silicon Deposition" was presented at the 17th IEEE PV Specialist Conference, Florida, May 1-4, 1984. In this paper, the grown particles were shown to be crystalline and to have a structure that has been interpreted to indicate growth by chemical vapor deposition as well as by the scavenging of Si clusters on seed particle surfaces.

Modeling of Silane Pyrolysis in Fluidized-Bed Reactors (Washington University at St. Louis)

The objective of this effort is to develop a comprehensive model for the preparation of Si by silane pyrolysis in fluidized-bed reactors. The model will be useful for the interpretation of experimental data, for the determination of the ranges of operating parameters for maximum throughput and yield, and for providing a basis for the design of scaled-up reactors for pilot plants.

After reviews of the homogeneous and heterogeneous paths for silane pyrolysis and of fluidized-bed technology, fluidized-bed model equations and the rate forms for the kinetics of silane pyrolysis were derived. A

simplified model for the process was developed assuming the reactor to be completely mixed; this model is directly applicable when the bed is particulately fluidized and can be useful to calculate the beginning of fine particle formation. The model was solved for batch and continuous feed modes. A computer program was developed for this model for the case of only a heterogeneous reaction occurring. Detailed equations based on population balance models were developed to predict particle size distribution when both homogeneous and heterogeneous reactions occur.

A backmixed model was used to simulate experimental data for the JPL fluidized-bed reactor. The model without an adjustable parameter was found to match the data at silane concentrations below 20%. The JPL data were predicted by a model involving a simplified treatment of nucleation that also included one undetermined parameter. The region of high silane concentrations is now being studied.

SUMMARY OF PROGRESS
Advanced Silicon Sheet Task

Shaped-Sheet Technology

Edge-Defined Film-Fed Growth (Mobil Solar Energy Corp.)

The primary goal of this program is to develop a model for obtaining temperature-field-residual stress relationships applicable to Si ribbon growth at high speeds and to apply this model subsequently to a growth system that has been modified and improved to produce low-stress ribbon at high speeds.

Attempts to verify aspects of the stress and temperature field modeling with the 10-cm cartridge system met with limited success. Due to the complexity of the growth interface environment, it has not been possible to use the fiber-optics sensor. The cartridge system has lacked flexibility to allow imposition of changes in growth conditions and system temperature fields in a known and controllable manner in order to study temperature field-stress relationships at a quantitative level.

A new EFG low-stress growth system without cold shoes that has the flexibility for testing of the stress analysis model was constructed. Preliminary analysis of this new system showed that the stresses predicted had a similar trend when compared to the cartridge system. The temperature gradient at the growth interface was clearly identified as a major control parameter to achieve reduced stress. Further model studies will continue to evaluate the role and sensitivity of other parameters and the effects of high and low temperatures on stress. Attempts to grow 5-cm-wide ribbon in this new EFG system (in Furnace 17) were successful. A number of changes have been made from the cartridge mode of growth to simplify the thermal environment of the sheet above the growth interface. This allows more straightforward thermal and stress analysis to be performed and also gives flexibility to change the post-solidification cooling profile through adjustments of insulation. The main problems to overcome in the initial trials were: establishment of a means of balancing ribbon-edge temperature gradients, and of a technique to ramp the main zone to compensate for latent-heat generation

while the growth speed was being attained. The former was accomplished by installation of movable radiation, or "tilt," shields at die-top level. The ramping of the main zone to establish growth was found to be manageable. The transients are much slower than those customarily found in the cartridge system, but accommodation can be made easily by adjusting the ramp rate. This is done manually at present. Initial growth of 5-cm-wide ribbon at speeds of 0.7 to 1.0 cm/min has produced material with a very low dislocation density. Evidence of Lueders strain, which produces bands with dislocation densities of up to $5 \times 10^6/cm^2$, is still found. Model results for this system were obtained to relate the growth and system design parameters to sheet stress.

Creep studies in FZ and Cz Si at high temperatures have established that Si sheet above $1200^\circ C$ responds as an essentially plastic material at the stresses and strain rates expected during growth. This creep information is being incorporated into the stress analysis to obtain new predictions for residual stress buildup in the EFG test system, using a temperature-independent creep rate at high temperatures and strain rate proportional to the 10th power of stress.

A task to characterize the electrical activity of stress-induced dislocations was started. Both room-temperature and low-temperature EBIC will be used to delineate the contribution of dislocation electrical activity to overall material quality limitations. Preliminary work is being carried out on deliberately stressed and dislocated FZ and Cz Si to attempt to quantify the measurements. Comparison of dislocation activity of this material and Si sheet with grown-in dislocations is also under way. The program will additionally study Si material property changes produced by increasing boron doping levels, which are shown to produce a greater deterioration in cell efficiency in the more highly defective sheet grown for terrestrial photovoltaic applications than in the best FZ Si available.

Through a contract extension currently being negotiated, during FY85, theoretical and experimental studies on thermally induced stress in EFG Si will be continued. In addition, correlation of defects produced by stress and their electrical activity and the influence of dopant concentration or defect structure will be undertaken.

Dendritic-Web Ribbon Growth (Westinghouse Electric Corp.)

A three-year program at Westinghouse for development of Si dendritic-web crystal growth and high-efficiency solar cells made from this material was started early in CY84. The purpose is to improve this technology and demonstrate capabilities that are consistent with utility requirements. The program is being supported jointly by DOE through both FSA and the Solar Energy Research Institute, and by Westinghouse, the Southern California Edison Co., the Electric Power Research Institute, and the Pacific Gas and Electric Co. The end-of-CY84 ribbon-growth goals of this augmented program are to demonstrate an area growth rate of at least 10 cm^2/min simultaneously with growing ribbon lengths of 10 meters or more, under conditions of continuous melt replenishment (constant melt level) on a routine basis.

MATERIALS AND DEVICES RESEARCH AREA

Early in 1984 the four furnaces that have been involved in the dendritic-web research program were moved from Westinghouse's R&D Laboratory, Pittsburgh, to their Advanced Energy Systems Division facility at Large, Pennsylvania, where most of the augmented program is being conducted and where Westinghouse's pre-pilot line of web growth and cell-processing demonstration, funded by prior agreements with Pacific Gas and Electric Co. and Southern California Edison Co., is located. The four furnaces that were moved are housed in a room called the Web Growth Development Laboratory, where they have been provided with individual power supplies, allowing each to be operated independently.

Late in March a ribbon was grown for eight and one half hours with continuous melt replenishment, producing a single piece of single-crystal ribbon a little more than 5 meters in length. This was by far the longest growth period to date with continuous melt replenishment (the longest previous one was about three hours). Since long-duration growth under conditions of constant melt level is a prerequisite for attaining the program goals, this test constituted a significant step. In the same period, another test was made in which a 9.6-meter-long ribbon was grown, the longest dendritic-web ribbon ever produced. The growth time was 13 1/2 hours, and melt replenishment was not employed. The ribbon was grown using a J435 growth configuration, which has been well characterized but which tends to produce material with higher stress than later configurations, such as the J460, and data indicate a stress build-up with time. The ribbon was the longest of four that were grown over a short period, each being at least 9 meters long. The week of June 25 to 29 was the first week in which ribbon growth in the Web Growth Development Laboratory was restricted to the J460L configuration (a high-performance design with width limiting set to produce 4-cm-wide ribbon) rather than the J435 configuration. Using the J460L, a 6-meter-long ribbon was grown with melt replenishment, this being about as long as the longest ribbon that had previously been grown using melt replenishment. An initial check was made at the center of the new ribbon at the 3-meter point, and it was found that there was essentially no residual stress present, confirming the good performance of the J460L design.

A review of the dynamic furnace element program was held in May. In this effort, web growth configurations having capability for dynamic positioning (i.e., movement during growth) of thermal elements were studied. Such a scheme can allow these thermal elements to be positioned initially to provide proper starting conditions and then enables positioning during growth to optimize steady-state growth. The conclusions from the review were that dynamic control can be most effectively applied if it affects the first 1 or 2 cm above the melt; no part of the upper stack warrants control; LIN (the vertical distance from the growth front to the bottom of the susceptor lid) is the most appropriate parameter to control; and no dynamic parameter, other than LIN, that can lead to improvements has been identified. Westinghouse rejected the concept of dynamic width-limiting as unnecessary.

In testing on the pre-pilot line in 1983, it had been found that during a growth run the vertical sides of the crucible can collapse inward, interfering with proper thermal control and crystal growth. As part of the augmented program, hardware was designed and constructed in which the

crucibles have walls that are sloped outward and that lie on sloping surfaces of the susceptor. Testing of these sloped-wall crucibles was initiated and, from the start, they gave excellent ribbon growth. The melt was extremely stable, and exceptionally smooth dendrites were grown. All four furnaces in the Web Growth Development Laboratory have now been furnished with rectangular crucibles having sloped walls. These new systems have larger melt-replenishment regions and more precisely built heating coils, factors that also will contribute to better thermal control.

Tests were conducted in which thermocouples were used to measure the temperature of the molten Si in crucibles having single and double barriers that thermally isolate the melt replenishment region from the growth region. The results indicated that the new double-barrier configuration has about four times the thermal impedance of the old, single-barrier design.

Testing was begun on a long version of the J460 growth configuration (a high-performance design that is being heavily used in the program). This new version, designated the J460LS, is designed to limit the ribbon width to about 5 cm, compared with the 4-cm width of the J460L system. Results were good; the best crystal was 5.5 m long and 5.1 cm wide, with continuous melt replenishment used for the entire run. However, the ribbon was grown at a relatively slow rate (1.3 to 1.5 cm/min) and was quite thick (about 200 micrometers), because the heating coil could not be optimally positioned.

A study was initiated to investigate the feasibility of using a non-contact procedure for monitoring dendrite thickness, to aid the operator during the web growth process. The systems being investigated must have closed-loop feedback capability for automated control.

The FSA contract that has been funding the web growth research program was extended in April, with the major technical goal being the demonstration of a quasi-steady-state (defined as ribbon lengths in the order of 30 to 100 cm) area growth rate of 20 cm^2/min or more; the maximum quasi-steady-state growth rate achieved to date is 13 cm^2/min. A new contract, which will provide the remaining FSA portion of the first year's funding for the ribbon growth work of the augmented program, was started in mid-September.

Low-Angle Silicon Sheet (Energy Materials Corp.)

A positive-pressure clean-room facility was constructed, and a new furnace designed for high-quality Si ribbon growth was put into operation. There are now two furnaces being used on the program. The major emphasis thus far has been in achieving a controlled melt circulation to suppress the natural convection in the melt, and in providing a reliable temperature profile close to the solid-liquid interface. Microstructural and electrical characterizations were carried out on the grown material. Minority carrier diffusion lengths (L_D) were measured as a function of depth through the ribbon. These results indicate that L_D decreases in value from the top surface to the bottom of the ribbon. Reasons for this L_D gradient are still being investigated. Annealing studies aimed at improving L_D have not yet advanced far enough to allow any conclusions to be drawn.

MATERIALS AND DEVICES RESEARCH AREA

Silicon Sheet Supporting Studies

Modification of Silicon Surface Properties by Fluid Absorption (University of Illinois at Chicago)

A report covering the results of the research effort from June 1981 through December 1983 was published. A follow-on effort was started. It has been emphasizing the Si surface property modification by various fluids that may be compatible for high-temperature and high-speed processing, and the measurement of residual stress in Si sheet by laser interferometery.

In previous indentation tests on Si in the presence of various sodium salts having different anions, of the salts tested NaI had the greatest effect in increasing identation damage and therefore would have the greatest effect in increasing abrasive wear.

During the present reporting period, indentation tests of {111} p-type silicon in 10^{-3} molar NaI solution were made. The indentation-tested Si samples were then annealed at 1373K for two hours. The indentation rosette lengths were measured as a function of indentation load. The results verified that dislocations were generated during room-temperature indentations and that the dislocation mobility may be obtained from subsequent annealing of indents. These data are being extended to encompass other concentrations of NaI.

An effort on measuring residual stress in Si sheet using laser interferometery was made in Mobil nonagon silicon ribbon and Westinghouse dendritic web Si ribbon. The data show that the centers of the sheets have tensile residual stress while the edges have compressive residual stresses. The measured maximum residual stresses for web ranged from 0.4 to 2.5 megapascals (MPa) while those for Mobil nonagon material were 5.0 to 9.0 MPa. Based on these data, web sheet appears to have significantly lower residual stresses than the Mobil nonagon sheet.

Analysis of Stress/Strain Relationships (University of Kentucky)

The University of Kentucky continued to develop stress/strain models for Si sheet growth processes and evaluate the relationship between Si growth structure and stress/strain. A major report titled "Viscoplastic Stress/Strain Model" (for Si ribbon) was delivered. The report describes the use of a model that handles plasticity, creep, and dislocation generation in Si as a function of strain rate, initial dislocation density, and oxygen concentration. This model is based on the work of Sumino and Yonenaga of Japan for Czochralski Si, but it has been modified to handle Si sheet products. Stress/strain plots were generated for Si material near its melting point.

Elastic stress and buckling analyses using constant material properties were completed. In these analyses, the critical (i.e., for onset of buckling) thickness versus Si sheet width were compared for four thermal profiles. The analytical results are reasonable consistent with experimental observation.

Work began in calculating the pre-buckled in-plane stresses for the plastic range of Si sheet material as a function of position along the length of the ribbon. When numerically convergent solutions are obtained, it was found that the plastic stresses do not change much from the elastic ones. These convergent analyses partly reflect the use of a very low (10^{-3} to 1 dislocation per square centimeter) assumed dislocation density at the melt interface. Also, depending on the temperature profile, σ_{yy} stresses and axial σ_{xx} stresses at the outer edge of the ribbon can be relatively large.

Work on a plastic buckling model started. Also, plans were developed for a high-temperature tensile-test-type program to determine experimentally the mechanical properties of Si near its melting point.

Solid/Liquid Interface Studies (Solar Energy Research Institute)

The work on investigating the stability and shape of the solid/liquid interface of high-speed-grown Si was drawn to a conclusion with the characterization of the material grown. Several ribbons that were grown by a crucible-free horizontal sheet technique were processed into solar cells resulting in efficiencies comparable to those of the Cz controls. These cells were obtained from the large-grained areas of the sheet. The crucible-free growth process resulted in a patent being issued for the technique.

In addition to the horizontally grown ribbon, material pulled by the ESP method from a cold crucible was also investigated. Again, the solar cells made from the large-grained regions of the ribbon had efficiencies equal to those of the Cz controls.

Analysis of High-Speed Growth of Silicon Sheets in Inclined-Meniscus Configurations (Massachusetts Institute of Technology)

This program started on June 20 as a two-year effort. The purpose is to study theoretically the factors that influence the quality of Si ribbon sheets grown in inclined-meniscus configurations. The finite-element program for the idealized inclined-growth system was completed. Calculations of unstable microscopic interface morphologies have reached the point where the prediction of cellular structures caused by constitutional undercooling is practicable.

Optimization of Silicon Crystals for High-Efficiency Silicon Solar Cells (Solar Energy Research Institute)

A new effort aimed at studying the influences of the float-zoning crystal growth parameters on the minority carrier diffusion length was begun. The objective of this research is to obtain long-lifetime single crystals for high-efficiency solar cells using heavily doped material (0.1 to 0.5 Ω-cm), and to understand and reduce the limitation to achieving the long lifetimes. Toward this end, a furnace was modified to grow float-zone crystals. Gallium-doped ingots of 0.1 and 5.0 Ω-cm resistivity were grown.

MATERIALS AND DEVICES RESEARCH AREA

Characterization of the material included spreading resistance, Hall mobility, and X-ray topography investigations. The lifetime measurements used to evaluate the material, photoconductive decay (PCD) techniques and a reflected microwave PCD method, are still under development at SERI.

Materials Properties Modification (JPL)

A high-temperature inert-gas tensile testing furnace and fixtures were ordered and received from Centorr Inc. This furnace was integrated into existing closed-loop hydraulic mechanical test equipment that is already in place in the Materials Test Laboratory at JPL. The furnace and mechanical test equipment will facilitate elevated-temperature testing of Si sheet material to determine tensile and yield strength, elastic modulus, and plastic creep behavior from 1000°C to 1400°C.

High-temperature Si sheet sample and grip designs as well as sample preparation techniques were investigated for the high-temperature test program. Reduced-cross-section Si test samples are being prepared from Si Czochralski and dendritic-web ribbon materials by a microgrit-blast technique. The extent of edge damage and need for additional or different sample preparation steps will be investigated. Also, ceramic-based adhesives were procured and will be evaluated with regard to sample grip requirements. Graphite tapered-lock grips were fabricated for initial sample tests.

Effort was continued on the evaluation of fracture properties and crack propagation in Si. An acoustic emission technique was used to monitor crack propagation in a single-crystal Si wafer loaded by the double-torsion method. Acoustic emission was demonstrated to be a useful tool to monitor the location of the crack and crack growth velocity in Si sheet. The test results indicate that the acoustic events occurred only at the critical stress intensity factor. This result suggests that Si does not undergo subcritical crack growth. A paper title "Acoustic Emission Monitoring Crack Propagation in Single Crystal Silicon" was presented by C. P. Chen (JPL) and S. Hsu (Dunegan Corp.) at a conference, Review of Progress in Quantitative Nondestructive Evaluation, held at the University of California, San Diego, July 8 to 13, 1984.

Two separate, complementary stress/strain modeling activities for Si ribbon were initiated in-house. One is a quasi-static approach using a NASTRAN computer code. The other is an in-process growth modeling program utilizing an ANSYS computer code. Parametric studies are possible in both of these models. Investigation into stress, buckling, material non-linearity, creep, and crystal imperfections were started or are planned. For example, residual stress contours were generated for web ribbon in which stress history was considered. Preliminary realistic-appearing residual stress values were predicted, ranging from approximately 1000 lb/in.^{2} tension to 1000 lb/in.^{2} compression.

Device Research Task

INTRODUCTION

The objective of this task is to identify and implement research and development activities in the photovoltaic device and measurements area to meet the near-term and long-term objectives of FSA. Task activities encompass research in device physics, device structure, material-device property interaction, and measurement techniques for physical, chemical and electrical evaluation of devices and materials.

Technical Approach, Organization and Coordination

To meet FSA objectives, efforts are now directed toward characterization of various silicon-sheet materials, material-device property interaction investigation, and measurement techniques. The program of the Task is structured accordingly.

The program of the Task also includes JPL in-house activities to conduct basic research in material and device characterization to support contractor needs and other Tasks of the Materials and Devices Area.

SUMMARY OF PROGRESS

University of Washington Joint Center for Graduate Studies

The objective of this work is to investigate the fabrication and operation of inversion-layer solar cells and to measure carrier lifetimes in those cells. Experiments to determine the effects of various RF power levels on surface-state densities, the effects of temperature of deposition, and the effects of surface passivation on surface-state densities have been completed.

Studies of SiN_x-Si interface properties have been conducted for SiN_x films grown on silicon for a range of film-growth conditions. Films were grown on silicon wafers having (100) orientation and resistivity of 2 ohm-cm. Two basic cleaning procedures were used: RCA cleaning procedure and an abbreviated process that omits the RCA peroxide steps. Substrates either had a native oxide or a thin oxide film (20 A) formed by heat treating the wafer at 500°C for 20 minutes in oxygen. Surfaces were either nitrided or not nitrided. Nitridation involves exposing a surface to a RF plasma and ammonia using 15 W RF power, 70 sccm NH_3 flow, and 270°C platen temperature. Thus, six initial surface conditions are defined by the various combinations of two chemical cleaning steps (RCA or abbreviated), two oxide films (native or 20 A), and whether nitrided or not.

After surface preparation, SiN_x films were deposited with an RF power of either 13 W or 75 W, and with the platen temperature at 150°C or 270°C. After deposition of the films, aluminum gates were deposited on a region of the substrate and the surface density obtained using high frequency C-V measurements. Effects of heat treatment were studied by annealing the films and depositing additional gates on another region of the substrate, and

then conducting C-V measurements. Some key results obtained from this study are: (1) SiN_x film deposition at low RF power (0.025 W/cm^2) leads to lower surface state densities; (2) deposition at 270° is preferable for low surface-state densities; and (3) nitriding the silicon surface before Si-N deposition results in low surface-state densities.

Some cells without AR coatings were provided by JPL for deposition of SiN_x. Measurements made on the cells after the SiN_x deposition indicate that the SiN_x layer has little effect on the surface recombination velocity of these cells. Efforts to utilize the Rosier method for determining the surface recombination velocity on completed n-p cells have also been initiated.

University of Southern California

The objective of this work is to develop a new laser measurement technique for studying deep-level traps and material defects in silicon. Results already obtained from this work clearly indicate that deep-level states can be measured using a one-micrometer-wavelength laser and a cryogenic calorimeter.

In the period since the last PIM, work has fallen into three categories: (1) development and testing of the cryogenic calorimeter, (2) optical absorption measurements on silicon carried out by means of laser calorimetric spectroscopy to determine the capability of the method for studying deep-level impurities, and (3) theoretical considerations of optical absorption techniques.

Operation of the calorimeter at liquid nitrogen temperatures was demonstrated. Measurements of the absolute accuracy of the apparatus were carried out, and it was determined that the principal limitation on its accuracy was uncertainty in the sample specific heat (which varies with temperature and free carrier concentration). A method for measuring the sample heat capacity by electrical heating was developed.

Optical measurements using 1.9 μm-wavelength light derived by coherent-Raman shifting of 1.06 μm-wavelength light from a Q-switched Nd:YAG laser were carried out. It was determined that band-to-band two-photon absorption dominated the signal. Consequently, the high intensity of the light derived from Q-switched lasers adds undesirable complications to the data analysis. This means that CW sources such as color-center lasers or incandescent lamps are preferable for spectroscopic studies of deep levels.

C.T. Sah Associates

The objective of this work is to determine the relationships of material properties in producing high-efficiency silicon solar cells.

Accurate measurements of the capture and emission rates of electrons and holes at one- or two-level recombination centers have been accomplished in one silicon p-n junction diode. The residual recombination levels are limiting the efficiency of high efficiency solar cells to values several

percentage points below the intrinsic (Auger and radiative) recombination-limited ultimate efficiency. A new method using minority carrier injection by forward biasing the p-n junction has been implemented. Detailed measurements have been completed and reported. The report describes the possibility of residual metallic recombination centers from titanium, zinc and gold which could be introduced either during crystal growth or subsequent high-temperature fabrication of the cells. Other possible residual impurities, defects, impurity-defect and defect-defect complexes, which may be recombination sites for the photogenerated electrons and holes, are being systematically measured.

Research Triangle Institute

The objective of this work is to develop a comprehensive silicon solar cell computer model. The first phase of programming has been completed and shows good agreement between the computer data and experimental data.

Coding of the simulation program has been completed, including the main program and a comprehensive set of phenomena submodels. All portions of the program have been debugged and the simulation results checked by hand calculations. Input parameters have been assigned several values, within their allowable or typical ranges, and simulation results checked for reasonableness. Simulation accuracy has also been investigated using experimental 10%. Initial studies show that the agreement between simulation and experimental data is significantly better than 5%.

The usefulness of the simulation program has been demonstrated in those cases where the cell's manufacturer is uncertain of the values of the material properties. Application of the program reveals the values of the parameters, separately or in combination, that result in agreement with the cell's electrical terminal or other device characterization parameters. For example, it can be shown for an n-type diffused or ion-implanted emitter region that Auger recombination is the dominant process. This result is obtained because the SRH process gives a collection efficiency of greater than 95%, whereas the experimental value is approximately 60%. This requires a lifetime value lower by 10^{-3} to overcome the strong aiding electrical field in this region. Auger recombination is the more reasonable process to represent lifetime values (i.e., $<10^{-10}$ sec.) required for these cases.

University of Florida

The objective of this work is to study effects of surface parameters on the performance of silicon solar cells and identify any allied properties that might affect performance. Initial work included an extensive literature search, which has been completed. The conclusion drawn from the search was that some of the Auger recombination measurement methods (Possin, Weaver, Swanson) have not taken the effects of doping dradient fields into account.

It was further concluded that photoluminescence is, by far, the only method likely to succeed in giving meaningful results from Auger lifetimes.

MATERIALS AND DEVICES RESEARCH AREA

Cornell University

The objective of this work is to investigate the physical structure and the chemical nature of defects in silicon sheet material. The study of precipitates has been the primary means of investigation, inasmuch as solar cell efficiency depends on junction perfection, which in turn is affected by the number of precipitates, information from these studies is expected to lead to a better understanding of the interaction between phosphorus and carbon diffusion in silicon.

A study of the defect structure of high-carbon Cz material is under way. This study will try to separate structural effects from chemical effects.

In Cz material with high carbon content, the junction region showed a high defect density. The spatial distribution of precipitation was uniform. The size distribution showed a peak at 400 A and tailed out at 1600 A as observed from analysis of 252 precipitates. FTIR measurements of oxygen concentration have been conducted and SIMS measurements and creep tests are planned in the near future.

Applied Solar Energy Corporation

This new contract will investigate solar processing techniques needed to produce high-efficiency solar cell structures. Work is currently directed at producing a high-efficiency cell structure proposed by C. T. Sah Associates.

State University of New York at Albany

The objective of this new contract is to study oxygen-related and carbon-related defects in silicon solar cells.

An extensive literature search on oxygen behavior in silicon has been performed. A study of the formation kinetics of oxygen precipitates in silicon is under way.

JPL (In House)

In the past, JPL had developed an electron-beam-induced current (EBIC) technique to measure recombination velocity at the back surface(s) of cells. Currently, JPL is performing a feasibility study of developing an EBIC method that will be capable of measuring recombination parameters in the front layer. The approach is to measure short-circuit current induced by electron beam as a function of electron energy (1-10 keV) and then to analyze the data with the aid of a sophisticated solar-cell simulation program, Solar-Cell Analysis Program in One Dimension (SCAP1D).

Oxidization of the front silicon surface of the cell has been demonstrated to be an effective approach for reducing surface recombination velocity. The recombination is mainly due to the existence of localized states at the oxide-silicon interface. JPL has established a capability of measuring the density of states at the interface using C-V measurements. The

preliminary result indicates that the density of states at the interface with the oxide grown by the existing process on p-type substrate is about $5 \times 10^{11}/cm^2$ eV. An effort to optimize the oxidation process for the front surface passivation is in progress.

The minority carrier diffusion length measuring system in the Devices and Materials Characterization Laboratory has been upgraded to include the capability of measuring spectral response.

A typical high-efficiency silicon solar-cell design reported in the literature is considered for performing sensitivity analyses with respect to various design parameters using Solar-Cell Efficiency Estimation Methodology and Analysis (SEEMA) scheme.

SEEMA uses SCAP1D (developed by Professor Richard Schwartz of Purdue University) for evaluating the performance of a solar cell of a given design. SEEMA also uses SUPREM-II (Stanford University Process Engineering Models) for obtaining the impurity profile data, given the diffusion process control parameters such as temperature and time. The impurity profile data supplied by SUPREM-II is used as input to SCAP1D as one of the doping profile options.

Sensitivity analysis is performed with respect to the following parameters: (1) various doping profiles such as complementary error function, step, profile generated by SUPREM-II; (2) front-surface concentration; (3) junction depth, and (4) surface recombination velocity at the front surface.

Solar-cell parameters such as short-circuit current, open-circuit voltage and efficiency predicted by the simulation model are in close agreement with the experimental results of the cell considered.

PROJECT ANALYSIS AND INTEGRATION AREA

INTRODUCTION

The objective of the Project Analysis and Integration Area (PA&I) is to support the planning, analysis, integration, and decision-making activities of FSA. Accordingly, PA&I supports the Project by developing and documenting Project plans based, in part, on the technical and economic assessments performed by PA&I of the various technical options. Goals for module technical performance and costs, derived from National Photovoltaics Program goals, are established by PA&I for each of the major technical activities in the Project. Assessments of progress toward achievement of goals are made to guide decision-making within the Project.

SUMMARY OF PROGRESS

Flat-Plate Module Efficiency versus Cost Tradeoffs

This study was presented during the plenary session of the PIM. The viewgraphs are reproduced in the Proceedings.

The study objective was to use the five-year Research Plan energy cost methodology and to make an in-depth analysis based on the extensive data that are relevant to PV systems to facilitate the accomplishment of the 0.15/kWh energy cost goal.

Studies such as this are used by FSA management to formulate allocation guidelines that are used to monitor the accomplishment of the cost-reduction and efficiency-increase goals. These allocations are research targets (not projections) that appear to be achievable.

Analysis of a Float-Zone Manufacturing Sequence

Float-zone material has been investigated as an option for high-efficiency cells. The Standard Assembly-Line Manufacturing Industry Simulation (SAMIS) computer model has been used to compare PV module manufacturing based on float-zone crystal growth with a similar manufacturing sequence based on Czochralski crystal growth. The SAMIS computer runs indicate an economic advantage to float-zone growth even if the subsequent cells produced have an efficiency equivalent to Czochralski cells. If float-zone cells have higher efficiencies than Czochralski cells, the economic advantage of float-zone appears to be quite substantial, given further development of float-zone crystal growth techniques. Float-zone crystal growth is of renewed interest since the PV Program emphasis on high efficiency emerged. Most of the laboratory experimental high-efficiency cells have been made from float-zone material.

23

PROJECT ANALYSIS AND INTEGRATION AREA

Microcomputer Implementation of SAMIS

Cne of the principal impediments to widespread use of FSA-developed models has been the cumbersome procedures required to run them on time-sharing mainframe computers. Microcomputers have now developed so far that these models can be transferred to them from mainframes with very little loss in model scope. To permit access by industry to the Solar Array Manufacturing Industry Costing Standards (SAMICS) model developed by FSA, it is currently being implemented on a microcomputer. As part of the effort to implement SAMICS, IPEG has been converted as a test case. IPEG can now be run on an IBM PC-XT and will soon be available through the Computer Software Management Information Center (COSMIC).

Metallization Cost Analysis

The metallization cost analysis is being updated. A review and update of the original data is near completion and the analysis is being expanded to include reliability as part of a performance ratio.

Allocation Guidelines

The updated Allocation Guidelines for flat-plate PV modules have been completed. Baseline allocations are 15% efficiency at standard test conditions (STC) for modules costing $90/m^2$, equivalent to $0.15/kWh given 2400 kWh/$m^2$·yr insolation for a one-axis tracking option. Alternative insolation levels of 2700 kWh/m^2·yr and 2250 kWh/m^2·yr have been used to derive allocation guidelines that are otherwise identical with the baseline allocations. An insolation level of 2700 kWh/m^2·yr is typical, for example, of areas such as Southern California, Arizona, New Mexico and Nevada. Florida, on the other hand, would be most representative of the 2250 kWh/m^2·yr insolation level. Each set of allocations is parametric with efficiency. It appears that the efficiency/cost goals established by the PV Program for flat-plate modules are technically feasible.

Photovoltaic Systems Sensitivity Analysis

The PV system sensitivity analysis has been expanded to incorporate new sets of baseline parameters. In particular, baseline insolation levels of 2000 kWh/m^2·yr and 1850 kV./m^2·yr have been used to extend the results of the 2250 kWh/m^2·yr analysis. Additionally, the choice of an appropriate indirect cost multiplier is being investigated. Analysis of marketing and distribution costs, taxes, and interest during construction have been completed; however, information is required to access contingency, engineering, and owner's cost markups and their contribution to the indirect multiplier.

Photovoltaic Energy Payback

In a Science Magazine article, R. Kaufman of Complex Systems Research Center, University of New Hampshire, compares PV with other energy options.

Kaufman reports a ratio of energy produced to energy consumed of about 10 which, assuming a 30-year lifetime, gives an energy payback time of a PV system today of about three years. This reflects actual progress in silicon purification, encapsulants, system design, and module efficiency. Information regarding PV energy payback times had been sent to Kaufman by PA&I before publication.

Inflation Values

Current values for inflation for the years 1975 to 1984 have been distributed within the PV Program. Inflation from January 1982 to January 1984 was only 8%. This is an average annual rate of about 4% and represents a significant decline from earlier years.

PROCESS DEVELOPMENT AREA

INTRODUCTION

The objective of the Process Development Area is, by conducting research in appropriate critical technology areas, to improve high-efficiency PV-cell and module formation. Process research is grouped into three areas for convenience of reporting: junction formation, metallization and directed-energy technology.

SUMMARY OF PROGRESS

Process research efforts have shifted from surface preparation techniques to directed-energy technologies. Various laser and microwave investigations have been started. Some early results are encouraging.

A spectrophotometer has been obtained and installed to assist in film deposition measurement.

Seven papers, one new technology report and one patent application were submitted during this reporting period.

JUNCTION FORMATION

Westinghouse Electric Corp., Advanced Energy Systems Division, has not been able to overcome the cross-contamination problem during simultaneous front and back diffusion of polymer dopants. Other junction formation techniques such as laser drive-in are being explored as alternatives.

Spire Corp., has achieved good cell efficiencies by laser-annealing ion-implanted cells. Both polished and texture etched cells are being studied with non-AR-coated efficiencies of 10.5% (polished) and 12% to 13% (textured) being reported.

METALLIZATION

Purdue University has improved adhesion of silver deposited from silver neodecancate by changing to a benzene solvent with higher vapor pressure. Furnace profile changes also helped. Addition of other metallo-organic compounds is being considered.

Spectrolab Division of Hughes Aircraft Corp. has completed its study of the molybdenum-tin thick-film ink system. Good adhesion was obtained but an overprint of silver was needed to ensure good solderability.

An ion cluster beam (ICB) deposition system has been demonstrated with application of silver to both silicon and gallium arsenide surfaces.

Investigation of amorphous metal films at the California Institute of Technology (Caltech) has been improved thermal stability of tungsten-zirconium films over the earlier tungsten-nickel films. Addition of nitrogen by

PROCESS DEVELOPMENT AREA

reactive sputtering can mitigate the chemical activity between the amorphous film and the substrate or metal overlayer.

DIRECTED-ENERGY TECHNOLOGY

ARCO Solar, Inc., is investigating the use of excimer lasers as an energy source for annealing ion-implanted cells and for metallization. The metal deposition approach is ultraviolet (UV) photolysis of gas-phase reactants.

Spire Corp., is also using an excimer laser (reported above, under Junction Formation). Westinghouse Electric Corp., R&D Division, is using an argon-ion laser for metallization.

Superwave Technology Inc., has successfully deposited silicon by using a microwave energy source rather than the conventional RF source.

RELIABILITY AND ENGINEERING SCIENCES AREA

INTRODUCTION

The objectives of the Reliability and Engineering Sciences Area are to develop the reliability-durability technology base required to achieve 30-year-life flat-plate photovoltaic modules and to develop the engineering sciences base required to integrate low-cost cell and module technologies into cost-effective and safe arrays that meet the operational requirements of future large-scale applications. Elements of the first objective include: failure mechanism identification and understanding; module reliability prediction tools; test, measurement and failure analysis technologies, and 30-year-life materials and designs. Elements of the second objective include operational and safety requirements, electrical and fire safety technologies, structural design technologies, temperature control technologies, and electrical circuit technologies.

These items are addressed in the context of the DOE Five-Year Research Plan and are reported herein in a structure corresponding to the organization of the Plan.

SUMMARY OF PROGRESS

Materials Research: Testing of Thin-Film Cells and Modules

A test program is under way at Clemson University to investigate first-order failure mechanisms on thin-film cells. At least three different cell types have been obtained to initiate the program. Initial tests are identical with those developed by Clemson for use with crystalline-silicon cells, to get baseline data.

After a Request for Quotation was issued to five contractors for amorphous-silicon modules, quotations were received from Chronar Corp. and from Hughes Aircraft Co. Purchase orders have been issued to both companies. Module deliveries are expected from Chronar in October and from Hughes in January.

A research forum on Reliability and Engineering of thin-film modules will be held in February 1985.

Collector Research: Advanced Module Development

Work is continuing at Spire Corp. on the development of a high-efficiency silicon cell module. With one processing regime a batch of module cells has been manufactured having average efficiency of 15.5%. Other regimes will be tried to optimize the process for maximum efficiency at NOCT.

Minimodules are being ordered using the basic designs expected for high-efficiency modules. These minimodules will be used for a reliability test program aimed at identifying failure mechanisms inherent in the high-efficiency module designs.

RELIABILITY AND ENGINEERING SCIENCES AREA

Systems Research: Module Reliability

Reliability and Physics Studies

1. Electrochemical Corrosion Research

    A series of 60-volt and 500-volt tests conducted on polymer-
    encapsulated two-electrode cell-frame samples exposed to several
    temperature-humidity environments has yielded a wealth of information
    relating leakage current levels integrated over exposure times with
    cell power output reduction as a measure of photovoltaic electro-
    chemical degradation. These data, together with reduced SOLMET
    weather data, provided the input to test a photovoltaic array
    life-prediction algorithm developed to determine yearly average
    module field failure rates.

    More recent experiments have refined the definition of mean cell
    failure charge transfer level and have focused on the mechanisms of
    electrochemical degradation. In particular, it has been observed
    that for positive and negative cell polarities (with respect to the
    grounded frame) the degradation mechanisms differ, but the degradation
    rates are of comparable magnitude.

    In another experiment PVB- and EVA-encapsulated modules, hermetically
    sealed and unsealed, were "piggybacked" onto the humidity-freeze
    test, a part of the standard JPL module qualification test, to
    determine if module qualification tests can spot potential
    electrochemical failures. It was learned that sealed modules,
    responding only to temperature stresses, experienced degradation
    equivalent to one to two years of exposure in a field environment
    such as Miami, whereas unsealed modules experienced four to 84 years
    of equivalent field exposure, depending upon the module encapsulation.

    These results have stimulated present research focusing on determining
    equilibrium leakage current levels of fielded modules and determining
    the effect on module electrical conductivity—hence electrochemical
    corrosion—of hermetic and non-hermetic substrate films.

2. Reliability and Durability of Bonded Material

    Chemical bonding work (Dow Corning Corp., Case Western Reserve
    University, University of Cincinnati) is continuing in the
    development of a reduced number (no more than three) of
    general-purpose primers for all photovoltaic module interfaces.
    Separately, investigative work is continuing to arrive at routine
    laboratory capabilities to monitor interfaces spectroscopically for
    fundamental information related to chemical debonding mechanisms and
    aging kinetics for assessing bond life potential.

    Dow Corning has observed that EVA bonds strongly to aluminized back
    surfaces of solar cells, when using the standard EVA-glass primer
    system. Ordinarily, EVA bonds weakly to aluminum foil or sheet
    stock, using the same primer; therefore, this observation with the
    solar cells was not expected. The chemistry of the aluminized

30

back surface is now being examined by combined scanning electron
microscopy (SEM) and electron dispersion spectroscopy (EDS) analysis
at the University of Cincinnati, where initial observations are
finding that the back surface is a mixture of aluminum and silicone.
If it can be assumed that the silicon may be present as an oxide, or
as a hydroxide, then perhaps the back surface has glass-like
chemistry, which would help to explain the Dow Corning observation.
If true, and if the process of aluminizing the back surface of a
solar cell generally results in a glass-like chemistry, then the task
of bonding a pottant to a solar cell may be simplified significantly.

3.   Photothermal Degradation Research

Data obtained from flash electron spin resonance studies has shown
that chemical intermediates of polymer outdoor photothermal
degradation behaved non-linearly with respect to light intensity. It
is important to determine quantitatively this non-linear relationship
to design meaningful accelerated testing procedures. During the past
quarter photothermal aging of EVA specimens at 2 suns and 6 suns were
carried out. Yellowing (loss of transmittance of EVA) had been
monitored as a function of time. The rate of EVA yellowing at 6 suns
is approximately 1.7 times faster than that obtained at 2 suns.
These data support a model in which the rate of EVA yellowing due to
photothermal aging is proportional to the square root of light
intensity.

Other data obtained show that the overall rate of photothermal
yellowing is governed by three mechanisms:

(1)   Thermal-induced yellowing

(2)   Photo-induced bleaching

(3)   Photo-induced yellowing

The photo-induced bleaching contribution is significant; rate of
thermal yellowing is found to be faster than that of photochermal
yellowing. Individual rates of these reactions are being determined
to develop a quantitative model measuring transmittance loss as a
function of environmental stress parameters.

Springborn Laboratories has prepared a draft of its annual report.
New work at Springborn will involve encapsulation process sensitivity
analysis, module flammability, electrical insulation life prediction,
polymeric and reactive protection stabilizers for high-temperature
pottant service, and increased use of outdoor heating racks for
accelerated aging in the natural terrestrial environment. A two-year
contract extension for Springborn has been issued.

All technical work at Spectrolab on encapsulation engineering modeling and analysis, as contractually required, has been completed and a final report is being prepared. An 18-month contract extension was issued in September.

Polytechnic Institute of New York has started synthetic work on a new class of UV stabilizers with carboxyl groups in the benzotriazole group. It is proposed that the compound 2,4-(2H-carboxybenzotriazole-2-yl) 1,3-dihydroxybenzene (DCBDH) be prepared from the diazonium salt of 4-amino-3-nitrobenzoic acid and resorcinol. The Institute is also working on the incorporation of previously synthesized UV stabilizers into polyesters and polycarbonates, and has initiated a study on the incorporation of these stabilizers in epoxy resins.

The University of Toronto is continuing its efforts on computer modeling of the photodegradation of polymeric materials. Polyethylene was used as the model compound for previous EVA photodegradation modeling, because of the similarity in chemical structure between polyethylene and ethylene vinyl acetate copolymer (EVA). It was assumed that the addition of the vinyl acetate group would act only as a perturbation to the polyethylene system. In the past quarter, computation of EVA was initiated. The time to failure required for an unstabilized EVA was found to be similar to that of an unstabilized polyethylene. These data lend support to the assumption that polyethylene is a valid model for EVA photodegradation.

4. Reliability Prediction and Management

Efforts focused on summarizing the overall status of module reliability from mechanism and circuit-redundancy perspectives. A paper titled "Technology Developments Toward 30-Year-Life," by R.G. Ross, Jr., was presented in a plenary session at the 17th IEEE Photovoltaic Specialists Conference on May 2. The present work updates the reliability goals for 13 principal failure mechanisms and defines the research status of each. Detailed life-prediction modeling efforts are nearing completion on electrochemical corrosion. Recent work on temperature-humidity aging was presented at the 1984 IES meeting in a paper titled "Assessing Photovoltaic Module Life from Long-Term Environmental Tests," by D.H. Otth and R.G. Ross, Jr.

In developing techniques to extrapolate accelerated photothermal test data to simulate 30-year field exposure, an analytical model was developed that incorporated the measured dependency between transmittance loss and UV and temperature exposure levels. This model was exercised using SOLMET weather data extrapolated to 30 years for various sites and module-mounting configurations. Preliminary results indicate that ground-mounted arrays using an encapsulant such as EVA should undergo degradation within the 30-year allocation of 6%; roof-mounted arrays produce marginal results. The

conclusions are that temperature is a key driver to photothermally induced transmission loss (approximate doubling of rate per 10°C) and that the sensitivity of transmission loss to UV level is highly nonlinear with the minimum in the curve near 1 sun. Future work includes refinement of the analytical model using additional data taken in the region of 1-sun UV exposure and repeating the thermal-UV exposure tests with the addition of humidity to study the impact of this variable.

Module and Array Engineering Sciences

The proceedings of the Central-Station Array Research Forum held at Sacramento, California, December 5-8, 1983, has been issued as JPL Document No. 5101-247, titled "Proceedings of the Flat-Plate Solar Array Project Research Forum on the Design of Flat-Plate Photovoltaic Arrays for Central Stations."

1. Operating Temperature Characterization of Roof-Mounted Arrays

    This activity evaluates the influence of environmental parameters on module thermal performance. Some results were reported in a paper titled "Thermal Performance of Residential PV Arrays," by L. Wen, presented at the ASES Annual Meeting June 5 in Anaheim, California. A report titled "The Influence of Environmental Parameters on the Thermal Performance of Photovoltaic Modules" is being prepared; it focuses on reducing uncertainties involved in NOCT testing and analytical predictions. Also, work is continuing on simplifying the procedure for determining the NOCT value of a PV module. This effort is supported by the environmental test activity and indicates that adequate NOCT values can be obtained from comparative measurements from a module and a reference plate.

2. Hot-Spot Heating with Complex Series-Parallel Source Circuits

    Hot-spot testing data were used to develop guidelines for future testing of modules to determine hot-spot susceptibility in central-station applications where multiparallel cell strings are prevalent, leading to a risk of current imbalance and severe hot-spot heating. The results of this effort, including guidelines for circuit-design strategies to reduce the risk of hot-spot problems, were summarized in a paper titled "Determination of Hot-Spot Susceptibility of Multistring Photovoltaic Modules in a Central-Station Application" by C.C. Gonzalez, et al, for the IEEE Photovoltaic Specialists Conference in Orlando, Florida in May. The paper was jointly written with ARCO Solar, Inc., and Acurex Corp.

3. Bypass Diode Integration Studies

    The General Electric Co. (GE) final report on the integration of bypass diodes in photovoltaic modules and arrays was distributed in May, 1984. GE prices for field-installed diode packages, when

revised to include only costs associated with the bypass function, were found to be of the same order of magnitude as those of other organizations. A technical paper on this work, titled "The Integration of Bypass Diodes with Terrestrial Photovoltaic Modules and Arrays," by N.F. Shepard, Jr., and R.S. Sugimura, was presented at the IEEE Conference of May 1-4, 1984, in Kissimmee, Florida.

Experiments are planned to develop a qualification procedure for determining the relative reliability of module bypass diodes. This effort will also help to define heat-sink requirements for diodes to determine whether low diode-attributed costs are attainable while maintaining diode reliability.

4. Module Flammability Research

In collaboration with ARCO Solar, Inc., a series of exploratory tests were completed at Underwriters Laboratories, Northbrook, Illinois, to characterize module back-cover temperature during fire testing and to increase fire resistance by material selection. Class A spread-of-flame tests and Class A burning-brand tests were conducted on July 24-25 on experimental modules made with improved construction techniques and using the following back cover materials: Kapton (2 and 3 mils), thermoseal mica plate, fiberglass-silicone rubber, and fiberglass-neoprene rubber. A preliminary conclusion is that the Class A burning-brand test is more severe than the Class A spread-of-flame test or the Class B burning-brand test.

Plans were completed for the next series of module flammability tests at Underwriters Laboratories, scheduled for October 23-25, 1984. Discussions with Gila River Products, Phoenix, Arizona, and HITCO Materials Division, Gardena, California, on high-temperature materials resulted in delivery of sample proprietary back covers to ARCO Solar, Inc. and Solavolt International for incorporation into test modules. The primary objective of the next series of tests is to identify non-conductive, back-surface materials and module configurations that can withstand Class A burning brands.

Results of initial research efforts that focused on Class B burning-brand tests were summarized in an IEEE paper titled "Flammability of Photovoltaic Modules," by R.S. Sugimura, et al, for the May 2 conference in Kissimmee, Florida.

MODULE PERFORMANCE AND FAILURE ANALYSIS

1. Solar-Cell Parametric Reliability Testing

Cell parametric reliability testing continues at Clemson University on encapsulated and unencapsulated cells in two areas: real-time rooftop testing and Arrhenius-type temperature-humidity testing. Clemson research on failure analysis of single-crystal cells has identified one potential cell failure mechanism, found in accelerated stress testing of p-on-n type cells: Schottky barrier formation on

the back-side contact. A paper titled "Degradation in Silicon Solar Cells Caused by the Formation of Schottky Barrier Contacts During Accelerated Testing," by J.W. Lathrop, et al, was presented at the IEEE Photovoltaic Specialists Conference in May 1984.

In a separate cell reliability research testing activity, cells are being exposed to the outdoor environment, in situ on test racks on the roof of an engineering building at Clemson University. The unique aspect of this test is that both encapsulated and unencapsulated cells are included. There are special jigs for holding individual unencapsulated cells. Preliminary data developed in this test will provide new insight into reliability attributes of unencapsulated silicon solar cells.

Renewed interest in high-efficiency silicon cells has led to a new round of cell-reliability testing. Test samples of new versions of high-efficiency cells from two manufacturers have been obtained. These samples are now undergoing accelerated stress testing in the Clemson test program and will be compared with earlier, lower-efficiency cells.

2. Module Parametric Reliability Testing

The development of humidity degradation rates and the identification of key electrochemical failure mechanisms continues for generic module designs based on temperature-humidity testing cycles and data from SOLMET weather tapes. Block V and several commercial designs have been combined in the minimodule test set for endurance testing at Wyle Laboratories. Although EVA encapsulants have been well represented, aliphatic polyurethane silicone samples have been involved as have samples from specific large-application experiments such as SMUD and Georgetown. To study the long-term effects of electrochemical cell corrosion, dual-polarity tests have been included in the six environments (55°C/40% RH and 85°C/85% RH; 70°C/40% RH and 70°C/85% RH; 85°C/40% RH and 85°C/85% RH).

3. Module Environmental Testing

The environmental test activity has continued with its three current major module groups: Block V modules, commercial modules procured under Block V type contracts, and commercial modules procured to investigate module developments.

Tests on the Block V Group 1 modules have been completed. The initial round of tests on the Block V Group 2 modules (ARCO Solar, Inc., Mobil Solar Energy Corp., and Solarex Corp.) has been completed only on the ARCO modules. However, some retesting must be performed on ARCO modules that have not yet been delivered. Furthermore, because of a series of problems (glass delivery, glass breakage, cell breakage during lamination) Solarex has not delivered all of its modules.

RELIABILITY AND ENGINEERING SCIENCES AREA

For the commercial modules procured under Block V-type contracts, the only significant remaining tests are those to be performed on the Solenergy Group 2 modules. For this group, Solenergy has changed to a laminated design with EVA encapsulant, for which a design review was held on August 22, before approval for module fabrication.

Results of environmental testing performed during the report period:

Vendor Code	Quantity	Test	Results
GR5H	4	Wind	Asphalt shingles at top of roof lifted by wind
YL5H	2	T-200	More touching and sagging of cells; diode short and 1/3 loss in power
US5P	6	Final Hipot, Cont'y	Satisfactory; four more modules to be submitted for retest of J-boxes
YL5P	4	T-50	Satisfactory
	4	HF-10	Some discoloration
	4	M-10K	String resistance increased 0%, 10%, 58% and 64% respectively; one edge gasket came loose at one end, bowing out end rail
LS5P	4	T-50	Slight back-surface material shrinkage; modules installed in JPL roof frames per vendor design; modules slid out of position in frames
	2	T-200	Fatigue stress marks on 20% of the interconnects
	4	HF-10	One module had bubbles in encapsulant
	2	M-10K	Satisfactory (2 are still to be tested)
BQ4H	2	T-200	Electrical failure: 52 and 37 interconnects broken, respectively; both modules showed discolorations around frame, J-boxes loose and air bubbles
BM2H	6		
BMOH	6	Final	

Vendor Code	Quantity	Test	Results
BEOH	6	Hipot,	Satisfactory
BQ4H	6	Cont'y	
BR2H	2		
BFOJ	5	Final Hipot, Cont'y	Tests were to back metal panel only; one module failed hipot, 5 failed continuity
BZOH	4	Final Hipot/ Cont'y	Hipot satisfactory, no continuity by design
BX2H	6	Final Hipot, Cont'y	Hipot satisfactory; all failed continuity
BX3H	1	HS-100	Satisfactory
BD2H	2	T-50	Satisfactory
		T-200	Electrical failure, one module; 11 and 13 interconnects cracked, respectively
BQ3H	1	HS-100	Satisfactory
BR2J	2	T-50	Satisfactory (retest of J-box adhesive)
SR5H	2	T-200	3 interconnect cracks, 1 module; more delamination with small Tedlar tears, some discoloration
	1	HS-100	Satisfactory
	1	T-50	Improved laminate process module showed no delamination

Notes:

T-50	=	50 thermal cycles, $-40^{\circ}C$ to $90^{\circ}C$
T-200	=	150 additional thermal cycles
HF-10	=	Humidity, $85^{\circ}C/85\%$ RH, $-40^{\circ}C$, 10 cycles
M-10K	=	Mechanical cycling, 50 lb/ft^2, 10,000 cycles
HS-100	=	Hot-spot test, 100 cycles

4. **Module Field Testing**

A report of the field test results at the sites monitored by JPL since 1981 has been published in JPL Document No. 5101-254, FSA Field Test Annual Report, August 1981-January 1984.

RELIABILITY AND ENGINEERING SCIENCES AREA

5. Electrical Measurements Technology Development

A series of silicon reference-cell performance measurements conducted by JPL and SERI has ultimately resulted in data showing that the SERI calibration values now match the JPL values very closely.

JPL has assembled and calibrated a set of four reference cells that will be included in a round robin of measurements being conducted by the Commission of European Communities (CEC). The cells were shipped to the CEC Research Centre, Ispra, Italy. A total of 128 cells from five countries will be measured in seven countries. JPL is scheduled to receive the cells for measurement next February.

JPL is also participating in a round robin of reference cell and module measurements being conducted by British Petroleum. The measurements at JPL, in progress, will be followed by measurements at the Royal Aircraft Establishment and at the Ispra Research Centre.

A filter has been designed and ordered for installation in the LAPSS to provide an air mass 1.5 global spectrum. The modification will be useful for global spectrum measurement of both silicon modules and amorphous-silicon modules. Reference cells suitable for measurement of amorphous-silicon modules are being prepared.

6. Failure Analysis and Reporting

Failure analysis was performed on a Solenergy Corp. module that had a reported 15.2% power degradation after a series of thermal and mechanical tests. Non-destructive tests were performed with the solar-cell laser scanner (SCLS), Sun-U-Lator and corona discharge tester. Mechanical probes and cell isolation techniques were used to measure the performance characteristics of interior cells. The electrical degradation of the module was verified but it was found not to be associated with any particular cell or group of cells. This suggests the possibility of an optical degradation, such as increased reflection or absorption of incident radiation due to degradation of the RTV encapsulant or antireflective coating, or of delamination, but these modes were not directly confirmed. The fact that other Solenergy modules also showed appreciable degradation only after HF-10 and T-200 environmental tests in which discolorations and delamination were observed throughout the module lends more credence to the suggested failure mode.

As part of continuing efforts to establish failure-analysis techniques suitable for evaluating, characterizing and analyzing thin-film amorphous silicon solar cells, an argon laser was integrated into the existing SCLS. The laser's six selectable spectral lines significantly expand the capability of the SCLS and also provide the means for depth-profiling cell performance properties. Investigations on the commercial modules (Sanyo AM-7802 and AM-7703) are continuing and include performance characterization

and technology assessment with emphasis on developing the data base
needed for the investigation of failure modes and mechanisms. Power
output, shunt and series resistance and conductivity measurements
were made under various test conditions, such as optical and
thermal. One interesting result is that the energy conversion
efficiency of commercial-quality a-Si modules is less than 2%, which
is well below that reported for experimental cells (7.4% to 11.7%).
SCLS photocurrent images for two different laser lines clearly show
difference response characteristics. This indicates that different
lines could be used to obtain information on different parts of the
device. This study is continuing.

A paper titled "Discoloration of Poly (Vinyl Butyral) in Cells
Exposed to Real and Simulated Solar Environments," by Q. Kim and A.
Shumka, was published in Solar Cells, in September, 1984.

RELIABILITY AND ENGINEERING SCIENCES AREA

RECENT TECHNICAL PUBLICATIONS

1. "Technology Developments Toward 30-Year-Life," R.G. Ross, Jr., 17th IEEE Photovoltaic Specialists Conference, Kissimmee, Florida, May 2, 1984.

2. "Assessing Photovoltaic Module Life from Long-Term Environmental Tests," D.H. Otth and R.G. Ross, Jr., IES 30th Annual Meeting, Orlando, Florida, April 30, 1984.

3. Proceedings of the Flat-Plate Solar Array Project Research Forum on the Design of Flat-Plate Photovoltaic Arrays for Central Stations, JPL Document No. 5101-247, Sacramento, California, December 5-8, 1983.

4. "Thermal Performance of Residential PV Arrays," L. Wen, presented at ASES Annual Meeting, June 5, 1984, Anaheim, California.

5. "Determination of Hot-Spot Susceptibility of Multistring Photovoltaic Modules in a Central-Station Application," C.C. Gonzalez, et al, IEEE Photovoltaic Specialists Conference, Orlando, Florida, May 2, 1984.

6. "The Integration of Bypass Diodes with Terrestrial Photovoltaic Modules and Arrays," N.F. Shepard, Jr., and R.S. Sugimura, IEEE Photovoltaic Specialists Conference, May 1-4, 1984, Kissimmee, Florida.

7. "Degradation in Silicon Solar Cells Caused by the Formation of Schottky Barrier Contacts During Accelerated Testing," J.W. Lathrop, et al, IEEE Photovoltaic Specialists Conference, May, 1984 Kissimmee, Florida.

8. "Flammability of Photovoltaic Modules," R.S. Sugimura, et al, IEEE Photovoltaic Specialists Conference, May, 1984, Kissimmee, Florida.

9. "Discoloration of Poly (Vinyl Butyral) in Cells Exposed to Real and Simulated Solar Environments," Q. Kim and A. Shumka, Solar Cells, Elsevier Sequoia S.A, Lausanne, Switzerland, September, 1984.

PROCEEDINGS

INTRODUCTION

The 24th Project Integration Meeting of the Flat-Plate Solar Array Project of the Jet Propulsion Laboratory was held at the Pasadena Center, Pasadena, California, on October 2 and 3, 1984.

The theme for the 24th PIM was High-Efficiency Photovoltaic Devices and Modules, reflecting recent increased emphasis on high efficiency by the national Photovoltaics Program, sponsored by the U.S. Department of Energy.

The results of the FSA Research Forum on High-Efficiency Crystalline Silicon Solar Cells, held at Phoenix, Arizona, July 9 through 11, 1984, were summarized. Plans and activities within FSA that are directed toward higher efficiency were presented, and specific key issues were discussed.

In addition, reports on progress in photovoltaic technologies in other areas were presented.

The FSA Project Integration Meetings continue to enable communication between the Government and the private photovoltaics community about present and future photovoltaics activities. This exchange is essential in assessing recent progress; in identifying trends and new developments; in integrating research activities, and in guiding near-term and long-term planning, decision making, and adjustments in Project priorities.

A summary of Plenary Session reports is presented below, followed by visual summaries of the reports given in the Technical Sessions.

Plenary Sessions

SUMMARY

W. T. Callaghan, Manager of the Flat-Plate Solar Array Project (FSA), opened the meeting by welcoming the participants to the Project Integration Meeting (PIM). He noted that FSA project activities directed toward higher-efficiency solar cells and modules are accelerating and supplement continuing efforts to develop technology that can be used by industry to reduce costs and increase reliability.

Morton B. Prince, Chief, Collector Research and Development Branch, National Photovoltaics Program, U.S. Department of Energy (DOE), presented the rationale for DOE's pursuit of high-efficiency crystalline-silicon technology activities, citing the National Photovoltaics Program Five-Year Research Plan. DOE is sponsoring R&D to advance technology that private enterprise can use to compete in U.S. lectric energy markets. The 30-year levelized cost of PV-generated electricity must descend to about $0.15 kWh in the long term, or, at today's cost, about $0.07/kWh. A trade-off of possible PV system parameters that should be attained in order to meet the cost goals are shown in the Plan, which makes obvious that cell and module efficiencies must be increased. To raise the efficiencies to the levels needed, considerable R&D is required.

How should DOE best use its limited budget resources to achieve technology advancements which industry can convert to the practical products required? In the near term, considering cost and efficiency leads to the conclusion that single-crystal silicon is the strongest contender for a single-junction PV device that may meet the objectives. Theoretically, it is possible to obtain higher efficiencies by stacking cells to make better use of the solar spectrum. To build successful high-efficiency stacked cells, it is necessary that each cell in the stack be efficient. Thus again, high-efficiency crystalline-silicon cell technology is the best-known PV technology, and could provide a component, sooner, for these very efficient systems.

A.H. Kachare, Manager of the FSA Device Research Task, described FSA high-efficiency cell activities supporting efforts to achieve the DOE Five-Year Plan goals. A specific goal is ". . .to establish the technologies by 1988 which industry can apply to the production of 15% efficient crystalline silicon modules. . . ." To achieve that goal it is necessary to identify and resolve key generic problems that limit cell efficiency. The major issues being addressed are surface losses, bulk losses, modeling, proof of concepts, and measurements. Achievement of 20%-efficient large-area solar cells using low-cost silicon sheet requires understanding of all aspects of carrier recombination losses, innovative designs based on sound modeling, and reliable measurement techniques. The research is showing promising results.

The High-Efficiency Crystalline-Silicon Solar Cell Research Forum held by FSA in July 1984 was summarized by Professor Martin Wolf, University of Pennsylvania. Twenty-six invited speakers gave presentations on high-efficiency concepts, surface and interface effects, bulk effects, modeling and high-efficiency device processing. The presentations focused on the best

efficiencies attained so far; the next improvements that can be expected; "ideal" cell efficiency; the ultimate expectable efficiency; the how and why of high-efficiency cells, and the knowledge required to attain high efficiencies. Each group working on increasing cell efficiency believes that it has not exhausted its present approach, has identified further optimization potentials, and has reason to believe that 20% (AM1.5) cell efficiency can be exceeded. Analysis of the contributions of the principal individual efficiency loss mechanisms in crystalline-silicon cells and experimental cell results were discussed in detail at the forum. Expectation of the achievement of efficiencies significantly above 20% is growing; however, major advances in material processing and in material quality will be required.

A presentation on nigh-quality crystalline-silicon ingot technology issues was presented by G. Schwuttke, University of Arizona. First issue: high-quality semiconductor silicon material research is needed, especially in the United States. This was the conclusion of a Defense Advanced Research Projects Agency study and of others in the field. Silicon wafers produced in the United States are not as good as some foreign-produced wafers. In the U.S. semiconductor industry the emphasis is on device technology, which has resulted in the evolution of many excellent people with excellent knowledge of device technology but with a weak comprehension of materials technology. Good materials research is sophisticated and requires long-term commitments with appropriate funding. The Japanese are doing better than the Americans at supporting long-term materials research. Second issue: in the United States there is a need for dynamic interaction between semiconductor-material specialists and producers and the material users, i.e., the device producers. Because of poor communications between these groups, the material suppliers don't really understand nor can they readily anticipate material user's future needs. Also, the users don't really understand the potentials and limitations of future materials. Third issue: high-quality semiconductor silicon material is a strategic material from both an economic and security viewpoint. These deficiencies could be changed with a joint effort by electronic and materials organizations to form and support a dynamic, advanced materials characterization capability.

High-efficiency module and array research activities were discussed by Ronald G. Ross, Jr., Manager of the FSA Reliability and Engineering Sciences Area. Continuing development of module technologies that contribute to high efficiency include high cell-packing factors, such as rectangular cells, narrow borders, close cell spacing and large modules, and low optical losses by use of antireflection coatings, antisoiling coatings and high light-transmittance encapsulants. Also included are low electrical-mismatch losses by use of series-paralleling and solar-cell performance sorting, and achieving low operating temperatures by good convective cooling of module rear surfaces, high thermal emittance and high reflectivity of module rear surfaces and low-IR-absorbance front surfaces. The research being performed during FY85 on the above items was summarized briefly.

Sensitivity analyses of PV systems that could meet the DOE energy cost goal of $0.15/kWh were presented by R.W. Aster of FSA's Project Analysis and Integration Task. Many parameters were varied during the study and comparisons were shown of the most important: module cost, module efficiency, insolation and energy cost. The relative impacts of energy costs were shown,

in which the $0.10/kWh value represented a worst-case competition against coal and $0.20 to $0.25/kWh represented competition with oil. Sensitivity to module efficiency is substantial; doubling efficiency allows the module cost to be five times higher. Sensitivity to site location is also strong; i.e., the insolation value has substantial influence on energy-generated costs. New FSA allocation guidelines for monitoring the progress of the various technical options toward achievement of cost-reduction and efficiency goals were presented.

Anthony F. Scolaro, Collector Research and Development Branch, DOE, gave a presentation on the future of crystalline silicon technology in the National Photovoltaics Program. There is a reasonable expectation that crystalline silicon will continue to dominate the PV market place through this decade because of its significant progress along the product growth curve, which positions it as a major contributor in PV market growth. Silicon has a very high potential efficiency, demonstrated reliability, and a significant potential for cost reduction. Therefore, it is important to resolve the critical problems that currently limit improvement of crystalline silicon technology. The perpetuation of the mutually beneficial Government-industry partnership can be encouraged by cost-shared research and prompt complete transfer of information. This will assist in maintaining a healthy growing PV industry. The Five-Year Research Plan includes work on silicon materials, advanced silicon sheet, flat-plate collectors and module reliability. The development of fluidized-bed reactor technology for commercial use in the deposition of high-purity silicon from silane is scheduled to be completed in FY85. Silicon-sheet efforts are directed toward obtaining a basic understanding of high-speed silicon crystallization; controlled crystallization to develop high-purity, low-defect-density sheet material during stable long-term growth is needed and is scheduled to be achieved in FY86. Flat-plate collector technology advancements needed include understanding of device parameter sensitivity to surface and bulk recombination mechanisms, and the identification and development of processes that are cost-effective and that result in high-performance cells. It is also necessary to develop and verify methods of extending module life to 30 years of reliable operation. There is a need to mitigate the effects of identified module degradation modes, e.g., electrochemical corrosion, bond delamination, photothermal oxidation, and electrical insulation breakdown; to develop an understanding of aging processes that will enable accelerated testing, and to complete these efforts in FY87. Crystalline silicon PV has a substantial knowledge base to draw upon, improving its chances of success in competition with other PV technologies.

The first phase of the Sacramento Municipal Utility District (SMUD) plan for 100 MW of PV generation capability was completed in July 1984. The completion, checkout, and initial operation of the 1 MW plant was described by D. Collier of SMUD. The plant consists of 896 8 x 16 ft panels of ARCO Solar, Inc., single-crystal silicon solar cells arranged in 112 single-axis tracking flat-plate arrays. The only major problem during construction and start-up was a dual ground fault that required replacement of some equipment. Performance monitoring data will be reduced on site and disseminated by SMUD, and will be sent to Boeing for evaluation in accordance with a contract with the Electric Power Research Institute (EPRI). The initial performance evaluation: The array field appears to be meeting design expectations, PCU

acceptance testing indicates compliance with specification, and electrical switchgear problems delayed early operation but now appear to be resolved.

Mark Anderson, manager of PV activities at SMUD, presented the current status and plans for the second and third phases of the SMUD PV plant. The second phase is also a 1 MW plant at a planned cost of $10,400,000, which is exactly the contracted cost. Nine hundred kW of modules assembled into 8 x 16 ft panels will be supplied by ARCO Solar Electric. Solarex Corp. will supply 200 kW of modules assembled into panels of similar size. Mobil Solar Energy Corp. will supply 37 kW of modules with solar cells made from EFG silicon ribbon. The plant is to be operational late in 1985, and will use single-axis tracking arrays similar to the first-phase arrays.

The third phase is to be a 5 MW ac (6 MW dc) plant, scheduled for operation by the end of 1987. This 5 MW unit is seen as a potential building-block unit for future PV additions. SMUD's target price for the entire PV system installed is $8,000/kW. Stone and Webster has been selected as the A&E contractor and is conducting a review, with SMUD, of design options, which include tracking flat-plate and concentrator units; SMUD plans to issue an RFP for PV collector panels on January 1, 1985. It will request bidder response by February 1, with the intent of awarding contracts to two panel vendors on March 1, 1985. The panel target price is $4,000/kW, with deliveries scheduled for June 1986 to November 1, 1987. The SMUD maximum-demand periods are 2:00 p.m. to 10:00 p.m. from May to October. Assessment of the value to the utility of PV versus generator units such as gas-fired turbines continues.

The largest rooftop PV array in the world, 300 kW, became operational in September 1984. N. Marshall of Hughes Aircraft Co. (the A&E) described the National Exemplar Facility at Georgetown University, Washington D.C., and showed photographs of its construction. The watertight array covers about 36,000 ft^2 of roof and meets safety, monitoring, and maintenance and repair requirements. The array is bipolar, neutral-resistivity-grounded, and has r output voltage of +228 Vdc. The 2 x 4 ft frameless laminated modules, manufactured by Solarex Corp., exceeded the 72 W minimum average power requirement. The modules had encapsulated bypass diodes, 3000 V electrical insulation, and passed the JPL Block V tests. The modules were matched in subpanels by 12 grades of electrical current outputs and arranged on the roof by grades. Test equipment for measuring performance on the roof was devised. During initial operation the PV system exceeded the system requirements.

An overview of the FSA Block V module activities was presented by M. Smokler, Manager of the FSA Module Performance and Failure Analysis Task. In the first phase, each manufacturer designed and fabricated 10 advanced modules, which were tested by FSA. During the second phase, each manufacturer submitted its module design, modified as determined by the test results, to JPL for a collaborative design review. Then 10 modules of each modified design were fabricated and tested. Where needed, further module modifications and tests were performed. During the Block V efforts the following continuing problems had to be corrected: uncured encapsulant, delamination, frame or mounting degradation, high-voltage breakdown, inadequate ground continuity and junction-box warpage. A number of persistent electric-power measurement problems were solved concurrently with the Block V activities. Solar cell and

circuit characteristics, module physical characteristics and electrical performance of the modules from the five second-phase contractors were presented in table form. The changes in Block I through Block V products were summarized by trend charts of module power, module packing factors, solar-cell efficiency, module efficiency and module costs. Block V activities will be completed early in 1985. The principal improvements of the Block V efforts: modules are larger, higher performance is more common, and several design problems have been solved, as evidenced by Block V test results.

A number of PV specialists toured China recently; Ishaq Shahryar, President of Solec International, presented his impressions of the tour. China is modernizing as rapidly as is possible, and is interested in all kinds of energy, especially renewable. People in many rural areas are aware of and want PV. Individuals can now own their own homes or small businesses. Capital is scarce, so hardware must be simple and inexpensive. Decentralization now permits small companies to arrange business deals with foreigners. Many of these companies want to learn about modern technology by means of joint ventures with foreign companies. They are good business people and they move fast; Shahryar noted that he lost a business deal because he expected that the Chinese would move slowly.

HIGH-EFFICIENCY CRYSTALLINE SILICON TECHNOLOGY DEVELOPMENT

U.S. DEPARTMENT OF ENERGY

Morton B. Prince

I have been asked to give the rationale for pursuing high-efficiency crystalline silicon technology research and development activities.

Let me start by quoting the purposes of the National PV Program from the latest Five-Year Research Plan.

"In accordance with legislative mandates and recent policy guidance, the National Photovoltaics Program sponsors high risk, potentially high payoff research and development in photovoltaic energy technology which will result in a technology base from which private enterprise can choose options for further development and competitive application in U.S. electrical energy markets."

In order for the private sector to compete in the U.S. electrical energy markets, photovoltaic energy systems must be able to produce electricity at or about the same cost as other competing energy systems such as oil, gas, coal, nuclear or any other source of energy. PV may be able to command a slightly higher price than some of the other sources because of its safety, non-pollution and other benefits. However, this premium should not blind us to the brutal fact that cost is the main driving force in our society in selecting its energy sources.

Energy cost analysts at JPL, Sandia, EPRI and the Aerospace Corp. have come up with essentially the same results regarding the necessary costs that must be reached. The 30-year levelized cost of electricity must get down to about 15¢/kWh, or at today's cost about 7¢/kWh.

The analysis has ended up with several graphs (which are in the Five-Year Plan) that relate module costs (in $/m^2$ and in $/W_p$), module efficiency and levelized electricity costs (¢/kWh). These graphs have been made w th many assumptions that differ in some parameters for flat-plate modules and concentrator modules

These parameters include system life, the ratio of system efficiency to module efficiency, capacity factor, average peak insolation, annual O&M costs, indirect cost multiplier, present worth factor, fixed charge rate, capital recovery and balance-of-system costs, both area-related and power-related. I refer to the Plan appendix which describes all of these parameters in detail and gives numerical data for them. I personally have some questions about some of the numbers, but the differences do not significantly change the results. Let us look at two of the figures from the Plan.

The first figure is for flat-plate PV systems with $75/m^2$ for area-related BOS costs (Figure 1). As you can see, in order for the PV system to meet the 15¢/kWh line, the module efficiency must be greater than 15%, and

even then the module cost must be less than $35/m^2 (or approximately
20¢/watt). If the module efficiency can be increased to 20%, the cost of the
module in the system can be up to $75/m^2 (or about 37¢/watt). Thus, one can
start to see the pressure on obtaining high efficiency.

Figure 2 shows similar information for a concentrator system with
$125/m^2 area-related BOS cost. In this case, one can see that the minimum
meaningful cell efficiency is 25%, which will allow a module cost of $50/m^2
of aperture. The $50/m^2 level will be extremely difficult to meet. A more
realistic set of numbers is efficiency of 35% and module cost of $135/m^2 of
aperture.

Thus, it is necessary to get to flat-plate module efficiencies of
approximately 20% (and thus cell efficiencies of 22%) and concentrator cell
efficiencies of about 35%. Also, you now have a better idea of what some of
our problems are in designing the PV program within the limited budgets that
we have been working with during the past few years. It is possible to trade
off lower BOS costs to allow lower cell and module efficiencies, but unless
some breakthrough is made in the BOS area of work, I believe the BOS costs
assumed above will be difficult to beat. Besides the PV Five-Year Plan, I
recommend that you read the EPRI Report AP-3351 titled "PV Power Systems
Research Evaluation," especially Section 2, if you are interested in more
detailed information on the economic requirements for PV systems.

The Program Office has, with the help of the three lead lab ~tories,
come up with a set of activities that, we believe, will help industry reach
these high efficiencies. This set includes work on silicon devices,
single-junction multielement devices, multijunction thin-film devices (for
flat-plate modules) and multijunction structures for concentrator modules.

Data on single-junction cells are shown in Figure 3. These data are for
laboratory devices. The expected near-term efficiencies are given in the
right hand columns. As you can see, none of these single-junction cells will
ever meet the 35% efficiency needed for the concentrator module. Only a
couple of materials have the potential for meeting the flat-plate cell
efficiency of 22% or more. In the near term, tying costs with efficiency
results in the fact that single-crystal silicon is the strongest contender for
a single-junction device that may meet the objectives discussed above.

As most of you know, it is possible to obtain higher efficiencies by
stacking more than one cell on top of another to make better use of the solar
spectrum. Several analyses have been made that indicate that the efficiency
can be increased to over 55% with about 10 to 20 junctions of different
materials stacked upon one another. However, the difficulties of developing
such a structure are so horrendous that we can only think in terms of two-cell
and three-cell stacks at this time. These smaller stacks obtain the major
increase of efficiency over the single-junction device efficiencies in any
case. Figure 4 shows what is possible theoretically for single-junction,
two-cell stack, and three-cell stack material systems for flat-plate modules
and 500X concentrator modules. This chart also shows the optimum band gaps
that should be used. Note the bottom line combination which uses silicon as
the lower cell. Figure 5 (from John Fan) shows that the band-gap selection is
not very critical. Thus many combinations of materials are possible that will
meet both the flat-plate module and concentrator-module requirements.

50

To build successful stacks with these efficiencies, it is necessary for each cell in the stack to be efficient in its own right. Thus, again, silicon appears to be a relatively near-term component for a useful system, and it must be highly efficient.

Now that I have developed the rationale for the need to maximize the efficiency of crystalline silicon PV devices, let me very briefly set the background for the other speakers of this morning's program.

Figure 6 lists many of the factors that must be considered in the design of a high-efficiency device. Many of these factors can only be optimized at the expense of other factors, and it is this complex overall optimization that has given us difficulties over the past many years. However, we are gradually closing in on the optimal trade-offs, and as you know cells with over 19% have been obtained for silicon.

The last figure (Figure 7) shows how many of these factors fit in the conceptual photovoltaic cell.

Figure 1. Module Costs and Efficiencies vs 30-Year
Levelized Electricity Costs for Flat-Plate
Photovoltaic Systems (175/m^2 Area-Related BOS)
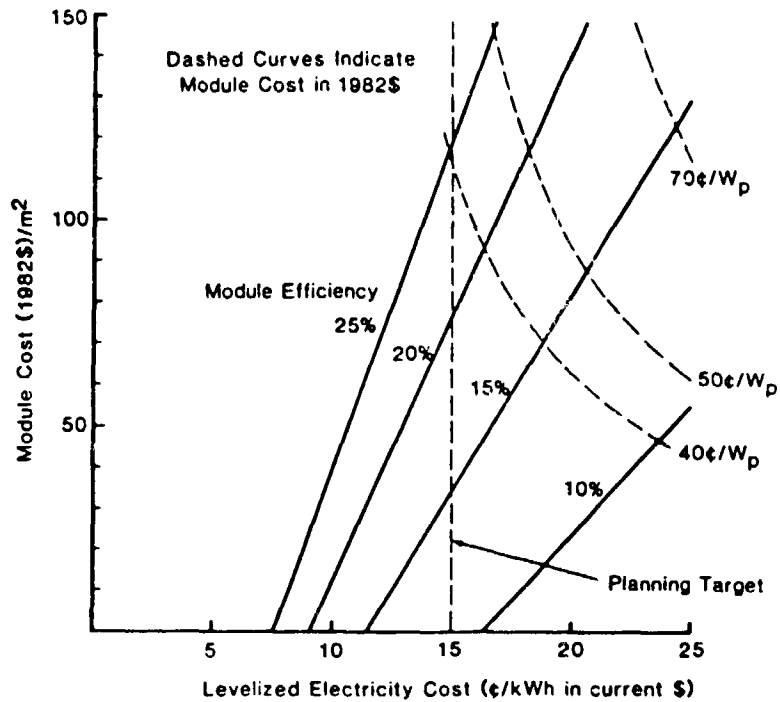
Figure 2. Module Costs and Cell Efficiencies vs 30-Year
Levelized Electricity Costs for Concentrator
Photovoltaic Systems ($125/m^2 Area-Related BOS)
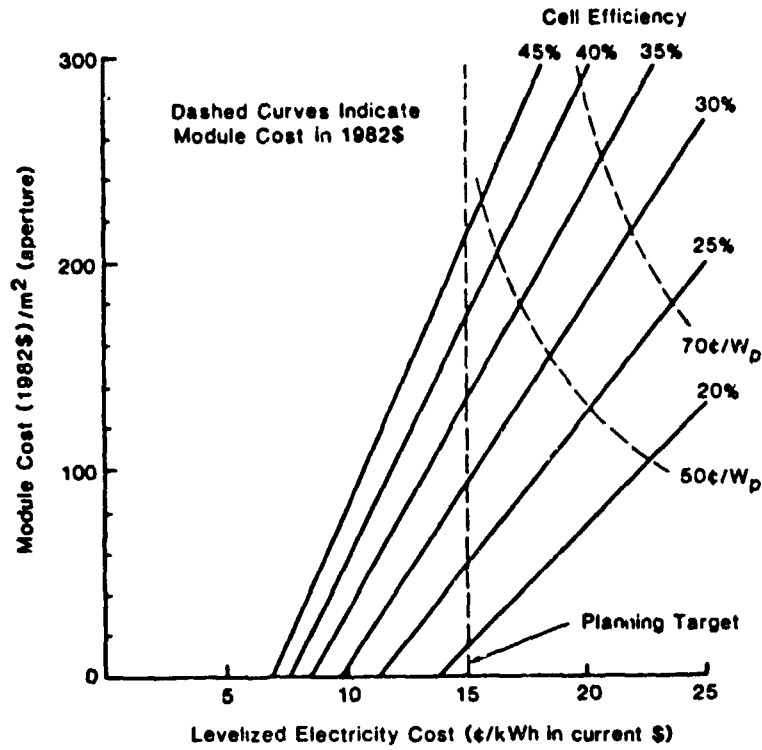
Figure 3. Single-Junction Photovoltaic Cells

CELL MATERIALS	LABORATOR CELL EFFICIENCY (%)[*]			
	η (1983)	η (THEORY)	η (1986-8)	η (1990's)
SINGLE-CRYSTAL				
SILICON	19	25	20-21	22
SILICON (500X)	20	28	21-23	26
GaAs THIN FILM (THICK)	17(23)	28	20-24	25
GaAs (500X)	24	32	26-28	30
AMORPHOUS SILICON	10	20	12-14	15
$CuInSe_2/CdS$ [**]	11	25	14-17	19
$CdTe/CdS$ [**]	11	28	14-19	22

[*] CONCENTRATION RATIO = 1 SUN (1X) UNLESS DESIGNATED OTHERWISE
(500 SUN CONCENTRATION RATIO = 500X)

[**] POLYCRYSTALLINE THIN FILM CELLS

Figure 4. Theoretical Efficiencies

	OPTIMAL BANDGAP(S) (TOP TO BOTTOM)	η (THEORY) 28°C
SINGLE-JUNCTION CELL (1 SUN)	1.45 EV	28%
SINGLE-JUNCTION CELL (500X)		32%
TWO-CELL STACK (1 SUN)	1.6 → 0.95 EV	35%
TWO-CELL STACK (500X)		40%
THREE-CELL STACK (1 SUN)	2.0 → 1.5 → 0.95 EV	42%
THREE-CELL STACK (500X)		47%
TWO-CELL STACK (1 SUN) (LOWER CELL-SILICON)	1.8 → 1.1 EV	34%

Figure 5. Two-Junction Photovoltaic Converter
Iso-Efficiency Lines

Independent cells
T = 300°K
C = 1000 AM2 suns

Bottom Cell Bandgap (eV)

Top Cell Bandgap (eV)
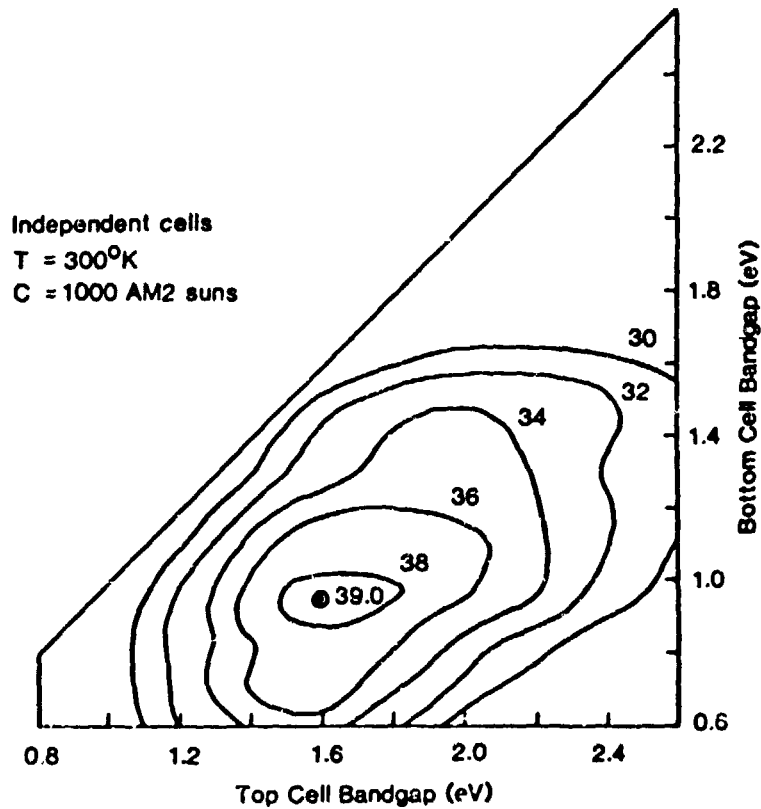
Figure 6. Factors Affecting Efficiency

MECHANICAL FACTORS

Depth of Junction (w)
Thickness of Wafer (d)
Series Resistance (contact geometry)
Front Surface Roughness (light trapping)
Contact Shadowing
Operating Temperature

PHYSICAL FACTORS

Base Resistivity
$(\tau_n, D_n, \mu_n, L_n, n_p)$

Emitter Impurity Distribution
$(\tau_{p_{eff}}, \mu_{p_{eff}}, p_{n_{eff}})$

Back Surface Impurity Distribution

Recombination and Scattering Centers
in Base and Emitter

DEVICE FACTORS

Surface Recombination Velocity (front,
back, under contacts)

Reflecting Back Surface

AR Coating

High Eg Window (oxide, etc.)

Series Resistance

Shunt Resistance

Reverse Saturation Current
(I_0)

Figure 7
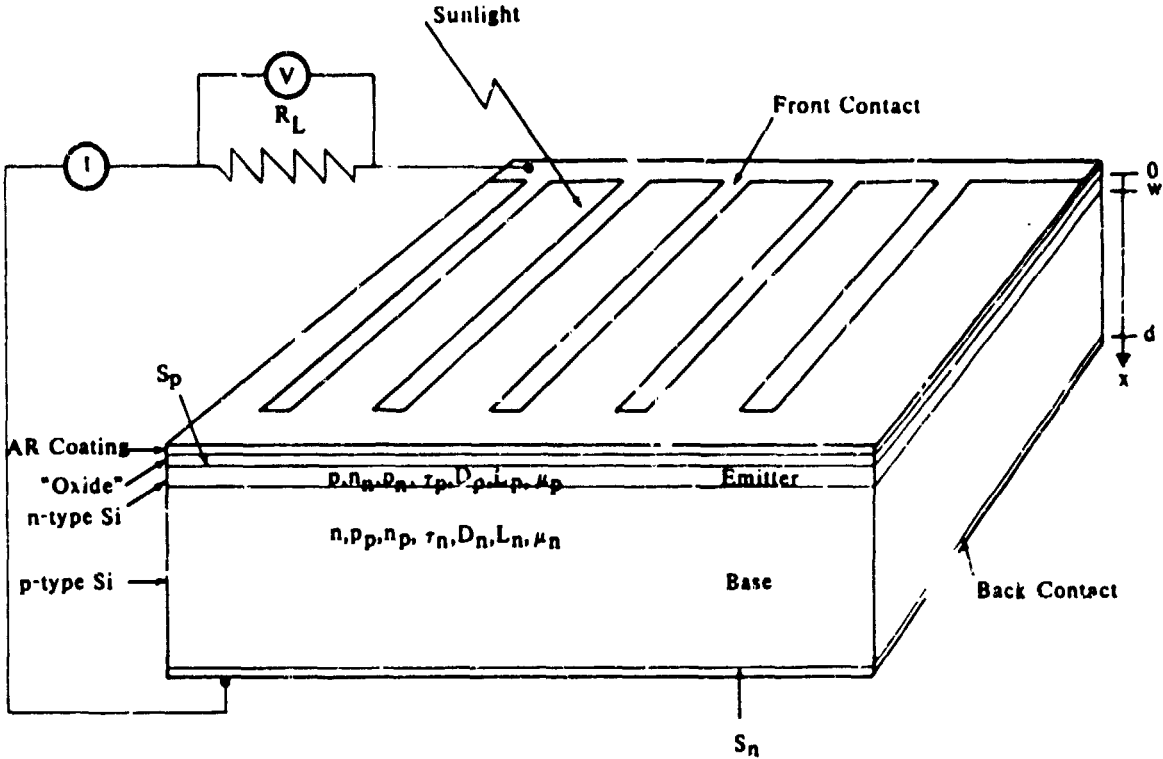
SUMMARY OF THE HIGH-EFFICIENCY CRYSTALLINE SOLAR CELL RESEARCH FORUM

UNIVERSITY OF PENNSYLVANIA

M. Wolf

Session I: OVERVIEW

P. Landsberg	Some Aspects of the Minority Carrier Lifetime in Silicon.
C.T. Sah	Review of Recombination Phenomena in High-Efficiency Solar Cells.

Session II: HIGH EFFICIENCY CONCEPTS

M. Wolf	Silicon Solar Cell Efficiency Improvement: Status and Outlook.
A. Lesk	Some Practical Considerations for Economical Back Contact Formation on High-Efficiency Solar Cells.
R. Bell	High-Efficiency Cell Concepts on Low-Cost Silicon Sheet.
R. Swanson	High Lifetime Silicon Processing.
L. Olsen	Silicon MINP Solar Cells.

Session III: SURFACE/INTERFACE EFFECTS

D. Chadi	Atomic Structure of the Annealed Si (111) Surface.
L. Kazmerski	Surface and Interface Characteristics.
S. Lai	Nitridation of SiO_2 for Surface Passivation.
S. Fonash	Surface Passivation and Junction Formation Using Low-Energy Hydrogen Implants.
P. Grunthaner	Chemical Structure of Interfaces.

Session IV: BULK EFFECTS

E. Sirtl	Structural Defects in Crystalline Silicon.
C. Pierce	Oxygen and Carbon Impurities and Related Defects in Silicon.
T. Tan	Current Understanding of Point Defects and Diffusion Processes in Silicon.
G. Schwuttke	Defects in Web Dendrite Silicon Ribbon Crystals and Their Influences on Minority Carrier Lifetime.
J. Hanoka	EBIC Characterization and Hydrogen Passivation in Silicon Sheet.
A. Neugroschel	Measurement of Electrical Parameters and Current Components in the Bulk of Silicon Solar Cells.

Session V: MODELING

R. Schwartz	Current Status of One and Two Dimensional Numerical Models: Successes and Limitations.
M. Lamorte	Application of Closed-Form Solution Using Recursion Relationship in Silicon Solar Cells.
F. Lindholm	Phenomena Simulation for Heavy Doping and Surface Recombination Velocity.

Session VI: HIGH EFFICIENCY DEVICE PROCESSING

S. Johnson	High-Efficiency Large-Area Polysilicon Solar Cells.
P. Iles	High-Efficiency Solar Cell Processing.
A. Rohatgi	Process and Design Considerations for High-Efficiency Silicon Solar Cells.
M. Spitzer	Processing Technology for High-Efficiency Silicon Solar Cells.
L. Dyer	Texture Etching of (100) Silicon for Solar Cells.

Questions Relating to the Attainment of
Higher-Efficiency Crystalline Silicon Solar Cells

1. WHAT ARE THE BEST EFFICIENCIES ATTAINED SO FAR?

2. HOW WERE THESE CELLS DESIGNED AND FABRICATED?

3. WHAT IS THE NEXT IMPROVEMENT STEP?

4. HOW CAN IT BE ACHIEVED?

5. WHAT IS THE REALISTICALLY EXPECTABLE "ULTIMATE" EFFICIENCY?

6. WHAT IS NEEDED TO GET BEYOND THE NEXT STEP?

    A. Reduced recombination
    B. Other design parameters
    C. Is heavy doping needed?
    D. Auger recombination as limiter.

7. HOW CAN RECOMBINATION BE REDUCED?

    A. Bulk recombination
    B. Surface recombination.

8. DO WE UNDERSTAND THE DEVICE PHYSICS ADEQUATELY?

    A. Band-Gap narrowing
    B. Auger recombination
    C. High level injection
    D. 2- and 3- dimensional interactions.

9. DO WE UNDERSTAND THE ORIGINS OF RECOMBINATION CENTERS?

10. HOW CAN ONE PROCESS TO ACHIEVE REDUCED RECOMBINATION?

11. ARE OTHER NEEDED TOOLS ADEQUATE?

    A. Modeling
    B. Analysis

12. WHAT ARE THE INHERENT PERFORMANCE LIMITATIONS
    IN "LOW COST" CRYSTALLINE SI?

PRIMARY CAUSES OF LOSSES	SYMBOL	DESIGN PARAM	1970 COM'L CELL	VIOLET CELL	"BLACK CELL"	1978 SPACE CELL	SPIRE (1984 EXPER'L)	STR'GH/GH (1984 EXPER'L)	M.A.GREEN (1984 EXPER'L)	GOALS 20%	GOALS 22.6%
1. LIGHT GENERATED CURRENT											
FUNDAMENTAL LIMIT (AM1)	$I_{L,\mu}$					44 mA cm^{-2}					
A. OPTICAL SURFACE PROPERTIES (REFLECTION)	(1-R)	BASE WIDTH	0.905	0.90	0.97	0.98	0.975	0.966	0.954	0.97	0.97
B. CONTACT COVERAGE	S	$\tau_{n,p}$ / $\tau_{n,p}^+$	0.96	0.95	0.95	0.96	0.965	0.97(A)	0.948	0.966	0.966
C. INCOMPLETE ABSORPTION (THICKNESS)			0.72	0.95-0.90	0.96	0.96(A)	0.956	0.956	0.973	0.92	0.95
D. RECOMBINATION OUTSIDE DEPLETION REGION (BULK AND SURFACE, INCLUDING CONTACTS)	η_{coll}	FRONT WIDTH $\tau_{p,n}$ / S		0.95	0.94	0.94	0.91	0.915	0.93		
E. (DEAD LAYERS)	(1-A)	TREATM.	1.0	1.0	1.0	1.0	1.0	1.0	1.0	1.0	1.0
OVERALL COLLECTION EFFICIENCY	γ		0.63	0.77	0.84	0.84	0.82	0.82	0.82	0.86	0.89
LIGHT GENERATED CURRENT (AM1)	$I_L = \gamma \cdot I_{L,\mu}$ (mA cm^{-1})		28.1	34.0	37.1	37.0	36.2	36.0	36.0	37.9	39.2
2. OPEN CIRCUIT VOLTAGE											
FUNDAMENTAL LIMIT	$(VF)_{fund} = 0.76$		0.836 V ($I_o = 4.2 \cdot 10^{-10}$ A cm^{-2})								
A. RECOMBINATION OUTSIDE DEPLETION REGION (BULK AND SURFACE, INCLUDING CONTACTS)	$(VF) = (VF)_{rechm} \cdot (VF)_{fund}$		0.522	0.528	0.533	0.555	0.565	0.57	0.59	0.60	0.65
B. BANDGAP NARROWING											
C. CURRENT LEAKAGE	(R_{sh})		1.0	1.0	1.0	1.0	1.0	1.0	1.0	1.0	1.0
OPEN CIRCUIT VOLTAGE	$V_{oc} = (VF) \cdot E_o$ (V)		0.574	0.581	0.586	0.610	0.622	0.627	0.653	0.661	0.715
3. FILL FACTOR											
FUNDAMENTAL LIMIT	$(CF)_{fund}$		0.865								
A. / B. SAME AS OPEN CIRCUIT VOLTAGE	$(CF) = (CF)_{rechm} \cdot (CF)_{fund}$		0.82	0.823	0.823	0.824	0.83	0.833	0.839	0.84	0.85
C.	(R_{sh})		1.0(A)	1.0	1.0	1.0	1.0	1.0	1.0	1.0	1.0
D. RECOMBINATION IN DEPLETION REGION	$(CF)_{add'l}$		0.91	0.97	0.97	0.97	0.985	0.98	0.982	0.97	0.97
E. SERIES RESISTANCE	(R_s)		0.96	0.985	0.984	0.98(A)	0.98	0.98	0.984	0.98	0.98
FILL FACTOR	(FF)		0.716	0.78	0.78	0.78	0.801	0.800	0.811	0.80	0.81
RESULTING CONVERSION EFFICIENCY	η		11.6	15.4	17.0	17.6	18.1	18.1	19.1	0.200	0.226

(A) = ASSUMED

The Recent Approach

a. THOUROUGH DEVICE ANALYSIS COUPLED WITH MODELING:

- TO DETERMINE ALL LOSS CONTRIBUTIONS

- TO IDENTIFY POSSIBILITIES FOR IMPROVED DEVICE DESIGN.

b. GLOBAL DESIGN VIEW OF DEVICE:

- OPTIMIZED CONTACT DESIGN

- DUAL AR OR TEXTURED FRONT SURFACE

- FRONT SURFACE PASSIVATION (AT LEAST PARTIAL)

- BSF AND/OR BSR DESIGN (LIMITED EFFECT)

- SELECTION OF LOW RESISTIVITY FZ Si

- PROCESSING TO MAINTAIN HIGHER FRACTION OF ORIGINAL L_b

- OPTIMIZATION OF EMITTER IMPURITY CONCENTRATION FOR

  PRESENT DESIGN

IN SUMMARY:

SQUEEZE A LITTLE MORE PERFORMANCE OUT,

WHEREVER CURRENT TECHNOLOGY PERMITS.

Status of Solar-Cell Technology

- TECHNOLOGY IS AVAILABLE TO REDUCE THE CONTRIBUTION OF EACH SECONDARY LOSS MECHANISM (REFLECTION, CONTACT SHADING, SERIES RESISTANCE, ETC.) TO THE MAXIMALLY 2-3% LEVEL.

- INTERNAL COLLECTION EFFICIENCY IS GENERALLY >90%; "SATURATES" WITH FURTHER REDUCED RECOMBINATION.

- OPEN CIRCUIT VOLTAGE CONTINUES TO SUBSTANTIALLY INCREASE WITH DECREASING MINORITY CARRIER RECOMBINATION, UP TO BASIC RECOMBINATION LIMIT (RADIATIVE AND AUGER).

- CURVE FACTOR (FUNDAMENTAL PART OF FILL FACTOR) CAN INCREASE (WITH V_{oc}) BY A FEW PERCENT.

HIGH EFFICIENCY REQUIRES

A GLOBAL VIEW OF THE DEVICE, SO THAT
ALL TECHNOLOGY-DETERMINED LOSSES
WILL BECOME LOW.

IF ONE LOSS MECHANISM DOMINATES ⟶ NOT OPTIMIZED
⟶ REDUCE IT

The Next Step

EACH OF THE GROUPS ACTIVE IN EFFICIENCY IMPROVEMENT FEELS THAT THEY HAVE:

a. NOT EXHAUSTED THE PRESENT APPROACH

b. IDENTIFIED POSSIBILITIES FOR FURTHER OPTIMIZATION IN THEIR PARTICULAR DESIGNS.

c. REASON TO BE CONFIDET OF REACHING 20% (AM 1.5) EFFICIENCY SOON.

"n on p" $x_j = 2\,\mu m$
uniform doping each region
$\tau_{p,n} = \tau_{n,p}$ (Auger recomb'n.
causes difference at
3 higher values)

Surface Recombination
Velocity Values
for Curve (2) of
η vs. $\tau_{n\,p}$ plot.
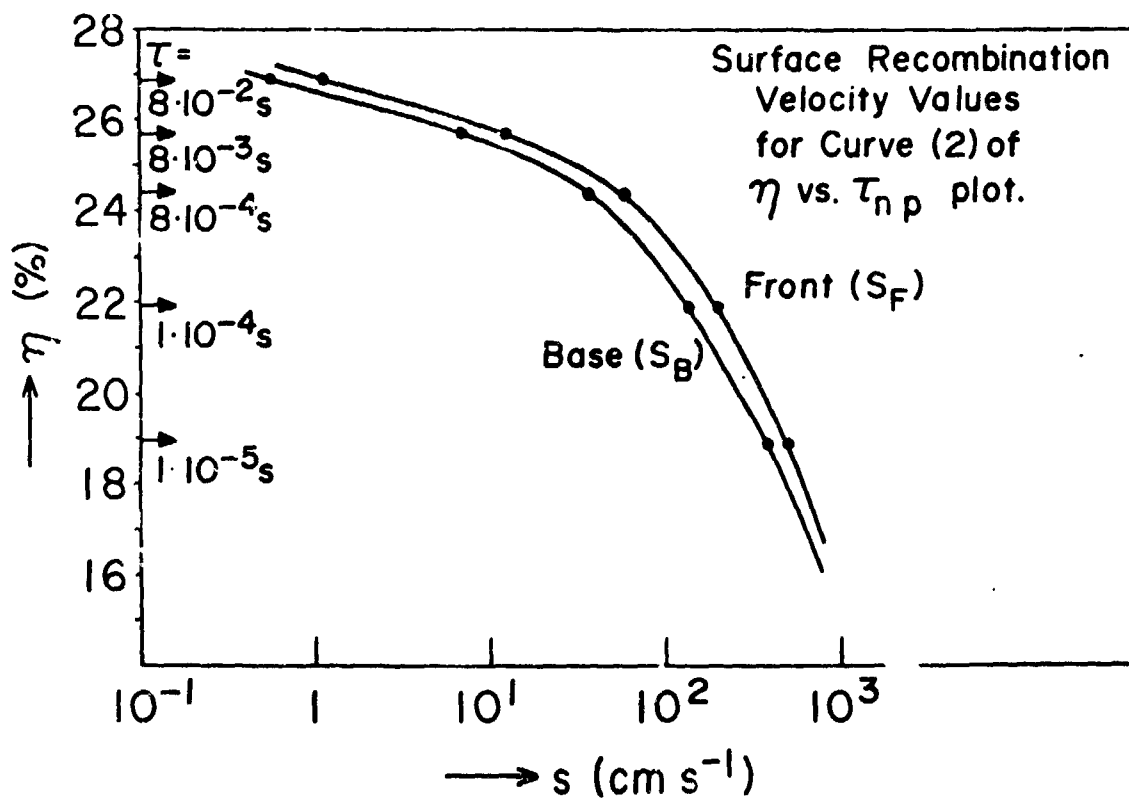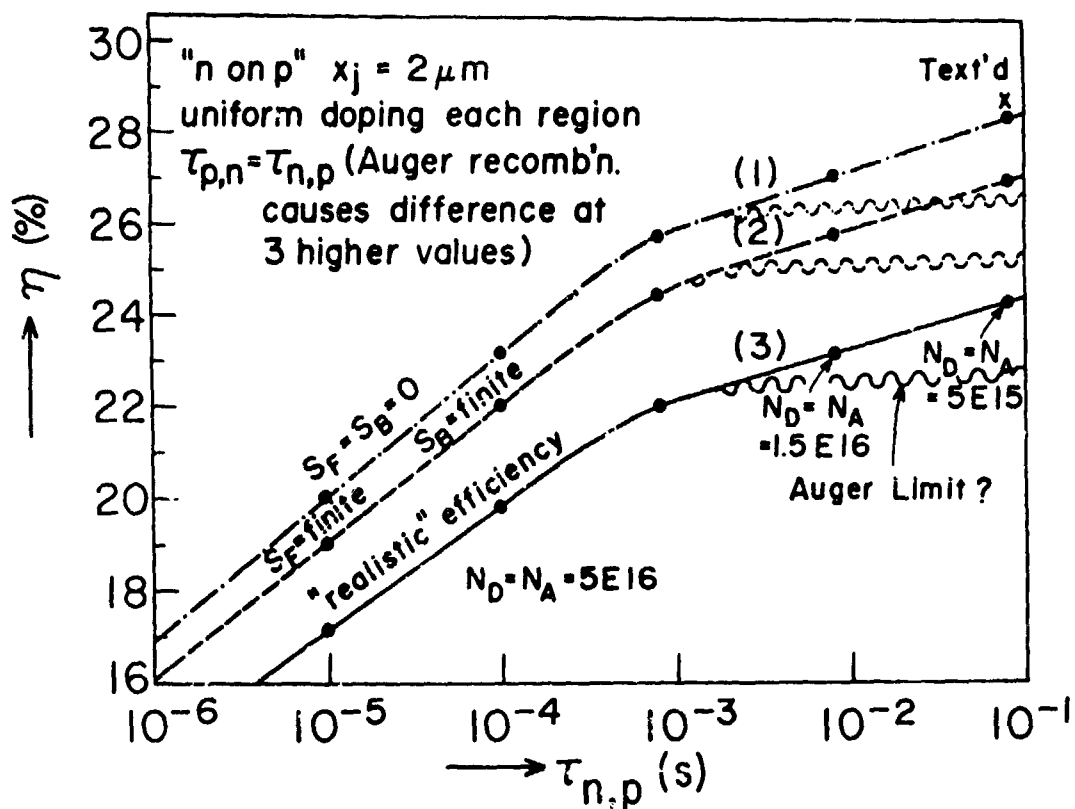
Schematic View of the Solar Cell That Has Everything

Photon Flux ↓ ↓ ↓ ↓ ↓ ↓ ↓ ↓ ↓

- Contact Grid Structure
- Isolating Layer
- Textured Surface
- AR Coating
- Passivating Layer
- Potential Step
- Main Potential Barrier
- Potential Step
- Optical Reflector
- Passivating Layer
- Isolating Layer
- Reduced Contact Area

The Basic Solar Cell
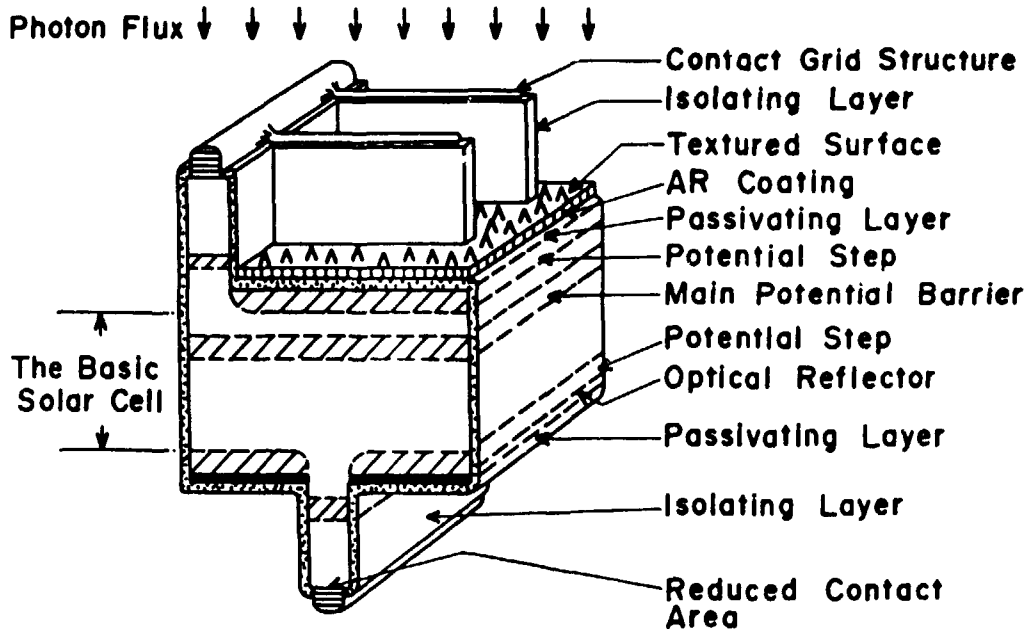
Is Heavy Doping Needed?

ITS PERFORMANCE-INCREASING APPLICATIONS:

- REDUCE SHEET RESISTANCE
- OBTAIN LARGER HIGH/LOW JUNCTION POTENTIAL STEP, OR HIGHER DRIFT FIELD.

ITS PERFORMANCE DECREASING ATTRIBUTES:

- AUGER RECOMBINATION
- BAND-GAP NARROWING.

The Three Principal Paths to Reduced Recombination

DECREASE

1. DENSITY OF RECOMBINATION CENTERS

   - IN BULK N_t [cm^{-3}] $\longrightarrow$ HIGHER τ
   - AT SURFACES $N_{s,t}$ [cm^{-2}] $\longrightarrow$ LOWER s

2. VOLUME OR AREA CONTAINING RECOMBINATION CENTERS:

   - "THIN" LAYERS
   - "DOT CONTACTS"

3. DENSITY OF EXCESS MINORITY CARRIERS

   - FAST REMOVAL TO OUTSIDE
   - "SHIELDING" WITH POTENTIAL STEPS $\left.\right\}$ FOR n_{coll}
   - "ISOLATING" FROM HIGHER RECOMBINATION RATE $\left.\right\}$ FOR V_{oc}
   - HIGH DOPANT CONCENTRATION

Shielding With Potential Steps

GENERALLY REDUCES TRANSPORT VELOCITIES (FOR RECOMBINATION CURRENTS)

BY: $\dfrac{u_1}{u_2} = e^{-\dfrac{q\Delta(E_F - E_V)}{kT}} = \dfrac{P_p(x_1)}{P_p(x_2)}$; (FOR p-TYPE)
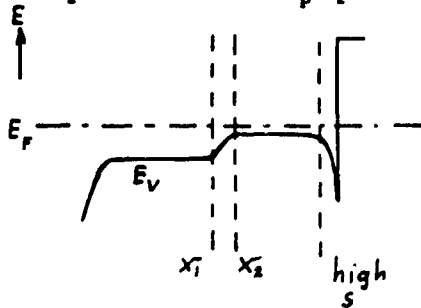
$j_r(x_1) = q n_p(x_1) u_1(x_1)$

$= q n_p(x_1) \dfrac{P_p(x_1)}{P_p(x_2)} u_2(x_2)$

FORMS OF POTENTIAL "STEPS":

   - DRIFT FIELD REGIONS
   - HIGH/LOW JUNCTIONS
   - ACCUMULATION LAYERS (USUALLY UNDER INSULATORS, INCLUDING "TUNNEL CONTACTS").
   - "FLOATING" pn JUNCTIONS (OR INVERSION LAYERS).
   - BANDGAP CHANGES (USUALLY ΔE_G WITH HIGH/LOW JUNCTION, "WINDOW LAYER").

LIMITS:

   - INCREASED DOPING AT "LOW" SIDE REDUCES AVAILABLE STEP HEIGHT.
   - "HEAVY DOPING" EFFECTS ON "HIGH SIDE" LIMIT USEFUL STEP HEIGHT.
   - ABSORPTION W/O COLLECTION IN "WINDOW LAYERS."
   - INTERFACE STATES AT TRANSITION TO "WINDOW LAYER."

Isolating With Thick Layers

PRINCIPLE:
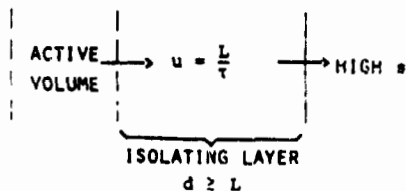
LIMITS: ● ADEQUATELY HIGH L/τ.

             ● AFFECTS COLLECTION EFFICIENCY,
               IF IN IPTICAL PATH.

Effective Bulk Recombination Mechanisms

INTRINSIC (INTERBAND) RECOMBINATION:

RADIATIVE	ULTIMATELY
	LIMITS
AUGER?	EFFICIENCY

EXTRINSIC (BAND-TO-BOUND STATE) RECOMBINATION:

THERMAL (PHONON ASSISTED)   SRH

(AUGER?)

EXTRINSIC RECOMBINATION CAN BE DECREASED BY REDUCING THE NUMBER OF BOUND

STATES (RECOMBINATION CENTERS, "DEFECTS").

Knowledge of Defects

a. ARE SOME DEFECTS "INTRINSIC"?

(NEUTRAL DEFECT WITH ACTIVATION ENERGY E_a AT PROCESS TEMPERATURE "FROZEN IN."
IONIZED FRACTION AT DEVICE OPERATION TEMPERATURE FORMS RECOMBINATION CENTER,
PARTICULARLY IN N-TYPE).

b. TRUELY EXTRINSIC (PROCESS-INDUCED) DEFECTS

* IMPURITIES (O, C, Au, Ti, Mo, Fe, ...)

    - BIG PROGRESS MADE IN DETECTING PRESENCE, DETERMINING CONCENTRATION.
      OPEN QUESTION OFTEN IS: INTERSTITIAL, SUBSTITUTIONAL, COMPLEXED, OR
      PRECIPATED?

    - O: PRIMARY SOURCE: CRUCIBLE IN Cz PROCESS. TECHNIQUES KNOWN TO REDUCE
      O-CONTENT TO 0.1 OF STANDARD LARGE-CRUCIBLE Cz PROCESS.
      O-CONTENT INCREASES WITH C- OR B-CONTENT.

* CRYSTAL GROWTH DEFECTS.

    - BIG PROGRESS MADE IN DETECTION, IDENTIFYING CRYSTAL GROWTH DEFECTS.

    - STRONGLY CONNECTED WITH THE CRYSTAL GROWTH TECHNOLOGY APPLIED;
      TECHNOLOGY APPLIED SEEMS PRIMARILY DETERMINED BY THROUGTHPUT, PRICE,
      AND WHAT THE MAJORITY OF USERS ARE WILLING TO ACCEPT.

Reduce Volume Recombination Center Density

* ORIGINAL MATERIAL PROCESSING:

    - FEWER IMPURITIES

    - ROLES OF OXYGEN, CARBON?

    - FEWER CRYSTAL DEFECTS   (THERMAL ENVIRONMENT IN X-TAL GROWTH?)

    - ROLES OF DEFECT COMPLEXES

* DEVICE PROCESSING:

    - NO NEW IMPURITY INTRODUCTION

    - REMOVE EXISTING DEFECTS (GETTERING)

    - AVOID TRANSFORMATION OF DEFECTS TO RECOMBINATION CENTERS
      (EFFECTS OF THERMAL PROCESSES?)

    - FOSTER TRANSFORMATION OF RECOMBINATION CENTERS TO HARMLESS
      DEFECTS (PASSIVATION; CHANGES OF COMPLEXES?; ROLE OF HYDROGEN?)

Steps toward Reduced Number of Recombination Centers

1.	IDENTIFY "DEFECT(S)" WHICH FORM RECOMBINATION CENTER(S)	- BROAD RANGE OF DEFECTS AND OF ENERGY LEVELS IDENTIFIED
		- INTERCONNECTION AND RELATIONSHIP TO RECOMBINATION CENTERS MADE IN ONLY A FEW CASES.
2.	IDENTIFY SOURCE(S) OF DEFECT(S)	- USUALLY NOT KNOWN.
3.	FIND WAYS FOR ELIMINATING SOURCE(S) OF DEFECT(S)	- STILL MOSTLY "BLACK ART."
4.	PASSIVATE EXISTING DEFECTS	- LITTLE KNOWN. IS H^+ THE BROAD SPECTRUM ANTIBIOTIC"?

Swanson's Prescription for Processing for Reduced Recombination

a. NEVER USE METAL TWEEZERS ON WAFERS

b. ALWAYS PERFORM RCA CLEANING BEFORE HIGH TEMPERATURE PROCESS STEPS.

c. PROCESS IN A CLASS 100 CLEAN AREA

d. PERIODICALLY CLEAN FURNACE TUBES WITH HCl.

Passivation With Hydrogen

- IT CAN NEUTRALIZE RECOMBINATION CENTERS, APPARENTLY EVEN DEEP IN THE BULK, PARTICULARLY AT GRAIN BOUNDARIES.

- HYDROGEN IMPLANTS PASSIVATE DANGLING BONDS, WHEREVER HYDROGEN IONS REACH THEM.

- HYDROGEN IMPLANTS MAY POSSIBLY ALSO PASSIVATE DEEP LEVELS (IMPURITIES) in Si.

- THE "IMPLANTATION" OF HYDROGEN IONS, EVEN AT LOW ENERGIES CAUSES SPUTTER ETCHING, LATTICE DAMAGE (200 A DEEP AT 400eV).

- HYDROGEN CAUSES MORE LATTICE DAMAGE THAN ARGON, EVEN AMORPHIZES SURFACE LAYER, BUT FEWER DANGLING BONDS ("PASSIVATES ITS OWN DAMAGE")

- WHETHER PASSIVATION DOMINATES OVER INTRODUCED DAMAGE DEPENDS ON IMPLANTATION ENERGY, PRIOR PROCESS HISTORY.

- HYDROGEN IS ALSO KNOWN TO NEUTRALIZE B AS AN ACCEPTOR.

Reducing Surface Defects

1. OXIDATION

- MOST HIGH EFFICIENCY CELLS NOW USE SOME FORM OF OXYDE PASSIVATION.

- REMAINING SURFACE RECOMBINATION VELOCITY IS FUNCTION OF PREPARATION PROCEDURE FOR FORMING OXIDE LAYER.

- DRY THERMAL OXIDE FOLLOWED BY LOW TEMPERATURE HYDROGENATION CAN YIELD MID-GAP STATE DENSITIES NEAR $1.10^{10}/(CM^2 \ eV)$, BUT OXIDATION FOLLOWED BY AN INERT ATMOSPHERE ANNEAL CAN YIELD $1.10^9/(CM^2 \ eV)$, i.e $\approx 2 - 5$ cm/s IN HIGH LEVEL INJECTION.

- NITRIDING OXIDE LAYERS MAY IMPORVE STABILITY, RADIATION RESISTANCE OF PASSIVATION LAYERS.

Si (100)
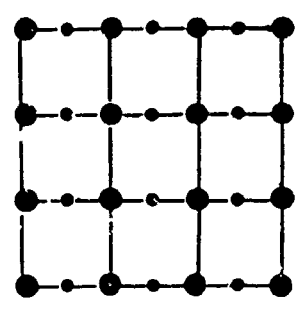
Top View
- **●** Surface Layer
- **·** Second Layer
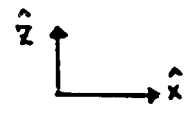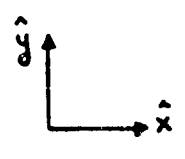
Side View
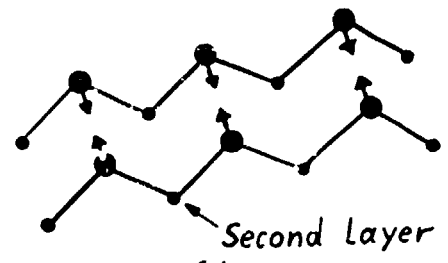
Pairing or Dimer Model

Second layer

Top Layer
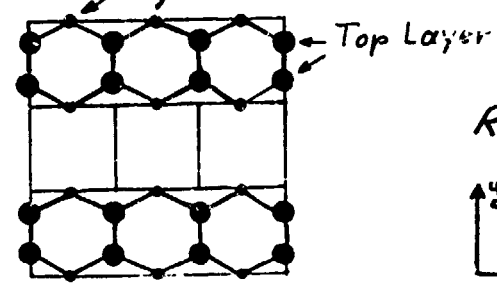
2×1 Reconstruction
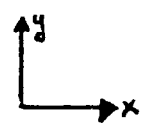
Top View
Si (100)
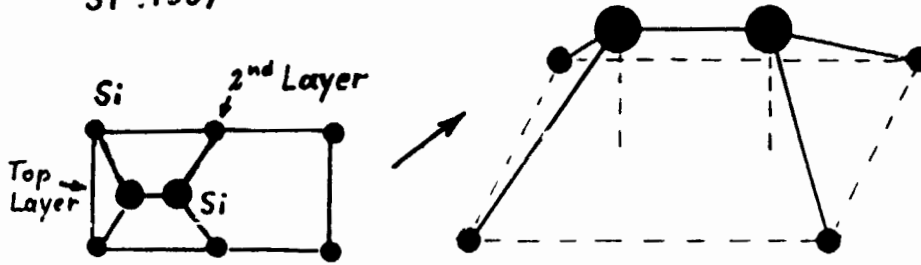
Symmetric Dimer Unstable
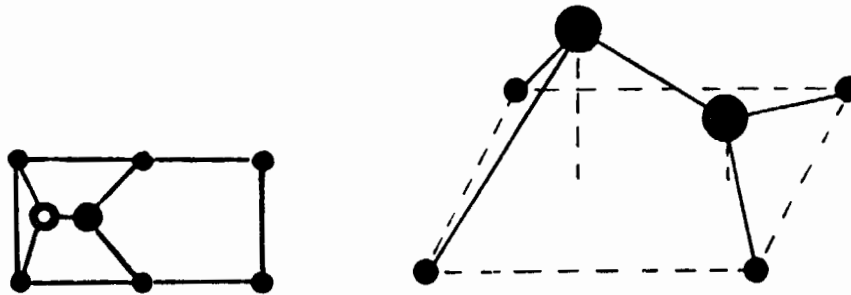
Asymmetric Dimer Stable

Buckling of symmetric dimer lowers
energy by 0.16 eV/dimer
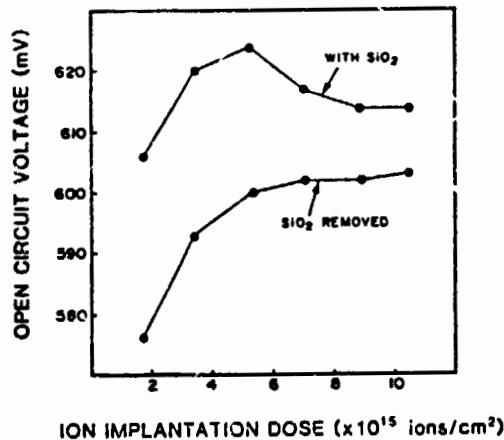
Modeling

- THE "MODELERS" CAN ONLY INCORPORATE THE PHYSICS AS PRESENTLY UNDERSTOOD.
- DIFFUSION PROFILES CAN BE "ANOMALOUS," DEPEND ON MATERIAL PERFECTION.
- THE ACHIEVEMENT OF THE ULTIMATE EFFICIENCIES WILL REQUIRE THE DETAILED SIMULATION OF ALL EFFECTS. THIS NEEDS 2- AND 3-DIMENSIONAL CAPABILITIES.
- SUCH SIMULATION CANNOT BE ANALYTICAL, BUT MAY, FOR SPEED AND COST-SAVINGS, BE QUASI-NUMERICAL.

ANALYSIS

- MATERIAL ANALYSIS HAS REACHED IMPRESSIVE CAPABILITIES.
- IN DEVICE ANALYSIS, THE SEPARATION OF BASE AND EMITTER CONTRIBUTIONS TO SATURATION CURRENT IS STILL TENUOUS, OFTEN LEADING TO CONFLICTING RESULTS.
- PROGRESS IS BEING MADE IN DEVELOPING METHODS TO PERMIT DETERMINATION OF RECOMBINATION RATES IN DIFFERENT PARTS OF THE DEVICE, BUT FURTHER ADVANCES ARE NEEDED.
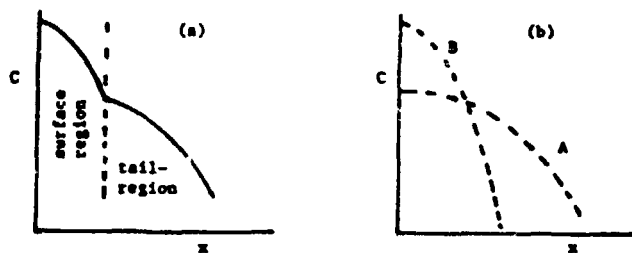
(a) Schematic drawing of the kink-tail structure of P profile, which, hypothetically, may be obtained by adding (b) profiles of physically distinguishable A and B atoms diffusing independently.

Low-Cost Crystalline Si Is Primarily:

- "CAST" INGOT MATERIAL   (SEMIX, SILSO, HEM, etc.)
- NOT-SINGLE CRYSTALLINE RIBBON   (EFG, LASS, etc.)

> EFFORTS TO INCREASE GRAIN SIZE, REDUCE DEFECTS,
> PASSIVATE REMAINING ONES, ALL SHOW PROGRESS.

BUT: IT SEEMS IMPOSSIBLE TO COMPLETELY PASSIVATE
      ALL THE DEFECTS ASSOCIATED WITH GRAIN BOUNDARIES

ALSO: FASTER, LESS CONTROLLED GROWTH MAY ALWAYS RESULT
       IN INCREASED NUMBERS OF IMPURITIES, CRYSTAL DEFECTS.

CONSEQUENTLY: THE ULTIMATELY ACHIEVABLE PERFORMANCE MARGIN
               RELATIVE TO THAT OF SINGLE CRYSTAL DEVICES IS
               NOT KNOWN.

- WEB-DENDRITE RIBBON IS IN A CLASS BY ITSELF.
  MAY HAVE POSSIBILITY, WITH INTERNAL GETTERING AT TWIN
  PLANES, TO SURPASS THE QUALITY OF SINGLE CRYSTAL WAFERS.

IN ALL METHODS, THE CONTROL OF THE THERMAL ENVIRONMENT
DURING AND SHORTLY AFTER GROWTH APPEARS IMPORTANT.

Final Discussion

- FOR HIGHER EFFICIENCIES (AT LEAST > 20%), BETTER SINGLE CRYSTAL Si IS NEEDED.

- IT SHOULD BE POSSIBLE TO BRING Cz Si TO THE SAME LOW-RECOMBINATION LEVEL AS Fz Si.

- HOW CAN DEVICES BE FABRICATED FROM THIS Si WITHOUT GREATLY INCREASING THE RECOMBINATION CENTER DENSITY?

- ARE SPECIAL Si QUALITIES NEEDED TO PERMIT SUCH PROCESSING?

- HOW CAN THE PROGRESS MADE IN MATERIAL SCIENCE BE TRANSLATED INTO BETTER PROCESSING METHODS?

- IF SOLAR CELL FABRICATORS WOULD SPECIFY THE QUALITY OF Si THEY NEED, WOULD Si MANUFACTURERS DELIVER TO THESE SPECIFICATIONS?

- DO SOLAR CELL FABRICATORS KNOW WHAT SPECIFICATIONS TO WRITE?

HIGH-EFFICIENCY MODULE AND ARRAY RESEARCH

JET PROPULSION LABORATORY

R.G. Ross, Jr.

Module High-Efficiency Research Thrusts

- Development of module technologies contributing to high efficiency
  - High cell packing factors
  - Low optical losses
  - Low electrical mismatch losses
  - Low operating temperatures

- Development of reliability technologies required to maintain high efficiency of:
  - Cells
  - Optical coatings
  - Encapsulants

Module Technologies Contributing to High Efficiency

- High cell-packing factors
  - Narrow borders, close cell spacing
  - Large modules

- Low optical losses
  - Antireflection coatings
  - Antisoiling coatings
  - High-transmittance encapsulants

- Low electrical-mismatch losses
  - Series-paralleling
  - Cell sorting

- Low operating temperatures
  - Good convective cooling of module rear surface
  - High-emittance, high-reflectance rear surface
  - Low IR-absorptance front surface

Unique Issues Associated With Reliability
of High-Efficiency Modules

- Reliability of:
    - High-efficiency cells
    - Narrow module borders
    - Antisoiling coatings
    - Antireflection coatings on glass-air interfaces

FY85 Research Related to High-Efficiency Modules

- Module temperature reduction with IR-reflecting cells (Spire)

- Reliability of antisoiling coatings (Springborn)

- Reliability of modules with narrow borders (JPL, Wyle)

- Reliability of high-efficiency cells (Clemson)

- Verification of overall module performance
  (JPL, Spire, Westinghouse)

FLAT-PLATE MODULE EFFICIENCY VS COST TRADEOFFS

JET PROPULSION LABORATORY

R.W. Aster

Objective

The study objective is to use the Five-Year Research Plan energy cost methodology and to perform in-depth analyses based on the extensive data that are relevant to PV systems to facilitate the accomplishment of the $0.15/kWh energy cost goal

The basis for the Five-Year Research Plan energy cost methodology is the equation:

$$\overline{EC} = \left[\frac{FCR}{INSOL}\right][INDC][A(\$MSQMD + \$MSQBS) + \$KWBS] + A \cdot G \cdot CRF \left[\frac{\$MSQOM}{INSOL}\right]$$

Parameters Varied in the Study

Parameter	Range	Nominal Value
Module efficiency* (25°C)	3% - 30%	15%
Module cost,* $/m^2	30-500	90
Type**	Fixed, one-axis, two-axis	
Insolation		2000 (F), 2400 (1), 2600 (2)
Energy cost,* ¢/kWh	10-25	15
Fixed charge rate	0.11-0.203	0.153
Indirect costs	1.3-2.1	1.5
O&M Cost, $/m^2	0.11-8.82 (F), 0.19-10.02 (T)	1.1 (F), 1.4 (1&2)
Area-related BOS, $/m^2		50 (F), 58 (1), 90 (2)
BOS efficiency, %	0.755-0.930	0.865
Module degradation rate	0.45% - 0.75%/yr	0.5%/yr
Module replacement rate	0.05-0.00001/yr	0.004/yr
Module cleaning frequency	0-12/yr	None

*Indicates sensitivities shown in this presentation
**F = Fixed, T = Tracking

Other Baseline Parameters

Values for the other baseline parameters were described at the 23rd PIM. However, since that time the baseline values for insolation have changed:

Tracking Option	Insolation Values (kWh/m^2/yr)	
	23rd PIM	Current Baseline
Fixed	2250	2000
One-axis	2700	2400
Two-axis	2925	2600

Allowable Module Cost, $/m^2, vs Module Efficiency and Energy Cost

Module Efficiency, % (STC)	Energy Cost, $/kWh				
	0.10	0.15*	0.20	0.25	0.30
9	-11	25	61	97	132
12	10	57	105	153	201
15*	30	90*	150	209	269
18	51	122	194	265	337

*DOE goals and JPL milestones.

Allowable Module Costs for Various Energy Costs
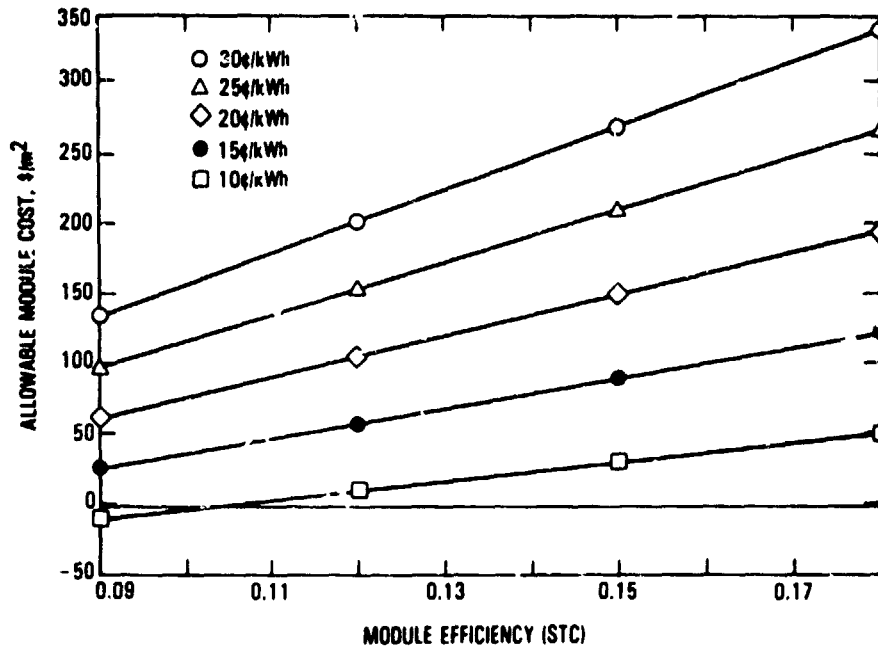
Allowable Module Cost vs Module Efficiency and Insolation, $/m^2

Module Efficiency, % (STC)	Annual Insolation (kWh/m^2/yr)			
	Fixed:	1833[1]	2000[2]	2250[3]	2400[4]
	One-axis:	2200	2400		2890
	Two-axis:	2380	2600		3130
9		1	25		17
12		45	57	5	7
15		75	90	1	2
18		104	122	14	8

[1]Typical for the Southeast

[2]Typical for the greater Southwest region

[3]Typical for Nevada, Arizona, New Mexico, southern Utah, portions of California and Texas

[4]Phoenix, Albuquerque

Allowable Module Costs for Various Insolation Levels
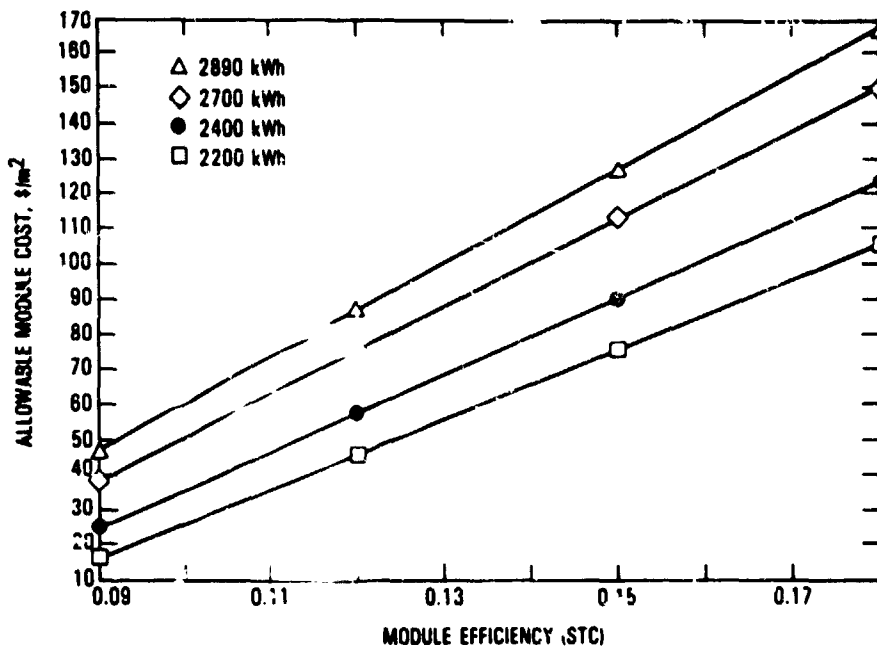
Energy Cost vs Module Cost and Efficiency, $/kWh

Module Efficiency, % (STC)	Module Cost, $/m²				
	30	60	90	200	500
3	0.44	0.57	0.69	1.15	
6	0.23	0.29	0.35	0.58	
9	0.16	0.20	0.24	0.39	
12	0.12	0.15	0.19	0.30	0.61
15		0.13	0.15*	0.24	0.49
18			0.13	0.20	0.41

*DOE goal and JPL milestone.

Flat-Plate Allocation Guidelines

The Allocation Guidelines are a working tool of FSA Project management. They provide targets for PV R&D that are consistent with the accomplishment of DOE milestones for FSA and the overall energy cost goal of the PV Program

Alignment of the Allocation Guidelines to the DOE energy goal produces module cost guidelines that are parametric with module efficiency. This provides researchers with a tool to make appropriate tradeoffs between cost and efficiency at the subsystem level

Baseline Allocation Guidelines ($0.15/kWh)

	Module Efficiency (STC)			
	0.13	0.14	0.15	0.16
Sheet, $/m^2 sheet *	24	30	36	37
Cells, $/m^2 cell **	20	25	30	40
Encapsulants, $/m^2 module	14	14	14	14
Fabrication, $/m^2 module	12	12	12	12
Total, $/m^2 module	68	79	90	100

*To convert to $/m^2 module, multiply by 0.990 to account for yields and packing efficiency.

**To convert to $/m^2 module, multiply by 0.927 to account for packing efficiency and module yield.

Conclusion

The Allocation Guidelines are designed to be consistent with FSA milestones for module cost ($90/m^2), module efficiency (15%, STC), and the programmatic goal for energy cost ($0.15/kWh)

They are research targets that appear to be achievable, given prior accomplishments and planned activities in the areas of:

- Low-cost silicon purification
- Low-cost sheet material
- High-efficiency cell processing
- Low-cost, long-life encapsulants
- Automated fabrication methods

Extensive sensitivity analysis work has been performed that shows that these guidelines represent an efficient way to meet the intent of the DOE program

C-2

THE FUTURE OF CRYSTALLINE SILICON TECHNOLOGY IN THE U.S. DEPARTMENT OF ENERGY PROGRAM

U.S. DEPARTMENT OF ENERGY

Anthony F. Scolaro

- THE POTENTIAL ENERGY CONVERSION EFFICIENCY OF CRYSTALLINE SILICON SOLAR CELLS IS AMONG THE HIGHEST OF POTENTIAL EFFICIENCIES FOR ONE JUNCTION CELLS.
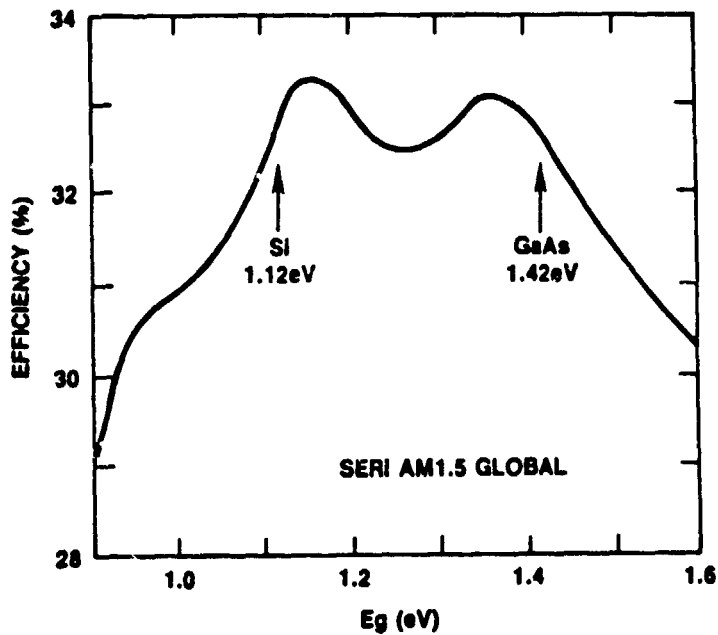
Five-Year Research Plan Goals for Crystalline Silicon

		1984	1985	1986	1987	1988
		FY 84	FY 85	FY 86	FY 87	FY 88
MATERIALS RESEARCH	SILICON MATERIALS	/////	///// < $20/kg			
	ADVANCED SILICON SHEET	/////	/////	/////	Resolve Generic Growth Problems	
COLLECTOR RESEARCH	FLAT PLATE COLLECTORS	Si Cell 18% (1cm²)	Si Mod. 12% ($100/m²)	Si Cell 20% (1 cm²)	Si Mod. 14% ($90/m²)	T.F. Mod. 12% ($70/m²) / Si Mod. 15% ($90/m²)
SYSTEMS RESEARCH	MODULE RELIABILITY	Complete 30-Yr. Model	Define T.F. Encapsulation Requirements	Complete Environmental Tests	Verify Cryst.-Si 30-Yr. Life	Assess Life of T.F. Modules

▲ Program Milestone *

*Cost Milestones Assume Further Industrial
Development and Scale-up, Efficiencies
Are Measured at 28°C and AM 1.5.

Issues to Be Addressed: Silicon Materials

- DEVELOP A PRODUCT WITH ACCEPTJLE PURITY FROM A FLUIDIZED BED REACTOR

- COMMERCIALIZE FLUIDIZED BED REACTOR TECHNOLOGY

- TO BE COMPLETED IN FY 1985

Issues to Be Addressed: Advanced Silicon Sheet

- DEVELOP BASIC UNDERSTANDING OF THE HIGH SPEED SILICON CRYSTALLIZATION

- CONTROL CRYSTALLIZATION TO DEVELOP HIGH PURITY/LOW DEFECT DENSITY MATERIAL

- DEVELOP THE TECHNOLOGY TO SENSE AND MITIGATE CHANGES IN THE GROWTH ENVIRONMENT, ENABLING LONG-TERM GROWTH

- TO BE COMPLETED IN FY 1986

Issues to Be Addressed: Flat-Plate Collectors

- UNDERSTAND DEVICE PARAMETER SENSITIVITIES, I.E. SURFACE AND BULK RECOMBINATION

- IDENTIFY AND DEVELOP PROCESSES TO OBTAIN THE DESIRED DEVICE PARAMETERS

- PERFORM RESEARCH TO DEMONSTRATE THAT HIGH EFFICIENCY CELL PROCESSES CAN BE COST-EFFECTIVE

- CONTINUING EFFORT

Issues to Be Addressed: Module Reliability

- MITIGATE THE EFFECTS OF ALREADY IDENTIFIED MODULE DEGRADATION MODES, I.E. ELECTROCHEMICAL CORROSION, BOND DELAMINATION, PHOTOTHERMAL OXIDATION, ELECTRICAL INSULATION BREAKDOWN

- DEVELOP AN UNDERSTANDING OF AGING PROCESSES, INCLUDING SYNERGISTIC EFFECTS, TO ENABLE ACCELERATED TESTING

- TO BE COMPLETED IN FY 1987

PV Product Growth Stages

● THE SIGNIFICANT PROGRESS OF CRYSTALLINE SILICON TECHNOLOGY DEVELOPMENT ALONG THE PRODUCT GROWTH CURVE POSITIONS THE TECHNOLOGY TO BE A MAJOR CONTRIBUTOR TO PV TECHNOLOGY MARKET GROWTH.
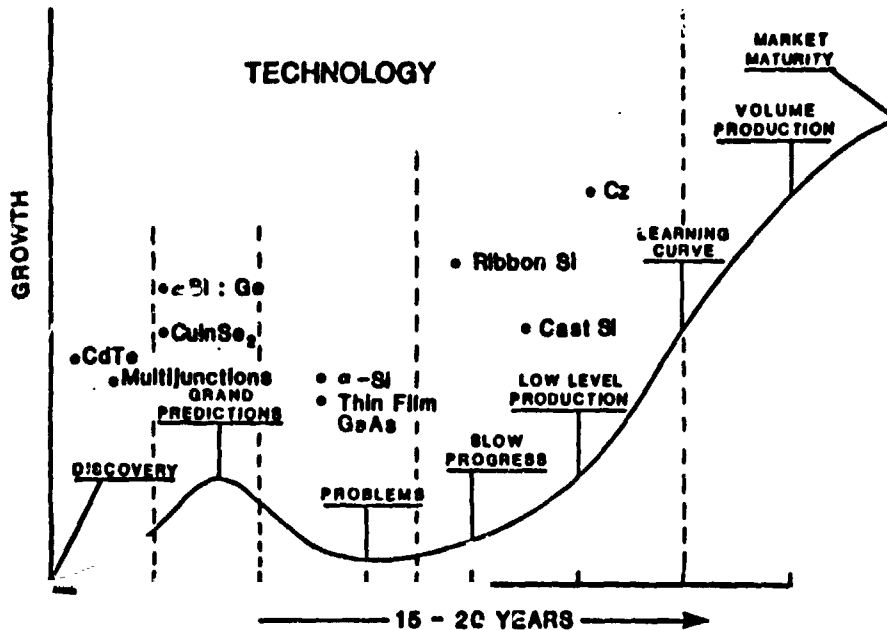
Summary

● SILICON HAS A VERY HIGH POTENTIAL EFFICIENCY, DEMONSTRATED IMPROVEMENT IN RELIABILITY AND A SIGNIFICANT POTENTIAL FOR COST REDUCTIONS.

● THE PHOTOVOLTAIC TECHNOLOGY DEVELOPMENT PROCESS IS HIGHLY UNCERTAIN, BUT CRYSTALLINE SILICON TECHNOLOGY HAS A SUBSTANTIAL KNOWLEDGE BASE TO DRAW FROM, IMPROVING ITS CHANCES OF SUCCESS.

GEORGETOWN UNIVERSITY PHOTOVOLTAIC HIGHER EDUCATION NATIONAL EXEMPLAR FACILITY (PHENEF)

HUGHES AIRCRAFT CO.

Neil Marshall
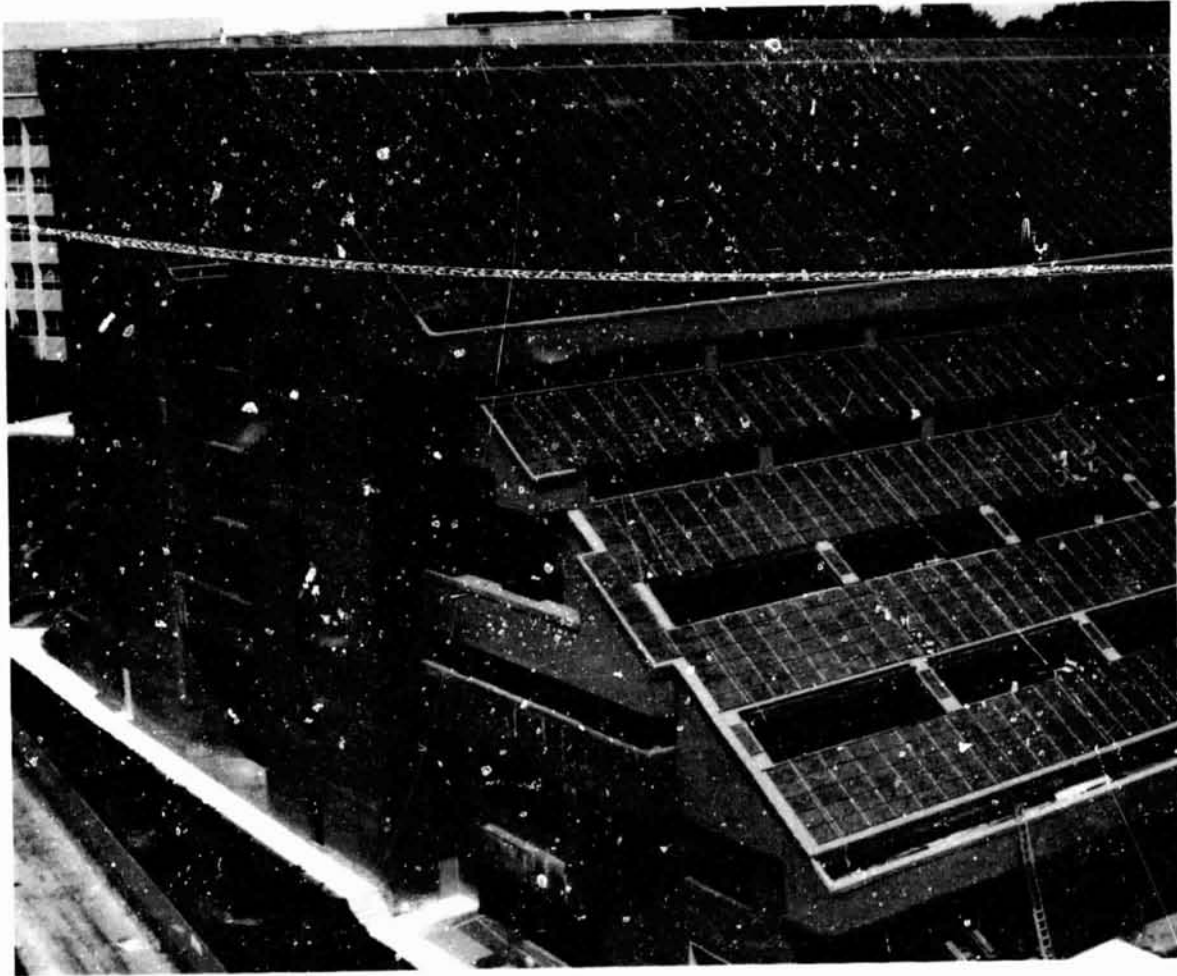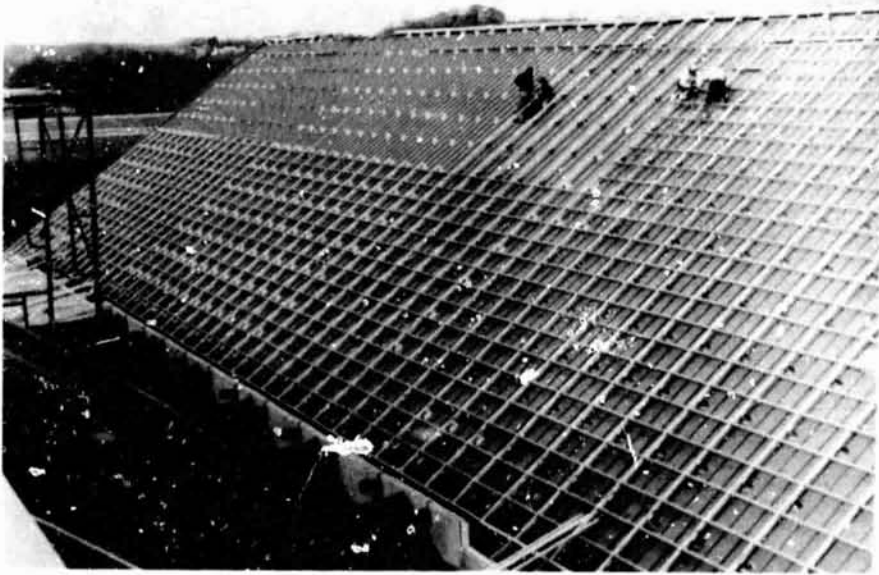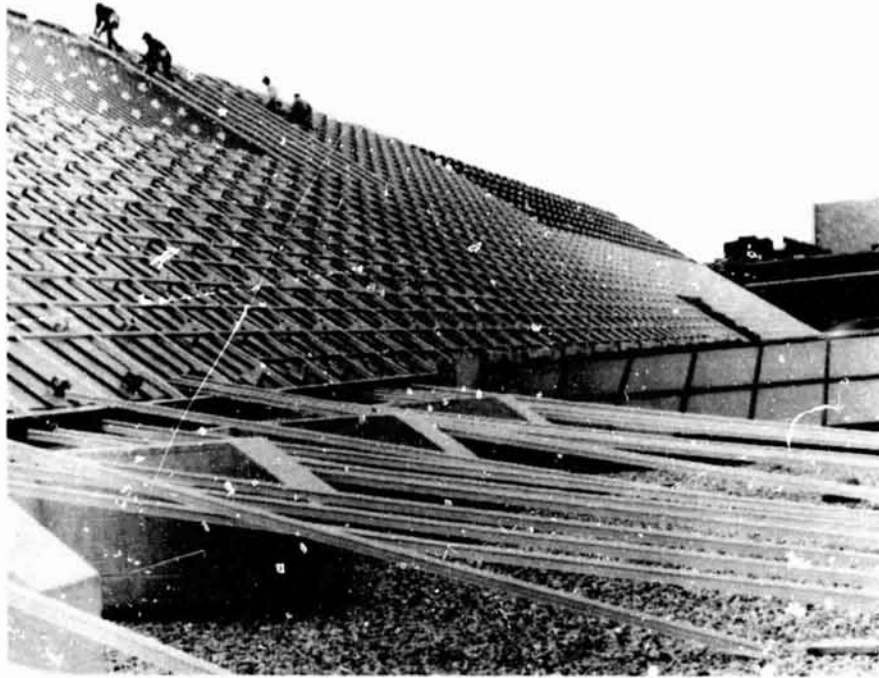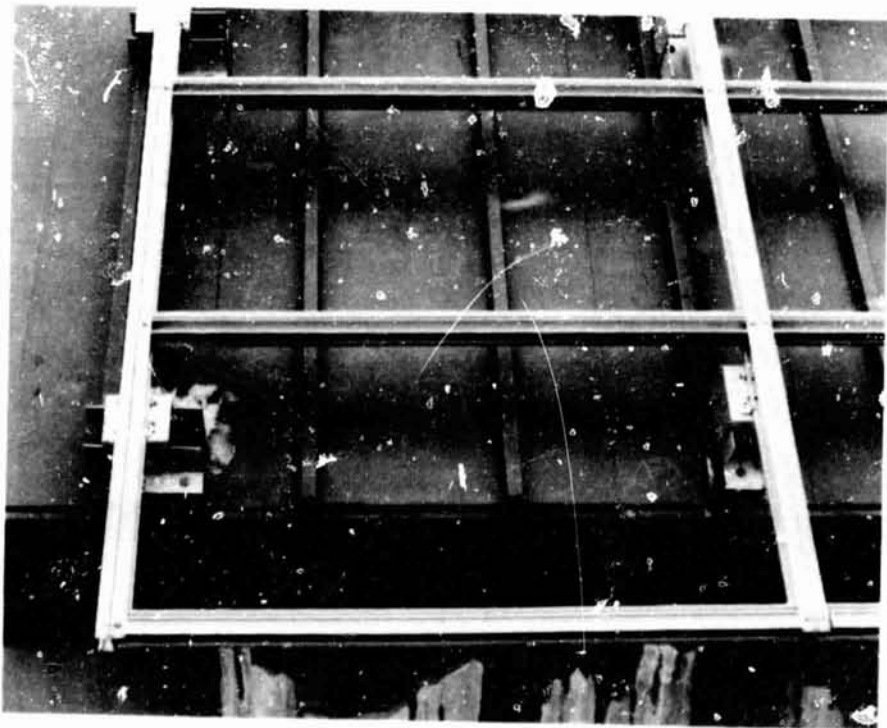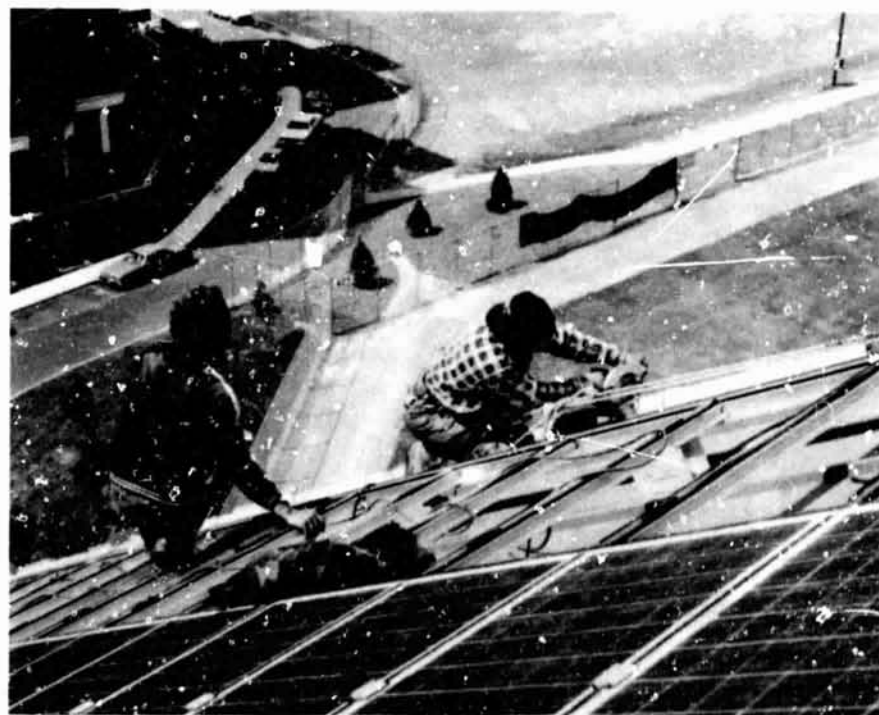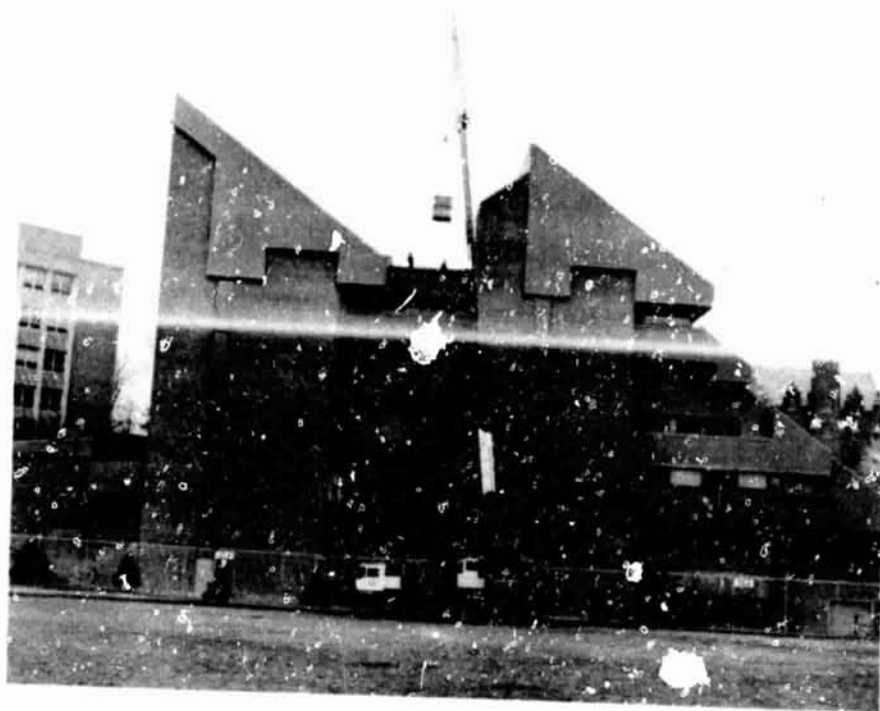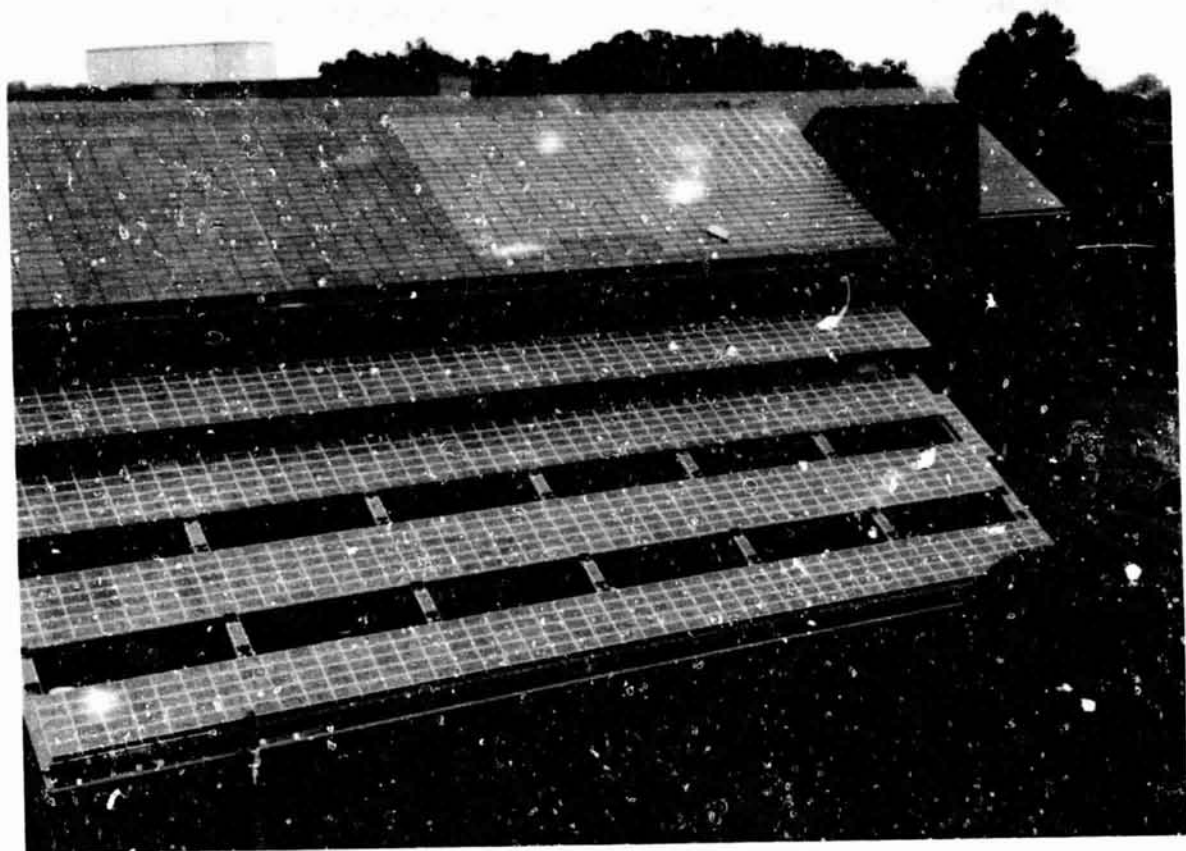
Systems Requirements

- PV ARRAY DESIGN LIFETIME — 20 YEARS MINIMUM

- AVAILABLE ROOFTOP AREA — ABOUT 36,000 SQ. FT.

- ARRAY ROOFTOPS — WATERTIGHT

- INSTRUMENTATION NETWORK — ODAS; WEATHER STATION; MODULES AND ROOFTOP TEMPERATURE

- MAINTENANCE AND REPAIR — MODULE REMOVAL; TEST EQUIPMENT; REMOTE MONITOR; ALARMS

- SAFETY — ELECTRICAL; MECHANICAL; SNOW/ICE

SYSTEM DESIGN AND WIRING TOPOLOGY

System Design and Performance

- **PEAK POWER AT STANDARD CONDITIONS**   —   300 kw, MIN.

- **ARRAY ELECTRICAL DESIGN**   —   BIPOLAR, NEUTRAL RESISTIVELY GROUNDED

- **ARRAY OUTPUT VOLTAGE**   —   ± 228 VDC

- **MAIN BUS CURRENT AT PEAK POWER**   —   660 ADC

PHENEF Simplified Block Diagram
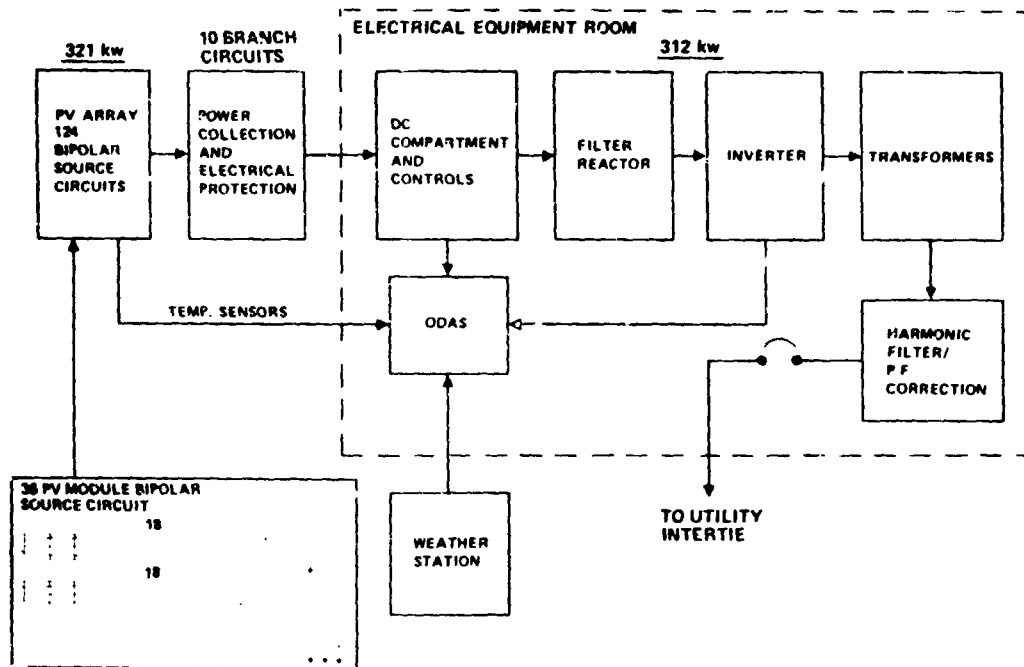
Module Electrical Characteristics

- 72 WATTS MINIMUM LOT AVERAGE AT 16.2 VOLTS

- 67 WATTS MODULE MINIMUM

- MEASURED AT 1000 W/M^2, AM 1.5, 28°C

- 3000 VOLT ELECTRICAL VOLTAGE INSULATION

- 3 ENCAPSUALTED BYPASS DIODES (12 CELLS/DIODE)

- SOLARLOK CONNECTORS (UL RECOGNIZED)

- SIZE: TWO FT. BY FOUR FT. LAMINATE

PV Module

- FULLY TESTED BY JPL PER BLOCK V 5101–162

- PRODUCTION ADHERES TO PREDETERMINED MANUFACTURING PROCESSES

- MODULES SUBJECTED TO UL–790 FIRE RESISTANCE TEST

- FULL MECHANICAL/VISUAL INSPECTION

- PREDETERMINED ACCEPTANCE TEST PROCEDURES

  - HUGHES–FURNISHED REFERENCE CELL STANDARDS (DSET/ASTM #178)

  - CALIBRATED MODULES

  - SOURCE INSPECTION/LOT SAMPLES

- SOLAREX HAS DELIVERED MODULES ABOUT 4 PERCENT ABOVE SPECS.

PV Module Matching

- MODULES SEGREGATED INTO 12 CURRENT GRADES

- MODULES MATCHED TO WITHIN $\pm$ .025 AMPS PER GRADE

- MODULES PACKAGED 18 PER BOX: SAME GRADE

  - ONE HALF BIPOLE

- ROOFTOP MODULE CIRCUIT LAYOUT MAPPED BY GRADE

  - LOWER PERFORMANCE GRADES INTO SHADOW PRONE AREAS

TEST EQUIPMENT
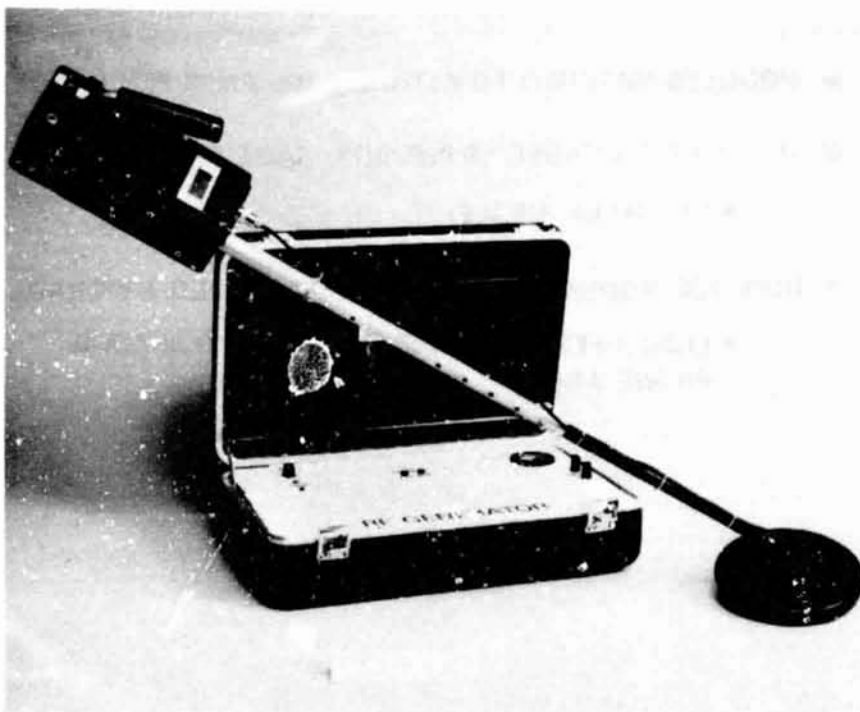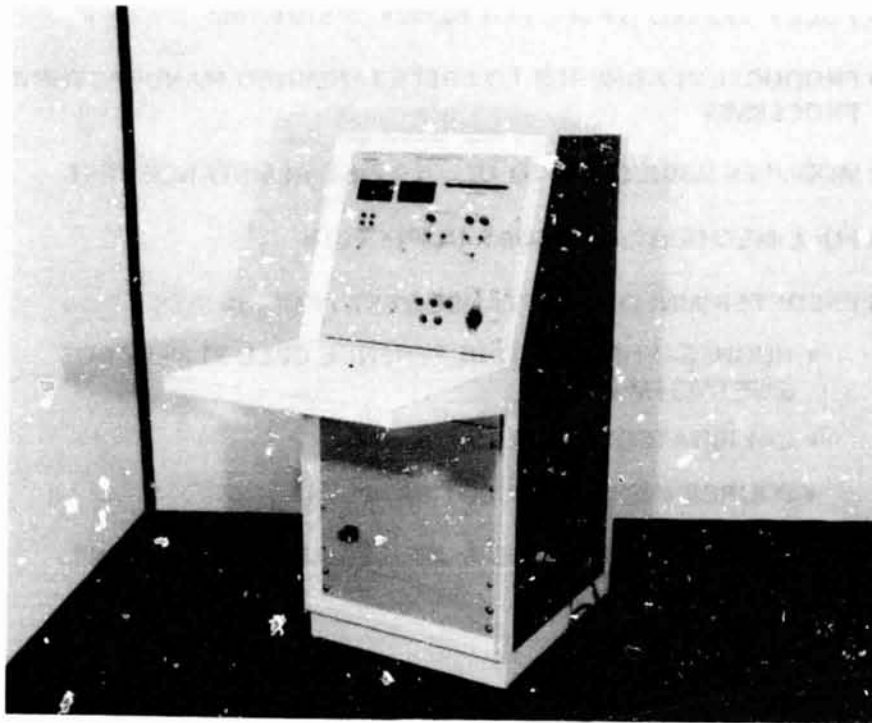
BLOCK V MODULE PROGRAM

JET PROPULSION LABORATORY

M.I. Smokler

Program Configuration

- Perform module design

- Manufacture 10 modules

- Conduct Block V qualification test sequence

- Modify design to correct problems, as necessary

- Conduct design review

- Manufacture 10 modules

- Conduct Block V qualification test sequence

- Modify design, as necessary, and supply modules for retest

- Prepare final report

Program Status: Remaining Events

Item	Expected
Qualification tests completed	12/84
Final reports submitted	2/85
JPL user handbook issued	3/85

Test Experience

- Negligible problems
    - Hail damage
    - Unacceptable cell cracks
    - Interconnect failure
    - Hot spot failure

- Continuing problems
    - Uncured encapsulant
    - Delamination
    - Frame/mounting degradation
    - High-voltage breakdown
    - Inadequate ground continuity
    - Junction box warp

Measurement Problems Solved

Problem	Solution
Current up to 27A	High current electronic load (to 50 A nominal)
Module diagonal up to 2.2 m	Uniform irradiance field (< 2% non-uniformity)
No custom-made reference cells	AM1.5 simulator spectrum (1% max mismatch)

Module Power Trend

CELL TEMP: 25°C
INSOLATION: 100 mW/cm^2, AM1.5
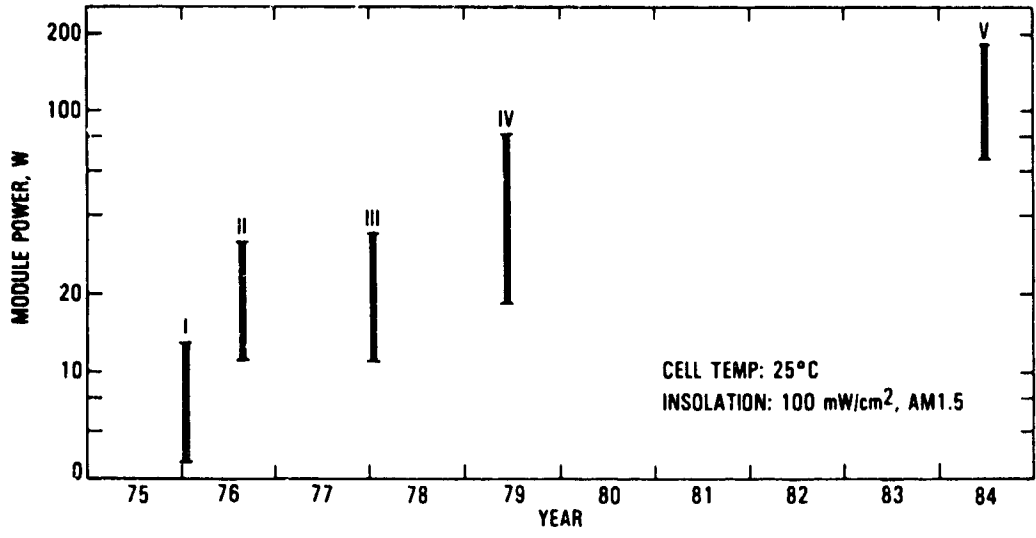
Packing Factor Trend
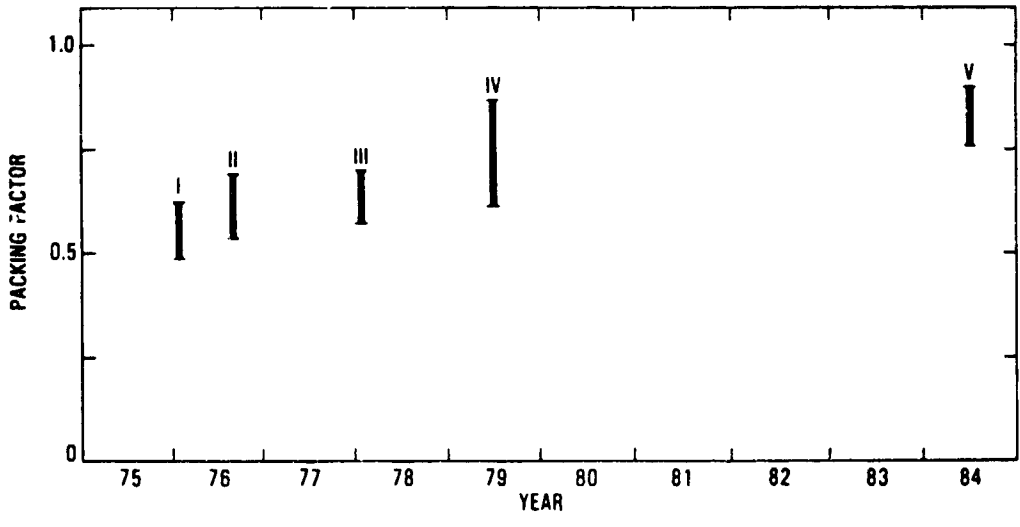
Cell and Circuit Characteristics

	Cell				Circuit	
	Qty	Size, mm	Shape	Base Material	Parallel Cells	Bypass Diodes
ARCO	72	97 × 97	"Square"	Cz	6	0
GE	72	100 × 100	"Square"	Cz	2	3
MSEC	432	48 × 95	Rect.	EFG	12	0
SOLAREX	117	101 × 101	Square	Sem:	9	0
SPIRE	72	91 × 91	"Square"	Cz	2	3

Module Physical Characteristics

	Size, m		Super-Strate	Encap.	Bottom Cover	Pack. Fctr
	Length	Width				
ARCO	1.22	0.61	Glass	EVA	TED/POLY/TED	0.90
GE	1.85[a]	0.81[a]			TED/POLY/AI/TED	0.90
MSEC	1.79	1.20			POLY/AI/TED	0.89
SOLAREX	1.39	0.96			POLY/MYLAR/TED	0.88
SPIRE	1.13	0.60	↓	↓	TEDLAR	0.76

[a]Includes roofing material

Electrical Performance

| | INSOLATION: 100 mW/cm² CELL TEMP: 25°C | | | | |
	P_{max}, W	$V_{P_{max}}$, V	$I_{P_{max}}$, A	Mod. Eff., %	Cell[a] Eff., %
ARCO	84.1	5.82	14.4	11.3	12.6
GE	81.4	16.9	4.82	10.5	11.7
MSEC	182	15.3	11.9	8.3	9.3
SOLAREX	139	5.84	23.8	10.3	11.7
SPIRE	71	16.1	4.38	10.1	13.3

[a]Encapsulated

Cell Efficiency Trend

CELL TEMP: 25°C
INSOLATION: 100 mW/cm², AM1.5
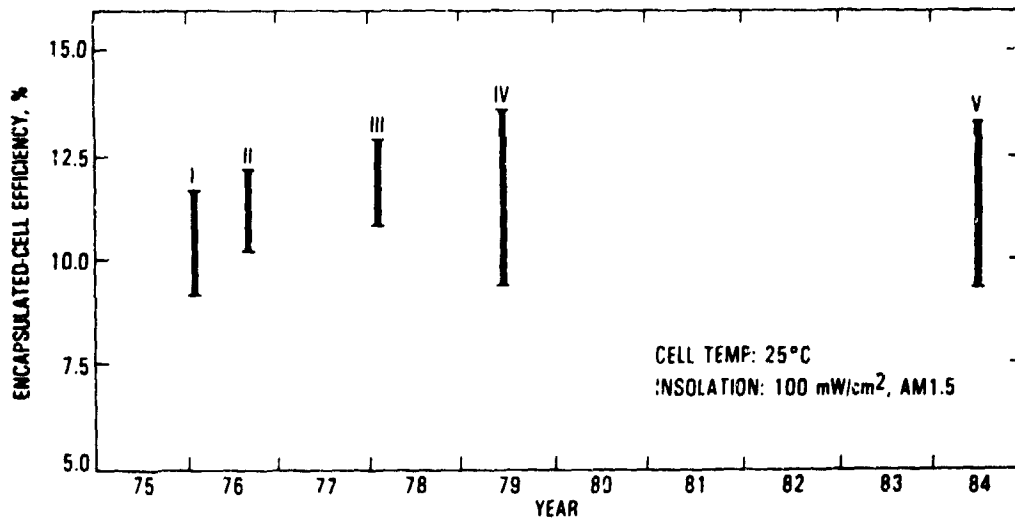
Module Efficiency Trend

Module Efficiency Trend graph: MODULE EFFICIENCY, % (vertical axis, 0 to 12.5) vs YEAR (horizontal axis, 75 to 84). Data points labeled I, II, III, IV, V. CELL TEMP: 25°C. INSOLATION: 100 mW/cm², AM1.5

Module Cost Trend

Module Cost Trend graph: 1980 $/W (vertical axis, 0 to 40) vs YEAR (horizontal axis, 75 to 84). Data points labeled I, II, III, IV (ESTIMATED), V. CELL TEMP: 25°C. INSOLATION: 100 mW/cm², AM1.5
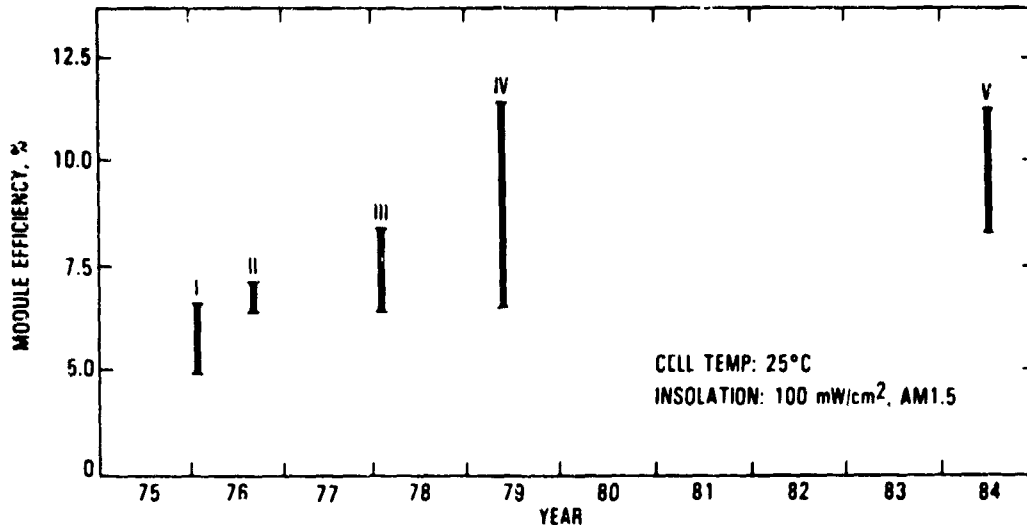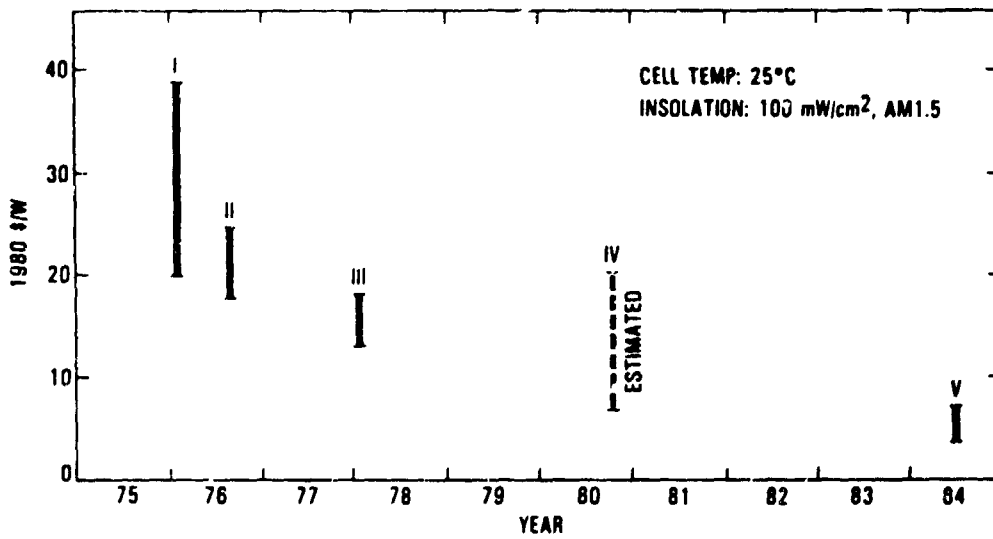
Summary

- The Block V Module Program will be completed in early 1985

- The principal improvements are

    Large modules

    High performance more common

    Several former design problems solved

Technical Sessions

RELIABILITY PHYSICS

Edward F. Cuddihy and
Ronald G. Ross, Jr., Chairmen

Ranty H. Liang of JPL reported on Studies of Photothermal Degradation in Encapsulants. The fundamental mechanisms and associated reaction kinetics of the thermal and photothermal yellowing of EVA are described. EVA will yellow during dark-oven aging at elevated temperatures, and will also yellow in the presence of UV. But the UV will induce a partial photobleaching of the thermal yellowing. Because the kinetics of the thermal yellowing, UV yellowing, and UV bleaching are different, the overall yellowing of EVA is not simply related to UV intensity and temperature. The work described seeks to derive the overall reaction kinetics of EVA yellowing as part of the development of a life-prediction methodology.

C.C. Gonzalez and R.G. Ross, Jr., of JPL reported on Predicting Photothermal Field Performance. A preliminary kinetics model of EVA yellowing was generated from the fundamental work described in the previous presentation. Using this model and SOLMET weather data, predictions of the level of weather-induced yellowing in EVA from 30 years of simulated outdoor exposure in Phoenix were generated. Yellowing of EVA results in optical absorption of transmitted sunlight, thereby reducing the power output of solar cells encapulsated in EVA. This preliminary work indicated power losses amounting to near 3.5% for ground-mounted arrays, and power losses approaching 7.9% for roof-mounted arrays, which typically operate at higher temperatures than ground-mounted arrays.

J. Guillet of University of Toronto reported on Micromolecular Modeling. This contract work seeks to develop a reaction-kinetics-based model of the overall photodegradation process experienced by encapsulatants in an outdoor weather environment. Inasmuch as well over 50 individual reaction mechanisms have been identified, part of this work is to develop a computer ability to solve all of the rection kinetic equations simultaneously for life-prediction purposes, and for chemical information related to the selection of the most effective stabilizing additives for weather-sensitive encapsulants such as EVA. The computerized model indicates that a combination of a UV absorber and a hindered amine light stabilizer (HALS) would be an effective stabilizing system.

P. Gomez, S.K. Fu, and O. Vogl of the Polytechnic Institute of New York reported on Polymerizable Ultraviolet Stabilizers. Polytechnic Institute of New York carries out chemical synthesis of advanced polymeric and reactive stabilization additives for polymeric materials, such as EVA. These additives, such as protective UV-absorbing agents, are resistant to high-temperature physical losses. The latest developments in this area were presented.

P. Willis of Springborn Laboratories, Inc., reported on Encapsulated Materials Research. Springborn Laboratories updated its continuing work on long-life, weather-stable encapsulation materials for photovoltaic modules.

RELIABILITY PHYSICS

The program emphasis at Springborn has shifted from material development and identification to life-assessment experiments, and to the identification and/or development of stabilization additives for encapsulation materials. Two items of significance were presented: (1) preliminary experimental testing is supporting the combination of a UV absorber and HALS as an effective stabilization system, as theoretically derived at the University of Toronto, and (2) the significant usefulness of the outdoor heating racks (called OPTs in the Springborn presentation) as an accelerated weathering technique.

J. Koenig of Case Western Reserve University reported on EVA-Glass Interface Bond Stability. Koenig and Boerio (see below) have developed the technology to investigate a chemically bonded interface for direct acquisition of chemical information on both bonding and aging mechanisms. The technology is based on Fourier transform infrared techniques (FTIR). Koenig presented FTIR spectra of the bonded interface between EVA and glass, which had been hydrolytically aged for at least one week in 80°C water. The early results indicate strong possibilities for a long-term weather-stable interfacial bond. The EVA-glass primer system is the one developed by Dow Corning Corp. for FSA, of which experimental quantities can be obtained from Springborn Laboratories under the designation A-11861.

J. Boerio of the University of Cincinnati reported on Interface Bonding Stability. Boerio's efforts are identical with those of Koenig, except that the emphasis of his study is on polymers and metals, such as EVA and aluminum. These interfacial chemistries can be quite distinct from those between EVA and glass, for example. Recently Dow Corning observed that EVA bonds strongly to aluminized back surfaces of solar cells, when using the standard A-11861 EVA-glass primer system. Ordinarily EVA bonds weakly to aluminum foil or sheet stock, using the same primer, and therefore this observation with the solar cells was not expected. Boerio described his examination of the aluminized back surface using SEM and EDS, and reported his initial findings that the back surface appears to be a mixture of aluminum and silicon. If it can be assumed that the silicon may be present as an oxide or hydroxide, then perhaps the back surface has glass-like chemistry, which would help to explain the Dow Corning observation. If true, the self-priming EVA being developed jointly by Dow Corning and Springborn for glass would also work with solar cells. More work in this area is planned.

G.R. Mon of JPL reported on Topics in Electrochemical Degradation of Photovoltaic Modules. Various topics related to the potential for electrochemical degradation of photovoltaic modules during 30 years of service in the natural outdoor weathering environment were presented. These included (1) the relationship between leakage current and electrochemical degradation, with emphasis on the efforts of positive and negative polarity, and the dependency of temperature and humidity; (2) a discussion of leakage current response mechanisms, and (3) considerations related to laboratory simulation of outdoor behavior to derive acceleration factors for module life prediction, and module qualification tests related to electrochemical susceptibility.

J. Orehotsky of Wilkes College reported on Polymer-Water Interaction Studies. Electrochemical susceptibility requires absorption of water by the encapsulation pottants, such as EVA and PVB. A new contract activity has been initiated at Wilkes College to determine experimentally the magnitudes and

rates of the absorption and desorption of atmospheric water vapor by pottant materials. This study includes the dependency on magnitude and change rate of temperature and relative humidity. The discussion included the background for the experimental studies, details of the experimental techniques, and preliminary experimental data related to (1) water absorption and desorption kinetics in EVA and PVB, (2) humidity dependence of electrical properties of EVA and PVB, and (3) influence of plasticizer in PVB on water absorption and electrical properties.

PHOTOTHERMAL DEGRADATION STUDIES OF ENCAPSULANTS

JET PROPULSION LABORATORY

Ranty H. Liang

Objectives

- DEVELOP TECHNOLOGY BASE FOR MATERIALS WITH 30 years LIFE WITH RESPECT TO PHOTOTHERMAL DEGRADATION

    - DEVELOP VALID ACCELERATED PHOTOTHERMAL TESTING PROCEDURES FOR EVALUATION OF ENCAPSULANTS

    - DEVELOP DATA BASE OF PHOTOTHERMAL REACTION RATES WITH RESPECT TO PHOTOTHERMAL STRESSES

    - DEVELOP MODEL TO PREDICT LIFE TIME OF ENCAPSULANTS WITH RESPECT TO PHOTOTHERMAL DEGRADATION

    - DEVELOP NECESSARY STABILIZERS TO ACHIEVE 30 years LIFE

Approach

- PARAMETRIC PERFORMANCE CHARACTERIZATION OF MATERIALS WITH RESPECT TO PHOTOTHERMAL STRESSES

C. GONZALEZ
- MARCO - PERFORMANCE MODELLING

- MECHANISTIC STUDIES OF PHOTOTHERMAL DEGRADATION AT MOLECULAR LEVEL

U. OF TORONTO
- MICROMOLECULAR KINETIC MODELLING

BROOKLYN TECH
- SYNTHESIS OF STABILIZERS BASED ON MOLECULAR UNDERSTANDING OF DEGRADATION MECHANISMS

Mechanistic Studies of Photothermal Degradation

- OBJECTIVES

    - TO STUDY MECHANISTIC PATHWAYS OF PHOTOTHERMAL DEGRADATION

    - TO DETERMINE PHOTOTHERMAL REACTION RATES FOR MICROMOLECULAR KINETIC MODELLING

- APPROACH

    - LASER – FLASH ESR SPECTROSCOPY TO DETERMINE KEY REACTION INTERMEDIATES AND THEIR KINETICS

ESR Spectrum of Photogenerated Carbon Radical in Vacuum at Room Temperature

20 G
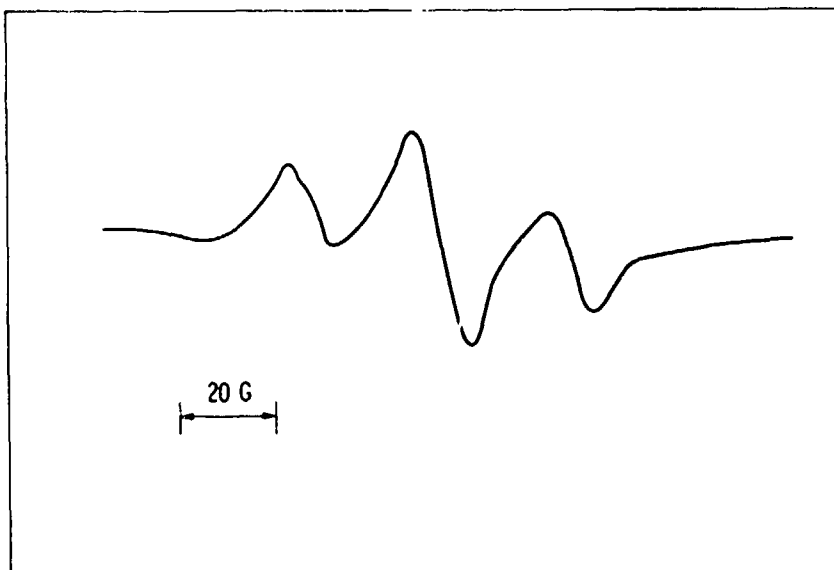
Time Profile of Tertiary Carbon Radical
at Room Temperature
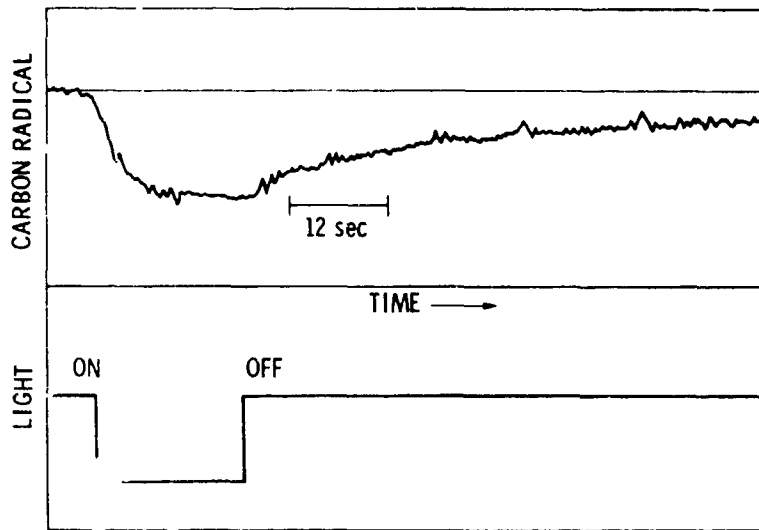
ESR Spectra of Photogenerated Radicals
in Air at Room Temperature
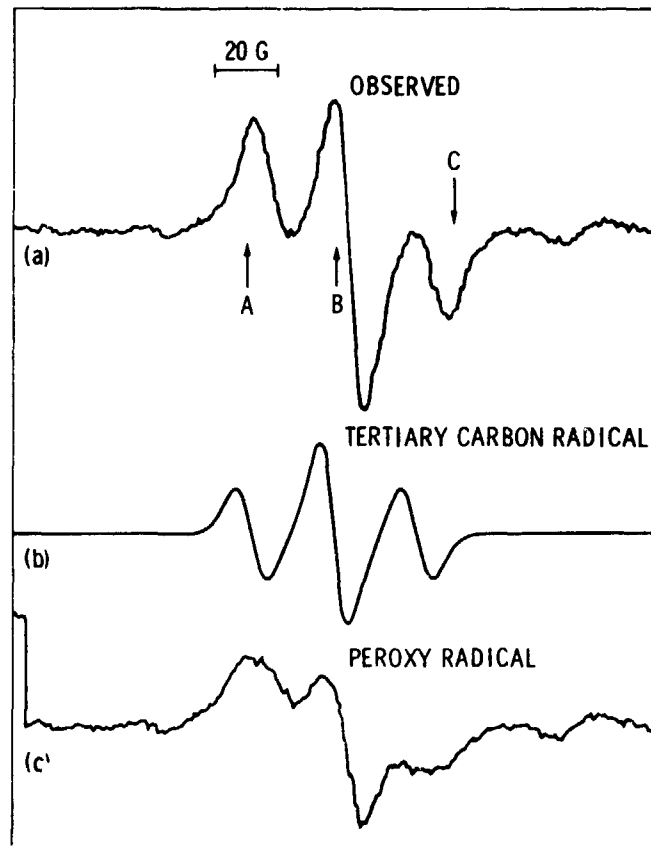
Kinetic Studies of Photogenerated Tertiary Carbon Radicals as a Function of Oxygen Concentration

$[O_2]$ CONCENTRATION
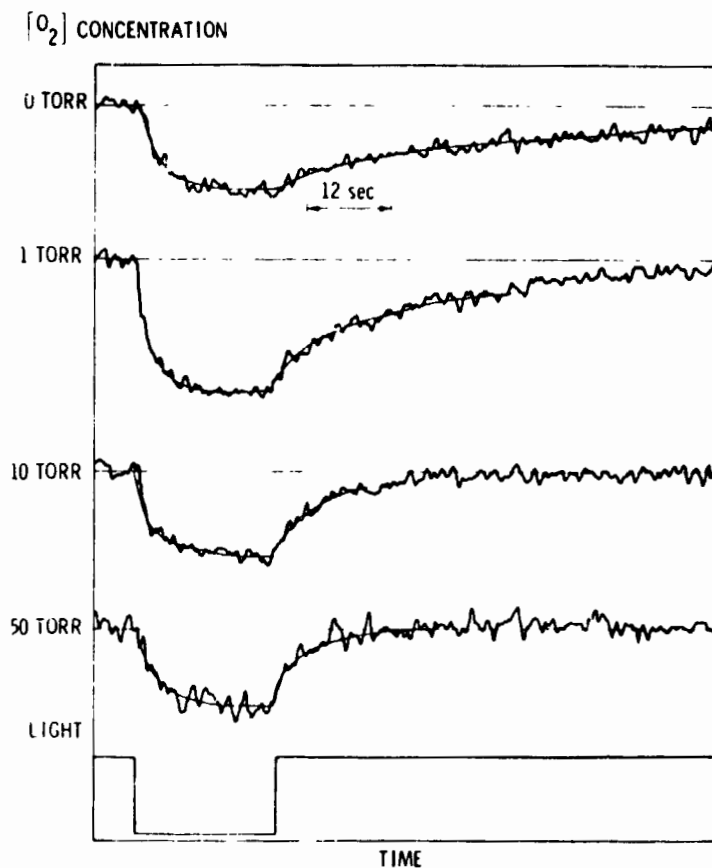
Mechanism of Photooxidation

$$R - R \xrightarrow{\ h\nu\ } R\cdot$$

$$R\cdot + R\cdot \xrightarrow{\ k_1\ } R - R \qquad \text{CROSSLINKING}$$

$$R + O_2 \xrightarrow{\ k_2\ } RO_2\cdot \qquad \text{OXIDATION}$$

$$RO_2\cdot + RH \xrightarrow{\ k_3\ } R\cdot$$
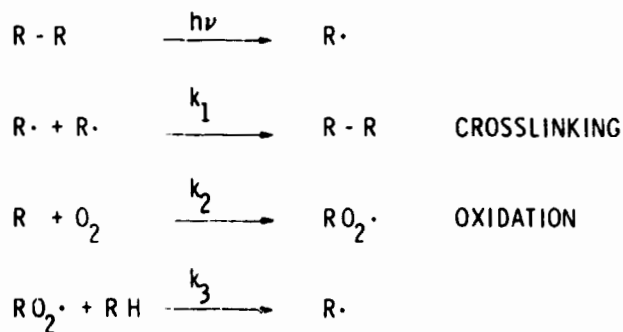
PRELIMINARY RESULTS

$k_1 = 10^{-2}$ liter/mole sec

$k_2 = 1.3 \times 10^{-2}$/sec

$k_3 = 10^{-1}$/sec

Conclusions

- IDENTIFIED KEY REACTION INTERMEDIATES

- DETERMINED RATES OF KEY DEGRADATION REACTIONS

- THERMAL EFFECTS ON PHOTOOXIDATION ARE BEING EVALUATED

Performance Characteristics of Materials With Respect to Photothermal Stresses

- OBJECTIVE

  - IDENTIFY PERFORMANCE CRITERIA

  - GENERATE DATA BASE FOR MACRO PERFORMANCE MODELLING

- APPROACH

  - PHOTOTHERMAL AGING OF MATERIAL SPECIMENS

    - UV   0 SUN, 2 SUNS, 6 SUNS

    - TEMPERATURE   50°C, 70°C, 85°C, 105°C
      120°C, 135°C

    - PARAMETERS MONITORED   TRANSMITTANCE, WEIGHT
      LOSS, TENSILE MODULUS

Transmittance Spectra of Sunadex/EVA/Pyrex
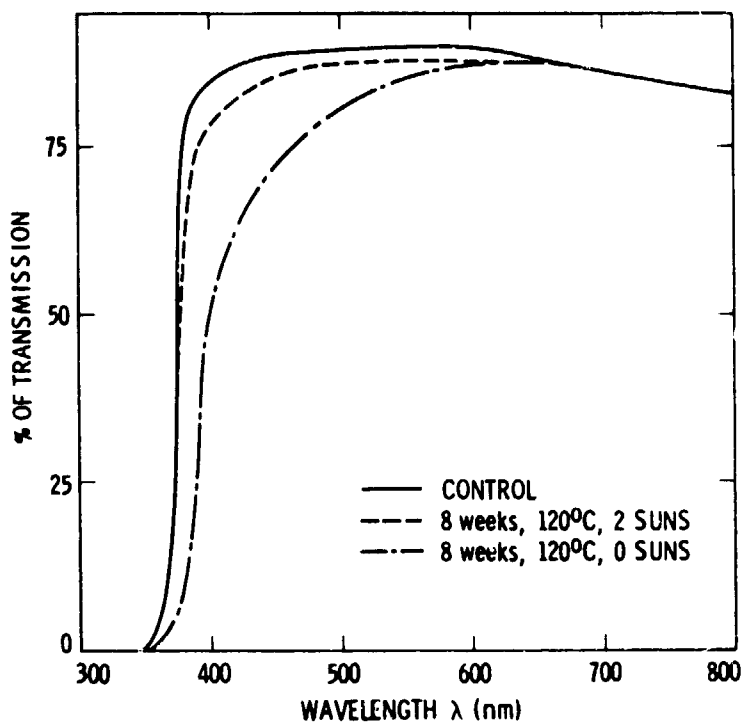
Mechanisms of Photothermally Induced Yellowing

- THERMAL INDUCED YELLOWING

- PHOTO INDUCED YELLOWING

- PHOTO INDUCED BLEACHING

Photothermally Induced Yellowing of EVA

$$K(T) = k_\Delta(T) + k_{h\nu}(T) - k'_{h\nu}(T)$$

WHERE

K · RATE OF OVERALL YELLOWING

k_Δ · RATE OF THERMAL INDUCED YELLOWING

$k_{h\nu}$ · RATE OF PHOTO INDUCED YELLOWING

$k'_{h\nu}$ · RATE OF PHOTO INDUCED BLEACHING

T · TEMPERATURE

i) IF $k'_{h\nu} = k_{h\nu}$

RATE OF YELLOWING IN DARK OVEN · RATE OF YELLOWING IN CER

ii) IF $k'_{h\nu} < k_{h\nu}$

RATE OF YELLOWING IN DARK OVEN > RATE OF YELLOWING IN CER

iii) IF $k'_{h\nu} > k_{h\nu}$

RATE OF YELLOWING IN DARK OVEN < RATE OF YELLOWING IN CER

Evaluation of k_Δ, $k_{h\nu}$, $k_{h\nu}$

- THERMALLY AGED VIRGIN SAMPLE IN DARK OVEN AT 120°C TO GENERATE YELLOWING

- THE YELLOW SAMPLE IS THEN PHOTOTHERMALLY AGED IN CER AT 6 SUNS AND 50°C TO EVALUATE THE BLEACHING RATE $k_{h\nu'}(50°)$

$$K(50°C) = k_\Delta(50°C) + k_{h\nu}(50°C) - k'_{h\nu}(50°C)$$

SINCE

$$k_\Delta(50°C) \text{ AND } k_{h\nu}(50°C) \text{ ARE SMALL}$$

THEREFORE

$$K(50°C) \approx -k'_{h\nu}(50°C)$$

SUNADEX / EVA / PYREX
DARK THERMAL AGING
AT 120°C, 0 SUN

SUNADEX / EVA / PYREX
PHOTOTHERMAL AGING
AT 50°C, 6 SUNS

T/T$_0$ AT 440 nm (%)

AGING TIME (weeks)

ABSORBANCE AT 440 nm DUE TO YELLOWING (x 10^2)

SUNADEX / EVA / PYREX
DARK THERMAL AGING
AT 120°C, 0 SUN

SUNADEX / EVA / PYREX
PHOTOTHERMAL AGING
AT 50°C, 6 SUNS

k_Δ

AGING TIME (weeks)
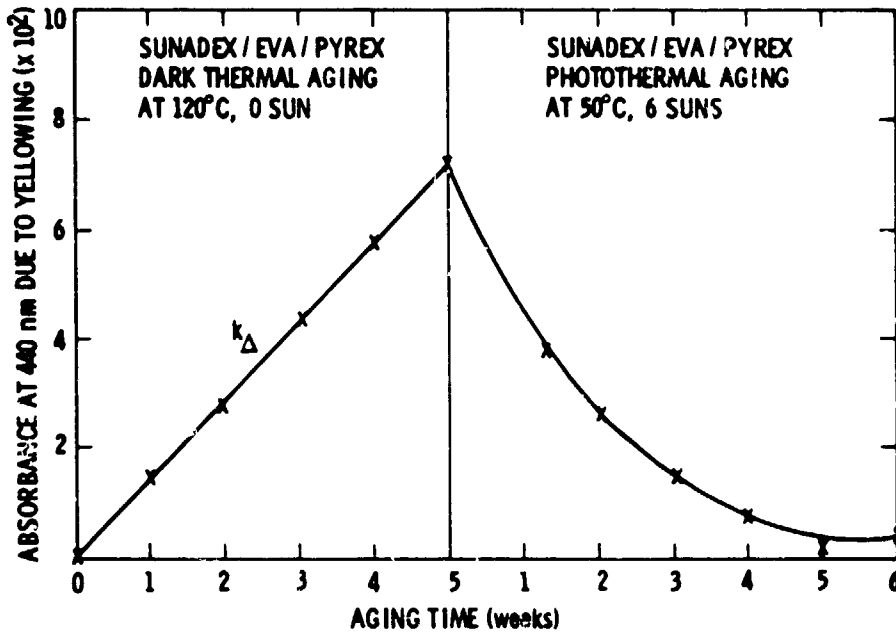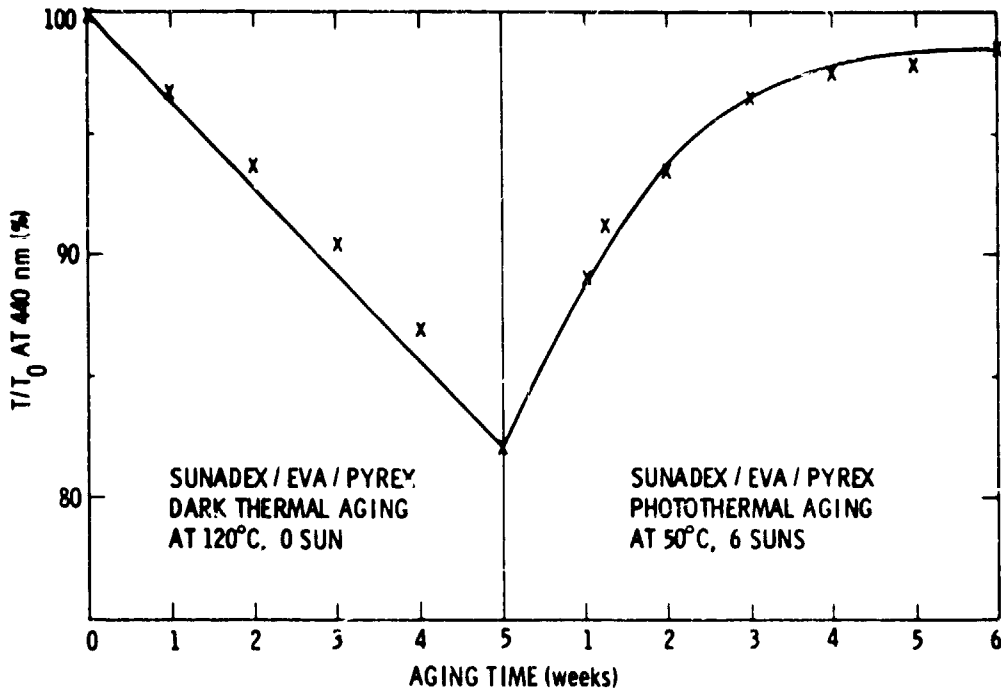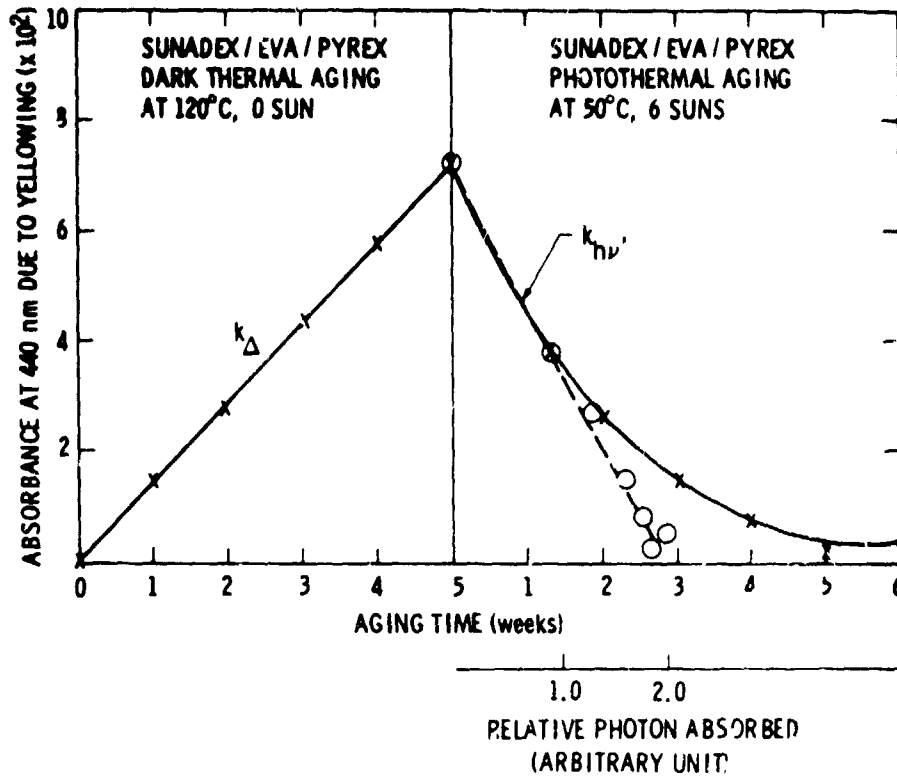
Conclusions

- IDENTIFY MECHANISMS OF PHOTOTHERMAL YELLOWING

- DEVELOP TECHNIQUES TO MONITOR DIFFERENT MODES OF YELLOWING

- STUDIES OF TEMPERATURE EFFECT ON RATES OF YELLOWING AND BLEACHING ARE BEING INITIATED

PREDICTING PHOTOTHERMAL FiELD PERFORMANCE

JET PROPULSION LABORATORY

C.C. Gonzalez

R.G. Ross, Jr.

Objective and Approach

- Extrapolate photothermal accelerated test data to simulate 30-year field exposure

    - Develop an analytical model incorporating the measured dependency between transmittance loss and UV and temperature exposure levels

    - Exercise the model using SOLMET weather data extrapolated to 30 years for various sites and module-mounting configurations

Analytical Model Assumptions and Characteristics

- Encapsulant optical transmittance can be expressed as a function of the concentration of a given reactive species, Q

- Rate of variation of concentration, Q/t, is a reaction rate

- Standard reaction-rate equations, Arrhenius and power-law relationships are used to relate Q/t to the stress levels

- Two competing reactions occur simultaneously, one causing the increase of yellowing and one bleaching out the yellowing
    - Principle of superposition is assumed; order in which environmental levels occur not important

- Arbitrary constants a_1 to a_{10} determined by least-squares fitting of experimental optical transmittance (as a function of temperature and UV) versus time data

Ana' ical Model

- Two equations developed:

$$\tau/\tau_O = 1 + a_1Q + a_2Q^2 + a_3Q^3$$

$$Q/t = e^{(a_4/T)} + a_5e^{(a_6/T)} S^{a_7} - a_8e^{(a_9T)} S^{a_{10}}$$

Where:

τ = transmittance at 440 nm
τ_O = initial transmittance at 440 nm
Q = concentration
a_i = constant
t = time
T = temperature in °K
S = UV level in suns

Reaction Rate (Q/Time) vs UV Level
As a Function of Temperature (EVA)
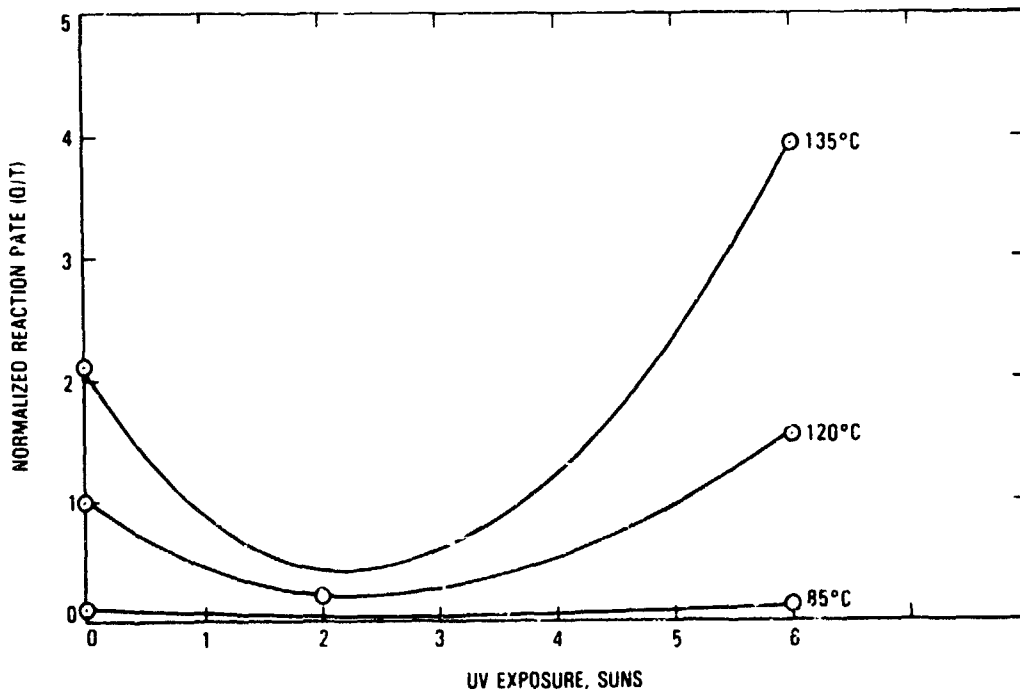
Transmittance Loss vs Concentration, Q (EVA)

The x-axis is labeled CONCENTRATION (Q) ranging from 0 to 0.80, and the y-axis is labeled RATIO OF TRANSMITTANCE TO INITIAL TRANSMITTANCE (τ/τ_0) ranging from 0 to 1.00.
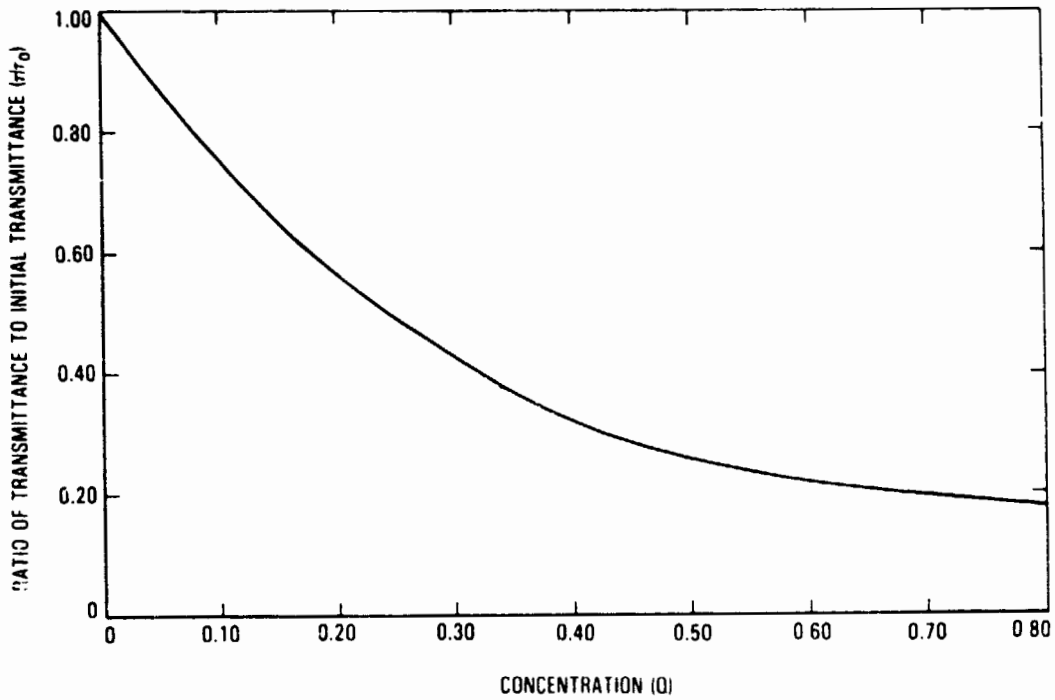
Transmittance Loss vs Time (EVA)

TEMPERATURE - 135°C

The x-axis is labeled TIME, HOURS ranging from 0 to 1600, and the y-axis is labeled RATIO OF TRANSMITTANCE TO INITIAL TRANSMITTANCE (τ/τ_0) ranging from 0 to 1.00. Curves are labeled UV, SUNS: 2, 1, 0, 6.
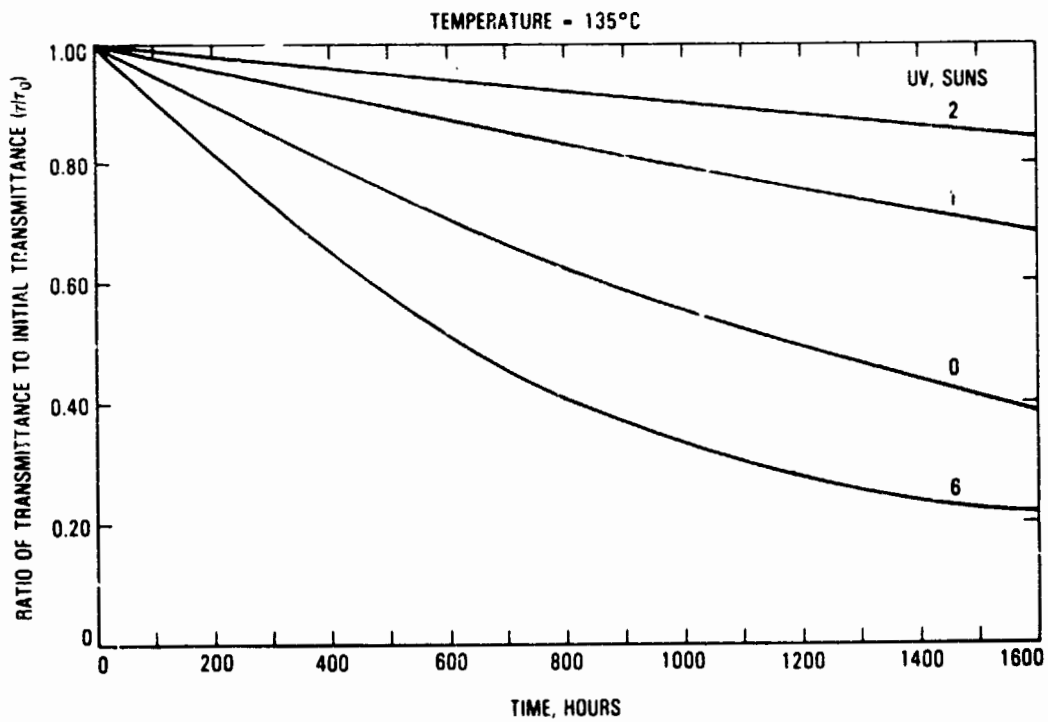
Arrhenius Plot of Reaction Rate (Q/Time) vs Temperature (EVA)
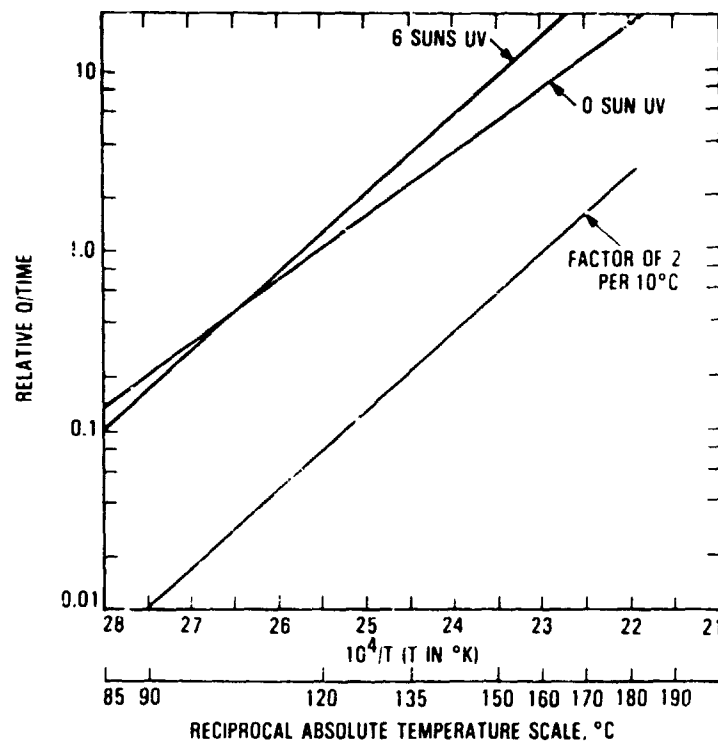
Derivation of Photovoltaic Degradation
From 440-m Transmittance Loss

- 440-nm transmittance loss defines unique spectral transmittance curve for encapsulant

- Photovoltaic response requires convolution of encapsulant transmittance curve, cell spectral response curve, and solar distribution curve (global spectrum)

- Two-cell spectral response models used, one for crystalline silicon and one for amorphous silicon cells

124

30-Year Transmittance, %, vs Wavelength for EVA
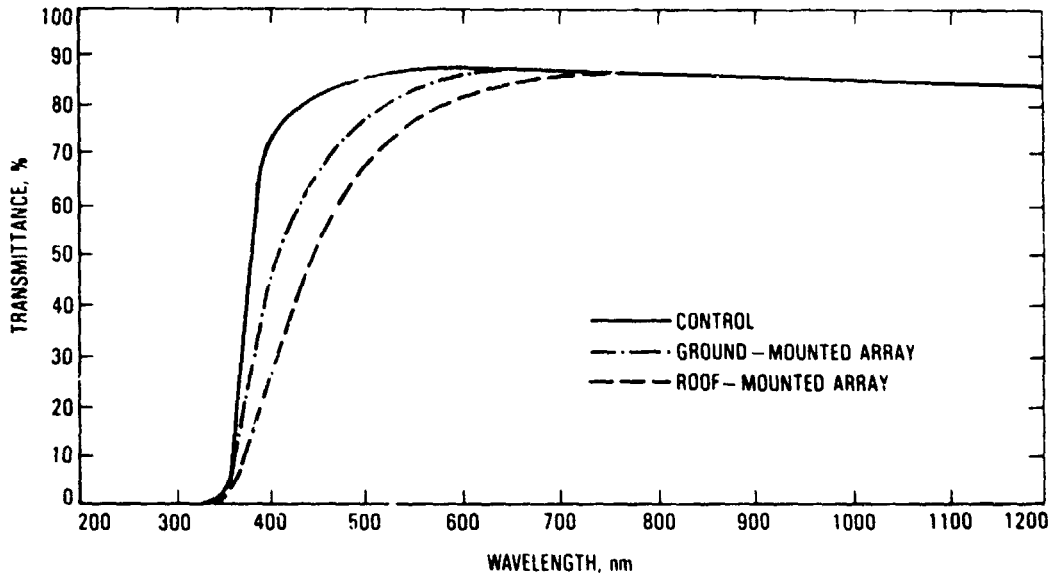
Spectral Response Curves of Crystalline and Amorphous Silicon Cells
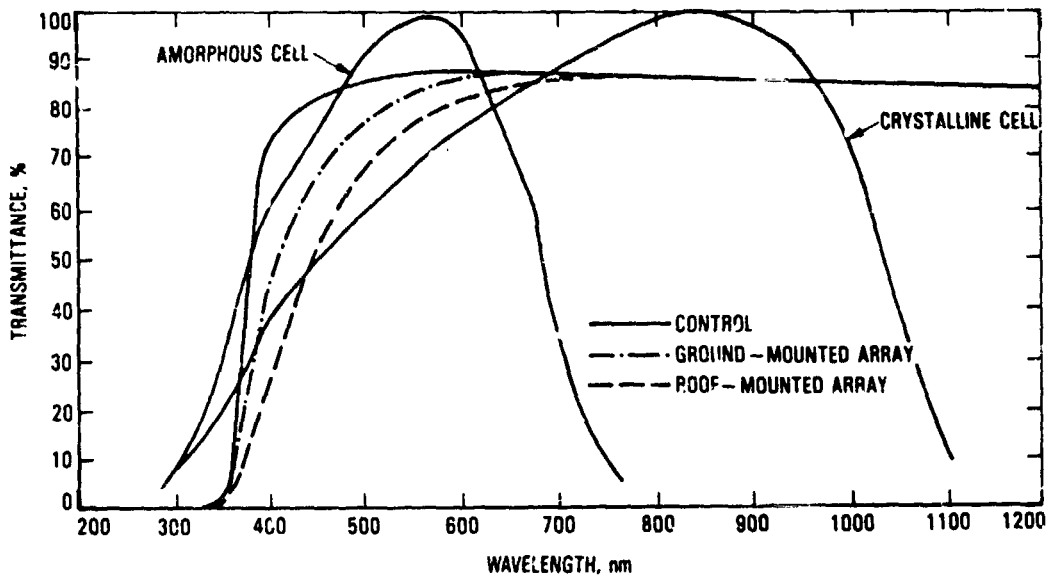
Determining 30-Year Degradation Using Photothermal Degradation Simulation Model

- Calculate 30-year field exposure environment using hourly SOLMET weather data tapes

  - Encapsulant operating temperatures computed as a function of irradiance level on tilted surface and ambient air temperature

  - UV level computed as a fixed 5% of the solar irradiance level

  - Results presented as matrix of annual number of exposure hours at each combination of temperature and UV level

- Simulate 30-year photothermal degradation using simulation model and environmental stress matrix

  - Matrix of reaction rates, Q/t, determined for temperature and UV levels in exposure-hours matrix

  - The product is taken of the two matrices

  - The sum of the values in each element of the last matrix yields the concentration Q at the end of a year

  - 30-year concentration is 30 times annual value

Annual Hours of Exposure of a Ground-Mounted Array to Various Cell Temperatures and UV Levels (Phoenix)

Cell temper-ature, °C	Annual hours of exposure											
	UV level in suns											
	0.05	0.15	0.25	0.35	0.45	0.55	0.65	0.75	0.85	0.95	1.05	1.15
75	0	0	0	0	0	0	0	0	0	11	4	0
65	0	0	0	0	0	1	17	24	107	294	167	6
55	0	0	0	32	18	56	130	81	201	142	177	17
45	22	74	32	110	62	84	144	73	172	154	55	1
35	134	131	63	124	97	93	113	49	53	17	0	0
25	190	129	92	86	53	21	22	0	0	0	0	0
15	129	94	36	35	8	0	0	0	0	0	0	0
5	55	20	3	0	0	0	0	0	0	0	0	0

Relative Values of Reaction Rates (Q/Time) for Various Cell Temperatures and UV Levels

Cell temper-ature, °C	Relative values of reaction rates, Q/time											
	UV level in suns											
	0.05	0.15	0.25	0.35	0.45	0.55	0.65	0.75	0.85	0.95	1.05	1.15
75	65	61	58	55	52	49	46	44	41	39	37	35
65	33	31	29	28	26	25	24	23	21	20	19	18
55	16	15	14	13	13	12	12	11	11	10	10	9
45	7	7	7	6	6	6	6	5	5	5	5	4
35	3	3	3	3	3	3	2	2	2	2	2	2
25	1	1	1	1	1	1	1	1	1	0.9	0.9	0.9
15	0.5	0.5	0.5	0.5	0.4	0.4	0.4	0.4	0.4	0.4	0.4	0.4
5	0.2	0.2	0.2	0.2	0.2	0.2	0.2	0.1	0.1	0.1	0.1	0.1

Photovoltaic Power Loss After 30 Years in Phoenix* (EVA)

Cell type	Ground-mounted array	Roof-mounted array
Crystalline cell	3.5%	7.9%
Amorphous cell**	8.1%	17.8%

30-year allocation for this degradation mode is 6%

*Based on assumed UV acceleration factor distribution near one sun

**Only when EVA is between module front surface and cells

Conclusions

- Temperature is key driver to photothermally induced transmittance loss (approximate doubling of rate per 10°C)

- Sensitivity of transmittance loss to UV level is highly nonlinear with minimum in curve near one sun

- EVA results consistent with 30-year life allocation

Future Work

- Refine analytical model using additional data taken in region of one sun

- Repeat the thermal-UV exposure tests with the addition of humidity to study the impact of this variable

- Investigate the use of techniques similar to those discussed here for determining the photothermal degradation of encapsulant mechanical properties over 30-year life

MICROMOLECULAR MODELING

UNIVERSITY OF TORONTO

James Guillet

- DEVELOP A REACTION KINETICS BASED MODEL OF THE PHOTODEGRADATION PROCESS EXPERIENCED BY ENCAPSULANTS

- DEVELOP A COMPUTER CAPABILITY TO UTILIZE THE REACTION KINETICS MODEL FOR PREDICTIVE PURPOSES

Goal

DEVELOP A REACTION KINETICS BASED MODEL OF
THE PHOTODEGRADATION PROCESS EXPERIENCED
BY ENCAPSULANTS, MEASURE ALL IMPORTANT
RATE CONSTANTS, DEVELOP A COMPUTERIZED ~~PREDICTING~~
MODEL CAPABLE OF PREDICTION OF PHOTODEGRADATION
RATE AND FAILURE MODES ASSOCIATED WITH IT
OVER A THIRTY YEAR PERIOD, AND VALIDATE THE
MODEL

FY84-85 Objectives

- EXTEND THE COMPUTERIZED DEGRADATION
  MODEL DEVELOPED FOR POLYETHYLENE
  TO EVA AND EVA (A-9918)

- EVALUATE THE EFFECT OF STABILIZERS ON
  PHOTODEGRADATION RATE

- PROVIDE GUIDELINES FOR SELECTION OF MOST
  EFFECTIVE CLASSES OF UV ~~ABSO~~ STABILIZER

- INITIATE ~~THE~~ STUDY OF THE EFFECT OF
  TEMPERATURE VARIATION ON THE MODEL

Accomplishments

- THE COMPUTERIZED PHOTODEGRADATION MODEL FOR POLYETHYLENE IS SHOWN TO CORRECTLY PREDICT FAILURE (EMBRITTLEMENT) OF ELVAX 150 ON OUTDOOR EXPOSURE, AND CROSS LINKED ELVAX 150 ON OUTDOOR EXPOSURE

- OUTDOOR EXPOSURE AND ACCELEROMETER TESTS INDICATE THAT CROSS-LINKING EVA DOES NOT SIGNIFICENTLY CHANGE ITS DEGRADATION RATE

- PARALLEL TESTS ON STABILIZED POLYTHYLENE AND EVA (A 9918) SHOW THAT THE EFFECT OF THE STABILIZER PACKAGE IS APPROXIMATELY EQUIVALENT ON BOTH POLYMERS — IC THE PE MODEL CAN BE USED FOR A-9918 WITH MINOR CHANGES, AND STABILIZER CONSUMPTION RATE IS A USEFUL DIAGNOSTIC MEASURE FOR EARLY PHOTODEGRADATION

- COMPUTERIZED MODEL INDICATES THAT PEROXIDE (HYDROPEROXIDE) DECOMPOSERS AND UV ABSORBERS ARE MOST EFFECTIVE STABILIZERS — BETTER THAN ANTIOXIDANTS

- EFFECT OF TEMPERATURE CYCLING IS BEING INVESTIGA...

Elementary Reactions in Polymer Photooxidation and Corresponding Rates

Reaction	Rate constant
$RO_2 + RH \longrightarrow ROOH + RO_2$	0.1×10^{-2}
$RO_2 + RO_2 \longrightarrow ROH + Ketone + SO_2$	0.1×10^{2}
$RO_2 + ROH \longrightarrow ROOH + \ldots tone + HOO$	0.5×10^{-1}
$HOO + RH \longrightarrow HOOH + RO_2$	0.5×10^{-2}
$HOO + RO_2 \longrightarrow ROOH + SO_2$	0.1×10^{8}
$RO_2 + Ketone \longrightarrow ROOH + PeroxyCO$	0.5×10^{-2}
$RO_2 + ROOH \longrightarrow ROOH + Ketone + OH$	0.5×10^{-1}
$RO_2 + SMROH \longrightarrow ROOH + Aldehyde + HOO$	0.5×10^{-2}
$RO_2 + Aldehyde \longrightarrow ROOH + SMRCO$	0.1×10^{3}
$OH + RH \longrightarrow RO_2 + Water$	0.3×10^{9}
$Ketone \longrightarrow KET^{*}$	0.3×10^{-5}
$SMKetone \longrightarrow KET^{*}$	0.3×10^{-5}
$KET^{*} \longrightarrow SMRO_2 + SMRCO$	0.5×10^{7}
$SMRCO \longrightarrow SMRO_2 + CO$	0.5×10^{6}
$KET^{*} \longrightarrow Alkene + SMKetone$	0.5×10^{8}
$KET^{*} + O_2 \longrightarrow Ketone + SO_2$	0.1×10^{8}
$KET^{*} + ROOH \longrightarrow Ketone + RO + OH$	0.1×10^{2}
$KET^{*} \longrightarrow Ketone$	0.1×10^{10}
$SO_2 \longrightarrow O_2$	0.6×10
$SO_2 + Alkene \longrightarrow ROOH$	0.1×10^{4}
$SMRO_2 + RH \longrightarrow SMROOH + RO_2$	0.1×10^{-3}
$SMROOH \longrightarrow SMRO + OH$	0.3×10^{-4}
$SMRO + RH \longrightarrow SMROH$	0.1×10^{6}
$SMRCO + O_2 \longrightarrow SMRCOOO$	0.1×10^{2}
$SMRCOOO + RH \longrightarrow SMRCOOOH + RO_2$	0.1×10^{-1}
$SMRCOOOH \longrightarrow SMRCO_2 + OH$	0.1×10^{-3}
$ROOH \longrightarrow RO + OH$	0.3×10^{-4}
$RO \longrightarrow SMRO_2 + Aldehyde$	0.1×10^{6}
$RO + RH \longrightarrow RO_2 + ROH$	0.1×10^{6}
$SMRCO_2 + RH \longrightarrow Acid + RO_2$	0.1×10^{6}
$RO_2 + RO_2 \longrightarrow ROOR$	0.1×10^{-6}

Effect of Termination Rate on Product Formation During Photooxidation
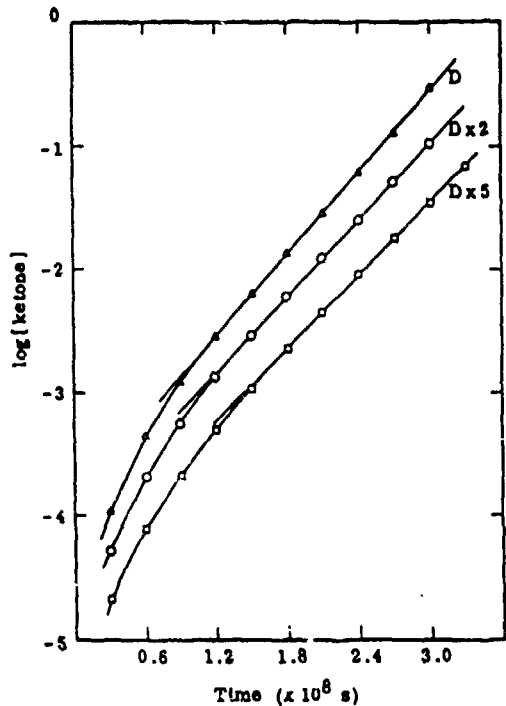
Stabilization of PE

$$ROOH + QD \xrightarrow{10^6} Products$$

$$KET^* + Q1 \xrightarrow{10^6} Ketone + Heat$$
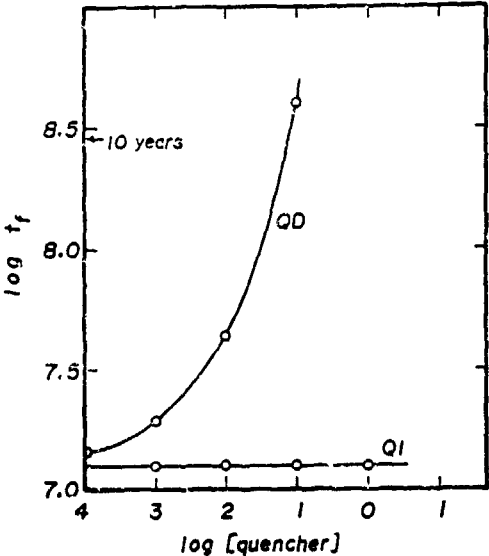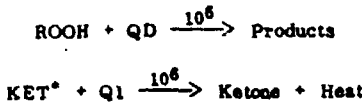
Effect of Intensity on Product Formation During Photooxidation
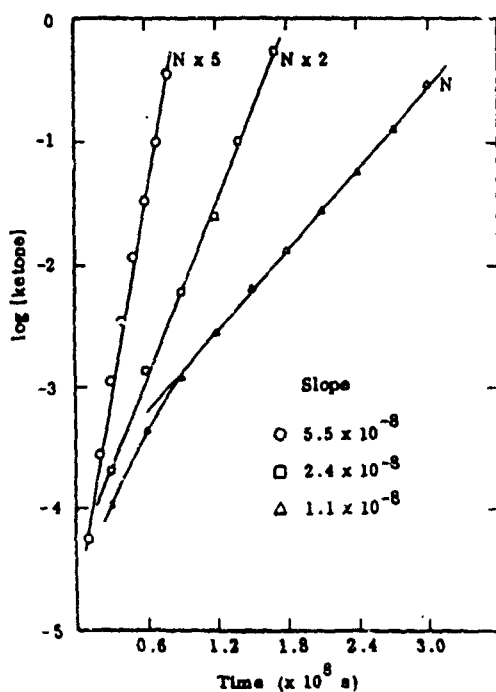
Photooxidation as a Function of Intensity of Light
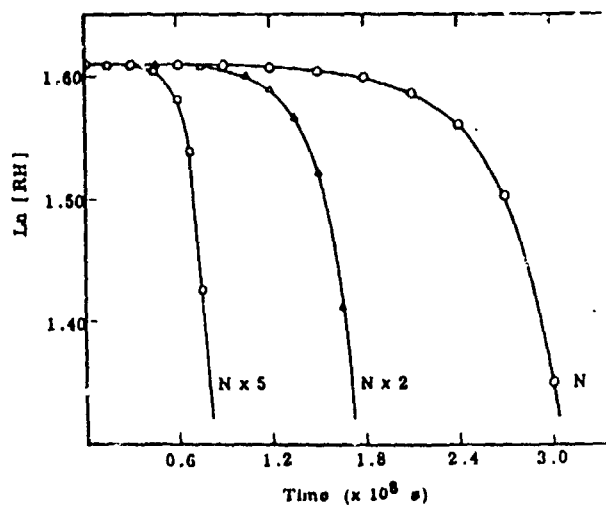
Equivalent Solar Exposure (Summer Days) vs Actual Accelerated Ager Exposure Time
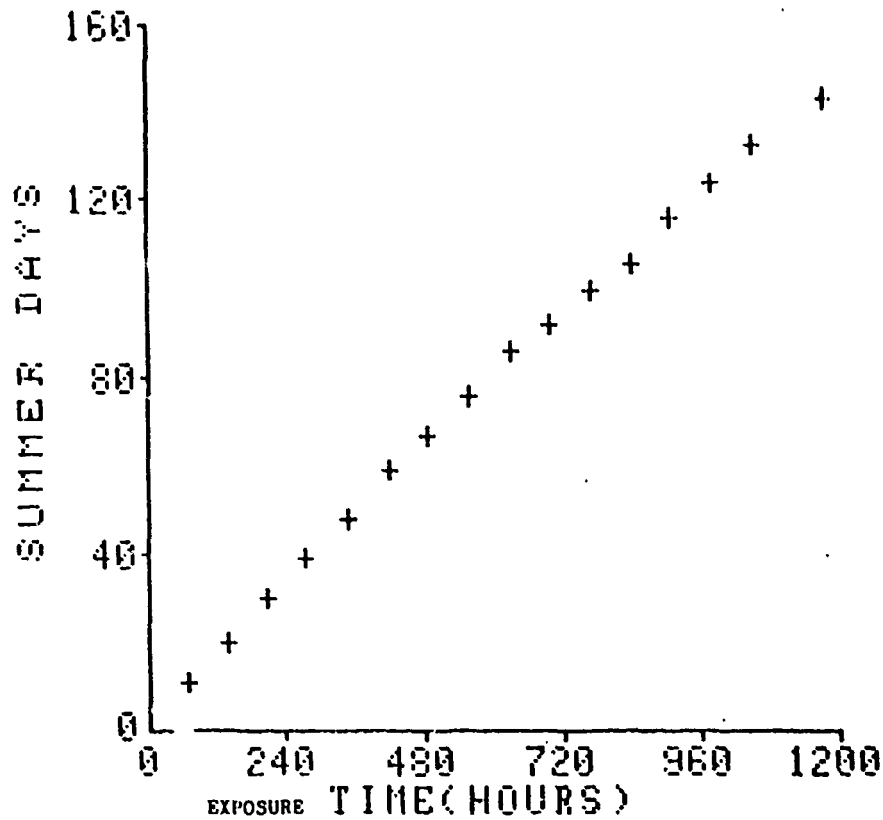
Key Finding

THE COMPUTERIZED MODEL INDICATES THAT A COMBINATION OF A UV ABSORBER AND A HINDERED AMINE LIGHT STABILIZER (HALS) IS THE MOST EFFECTIVE STABILIZER SYSTEM

POLYMERIZABLE ULTRAVIOLET STABILIZERS

POLYTECHNIC INSTITUTE OF NEW YORK

P. Gomez
S.K. Fu
O. Vogl

Objectives

A: SYNTHESIS OF POLYMERIZABLE UV MONOMERS
   (BENZOTRIAZOLES)

- VINYL AND ISOPROPENYL DERIVATIVES OF
  DIBENZOTRIAZOLE SUBSTITUTED RESORCINOL
  AND PHLOROGLUCINOL.

- MONO- AND DIMETHOXY AND HYDROXYBENZOTRIA-
  -ZOLE DERIVATIVES OF RESORCINOL AND
  PHLOROGLUCINOL.

- CARBOXY, CARBOMETHOXY AND ACETOXY
  SUBSTITUTED DERIVATIVES OF RESORCINOL.

B: INCORPORATION OF POLYMERIZABLE UV
   STABILIZERS (BENZOTRIAZOLES) INTO POLYMERS.

- ADDITION POLYMERS — STYRENES, ACRYLICS

- CONDENSATION POLYMERS — POLYESTERS,
                          POLYCARBONATES,
                          POLYURETHANES,
                          POLYAMIDES
                          EPOXIES.

$R = CH_3$, H

$R' = C_6H_5$, $COOCH_3$, $COOC_4H_9$

138

$R = H$, $R = CH_3$

HBr, DMF, 130°C

λmax 337 nm

λmax 341 nm.

-O-Bzt

1%
3%

-O-Bzt   Bzt-O-

1%
3%
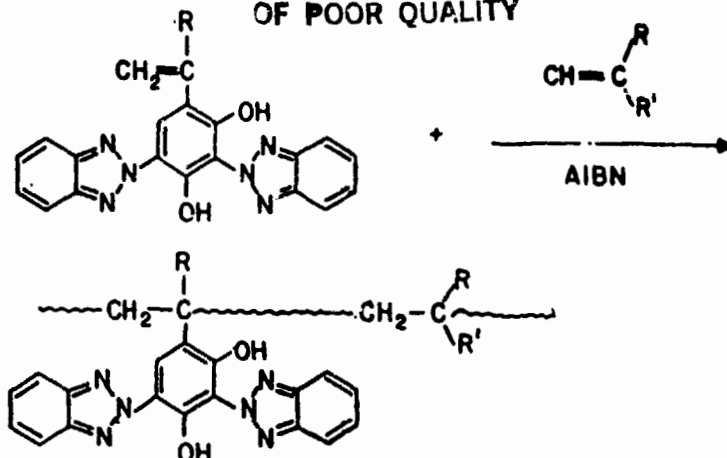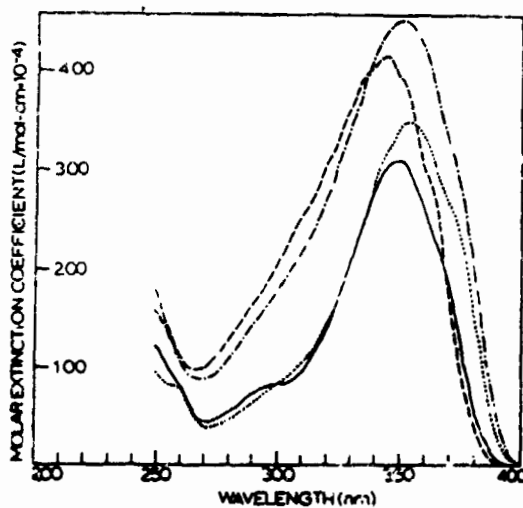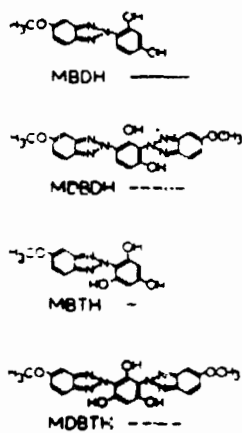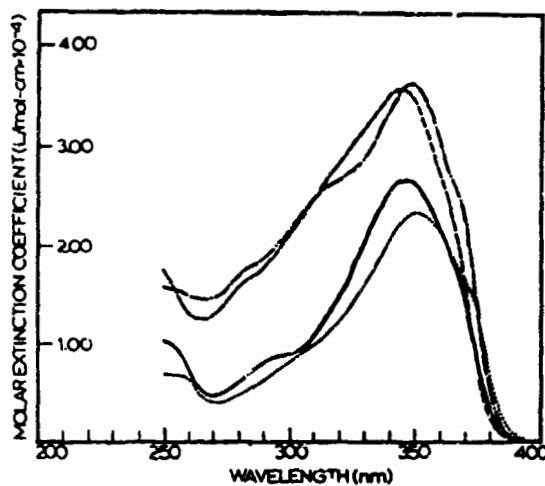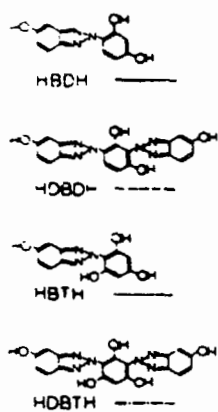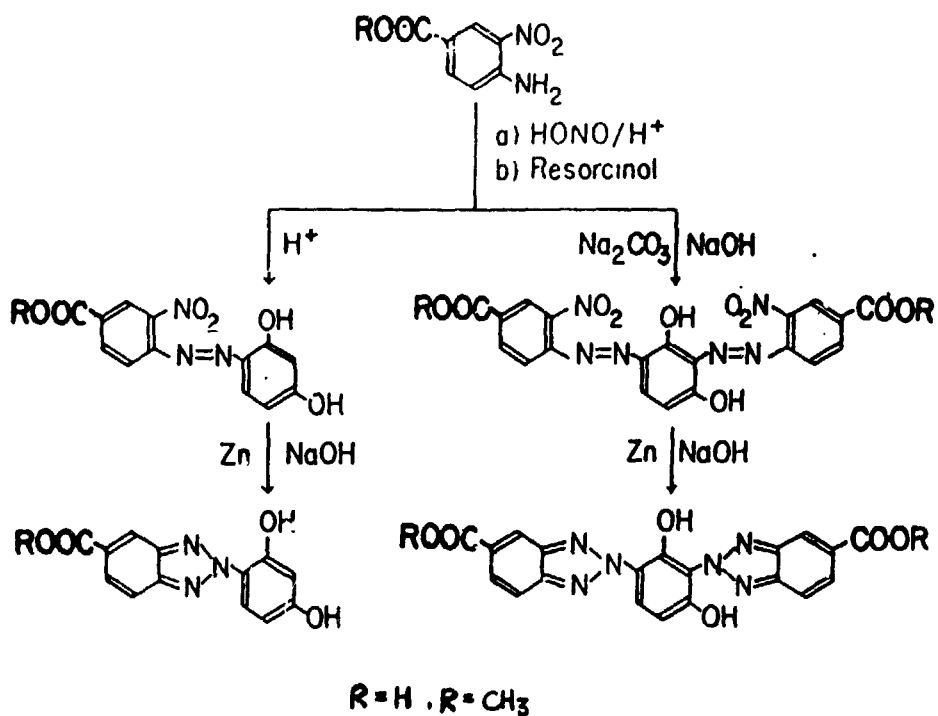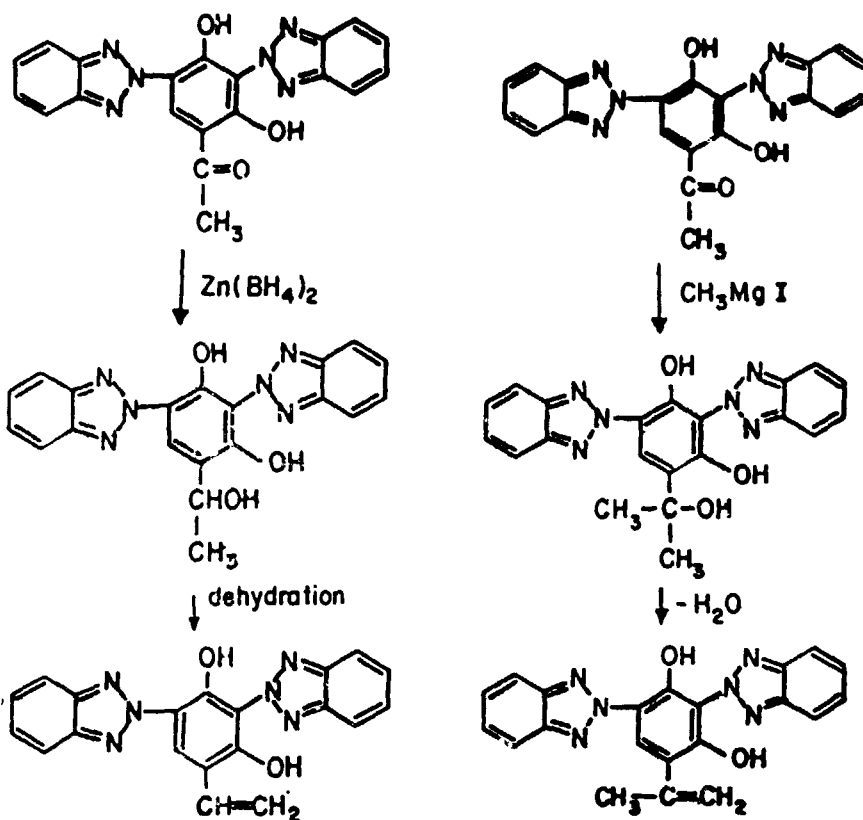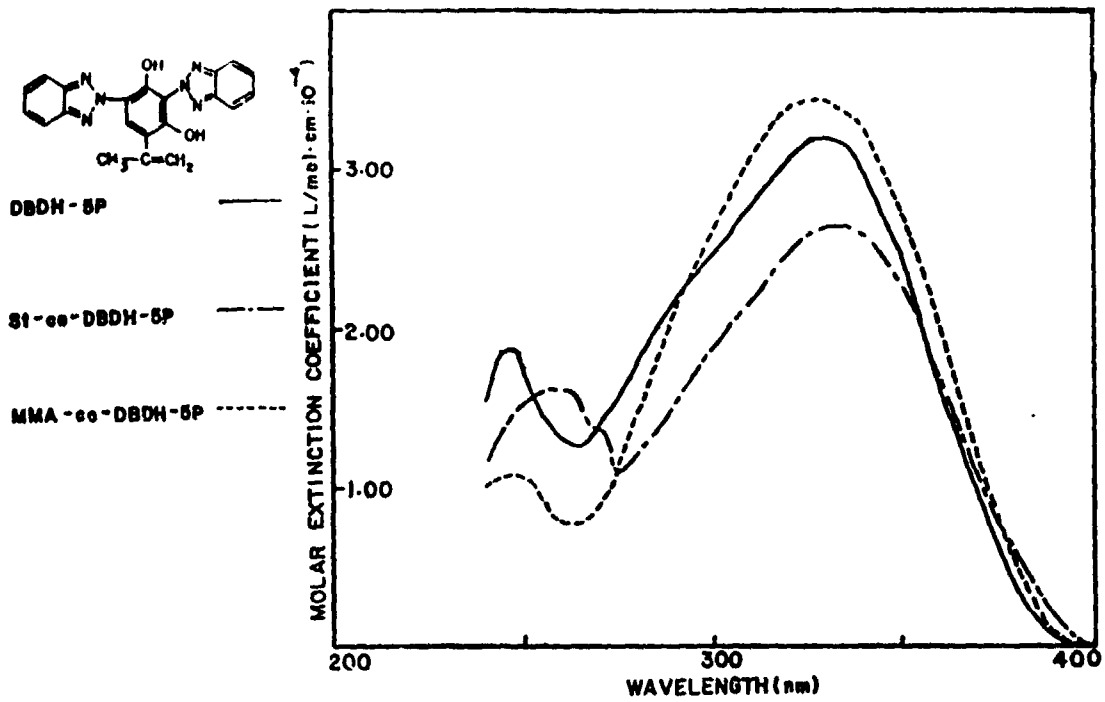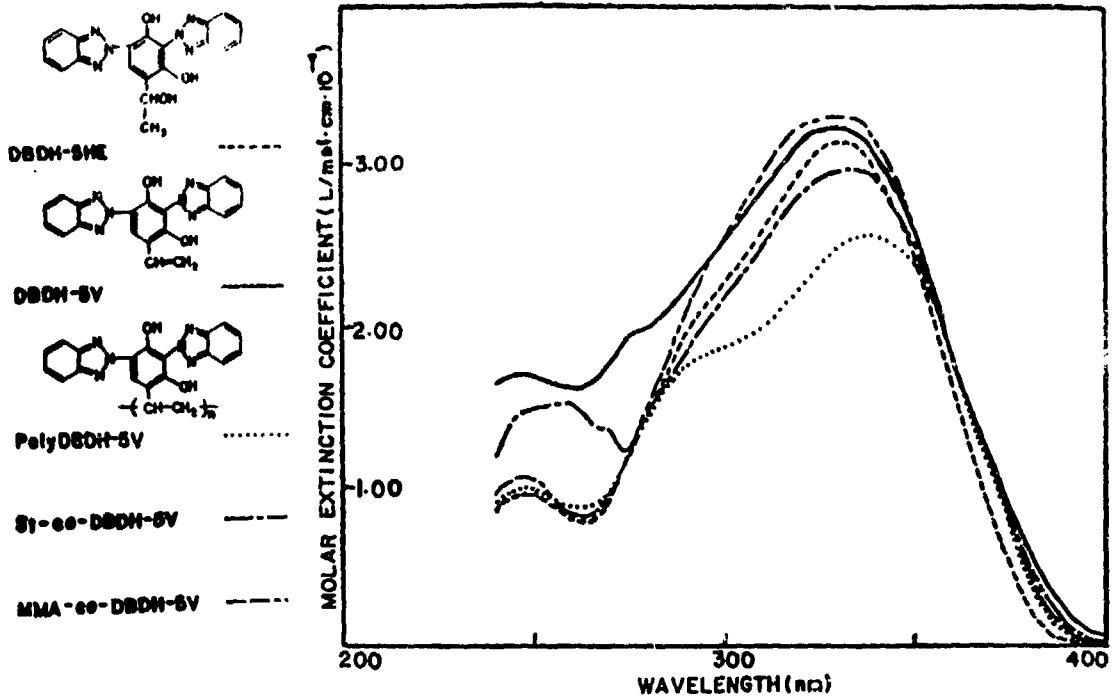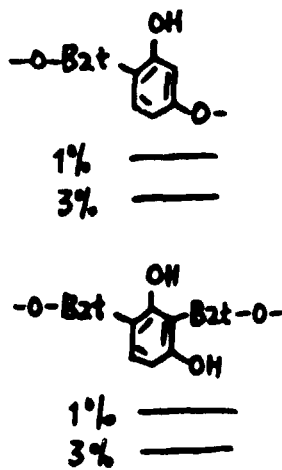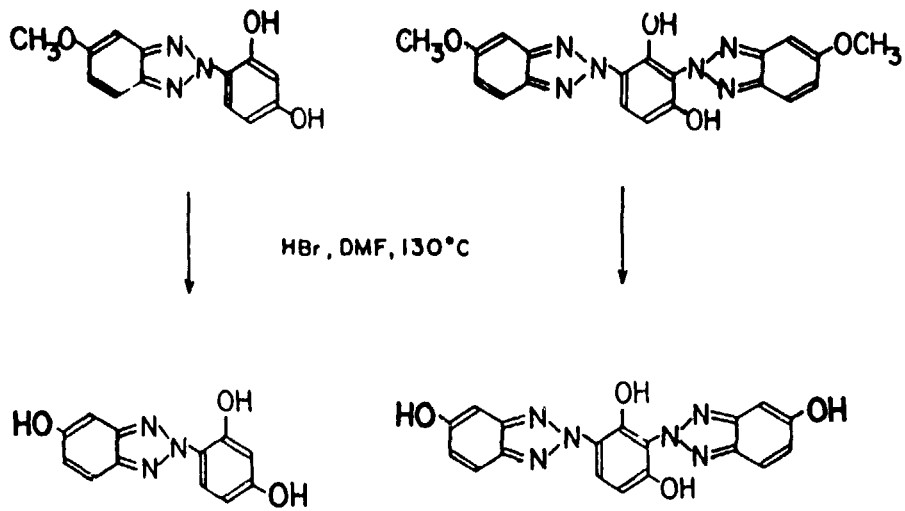
* CALCULATED FROM
FEED RATIO.

* APPROX. MOLAR EXTINCTION COEFFICIENT (L/Mol.cm ×10⁻⁴)

3.0

2.0

1.0

250   300   350   400

WAVELENGTH (nm)

141
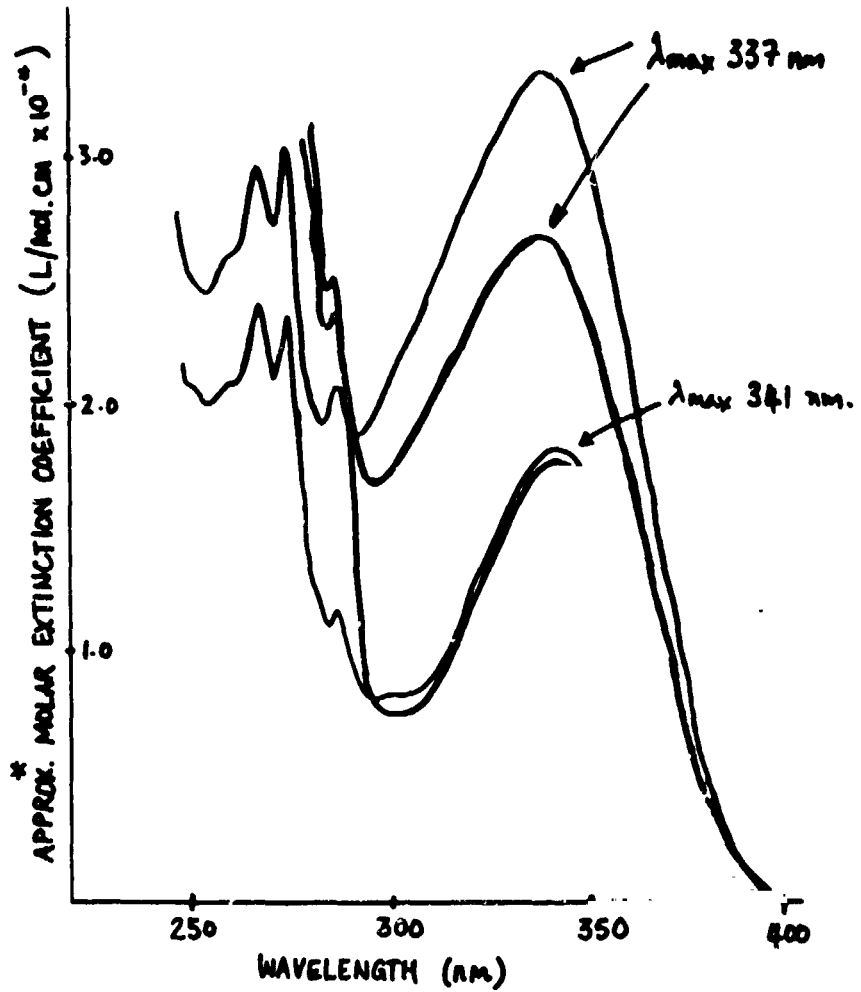
Polycarbonates With UV Stabilizers
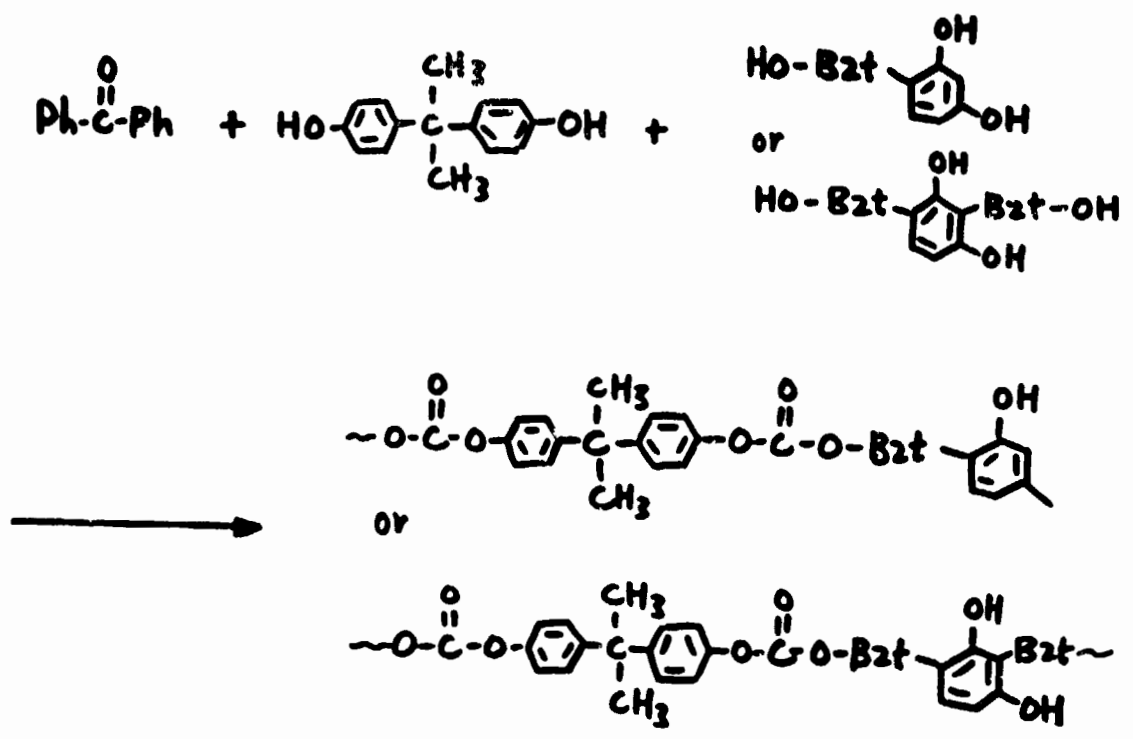
Polyesters With UV Stabilizers

$$HO\text{-}Bzt\text{-}(Ac) \text{ (resorcinol with OH, OH)} + X\text{-}\overset{O}{\underset{\|}{C}}\text{-}R\text{-}\overset{O}{\underset{\|}{C}}\text{-}X + HO\text{-}R'\text{-}OH \longrightarrow$$

$$\sim R'\text{-}O\text{-}\overset{O}{\underset{\|}{C}}\text{-}R\text{-}\overset{O}{\underset{\|}{C}}\text{-}O\text{-}Bzt\text{-}(ring\ OH)\text{-}O\text{-}\overset{O}{\underset{\|}{C}}\text{-}R\text{-}\overset{O}{\underset{\|}{C}}\text{-}O\sim$$

$$\sim R'\text{-}O\text{-}\overset{O}{\underset{\|}{C}}\text{-}R\text{-}\overset{O}{\underset{\|}{C}}\text{-}O\text{-}Bzt\text{-}(ring\ OH\ OH)\text{-}Bzt\text{-}O\text{-}\overset{O}{\underset{\|}{C}}\text{-}R\text{-}\overset{O}{\underset{\|}{C}}\text{-}O\sim$$

$$Bzt = -N\overset{N}{\underset{N}{\diagdown}} \text{ (benzotriazole ring)}$$
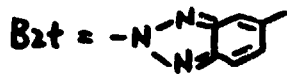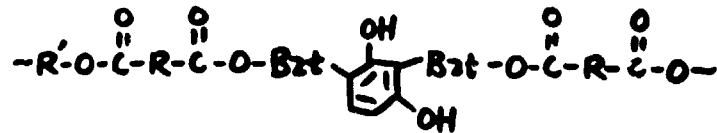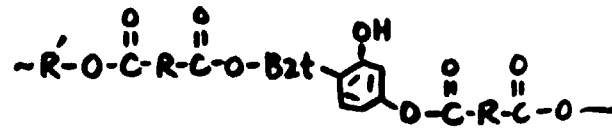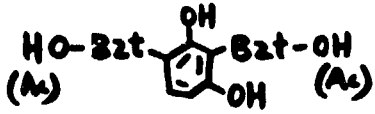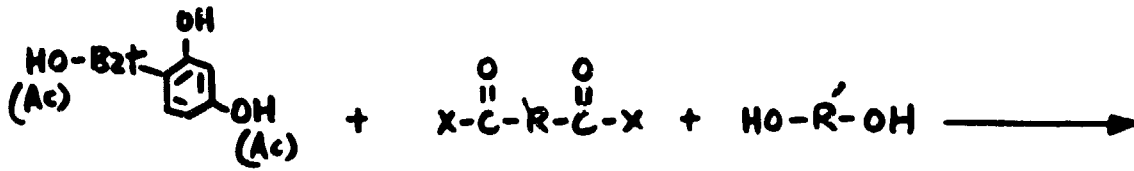
$$R, R' = \{CH_2\}_n, \text{ (phenyl)}, \text{ (phenyl)}, \text{ Bisphenol A}$$

$$X = Cl, -OCH_3, -OPh$$

ENCAPSULATION MATERIALS RESEARCH

SPRINGBORN LABORATORIES, INC.

P. Willis

<u>PHASE I</u>

IDENTIFY AND DEVELOP LOW COST
MODULE ENCAPSULATION MATERIALS

- POTTANTS
- COVER FILMS
- SUBSTRATES
- ADHESIVES/PRIMERS
- ANTI-SOILING TREATMENTS

<u>PHASE II</u>

MATERIALS RELIABILITY

- AGING AND LIFE ASSESSMENT
- ADVANCED STABILIZERS
- CHEMICAL DIAGNOSTICS
- FLAMMABILITY
- ELECTRICAL ISOLATION

<u>PHASE III</u>

PROCESS SENSITIVITY

- INTERRELATIONSHIPS OF
  - FORMULATION VARIABLES
  - PROCESS VARIABLES
- MANUFACTURING YIELD ANALYSIS

(PROCESS DEVELOPMENT SECTION)

Module Components

SURFACE

OUTER COVER
(OR GLASS)

POTTANT

BACK COVER
(OR SUBSTRATE)

GASKET/SEALANT
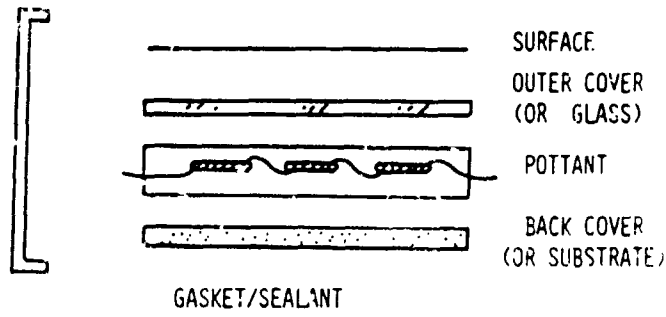
CURRENT EMPHASIS ON MATERIALS AND MODULE
PERFORMANCE CHARACTERISTICS

- DETERMINE CURRENT LEVEL OF PERFORMANCE
- ENHANCE PERFORMANCE (E.G. REFORMULATION)
- SERVICE LIFE PROGNOSIS

PERFORMANCE CRITERIA

- ENVIRONMENTAL DEGRADATION
- ADHESIVE BOND DURABILITY
- ELECTRICAL INTEGRITY
- FLAMMABILITY

Module Flammability

- MOST MODULES CONSTRUCTIONS NOT PASSING UL-,90 BURNING BRAND TEST
- MECHANISM: APPEARS TO BE RUPTURE OF THE BACK COVER WITH THE EVOLUTION OF BURNING GASSES
- MODULES CAN BURN BUT MUST NOT SERVE AS AN IGNITION SOURCE TO OTHER STRUCTURES
- MODULES WITH KAPTON BACK COVERS (HIGH STRENGTH) PASS TEST DUE TO ABILITY TO RETAIN COMBUSTIBLE GASSES

PYROLYZING POLYMER

COMBUSTIBLE GASSES
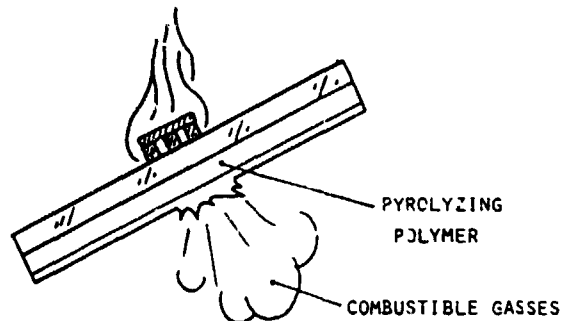
- KAPTON IS VERY EXPENSIVE
- INEXPENSIVE HIGH STRENGTH HIGH TEMPERATURE BACK COVER NEEDED

Module Flammability

GOAL:

- PREVENT SPREAD OF FLAME
- PASS UL-790

APPROACHES:

(1) HIGH STRENGTH HEAT RESISTANT BACK COVERS

- CERAMIC PAPER
- POLYMER FILM LAMINATES WITH GLASS SCRIM REINFORCEMENT
- METAL FOILS
- RESIN IMPREGNATED GLASS CLOTH

(2) REDUCTION OF COMBUSTIBLE MATERIALS

- THINNING OF POTTANT LAYER

(3) FIRE RETARDANT ADDITIVES

- INERT DILUENTS (TALC, CALCIUM CARBONATE)
- RELEASE OF WATER WITH HEAT ALUMINA TRIHYDRATE (35% WATER)
- FIRE RETARDANTS (FREE RADICAL TRAPS)
  ANTIMONY OXIDE, ZINC BORATE
  BROMINATED ORGANICS
  ORGANIC PHOSPHATES

(4) COMBINATION OF ALL THREE

EVALUATION OF CANDIDATE TECHNIQUES

CONVENTIONAL:

- UL-94 VERTICAL BURN TEST
- ASTM E-262 FLAME SPREAD INDEX
- ASTM D-2863 LIMITING OXYGEN INDEX

FOR BACK COVERS:

- CONSTRUCT SPECIAL APPARATUS
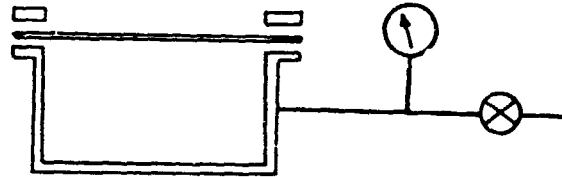
- DETERMINE BURST STRENGTH AS FUNCTION OF TEMPERATURE AND PRESSURE
- CORRELATE TO ACTUAL EFFECTIVENESS UNDER FIRE CONDITIONS
- DETERMINE ADD-ON COST FOR IMPROVEMENT IN FIRE RATING
- RECOMMEND CANDIDATES FOR UL-790 TESTING

149

Electrical Isolation

- POTTANTS AND COVER FILMS SERVE AS ELECTRICAL INSULATION
- NEED TO KNOW THICKNESS REQUIRED FOR VOLATAGE STANDOFF
- VARIATION WITH TEMPERATURE, ABSORBED WATER
- NEED TO KNOW VARIATION DIELECTRIC STRENGTH WITH AGING:

  LIGHT, HEAT, HUMIDITY, FIELD STRESS

METHOD:

- USE DC DIELECTRIC TEST APPARATUS
  TIP TO TIP SYMMETRIC ELECTRODES
- SPECIFIED RATE OF RISE
- PLOT AVERAGE BREAKDOWN VOLTAGE, V_A VS THICKNESS
- STRAIGHT LINE RELATIONSHIP:
  SLOPE CONSIDERED TO BE THE INTRINSIC
  DIELECTRIC STRENGTH, DV/DT
- MEASUREMENTS TO DATE:

  EVA DV/DT = 3.65 KV/ MIL

- REMEASURE DV/DT :
  - THERMAL AGING
  - WATER ABSORPTION
  - ENVIRONMENTAL EXPOSURE
  - FIELD STRESS AGING
- RECALCULATE THE REQUIRED INSULATION THICKNESS
  FOR SERVICE LIFE OF THE MODULE

Adhesion Experiments

SELF-PRIMING FORMULATIONS
(TO SUNADEX GLASS)

POTTANT/PRIMER	LEVEL (PHR)	BOND STRENGTH, LBS/IN	
		CONTROL[*]	12 MONTHS[*] STORAGE
EVA A9918	0.25	42	31
Z-6030	0.05	29	20
EVA 15295/	0.25	31	28
Z-6030	0.05	10.9	5
EMA 15257/	0.25	57.4	41
Z-6030	0.05	49.0	26

[*]BONDS ALSO STABLE TO WATER IMMERSION AND BOILING WATER

- STABLE TO STORAGE CONDITIONS (12 MO. TO DATE) AT 0.25 PHR LEVEL, .05 PHR NOT AS STABLE

- NOW COMMERCIALLY AVAILABLE (SPRINGBORN)

    EVA A9918-P   (LUPERSOL 101 CURE)
    EVA 15295-P   (TBEC CURE)

- WORKING ON INTERNAL PRIMING FOR CELL STRING AND METALLIZATION (MORE DIFFICULT TO PRIME)

CONTINUED PRIMER STUDIES:

- EVALUATE THE THREE "BASIC" PRIMERS -
  DR. PLUEDDEMANN - DOW CORNING
    - POLYMER/METAL
    - POLYMER/INORGANIC
    - POLYMER/ORGANIC

- METAL PRIMER (ALUMINUM) RECOMMENDATIONS
  DR. JIM BOERIO - UNIVERSITY OF CINCINNATI

ADHESION DIAGNOSTICS:

- HOW DURABLE ARE ADHESIVE BONDS?
  UNDER WHAT CONDITIONS?

- SUCCESSFUL SPECTROSCOPIC EXAMINATION OF GLASS/
  PRIMER INTERFACE - DR. JACK KOENIG -
  CASE WESTERN RESERVE

- EVA COMPOUNDED WITH HIGH LOADINGS OF SILANE
  TREATED GLASS BEADS
    - SPECIMENS AT CASE WESTERN FOR "DRIFT"
      ANALYSIS (CHEMICAL)
    - IDENTICAL SPECIMENS AT SPRINGBORN FOR
      MECHANICAL ANALYSIS
    - HYDROLYTIC AGING
    - CORRELATE CHEMICAL OBSERVATIONS WITH
      MECHANICAL PERFORMANCE
    - DETERMINE DEGRADATION RATES
    - ASSESS SERVICE LIFE

Accelerated Aging

OUTDOOR PHOTOTHERMAL AGING DEVICES
(OPT)

- USE NATURAL SUNLIGHT, AVOIDS SPECTRAL DISTRIBUTION PROBLEMS WITH ARTIFICIAL LIGHT SOURCES

- USE TEMPERATURE TO ACCELERATE THE PHOTO-THERMAL REACTION

- INCLUDES DARK CYCLE REACTIONS

- INCLUDES DEW/RAIN EXTRACTION

- INTENDED PRIMARILY FOR MODULE EXPOSURE

- EXTRAPOLATE EFFECTS TO LOWER TEMPERATURES
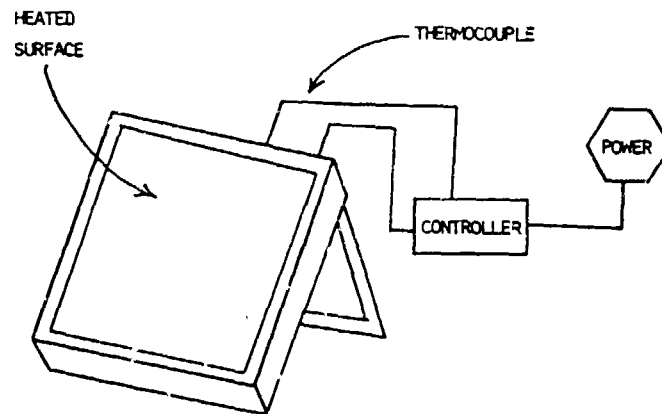
RELIABILITY PHYSICS

- MODULE EXPOSURE: OPT 105°C, 7,000 HRS

- ALL SHOW SEVERE COPPER REACTION

- BEST PERFORMANCE: EVA-ADVANCED STABILIZER
  TBEC, UV-2098, TINUVIN 770
  VIRTUALLY NO DEGRADATION APPARENT

- CONSPICUOUS DEGRADATION IN OTHERS

- GLASS FRACTURE - THERMAL SHOCK

- MODULE EXPOSURE: OPT 70°C, 7000 HRS.
- SOME COPPER REACTION W/EVA 9918
- NO OTHER EFFECTS NOTICEABLE

- USEFUL FOR EVALUATING CANDIDATE
  FORMULATIONS - COMPARISON
- EVALUATES WHOLE MODULES
- DETERMINE UPPER LEVEL SERVICE
  TEMPERATURES
- MODELLING:
  - ARRHENIUS : LOG P VS. 1/K°
  - PREDICT SERVICE LIFE BY EXTRAPOLATION
    TO LOWER TEMPERATURES
  - TIME TO ONSET OF DEGRADATION
    (INDUCTION PERIOD)
  - PROBABILITY DISTRIBUTION-FAILURE
- EXAMPLE: POLYPROPYLENE - INDUCTION TIME

TIME, HOURS

Advanced Stabilizers

```
GENERAL DEGRADATION                    STABILIZATION
    MECHANISM                            ADDITIVE

 LIGHT (UV)    ~~~~~>

   ABSORPTION ─────────────────────> SCREENERS
       │
       ↓
 EXCITED SPECIES ───────────────────> QUENCHERS
 (ACTIVATED KETONES)
       │
       ↓
    RADICALS   ──────────────────────> FREE RADICAL
    P•,  H•                            SCAVENGERS
       │
       │          + O₂
       ↓
    ROOH      ──────────────────────> HYDROPEROXIDE
 (HYDROPEROXIDES )                    DECOMPOSERS
       │
       ↓
   P•,   RO•, HO•
```
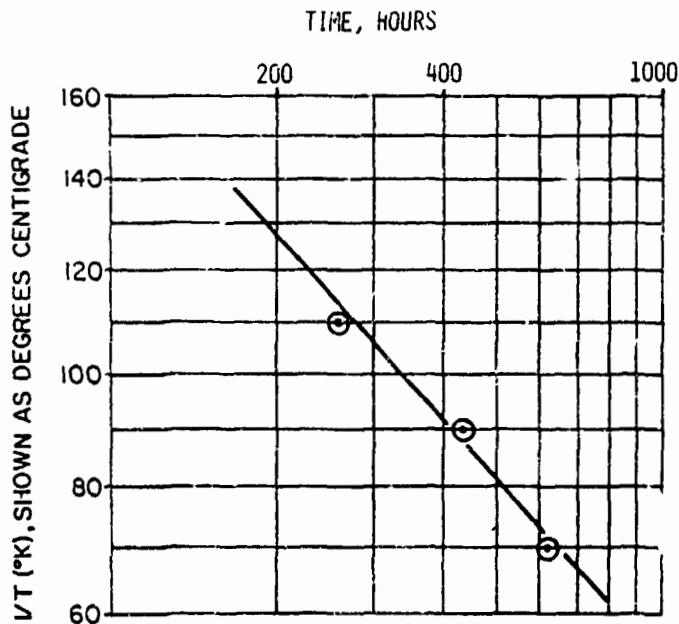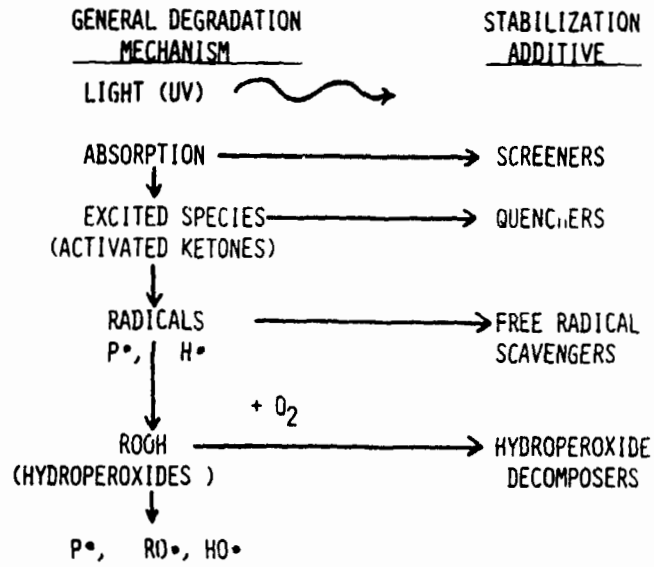
AUTOCATALYTIC DEGRADATION

- QUENCHERS STRONGLY COLORED - NOT USED

- LONG TERM STABILIZERS:
  - OXIDATIVELY STABLE
  - NON-FUGITIVE

- UV-2098 (AMERICAN CYANAMIDE) BEST SCREENER
  FOUND TO DATE   (CO-REACTIVE BENZOPHENEONE)

- HINDERED AMINE LIGHT STABILIZERS (HALS)
  FREE RADICAL TRAPS AND HYDROPEROXIDE
  DECOMPOSITION

- COMBINATION OF SCREENER AND HALS BEST
  STABILIZER PACKAGE

CANDIDATE HINDERED AMINES (HALS)

- HIGH EFFICIENCY FROM REGENERATIVE CHEMISTRY:
  ACTIVE SPECIES RECYCLES - NON SACRIFICIAL

- EVALUATION OF CANDIDATES:
  - EVA, TBEC CURE, 0.1% HALS
  - % ELONGATION VERSUS TIME
  - OPT DEVICE, 90 °C
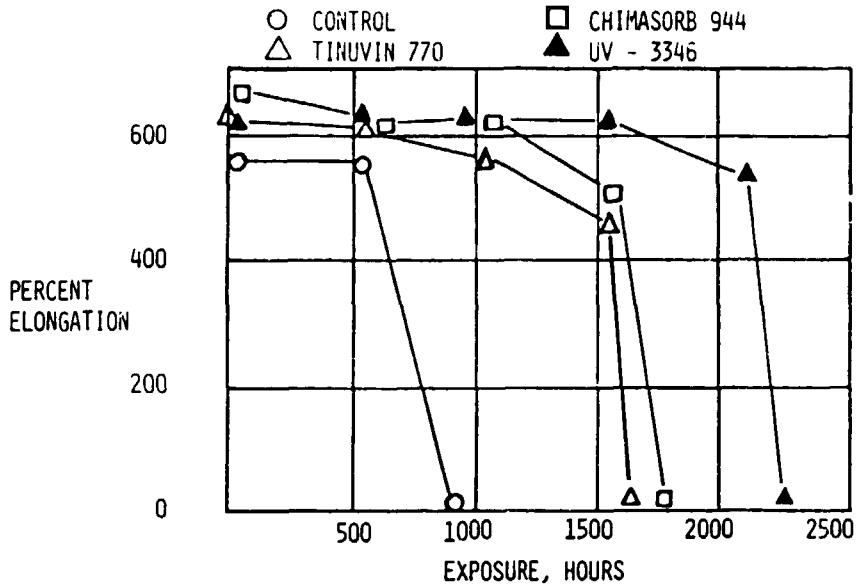
- FAILURE: LOSS OR CONSUMPTION OF CHEMISTRY?
  NEED FOR ANALYTICAL METHOD

- CYASORB UV-336 (CYANAMIDE) CLEARLY BETTER
- SYSTEM EVALUATION: EVA/TBEC/UV-2098/UV-3346
  MODULES, ADHESION, FLAMMABILITY, ETC.

Antisoiling Treatments

SURFACE CHEMISTRY:

- HARD
- SMOOTH
- HY ROPHOBIC
- OLEOPHOBIC
- ION FREE
- LOW SURFACE ENERGY

SURFACE INVESTIGATED:

- SUNADEX GLASS
- TEDLAR (100 BG 30 UT)
- ACRYLAR (ACRYLIC FILM)

TREATMENTS REMAINING:

- L-1668 FLUOROSILANE (3M)
- E-3820 PERFLUORODECANOIC ACID/
  SILANE   (DOW CORNING)
- STILL EFFECTIVE AT 38 MONTHS
  OUTDOOR EXPOSURE
- RESULTS IN IMPROVED POWER OUTPUT
- FLUOROALKYL SILANE CHEMISTRY
  APPEARS TO BE MOST EFFECTIVE

Soiling Experiments

THIRTY-TWO MONTHS EXPOSURE
ENFIELD, CONNECTICUT

% LOSS IN I_{sc} WITH STANDARD CELL TREATED
TEDLAR 100BG300UT

(SUPPORT ON GLASS)
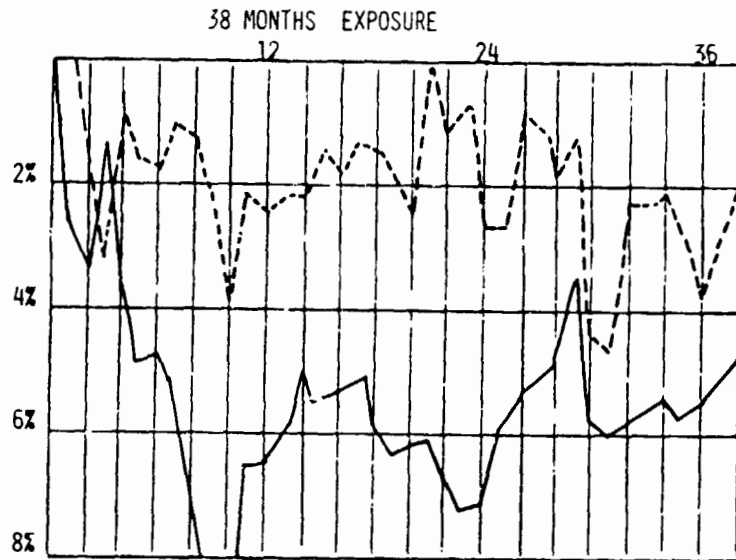
38 MONTHS EXPOSURE

CONTROL, NO COATING

E-3820 COATING (BEST)

ESTIMATED AVERAGE POWER IMPROVEMENT, 3.8%

THIRTY-TWO MONTHS EXPOSURE
ENFIELD, CONNECTICUT

% LOSS IN I_{sc} WITH STANDARD CELL TREATED ACRYLAR
(SUPPORTED ON GLASS)

38 MONTHS EXPOSURE

CONTROL, NO TREATMENT

OZONE WITH E-3820 (BEST)
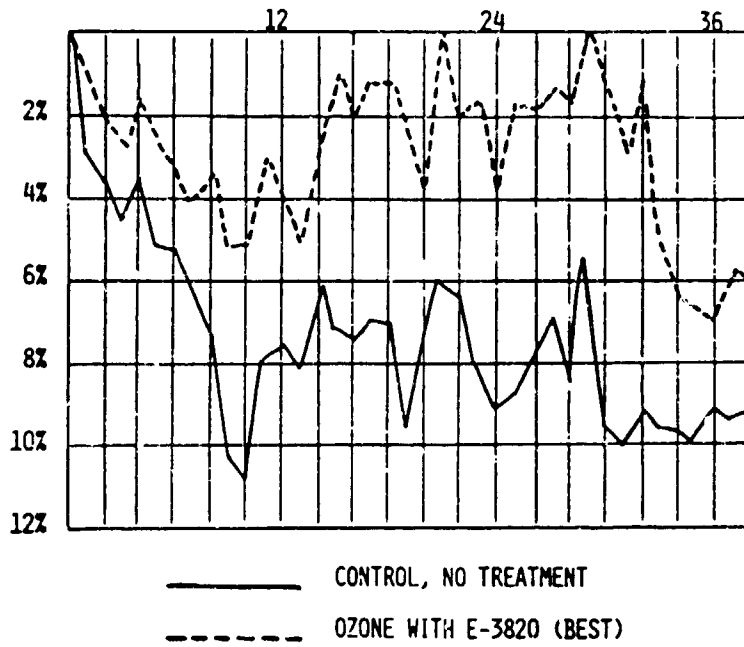
ESTIMATED AVERAGE POWER IMPROVEMENT, 3.9%

159

THIRTY-TWO MONTHS EXPOSURE
ENFIELD, CONNECTICUT

% LOSS IN I_{sc} WITH STANDARD CELL TREATED
SUNDEX GLASS

38 MONTHS EXPOSURE

CONTROL, NO TREATMENT

E-3820 (BEST)

RAINFALL, INCHES
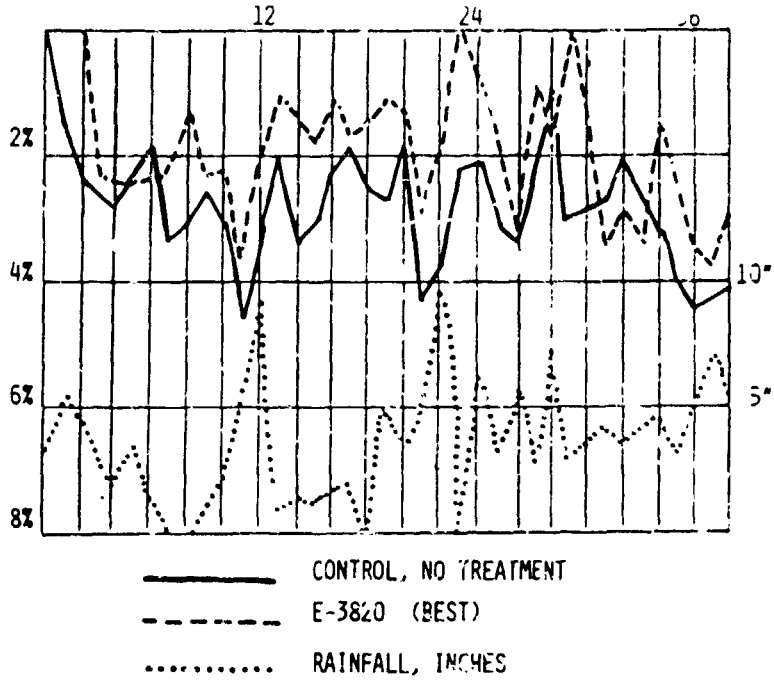
ESTIMATED AVERAGE POWER IMPROVEMENT, 1%

Antisoiling Coatings

- STILL EFFECTIVE AFTER THREE YEARS OUTDOOR EXPOSURE
- PERMANENCE APPEARS TO BE GOOD
- POSSIBILITY FOR IMPROVED PERFORMANCE BY INCREASING SOIL REPLELLANCY

NEW CANDIATE(S):

- LOWEST SURFACE ENERGY EVER REPORTED: POLYMER OF PERFLUORO-OCTYL METHACRYLATE

    $\gamma_c = 10.6$ DYNE CM^{-1}

- REACT WITH TRIMETHOXY HYDROGEN SILANE TO FORM ADDUCT WITH GLASS-REACTIVE GROUP

- EVALUATE IN SOILING TESTS
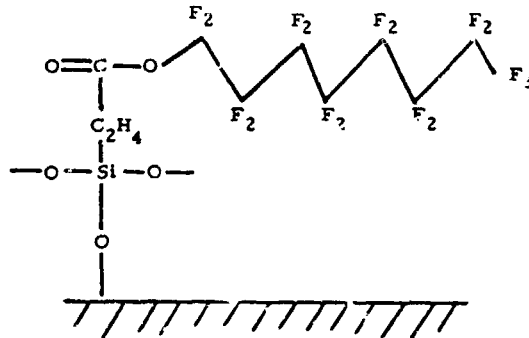
Outer Covers (Substrate Design)

- LOW COST UV SCREENING FILMS COMMERCIALLY AVAILABLE
- PROBLEMS: SHRINKAGE, STABILIZER EXTRACTION ADHESION, WEATHER STABILITY
- POTTANTS APPEAR TO HAVE GOOD STABILITY
- NON-SCREENING CANDIDATE FILMS CLEAR, WEATHERABLE, BONDABLE ?

FILM	REF. INDEX	% T	COST $/FT^2/MIL
TEFZEL	1.403	85.6	0.128
KAYNAR	1.420	88.8	0.055
HALAR	1.40	85.3	0.096
PFA	1.30	88.4	0.123
FEP	1.34	93.6	0.109

- FEP MAY BE GOOD CHOICE:
    - HIGH TRANSPARENCY
    - OUTSTANDING WEATHERABILITY
    - MAY IMPROVE OPTICAL THROUGHPUT BY 2% DUE TO OPTICAL COUPLING
    - REQUIRES PRIMER TECHNOLOGY
    - WILL BE EVALUATED IN MODULE FABRICATION AND OUTDOOR EXPOSURE EXPERIMENTS

Conclusions

- OUTDOOR PHOTOTHERMAL AGING DEVICES (OPT)
  - BEST ACCELERATED AGING METHOD DISCOVERED YET
  - SIMULATES WORST CASE FIELD CONDITIONS
  - EVALUATE FORMULATIONS
  - EVALUATE MODULE PERFORMANCE
  - POSSIBLITY FOR LIFE ASSESSMENT

  AVOID METALLIC COPPER EXPOSURE

- SELF PRIMING FORMULATIONS HAVE GOOD STORAGE STABILITY AT 0.25 PHR)

- STABILIZERS - ENHANCED PERFORMANCE
  - UV-2098 UV SCREENER
  - UV-3346 HINDERED AMINE (HALS)

- SOIL RESISTANCE TREATMENTS STILL EFFECTIVE

Future Work

- FLAMMABILITY: FIRE RETARDANTS
  AND FLAME RESISTANT WORK COVERS

- ELECTRICAL INTEGRITY: DIELECTRIC
  STRENGTH VERSUS AGING OF
  ENCAPSULATION MATERIALS

- ADHESION DIAGNOSTICS AND SERVICE
  LIFE ASSESSMENT

- MODULE EVALUATION: EVA POTTANT
  WITH ADVANCED STABILIZER PACKAGE

- NEW ANTI-SOILING CONCEPTS

- MODULE SERVICE LIFE ASSESSMENT

     (PHASE III)

- PROCESS AND MANUFACTURING VARIABLES

EVA-GLASS INTERFACE BOND STABILITY

CASE WESTERN RESERVE UNIVERSITY

Jack L. Koenig

1. DEVELOP SPECTRAL METHODS FOR DETERMINING STRUCTURE OF POLYMER/GLASS INTERFACE   (ACCOMPLISHED)

2. EXAMINE STRUCTURAL CHANGES ASSOCIATED WITH HYDROTHERMAL DEGRADATION OF POLYMER/GLASS INTERFACE (IN PROGRESS)

3. DEVELOP METHODS OF INHIBITING THE DEGRADATION REACTION OCCURRING AT POLYMER/GLASS INTERFACE   (FUTURE)
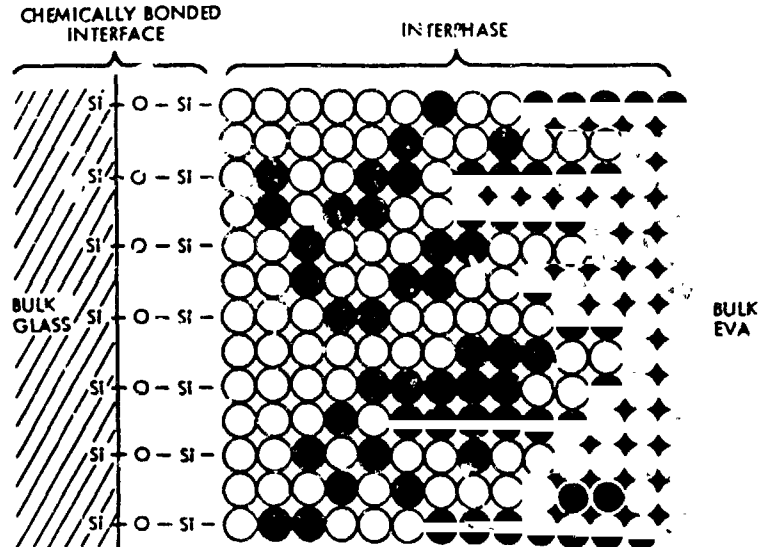
Figure 13. Schematic Representation of the Interdiffusion Model for a Silane-Primed Glass-EVA Joint; Open Circles Indicate Regions of Coupling Agent, Filled Circles Indicate Regions of EVA
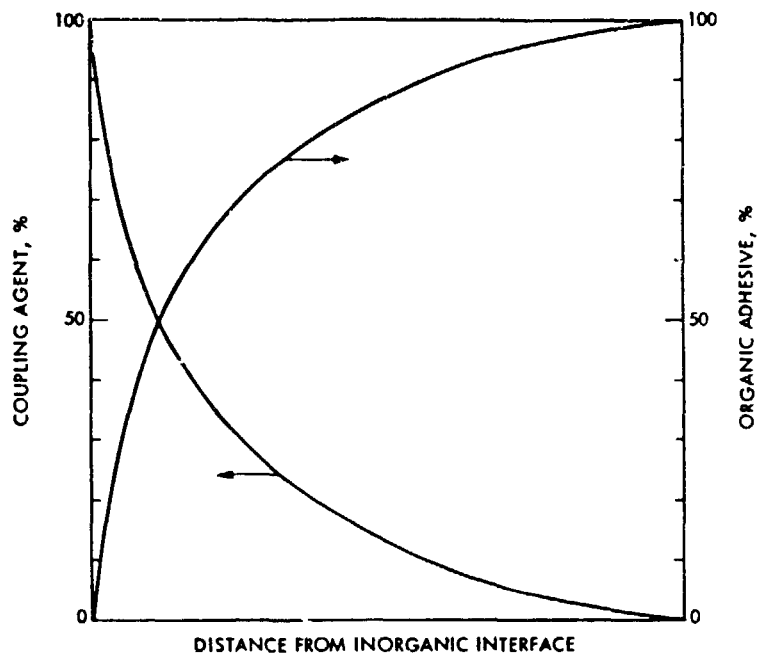
Figure 14. Plot of Silane-Adhesive Concentration Gradient as a Function
of Distance From Inorganic Interface

166

a)

CHEMICALLY
BONDED
INTERFACE

BULK
GLASS | CHEMISORBED
LAYERS | PHYSISORBED
LAYERS

b)

STRENGTH

DISTANCE

1 7 4 8 2 - 4
DRIFT
EVA / no MPS / PEROXIDE
NO HYDROTHERMAL

1 7 4 8 2 - 3
DRIFT
EVA / MPS / PEROXIDE
NO HYDROTHERMAL

1 7 4 8 2 - 4

DRIFT

EVA / no MPS / PEROXIDE

HYDROTHERMAL RECYCLE 85°C 2 MONTHS

DRYING at ROOM TEMPERATURE AND PRESSURE

17482-4

DRIFT

EVA / no MPS / PEROXIDE

HYDROTHERMAL CYCLING 85°C 2 MONTHS

DRYING 36 HRS 100°C VACUUM

1 7 4 8 2 - 3
DRIFT
EVA / MPS / PEROXIDE
HYDROTHERMAL CYCLING 85°C   2 MONTHS
DRYING   ROOM TEMP AND PRES

1 7 4 8 2 - 3
DRIFT
EVA / MPS / PEROXIDE
HYDROTHERMAL RECYCLE 85°C 2 MONTHS
DRYING 36 HRS 100°C VACUUM

EVA / MPS / PEROXIDE

WITH AND WITHOUT HYDROTHERMAL CYCLING

WAVENUMBER (CM-1)

C-3

WATER IN O-H STRETCHING REGION

EVA / no MPS / PEROXIDE

EVA / MPS / PEROXIDE

EVA / no MPS / PEROXIDE   HYDROTHERMAL CYCLING

EVA / MPS / PEROXIDE   HYDROTHERMAL CYCLING

3800   3600   3400   3200   3000   2800   2600

WATER in O-H BENDING REGION 1640 cm

17388A

DRIFT

EVA / MPS / no PEROXIDE

17488-B

DRIFT

PE / MPS / no PEROXIDE

NO HYDROTHERMAL

CM-1

17488C
DRIFT
PE / MPS / PEROXIDE
NO HYDROTHERMAL

ORIGINAL PAGE IS
OF POOR QUALITY

FILE LUP101

PEROXIDE

PE / MPS / PEROXIDE COMPOSITE

1363

PE / MPS / no PEROXIDE COMPOSITE

1368

1353

methyl end group

1377

weak MPS bands

PE CH_2 wag   amorphous

1400 1380 1360 1340 1320 1300 1280 1260 1240

0.447

$1363 cm^{-1}$ BAND

0.358

PEROXIDE

OBTAINED FRCM DIFFERENCE SPECTRUM

0.268

PE/MPS/ PEROXIDE - PE/MPS/no PEROXIDF

0.179

0.089

MPS

0.000

1400 1380 1360 1340 1320 1300

CM-1

COMPOSITE INTERFACE

MPS Reaction in PE

	C=C / C=O	%
MPS neat	0.138	100
PE / MPS	0.107	77.5
PE / MPS / peroxide	0.027	19.6

Weaker Interfacial Bands

181
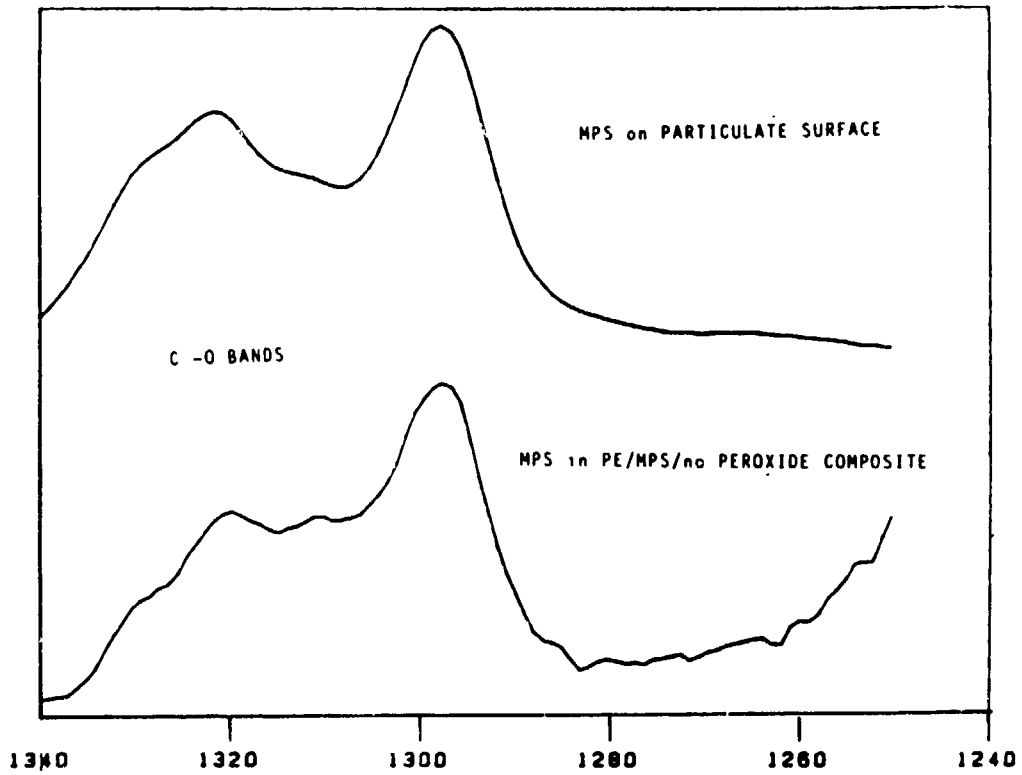
INTERFACIAL BONDING STABILITY

UNIVERSITY OF CINCINNATI

J. Boerio

IN-SITU ELLIPSOMETRY
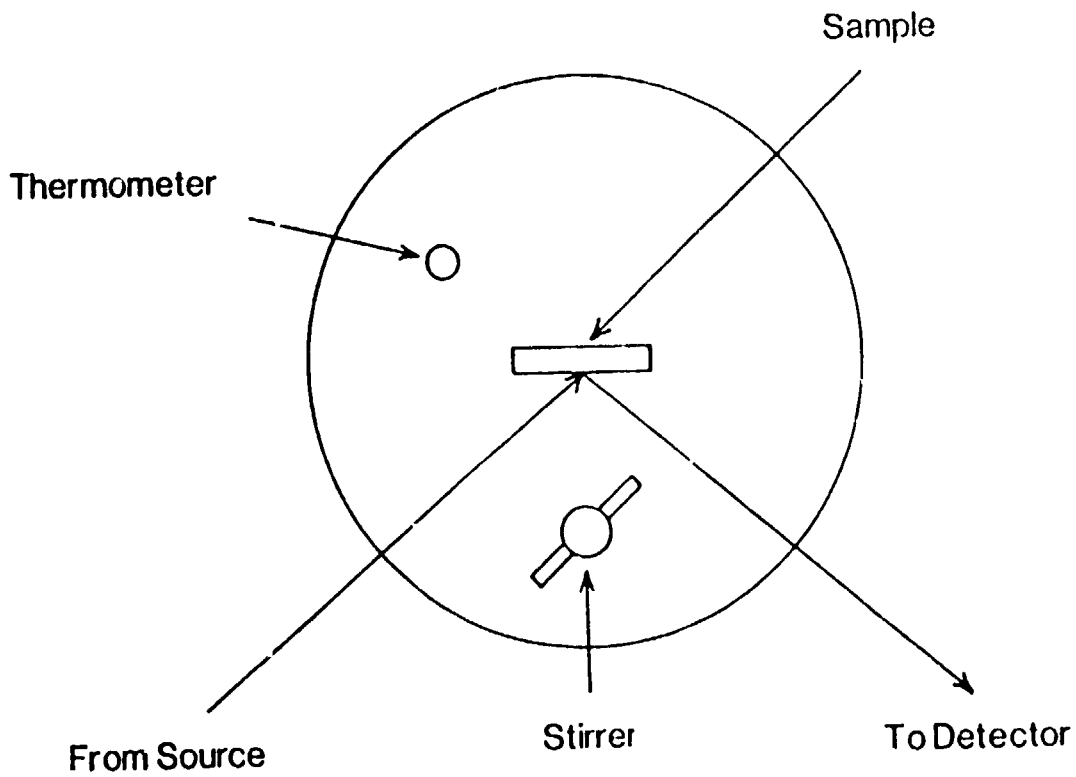
Figure 2. Sample cell for in-situ ellipsometry of metals exposed to water.
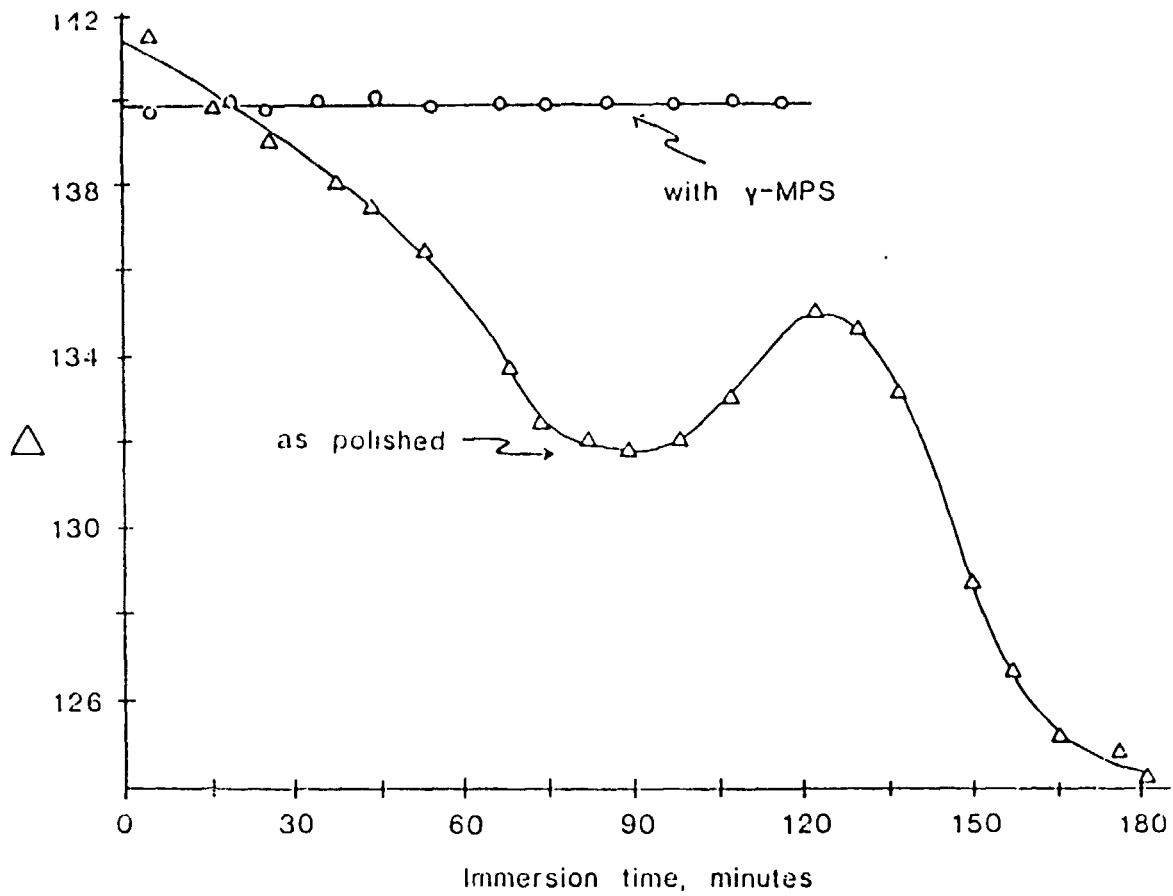
Figure 8. In-situ ellipsometry for (Δ) - polished aluminum and (o) - polished aluminum primed with γ-MPS undergoing hydration in water at 40°C.
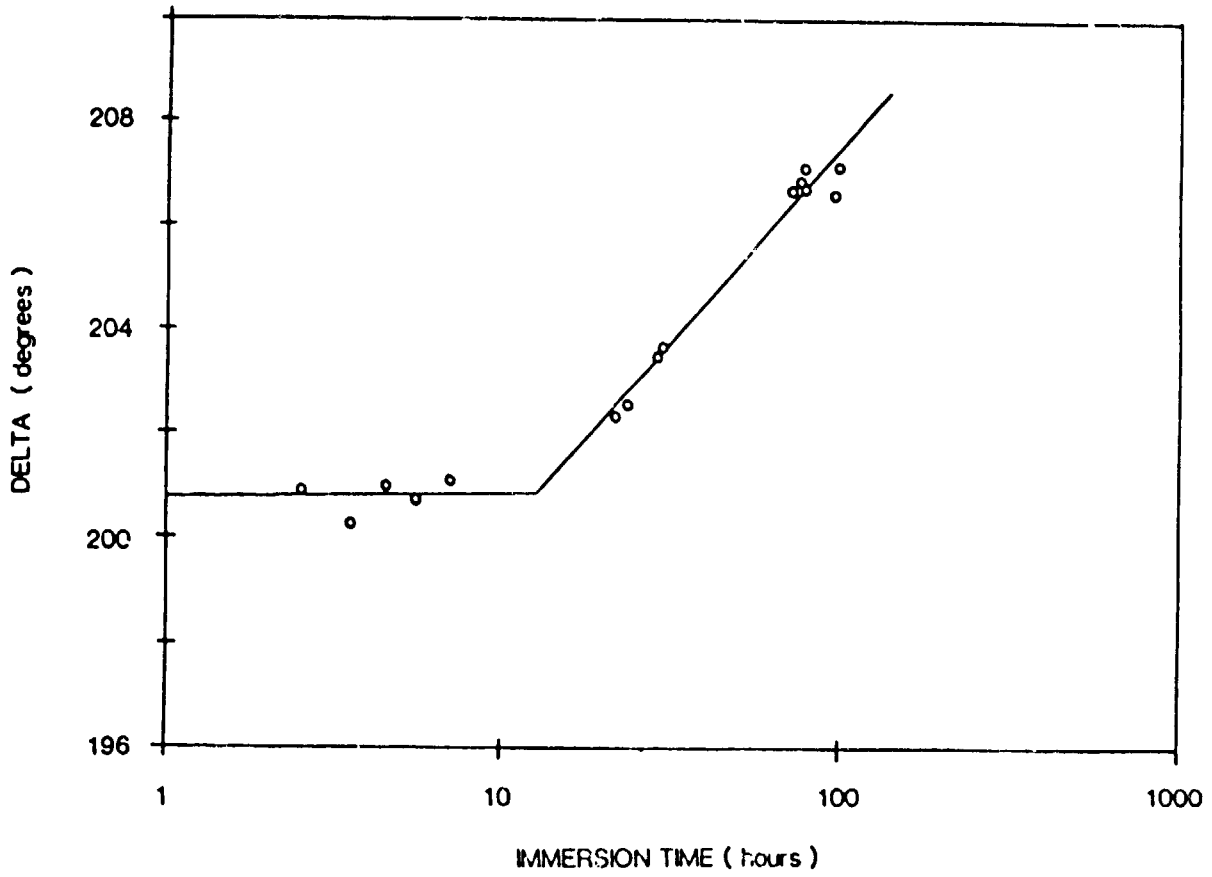
Figure 4. In-situ ellipsometry for EVA/Al in water at 40°C; no pr ..
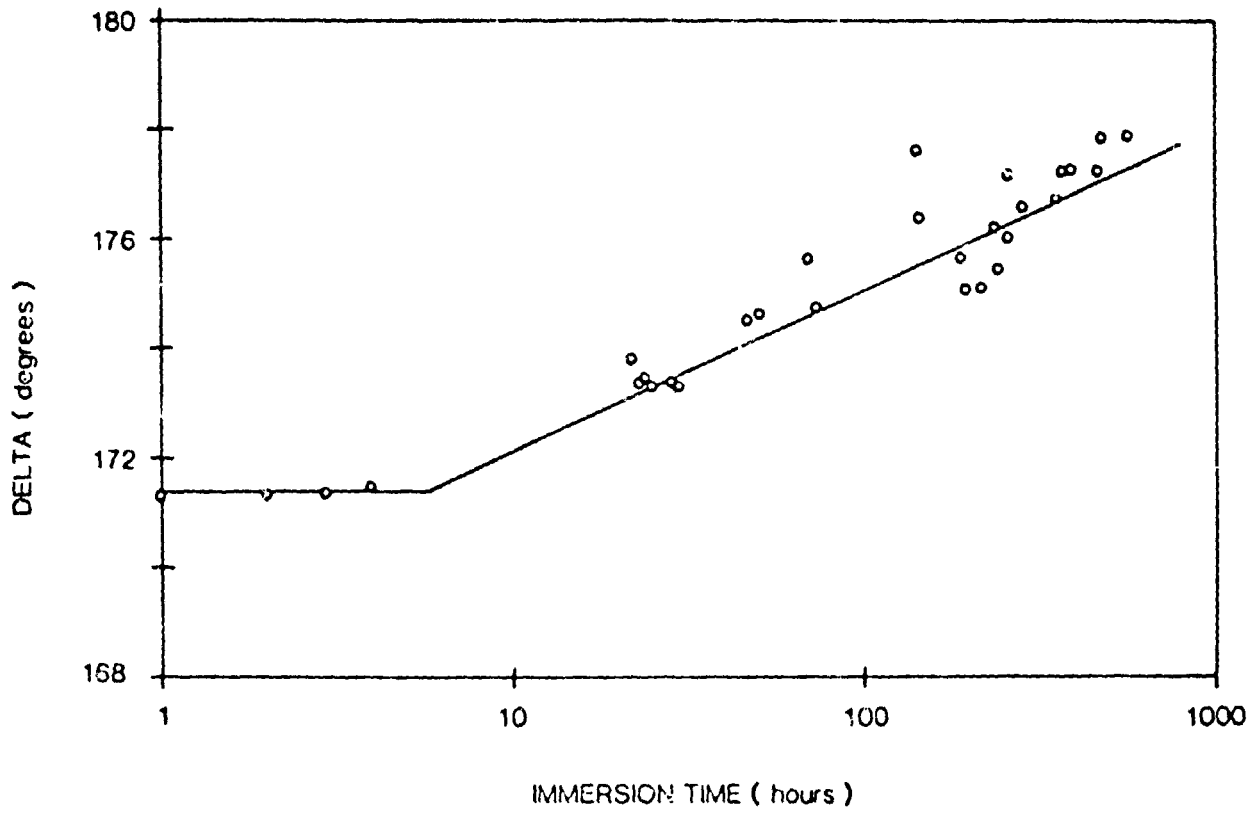
Figure 5.   In-situ ellipsometry for EVA/Al in water at 40°C;
A-11861 primer.

AUGER ELECTRON SPECTRA
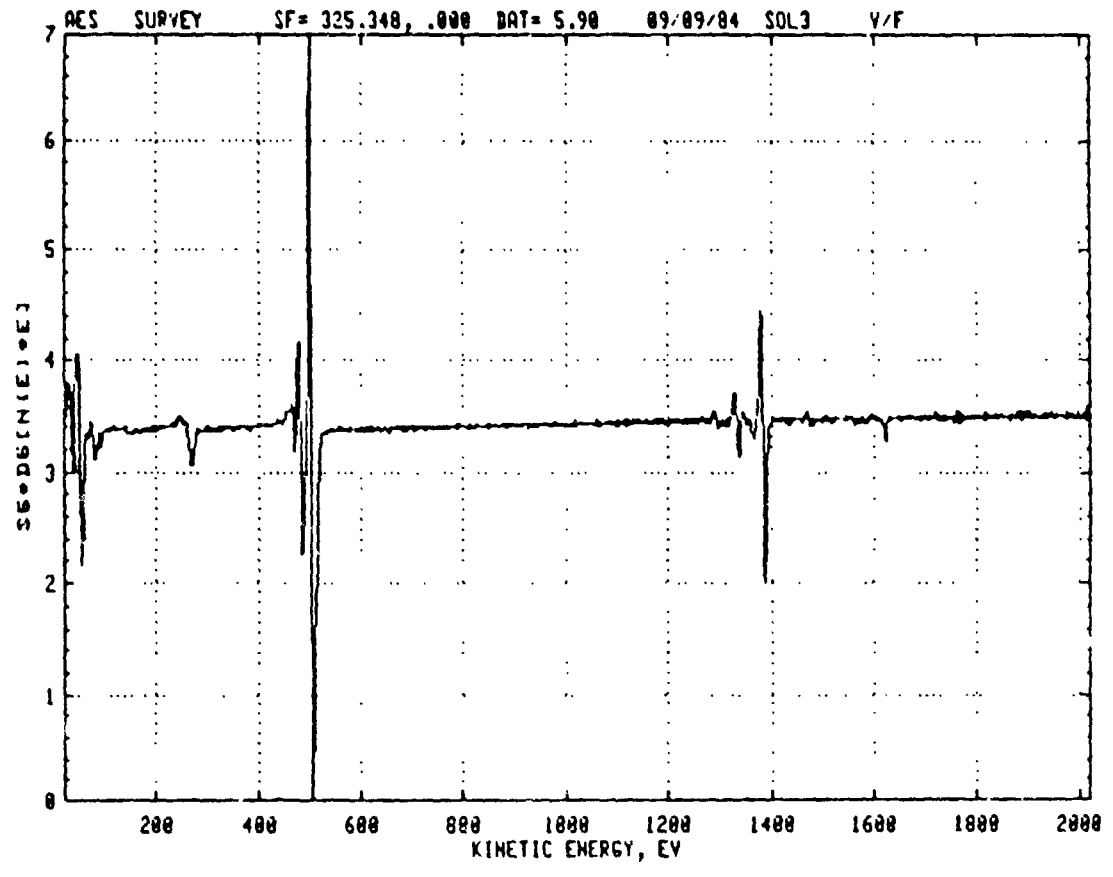
Figure 1. Auger electron survey spectrum from back surface of silicon wafer.
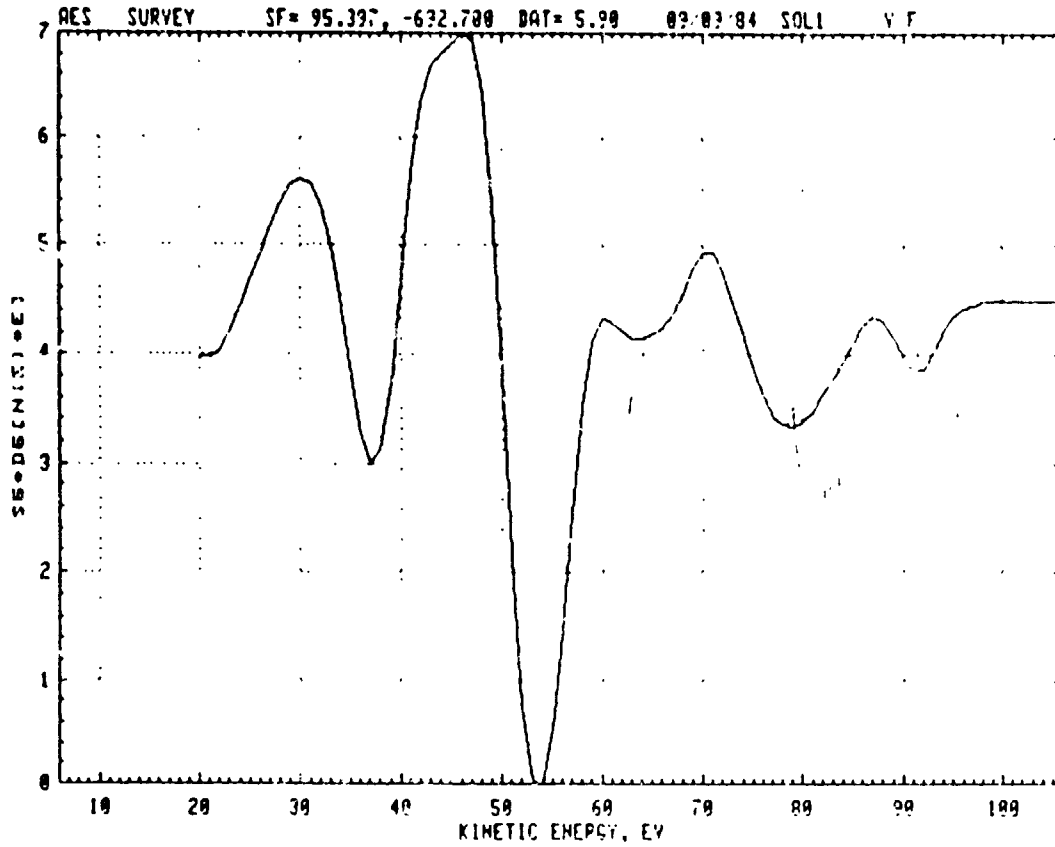
Figure 2.   Aluminum and silicon Auger electron spectra from
back surface of silicon wafer.
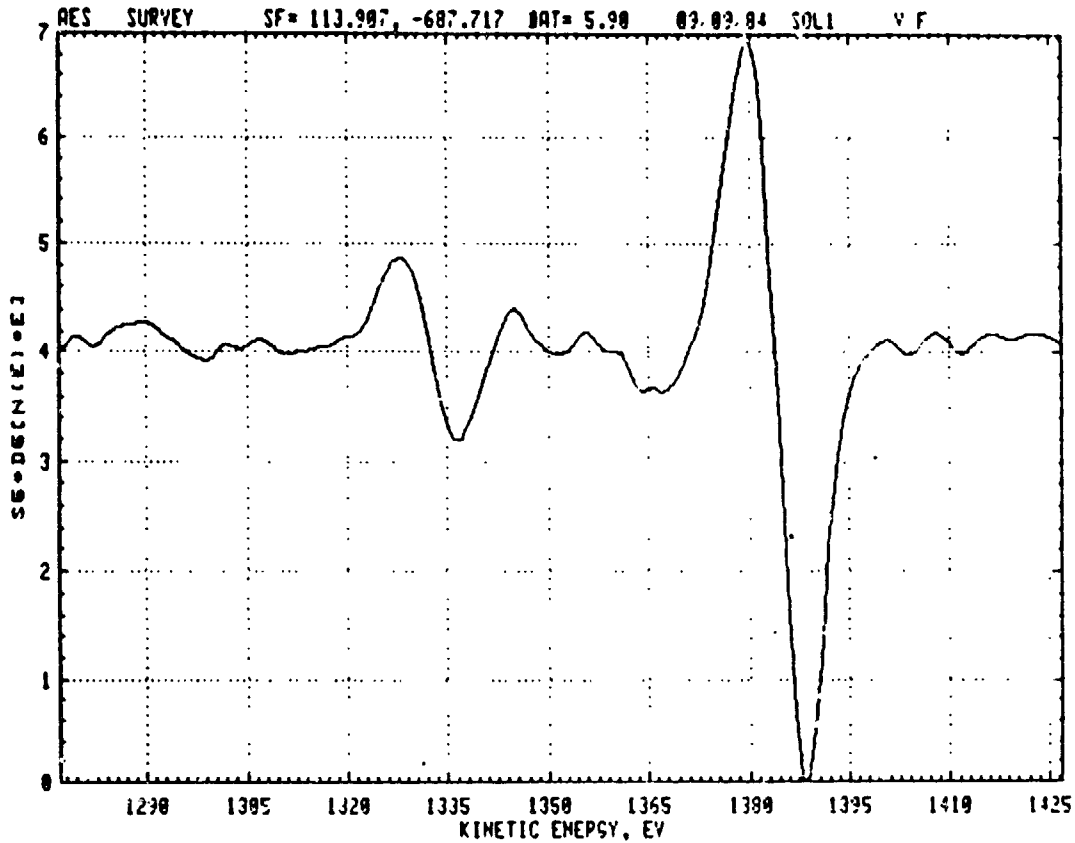
Figure 3: Aluminum Auger electron spectra from back surface of silicon wafer.

Conclusions

1. γ-MPS is an effective primer for bonding EVA to aluminum.

2. Ellipsometry is an effective in-situ technique for monitoring the stability of polymer/metal interfaces.

3. The aluminized back surface of silicon wafers contain significant amounts of silicon and may have glass-like properties.

TOPICS IN ELECTROCHEMICAL DEGRADATION
OF PHOTOVOLTAIC MODULES

JET PROPULSION LABORATORY

G.R. Mon

Topics

- The relationship between leakage current and electrochemical degradation
    - . ositive and negative polarity
    - Dependence on temperature and humidity

- Leakage-current response mechanisms
    - Experimental observations
        - The effect of non-metallized substrate films
        - The effect of cell-frame gap dimension
        - The effect of applied voltage magnitude
        - The effect of pottant ion mobility
    - Physical deductions

- Laboratory-field equivalence -- acceleration factors
    - Module life prediction
    - Module (electrochemical) qualification test

PRECEDING PAGE BLANK NOT FILMED

The Relationship Between Leakage Current and Electrochemical Damage
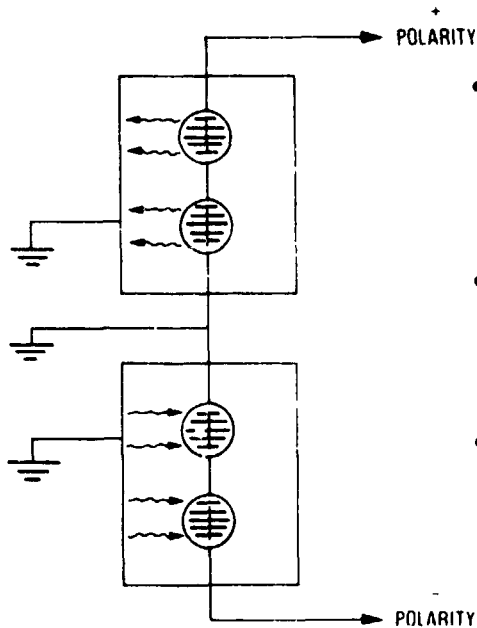
- Cell string and frame behave as opposite-polarity electrodes; the intervening pottant behaves as a solid-state electrolyte

- Module leakage current increases with increasing temperature and relative humidity

- Observed and electrically measured electrochemical damage increases with increasing accumulated charge transfer

Electrochemical Damage: Positive and Negative Polarity

■ **Positive polarity**
  - **Metallization dissolution and migration (from cell to frame)**
  - Cathodic dendrite formation (from frame to cell)
  - Evolution of gas at cathode (frame)

■ **Negative polarity**
  - **Evolution of gas at cathode (cell) between metallization and silicon substrate -- metallization delamination**
  - **Formation of corrosion salts at anode (frame)**

■ **Both polarities**
  - **Reduction of cell power output**
  - **Increase in cell series resistance**

Power Reduction and Series Resistance vs Time, Showing Effects of Polarity and Non-Metallized Substrate Films
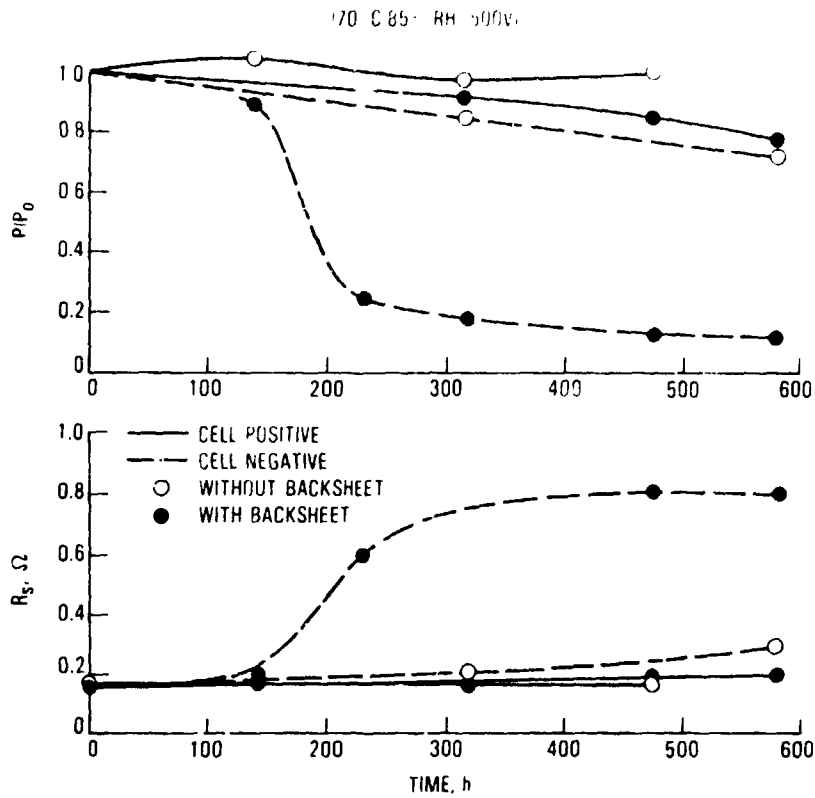
Influence of Electrochemical Damage
on Cell I-V Performance

(UNPROTECTED PVB Ag METALLIZATION)
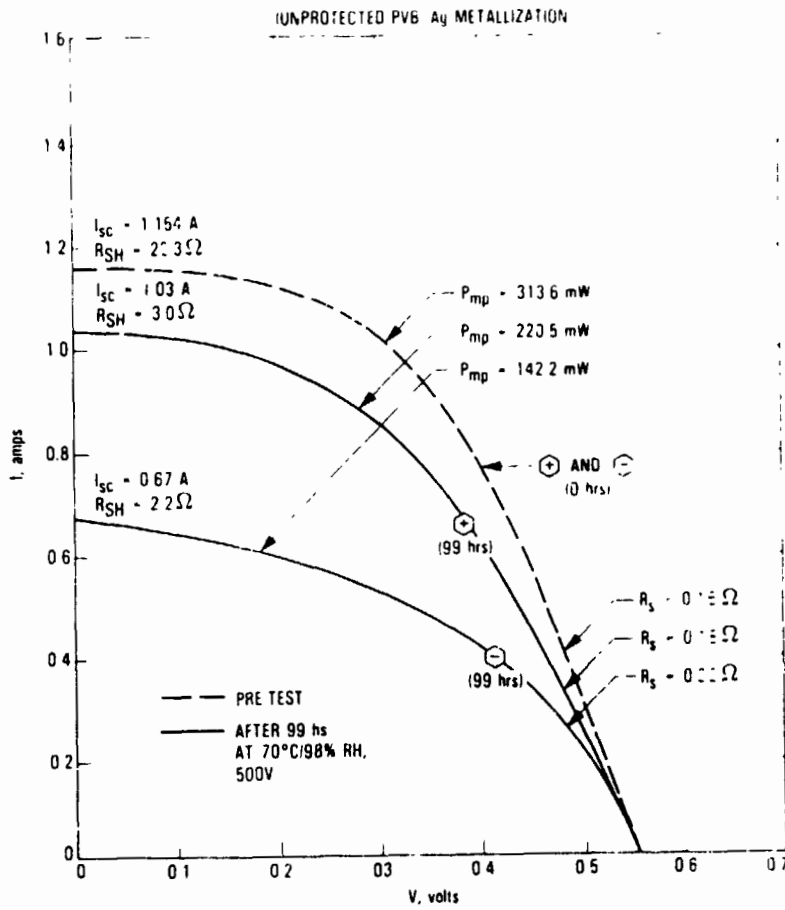
Observed Current Paths
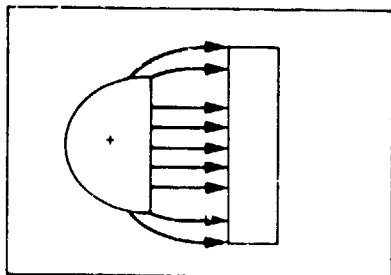
- Metallization ions follow electric field lines

GLASS

POTTANT
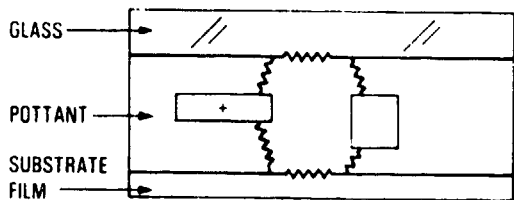
SUBSTRATE
FILM

- Metallization ions often proceed to, and then along, interfacial surfaces

Current Response for Small-Gap Samples and the Effect of Non-Metallized Polymer Substrate Films

Ag PRINT CELL, Al FRAME, PVB, 55-MIL GAP (70°C/85% RH)

500 V

NO TEDLAR BACK SHEET

TEDLAR BACK SHEET

TIME, h
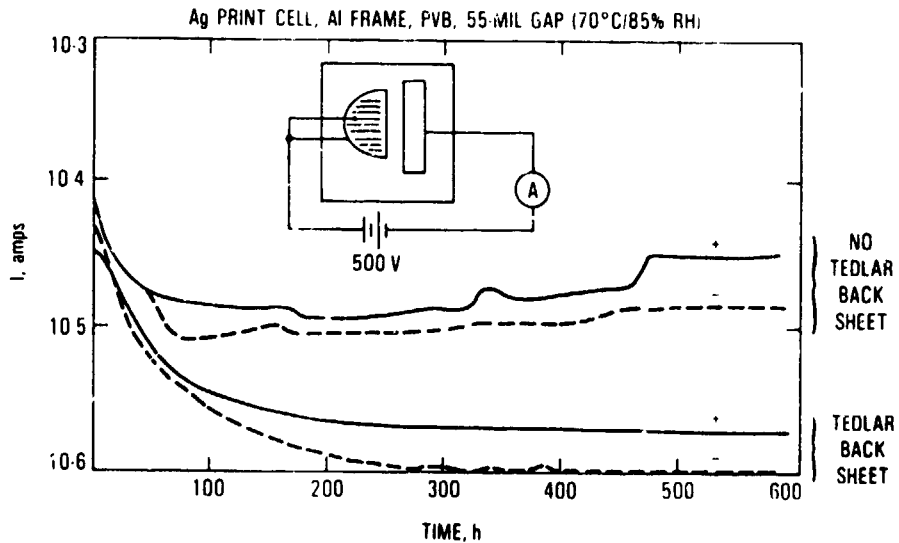
Current Response for Large-Gap Sample

Ag PRINT CELL, Al FRAME, PVB, 500 MIL GAP (70°C/85% RH, 500 V)
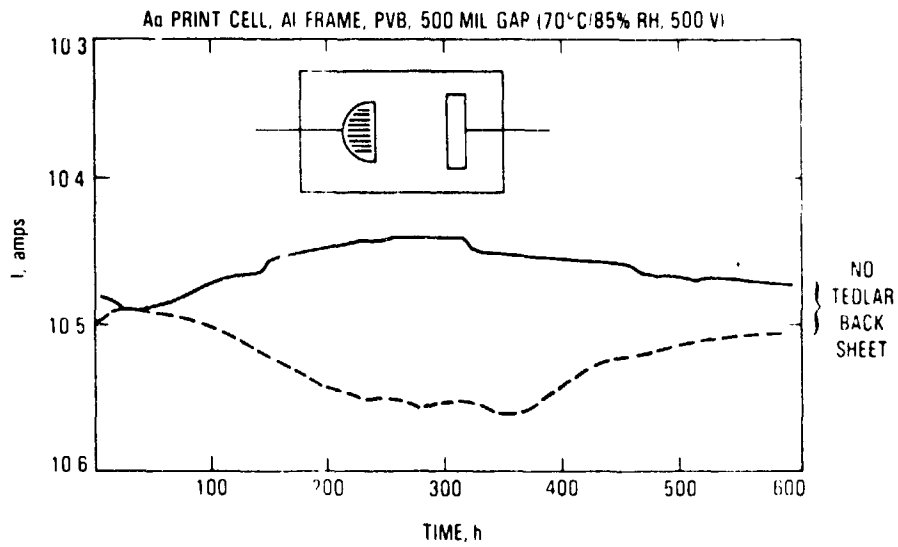
Current Response of Minimodules, Comparing PVB and EVA Encapsulants

85°C/85% RH, 500 V
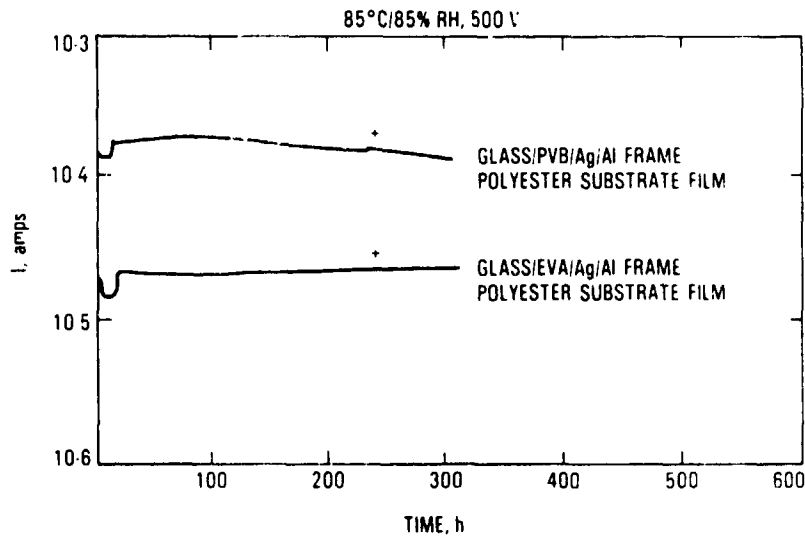
Physical Deductions

- At large cell-frame gaps and/or low voltages, capacitive charging and polarization currents are absent because
    - Interelectrode capacitance is small
    - Electrode forces on interelectrode dipoles are weak

- Equilibrium current is independent of gap, other things being equal, because of the relatively low-resistance surface-active paths

- The magnitude of the equilibrium current is directly proportional to the pottant volume conductivity (actually, ion mobility) along paths in the bulk of the pottant

- Independent of voltage breakdown considerations, substrate polymer films provide higher surface resistance paths, hence lower equilibrium current levels

Electrochemical Damage: Laboratory-Field Equivalence

- Assumption: Equal quantities of charge transfer in the field and test environments produce equivalent amounts of electrochemical degradation

- Ohm's law: $Q = I\tau = V \cdot (\sigma\tau) \cdot (\text{geometric terms})$

- Field time in years equivalent to τ_T hours at test conditions:

$$Y_{EQ} \approx \frac{Q_T}{Q_F} = \left(\frac{V_T}{V_F}\right) \cdot \frac{(\sigma\tau)_T}{\left(\sum \sigma_i \tau_i\right)_F}$$

ratio of test to field conductivity — time product

test to field voltage ratio

test to field charge transfer unit

- Field values are based on yearly compilations from reduced SOLMET weather data

Test Chamber Time Equivalent To 30 Years In The Field

Test Chamber Time τ Equivalent to 30 Years in the Field: EVA
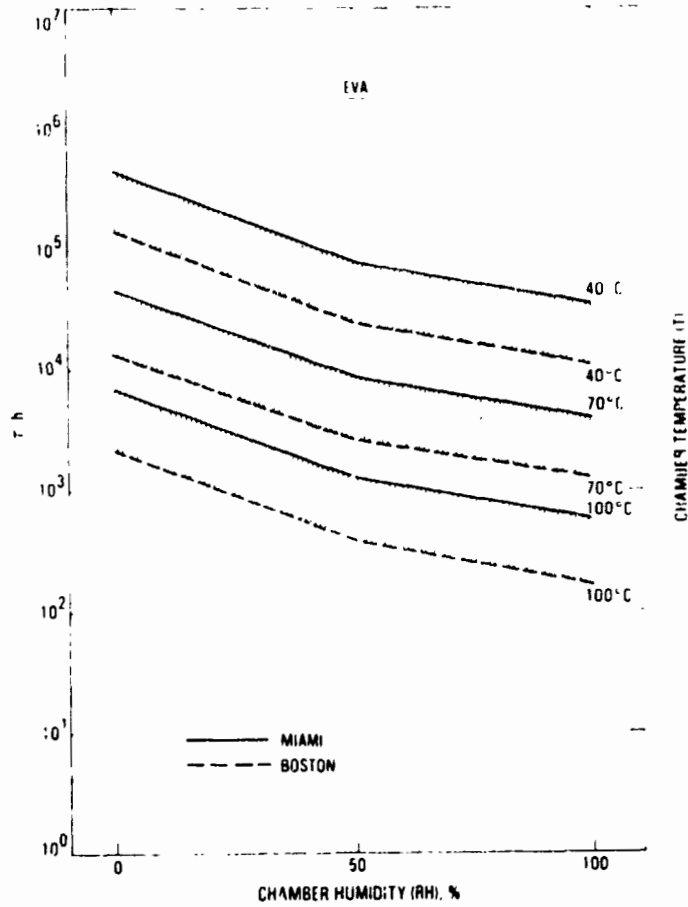
Module Life Prediction

- Median cell failures are experimentally determined to occur with the passage of about $Q_T = 1 - 2$ C/cm of charge between cell and frame

- Median time to cell failure is $T_M = \dfrac{Q_T}{Q_F}$

    - Calculate charge transfer in the field, Q_F, using known dependencies on T and RH and SOLMET weather data

    - Assume a log-normal distribution of cell failures

- Calculate average module field failure rate

    - Without replacement (23rd PIM)

    - With replacement (this PIM)

Power Output Reduction vs Accumulated Charge Transfer
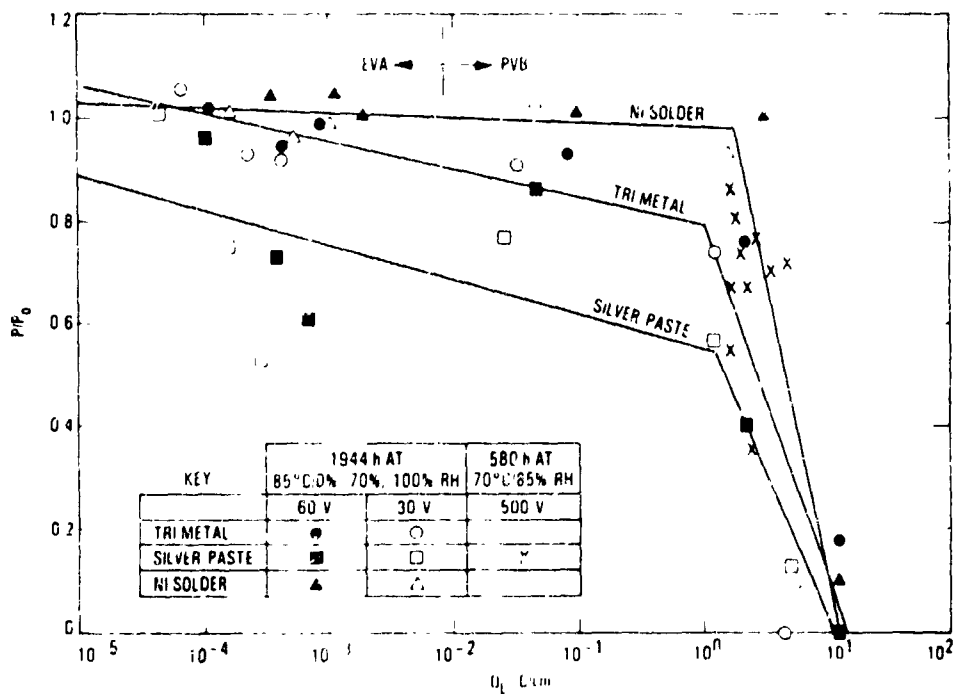
Module Failure Rate vs Time for 4 × 4-ft-Square-Celled Modules at Miami
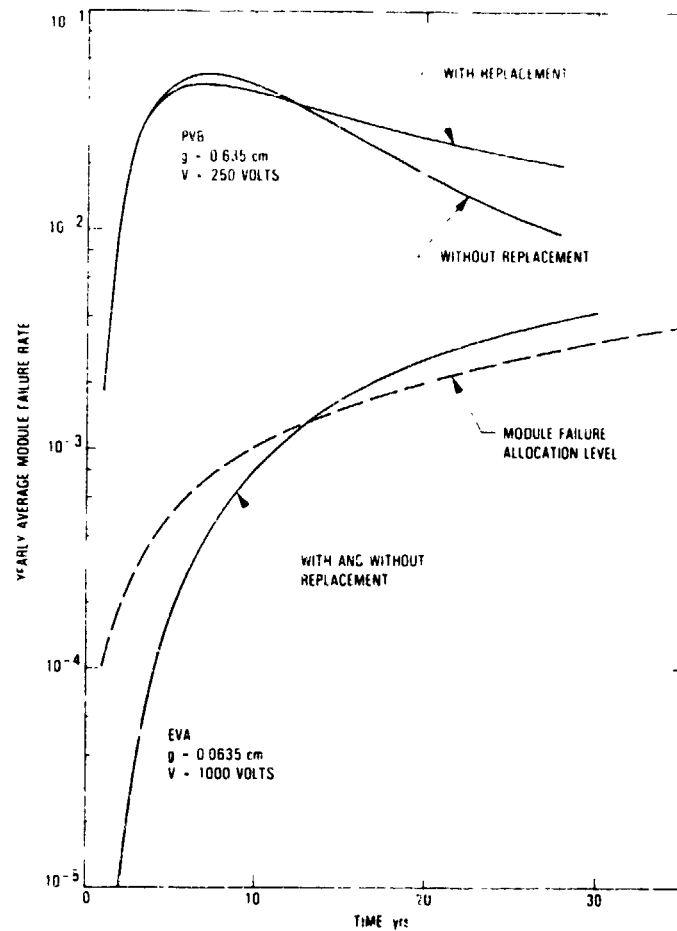
Conclusions

- Calculated failure rates for unprotected PVB modules exceed allocation levels

- Failure rates for EVA modules fall within allocation guidelines

- Added mathematical rigor engendered by considering that replacement minimally impacts computed module failure rate results

Block V Qualification Test Temperature-Humidity Profile
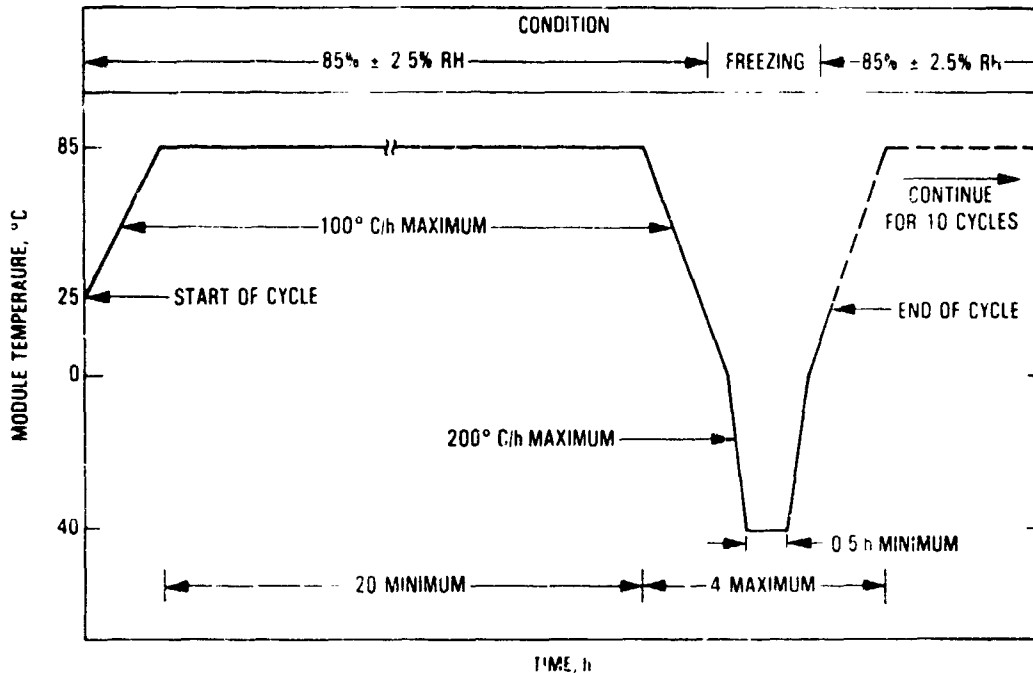
Electrochemical Qualification Test Results: 500 Vdc, 85°C/85% RH for 20 h, −40°C for 4 h, 10 24-h Cycles

Sample	Polarity	Metallization	Encapsulation	Metal Substrate Foil?	Q200, C/cm	P/P₀	I/I₀	Equivalent 500-V Field Exposure Miami, yr*
MO 5107	P	Pd/Ni-solder	PVB	Y	1.17	0.95	0.91	1.8
PW 5222	P	Ni-solder	PVB	Y	1.53	0.97	0.96	1.8
AS 200307	P	Print Ag	PVB	Y	3.61	0.96	0.96	1.8
AS 107461	P	Print Ag	PVB	N	2.91	0.17	0.32	84.0
MO 5117	N	Pd/Ni-solder	PVB	Y	0.737	0.79	0.97	1.8
PW 5224	N	Ni-solder	PVB	Y	0.0034	1.0	1.0	18
AS 200303	N	Print Ag	PVB	Y	0.181	0.99	1.01	1.8
AS 107449	N	Print Ag	PVB	N	1.41	0.88	0.94	84.0
MS 4887	P	Ni-Cu-Sn	EVA	Y	0.031	0.98	0.99	1.0
SP 58494	P	Ni-Sn	EVA	Y	0.072	0.93	0.98	1.0
SO 009	P	Print Ag	EVA	N	0.202	0.9	0.8	4.3
AS 022	P	Print Ag	EVA	N	0.534	0.96	0.97	4.3
MS 4954	N	Ni-Cu-Sn	EVA	Y	0.052	0.53	1.0	1.0
SP 58487	N	Ni-Sn	EVA	Y	0.006	1.06	0.98	1.0
SO 011	N	Print Ag	EVA	N	0.346	0.73	0.9	4.3
AS 021	N	Print Ag	EVA	N	0.205	0.94	0.96	4.3

* Values in last column assume that foil modules are water-free (temperature acceleration only) and that non-foil modules instantly track the environmental temperature and humidity

Conclusions

- An equivalence relationship for electrochemical degradation, based upon equal charge transfer levels, establishes a correspondence between years in the field and hours in an accelerated stress test chamber

- Adding voltage to the Block V temperature-humidity test provides an electrochemical qualification test of modules
  - Equivalent to 1 to 2 years for foil-back modules
  - Equivalent to 4 to 80 years for non-foil-back modules
  - Equivalent field years are inversely proportional to the test voltage

- Temperature acceleration ratios are similar for a wide variety of module constructions and materials (factor of 2 per 10°C)

- Humidity acceleration ratios vary considerably (40 to 1), depending upon module construction and materials

Summary and Conclusions

- The extent of electrochemical damage is dependent on the integrated leakage current

- PV electrochemical degradation mechanisms in the two polarities are different
  - Degradation rates in the two polarities are of the same order of magnitude
  - Center-tapped grounded arrays appear to be a preferred system configuration to minimize electrochemical degradation

- There is encouraging agreement between theory and experiment in regard to leakage current response to applied voltage, gap magnitude, and encapsulant ion mobility

Summary and Conclusions (Cont'd)

- Path resistance considerations suggest the use of thicker pottant layers and polymer substrate films to reduce equilibrium leakage current values

  - A metallized substrate layer, if used, should be isolated from the pottant and the frame by polyester layers

  - EVA modules appear to be consistent with 30-year-life allocation levels for electrochemical damage

- Temperature acceleration factors are well behaved and moderately well understood; humidity acceleration factors vary radically with module construction and materials and require additional research

Additional Work Required to Finalize Understanding of Photovoltaic Electrochemical Corrosion

- Quantify temperature-humidity dependency of equilibrium leakage currents

- Quantify temperature-humidity levels of encapsulants in fielded modules

Leakage Current Response Mechanisms
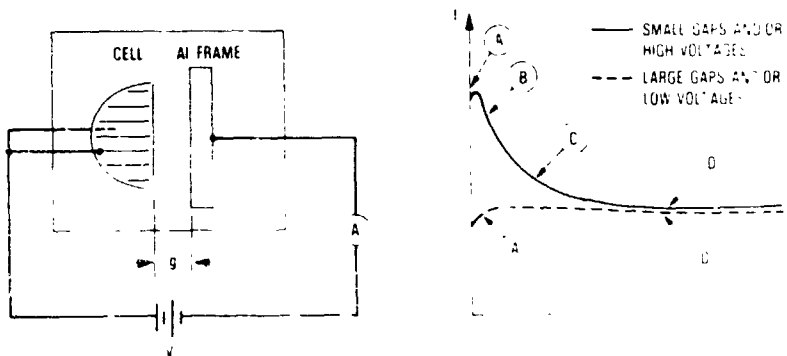
Current response characteristics

(A) ⟶ Water absorption current (impurity ion removal)

(B) ⟶ Capacitive charging current

(C) ⟶ Polarization currents (polymer and water dipoles)

(D) ⟶ Equilibrium ion current (metallization ion diffusion)

POLYMER-WATER INTERACTION STUDIES

WILKES COLLEGE

John Orehotsky

Corrosion in Solar Cells

REQUIREMENTS FOR CORROSION

- DISSIMILAR MATERIALS

- CELL-TO-CELL POTENTIAL DIFFERENCES

- ELECTRICALLY CONNECTED CELLS

- IONIC CONDUCTING ELECTROLYTE (POLYMER)

Ions in Polymers

- ABSORBED WATER IONS

- POLYMER IONS

- PLASTICIZER IONS

- UV ABSORBER AND STABILIZER IONS

- CROSS – LINKING AGENT IONS

- CHAIN SCISSION (IONIZING RADIATION) IONS

Studies

I – WATER ABSORPTION AND DESORPTION
KINETICS IN EVA AND PVB

II – HUMIDITY DEPENDENCE OF ELECTRICAL
PROPERTIES OF EVA AND PVB

III – PLASTICIZER EFFECTS IN PVB

IV – RADIATION EFFECTS IN PVB AND EVA

WATER ABSORPTION AND DESORPTION KINETICS IN PVB AND EVA

Weight Characteristics of EVA During Absorption and Desorption

Temperature Humidity Conditions T(°C)/H(%)	Woe: Expected Starting Weight (gms)	Woa: Measured Starting Weight (gms)	Wao: Measured Final Weight (gms)	Wao-Woa: Apparent Weight Change (gms)	Wao-Woe: True Weight Change (gms)	Woa-Woe: Weight of Initially Formed Surface Layer (gms)	Woe-Woa: Weight of Initially Lost Surface Layer (gms)
88/0→88/100 absorption	1.600*	1.691	2.366	.675	.746	.091	—
88/100→88/0 desorption	2.366	1.750	1.599	.151	.767	—	.616
75/0→75/100 absorption	1.821*	1.914	2.804	.890	.983	.093	—
75/100→75/0 desorption	2.804	2.388	1.824	.564	.980	—	.416
60/0→60/100 absorption	1.520*	1.575	2.593	1.018	1.073	.55	—
60/100→60/0 desorption	2.593	2.092	1.519	.573	1.074	—	.501
50/0→50/100 absorption	1.600*	1.647	2.565	.918	.965	.047	—
50/100→50/0 desorption	2.565	2.198	1.602	.596	.963	—	.367
40/0→40/100 absorption	1.608*	1.613	2.295	.682	.695	.013	—
40/100→40/0 desorption	2.295	2.149	1.603	.546	.692	—	.146

Original weight of desiccated dried sample.

208

TEMPERATURE DEPENDENCE OF THE NORMALIZED WEIGHT FOR THE INITIALLY FORMED SURFACED LAYER OF WATER DURING WATER ABSORPTION IN EVA
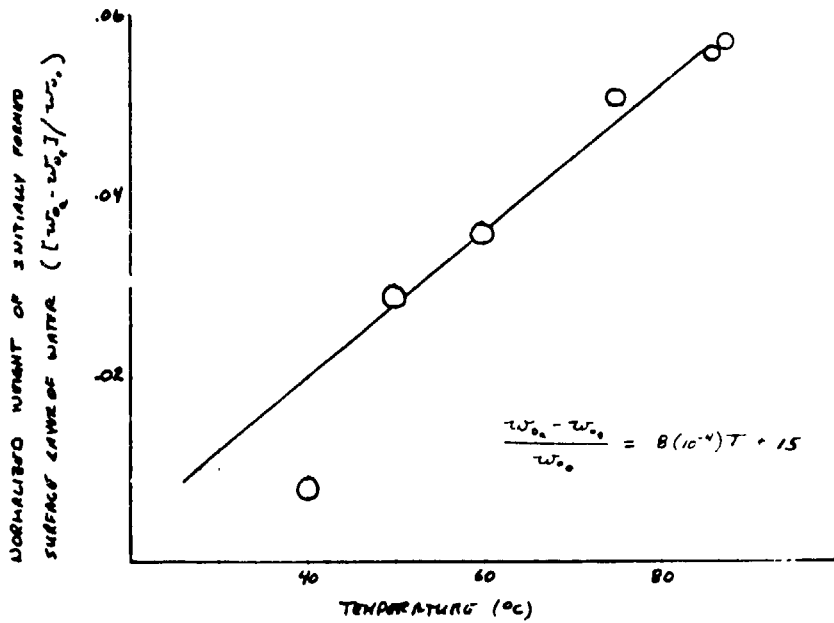
Temperature Dependence of the Normalized Weight
for the Initially Lost Surface Layer of
Water During Desorption in EVA

$$\frac{w_{o_e} - w_{o_e}}{w_{o_e}} = 3.7(10^{-3})T + 20$$
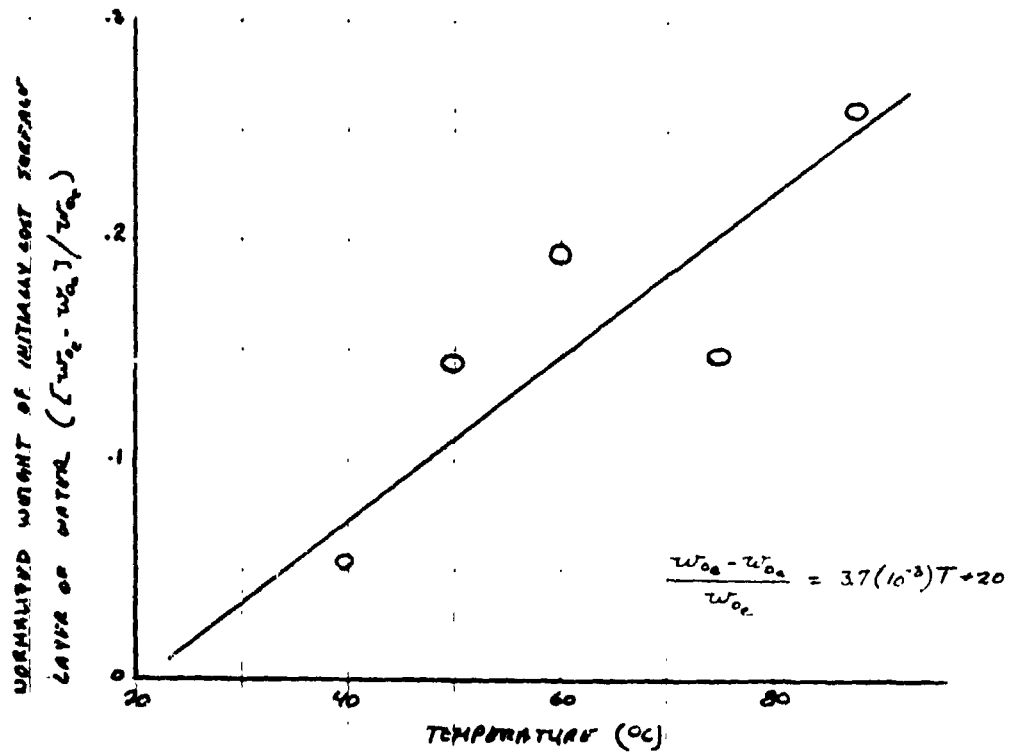
Normalized Weight Change During Absorption and Desorption in EVA
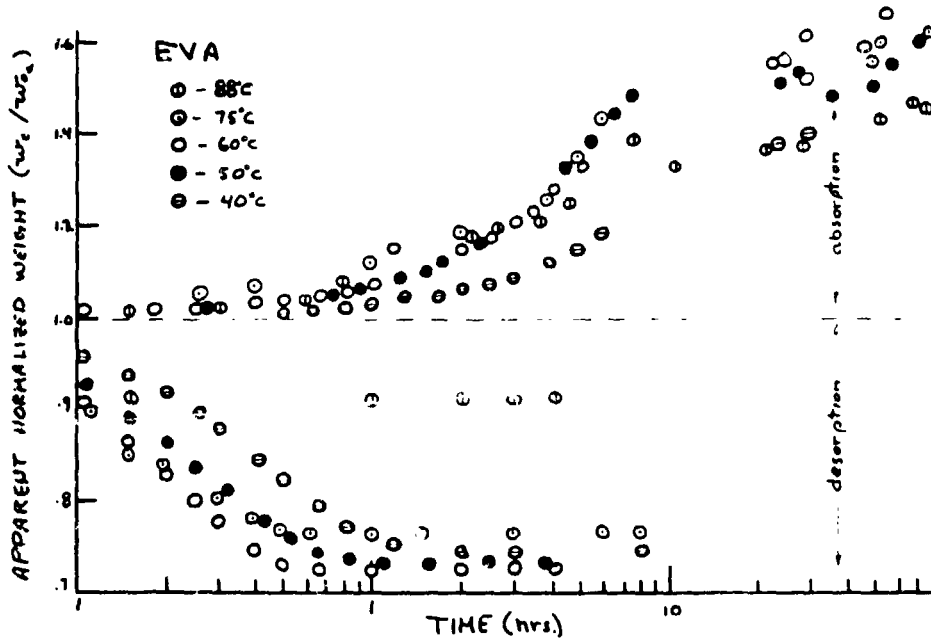
Time Dependence of Normalized Weight Gain in EVA Due to Water Absorption (40°C)
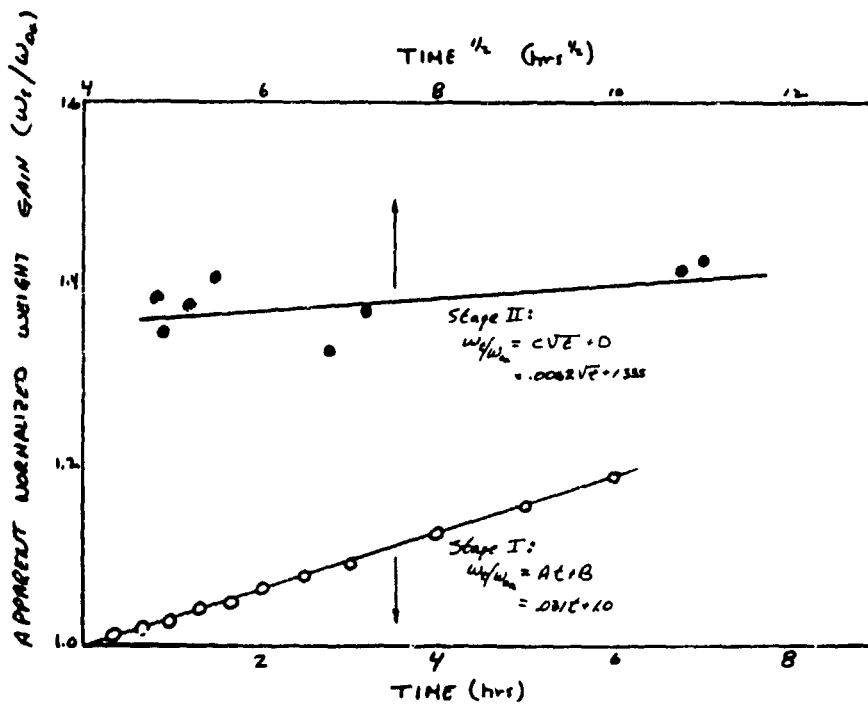
Time Dependence of Normalized Weight Loss
in EVA Due to Water Desorption (40°C)
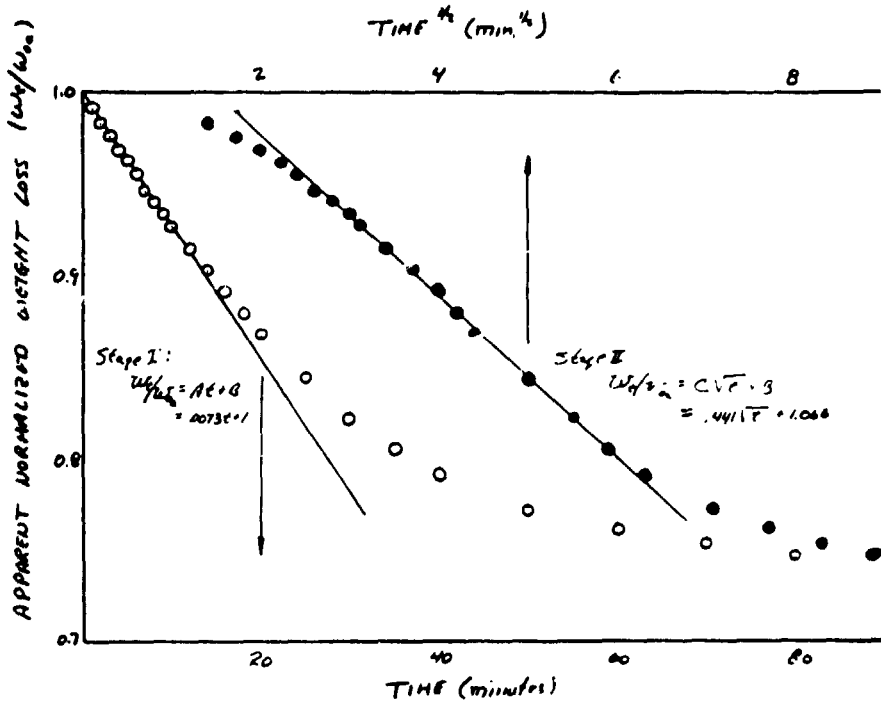
Characterizing Rate Constraints for Water Absorption and Desorption in EVA

	STAGE I		STAGE II	
	$\frac{Wt}{Woa}$	$At + B$	$\frac{W_t}{W_{oa}}$	$C_t{}^{1/2} + D$
Temp.	A	B	C	D
	(hrs.$^{-1}$)	**Absorption**	(hrs.$^{-1/2}$)	
88°C	.080	1.0	.0190	1.24?
75°C	.080	1.0	.0125	1.4?0
60°C	.068	1.0	.010	1.5?0
50°C	.071	1.0	.0082	1.440
40°C	.031	1.0	.0062	1.?5

	Desorption			
	(min.$^{-1}$)		(min.$^{-1/2}$)	
88°C	.030	1.0	—	—
75°C	.021	1.0	.0723	1.?6?
60°C	.0175	1.0	.0690	1.?70
50°C	.0130	1.0	.0605	1.?71
40°C	.0073	1.0	.441	1.?6?

Temperature Dependence of the Rate Constant for First-Stage Water Absorption and Desorption in EVA
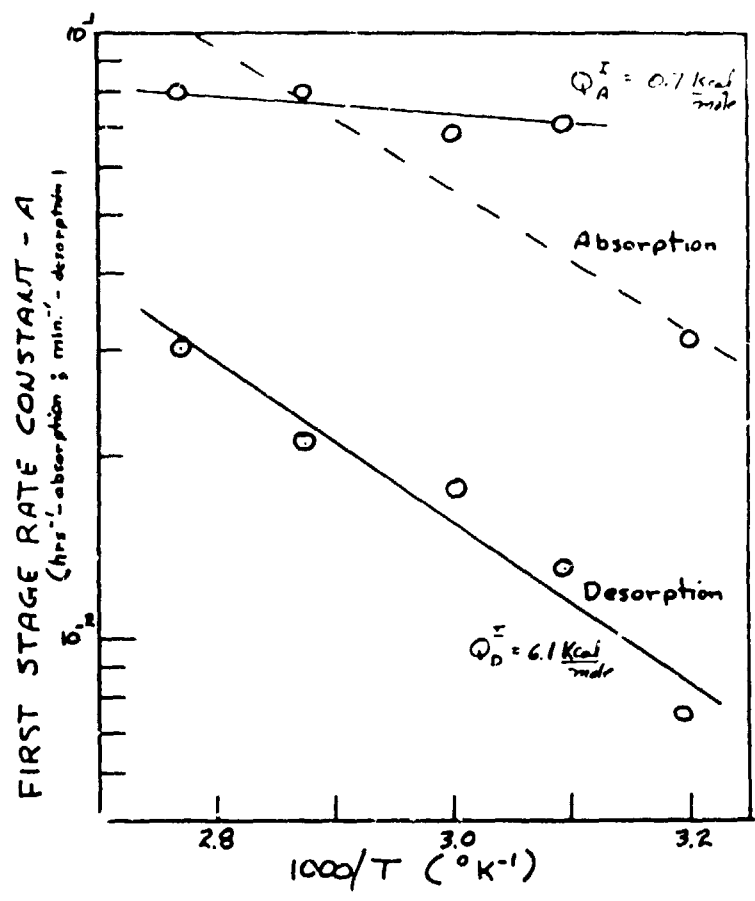
Temperature Dependence of the Rate Constant for the Second-Stage Water Absorption and Desorption in EVA

$$Q_D^{II} = 5.1 \frac{kcal}{mole}$$

Desorption

$$Q_A^{II} = 5.1 \frac{kcal}{mole}$$

Absorption

SECOND STAGE RATE CONSTANT - c (hrs$^{-1/2}$ - absorption ; min.$^{-1/2}$ - desorption)

$1000/T \ (^\circ K^{-1})$
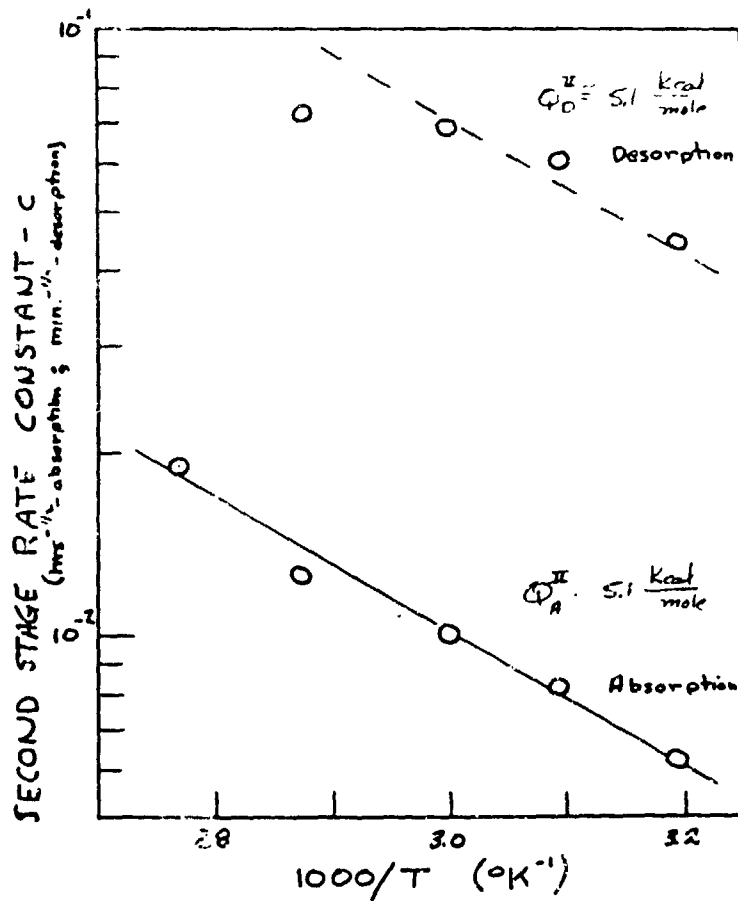
Activation Energies and Pre-Exponential Factors for Water Absorption and Desorption in EVA

STAGE I ← Surface Film

	Q^I (kcal/mole)	A_o (min.$^{-1}$)
Absorption	0.7 (=Q^I_A)	.0033 (0.2 hrs.$^{-1}$)
Desorption	6.1 (=Q^I_D)	167

STAGE II - Volume Diffusion

	Q^{II} (Kcal/mole)	C_o (min$^{-\frac{1}{2}}$)
Absorption	5.1 (=Q^{II}_A)	3 (23 hrs. $^{-\frac{1}{2}}$)
Desorption	5.1 (=Q^{II}_D)	159

EVA Water Absorption Model

SEQUENTIAL
REACTION STEPS:

STEP 1: CONDENSATION OF ATMOSPHERIC WATER AS A MONOLAYER ON SURFACE

REACTION: H_2O (in atmosphere) $\longrightarrow$ H_2O (monolayer on surface)

SCHEMATIC
ILLUSTRATION: H_2O vapor + | dehydr. polymer | $\longrightarrow$ | dehydr. polymer | adsorbed water monolayer
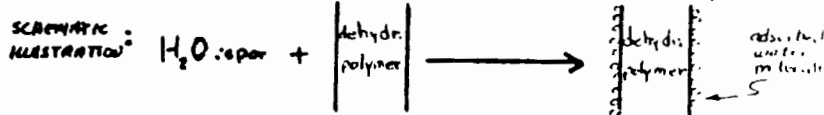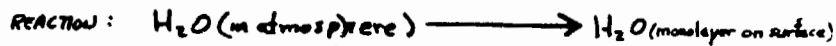
STEP 2a: CONDENSATION OF SUCCESSIVE MONOLAYERS TO FORM A SURFACE FILM

REACTION: H_2O (in atm.) + H_2O (monolayer) $\longrightarrow$ H_2O (surface film)

SCHEMATIC
ILLUSTRATION: H_2O vapor + | dehydr. polymer | $\longrightarrow$ | dehydr. polymer | water film
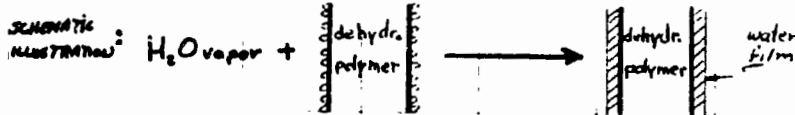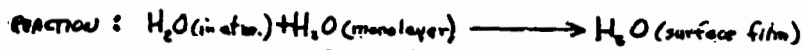
STEP 2b: DIFFUSION OF MONOLAYER INTO POLYMER

REACTION: H_2O (monolayer on surface) $\longrightarrow$ H_2O (in polymer)

SCHEMATIC
ILLUSTRATION: | dehydr. polymer | $\longrightarrow$ | hydrated polymer |

OVERALL REACTION:

H_2O (in atmosphere) $\longrightarrow$ H_2O (in polymer and in surface film)

H_2O vapor + | dehydr. polymer | $\longrightarrow$ | hydrated polymer |

EVA Water Desorption Model

SEQUENTIAL
REACTION STEPS:

STEP 1: EVAPORATION OF THE ADSORBED WATER FILM ON SURFACE

REACTION: H_2O (in polymer and in surface film) $\longrightarrow H_2O$ (in polymer) + H_2O (in ...

SCHEMATIC
ILLUSTRATION
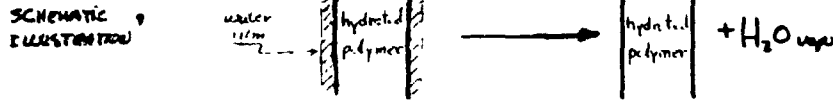
STEP 2: VOLUME DIFFUSION OF WATER OUT OF POLYMER TO SURFACE

REACTION: H_2O (in polymer) $\longrightarrow H_2O$ (monolayer on surface)

SCHEMATIC
ILLUSTRATION
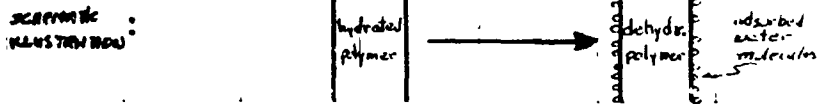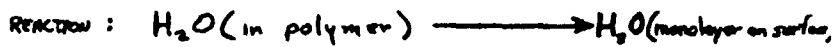
STEP 3: EVAPORATION OF WATER MONOLAYER ON SURFACE

REACTION: H_2O (monolayer on surface) $\longrightarrow H_2O$ (in atmos.)

SCHEMATIC
ILLUSTRATION

OVERALL REACTION:

H_2O (in polymer and in surface film) $\longrightarrow H_2O$ (in atmos.)
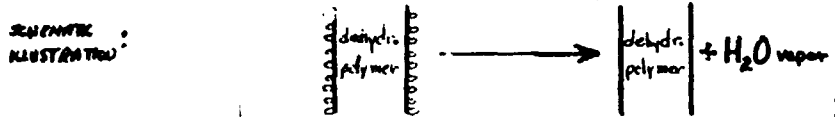
Weight-Gain Characteristics of EVA in Water Absorption
Due to Surface-Film Formation and Volume Absorption

Temperature	W_∞ Woa: Total normalized weight gain	W_∞: total weight gain per gram EVA (gms)	Ws/Woa: Total Normalized Weight Gain Due to Surface Film Formation (gms)	Ws: Weight Gain per Gram. EVA due to Surface film Formation (gms)	Wv: Weight Gain per Gram. EVA Due to Volume Absorption (gms)	W%: Weight Percent Solubility of water In EVA (%)
88 °C	1.45	.45	1.285*	.285	.195	16.5
75 °C	1.70	.70	1.160^	.460	.240	19.5
60 °C	1.65	.65	1.570*	.570	.110	4.5
50 °C	1.58	.58	1.490*	.430	.040	8.2
40 °C	1.42	.42	1.335*	.335	.085	7.5

* Determined from data in Table I

^ Taken from extrapolated D intercept values in Table II

Solubility of H_2O in EVA as a Function of Temperature

218
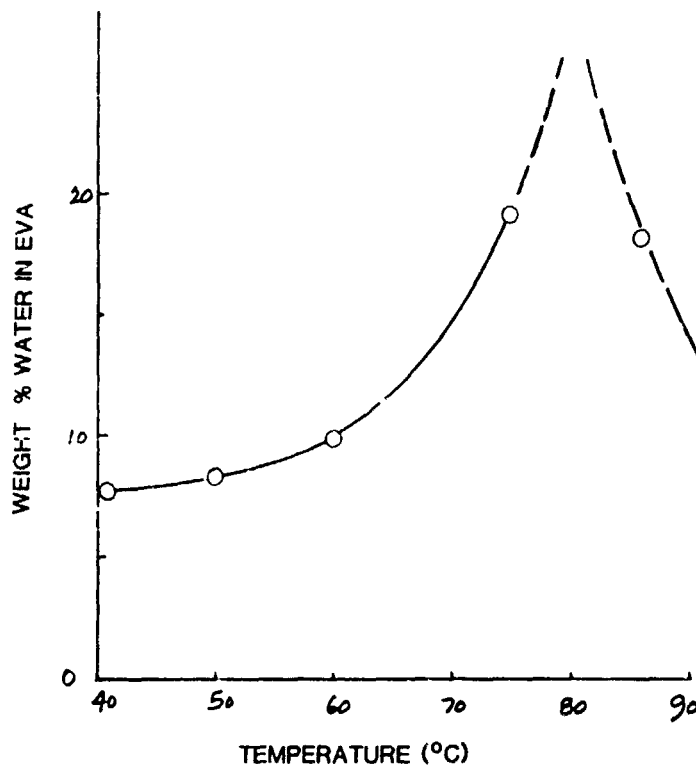
Equilibrium Thickness of Absorbed Water Film on EVA as a Function of Temperature
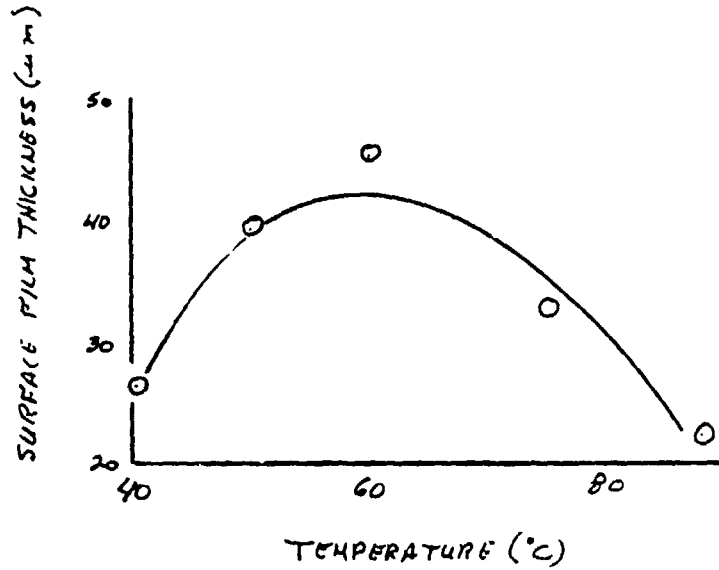
Energy Barrier for Condensation and Evaporation During the Stage I Kinetic Response in Water Absorption and Desorption on EVA

CONDEUSATION

EVAPORATION
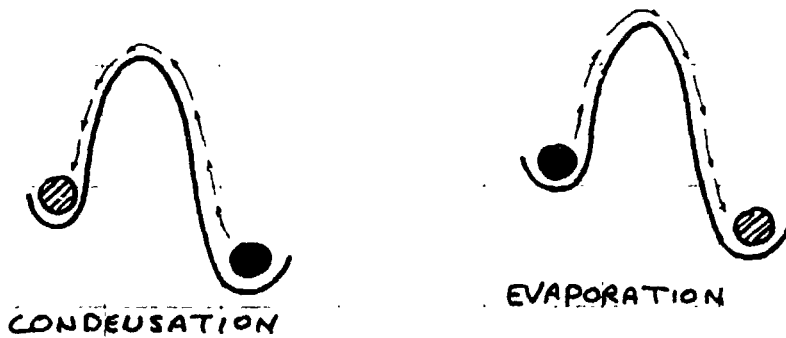
Water Interaction Comparison of EVA and PVB

	PVB	EVA
WATER SOLUBILITY AT 60°C (w/o)	38	10
ACTIVATION ENERGIES (Kcal/mole)		
ABSORPTION		
STAGE I	4.2	0.7
STAGE II	6.3	5.1
DESORPTION		
STAGE I	16	6.1
STAGE II	7.1	5.1
STAGE I ABSORPTION RATE OF WATER PER GRAM OF POLYMER AT 25°C (gms/hr)	$2.5(10^{-4})$	$6.1(10^{-2})$
STAGE I DESORPTION RATE OF WATER PER GRAM OF POLYMER AT 25°C (gms/hr)	$9.9(10^{-2})$	$5.5(10^{-3})$

HUMIDITY DEPENDENCE OF THE ELECTRICAL
PROPERTIES OF EVA AND PVB

Current Response to a 390-V Step Voltage for PVB (80°C)
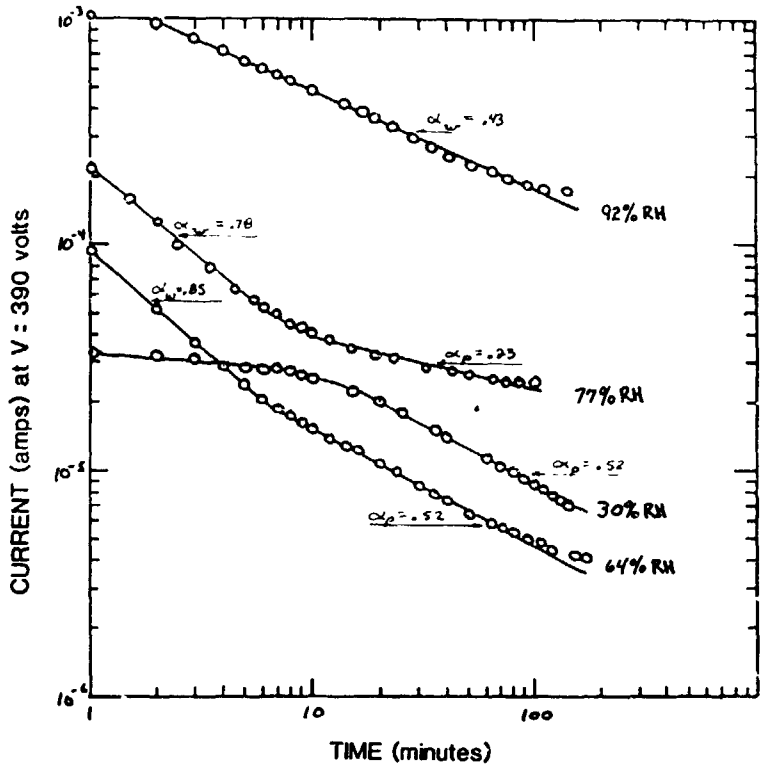
Current Response to a 390-V Step Voltage for PVB (68°C)
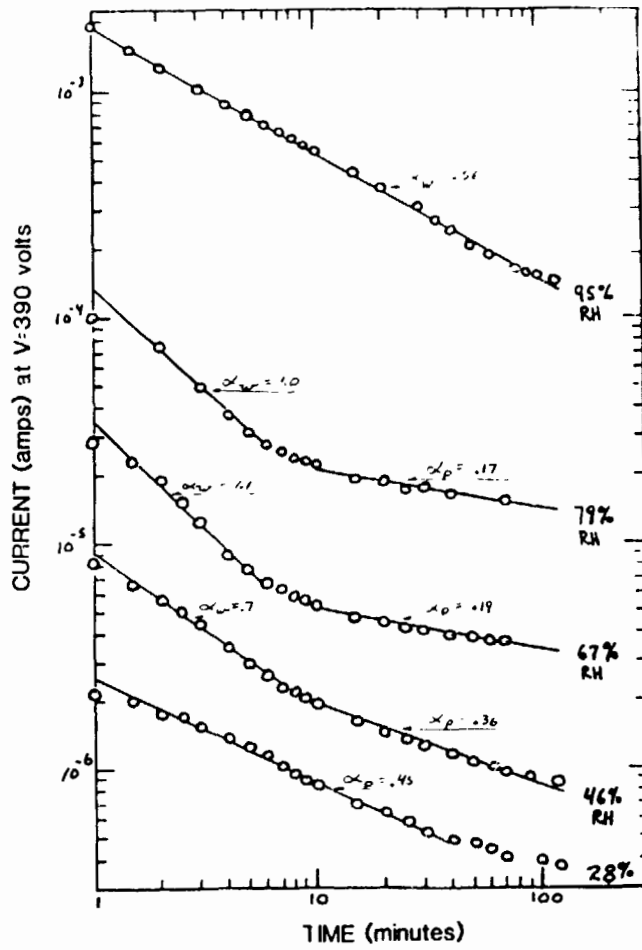
Initial Transient Behavior for the Current Response
to a 390-V Step Voltage for PVB (68°C)
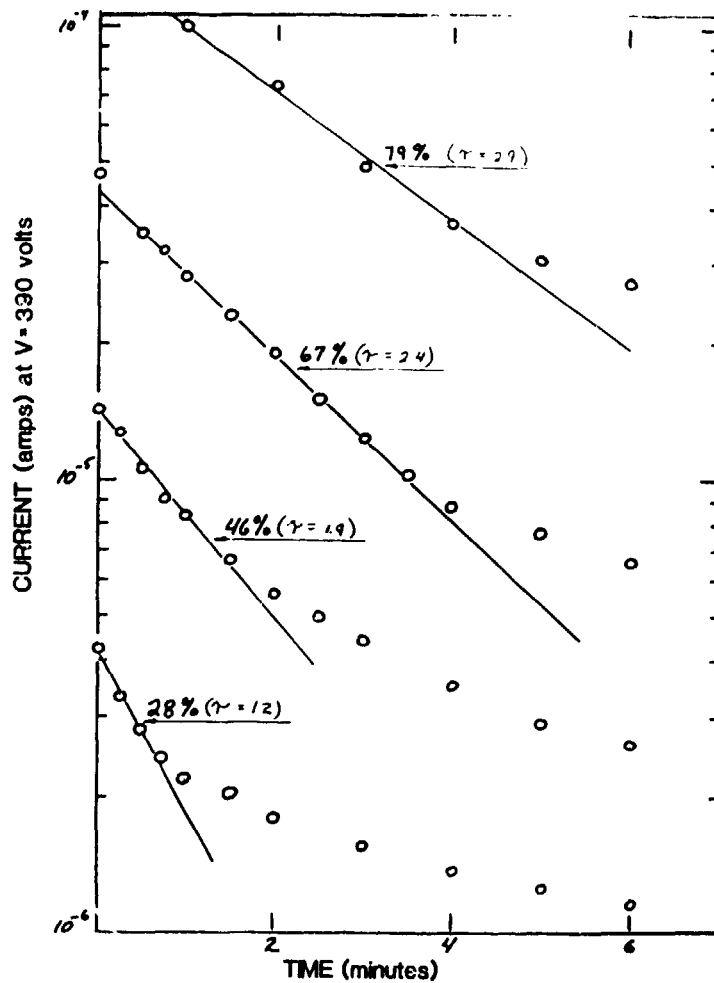
Proposed Current Response to a Step Voltage

CAPACITIVE CHARGING

$$I_c = 390 \exp(-t/\tau)/R_o$$

$R_o \sim H^{-1}$

$\tau \sim H^{-1}$

WATER POLARIZATION

$$I_w = I_{w_o} t^{-\alpha_w}$$

$I_{w_o} \sim H$

$\alpha_w \neq fct(H)$

POLYMER POLARIZATION

$$I_p = I_{p_o} t^{-\alpha_p}$$

$I_{p_o} \neq fct(H)$

$\alpha_p \neq fct(H)$

IONIC MIGRATION

$$I_i = 390/R_i$$

$R_i \sim H^{-1}$

RESPONSE CURRENT — TIME

$I_{w_o} \cdot I_{p_o} \cdot I_i$

I_w

$I_{p_o} \cdot I_i$

I_p

I_i
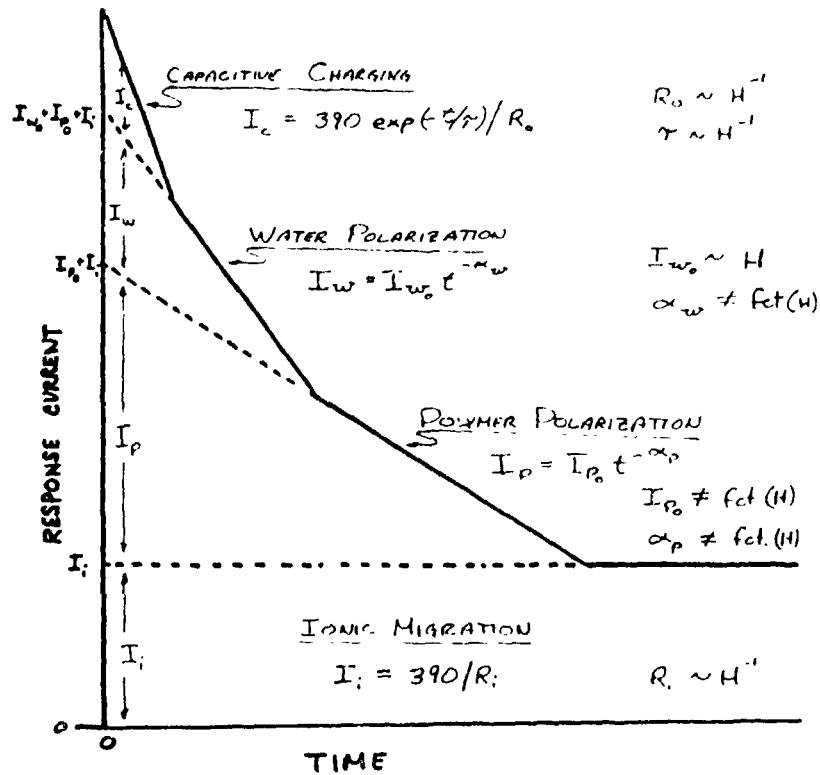
Current Response Parameters for PVB (80°C)

RELATIVE HUMIDITY (%)	TIME RANGE (min.)	CURRENT COMPONENTS	TIME DEPENDENCE $I = A\,t^{-\alpha}$		I_{w_o}	I_{p_o}	I_i
			$A\ (=I_{w_o}, I_{p_o}, I_i)$	α			
92	$0 < t < 100$	$I_w \cdot I_i$	$1.3(10^{-3})$	$.43(=\alpha_w)$	$1.2(10^{-3})$	—	—
	$t > 100$	I_i	—	—	—	—	$1.7(10^{-4})$
77	$0 < t < 10$	$I_w \cdot I_p \cdot I_i$	$2.1(10^{-4})$	$.78(=\alpha_w)$	$1.5(10^{-4})$	—	—
	$10 < t < 100$	$I_p \cdot I_i$	$6.5(10^{-5})$	$.23(=\alpha_p)$	—	$4.1(10^{-5})$	—
	$t > 100$	I_i	—	—	—	—	$2.5(10^{-5})$
64	$0 < t < 7$	$I_w \cdot I_p \cdot I_i$	$9.5(10^{-5})$	$.85(=\alpha_w)$	$4(10^{-5})$	—	—
	$7 < t < 100$	$I_p \cdot I_i$	$5.0(10^{-5})$	$.52(=\alpha_p)$	—	$4.6(10^{-5})$	—
	$t > 100$	I_i	—	—	—	—	$4(10^{-6})$
30	$20 < t < 100$	$I_p \cdot I_i$	$4.7(10^{-5})$	$.52(=\alpha_p)$	—	—	—
	$t > 100$	I_i	—	—	—	—	$7(10^{-8})$

Current Response Parameters for PVB (68°C)

RELATIVE HUMIDITY (%)	TIME RANGE (min)	CURRENT COMPONENTS	I_i (amps)	R_i $\cdot 3\%/I_i$ (Ω)	TIME DEPENDENCE			
					$I = At^{-\alpha}$		$I = [3\%/R_o][\exp(-t/\tau)]$	
					A (amps)	α	$3\%/R_o(amp)$ $R_o(\Omega)$	τ (min)
95	0 < t < 100	$I_w + I_i$			$1.9(n^{-1})$	$.56(=\kappa_w)$	— —	—
	t > 100	I_i	$2(n^{-4})$	$1.9(n^6)$				
79	0 < t < 4	$I_c + I_w + I_p + I_i$			—	—	$1.4(10^{-1})$ $2.8(n^6)$	2.9
	2 < t < 6	$I_w + I_p + I_i$			$1.4(10^{-1})$	$1.0(=\kappa_w)$	— —	—
	10 < t < 100	$I_p + I_i$			$3.2(n^{-5})$	$0.17(=\kappa_p)$		
	t > 100	I_i	$1.5(n^{-5})$	$2.6(n^7)$				
67	0 < t < 4	$I_c + I_w + I_p + I_i$			—	—	$4.3(10^{-1})$ $9.0(10^6)$	2.4
	2 < t < 6	$I_w + I_p + I_i$			$6.9(10^{-5})$	$1.1(=\kappa_w)$	— —	—
	10 < t < 100	$I_p + I_i$			$8.0(10^{-5})$	$0.14(=\kappa_p)$		
	t > 100	I_i	$3(n^{-5})$	$1.3(n^8)$				
46	0 < t < 2	$I_c + I_w + I_p + I_i$			—	—	$1.4(10^{-1})$ $2.8(10^7)$	1.9
	2 < t < 10	$I_w + I_p + I_i$			$9.4(10^{-5})$	$0.72(=\kappa_w)$	— —	—
	10 < t < 100	$I_p + I_i$			$4.5(10^{-5})$	$0.36(=\kappa_p)$		
	t > 100	I_i	$8(n^{-7})$	$4.9(n^8)$				
28	0 < t < 1	$I_c + I_p + I_i$			—	—	$4.2(10^{-1})$ $9.2(10^7)$	1.2
	2 < t < 50	$I_p + I_i$			$2.4(10^{-4})$	$0.45(=\kappa_p)$	— —	—
	t > 50	I_i	$4(n^{-7})$	$9.6(n^8)$				

Dependence on Relative Humidity of the Current Response Coefficients κ_p and κ_w
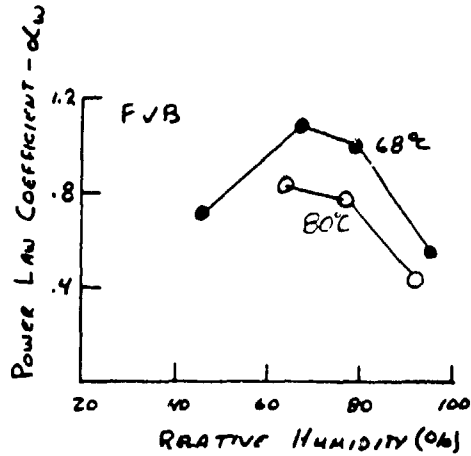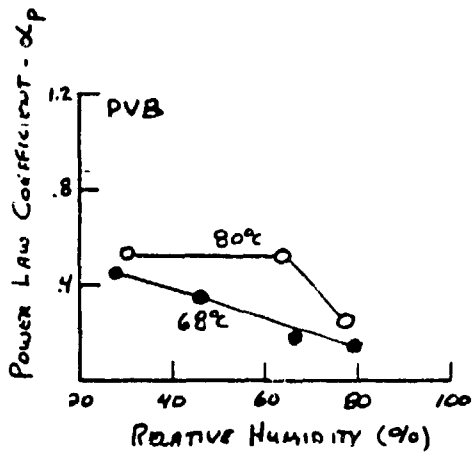
Ionic and Polarization Components of the Response Current vs RH (PVB at 80°C)

$$I_i = 5(10^{-10}) \exp(.15H)$$
$$I_{w_o} = 1.24(10^{-8}) \exp(.124H)$$

226
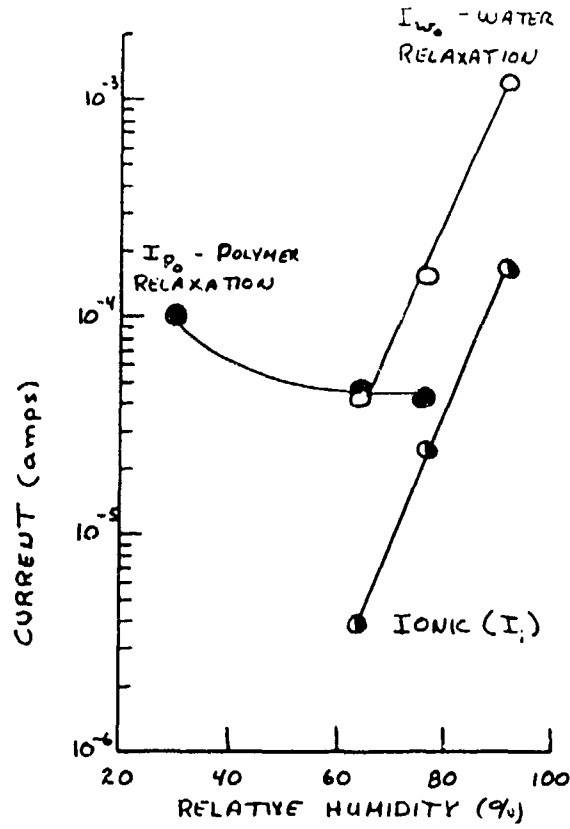
Ionic Resistance vs Relative Humidity (80°C and 68°C)

$$68°C : \quad R_i = 1.1(10^{10}) \exp(-.078 H)$$
$$80°C : \quad R_i = 1.5(10^{12}) \exp(-.15 H)$$

227
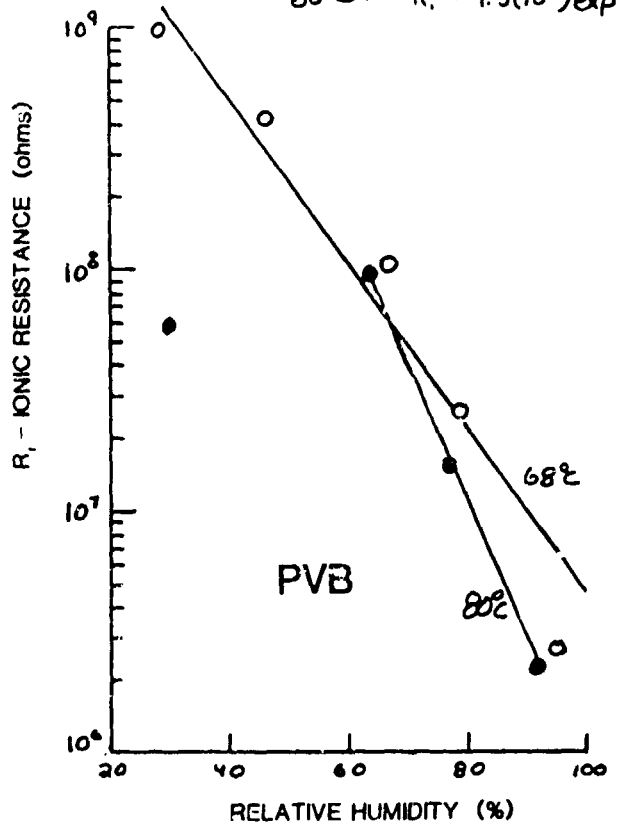
Time Constants vs Relative Humidity for PVB (68°C)

$$\tau = .033 H + 0.3$$
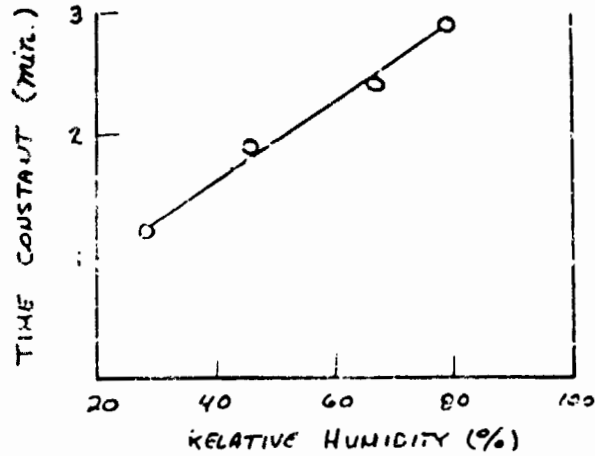
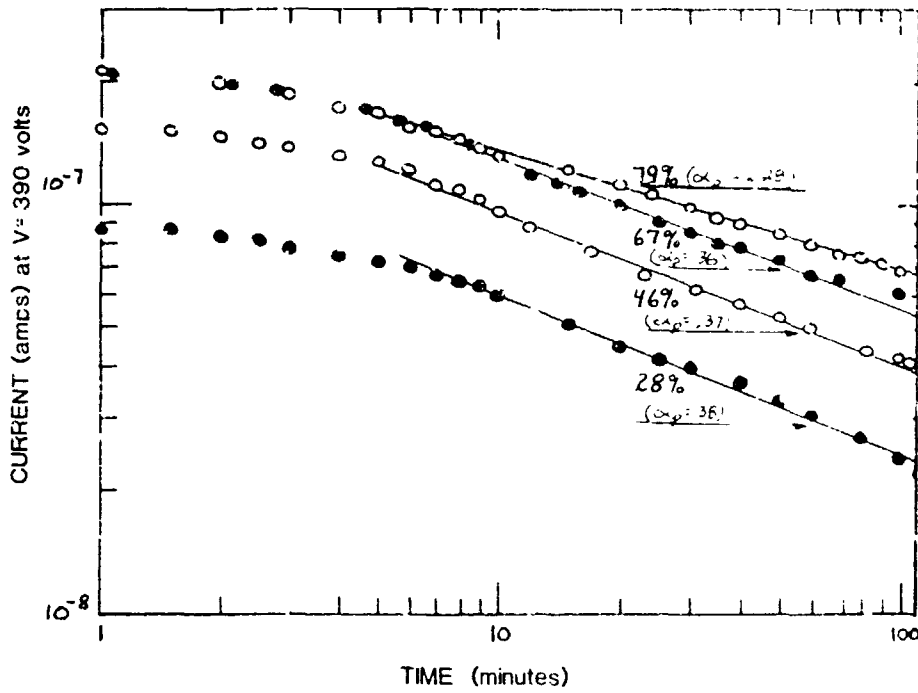## Humidity Dependence of the Initial Resistance for PVB (68°C)

$$R_0 = 11(10^9) exp(-.078 H)$$
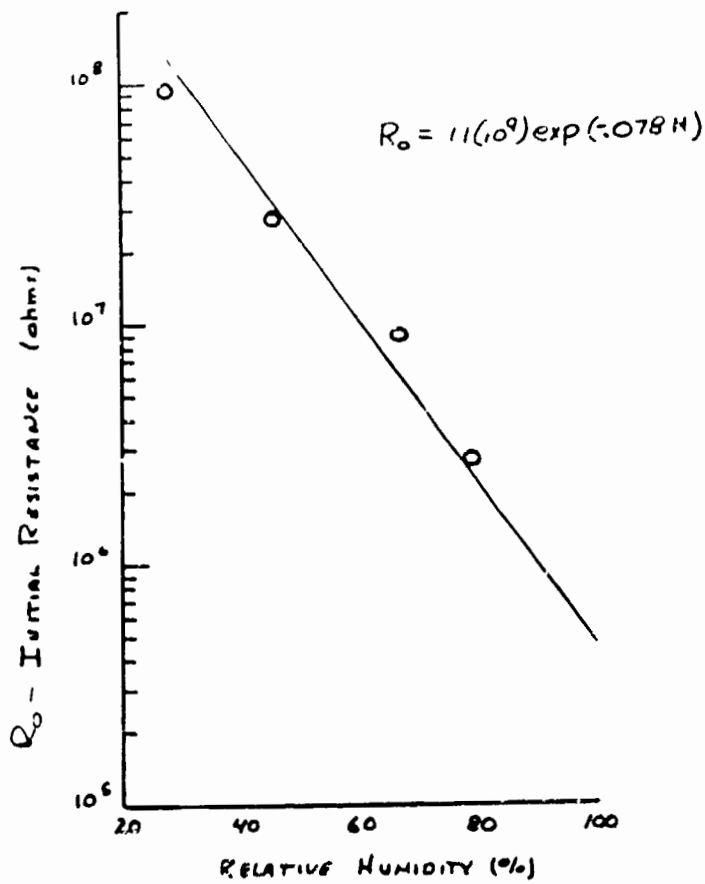
Capacitance and (tan δ) vs RH (500 Hz and 68°C)

PVB : $C = 2.8 H + 190$

EVA : $C = 0.15 H + 102$

PVB: $\tan \delta = 5(10^{-3}) H$

EVA: $\tan \delta = 7(10^{-5}) H$
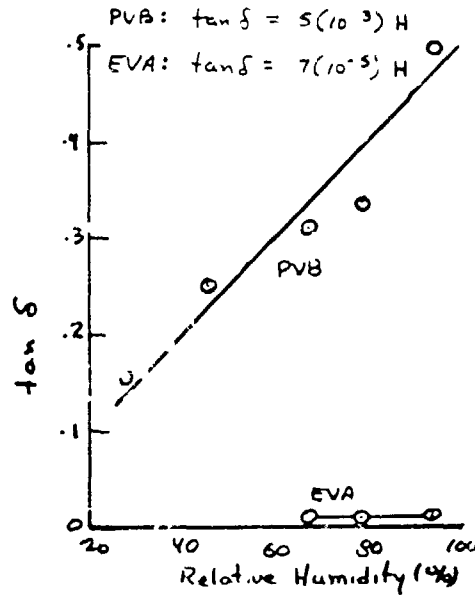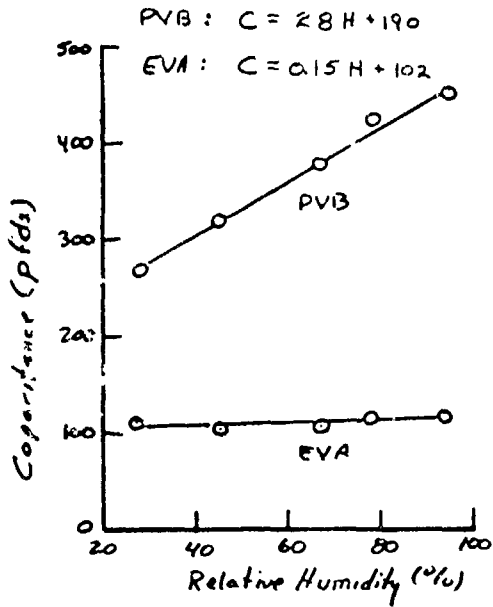
Capacitance and (tan δ) vs Frequency (68°C/95% RH)
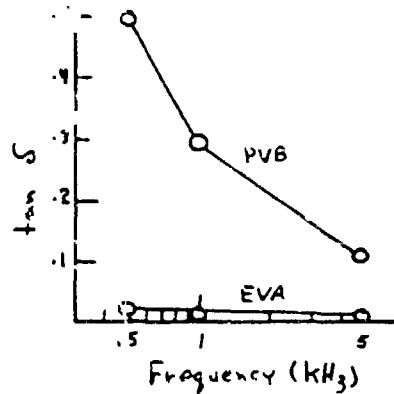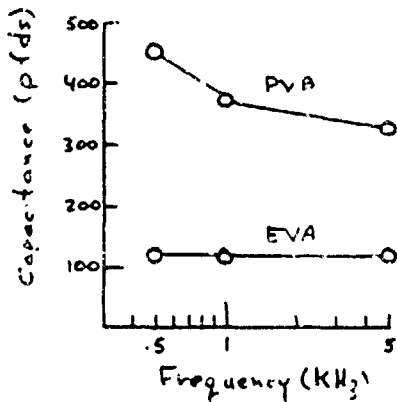
Current Response to a 390-V Step Voltage for EVA at Various RH (%) Levels (68°C)

Initial Transient Current Response to a 390-V Step Voltage for EVA (68°C)
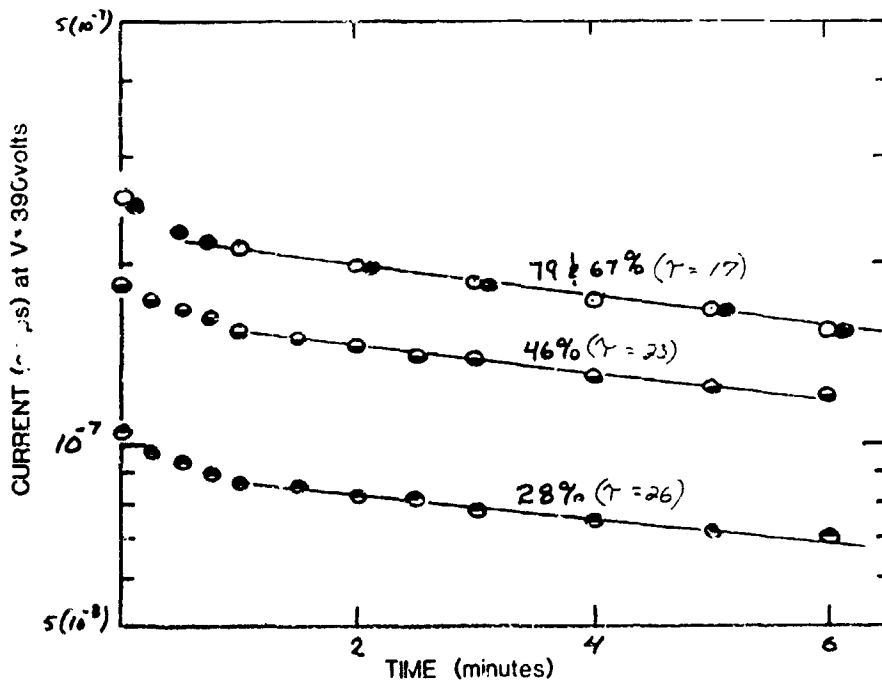
Current Response Parameters for EVA (68°C)

RELATIVE HUMIDITY (%)	TIME RANGE (min)	CURRENT COMPONENTS	I_i (amps)	R_i .390/I_i (Ω)	TIME DEPENDENCE				
					$I = At^{-\alpha}$		$I = [390/R_o][exp(-t/\tau)]$		
					A (amps)	α_p	$1/R_o$ (R$_o^{-1}$)	R_o (Ω)	τ (min)
79	$1 < t < 6$ $6 < t < 100$ $t > 100$	$I_c + I_p + I_i$ $I_p + I_i$ I_i	$\sim 7(10^{-9})$	$\sim 55(10^{9})$	$2.6(10^{-7})$	.28	$2.2(10^{-7})$	$18(10^{6})$	17
57	$1 < t < 6$ $6 < t < 100$ $t > 100$	$I_c + I_p + I_i$ $I_p + I_i$ I_i	$\sim 6(10^{-9})$	$6.5(10^{9})$	$3.0(10^{-7})$	.36	$2.2(10^{-7})$	$18(10^{6})$	17
46	$1 < t < 6$ $6 < t < 100$ $t > 100$	$I_c + I_p + I_i$ $I_p + I_i$ I_i	$4.2(10^{-9})$	$9.2(10^{9})$	$2.3(10^{-7})$	.37	$1.6(10^{-7})$	$24(10^{6})$	23
28	$1 < t < 6$ $6 < t < 100$ $t > 100$	$I_c + I_p + I_i$ $I_p + I_i$ I_i	$\sim 25(10^{-9})$		$1.5(10^{-7})$	.38	$8.8(10^{-8})$	$44(10^{6})$	26

Power-Law Coefficient κ and Time Constant τ vs RH for Current Response of EVA to a 390-V Step Voltage (68°C)

$$\tau = -.19H + 31$$

$$\alpha_p = -1.5(10^{-3})H + .43$$
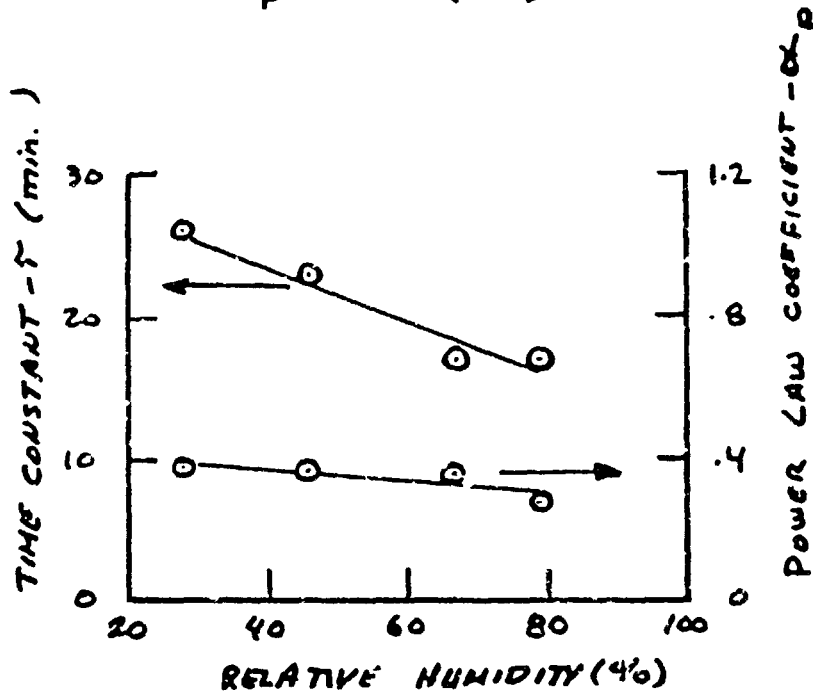
Ionic Resistance and Initial Conductance vs Relative Humidity for EVA (68°C)

$$R_i = -1.13(10^8)H + 1.4(10^{10})$$

$$R_0 = \frac{1}{\sigma_0} = \frac{1}{8(10^{-12})H + 4(10^{-11})}$$
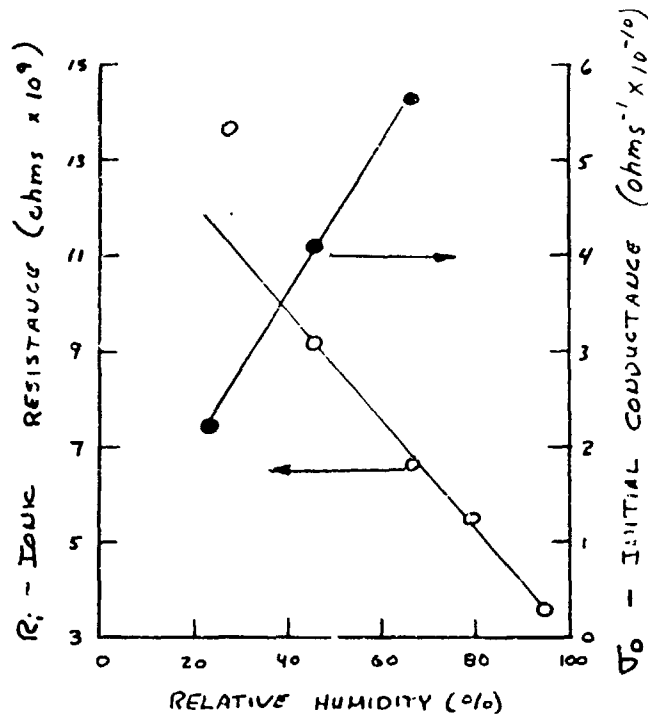
Measure and Calculated Time Constants for Capacitive Charging of EVA and PVB (68°C)

Humidity %	Time Constants (min.)			
	PVB		EVA	
	measured	calculated	measured	calculated
79	2.9	$1.0(10^{-5})$	17	$3.5(10^{-3})$
87	2.4	$5.0(10^{-5})$	17	$3.5(10^{-3})$
46	1.9	$1.4(10^{-4})$	23	$4.2(10^{-3})$
28	1.2	$4.0(10^{-4})$	26	$7.9(10^{-3})$

Humidity Dependencies of Selected
Properties of PVB and EVA (68°C)

Property	Expected Dependency	Experimentally Observed Dependencies PVB	EVA
$R_0(\Omega.)$	$=[\gamma H + \beta]$	$=1.1(10^9)\exp(-.078H)$	$=[8(10^{-8})H + 4(10^{-11})]^{-1}$
$R_i(\Omega)$	$=[\gamma H + \beta]^{-1}$	$=1.1(10^{10})\exp(-.078H)$	$=-1.13(10^8)H + 1.4(10^{10})$
α_w	$\neq fct(H)$	?	—
α_p	$\neq fct(H)$	$=-6.4(10^{-3})H + .64$	$=-1.5(10^{-3})H + .43$
$\tau_{(min.)}$	$=[\delta H + \eta]/[\gamma H + \beta]$	$=.033H + 0.3$	$=-.19H + 31$
$C \ (pfds)$	$=\delta H + \eta$	$=2.8H + 190$	$=0.15H + 102$
$\tan \delta$	$=\delta H + \eta$	$=5(10^{-3})H$	$=.7(10^{-4})H$

Effects of Plasticizer on the Resistivity of PVB

PVB	RESISITIVITY (Ω -cm)
UNPLASTICIZED	$3(10^{14})$
PHTHALATE PLASTICIZED	$5(10^9)$
PHTHALATE REMOVED	$6(10^{14})$

RADIATION EFFECTS IN PVB and EVA

Radiation Effects on EVA Resistivity

EVA
RADIATION EFFECTS
ON EVA RESISTIVITY
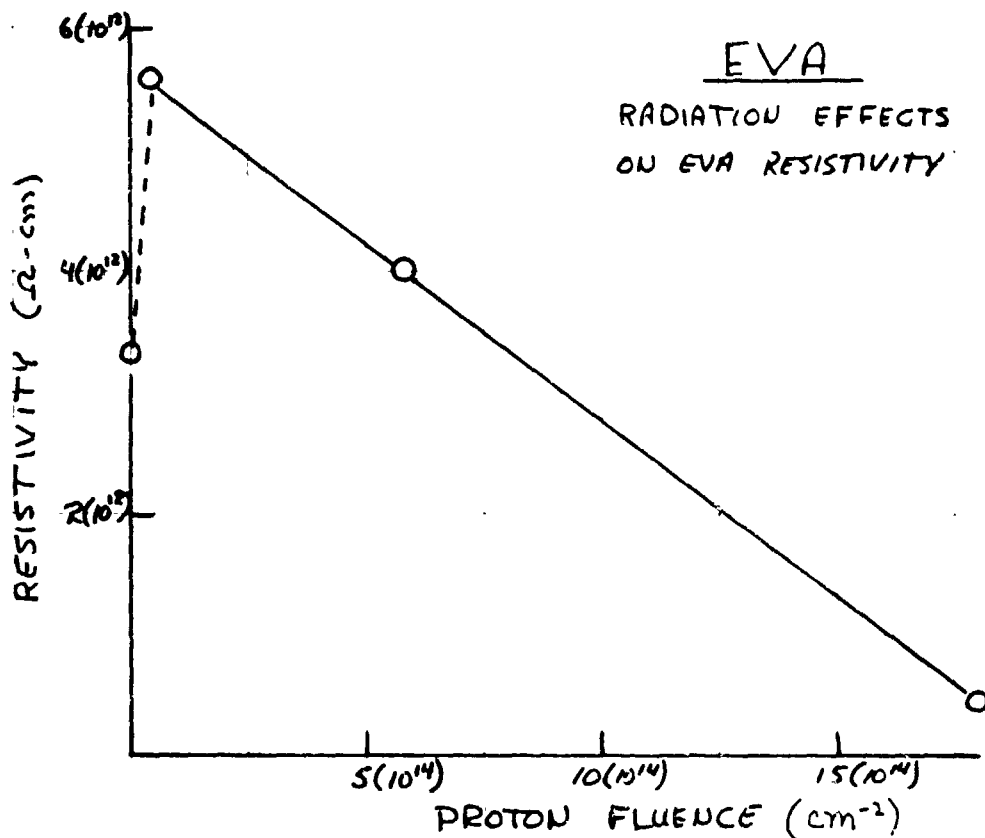
Radiation Effects on PVB Resistivity
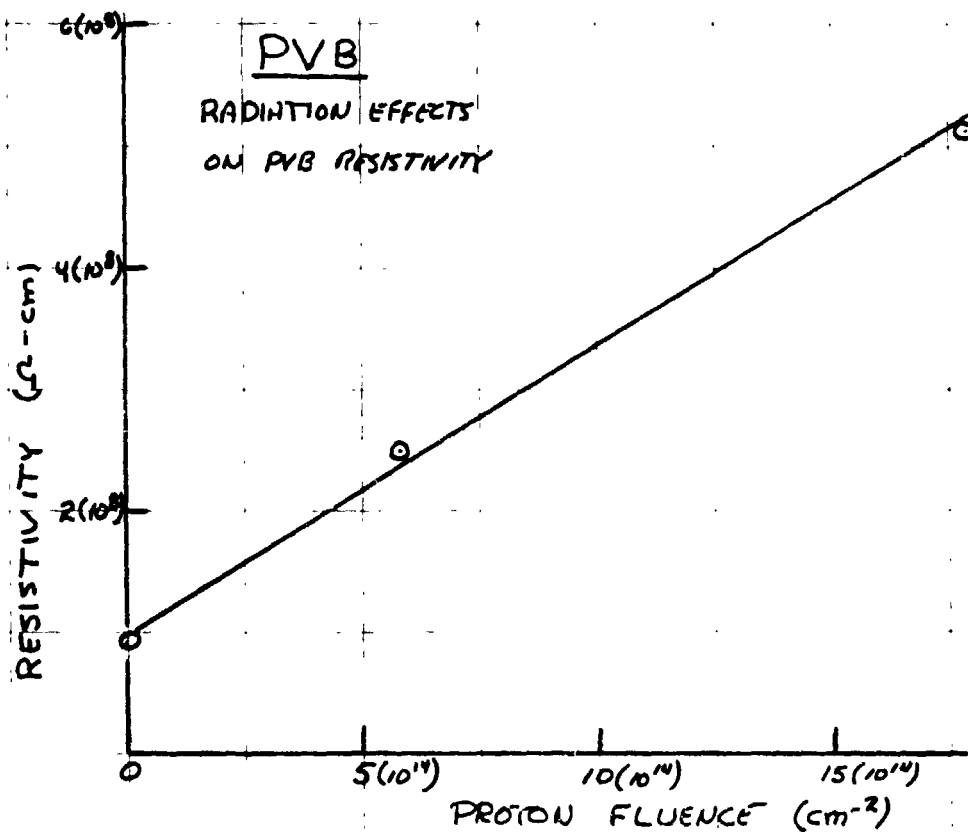
Conclusions

I. WATER ABSORPTION EXPERIMENTS

- FAST WATER DESORPTION KINETICS IN PVB AND EVA

- SLOW WATER ABSORPTION KINETICS IN PVB AND EVA

- WATER ABSORBED IN PVB IS LARGE

- WATER ABSORBED IN EVA IS SMALL

II. ELECTRICAL PROPERTIES OF PVB AND EVA

- IONIC RESISTANCE : $R_i^{PVB} < R_i^{EVA}$ 10^2

- CAPACITANCE : $C^{PVB} > C^{EVA}$ 10^1

- LOSS FACTOR : $\tan\delta^{PVB} > \tan\delta^{EVA}$ 10^1

- HUMIDITY DEPENDENCE : $PVB > EVA$

- WATER DIPOLE EFFECTS IN PVB

- NO WATER DIPOLE EFFECTS IN EVA

III. PLASTICIZER EFFECTS ON IONIC RESISTANCE OF PVB

- R_i UNPLASTICIZED $>$ R_i PLASTICIZED 10^5

IV. IONIZING RADIATION EFFECTS ON RESISTANCE OF PVB AND EVA

- PVB : $R_i \uparrow$ AS DOSE $\uparrow$

- EVA : $R_i \downarrow$ AS DOSE $\uparrow$

Future Work

- TEMPERATURE DEPENDENCE OF ELECTRICAL PROPERTIES
  OF EVA AND PVB

- UV LIGHT EFFECTS ON THE ELECTRICAL PROPERTIES OF EVA
  AND PVB AS A FUNCTION OF HUMIDITY AND TEMPERATURE

- EFFECT ON COMPOUNDING AGENTS ON ELECTRICAL
  PROPERTIES OF PVB AND EVA

- CORROSION EFFECTS IN SOLAR CELL MATERIALS

- THEORETICAL MODELS FOR HUMIDITY DEPENDENCY OF
  ELECTRICAL PROPERTIES

SILICON MATERIAL

Naresh Rohatgi, Chairman

This session comprised six presentations covering research on processes for refining silicon (Si).

Energy Materials Corp. reported on its program from a scaled-up demonstration of a fused-salt electrochemical cell for purifying metallurgical-grade Si feedstock. Attempts to operate the cell, which was designed to produce up to 50 g/h of Si, were unsuccessful.

The Solar Energy Research Institute discussed research on a chemical vapor transport process in which HCl is reacted with an alloy of copper and metallurgical-grade Si, forming predominantly trichlorosilane, and then Si is deposited by chemical vapor deposition on a heated filament. The Cu-Si alloy acts as a filter for impurities, allowing Si to diffuse relatively fast to the electrode surface.

Union Carbide Corp. described progress in its research on fluidized-bed reactor (FBR) silane decomposition technology for producing simiconductor-grade Si. Liners made of quartz of polysilicon were incorporated into the FBR to eliminate contamination of the product Si by the metal wall material. Improvements in product purity were obtained, but liners failed during cool-down after testing.

JPL reported on its program to investigate the deposition of Si from silane in FBRs. The six-inch-diameter reactor was provided with a quartz liner and tests with silane at concentrations as high as 50 mole % in hydrogen were successfully made with no liner cracking. Determination of product purity is under way.

Washington University at St. Louis described progress in modeling silane pyrolysis in FBRs. A preliminary comparison shows reasonable agreement of model predictions with experimental results from JPL FBR tests.

The California Institute of Technology presented results from a program for describing theoretically the growth of Si particles from silane in a free-space reactor and developing experimentally the conditions for growth of large particles. Progress was made in understanding how to avoid runaway nucleation.

SILICON REFINEMENT BY CHEMICAL VAPOR TRANSPORT

SOLAR ENERGY RESEARCH INSTITUTE

J. Olson

TECHNOLOGY	REPORT DATE
SILICON MATERIALS	OCTOBER 1, 1984

APPROACH	STATUS
VAPOR TRANSPORT PURIFICATION OF Si USING A Si:Cu$_3$Si SOURCE	-CASTING OF LARGE ALLOY PLATES HAS BEEN ACHIEVED -CHARACTERIZATION OF A LARGER RESEARCH SCALE REACTOR IS NEAR COMPLETION -REFINED SILICON PRODUCT HAS BEEN SHOWN TO YIELD SOLAR CELLS WITH NEAR STATE-OF-THE-ART CONVERSION EFFICIENCIES

CONTRACTOR
SOLAR ENERGY RESEARCH INSTITUTE

GOALS
STUDY THE OPERATING CHARACTERISTICS OF THE PURIFICATION PROCESS INCLUDING FACTORS AFFECTING THE RATE, THE PURIFICATION EFFICIENCY, AND THE PHOTOVOLTAIC QUALITY OF THE REFINED SILICON

SILICON MATERIAL

Impurity	mgSi (ppma)	CVT Refined (ppma)
Cu	—	0.12 - 0.15
B	117	< 0.26
P	15	0.16 - 1.8
Al	> 3400	< 0.1 - 0.98
Fe	> 2500	< 0.13 - 0.50
Mn	550	< 0.15
Ca	290	< 0.07 - 0.2
Ti	290	< 0.06
V	250	0.055 - 0.44
Ni	39	0.13 - 1.9
Zr	13	0.09
Mo	1.4	0.09

†R. H. Hopkins, et. al. (n-type base)
*p-type base

242

CVT Transport per Mole HCl
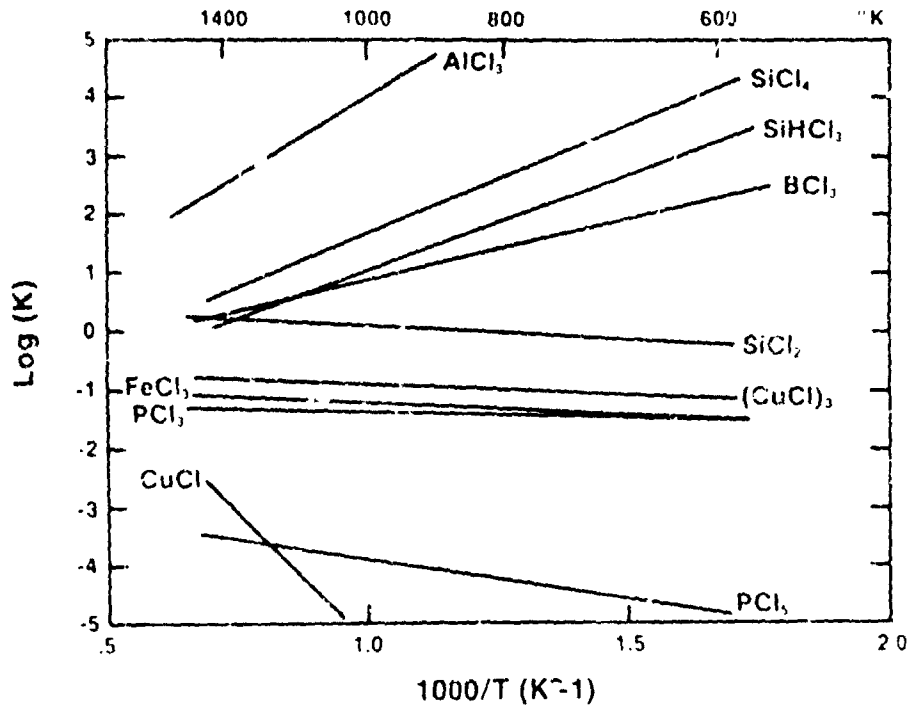
ORIGINAL PAGE IS
OF POOR QUALITY
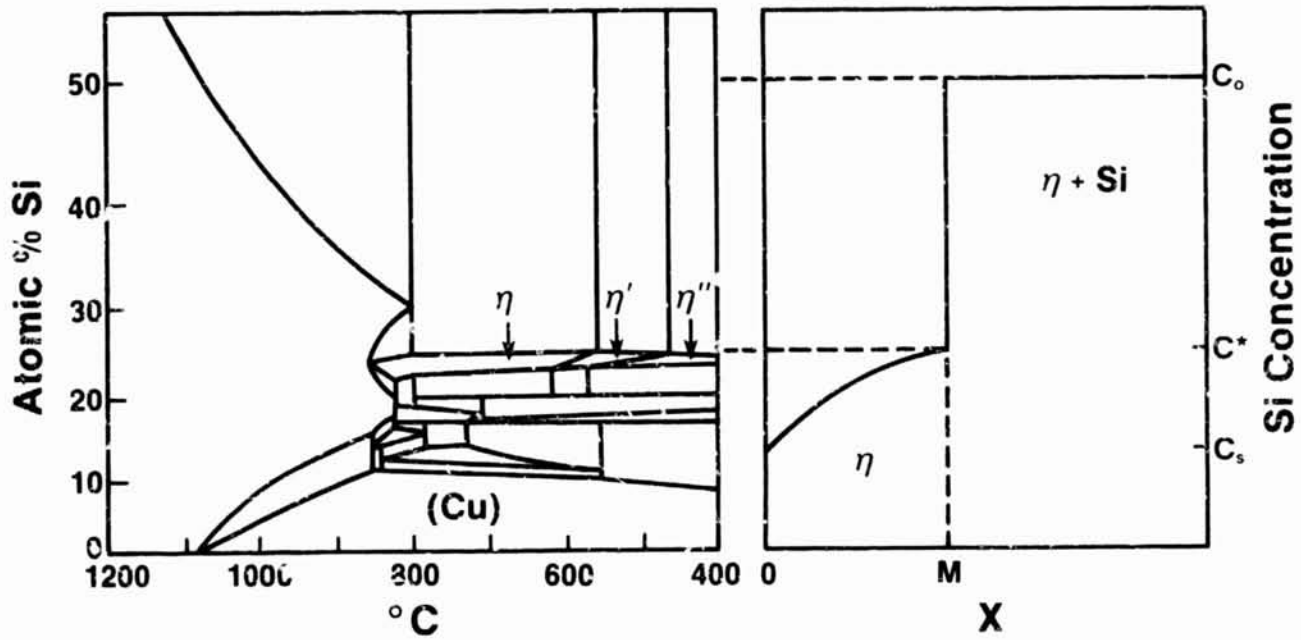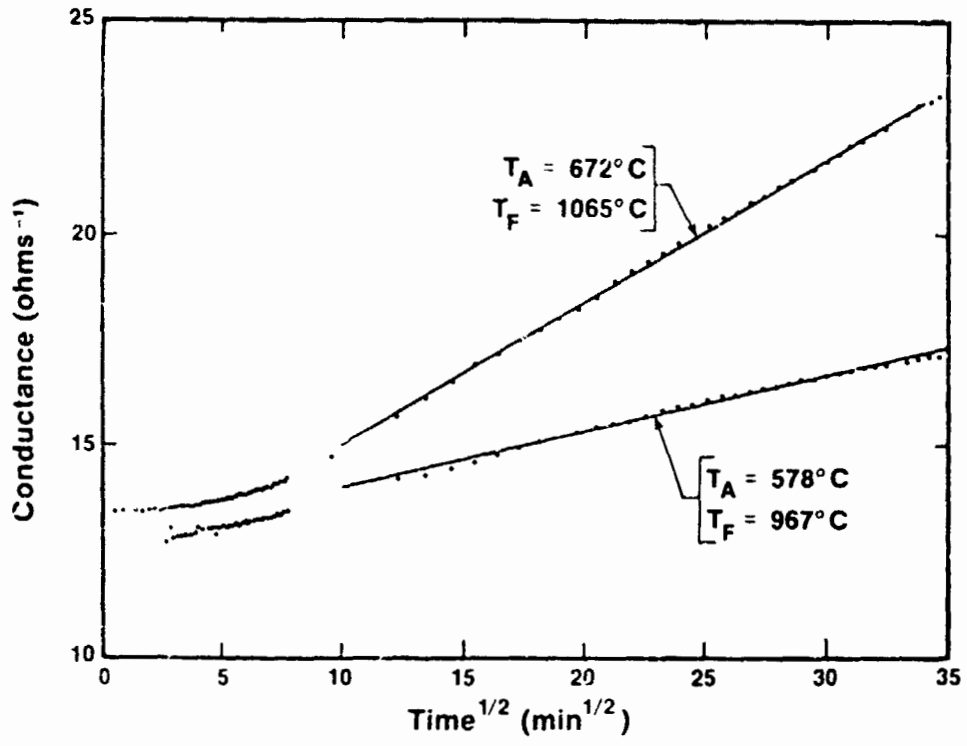
Electronic Properties

	RECRYSTALLIZED	AS DEPOSITED
RESISTIVITY	0.08.	0.1-1
HALL MOBILITY	524	
N_D-N_A	1.5×10^{17}	

PHOTOVOLTAIC CHARACTERISTICS
(NO AR COATING)

	VTF REFINED Si	CONTROL CELLS
V_{OC} (mV)	622	604
J_{SC} (mACM^{-2})	19.6	19.6
FF	0.81	0.81
EFFICIENCY	9.8%	9.6%
BASE RESISTIVITY	0.08	0.2

Sample: Si V_{oc} = 0.5945 volts
Date: APR 30 1984 17:00 J_{sc} = 19.71 mA/cm²
Temperature = 28.0°C   **Fill factor = 79.94%**
Area = 0.1000 cm²   **Efficiency = 9.37%**

V_{max} = 0.5070 V
I_{max} = 1.848 mA
I_{sc} = 1.971 mA

Current (mA) vs Voltage (volts)
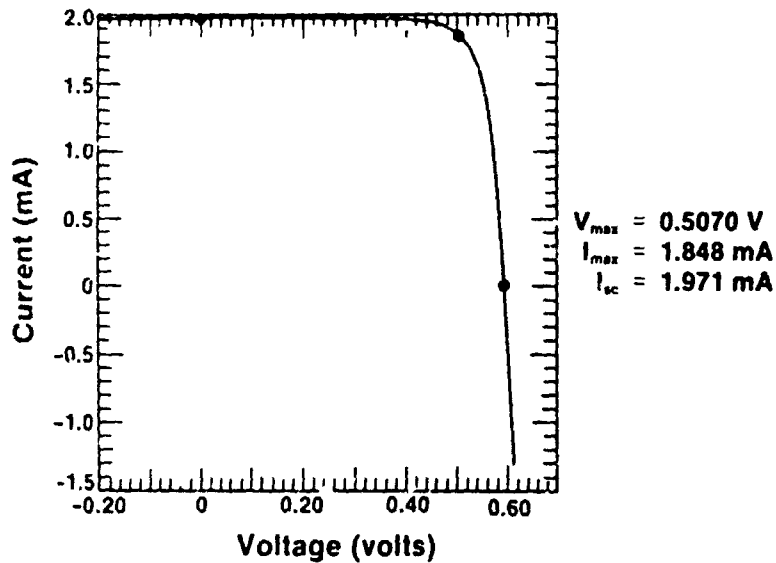
A FLUIDIZED-BED REACTOR FOR SILANE PYROLYSIS

UNION CARBIDE CORP.

S. Iya

TECHNOLOGY	REPORT DATE
POLYCRYSTALLINE SILICON R&D	OCTOBER 2, 1984
APPROACH SILANE DECOMPOSITION IN A FLUIDIZED BED REACTOR **CONTRACTOR** UNION CARBIDE CORPORATION	**STATUS** ● HIGH-PURITY LINER WAS INSTALLED IN THE FLUID BED REACTOR. ● LONG DURATION TEST RUNS WERE CONDUCTED. ● FBR PRODUCT WAS MELTED AND SINGLE CRYSTALLIZED. ● PRODUCT PURITY IMPROVEMENTS WERE NOTED.
GOALS ● DEMONSTRATE PROCESS FEASIBILITY. ● DETERMINE OPERATING WINDOW. ● CONDUCT LONG-DURATION TESTS. ● DEMONSTRATE SILICON PURITY.	

Summary of Activities

● PDU WAS MODIFIED TO INSTALL A HIGH-PURITY LINER.

● A SUITABLE LINER SUPPORT SYSTEM WAS DESIGNED AND IMPLEMENTED.

● SEED BED WAS PREPARED BY SCREENING AND ACID WASHING PURCHASED SILICON FINES.

● A LONG-DURATION TEST RUN WAS CONDUCTED USING POLYSILICON LINER. PRODUCT FROM THIS RUN WAS SINGLE CRYSTALLIZED AND ANALYZED FOR PURITY.

● A HIGH-THROUGHPUT TEST RUN WAS CONDUCTED USING QUARTZ LINER.

● A COLD MODEL WAS CONSTRUCTED TO INVESTIGATE COARSE PARTICLE WITHDRAWAL.

Run Summary: Long-Duration Test With Polysilicon Liner

- 56 HOURS RUN DURATION FOLLOWED BY VOLUNTARY SHUTDOWN.

- 280 μM SEED GROWN TO 500 μM PRODUCT.

- SILANE FEED CONCENTRATION IN THE RANGE 10 - 15%.

- AVERAGE DEPOSITION RATE APPROXIMATELY 1 KG/HR.

- BED TEMPERATURE 650 - 750°C.

- U/UMF 3.5 - 4.0.

- COMPLETE SILANE CONVERSION WITHIN THE BED.

- SEVERAL KG PRODUCT WAS WITHDRAWN.

- FINE POWDER 5.3 % OF SILANE FEED.

- POWER CONSUMPTION 25 KWH/KG.

Long-Duration Run: Mass Balance

INITIAL BED WEIGHT	=	26.7 KG
SILICON IN	=	63.0 KG
TOTAL	=	89.7 KG
BED MATERIAL WITHDRAWN	=	83.5 KG
POWDER IN FILTER HOPPERS	=	3.8 KG
TOTAL	=	87.3 KG
ERROR IN MASS BALANCE	=	2.7%

Run Summary: High Throughput Test With Quartz Liner

- 10 HOURS TOTAL RUN DURATION.

- MAXIMUM SILANE FEED CONCENTRATION 48%

- MAXIMUM DEPOSITION RATE 3.8 KG/HR.

- FINE POWDER 6.9% OF SILANE FEED

- POWER CONSUMPTION 8 KWH/KG.

- SHUT DOWN CAUSED BY HEATER FAILURE.

Test Product Characterization:
Long-Duration Run With Poly Liner

PARTICLE PROPERTIES

- 500 μM MEAN PARTICLE DIAMETER
- 100 LB/cFT. BULK DENSITY
- SMOOTH, ROUNDED SURFACE
- FREE FLOWING

PARTICLE MORPHOLOGY

- DENSE DEPOSITION LAYER
- LAYERED RING-LIKE GROWTH STRUCTURE
- GROWTH LAYER THICKNESS ~100 μM

PARTICLE PURITY

- FE, CR, NI NOT DETECTED BY EMISSION SPEC
  (FE < 20 PPM, CR < 5 PPM; NI < 5 PPM)
- SAMPLES OF SEED, INTERMEDIATE & FINAL PRODUCT
  WERE SENT TO JPL FOR NEUTRON ACTIVATION ANALYSIS
- SINGLE CRYSTAL RESISTIVITY 8 OHM-CM, P TYPE
- FTIR MEASUREMENTS SHOWED PPB LEVELS OF BORON AND
  PHOSPHOROUS

Plans

- ADDITIONAL PURITY RUNS STARTING WITH UNION CARBIDE
  SEED MATERIAL.

- PRODUCT PURITY EVALUATION.

- COARSE PRODUCT WITHDRAWAL TESTS.

- TECHNICAL AND ECONOMIC ASSESSMENT.

JPL IN-HOUSE FLUIDIZED-BED REACTOR RESEARCH

JET PRCPULSION LABORATORY

N.K. Rohatgi

Silicon Withdrawal System
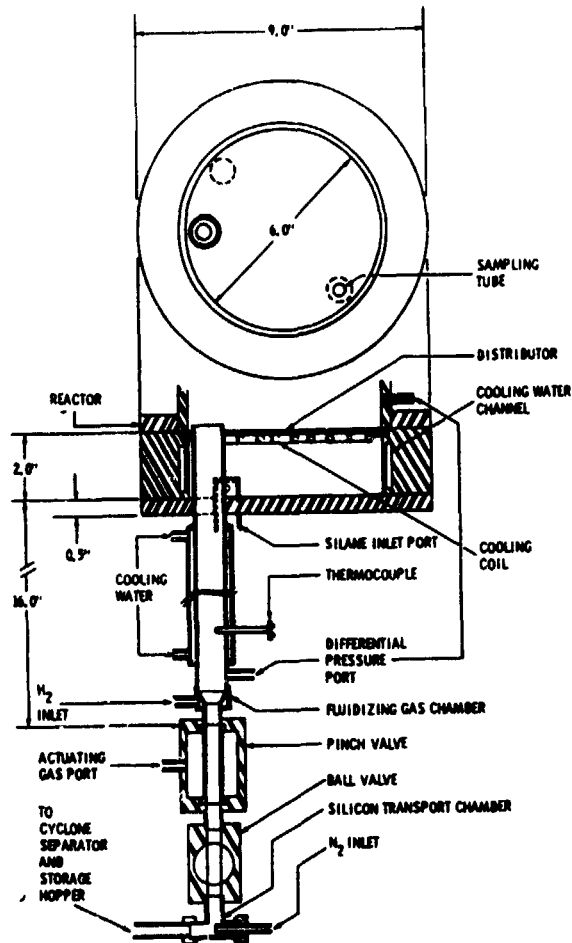
Quartz Liner System Design

- PROBLEM

  - POSSIBLE BREAKAGE OF QUARTZ LINER DURING THERMAL CYCLE

- DESIGN CRITERION

  - NO SILANE SHOULD BE ALLOWED TO FLOW IN BETWEEN QUARTZ LINER AND STAINLESS STEEL REACTOR WALL

251

Quartz Liner for FBR
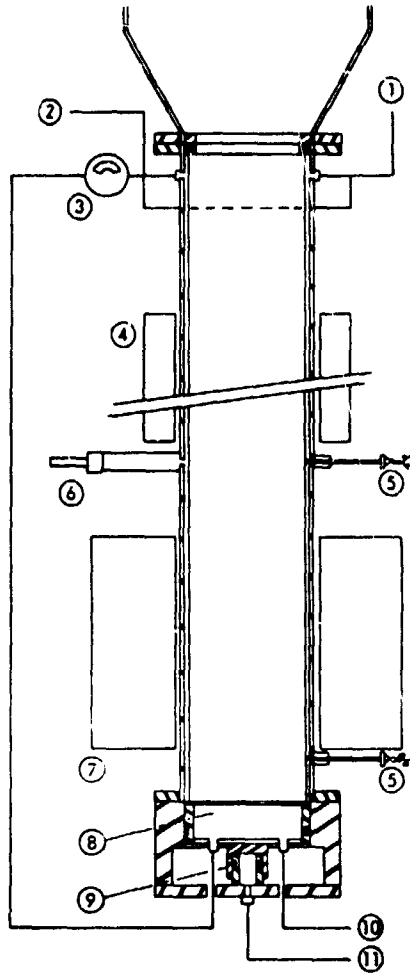
1. HYDROGEN EXHAUST
2. HYDROGEN INLET
3. DIFFERENTIAL PRESSURE GAGE
4. CLAMSHELL HEATER
5. THERMOCOUPLE
6. PYROMETER
7. SILICON CARBIDE HEATER
8. PISTON
9. PNEUMATIC CYLINDER
10. SILANE INLET
11. NITROGEN INLET

Quartz Liner After Exposure to Silane Pyrolysis
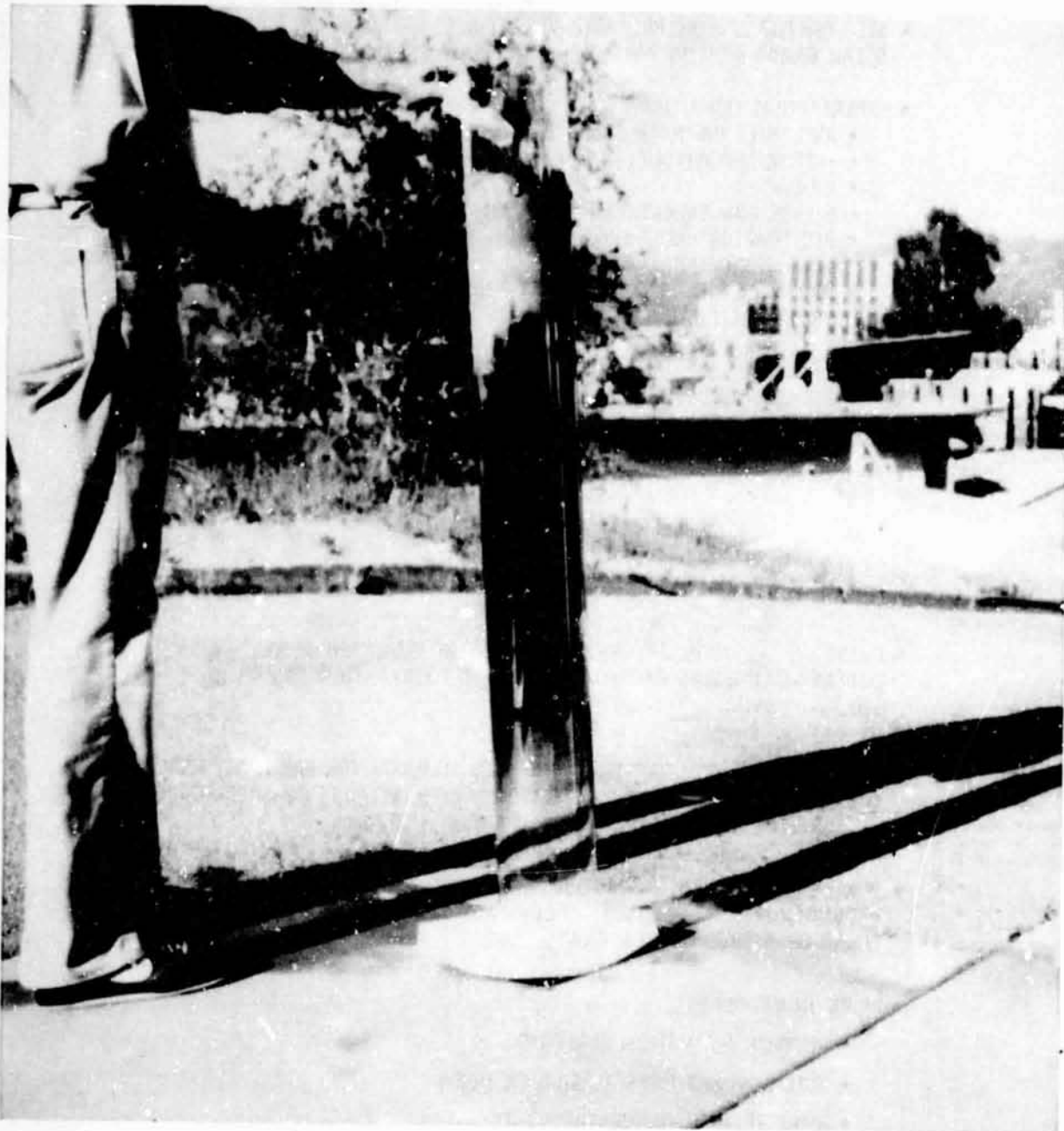
Purity Experiment

- SEED PARTICLES WERE PREPARED VIA JET MILL GRINDING OF 2 TO 4 mm SIZE SOLAR GRADE SILICON PARTICLES PURCHASED FROM THE DYNAMITE NOBEL

- EXPERIMENTAL CONDITIONS
    - AVG. SEED PARTICLE SIZE: 254 μm (+106 TO -425 μm)
    - INITIAL BED WEIGHT: 9 kg ($\approx$ 21" BED HEIGHT)
    - U / U_{mf} ⋅ 5
    - SILANE CONCENTRATION: 30% (IN H_2)
    - BED TEMPERATURE: 650°C
    - DURATION OF RUN: 4 hrs
    - PARTICLES WERE WITHDRAWN AT 2 hr INTERVALS EQUIVALENT TO PRODUCTION RATE

- MASS BALANCE
    - SILICON DEPOSITED ON THE PARTICLES IN BED ⋅ 90%
    - SILICON RECOVERED AS FINES ⋅ 7.2%

- PRODUCTION RATE: 1.7 kg/ hr

Purity of Silicon

- EMISSION SPECTROSCOPY WAS USED ONLY TO ESTABLISH IF ANY GROSS CONTAMINATION WAS CAUSED DURING SEED PREPARATION AND FLUIDIZED BED PROCESSING

- PURCHASED SILICON PARTICLES AND SEED MATERIAL FOR FBR HAVE METALLIC CONTAMINATIONS BELOW THE DETECTION LIMITS OF EMISSION SPECTROSCOPY, SUCH AS Fe ⋅ 30 ppmw, CR ⋅ 8 ppmw, AND Ni ⋅ 10 ppmw

- PURITY DATA DO NOT SHOW ADDITIONAL METAL CONTAMINATIONS IN THE PRODUCT SILICON. HOWEVER, IT DOES NOT MEAN THAT FBR PRODUCT IS OF SOLAR OR SEMICONDUCTOR GRADE

- WORK IN PROGRESS
    - NEUTRON ACTIVATION ANALYSIS
    - PULL A SINGLE CRYSTAL SILICON INGOT
    - MAKE RESISTIVITY MEASUREMENTS

SEM Photographs of FBR Product (650°C, 30% SiH$_4$, 4 h); Deposition ≈17 μm

Jet Mill for Silicon Seed Particle Preparation
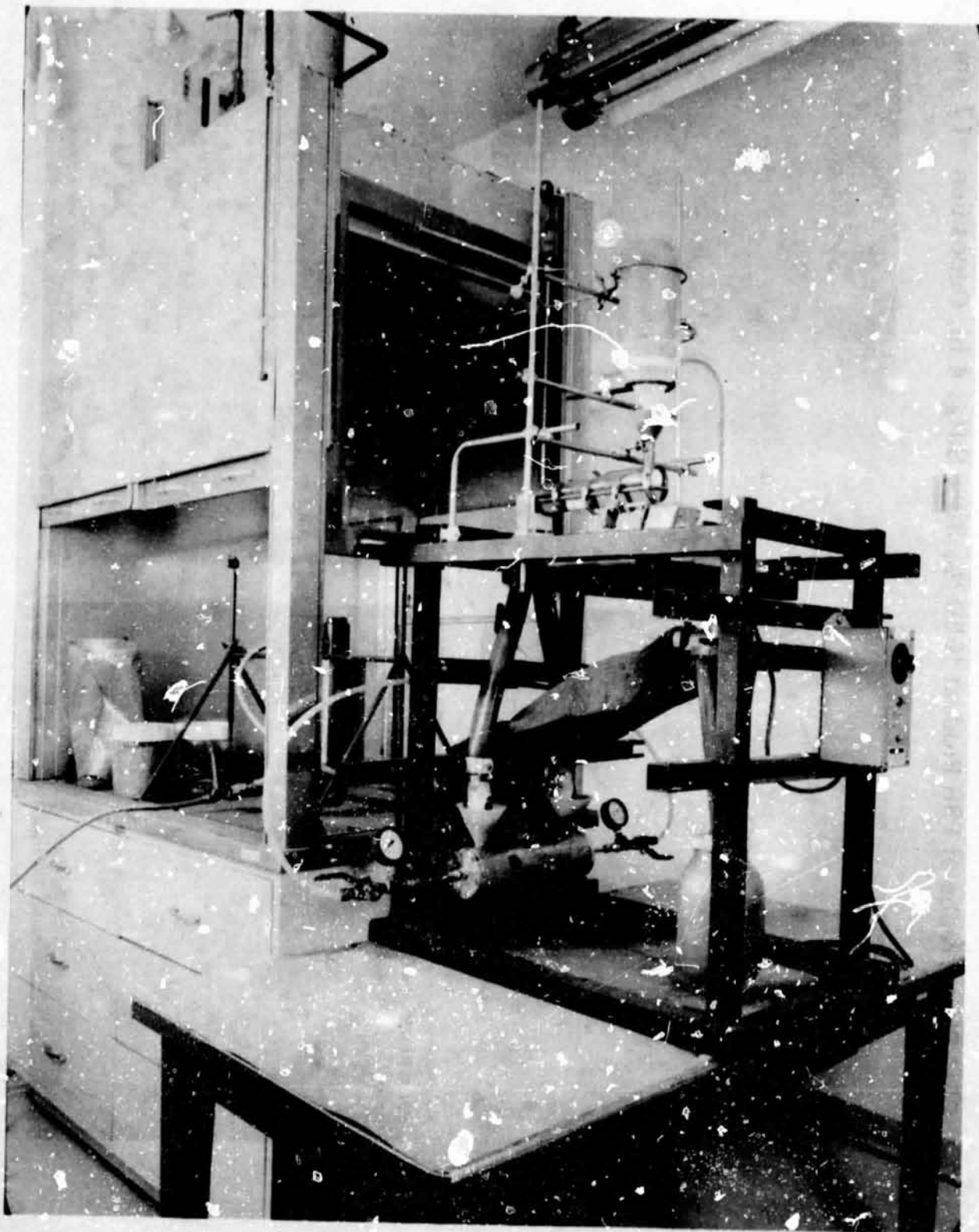
Recent Publications

- A PAPER TITLED "FINES IN FLUIDIZED BED SILANE PYROLYSIS" WAS PUBLISHED IN THE JL. OF ELECTROCHEMICAL SOCIETY, MARCH 1984.

- A PAPER TITLED "FLUIDIZED BED SILICON DEPOSITION" WAS PESENTED TO THE 17TH IEEE PV SPECIALIST CONFERENCE, FLORIDA, MAY 1-4, 1984.

- A PAPER TITLED "SILCION PARTICLE GROWTH IN A FLUIDIZED BED REACTOR," WAS SUBMITTED TO THE AICHE ANNUAL MEETING, SAN FRANCISCO, NOV. 25-30, 1984.

MODELING OF THE SILANE FBR SYSTEM

WASHINGTON UNIVERSITY

M.P. Dudokovic
P.A. Ramechandran
S. Lai

Objectives

- Development of a mathematical model for fluidized bed pyrolysis of silane that relates production rate and product properties (size, size distribution, presence or absence of fines) with bed size and operating conditions (temperature, feed concentration flow rate, seed size, etc.).

- Development of user oriented algorithm for the model.

- Parameter sensitivity study of the model.

Needed

- Assumptions on mixing pattern of gas and solids.

- Mass and energy balances for gas and solid phase.

- Constitutive relationships
    - Homogeneous nucleation rate

    - CVD growth

    - Fines interactions

    - Scavenging of fines by large particles

    - Transport properties in fluidized beds

Summary of Work Done

1. The kinetic studies on silane pyrolysis were reviewed
    and all pathways and rate models for Si formation via
    silane pyrolysis were summarized. A CVD growth and
    homogeneous rate form were selected.

2. A simplified model was developed assuming the
    reactor to be completely mixed. This model was
    solved for both batch as well as continuous feed
    of solids with/without homogeneous nucleation.

3. A computer program was developed for a more
    general fluidized bed model based on the modified
    two phase theory accounting for CVD growth only.

4. A detailed model based on population balance
    approach was developed for predicting particle
    size distribution of fines when CVD growth,
    coagulation, scavenging by seed particles and
    homogeneous nucleation take place.

Back-Mixed Reactor Model

(1) Balance on SiH_4 (g)

$$q_f C_{s,f} - q_e C_{s,e} = V\bar{r}_{HT,1} + V\bar{r}_{HT,2} + Vr_{HO}$$

where

$V\bar{r}_{HT,1} \equiv$ total rate of CVD on seed particles

$$= N_s \cdot 4\pi R^2 / \phi_s \cdot r_{HT}$$

$$r_{HT} = A \exp{(-\Delta E/R_g T_p)} \, C_{s,e}$$

$V\bar{r}_{HT,2} \equiv$ total rate of CVD on fines

$Vr_{HO} \equiv$ total rate of homogeneous nucleation

(2) Balance on seed solids (uniform particle size)

$$\frac{dR}{dt} = \frac{r_{HT}}{\phi_s} \frac{M_{si}}{\rho_{si}} + \frac{m_{sca}}{4\pi R^2 \, N_S \rho_{si}}$$

where $m_{sca} \equiv$ total rate of scavenging

$$= \rho_{si} \int_{v^*}^{v_{max}} v \, a(v) \, n(v,t) \, dv$$

(3) Energy balance

(4) Balance equation for fines

$$\frac{\partial \, n(v,t)}{\partial t} + R_{elu}(v,t) + \frac{\partial}{\partial v} \, \{I(v,t) \, n(v,t)\}$$

$$= \int_{v^*}^{v/2} \beta(v-\tilde{v},\tilde{v}) \, n(v-\tilde{v},t) \, n(\tilde{v},t) \, d\tilde{v}$$

$$- \int_{v^*}^{v_{max}} \beta(v,\tilde{v}) \, n(v,t) \, n(\tilde{v},t) \, d\tilde{v}$$

$$- R_{sca}(v,t) + S(v,t)$$

where

$I(v,t)$		rate of particle growth $= dv/dt$
$\beta(v,\tilde{v})$	$=$	the coagulation coefficient
$R_{elu}(v,t)$	$=$	rate of elutriation $= K(v) \cdot n(v,t)$
$R_{sca}(v,t)$	$=$	rate of scavenging $= \alpha(v) \cdot n(v,t)$
$S(v,t)$	$=$	rate of generation of fines by homogeneous nucleation $= S_o \cdot \delta(v-v^*)$

Define the total volume by the first moment:

$$M_1(t) = \int_{v^*}^{v_{max}} v \, n(v,t) \, dv$$

For t e special case:
$$K(v) = const. \; K$$
$$I(v,t) = \sigma_1 v$$
$$\beta(v,v) = \sigma_1 (v + \tilde{v})$$
$$\alpha(v) = const. \; \alpha$$

$$M_1(t) = [\frac{S_o \, v^*}{\sigma_1 - (\alpha + K)}] \, (e^{[\sigma_1 - (\alpha + K)]t} - 1)$$

Input Data (From JPL 6-in. FBR Experiments)

1. Reactor Specifications

    bed diameter $\quad$ = 15.4 cm (6.065" I.D.)

    no. of orifice holes = 4500

    orifice area $\quad$ = 0.02 cm^2

2. Operating Conditions

    total pressure of gas $\quad$ = 1.34 atm

    total volumetric flow rate $\quad$ = 600 cm^3/s - 1200 cm^3/s

    $\quad$ (1.97 moles/min -

    $\quad$ 3.94 moles/min)

    feed ratio of SiH$_4$ $\quad$ = 20% - 80%

    Initial total wt. of seed solids = 10 to 12 kg

    Initial diameter of seed solids $\quad$ = 200 - 240 µm

    $\quad$ entering gas temp. $\quad$ = 25°C

    $\quad$ wall temp. $\quad$ = 600 - 800°C

    $\quad$ distributor plate temp. $\quad$ = 200°C

Back-Mixed Reactor Model

Bed parameters needed

h_w - heat transfer coefficient
between bed and wall Wender and Cooper (1958)

h_d - heat transfer coefficient
between bed and
distributor plate

H_{mf} - bed height at minimum
fluidizing conditions Kunii and Levenspiel (1969)

$K(R)$ - elutriation constant Wen and Hashinger (1960)

Kinetic parameters needed

- CVD growth rate Iya et al. (1982)

- homogeneous nucleation
/reaction rate

Particle interaction parameters needed

- coagulation coefficient for fines

- scavenging coefficient

CSTR — Batch Solids (20%)

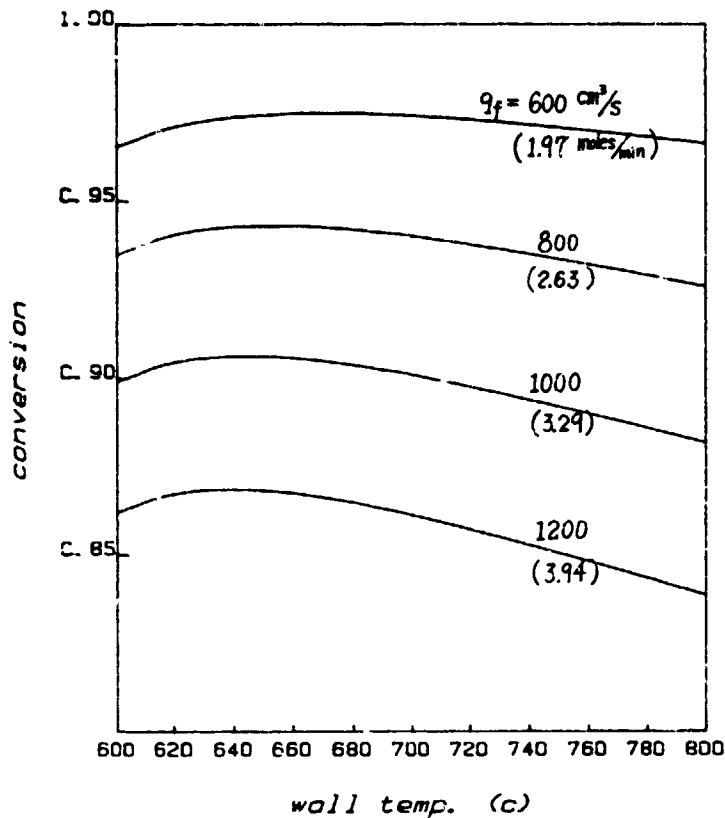$$T_{bed} \approx \frac{\left(\frac{h_p A_p}{h_w A_w}\right) T_p}{1 + \left(\frac{h_p A_p}{h_w A_w}\right)} + \frac{1}{1 + \left(\frac{h_p A_p}{h_w A_w}\right)} T_w$$
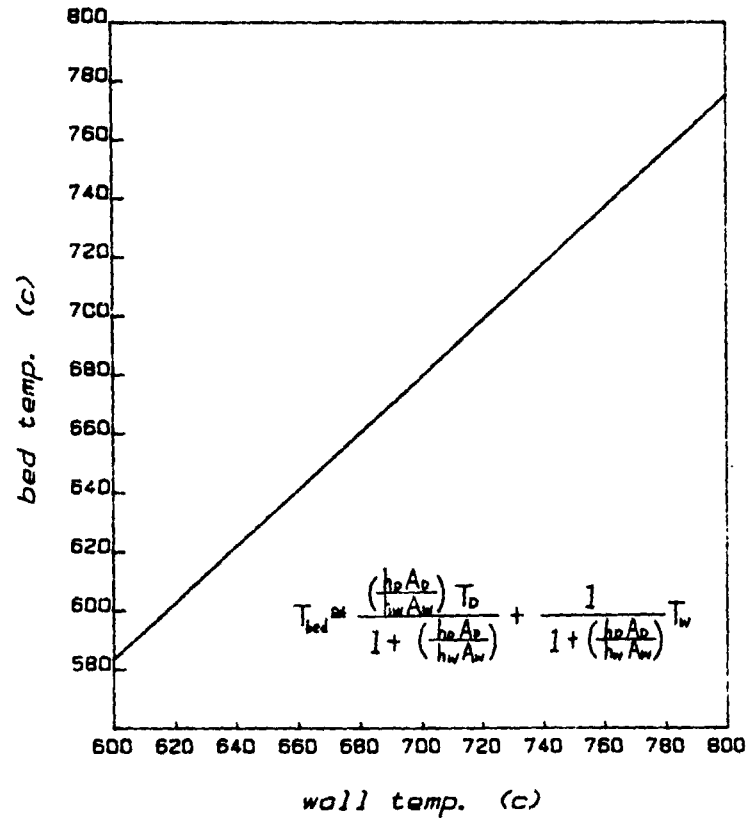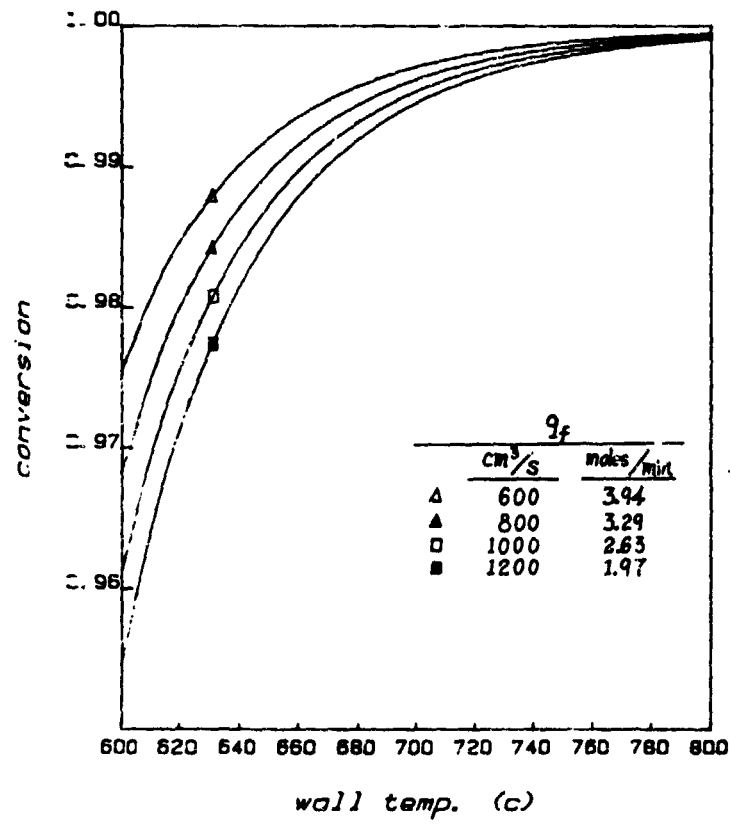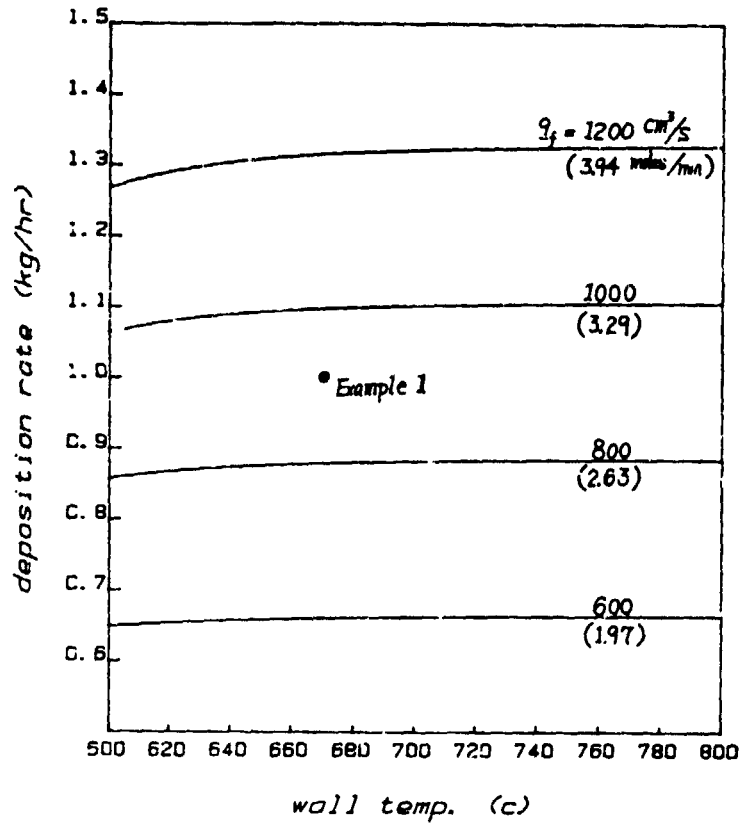
CSTR — Batch Solids (80%)

Bubbling Bed Model

```
Product        Entrained      Product
Particles      Particles      Gas
  ↑ (Si)         ↑ (Si)         ↑

Feed Particles      Particles
     (Si)            (CSTR)

                  Heterogeneous
                  reaction (r_HT)        Bubble
Transport Gas                            Phase
                 SiH₄(g) → Si(s)+2H₂(g)

                  Heat       Mass
                                         q_e
                                         heat
                 Interstitial Gas
        Heat       (CSTR)               Mass

                                    q_e
        Heat        Mass

                      Grid Region
                       (Plug)
```

$$SiH_4(g) \rightarrow Si(s) + 2H_2(g)$$
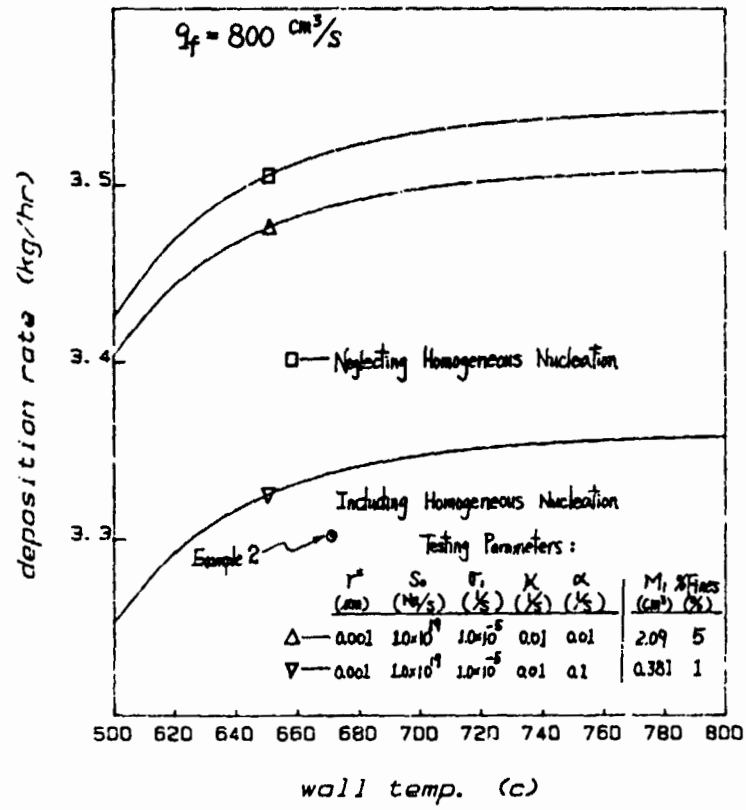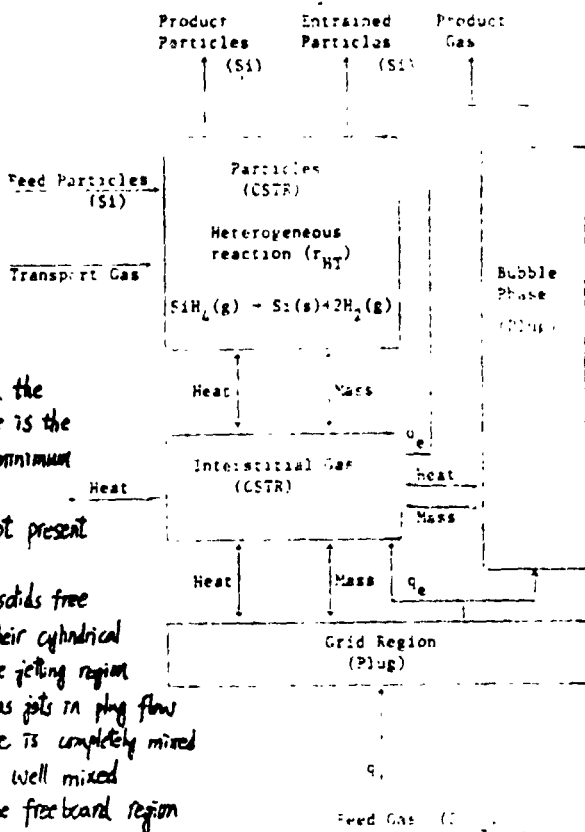
Assumptions:

1) The voidage in the emulsion phase is the same as at minimum fluidization

2) Particles are not present in bubbles

3) Gas jets are solids free and maintain their cylindrical shape within the jetting region

4. Bubbles and gas jets in plug flow

5 Emulsion phase is completely mixed

6 All solids are well mixed

7 Reaction in the freeboard region is ignored

8 Volumetric flow rate in the bubble and emulsion phase is const.

9) Temp. of the particles is the same as the temp. of the emulsion phase.

q_e

Feed Gas

Figure 1.1. Modified two-phase model with ... nucleation

Bed parameters needed

h_j –   jet penetration depth   Yang and Keairns (1979)

$\bar{d}_b$ –   average bubble diameter

$\bar{\delta}_b$ –   average volume fraction   Weimer and Clough (1981)

L_f –   expanded bed height

$\bar{U}_b$ –   average bubble velocity   Kunii and Levenspiel (1969)

U_e –   upward velocity of gas

            through the emulsion phase   ibis

$(K_{he})_b$, $(H_{be})_b$ –   overall mass and heat
           transfer coefficient
           between the bubbles
           and the interstitial
           gas   ibis

K_{je}, H_{je} –   overall mass and heat
           transfer coefficient
           between the jets and
           the interstitial gas   Weimer and Clough (1981)

h_w, h_d, L_{mf}, $K(R)$

Kinetic parameters needed

   – CVD growth rate   Iya et al. (1982)

   – homogeneous nucleation

     /reaction rate

Particle interaction parameters needed

   – coagulation coefficient for fines

   – scavenging coefficient

FBR — Batch Solids (20%)

$$T_{bed} \approx \frac{\left(\frac{h_p A_p}{h_w A_w}\right) T_p}{1 + \left(\frac{h_p A_p}{h_w A_w}\right)} + \frac{1}{1 + \left(\frac{h_p A_p}{h_w A_w}\right)} T_w$$

bed temp. (c)

wall temp. (c.)

deposition rate (kg/hr)

$q_f = 1200$ cm^3/s

(3.94 moles/min)

1000
(3.29)

• Example 1

800
(2.63)

600
(1.97)

wall temp. (c)
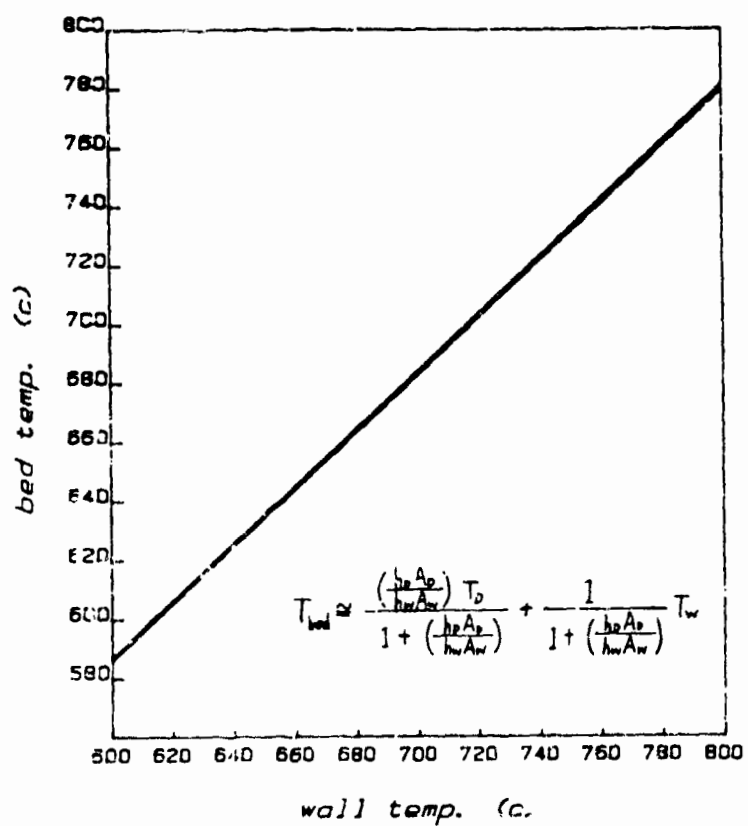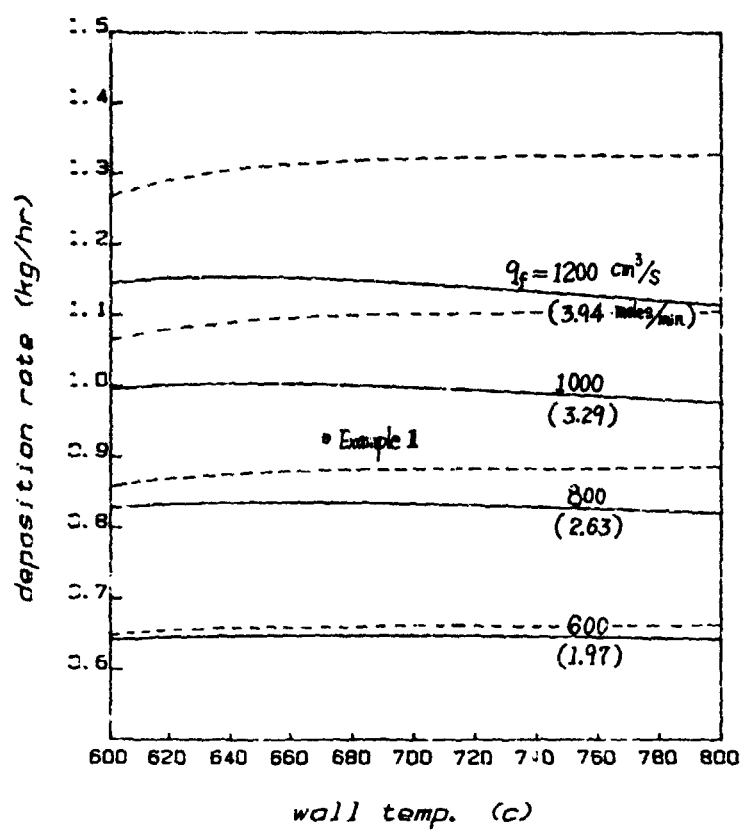
----- CSTR Model Prediction

——— FBR Model Prediction

C-24

$$q_f = 600 \text{ cm}^3/s$$
$$(1.97 \text{ moles/min})$$
$$800$$
$$(2.63)$$
$$1000$$
$$(3.29)$$
$$1200$$
$$(3.94)$$

wall temp. (c)

Selected Examples From JPL 6-in. FBR Experiments

	Silicon Seed		Experimental Conditions			
	Weight (Kg)	$\bar{d}_p$ (μm)	Silane Concen. (%)	Bed temp. (°C)	Total gas flow rate (moles/min)	Duration (min)
Example 1	10.50	227	20	650	3.0	90
Example 2	11.34	212	80	650	2.5	173

Product Comparison

	Experimental Data		Model Predicted (CSTR)		Model Predicted (FBR)	
	Production rate (Kg/hr)	$\bar{d}_p$ (μm)	Production rate (Kg/hr)	$\bar{d}_p$ (μm)	Production rate (Kg/hr)	$\bar{d}_p$ (μm)
Example 1	0.87	235.5	1.00	237.4	0.93	236.6
Example 2	3.50	241.5	3.35	260.3	3.15	257.7

Conclusion

-— A preliminary comparison with two experimental results
of JPL shows a reasonable agreement of model prediction
with experiments.

— The deposition rate and conversion of silane are found to
be lower for the two-phase fluidized bed model (FBR model)
compared to the well-mixed reactor model (CSTR model).
Only at low flowrates the performances from both model
predictions are close.

-— For the more general FBR model the deposition rate and
conversion go through a slight maximum as the bed
temperature is increased. Optimum Operating Conditions
for the bed temperature and flowrate can be simulated by
this model.

- The CSTR model which incorporates both homogeneous
and heterogeneous reaction was developed to predict
the generation, coagulation and scavenging of fines.
Preliminary results show that the performance is very
sensitive to the kinetic and interaction parameters.
The results can be improved by using a more realistic
FBR model and better estimates of parameters.

SILICON PRODUCTION IN AN AEROSOL REACTOR

CALIFORNIA INSTITUTE OF TECHNOLOGY

Jin Jwang Wu
M.K. Alam
B. Ellen Johnson
Richard C. Flagan

Siemens Process

BELL JAR

COOLING COILS

HEATED SUBSTRATE

GASEOUS REACTANTS

Silane Pyrolysis

$$SiH_4 + M \xrightarrow{1} SiH_2 + H_2 + M$$

$$SiH_2 + SiH_4 \overset{2}{\rightleftharpoons} Si_2H_6 \xrightarrow{3} Si_2H_4 + H_2$$

$$SiH_2 + Si_2H_6 \overset{4}{\rightleftharpoons} Si_3H_8 \overset{5}{\rightleftharpoons} Si_2H_4 + SiH_4$$

$$SiH_2 \xrightarrow{6} surface - SiH_2$$

$$surface - SiH_2 + SiH_4 \xrightarrow{7} surface - SiH_3 + SiH_3$$

$$SiH_3 + SiH_3 \xrightarrow{8} Si_2H_6$$

PRECEDING PAGE BLANK NOT FILMED
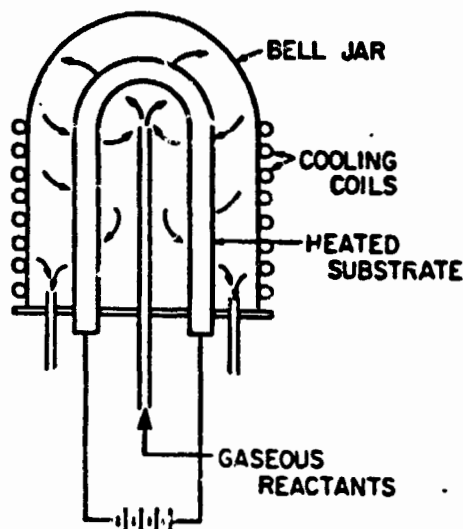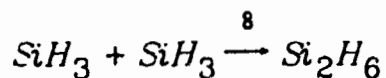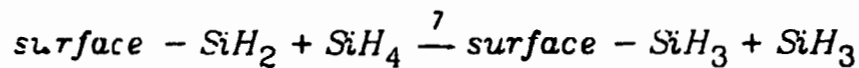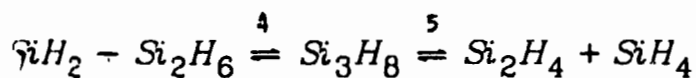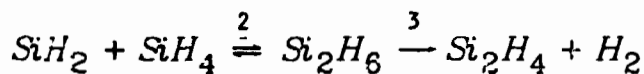
Aerosol Reactor

- Efficiency - energy & reactant usage
- Product purity
- Continuous rather than batch process
- Product particle size $D > 10{-}50\ \mu m$ to facilitate separation and subsequent processing

Simultaneous Nucleation and Particle Growth

$$\rho_g\,\frac{\partial n(a,t)/\rho_g}{\partial t} + \rho_g\,\frac{\partial}{\partial a}[\dot{a}n(a,t)/\rho_g] = J_c\delta(a-a^*)$$

$$\rho_g\,\frac{\partial C_v/\rho_g}{\partial t} = -C_p\int_{a^*}^{\infty}4\pi a^2 n(a,t)\dot{a}\,da\ -C_p\,\frac{4}{3}\pi a^{*3}J_c + R$$

Traditional approach:

$$J_c = J(\overline{c_v})$$

Clearance Volume approach:

$$J_c = \begin{cases} J(c_{v\infty})\cdot(1-\Omega) & 0 \le \Omega \le 1 \\ 0 & \Omega > 1 \end{cases}$$

where

$$\Omega = \int_0^{\infty}\frac{4}{3}\,\pi a^3\rho^3 n(a,t)\,da$$
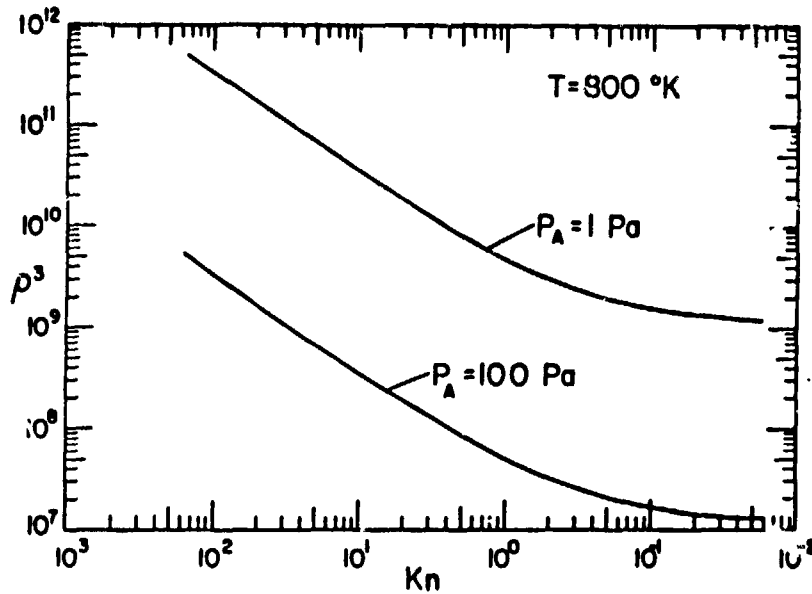
**Aerosol Reactor for Growth of Large
Silicon Particles by Silane Pyrolysis**

1. Generate seed particles by pyrolysis of
   a small amount of silane.

2. Mix seed aerosol with primary silane
   flow, limiting number concentration
   such that the amount of silane is
   sufficient to grow the desired size of
   particles from the seed.

3 React the silane at a rate which is con-
   trolled such that the seed particles
   scavenge the condensible vapors
   rapidly enough to inhibit further
   nucleation.

Reactor Optimization

- Control rate of condensible vapor production by limiting rate of temperature increase.

- Maintain $\Omega > \Omega^*$ to prevent nucleation.

- Ω depends on particle size and concentration so the growth history is important.

- Integrate rate equations to evaluate $\Omega(t)$. Adjust $T(t)$ to satisfy $\Omega_{min} > \Omega^*$ at all times.

- Use high temperature burn-off to guarantee complete reaction.

WHAT IS THE APPROPRIATE VALUE FOR Ω^* ?

D (μm)
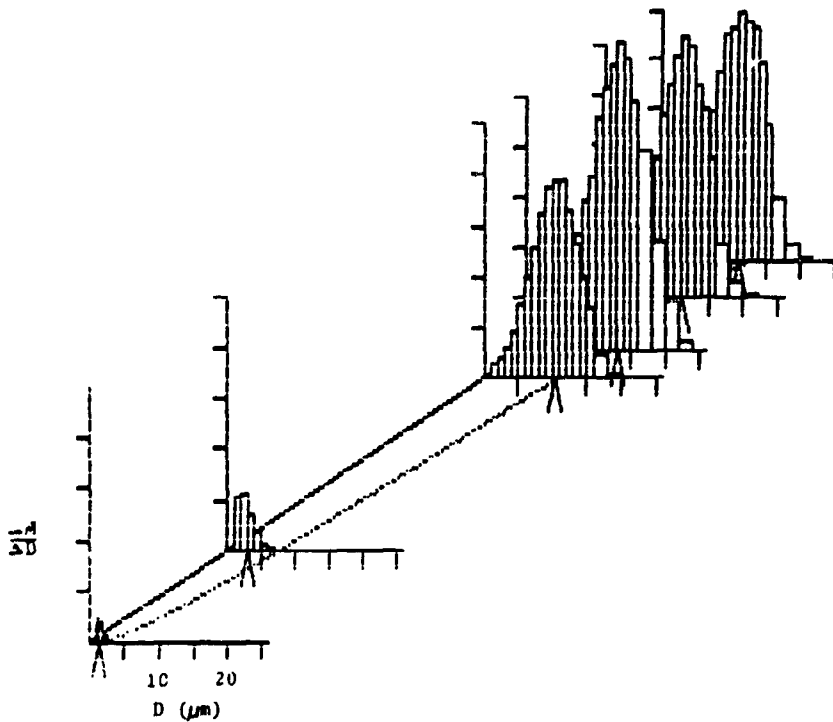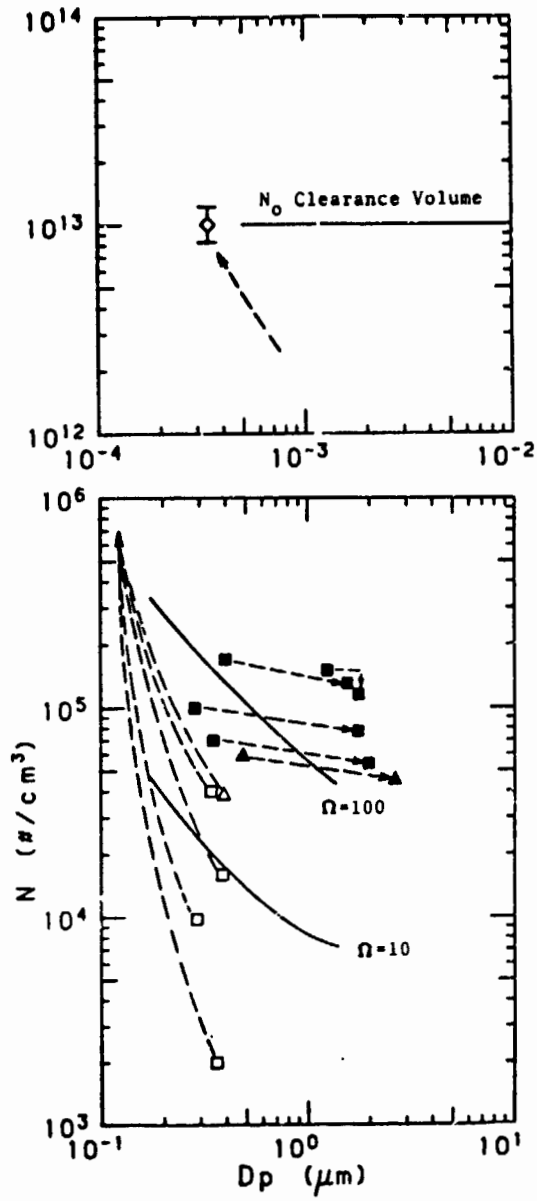
Conclusions

- Particles of low volatility materials can be grown to large size in aerosol reactors by controlling the reaction rates to minimize nucleation.

- The clearance volume model provides reasonable estimates of suitable operating conditions.

- The "total clearance volume fraction" must be large (order 20-40) to quench nucleation.

- Nucleation quenching by a growing aerosol is extremely sensitive to seed particle size.

HIGH-EFFICIENCY SILICON SOLAR CELL RESEARCH

Taher Daud, Chairman

Progress reports on research in high-efficiency silicon solar cells were presented by eight contractors and JPL. The presentations covered the issues of Bulk and Surface Loss, Modeling, Measurements, and Proof of Concept.

The University of Florida's theoretical work on heavily doped silicon included an energy-gap model, which was compared with photoluminescent and transport data. A majority carrier screening model, originally published by C.T. Sah in 1966, was presented with modifications. Improvement in the short-circuit current decay and open-circuit voltage decay measurement methods were described.

The University of Pennsylvania described and compared various methods of measurement of L or τ and s, specially in the front region of the cell. Basic requirements, types of parameters and classification of the methods regarding various options were given. Sensitivity analysis of light-beam-induced current (LBIC) method was presented.

Cornell University described its work on dislocations and grain boundaries using the electron diffraction technique. Cornell's studies on EFG showed that low concentrations of oxygen introduced a higher density of twins. Distribution and location of precipitates in processed EFG were also studied, using TEM and EDX.

A comprehensive review of oxygen-related and carbon-related defects was presented by State University of New York at Albany. It was pointed that oxygen is a bond-centered interstitial, which is mobile, whereas carb is relatively immobile, being a substitutional impurity in silicon. Data on diffusion of oxygen and various oxide precipitate formations were described along with their bonding behavior. Other impurities react with oxygen and carbon-related defects during processing and are therefore important for silicon solar cells.

Research Triangle Institute described its effort on the comprehensive modeling of solar cells and elaborated on its analysis of the charge distribution in the quasineutral region by considering a Gaussian doping profile in the emitter region. Results of measurement on cells made by Spire Corp. were compared with the simulated analysis, and a 6.4% correspondence was shown for data taken at temperatures varying from 28°C to 150°C. Other simulation plots of photo-excited hole concentration and net charge distribution were also discussed.

Anant Mokashi of JPL described studies using Purdue Research Foundation's SCAP1D simulation program. A good match was obtained between his result and MINP solar-cell data published in the literature. The doping profile in the front region was then altered to show its effect on efficiency. Sensitivity analysis with S, τ, BSF and cell thickness was also described.

HIGH-EFFICIENCY SILICON SOLAR CELL RESEARCH

The University of Washington described its study of the effects on SiN_x surface passivation of gas flow and temperature in the plasma enhanced CVD system. Special device structures for interface studies, along with a description of preparation techniques, were described. Surface state density results were good for devices prepared using the RCA cleaning procedure and fabricated with a thin oxide and nitride layer and annealed at 450°C. The layers were fabricated with a substrate temperature of 270°C. Spectral response analysis was also given for these devices. Results of electrical characterization and theoretical analysis were described for an MINP cell. A procedure for preparing 25% cells was described.

C.T. Sah Associates described its study of important loss mechanisms for >20% and <20% cells. For <20% cell', dark currents below 10^{-13} A/cm^2 will be required. Present cells are limited both by emitter and base recombination mechanisms. To reach 25% efficiency, SRH and interband Auger recombination mechanisms will have to be reduced.

In its effort on high-efficiency solar cells made from silicon web, Westinghouse has investigated loss mechanisms and formulated an analytical model to study the effect of a twin plane on V_{oc}. It shows a fail of V_{oc} by 20 mV with a twin plane having an interface recombination velocity of 10^6 cm/s. Electrical activity of a twin plane is studied on bevelled web material with the LBIC method. Further, it was shown that so web samples showed increases in diffusion length with temperature cycling. These diffusion length data were compared with those from similar temperature cycling of FZ silicon material.

PHYSICS OF HEAVILY DOPED SILICON AND SOLAR-CELL PARAMETER MEASUREMENT

UNIVERSITY OF FLORIDA

Fred A. Lindholm

CONTRACT: PHYSICS OF HEAVILY

DOPED SILICON AND SOLAR-CELL

PARAMETER MEASUREMENT

CONTRACTOR: UNIVERSITY OF

FLORIDA, FRED A. LINDHOLM

GOALS: THEORY & EXPERIMENT ON

ENERGY ΔE_G GAP, LIFETIME τ, RECOMB. S

VELOCITY, DIFFUSIVITY D, MOBILITY

IF N AND/OR P IS HIGH.

ALSO

ACCURATE DETERMINATION OF $\tau, S,$

IN QUASINEUTRAL REGIONS

REPORT DATE: 10/2/84 (3 MOS.)

Colored & Presented by

C. Tang Sah

Status (Briefly)

$$3 \; Parameters: \; \Delta E_G, \; \tau_B, \; S_{BSF}$$

1
- 1. ENERGY-GAP MODEL DEVELOPED, COMPARED WITH PHOTOLUMINESCENT AND TRANSPORT DATA. ΔE_G

2
- 2. ELECTRICAL SHORT-CIRCUIT CURRENT DECAY (ESCCD) DEVELOPED AND IMPROVED $\tau_B, \; S_{BSF}$
- 3. ESCCD AUGMENTED BY ADMITTANCE VS. ω AND V(FORWARD)
- 4. ESSCD+ADMITTANCE APPLIED TO MEASURE S AND τ FOR BASE OF MANY BSF SOLAR CELLS

Publications

2 [ESSCD IN TRANS ED. Y · ESSCD BEING WRITTEN. $\tau_B, \; S_{BSF}$

1 [ENERGY GAP MODEL IN PHOTOVOLTAICS CONF., ALSO DETAILED VERSION UNDER REVIEW, PHYS. REV. ΔE_G

CO-WORKERS: A. NEUGROSCHEL, ALL WORK: P.T. LANDSBERG, C.T. SAH, AND NEUGROSCHEL ON ENERGY GAP.

Remarks on Energy Gap Model

- ENERGY GAP = KEY PARAMETER

- SIMPLE USEFUL FORMULA

- REPRESENTS EXPERIMENTAL FACTS

    5K (OPTICAL = PL)

    300K (TRANSPORT DATA)

- HEAVILY DOPED (LARGE N OR P)

- HIGHLY EXCITED (LARGE N AND P)

    STRONG IRRADIATION

    P/N TRANSITION REGION

- T DEPENDENCE

    SOLAR CELLS AT 300K

    EXPERIMENTS, OTHER T

~~T/ TM PP P/U U NE AM E 5 T/ AM / AM L M~~

- *Simple understanble Theory:—*
    Debye (Carrier) Screening < *Electrostatic*
                                    Coulombic
    - *SAH (1966), Chapter 6*
    - *SAH, McNutt, Chan, TR28*
        (June 1974)
    - *SAH, etal., SOLAR CELL (1978)*
    - *LANDSBERG, N.L.S. (1984)*

HIGH-EFFICIENCY SILICON SOLAR CELL RESEARCH

TEMPERATURE DEPENDENCES OF

$$\sqrt{n_N p_P}/n, \ E_G, \ n_1 \ \text{and} \ L_D$$

OF SILICON

C. T. Sah, M. J. McNutt and C. N. Chan

Technical Report No. 28

June 27, 1974

The actual energy gap also includes the electron-hole, electron-electron and hole-hole electrostatic interaction energies which reduces the energy gap at high carrier concentrations. This effect is represented by Δ^r,

$$\Delta E_G = -e/4\pi\epsilon(\lambda_D + a) \tag{4}$$

$$= -1.23\times10^{-4}/(L_D + a) \quad \text{Volts} \tag{5}$$

1984 Landsberg Version

EXPRESSION FOR GAP SHRINKAGE

$$(1): \quad E_G(N,P) = W + \frac{e^2}{\epsilon a} e^{-k_D(N,P)a}$$

$$(2): \quad E_G = W + \frac{e^2}{\epsilon a}, \quad \text{for } N = P = 0$$

$$(3): \quad \Delta E_G = \frac{e^2}{\epsilon a} [1 - e^{-k_D(N,P)a}]$$

$$= \frac{e^2}{\epsilon} k_D(N,P)$$

$$\lambda_D = \frac{1}{k_D} = \text{Debye Screening Length}$$

1966 Sah Version: Screening by Majority carriers on minority carrier ΔE_G

NOTE: ΔE_G data is from minority carriers experiments!

P-Si

$$\Delta E_0 = E_G$$

$$-\frac{e^2}{4\pi\epsilon r}$$

$$\Delta E_i = E_G + \Delta E_G$$

$$\Delta E_G = \frac{-e^2}{4\pi\epsilon} k_D$$

$$-\frac{e^2}{4\pi\epsilon r} e^{-k_D r}$$
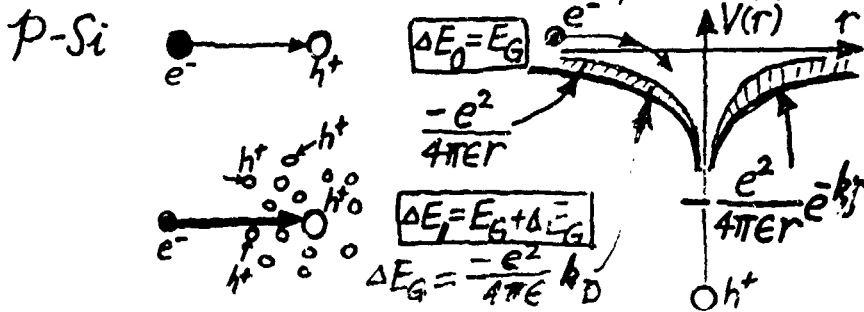
Screening Wave Number k_D

$$k_D^2 = \frac{e^2}{\epsilon k T} \left[N_C F_{-1/2}(\eta_F - \eta_C) + \ldots \right]$$

FOR GENERAL N AND P.

FOR LOW CONCENTRATIONS, FERMI
INTEGRALS BECOME EXPONENTIALS:

$$k_D^2 = \left[e^2 (N + P) / \epsilon k T \right]$$

OR, FOR DEGENERATE DENSITY N,

$$k_D^2 = (3/\pi)^{1/3} \left(e^2 m^*_n / \epsilon h^2 \right) N^{1/3}$$

MKS unit
(4π of CGS taken out.)
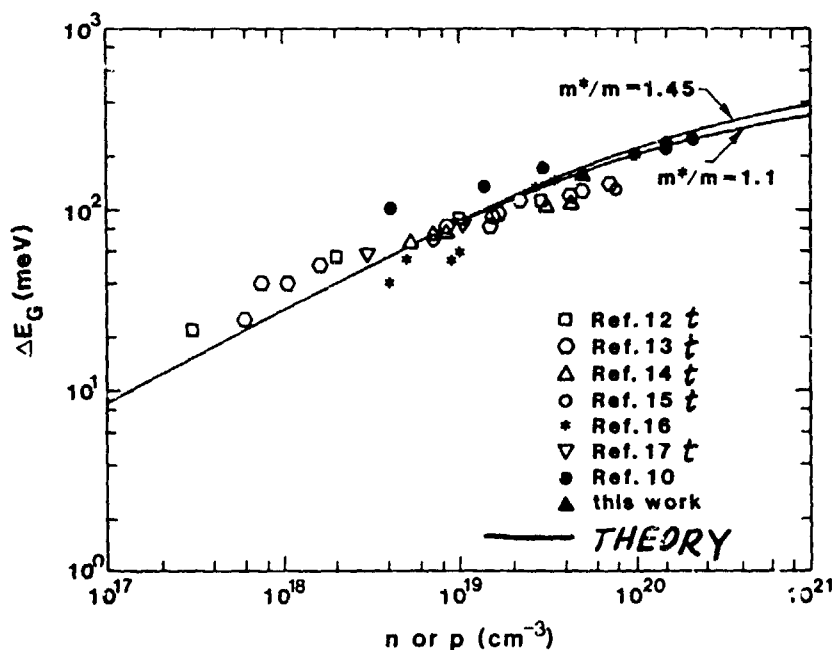
Comparison with minority carrier transport or 'pn' product measurements in bipolar devices: diodes, transistors.
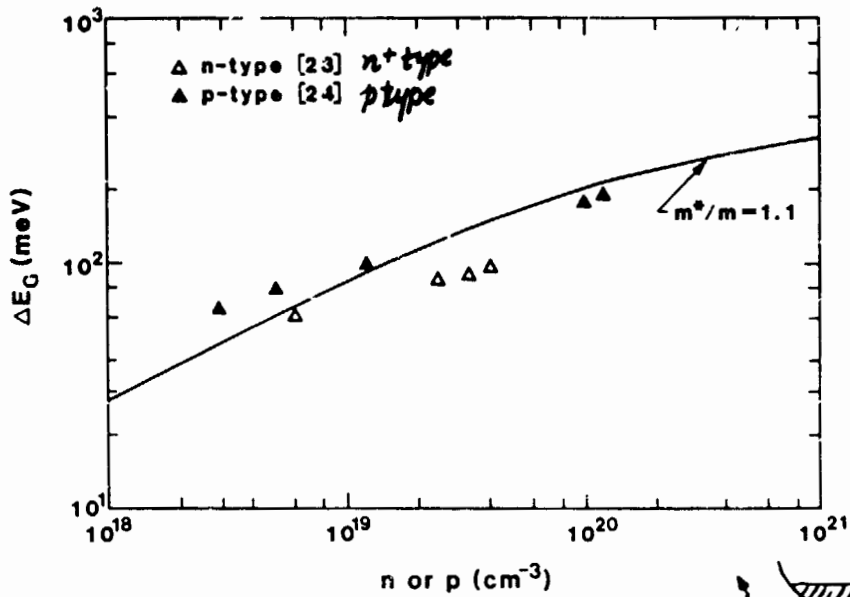
Luminescence data (Dumke) at 300K

23. Dumke, APL 42, 196 (1983)
24. Dumke, JAP 54, 3200 (1983)
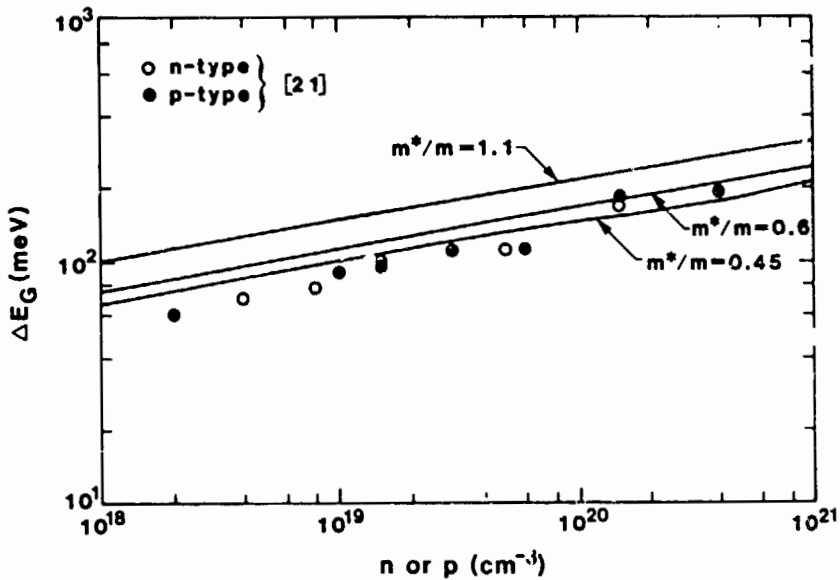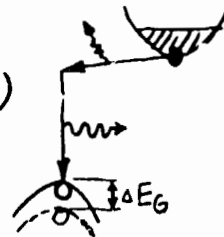
5K Photoluminescence and exitation data
Wagner PR B29, 2002 (1984)

2. MEASUREMENT OF $\underline{\underline{S}}_{BSF}$ AND $\underline{\underline{\tau}}_B$ IN QUASINEUTRAL BASE OF BSF CELLS

● — ESSCD ⟷ slope + intercept

● 1. REPORT IMPROVED ESSCD: ELECTRICAL SHORT-CIRCUIT CURRENT DECAY BY USE OF

FAST MOS TRANSISTOR SWITCH (10 ns.).

2. ADVANTAGE OF ESSCD VS OPEN-CIRCUIT VOLTAGE DECAY, REVERSE STEP RECOVERY, ETC. IT AVOIDS INFLUENCE OF HOLES & ELECTRONS IN P/N SCR BY FORCING DENSITIES TO EQUILIBRIUM VALUES IN 10 ps.

3. TO MEASURE S AND τ IN BASE YOU NEED SLOPE OF LOG V(t) AND ONE OTHER PIECE OF DATA. THIS IS BEST PROVIDED BY $\underline{Y(j\omega,V)=}$ ADMITTANCE MEASURED ON BRIDGE. Y PROVIDES TWO THINGS: (A) SEPARATION OF QNE I FROM QNB I BY CHANGING ω. (B) CONFINEMENT OF Y RESPONSE TO VOLUME (NOT SURFACE) FOR LARGE ω; THUS CAN GET τ EVEN IF DIFF. LENGTH > BASE THICKNESS.

ESSCD

G_{QN} vs ω
$C_{HF} - C_{LF} \rightarrow \tau_B$

$$Y(\omega) \text{ actually } - C_{HF} + C_{LF} = C_{QN} \text{ vs } \omega$$
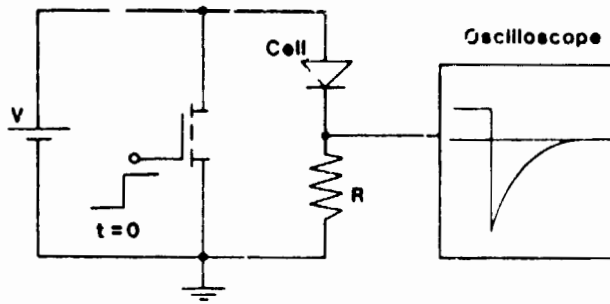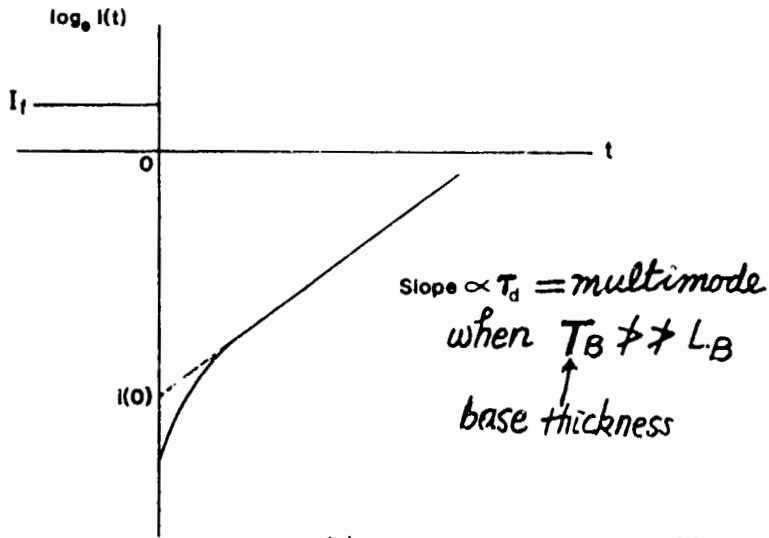
$$G_{QN} \text{ vs } \omega$$

(a)

Slope $\propto \tau_d =$ *multimode*

when $T_B \not\gg L_B$

base thickness

(b)

$\tau_d \rightarrow$ *multi-mode*
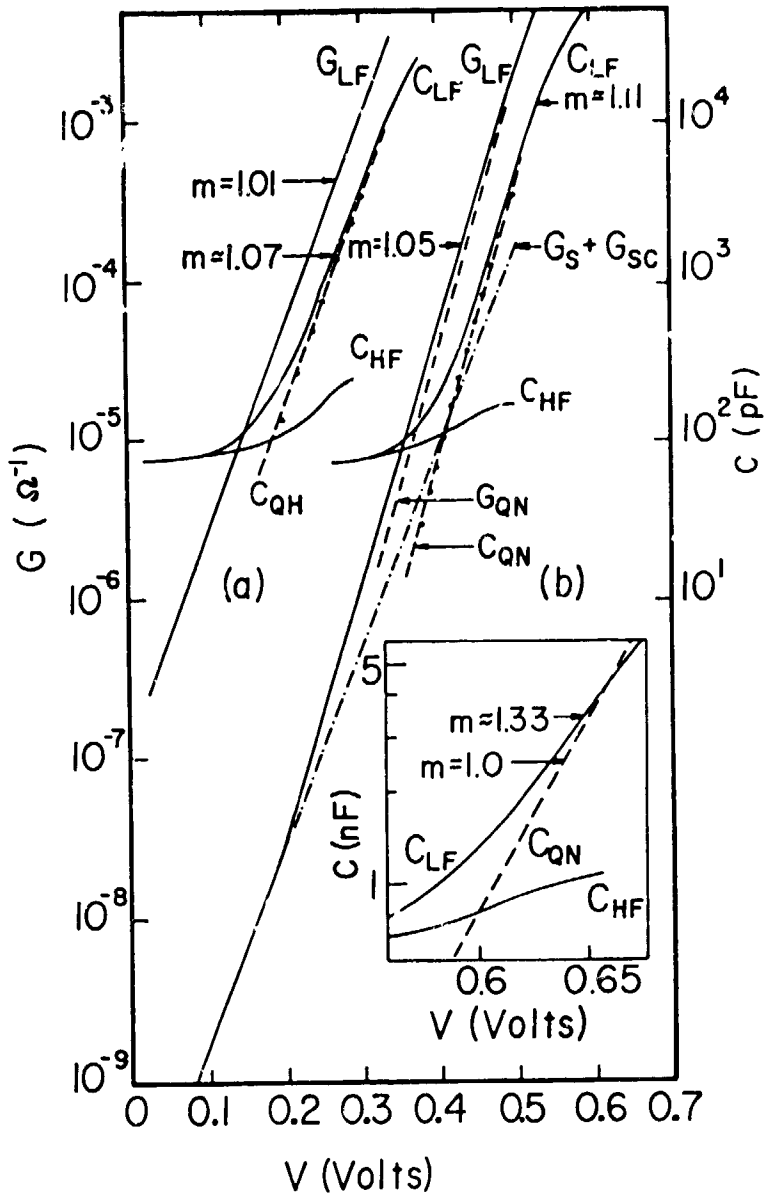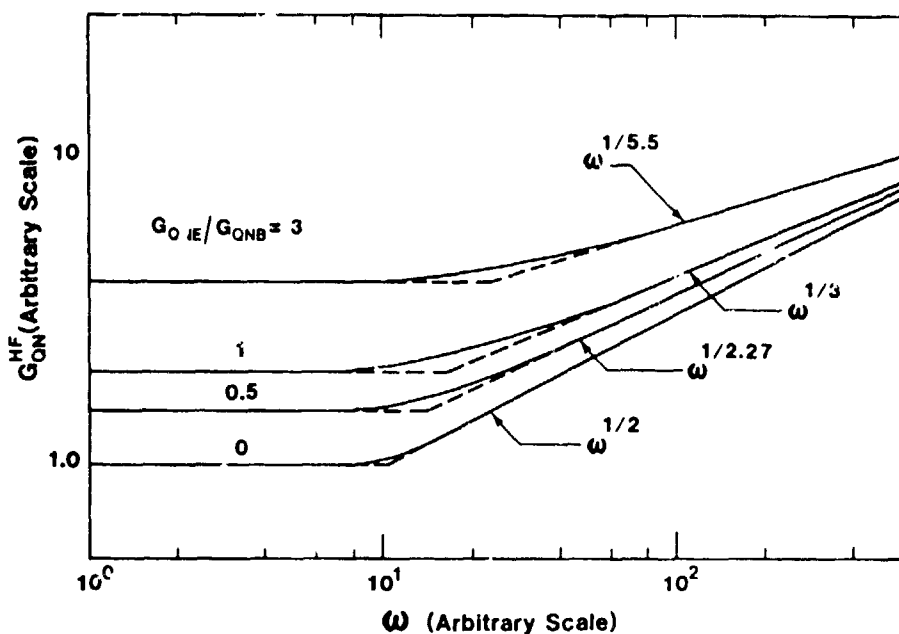
Recommendations

$OLD\text{-}RENEWED$

● 1. USE NEW ENERGY GAP MODEL
IN COMPUTER SIMULATION. ΔE_G

● 2. USE ESSCD + $Y(j\omega,V)$ FOR τ_B
AND S_{BSF} OF BACK SURFACE FIELD.

NEAR TERM EFFORTS:

● 1. NEW EXPERIMENTS TO EXPLORE
ENERGY GAP MODEL FURTHER. ΔE_G

● 2. ADAPT S_E AND τ_E MEASUREMENTS
TO EMITTER, USING $Y(j\omega)$.

● 3. THEORY TO ACCOUNT FOR $\Delta E_D \not{4} \Delta E_A$
IMPURITY BAND INFLUENCE FOR
MODERATELY HIGH DENSITIES: 10^{1-}

● 4. ACCOUNT FOR HOLES AND
AND ELECTRONS IN SCR TO C_{SCR}
IMPROVE ACCURACY OF OPEN-
CIRCUIT VOLTAGE DECAY G_{SCR}

● 1. $\Delta \bar{E}_G , \oplus \Delta E_D \not{4} \Delta E_A$

● 2. $S_{BSF}, \tau_B, \oplus S_E, \tau_E$

MEASURING BULK RECOMBINATION RATES AND BOUNDARY RECOMBINATION VELOCITIES

UNIVERSITY OF PENNSYLVANIA

M. Wolf

Measurement of L (or τ) and s

I.   ALL METHODS MEASURE SOME OTHER QUANTITY, DEDUCE L (OR τ) AND S.

II. IN MOST, THE MEASURED QUANTITY IS ALSO INFLUENCED BY OTHER PARAMETERS. THESE ARE SEPARATELY MEASURED, ASSUMED, OR NEGLECTED.

III. ALL METHODS HAVE RANGES OF L, S, OR THE OTHER PARAMETERS, WHERE THE DEPENDENCE OF THE MEASURED QUANTITY ON L AND/OR S IS WEAK.

IV. THERE ARE STEADY-STATE AND TIME-DEPENDENT MEASUREMENTS. SOME OF THE LATTER STILL DEPEND ON A TRANSPORT PROPERTY (L), NOT A TIME CONSTANT (τ).

V.   SOME METHODS FIND A CONDITION WHERE THE MATHEMATICAL RELATIONSHIPS BECOME SIMPLE, E.G. REAL AND IMAGINARY PARTS OF A NUMBER BECOME EQUAL.

Recombination in dept- region

MEASURED QUANTITIY:

			$A_1....A_I,$	$B_1....B_J,$	$C_1....C_K,$	$D_1....D_K)$
$M = M (L_{WANTED},$		$u_{WANTED},$	VARIABLE	VARIABLE	CONSTANT	CONSTANT
MAY BE			DEVICE	EXTERNAL	DEVICE	EXTERNAL
COMPLEX			PAPAMETERS	PARAMETERS	PARAMETERS	PARAMETERS
NUMBER						

EXAMPLE: L_{FI} $u_{FI} \div 1$

THICKNESSES	T	ANY OF A_1	ANY OF B_1
$S_{BJ}, S_{FJ},$	s-INFLUEN-	NOT	NOT VARIED
$L_{BJ}, L_{FJ}, u_{FJ},$	CING ENV'T	VARIED;	
u_{BJ}	EXCITATION:	R IN	
	LIGHT: λ, f	DEPL'N	
	VOLTAGE: V_1, f	REGION	
	TERMINAL		
	IMPEDANCE:		
	s.c., o.c., ETC.		

Basic Requirement for Determination of Both L and u

AT LEAST <u>2 INDEPENDENT MEASURED DATA</u> (M_1, M_2) NEEDED,

WHICH ARE <u>SENSITIVE TO u AND L</u> IN THEIR RANGE OF INTEREST.

(<u>ONE</u> MEASUREMENT MAY BE SENSITIVE TO <u>ONLY L OR u</u>, IF THE <u>OTHER</u>

IS SENSITIVE TO <u>BOTH</u>.)

---

2 INDEPENDENT DATA ARE AVAILABLE FROM:

- COMPLEX NUMBERS (ONE OPTION)

- VARIATION OF A SUITABLE PARAMETER (EACH PARAMETER = ONE OPTION)

FINDIT: A SENSITIVE DATA PAIR SEEMS THE MORE LIKELY, THE MORE OPTIONS

FOR OBTAINING 2 DATA POINTS EXIST.

Type of Parameters Varied

INTERNAL

EXTERNAL

MINORITY CARRIER
EXCITATION

GENERALLY
REQUIRES
ESPECIALLY
PREPARED
SAMPLES

LIMITED TO REGION
TO BE TESTED

BEYOND REGION
UNDER TEST

i.e NONPENETRATING
LIGHT, SHORT CIRCUIT
TECHNIQUES

WEAK INFLUENCE OF
OTHER REGIONS UNDER
SOME CONDITIONS

$$M = M(L, u, a...., b....)$$

RECOMBINATION
PARAMETERS AND
OTHER INTERNAL
PARAMETERS
OUTSIDE THE
REGION OF INTEREST
ELIMINATED
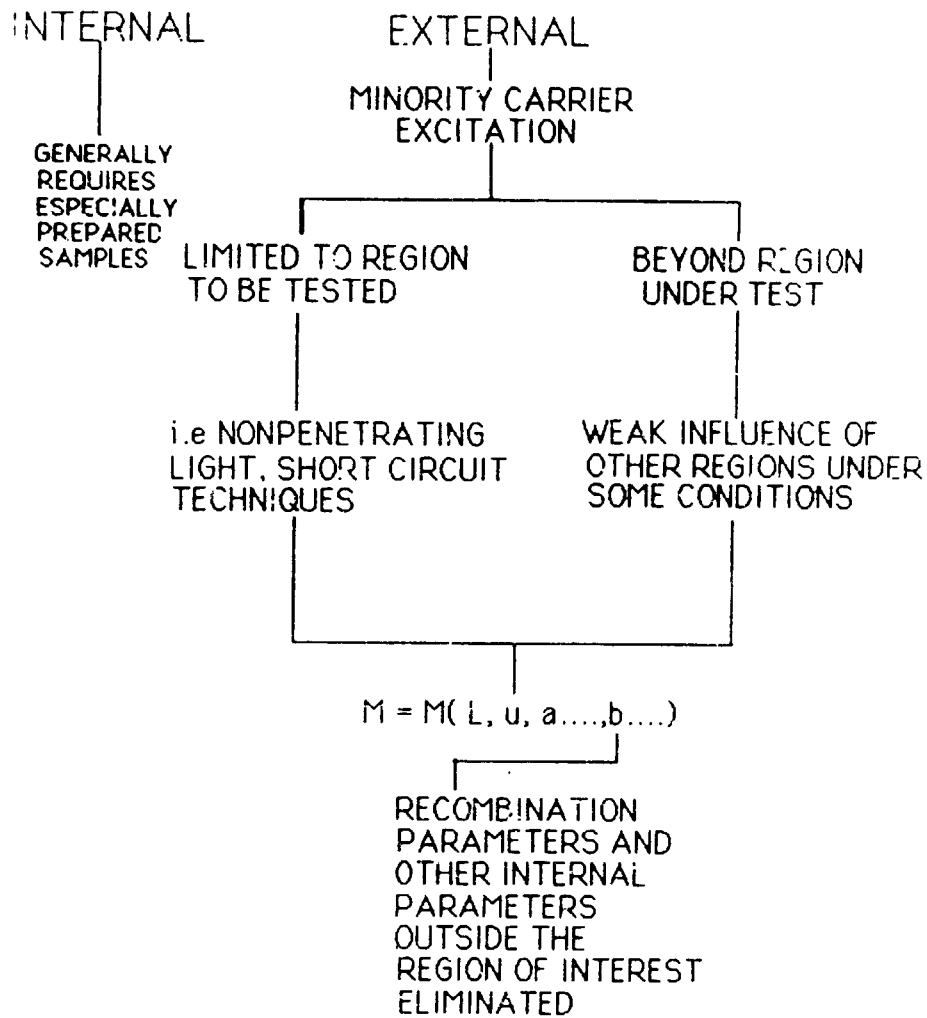
HIGH-EFFICIENCY SILICON SOLAR CELL RESEARCH

Classification of Methods

TYPE	EXCITATION	M	VARIED EXTERNAL PARAMETERS	NUMBER OF OPTIONS
ASLBIC	LIMITABLE	REAL	λ	1
MODULATED LIGHT METHOD	LIMITABLE	COMPLEX	ω, λ	3
IMPEDANCE	DEVICE DEPENDENT	COMPLEX	ω	2
I_{sc}, V_{oc} PAIR	DEVICE DEPENDENT	COMPLEX	CIRCUIT IMPEDENCE	1
SCCD	DEVICE DEPENDENT	REAL	CIRCUIT IMPEDENCE	1

Goal: Reduce the Number of Variable or Constant Parameters
(Requirements Listed in Order of Importance):

1. ELIMINATE INFLUENCE OF UNMEASURABLE PARAMETERS.

2. FIND SENSITIVE RELATIONSHIP BETWEEN L_{WANTED}, U_{WANTED}, AND M.

3. METHOD SHOULD BE APPLICABLE TO FINISHED, OR IN-PROCESS PRODUCT.

4. FIND EASILY MEASURABLE QUANTITY M, AND EASILY, REPEATABLY VARIABLE PARAMETERS.

5. REDUCE NUMBER OF INFLUENCING PARAMETERS.

6. FIND SIMPLE RELATIONSHIP.

The Basic Carrier Diffusion Expression

AN EXAMPLE FOR M: (ASLBIC):

$$M = \eta_{COLL} = \frac{B}{B+Y} E^{-B} \left\{ 1 + \frac{1}{B-Y} \frac{(1+A)}{COSH} \frac{YE^{-Y}}{Y +} \frac{-(B+A'')E^{B}}{A SINH} \right\}$$

(SIMPLEST FORM FOR SINGLE-LAYER FRONT REGION)

WITH THE BASIC VARIABLES:

$$Y = \frac{X_{J,F}}{L}; \qquad A = \frac{SL}{D}; \qquad B = \alpha(\lambda).X_{J,F}$$

VERY SIMILAR RELATIONSHIPS FOR OTHER METHODS.
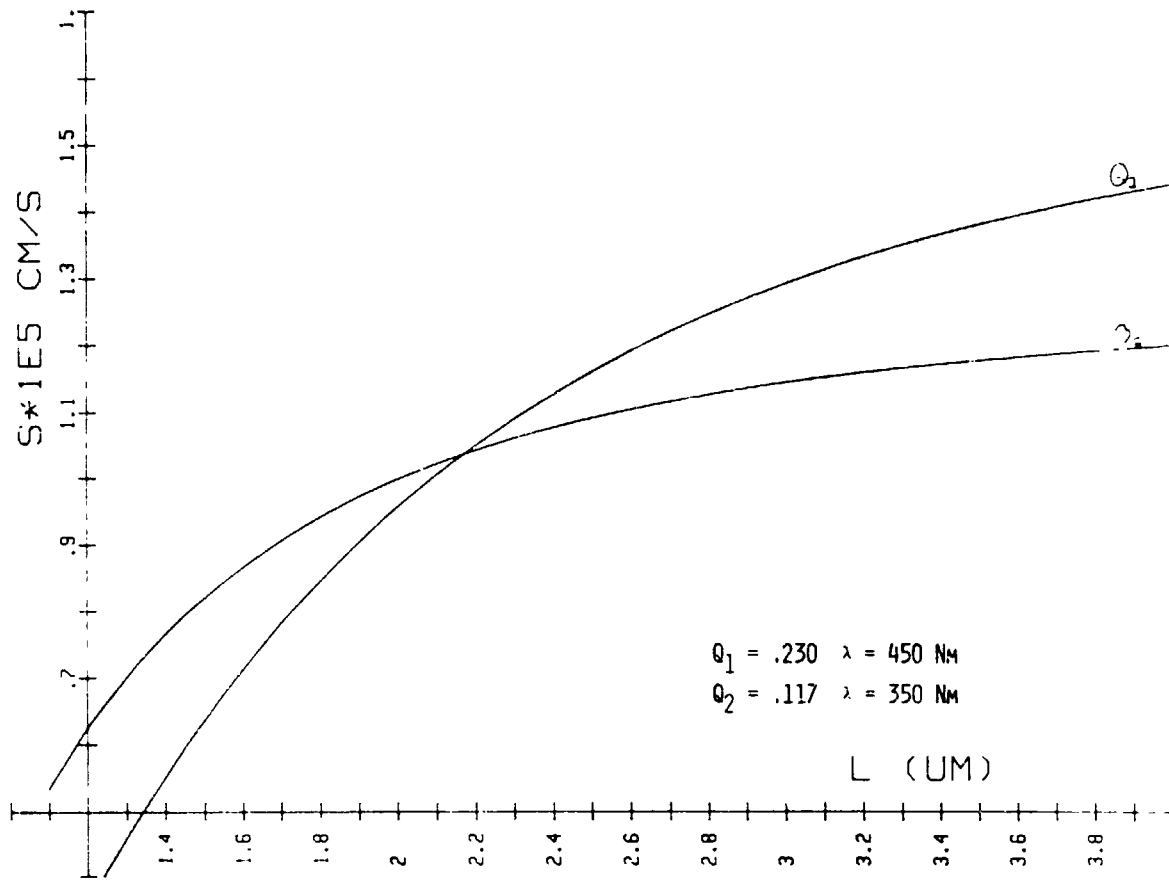
Plot with axes: vertical axis labeled "S*1E5 CM/S" with values 1., 1.5, 1.3, 1.1, .9, .7; horizontal axis labeled "L (UM)" with values 1.4, 1.6, 1.8, 2, 2.2, 2.4, 2.6, 2.8, 3, 3.2, 3.4, 3.6, 3.8. Annotations: $Q_1 = .230 \pm 2.5\%$, $Q_2 = .117 \pm 2.5\%$

$Q_1 = .09750$

$Q_2 = .06696$

$Q_1 = .08750 \pm 2.5\%$

$Q_2 = .06696 \pm 2.5\%$
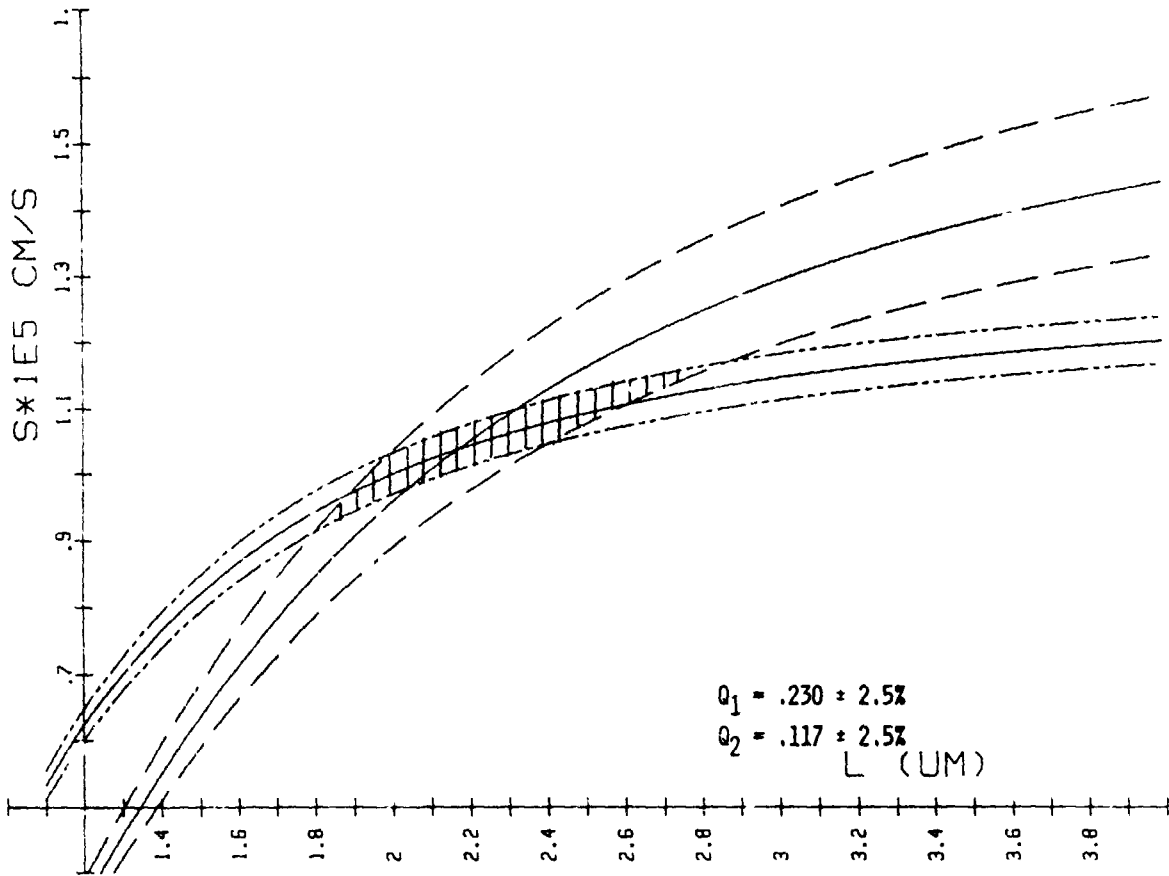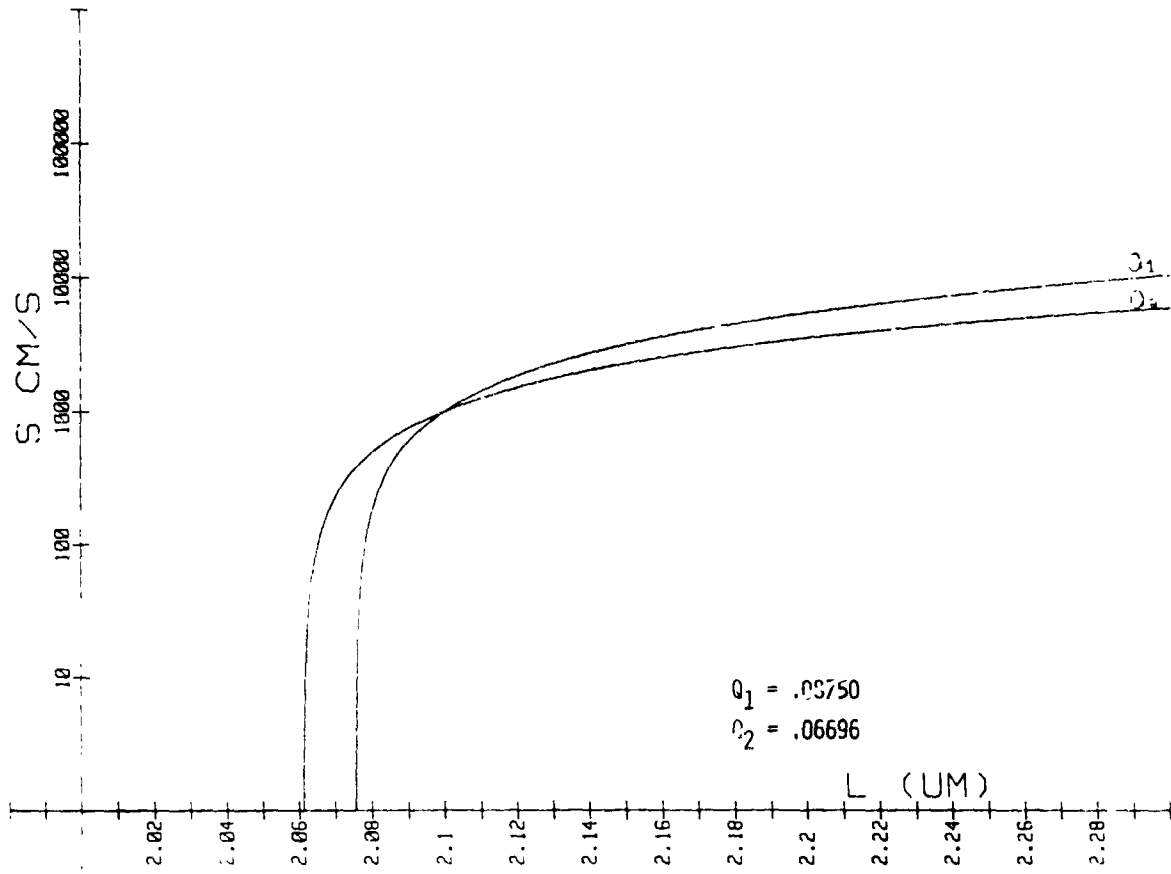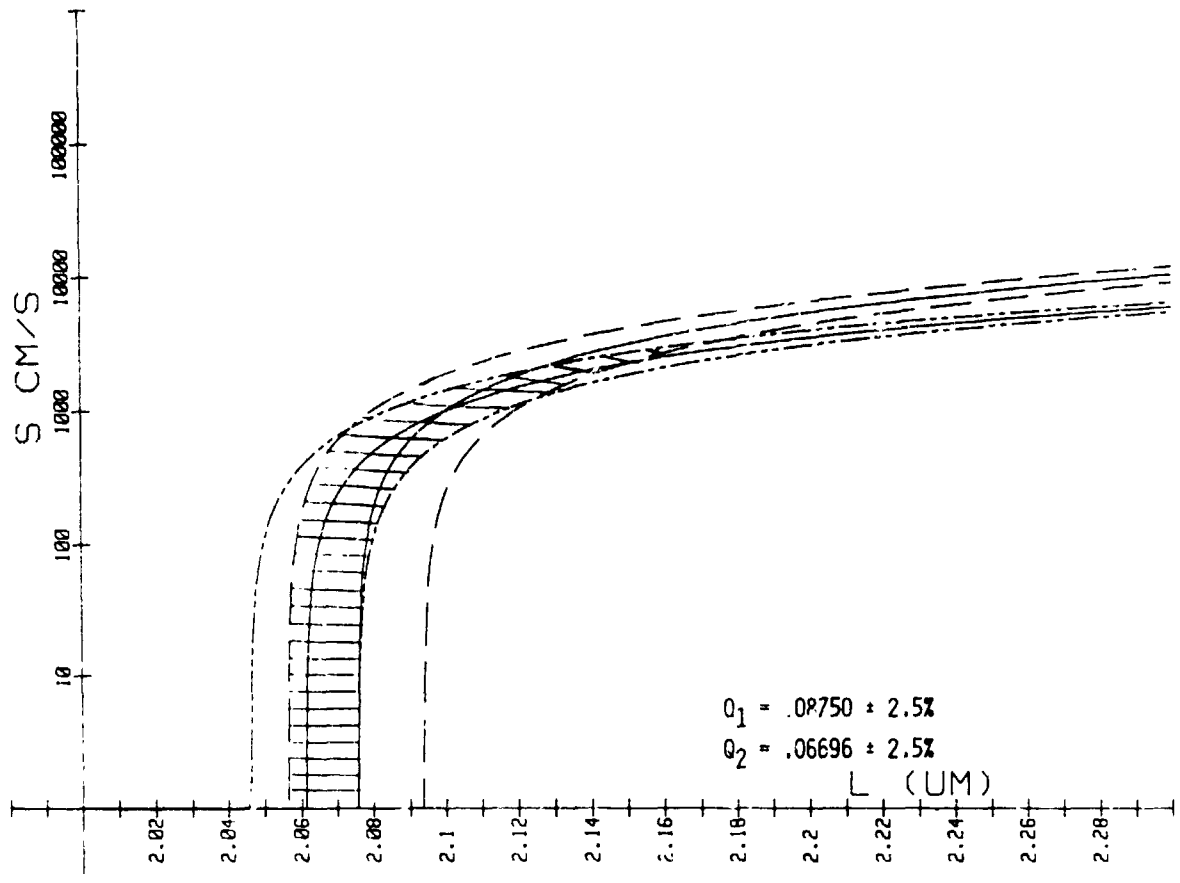
HIGH-EFFICIENCY SILICON SOLAR CELL RESEARCH

Measurement Comparison Criterion

SENSITIVITY ANALYSIS DETERMINES THE ERRORS IN CONSEQUENCE OF INACCURACIES IN THE MEASURED DATA AND THE PARAMETERS.

EXAMPLE ASLBIC:

$$M_1 = M (L, S, \lambda_1, A_2 \ldots) \tag{1}$$

$$M_2 = M (L, S, \lambda_2, A_2 \ldots) \tag{2}$$

IDEALLY, THESE EQUATIONS WOULD BE ANALYTICALLY INVERIABLE TO:

$$S = S (M_1, M_2, \lambda_1, \lambda_2, A_2 \ldots B_1 \ldots) \tag{3}$$

$$L = L (M_1, M_2, \lambda_1, \lambda_2, A_2 \ldots B_1 \ldots) \tag{4}$$

AND THEN PERMIT A SENSITIVITY ANALYSIS SUCH AS:

$$\Delta S = \left.\frac{\partial S}{\partial M_1}\right|_{M_2} \Delta M_1 + \left.\frac{\partial S}{\partial M_2}\right|_{M_1} \Delta M_2 \tag{5}$$

$$\Delta L = \left.\frac{\partial L}{\partial M_1}\right|_{M_2} \Delta M_1 + \left.\frac{\partial L}{\partial M_i}\right|_{M_1} \Delta M_2 \tag{6}$$

AS EQ. (1), (2) ARE TRANSCENDENTAL (3), (4) ARE NOT ANALYTICALLY EXPRESSABLE.
HOWEVER:

$$S = S (L, M, \lambda, A_2 \ldots, B_1 \ldots)$$

IS AVAILABLE, AND CONSEQUENTLY (6). FOR (5), NOTE

$$\left.\frac{\partial S}{\partial M_i}\right|_{M_i} \neq \left.\frac{1}{\frac{\partial M}{\partial S}}\right|_L$$

WHERE ANALYTICAL TREATMENT NOT POSSIBLE, LINEAR APPROXIMATIONS:

$$M_1 \quad M_0 (S_F, L_F, A_1 \ldots) + \left.\frac{\partial M}{\partial A_1}\right|_{S_F, L_F \ldots} \Delta A_{1, 1}$$

$$M_2 \quad M_0 (S_F, L_F, A_1 \ldots) + \left.\frac{\partial M}{\partial A_1}\right|_{S_F, L_F \ldots} \Delta A_{1, 2}$$

$$M_3 \quad M_1 + \left.\frac{\partial M}{\partial S_F}\right|_{L_F, A_1 + \Delta A_1, 1} \ldots$$

MAY YIELD SOME INFORMATION ON SENSITIVE RANGES.

STUDIES OF OXYGEN- AND CARBON-RELATED DEFECTS
IN HIGH-EFFICIENCY SILICON SOLAR CELLS

STATE UNIVERSITY OF NEW YORK AT ALBANY

J. Corbett

OXYGEN AND CARBON ARE ALMOST ALWAYS PRESENT IN SILICON.

[O] $\approx$ 10^{18} / CC ,   30 ppma

[C] $\lesssim$ 5 x 10^{17} / CC ,   10 ppma

Oxygen comes from the silicon source or from quartz boats.

Carbon comes from graphite susceptors in pullers.

WE KNOW THE CONFIGURATIONS OF THESE IMPURITIES:

OXYGEN IS A PUCKERED BOND-CENTERED INTERSTITIAL.
(OXYGEN IS QUITE MOBILE.)

CARBON IS A SUBSTITUTIONAL ATOM.
(CARBON IS RELATIVELY IMMOBILE.)

BOTH ARE ELECTRICALLY INACTIVE

IN THIS FORM.

HIGH-EFFICIENCY SILICON SOLAR CELL RESEARCH

ALTHOUGH THERE HAS BEEN A LOT OF CONTROVERSY AND UNCERTAINTY
CONCERNING THE DIFFUSION COEFFICIENT OF INTERSTITIAL OXYGEN,
WE NOW KNOW THIS QUANTITY VERY WELL, PRIMARILY BECAUSE OF THE
WORK OF STAVOLA AND OF MIKKELSEN.

$$D = 0.17 e^{-2.54 eV/RT}$$
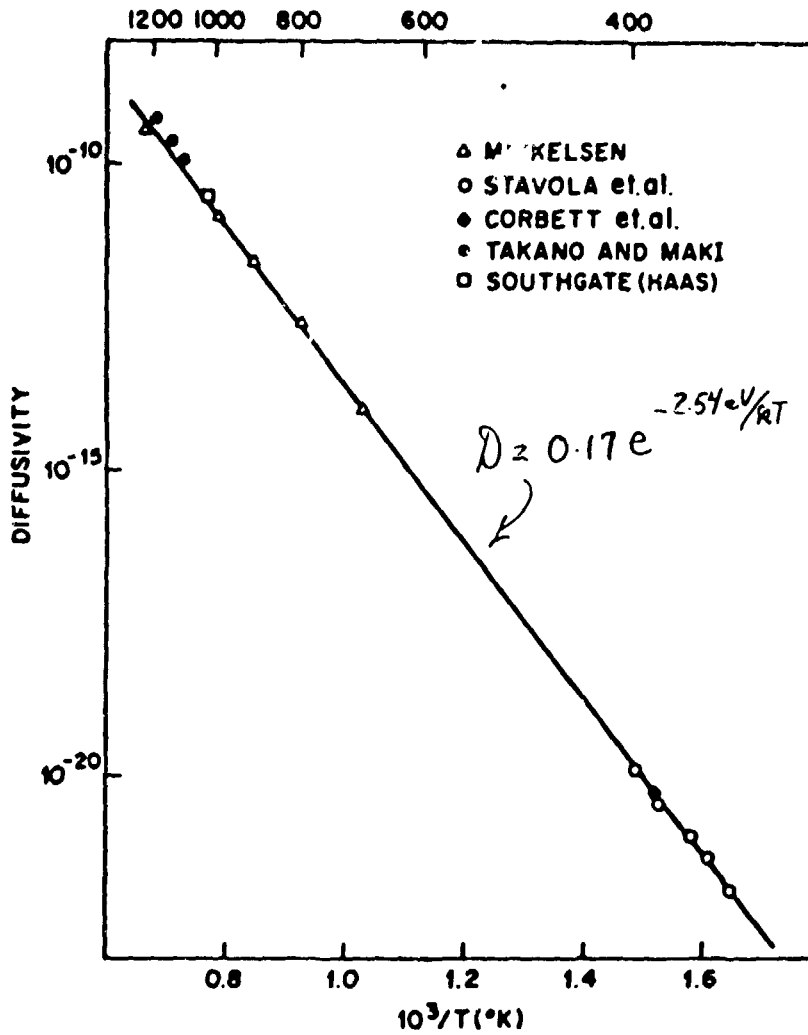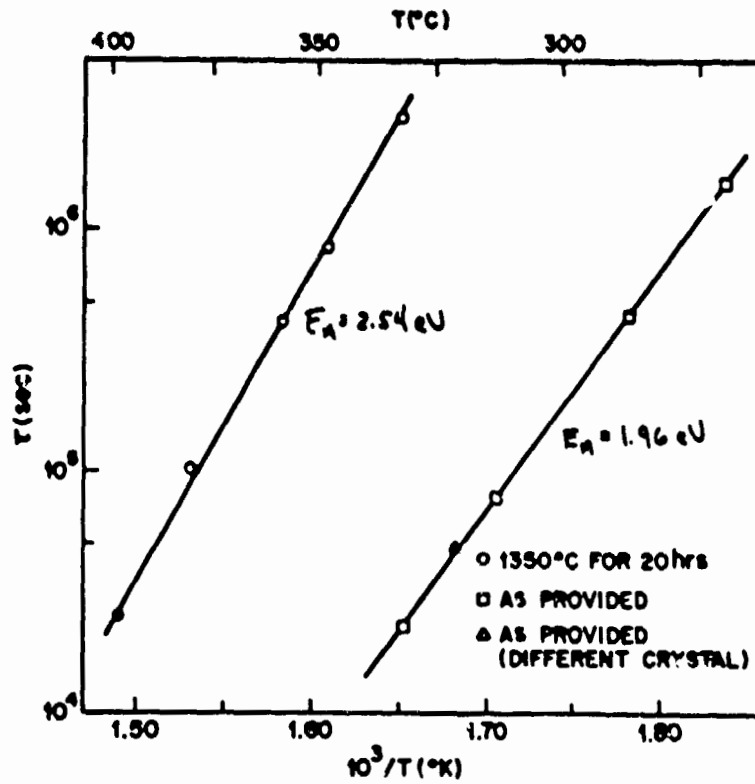
A MAJOR ADVANCE IS THAT MODERN QUANTUM CHEMICAL CALCULATIONS (SNYDER-ALBANY) CAN TREAT THE DIFFUSION OF OXYGEN QUANTITATIVELY.

BUT STAVOLA ALSO FOUND AN ANOMALOUS DIFFUSION PROCESS IN SAMPLE WHICH HAD A 2 HOUR HEAT-TREATMENT AT 900 C .

THIS ANOMALY REMAINS A MAJOR PROBLEM.

M Stavola et al.

WHY IS THIS DIFFUSION A CONCERN?

MOBILE OXYGEN PRECIPITATES IN A COMPLEX WAY,
AND CARBON MAKES THAT PRECIPITATION EVEN MORE COMPLEX.

CONSIDER A SAMPLE THAT HAS HAD A HIGH TEMPERATURE (E.G., 1300 C) ANNEAL WHICH DISPERSES THE OXYGEN AND CARBON.

FULLER ET AL. (1954 !) FOUND HEAT TREATMENT DONORS BEFORE IT WAS KNOWN THAT OXYGEN WAS IN SILICON.

KAISER, FRISCH AND REISS (1957) OUTLINED THE BROAD PICTURE OF THE PROCESSES:

$$O + O \longrightarrow O_2$$

$$O + O_2 \longrightarrow O_3$$

$$O + O_3 \longrightarrow O_4$$

$$O + O_4 \longrightarrow O_5$$
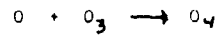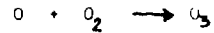
ETC.

SUBSEQUENT WORKERS USING IR, EPR AND DLTS STUDIES SHOWED THAT THERE IS A HIERARCHY OF DOUBLE DONOR DEFECTS.

SUEZAWA AND SUMINO (1984) SHOWED THAT

$$TD1 = O_3$$

$$TD2 = O_4$$

$$TD3 = O_5$$

$$TD4 = O_6$$

$$TD5 = O_7$$

$$TD6 = O_8$$

IR STUDIES REVEAL BOTH THE HYDROGENIC AND HELIUM-LIKE STATES
OF THESE NINE DOUBLE DONORS.

THE HELIUM-LIKE GROUND STATE IS AT (E - 0.15 eV) FOR THE
TD1 AND GETS PROGRESSIVELY SHALLOWER FOR THE REMAINING
DEFECTS. THE THEORY OF THIS PROGRESSION HAS BEEN ESTABLISHED
(CORBETT, FRISCH, AND SNYDER, 1994).

THE DONOR APPEARS TO HAVE A "CORE" WHICH CAUSES THE
ELECTRICAL ACTIVITY AND SUCCESSIVE OXYGENS CREATE THE
HIERARCHY OF DEFECTS.

"CORE" : n (OXYGENS) + TDn

THERE ARE A NUMBER OF MODELS FOR THE CORE, BUT THE
FRONT-RUNNERS ARE THE 'YLID" AND THE (VACANCY+ TWO-OXYGENS),
BOTH MODELS ARISING FROM STUDIES AT ALBANY

" Ylid "

oR

Split <110> Si-O
Interstitial

$(V \cdot O_2)$
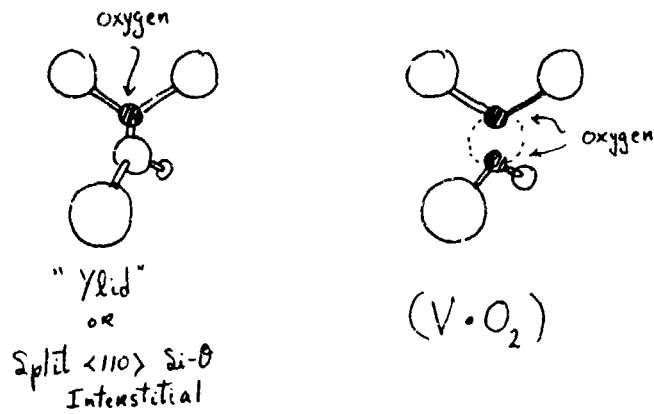
THERE HAS BEEN A GREAT DEAL OF PROGRESS IN THE STUDY OF OXYGEN IN SILICON, AND WE SHOULD SOON UNDERSTAND THIS OLD PROBLEM.

WE ALREADY KNOW ONE OF THE DIFFICULTIES: THE OXYGEN PRECIP-ITATION PROCESS GENERATES SILICON INTERSTITIALS AND THESE ARE VERY MOBILE AND REACTIVE.

$$(Si)_I + (C)_S \longrightarrow (C)_I$$

$$(Si)_I + (B)_S \longrightarrow (B)_I$$

etc.
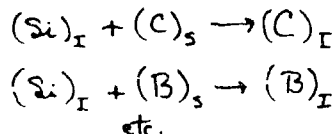
AND THE PRODUCTS OF THE REACTIONS, E.G., THE CARBON-INTERSTITIAL AND THE BORON-INTERSTITIAL ARE VERY MOBILE, REACTIVE AND ELECTRICALLY ACTIVE, AND CREATE OTHER DEFECTS THAT ARE ELECTRICALLY ACTIVE.

FURTHERMORE CARBON SUPPRESSES THE FORMATION OF THERMAL DONORS AT 450° C, BUT APPARENTLY AIDS THE FORMATION OF "NEW DONORS" AT 650° C, AND LITTLE HAS BEEN DONE IN STUDYING THOSE DEFECTS.

RETURN TO THE PRECIPITATION OF OXYGEN.

AFTER A 600 °C ANNEAL, THE THERMAL DONORS ARE GONE, AND (110) "RODS" AND "BLACK DOTS" ARE OBSERVED IN THE ELECTRON MICROSCOPE.

BOURRET ET AL. (1983) HAVE SHOWN, USING HIGH RESOLUTION ELECTRON MICROSCOPY, THAT THE RODS ARE COESITE, A HIGH PRESSURE PHASE OF SILICON-DIOXIDE, AND THE DOTS ARE AMORPHOUS SiO_x.
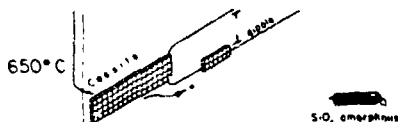
AFTER AN 850° C ANNEAL, THE RODS HAVE DISAPPEARED AND DISLOCATION LOOPS (WITH, PRESUMABLY, COESITE PRECIPITATES) AND LARGER SiO_x DEFECTS ARE OBSERVED IN ELECTRON MICROSCOPY.

AFTER AN 1100° C ANNEAL, LARGE STACKING FAULTS (AGAIN WITH
OCCASIONAL DECOR) (¨¨) OF PRECIPITATES) AND LARG¨ SILICON
DIOXIDE PRECIPI¨ ¨S ARE OBSERVED IN THE ELECTRON MICROSCOPE.
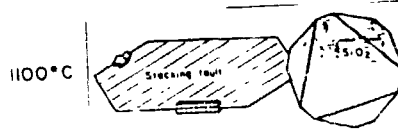
WHY IS ALL THIS PERTINENT TO HIGH EFFICIENCY SILICON SOLAR
CELLS?

WE NOW KNOW THAT THERE ARE MANY PROCESS-INDUCED DEFECTS IN
SILICON, SOME OF WHICH ARE THE FAST DIFFUSERS, Fe, Ni, Cu,
Au, ETC.

ALL OF THESE DEFECTS CAN INTERACT WITH THE OXYGEN- AND
CARBON-RELATED DEFECTS. INDEED THE OXYGEN PRECIPITATION IS
KNOW TO PROVIDE DEFECTS WHICH ARE HELPFUL IN GETTERING
IMPURITIES.

BUT THE NATURE OF THESE REACTIONS IS STILL LARGELY UNKNOWN.

COMPREHENSIVE SILICON SOLAR-CELL COMPUTER MODELING

RESEARCH TRIANGLE INSTITUTE

M.F. Lamorte

Synopsis of Significant Progress

1. Model and analysis of the net charge distribution in quasineutral regions (investigation continuing in collaboration with Professor F A. Lindholm, University of Florida)

2. Experimentally determined temperature behavior of Spire Corp. n^+pp^+ solar cells where n^+-emitter is formed by ion implantation of ^{75}As or ^{31}P (Acknowledgments: M. B. Spitzer, Spire Corp.; and Ward J. Collis, North Carolina A&T State University, Greensboro, N.C.)

3. Initial validation results of computer simulation program using Spire Corp. n^+pp^+ cells.

Model and analysis of the net charge distribution in quasineutral regions: a model and a corresponding analysis has been developed that describes the net charge distribution which gives rise to built-in electric fields. Conclusions derived from analysis are:

a. only the redistribution of majority carriers, from their charge neutrality distribution, may affect the establishment of high-intensity built-in electric fields

b. charge neutrality exits in quasineutral regions only for position-independent and exponential doping concentration profiles

c. all other doping profiles produce a net charge concentration distribution

d. new mass action law is developed that applies to quasineutral regions in which charge neutrality is not present.

Application to n+-region:

Electron concentration distribution:

$$n_n(x) = p_n(x) + N_D(x) - N_A(x) - \Delta N_n(x)$$

Net positive charge concentration:

$$\Delta n_n = \frac{E}{q} \frac{dE_n}{dx}$$

Mass action law:

$$p_n = \frac{N_D - N_A - \Delta n_n}{2} \left[\sqrt{1 + \left(\frac{2n_{ie}}{N_D - N_A - \Delta n_n} \right)^2} - 1 \right]$$

for charge neutrality $\Delta n_n = 0$, and $p_n = \dfrac{n_{ie}^2}{N_D - N_A}$

Substitute p_n into n_n:

$$n_n = \frac{N_D - N_A - \Delta n_n}{2} \left[\sqrt{1 + \left(\frac{2n_{ie}}{N_D - N_A - \Delta n_n} \right)^2} + 1 \right]$$

for charge neutrality $\Delta n_n = 0$, and $n_n = N_D - N_A + p_n$

Application to n+-region with Gaussian Donor Distribution:

Built-in electric field: $E_n = \zeta \dfrac{kT}{q} \dfrac{x}{2Dt}$

$$\zeta = \frac{1}{1 - \dfrac{N_A - \Delta n_n}{N_D}}$$

Far removed from the depletion region edge: $\zeta \quad 1$

$$E_n = \frac{kT}{q} \frac{x}{2Dt}$$

$$\frac{dE_n}{dx} = \frac{kT}{q} \frac{1}{2Dt} = \text{position independent}$$

$\Delta n_n -$ position independent (see Figure 1).

Figure 1. Representation of the Charge Distribution in the Quasi-Neutral n-Type Emitter Region of a Solar Cell that Establishes a Built-In Electric Field Attributed to a Gaussian Donor Concentration Profile.

Position in n-Type Emitter, cm
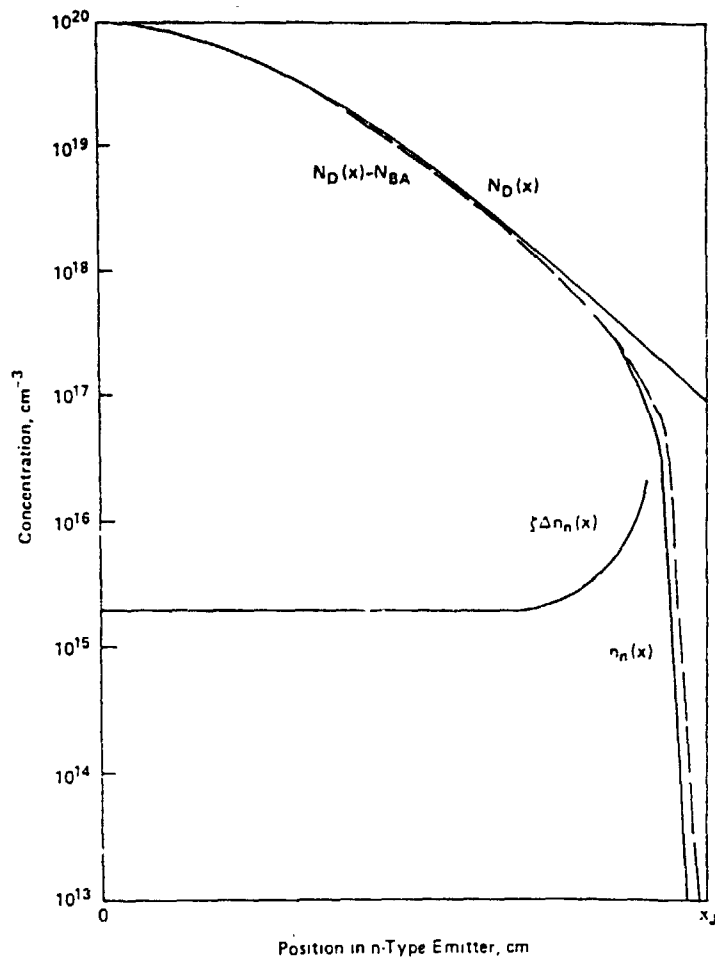
Experimental Data Obtained from n^+pp^+ Spire Corp. Solar Cells at 28°C

Cell # 4408-	Ion (As/P)	Dose (Ions/cm^2)	L_D (μm)	QE (@ 350 μm)	VOL (mV)	JSC (mA/cm^2)	FF (%)	EFF (%)
1B	P	1×10^{14}	48	.18	541	20.1	77.1	8.39
4C	P	2×10^{14}	46	.31	577	20.7	77.9	9.28
6F	P	4×10^{14}	46	.44	603	20.5	79.4	9.81
8C	P	8×10^{14}	56	.43	608	21.0	80.1	10.2
10F	P	1×10^{15}	78	.42	610	21.7	81.0	10.7
12C	P	2.5×10^{15}	94	.37	610	22.4	80.3	11.0
14C	As	1×10^{14}	37	.31	559	20.1	71.3	8.03
16B	As	2×10^{14}	41	.42	590	20.6	77.0	9.37
17F	As	4×10^{14}	3/	.44	603	20.6	77.5	9.61
20C	As	8×10^{14}	38	.47	605	20.6	79.5	9.91
22F	As	1×10^{15}	40	.46	603	20.8	80.7	10.1
24C	As	2.5×10^{15}	59	.44	595	22.8	74.1	10.1

Notes: cell area = 4 cm^2. T = 28°C. Insolation was AMI, 100 mW/cm^2. No AR coating.

Figure 2. Experimentally Determined Behavior of Efficiency versus
Temperature Obtained from n^+pp^+ Spire Corp. Solar Cells
Which Do Not Have AR Coatings.
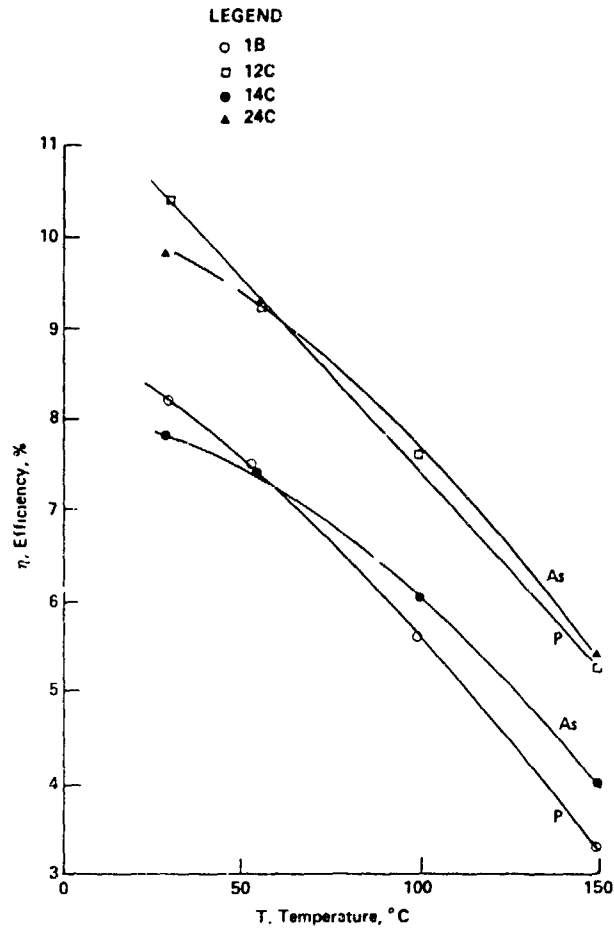
Figure 3. Experimentally Determined Behavior of Open-Circuit Voltage
versus Temperature Obtained from n^+pp^+ Spire Corp. Solar Cells
Which Do Not Have AR Coatings.
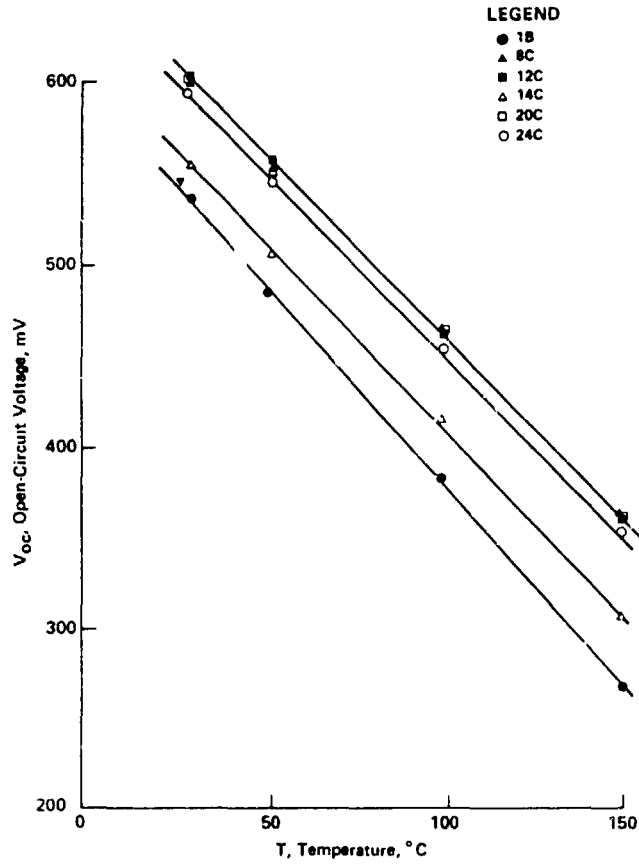
Figure 4. Comparison of Experimental Data and Simulation Results
Describing the Behavior of the Short-Circuit Current Density
Versus Temperatures for n^+pp^+ Spire Corp. Solar Cell No. 24C,
Which Does Not Have an AR Coating.
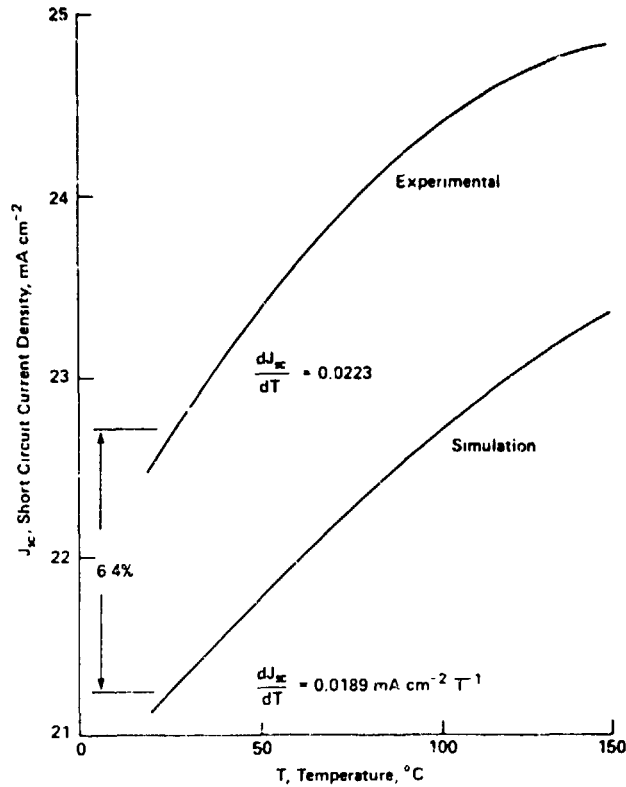
Calculated Normalized Temperature Coefficients of Efficiency,
Open-Circuit Voltage, and Short-Circuit Current Density Obtained
from n^+pp^+ Spire Corp. Solar Cell Experimental Data
Which Do Not Have AR Coatings

	Dose $= 1 \times 10^{14}$ cm^{-2}			Dose $= 2.5 \times 10^{15}$ cm^{-2}		
Figure of Merit*	^{31}P(1B)	^{75}As(14C)	Percent Change	^{31}P(12C)	^{75}As(24C)	Percent Change
$\frac{1}{\eta_o} \frac{\eta(150) - \eta_o}{\Delta T}$	-4.9×10^{-3}	-4.0×10^{-3}	$+22.5\%$	-4.1×10^{-3}	-3.71×10^{-3}	$+10.8\%$
$\frac{1}{(V_{oc})_o} \frac{V_{oc}(150) - (V_{oc})_o}{\Delta T}$	-4.1×10^{-3}	-3.7×10^{-3}	$+10.8\%$	-3.4×10^{-3}	-3.4×10^{-3}	0
$\frac{1}{(J_{sc})_o} \frac{J_{sc}(150) - (J_{sc})_o}{\Delta T}$	0.9×10^{-3}	1.1×10^{-3}	-18.2%	$+0.63 \times 10^{-3}$	0.76×10^{-3}	-17.1%
η_o (Spire Corp.)	8.39	8.03	4.5%	11.0	10.1	5.9%
η_o (NC A&T)	8.2	7.8	5.1%	10.4	9.8	6.1%

*No AR coating

Figure 5. Simulation of Electric Field Distribution in n$^+$ of Spire Corp. Solar Cell No. 24C With Temperature a Parameter.
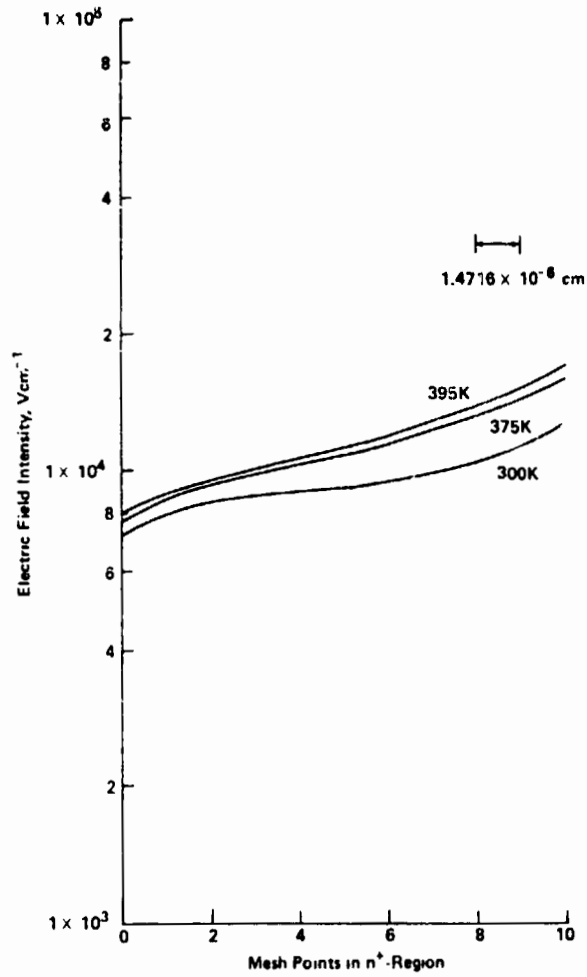
Figure 6. Net Charge Distribution in the n$^+$-Region of Spire Corp.
Solar Cell No. 24C With Temperature a Parameter.
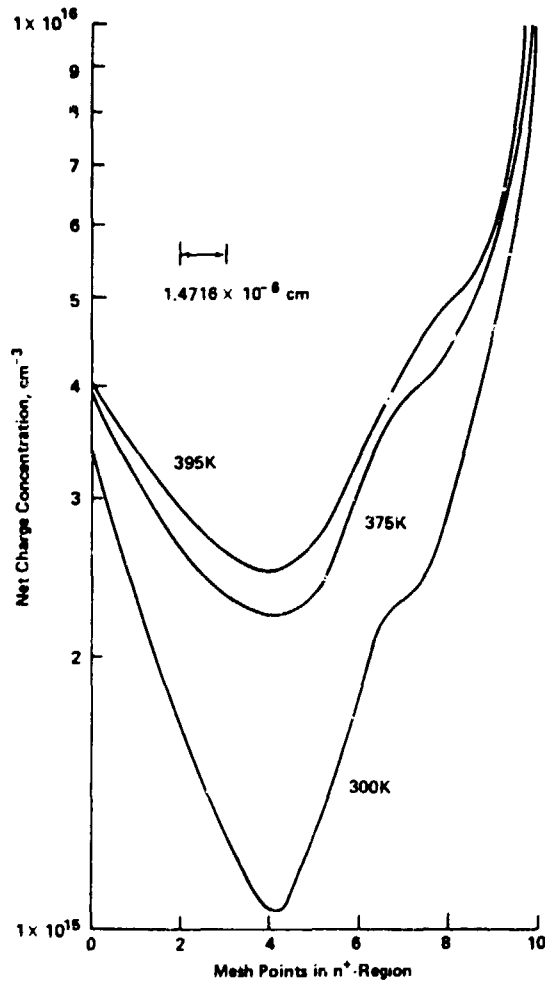
Figure 7. Simulation of Photoexcited Hole Concentration in the
n$^+$-Region of Spire Corp. Solar Cell No. 24C,
With Temperature a Parameter.
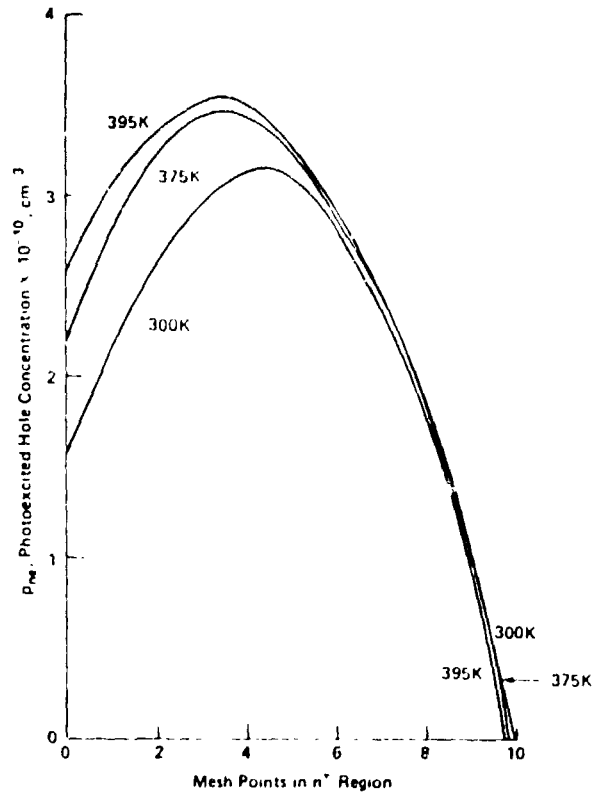
Figure 8. Lifetime and Transit Time Simulations of Holes in the n⁺-Region
of a n⁺pp⁺ Spire Corp. Solar Cell, No. 24C,
Under Short-Circuit and 27°C.
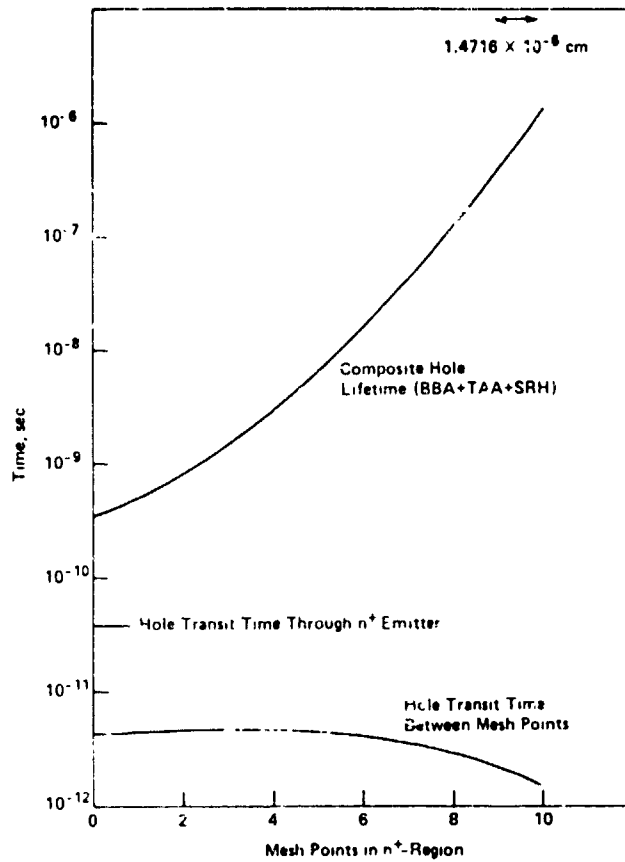
Figure 9. Short-Circuit Current Density versus Base Electron Diffusion Length Representing Spire Corp. n^+pp^+ Silicon Solar Cells and Computer Simulation Results of Cell No. 24C, no AR Coating, and 27°C.
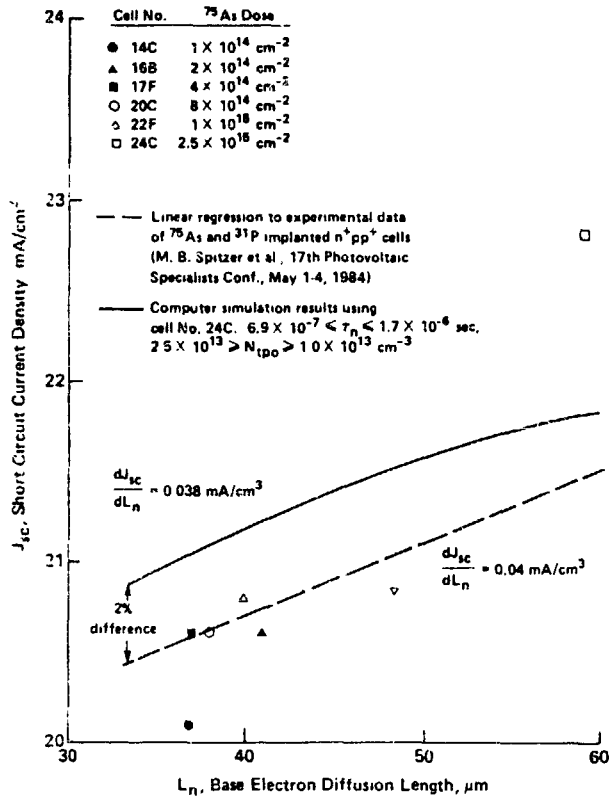
Figure 10. Behavior of Short-Circuit Current Density versus Base Electron Diffusion Length Obtained from Simulating Cell No. 24C, n^+pp^+, Provided by the Spire Corp., no AR Coating, and 27°C.
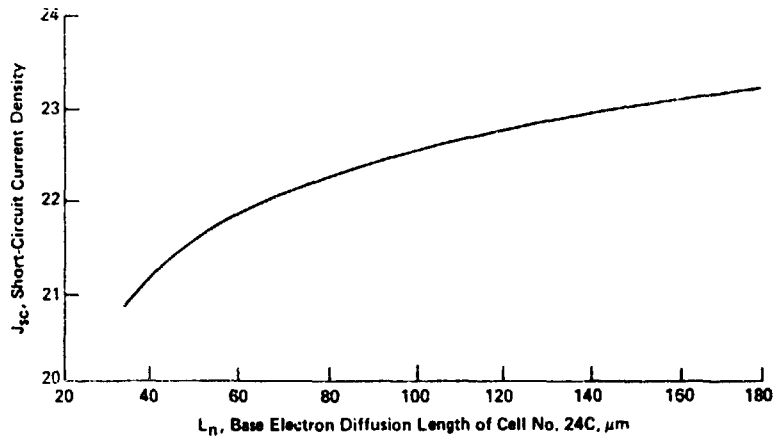
SENSITIVITY ANALYSIS OF HIGH-EFFICIENCY SILICON SOLAR-CELL DESIGN PARAMETERS

JET PROPULSION LABORATORY

Anant R. Mokashi

Outline

- EXPERIMENTAL VS SIMULATION RESULTS

- DOPING PROFILE MODIFICATIONS

- SENSITIVITIES OF CRITICAL PARAMETERS

- CONCLUSIONS

Cross Section of the Silicon Solar Cell Considered for Sensitivity Analysis
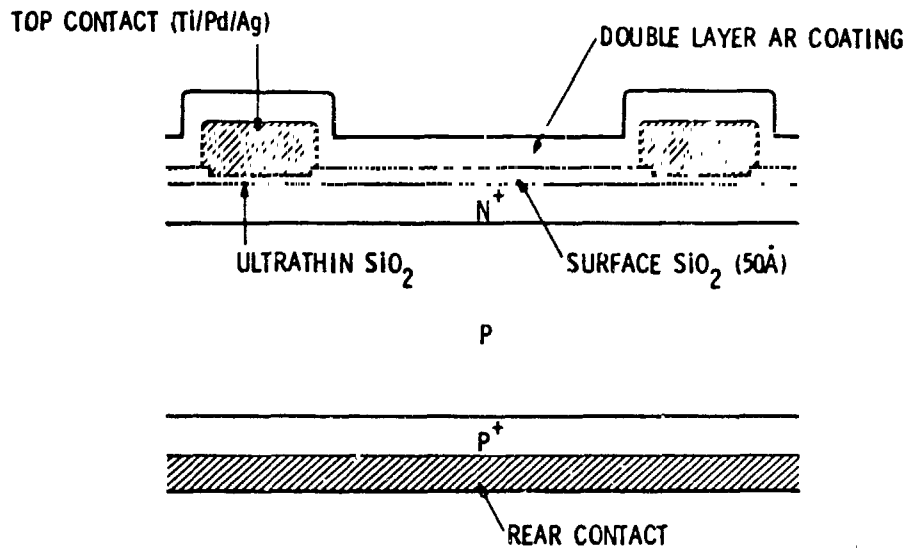
REF: IEEE TRANSACTIONS ON ELECTRON DEVICES, VOL ED-31, NO. 5, MAY 1984

Doping Profile of the Silicon Solar Cell

DEPTH (MICROMETERS)
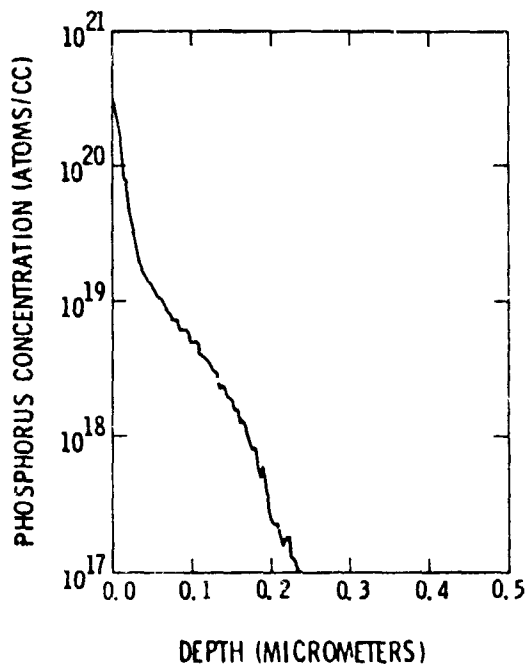
Solar-Cell Parameters

- BULK RESISTIVITY — 0.2 Ω-cm ($2.0 \times 10^{17}/cm^3$, B)
- MINORITY-CARRIER LIFETIME — 20.0 μsec
- CELL THICKNESS — 280.0 μm
- FRONT JUNCTION DEPTH — 0.23 μm
- FRONT SURFACE DOPING CONC. — $2.8 \times 10^{20}/cm^3$ (PHOS)
- FRONT SURFACE RECOMBINATION VELOCITY — $1,000$ cm/sec
- BACK SURFACE CONTACT — ohmic

Experimental vs Simulation Results

TYPE	V_{oc} (mV)	I_{sc} (mA)	FF	EFFICIENCY (%)
EXPERIMENTAL*	641.11	35.48	0.8220	18.70
SIMULATION (X)	638.76	35.08	0.8334	18.53

* MARTIN GREEN'S MINP CELL

(X) SOLAR CELL ANALYSIS PROGRAM IN 1 DIMENSION (SCAP1D)
DEVELOPED BY PURDUE UNIVERSITY FOR SANDIA LABORATORY

Doping Profile Modification
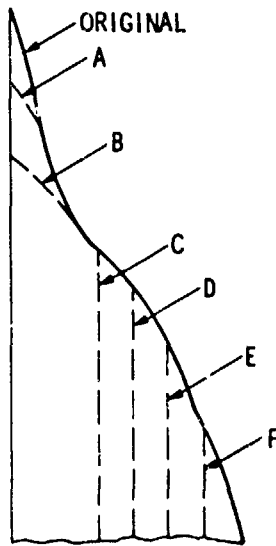
TYPE	FRONT SURFACE CONC.	FRONT JUNCTION DEPTH	EFFICIENCY (%)
ORIGINAL	2.8×10^{20}	$0.23 \mu m$	18.53
A	5.0×10^{19}	$0.23 \mu m$	19.21
B	2.0×10^{19}	$0.23 \mu m$	19.24
C	1.8×10^{19}	$0.21 \mu m$	19.27
D	1.6×10^{19}	$0.19 \mu m$	19.29
E	1.1×10^{19}	$0.17 \mu m$	19.28
F	7.5×10^{18}	$0.15 \mu m$	19.27

Complementary Error Function vs Profile-D
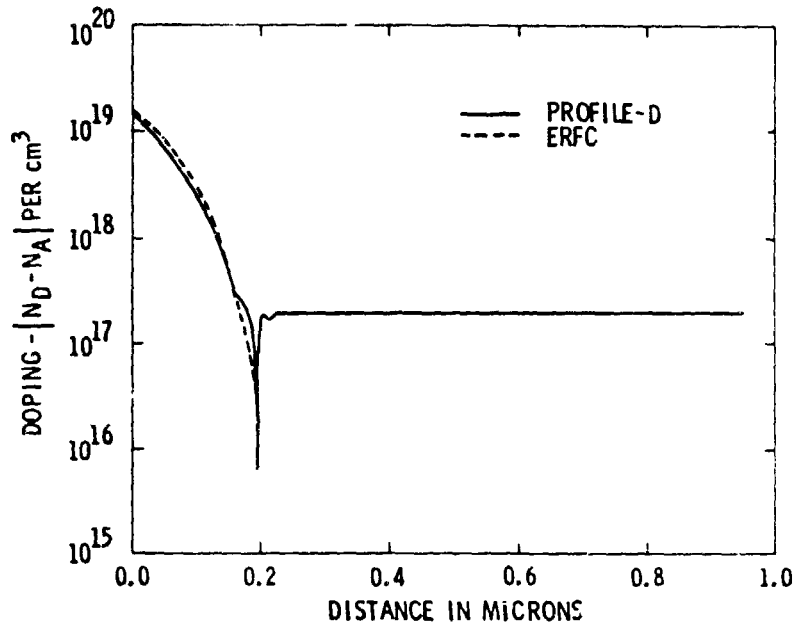
Sensitivity Analysis

CRITICAL PARAMETERS

- SURFACE RECOMBINATION VELOCITY

- MINORITY-CARRIER LIFETIME

- CELL THICKNESS

- BACK SURFACE FIELD

Front-Surface Recombination Velocity Sensitivity
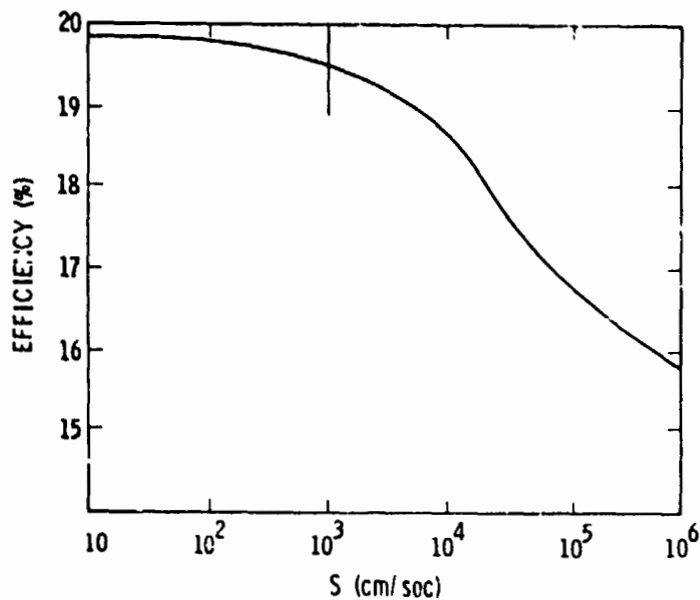
Minority-Carrier Lifetime Sensitivity
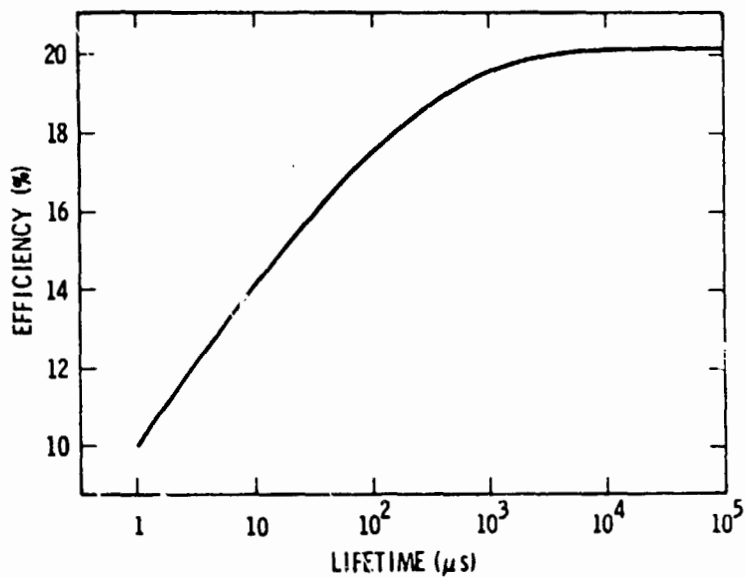
Cell Thickness Sensitivity
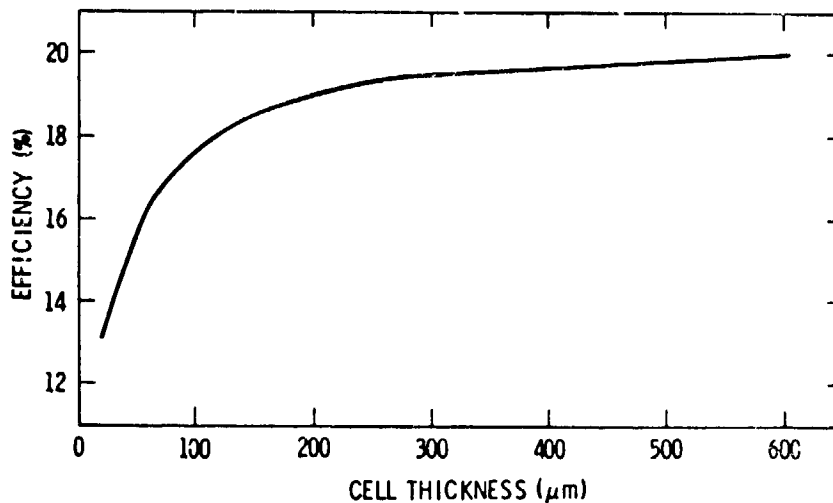
Effect of Back-Surface Field

BACK SURFACE CONC.	BACK JUNCTION DEPTH (μm)	EFFICIENCY (%)
2×10^{17}	0	19.55
1×10^{18}	2	19.57
	5	19.59
	10	19.63
1×10^{19}	2	19.61
	5	19.68
	10	19.76
1×10^{20}	2	19.67
	5	19.74
	10	19.78

Conclusions

- THERE IS GOOD AGREEMENT BETWEEN EXPERIMENTAL AND SIMULATION RESULTS

- SHEET MATERIAL QUALITY IMPROVEMENT IS NEEDED FOR HIGH EFFICIENCY CELLS

- 20% CELL OF THIS DESIGN IS FEASIBLE WITH 10 ms BULK LIFETIME MATERIAL

- FOR ACHIEVING EFFICIENCIES HIGHER THAN 20% NEW CELL DESIGNS INCLUDING THIN CELLS WITH LIGHT TRAPPING AND BACK SURFACE FIELD SHOULD BE CONSIDERED

SILICON SURFACE PASSIVATION BY
SILICON NITRIDE DEPOSITION

UNIVERSITY OF WASHINGTON

Larry C. Olsen

Objectives and Approach

OBJECTIVES
- TO INVESTIGATE THE USE OF PECVD SILICON NITRIDE FOR PASSIVATION OF SILICON SURFACES.
- TO INVESTIGATE MEASUREMENT TECHNIQUES FOR SURFACE RECOMBINATION VELOCITY.
- TO INVESTIGATE THE IMPORTANCE OF SURFACE PASSIVATION TO HIGH EFFICIENCY SOLAR CELLS.

APPROACH

SiN_x FILM DEPOSITION AND CHARACTERIZATION
- ESTABLISH PECVD SYSTEM
- DEVELOP DEPOSITION PROCEDURES

FILM CHARACTERIZATION
- OPTICAL CHARACTERIZATION -- N and K VS WAVELENGTH AND DEPOSITION PARAMETERS.
- PHYSICAL CHARACTERIZATION

PASSIVATION STUDIES
- SURFACE STATE DENSITY AT SiN_x/Si INTERFACE FOR MODERATELY DOPED SILICON SUBSTRATES.
- PHOTORESPONSE OF N/P SOLAR CELLS WITH PECVD SiN_x FILMS.
- CURRENT-VOLTAGE ANALYSES OF SILICON CELLS WITH SiN_x FILMS.
- ROSIER MEASUREMENT

PRECEDING PAGE BLANK NOT FILMED

SiN$_x$ Film Index of Refraction vs Silane-Ammonia Ratio
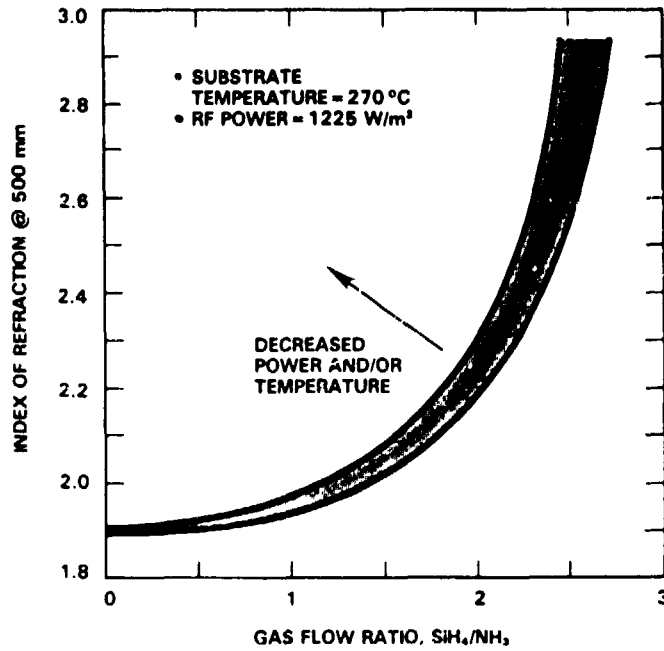
Optical Constants of SiN$_x$ Films From Ellipsometry Measurements
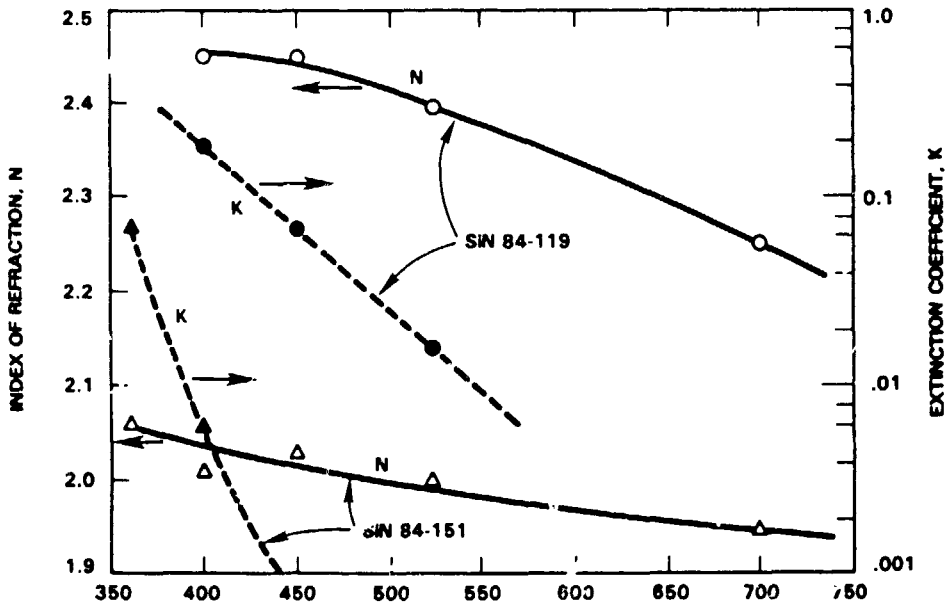
*MEASUREMENTS TAKEN ON EQUIPMENT PROVIDED BY BATTELLE NORTHWEST LABORATORIES

Approaches to Investigation of Surface Recombination in Solar Cells

M-SiN$_x$-pSi STRUCTURE

HIGH FREQUENCY AND
QUASI-STATIC C-V
MEASUREMENTS TO
OBTAIN INTERFACE
STATE DENSITY.
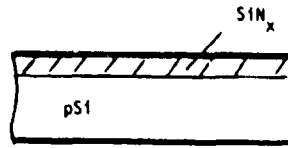
SOLAR CELL STRUCTURE

PHOTORESPONSE AT
SHORT WAVELENGTHS
CAN THEORETICALLY
YIELD RECOMBINATION
VELOCITY.

I-V CHARACTERIZATION
MAY ALLOW IDENTIFICATION
OF DOMINANT CURRENT
MECHANISMS.

SPECIAL STRUCTURES (ROSIER)

PHOTORESPONSE MEASUREMENT
WITH SURFACE POTENTIAL
VARIED MAY ALLOW
DETERMINATION OF S.

I-V CHARACTERIZATION
WITH SURFACE POTENTIAL
VARIED ALLOWS DETECTION
OF SURFACE RECOMBINATION
EFFECTS.
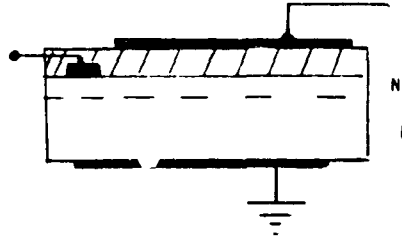
Results of Interface State Study of SiN$_x$ on p-Type Si

SURFACE TREATMENT	RF POWER = 212 $\frac{W}{m^2}$		RF POWER = 1225 $\frac{W}{m^2}$	
	SUBSTRATE TEMPERATURE		SUBSTRATE TEMPERATURE	
	150 °C	270 °C	150 °C	270 °C
ABBREV CLEAN				
RCA CLEAN				
ABBREV CLEAN & NITRIDED				
RCA CLEAN & NITRIDED				
RCA CLEAN & THIN OXIDE				
RCA CLEAN, THIN OXIDE & NITRIDED				

SURFACE STATE DENSITY (cm^{-2}eV)
−10^{13}
−10^{12}
−10^{11}
−10^{10}

AS GROWN   °C ANNEAL   450 °C ANNEAL
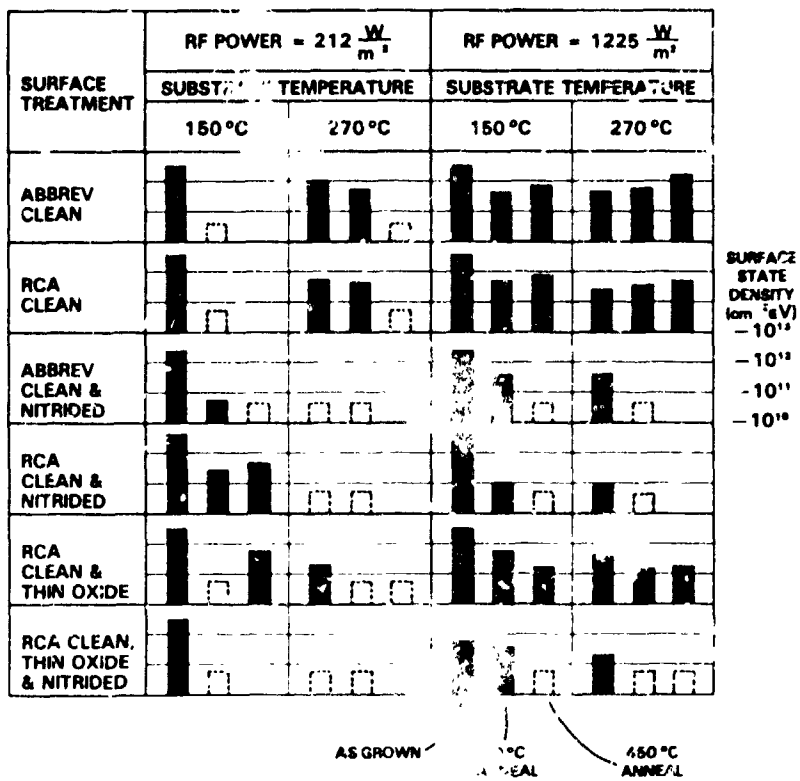
Interface State Density vs Annealing Temperature for SiN$_x$ on p-Type Si

○ RCA CLEAN/NITRIDED/DEPOSIT @150 °C
▽ RCA CLEAN/NITRIDED/DEPOSIT @270 °C (UPPER LIMIT)
□ RESULTS REPORTED BY HEZEL, et al.

MIDGAP INTERFACE STATE DENSITY (cm^{-2}eV^{-1})

ANNEALING TEMPERATURE (°C)
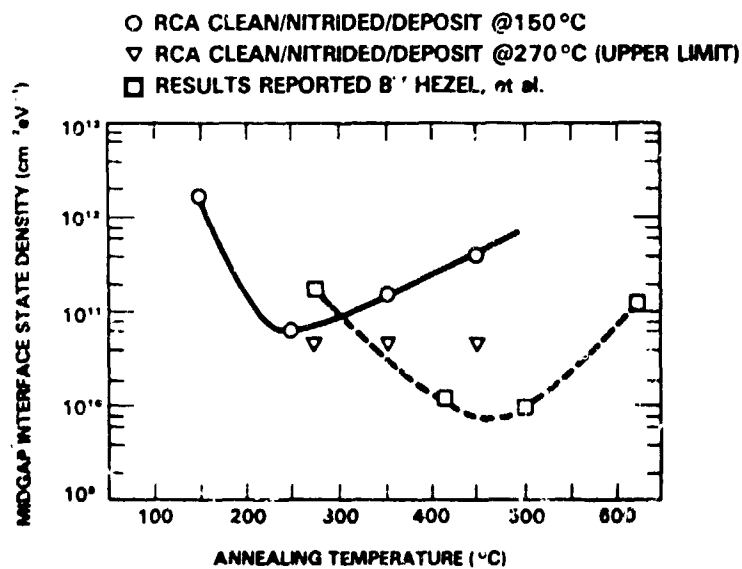
Internal Photoresponse Analysis

<u>THEORY</u>

$$J_{PH}(\lambda) = S_{INT}(\lambda) \cdot T_{\lambda} \cdot N_{\lambda} \cdot q$$

$$S_{INT}(\lambda) = (S_{INT})_{EMITTER} + (S)_{DEPL.\ WIDTH} + (S_{INT})_{BASE}$$

$$T_{\lambda} = T_{\lambda}(N_{AR}, K_{AR}, N_{Si}, K_{Si})$$
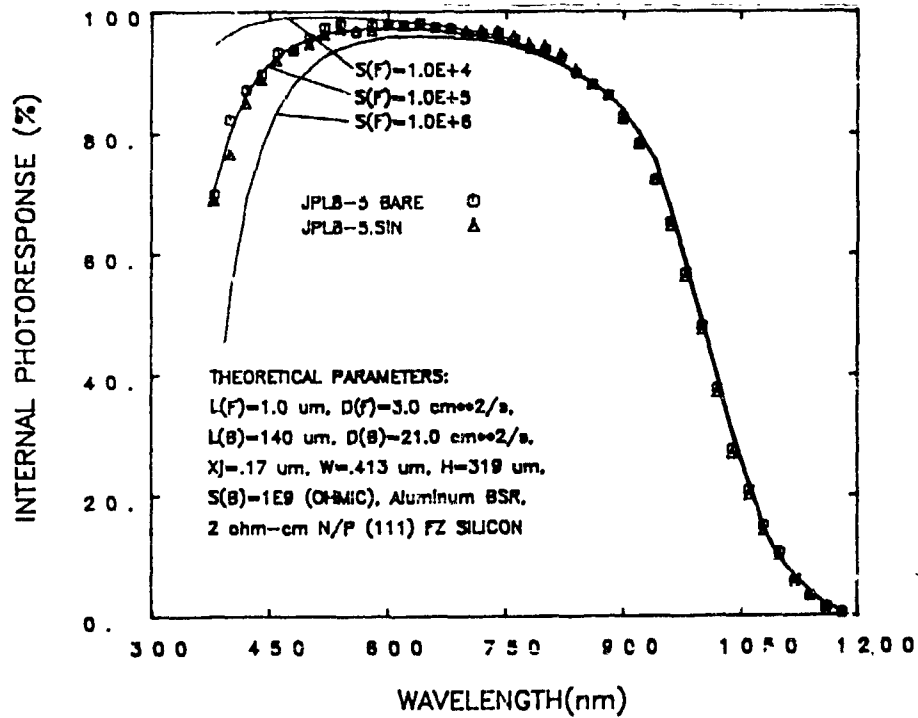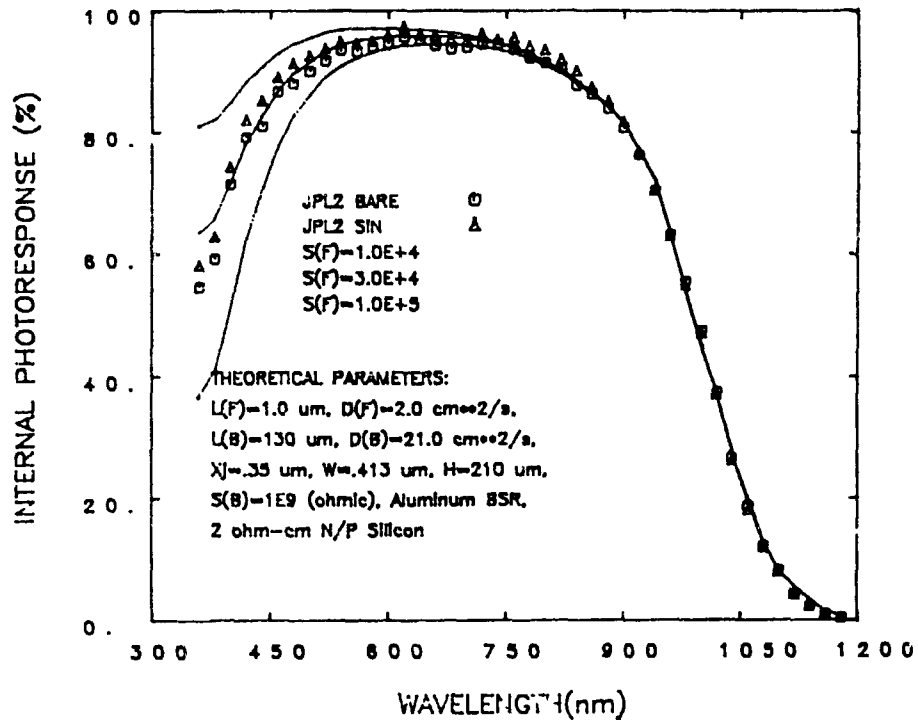
$$= 1 - R_{\lambda} - A_{\lambda}$$
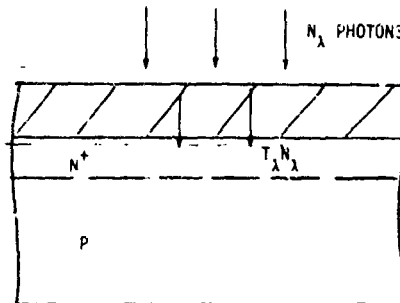
<u>EXPERIMENT</u>

MEASURE: $J_{PH}(\lambda)$, R_{λ}, N_{λ} and K_{λ} of SiN_x

ANALYSIS: HAVE OBTAINED $S_{INT}(\lambda)$ FOR CELLS WITH SiN_x LAYERS.
DETERMINED S_F ASSUMING A HOMOGENEOUS EMITTER.

Internal Photoresponse vs Wavelength for Si n-p Cell With 100 Angstroms SiO₂
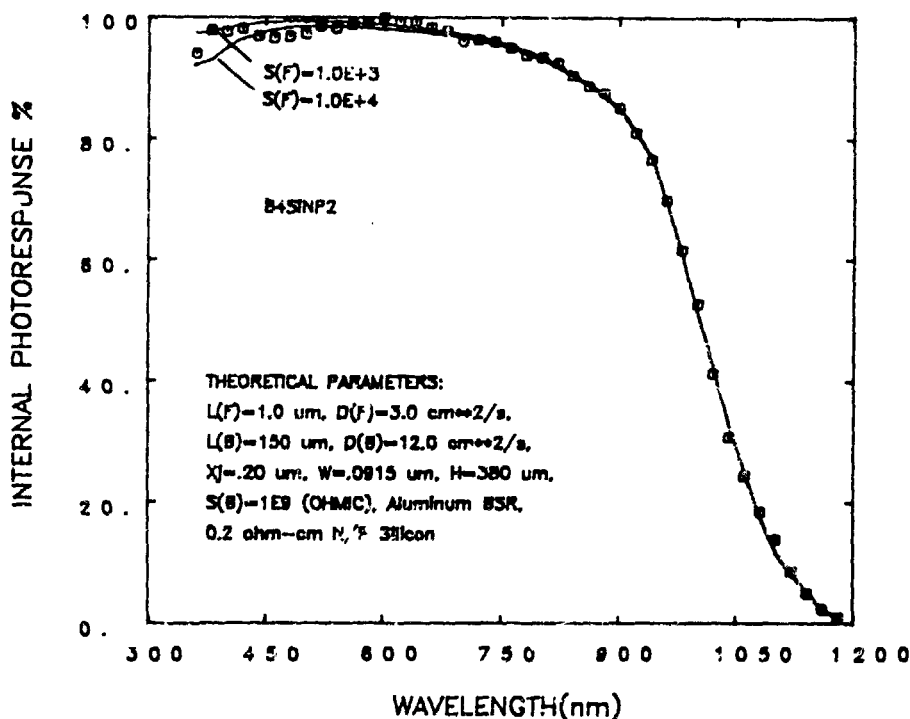
Internal Photoresponse vs Wavelength for JPL Cell

Illuminated Characteristics of JPL Cells
(Fabricated by ASEC)

CELL	ORIENTATION	AR LAYER	AM1* EFFICIENCY (%)	I_{SC} (mA)	V_{OC} (mV)	FF	TOTAL AREA J_{SC} (mA/cm²)
2-3	(100)	SiO_x	15.2	130	583	.798	32.6
4-1	(100)	SiO_x	14.7	129	579	.786	32.3
1-5	(100)	SiN_x	14.6	130	570	.793	32.7
2-6	(100)	SiN_x	14.7	130	571	.791	32.7
9-1	(111)	SiO_x	15.0	130	581	.795	32.5
10-2	(111)	SiO_x	15.7	134	588	.796	33.5
8-5	(111)	SiN_x	14.4	128	570	.786	32.0
9-2	(111)	SiN_x	14.8	130	573	.792	32.9

*EFFICIENCY MEASURED AT JCGS WITH ELH SIMILATOR. THE SIMULATOR HAS BEEN CALIBRATED BY EXCHANGING A REFERENCE CELL WITH SERI.

Effect of Reactive Ion Etching Cell Edges
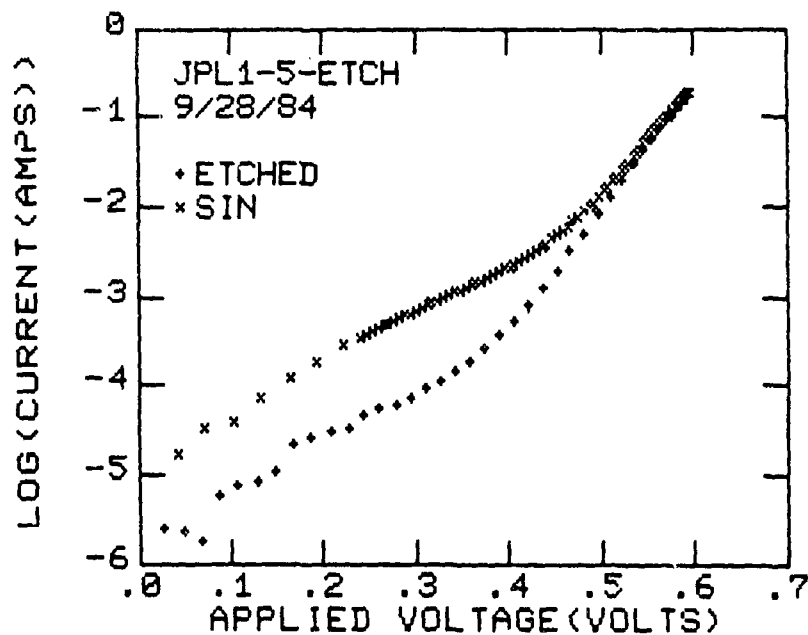
Approach to Dark I-V Analysis

<u>I-V RELATIONSHIP $(V_j \gg kT)$</u>

$$I_{MEAS} = I_j + V_j/nkT$$

$$V_j = V_{MEAS} - R_S I_{MEAS}$$

$$I_j = I_{o1} \exp(BV_j) + I_{o2} \exp(V_j/nkT,$$

<u>FITTING PROCEDURE</u>

1. SELECT R_S AND R_{SH}

2. GENERATE (I_j, V_j)

3. CONSIDER (I_j, V_j) FOR REGION 1

$$I_j = I_{o1} \exp(BV_j)$$

$$Log_e(I_j) = Log_e(I_{o1}) + BV_j$$

LEAST SQUARES FIT $\Rightarrow I_{o1}$, B

4. CONSIDER (I_j, V_j) FOR REGION 2

$$I_{j2} = I_j - I_{o1} \exp(BV_j)$$

$$= I_{o2} \exp(V_j/nkT)$$

LEAST SQUARES FIT $\Rightarrow I_{o2}$, B

5. ITERATE BETWEEN REGIONS 1 AND 2 UNTIL ACHIEVE CONVERGENCE.

6. CARRY OUT STEPS 1 THROUGH 5 FOR ARRAY OF R_S AND R_{SH} VALUES. SELECT VALUES OF PARAMETERS WHICH PROVIDE BEST FIT TO DATA.
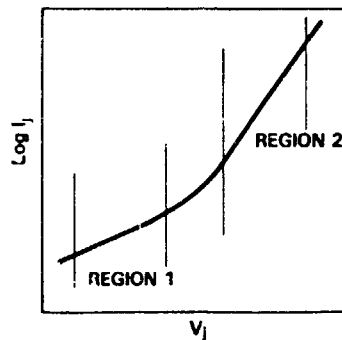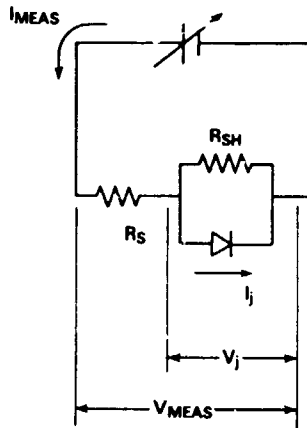
## Emitter J_O vs Surface Donor Concentration for Shallow-Junction n-p Cell
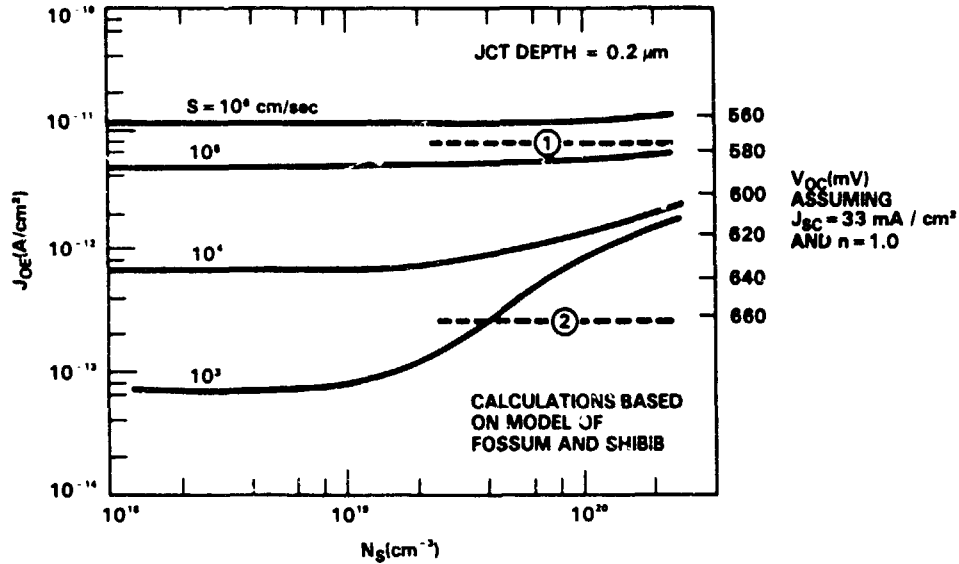
1 J_{OE} FOR 2 Ohm-cm N/P CELL WITH THICKNESS OF 15 MILS, L(BASE) = 130 μm, D = 21 cm²sec⁻¹ (APPROXIMATE CELLS PROVIDED BY JPL).
2 J_{OE} FOR 0.2 Ohm-cm N/P CELL WITH THICKNESS OF 15 MILS, L(BASE) = 150 μm, D = 21 cm²sec⁻¹.

I-V Parameters for Dark Characteristics

| CELL | JCT DEPTH (m) | BASE RESISTIVITY (Ohm-cm) | LARGE VOLTAGE MECHANISM | | | | ACTIVATION ENERGY (eV) | POSSIBLE CURRENT MECHANISM |
			ORDERS OF MAGNITUDE FOR FIT	AVERAGE ERROR (%)	J_0 (A/cm²)	n		
JPL 6 (SiN_x)	0.4	2	2.5	.30	2.1 E-11	1.07	0.96	DEPL LAYER RECOMB VIA SHALLOW TRAP
JPL 8-5 (SiN_x)	0.2	2	2.8	.20	1.7 E-11	1.02	1.00	EMITTER RECOMB WITH S = 10^5 to 10^6 cm/sec
JPL 9-1 (SiO_x)	0.2	2	2.8	.19	3.1 E-11	1.06	0.94	DEPL LAYER RECOMB VIA SHALLOW TRAP
JCGS MINP 84-2	0.2	0.2	2.0	.4	1.3 E-12	1.02	1.10	EMITTER RECOMB W' TH S = 10^3 to 10^4 cm/sec

Analysis of Temperature-Dependent
I-V Characteristics of JPL Cell
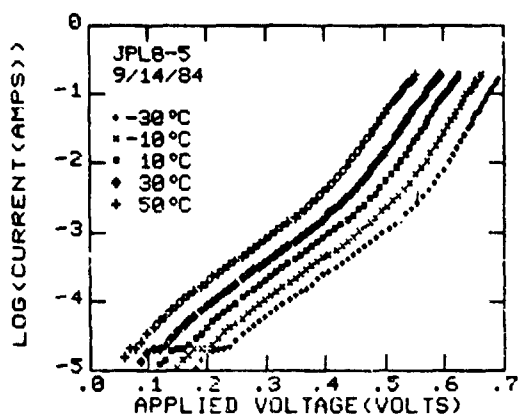
I-V DATA
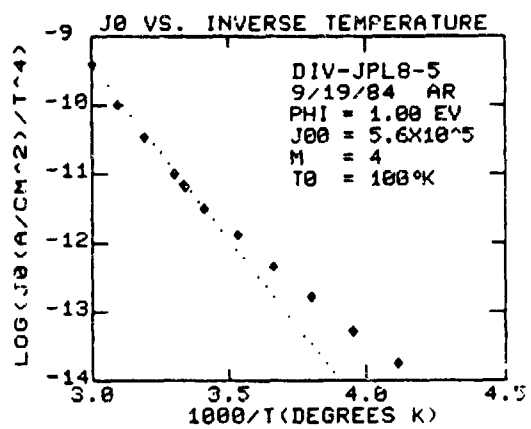
ACTIVATION
ENERGY
ANALYSIS

Theory for I-V Characteristics

1. **EMITTER RECOMBINATION CURRENT**

$$J = J_{OE} \left[\exp\left(\frac{V}{nkT}\right) - 1\right]$$
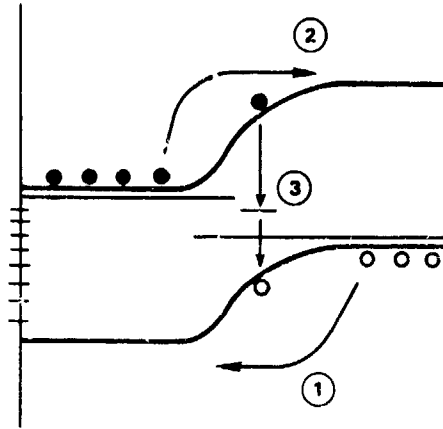
$$n = 1$$

FOR RM TEMP ANALYSIS:

$$J_{OE} = \frac{en_i^2}{N_D^{(Eff)}} \cdot GF$$

GF IS A FCT OF W_H, S_P, D_{PO} & τ_P

FOR INTERPRETATION OF TEMPERATURE DEPENDENT DATA:

$$J_{OE} = J_{OO}(T) \exp\left(\frac{-\phi}{kT}\right)$$

$$\phi = 1.20 - (\Delta E)\, \text{EMITTER BGN}$$

2. **BASE REGION RECOMBINATION CURRENT**

$$J = J_{OB} \left[\exp\left(\frac{V}{nkT}\right) - 1\right]$$

$$n = 1$$

$$J_{OB} = \frac{en_i^2}{N_A} \frac{L_n}{\tau_n} \cdot G_F$$

$$= J_{OO}(T) \exp\left(\frac{-\phi}{kT}\right)$$

$$\phi = 1.20 - (\Delta E)\, \text{BASE BGN}$$

4. **TUNNELING/RECOMBINATION**

$$J = J_{OT} \exp(BV) \quad V \gg kT$$

B TEMPERATURE INDEPENDENT

$$J_{OT} = J_{OO} \exp\left(\frac{-\phi}{kT}\right)$$

ϕ TYPICALLY 0 TO 0.5 eV

5. **FIELD EMISSION**

$$J = J_{OF} \exp(CV)$$

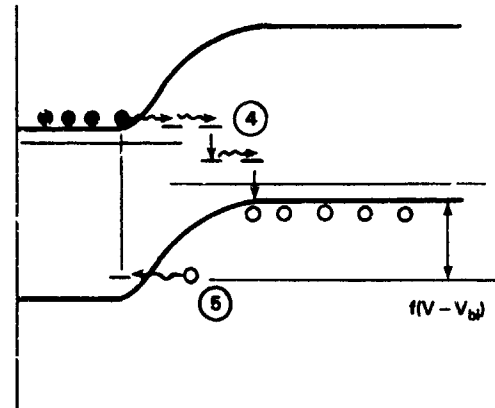$$C = \frac{1}{nkT} + B$$

$$J_{OF} = J_{OO} \exp(-\phi/kT)$$

$$\phi = fV_{bi} \quad f = n^{-1}$$

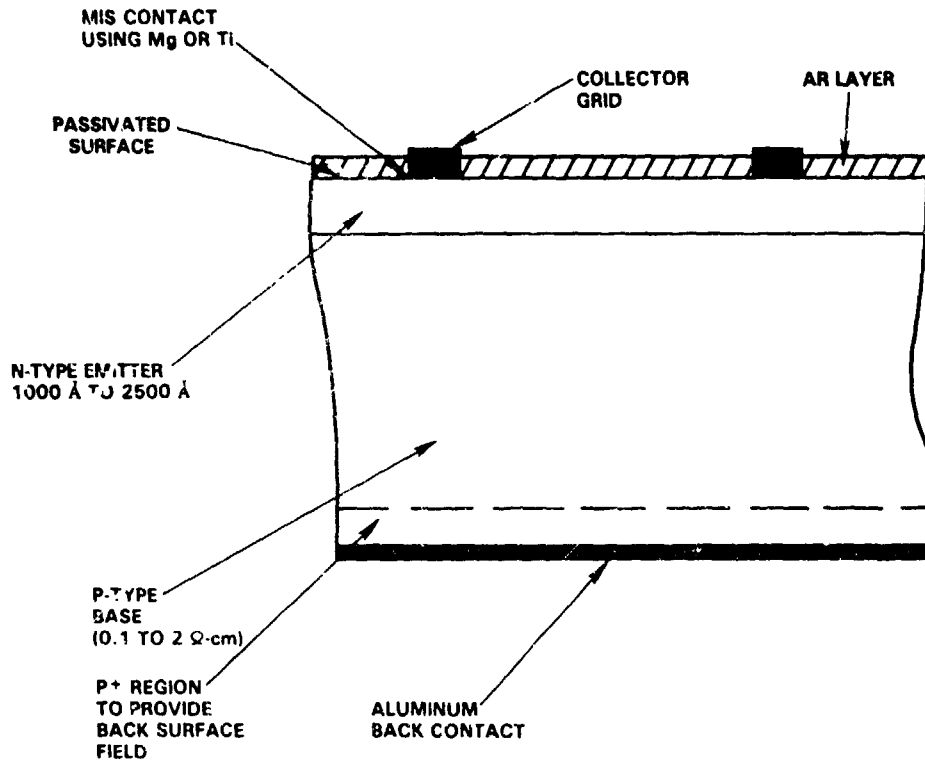6. **EDGE LEAKAGE CURRENTS**

CURRENT MECHANISMS (3), (4) OR (5)
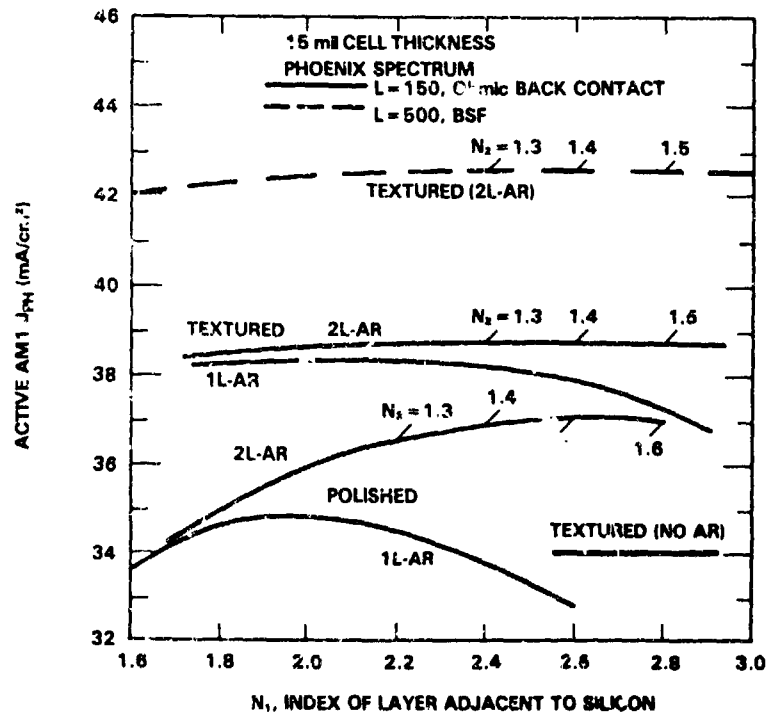
USUAL SHUNTING MECHANISM
$$J_{SH} = V/R_{SH}$$

3. **DEPLETION LAYER RECOMBINATION CURRENT**

$$J = J_{OR} \exp\left(\frac{V}{nkT}\right) \quad V \gg kT$$

$$J_{OR} = J_{OO} \exp\left(\frac{-\phi}{kT}\right)$$

$$\phi = (E_t - E_v) \text{ OR } (E_c - E_t) \qquad n = 1 \text{ TO } 2$$

FOR $n \approx 2$, $\phi \approx E_g/2$ \qquad FOR $n \approx 1$, $\phi \approx 0.8$ eV

MINP Cell Concept

## Calculated J_{ph} for Single and Double AR Layers

Projected Performance

TO ACHIEVE 20%
- MUST REDUCE J_{OE} BY DECREASING N_S AND S_p
- NEED SLIGHT IMPROVEMENT IN L

TO ACHIEVE 25%
- NEED F&P DIFFUSION LENGTH
- MUST REDUCE S_p TO 10^2
- WITH THESE VALUES OF L AND S_p, J_0 WILL BE DECREASED TO $\approx 3 \times 10^{-14}$ A/cm^2
- MUST USE DOUBLE AR WITH TEXTURED SURFACE OR WITH COMPLETE OPTICAL CONFINEMENT

Bar chart: AM1 EFFICIENCY vs projected performance — 18%, 19%, 20%, 25%
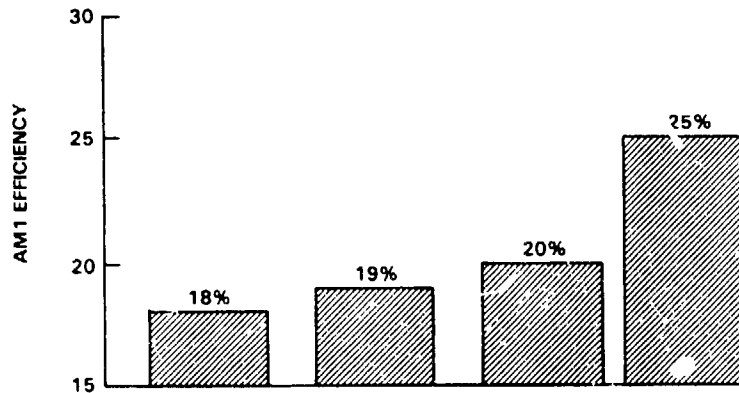
J_{SC}(mA/cm^2)	36.0	36.0	36.7	40.9
V_{OC}(mV)	630	650	670	720
FF	.794	.812	.820	.850
J_0(A/cm^2)	1×10^{-12}	4.5×10^{-13}	2×10^{-13}	3×10^{-14}
n-VALUE	1.0	1.0	1.0	1.0
N_S(cm^{-3})	6×10^{19}	4×10^{19}	2×10^{19}	2×10^{19}
SURF REC VEL	10^4	10^3	10^3	10^3
DIFF LENGTH	150	150	200	500 (F&P)
GRID SHADOW	4%	4%	3%	2%
CELL THICKNESS	15 mils	15 mils	15 mils	10 mils
BACK SURF	Ohmic	Ohmic	BSF	BSF

Key Results and Future Work

KEY RESULTS

ESTABLISHED PECVD SYSTEM.

DEVELOPED PROCEDURES FOR GROWTH OF SiN_x WITH APPROPRIATE OPTICAL PROPERTIES FOR SINGLE AR COATING.

DETERMINED APPROACH FOR ACHIEVING SURFACE STATE DENSITY $<5 \times 10^{10}$ cm^{-2}eV^{-1} ON MODERATELY DOPED SILICON.

DEVELOPED APPROACH FOR REACTIVE ION ETCHING CELL EDGES TO INCREASE CELL FF VALUES.

HAVE INITIATED STUDIES OR ROSIER MEASUREMENTS ON SOLAR CELLS.

CHARACTERIZED CELLS WITH SiN_x AND SiO_x AR COATINGS WITH I-V ANALYSIS AND PHOTORESPONSE TO OBTAIN ESTIMATED VALUES FOR S.

FUTURE WORK

INVESTIGATE EFFECT OF SiN_x ON SURFACE RECOMBINATION FOR MODERATELY DOPED N-TYPE MATERIAL.

INVESTIGATE FEASIBILITY OF ROSIER METHOD FOR MEASURING S ON SILICON SOLAR CELL STRUCTURES.

INVESTIGATE MINP SILICON SOLAR CELLS.

-- DEVELOP DBLAR AND REDUCE SHADOWING TO ACHIEVE $J_{sc} = 36$ mA/cm^2

-- REDUCE CURRENT LOSSES SUCH THAT $J_0 = 5 \times 10^{-13}$ A/cm^2 AND n = 1.0 TO ACHIEVE $V_{oc} = 650$ mV, FF = .81 and EFF = 19%.

IMPORTANT LOSS MECHANISMS IN HIGH-EFFICIENCY SOLAR CELLS

C.T. SAH ASSOCIATES

C. Tang Sah

Study of Material Properties and High-Efficiency Solar-Cell Performance on Material Composition

TASKS

(1) Impurity and Defect Levels Limiting High Efficiency Cells

- New CVCT - one p/n diode.
- Ti, Zn, Au, others.

(2) Computer Model - Exact

- Matured - 1978. Including All Recombination Mechanisms and ΔE_G.
- Applied - TR.1-5(78-81) - TR.1 (83)

(3) Fundamental Limitations on High Efficiency Cells.

- Mechanisms
- < 20% Cells.
- > 20% Cells.
- Ultimate Cells.

HIGH-EFFICIENCY SILICON SOLAR CELL RESEARCH

Outline

(1) RECOMBINATION LOSS MECHANISMS

(2) HIGH EFFICIENCY CELLS   (<20%)

(3) VERY HIGH EFFICIENCY CELLS (>20%)

(4) ULTRA HIGH EFFICIENCY CELLS (~25%)

Recombination Loss Mechanisms

* INTRINSIC - Interband

    # Auger   25%
    # Radiative 25%

* EXTRINSIC - Band-Bound

    # Impurities
    # Defects
    # Damages

* LOCATIONS

    # Bulk
    # Interfaces
    # Perimeters
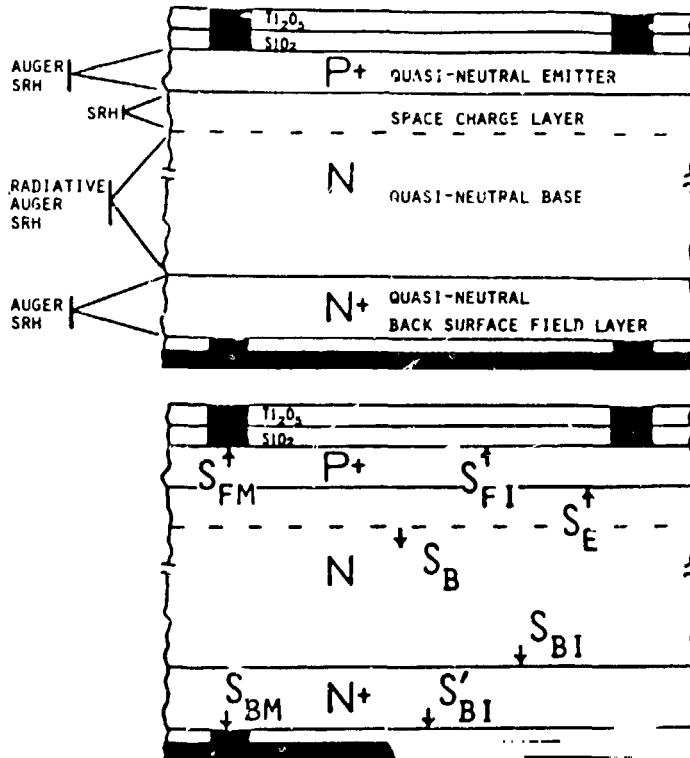
Performance Parameters of Very-High-Efficiency Ideal Diode Silicon Solar Cells (AM1 or AM1.5, 24°C)

SOURCE	J_1 (A)	J_{SC} (mA)	V_{OC} (mV)	FF	EFF (%)
Theory	2.0×10^{-16}	36.0	840	0.8664	26.0
Theory	2.0×10^{-15}	36.0	780	0.8588	24.0
Theory	2.0×10^{-14}	36.0	720	0.8501	22.0
Theory	2.0×10^{-13}	36.0	660	0.8402	20.0

SOLAR CELL EQUATIONS

$$J = J_L - J_1\left(e^{\frac{qV}{kT}} - 1\right) \quad \text{RAD H+L}$$
$$\text{AUG L}$$
$$\text{SRH L}$$

$$-J_{\frac{2}{3}}\left(e^{\frac{3qV}{2kT}} - 1\right) \quad \text{AUG H}$$

$$-J_m\left(e^{\frac{qV}{mkT}} - 1\right) \quad \text{SRH SEL}$$
$$\text{SRH H}$$
$$\text{Interface +}$$
$$\text{Surfaces}$$

—— CAN BE ELIMINATED

VG-8
24P1M

HIGH-EFFICIENCY SILICON SOLAR CELL RESEARCH

(1) RECOMBINATION LOSS MECHANISMS

(2) HIGH EFFICIENCY CELLS (<20%)

  ** BASE RECOMBINATION DOMINATED PERFORMANCE

  * CELL PERFORMANCE DATA AND BASE RECOMBINATION LOSS THEORY
    (Analyzed by author or/and Sah)

SOURCE (author)	CELL TYPE	RHO ohm-cm	THICK (um)	Lb (um)	TAU (us)	JSC (mA)	VOC (mV)	FF	EFF% AM1	Seff (cm/s)
Green C	1	0.2		170		36.0	660	0.840	19.7	850
Green Exp	M/T/N/P	0.2	280		20	36.0	653	0.811	19.1	
Spitzer Cal		0.3			13	36.2	627	0.834	18.8	1100
Spitzer Exp	N+/P/P+	0.3	380	150		36.2	622	0.801	18.0	
Rohatgi Cal		4.0			23	35.9	605	0.830	18.2	650
Rohatgi Exp	N+/P/P+	4.0	150	20		35.9	605	0.786	17.1	
ASEC Cal										
ASEC Exp	N+/P					34.75	620	0.793	17.1	
ASEC MaxExp	N+/p					34.85	623	0.799	17.1	

  * BASE DIFFUSION LENGTH AND BSF SURFACE RECOMBINATION VELOCITY DATA

SOURCE	TYPE	RHO	TBASE	LB	TAU	SRV	JSC	VOC	EFF%
Neugroschel	N+/P/P+	10	227	450	(60)	105	-	-	-
Neugroschel	N+/P/P+	10	92	600	(103)	180	-	-	-
Neugroschel	N+/P/P+	1.5	220	600	(136)	380	38*	6.7	-
Neugroschel	P+/N/N+	7.0	320	503	(200)	80	39*	605	-
Computed-Sah	P+/N/N+	0.6	50	320	39	(128)eff	36.0	660	20.0
Green	M/I/N/P	0.2	280	(170)	20	(850)eff	36.0	653	19.1
Spitzer	N+/P/P+	0.3	380	150	(13)	(1100)eff	36.2	622	18.0
Rohatgi	N+/P/P+	4.0	150	263	(23)	(652)eff	35.9	605	17.1
ASEC	N+/P						34.8	620	17.1

Legend: Dimensions: RHO(ohm-cm); TBASE, LB(microns); TAU(microsec.);
    SRV(cm/s); JSC(mA/cm^2); VOC(mV); Values in ( ) are compute.
    ( )eff is the effective value to give the J1. All at AM1.5
    except * at AM0.

(1) RECOMBIANTION LOSS MECHANISMS
(2) HIGH EFFICIENCY CELLS (<20%)

(3) VERY HIGH EFFICIENCY CELLS (>20%)

  * BASE RECOMBINATION ELIMINATED

    # REDUCE BULK RECOMBINATION
     * High Base Lifetime
     * Low Defects (Float-Zone)
     * Low Residual Impurities (FZ)

    # REDUCE BACK SURFACE RECOMBINA-
    TION LOSS
     * Thin Epitaxial Base.
     * Graded Base.
     * Back Surface Field.
     * Oxidized Back Surface.
     * Interdigited Back Contact.
     * Doped-diffused Back Contact.

(1) RECOMBINATION LOSS MECHANISMS

(2) HIGH EFFICIENC CELLS (<20%)

(3) VERY HIGH EFFICIENCY CELLS (>20%)

    * BASE RECOMBINATION ELIMINATED

    ** EMITTER RECOMBINATION LIMITING
       (Data yet to be obtained.)

       # BULK EMITTER
         = Auger (Hi Dop Effect)
         = SRH (with BGN Hi Dop Effect)
           o Residual Impurity Centers
           o Point-Pair Defects (Hi Dop)
         = Gross Defect (Hi Dop Effect)
           o Grain Boundary
           o Dislocation
           o Lattice Faults
           o Diffusion Piper

       # EMITTER/OXIDE INTERFACE
         = Interface States Monitoring
           o DOS by MOS HFCV (Terman's)
           o SRV by SCD DCIV (Sosier's)
         = Interface States Reduction
           o Dry/Low-Temp Oxide
           o Hydrogen Passivation (Stable?)

       # EMITTER/CONTACT INTERFACE
         = M/I/P Tunneling Oxide
           (Green)
         = Polysilicon Emitter
           (Ning-Isaac-Neugroschel)
         = Floating Emitter Transistor
           (TI & JPL/Cheng-Sah)
           o Epitaxial Base/Front-Back
             Contacts.
           o All Back Contacts.

Summary

(1) RECOMBINATION LOSS MECHANISMS

    * Residual Impurities.
    * Lattice Defects.
    * Interface States.
    * Interband Auger & Radiative.

(2) HIGH EFFICIENCY CELLS (<20%)

    * J1 > 2.0E-13 A/cm^2
    * Back Surface Recombination.
    ** Base Recombination LIMITING.

(3) VERY HIGH EFFICIENCY CELLS (>20%)

    * J1 < 2.0E-13 A/cm^2
    * Eliminate Base Recombination.
    * Eliminate Back Surface & BSF
       Layer Recombiantion Losses.
    * Emitter Recombination LIMITING.

(4) ULTRA HIGH EFFICIENCY CELLS (~25%)

    * J1 < 1.0E-16 A/cm^2
    * Eliminate All Extrinsic
       Recombination Losses.
         o Residual Impurities.
         o Lattice Defects.
    * Eliminate Perimeter Damage.
    * Design away Auger Emitter
       Recombiantion.
    ** Interband Auger and Radiative
       in base LIMITING.

DEVELOPMENT OF HIGH-EFFICIENCY SOLAR CELLS ON SILICON WEB
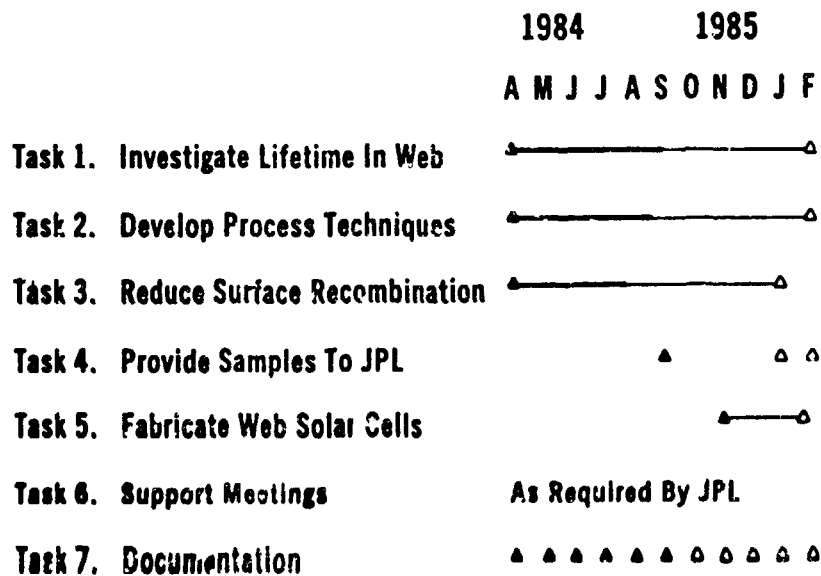
WESTINGHOUSE ELECTRIC CORP.

A. Rohatgi
D.L. Meier
R.B. Campbell
R.G. Seidensticker
P. Rai-Choudhury

Specific Tasks

- **Investigate The Heat Treatment Effects On Web Quality**

- **Investigate The Influence Of Twin Plane Lamellae, Trace Impurities And Stress On Minority Carrier Lifetime**

- **Fabricate High Efficiency Web Solar Cells**

Milestone Chart

		1984	1985
		A M J J A S O N D	J F
Task 1.	Investigate Lifetime In Web	●————————————————△	
Task 2.	Develop Process Techniques	●————————————————△	
Task 3.	Reduce Surface Recombination	●————————————△	
Task 4.	Provide Samples To JPL	▲	△ △
Task 5.	Fabricate Web Solar Cells		●———△
Task 6.	Support Meetings	As Required By JPL	
Task 7.	Documentation	▲ ▲ ▲ ▲ ▲ ▲ △ △ △ △ △	

Calculated AM1 Performance of Standard Web Cells
With Base Diffusion Length as a Parameter

Cell Base: 4 Ohm-cm (3.5e15/cm^3) P-Type, 150 Microns Thick

Ln (Microns)	J_{oe} (A/cm^3)	J_{ob} (A/cm^3)	J_{sc} (mA/cm^2)	V_{oc} (V)	FF	Eff (%)	Eff' (%)
10	1.6e-12	32.1e-11	24.6	.471	.793	9.2	8.3
30	1.6e-12	9.5e-11	30.6	.508	.802	12.5	11.2
60	1.6e-12	5.3e-11	33.2	.525	.809	14.1	12.7
150	1.6e-12	2.0e-11	36.5	.551	.815	16.4	14.8
300	1.6e-12	1.1e-11	37.6	.566	.819	17.4	15.7

Note:

1. Calculations Were Made Using Martin Wolf's Program SPCOLAY.BAS

2. Calculated Values Do Not Account For Grid Shadowing, Light Reflection. Or Resistive Losses. In Order To Estimate These Effect, The Calculated Efficiency (Eff) Was Multiplied By 90% To Give A More Realistic Efficiency (Eff').

3. The Model Accounts For Variation In Doping Density In The Emitter And In The Back Region. For Both The n+p And p+p Regions The Junction Depth Was Taken To Be 0.3 Microns With A Surface Concentration Of 8.0E19/cm^3.

4. The Surface Recombination Velocity Was Taken As 10,000 cm/sec On The Front (AR Coating On Bare Silicon) And 1,000,000 cm/sec On The Back (Metal On Silicon).

15% Baseline Web and Float-Zone Silicon Cell

n^+-p-p^+ With Single Layer AR And NO Oxide Passivation

Cell ID	J_{sc}	V_{oc}	FF	η	τ_{OCD}
4412-49W Cell 63A, 4 Ω-cm	31.8	0.588	0.80	15.0%	40 μs
FZ, 4 Ω-cm	33.4	0.584	0.78	15.2%	45 μs

τ_{OCD} Of 40 μsecs $\simeq$ 360 μm Diffusion Length In 4 Ω-cm Base

Scatter Plot for As-Grown Web

Development Furnaces J, N, R, and Z are Plotted as 10, 11, 12, and 13
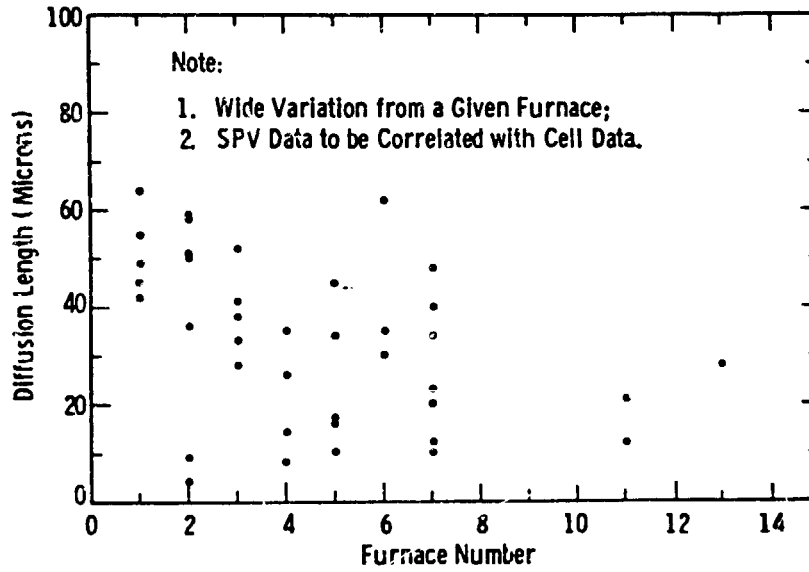
Effect of Quench Temperature and Cooling
Rate on Generation Lifetime

Table 4 — Effect Of Quench Temperature Of Lifetime And Defects In FZ Silicon[a]

Quench Temperature, °C	Lifetime, μs
500	2012
600	2000
700	850
800	73
900	40

[a]Oxidation Was Performed At 1100°C With 1% HCl By Using Back-Surface Damaged Wafers And A Cooling Rate Of 1°C/Min.
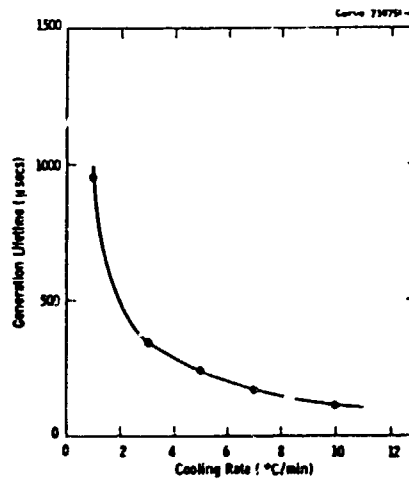
Effect of Process Sequence on Lifetime in FZ Silicon

Process	Lifetime (us)
1% HCl Oxidation At 1100°C Slow Cooled	2115
↓	
1 Hr Anneal in N$_2$ At 1100°C Quenched	50
↓	
1 Hr Anneal In N$_2$ At 1100°C Slow Cooled	1400
1% HCl Oxidation At 1100°C Quenched	60
↓	
1 Hr Anneal In N$_2$ At 1100°C Slow Cooled	1650
↓	
1 Hr Anneal In N$_2$ At 1100°C Quenched	40

Back Surface Of The Samples Was Damaged

HIGH-EFFICIENCY SILICON SOLAR CELL RESEARCH

Effect of Dry Oxidation Temperature on SPV
Diffusion Length for a Dendritic-Web Silicon Crystal

Silicon Dendritic Web Crystal 1-288-7.3

Heat Treatment :
Dry Oxidation for 1 Hour
Slow-Cool at 1°C/min to 600°C in Nitrogen

(As-Grown)

Diffusion Length (μm)

Oxidation Temperature (°C)
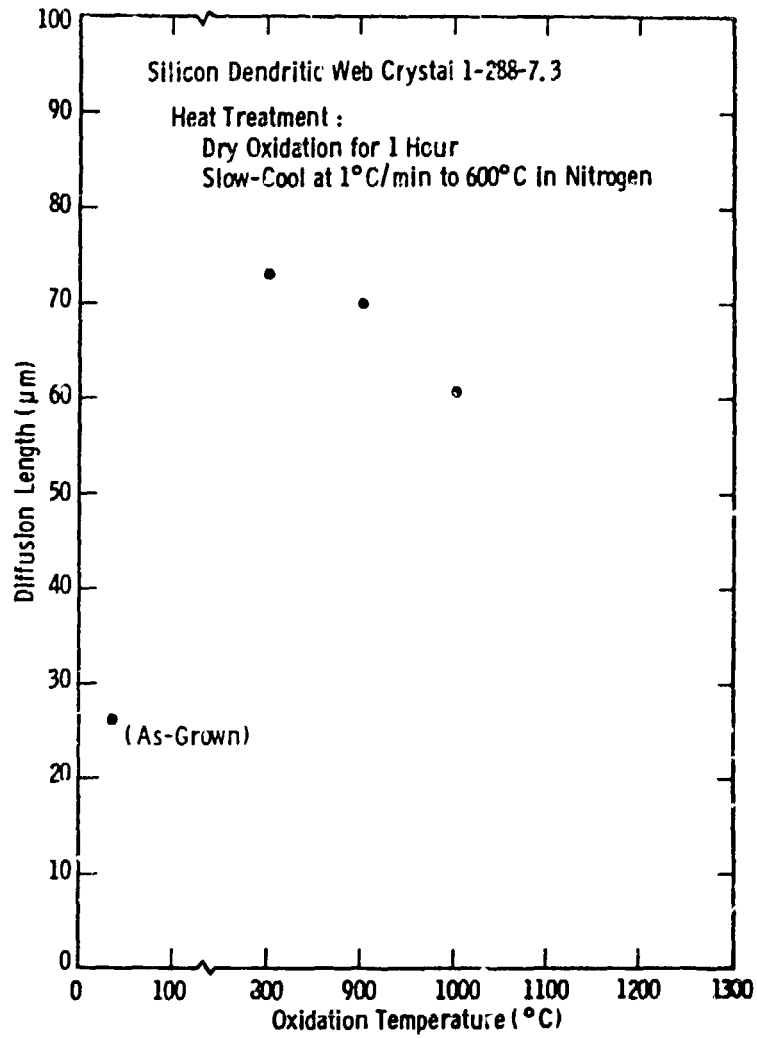
Diffusion-Length Map of Web Crystals
as a Function of Cell Processing

Sample ID	Crystal ID	As Grown L (μm)	After BSF L (μm)	After POCl$_3$ L (μm)	After Passivation L (μm)
#2	4.229 – 4.2 (0.5 Ω-cm)	27	51	41	30
#3	4.227 – 2.4 (1.0 Ω-cm)	27	51	22	26
#5	4.225 – 3.2 (1.5 Ω-cm)	23	–	9	40
#25	1.288 – 5.5 (4 Ω-cm)	24	–	52	76
#26	1.288 – 5.6 (4 Ω-cm)	28	–	124	60
#90	1.288 – 7.4 (4 Ω-cm)	26	–	110	88
#26	2.244 – 6.4 (4 Ω-cm)	25	40	71	63
#28	2.244 – 7.3 (4 Ω-cm)	22	74	76	80
#76	3.155 – 11.7 (4 Ω-cm)	19	151	124	73
#77	3.155 – 15.5 (4 Ω-cm)	23	50	78	–
#79	3.155 – 15.3 (4 Ω-cm)	16	–	91	103
FZ	Wacker 0.25 Ω-cm	216	220	220	225

Note: On 4 Ω-cm Web Crystals AESD Made Baseline Cells (n^+-p-p^+ With 14.5 – 15% Efficiencies

Effect of Residual Stress on Diffusion Length in Web Silicon Before and After 960°C Boron Diffusion

Crystal	Residual Stress Mdyne/cm^2	Diffusion Length As-Grown Microns	Diffusion Length After BBr$_3$ Microns
Z-025-3.4	14	19	16
Z-025-3.10	40	16	23
Z-025-3.15	42	16	12
Z-028-12.4	< 5	25	27
Z-028-12.10	< 5	40	–
Z-025-12.16	< 5	33	116
R-461-5.3	< 5	17	39
R-461-5.8	< 5	9	–
R-461-5.13	< 5	10	83

Note:
1. Crystal Z-025 Was Grown With J435 Configuration And Crystals Z-028 And R-461 Were Grown With J460L Configuration;
2. Web Was 4 Ohm-cm, P-type

Observations:
1. Diffusion Length For Web Crystal With High stress (Z-025) Did Not Improve After Boron Diffusion;
2. In Three Of Four Samples With Low Stress, The Diffusion Length Improved Appreciably After Boron Diffusion

Model Calculations for the Effect of Electrical Activity of the Twin Plane on V_{OC} in 4 ohm-cm Web Cells
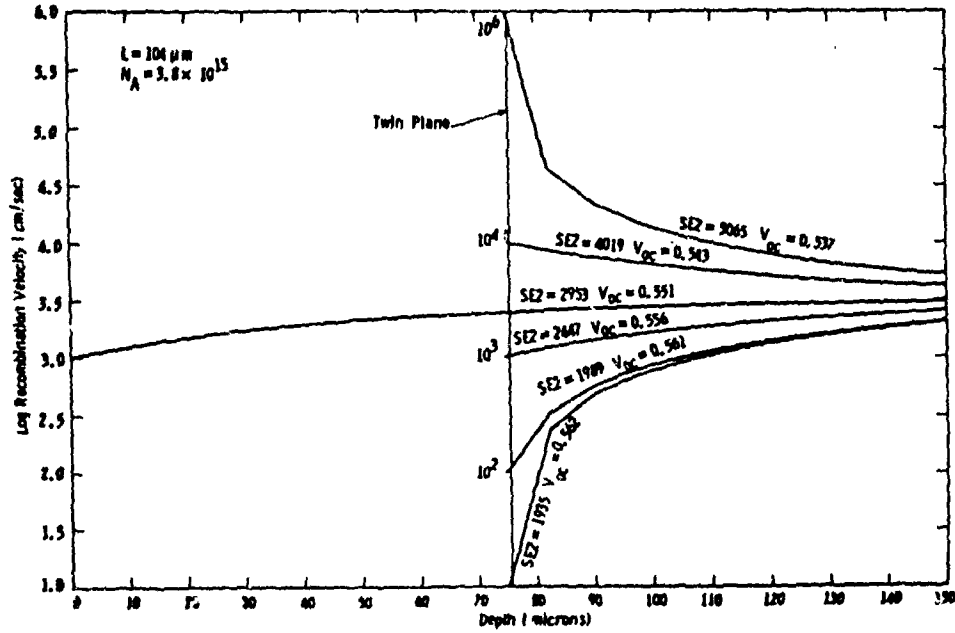
Cell Model Calculations
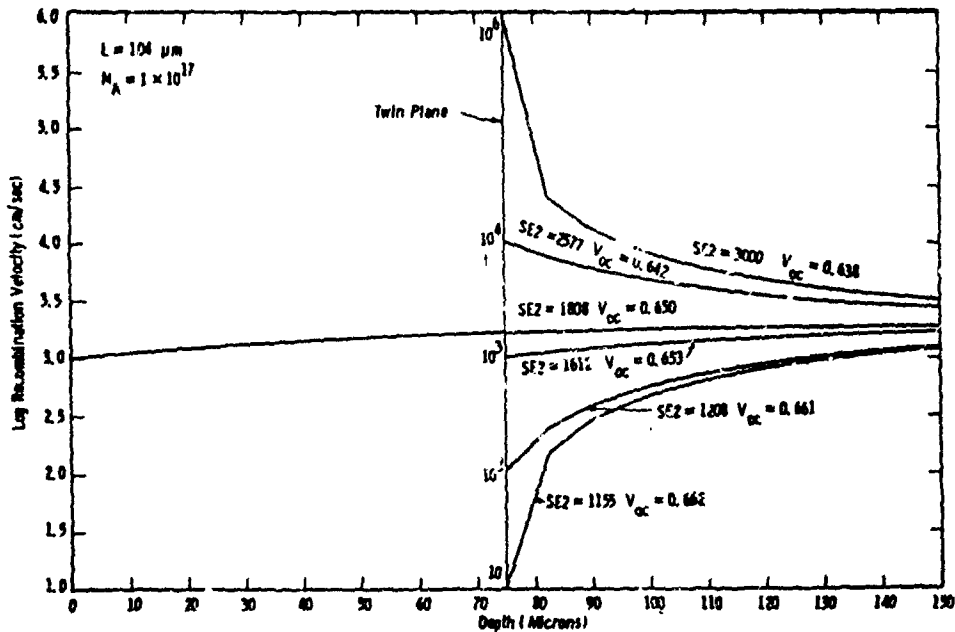
Calculated AM1 Performance of Standard and Low-Resistivity Web Cells With Base Diffusion Length as a Parameter

A. 4 Ohm-cm ($3.5e15/cm^3$) P-Type, 150 Microns Thick

Ln (Microns)	J_{oe} (A/cm^3)	J_{ob} (A/cm^3)	J_{sc} (mA/cm^2)	V_{oc} (V)	FF	Eff (%)	Eff' (%)
10	1.6e-12	32.1e-11	24.6	.471	.793	9.2	8.3
30	1.6e-12	9.5e-11	30.6	.508	.802	12.5	11.2
60	1.6e-12	5.3e-11	33.2	.525	.809	14.1	12.7
150	1.6e-12	2.0e-11	36.5	.551	.815	16.4	14.8
300	1.6e-12	1.1e-11	37.6	.566	.8'9	17.4	15.7

B. 0.2 Ohm-cm ($1.0e17/cm^3$) P-Type, 150 Microns Thick

Ln (Microns)	J_{oe} (A/cm^3)	J_{ob} (A/cm^3)	J_{sc} (mA/cm^2)	V_{oc} (V)	FF	Eff (%)	Eff' (%)
10	1.6e-12	7.5e-12	24.2	.563	.817	11.1	10.0
30	1.6e-12	2.5e-12	30.0	.589	.824	14.6	13.1
60	1.6e-12	1.2e-12	33.0	.601	.826	16.4	14.8
150	1.6e-12	0.6e-12	35.1	.609	.831	17.8	16.0
300	1.6e-12	0.5e-12	35.7	.611	.832	18.1	16.3

Note:

1. Calculations Were Made Using Martin Wolf's Program SPCOLAY.BAS

2. Calculated Values Do Not Account For Grid Shadowing, Light Reflection, Or Resistive Losses. In Order To Estimate These Effect, The Calculated Efficiency (Eff) Was Multiplied By 90% To Give A More Realistic Efficiency (Eff').

3. The Model Accounts For Variation In Doping Density In The Emitter And In The Back Region. For Both The n+p And p+p Regions The Junction Depth Was Taken To Be 0.3 Microns With A Surface Concentration Of $8.0e19/cm^3$.

4. $S_{front} = 10^4$ cm/sec (AR On Bare Si); $S_{back} = 10^6$ cm/sec (Metal on Si)

Effect of Oxide Passivation on 4 ohm-cm FZ Silicon

Table 1 - Baseline Unpassivated Solar Cells (n^+-p-p^+)
Fabricated On 4 Ohm-cm Float Zone Silicon

Cell ID	Short Circuit Current J_{sc} mA/cm^2	Open Circuit Voltage V_{oc} Volts	Fill Factor	Cell Efficiency %
1	33.3	0.582	0.767	14.8
4	32.9	0.581	0.772	14.7
6	33.4	0.583	0.780	15.2

Table 2 - Oxide-Passivated Solar Cells On Boron-Doped
4 Ohm cm Float-Zone Silicon

Cell ID	J_{sc} (mA/cm^2)	V_{oc} (Volts)	FF	η (%)
HIEFY 4-4	36.1	0.599	0.794	17.1
-5	36.2	0.600	0.793	17.2
-7	36.2	0.599	0.791	17.2

* Improvements: $\Delta J_{SC} \sim 3$ mA/cm^2, $\Delta V_{OC} \sim 20$ mV, $\Delta\eta \sim 2\%$
$\Delta J_0 \sim$ Factor Of Two

Solar-Cell Data on 4 ohm-cm Web With
and Without Oxide Passivation

Cell ID	Short-Circuit Current J_{sc} (mA/cm^2)	Open-Circuit Voltage V_{oc} Volts	Fill Factor	Cell Efficiency (%)
		Without Passivation		
W6	32.7	0.575	0.782	14.7
W7	33.1	0.577	0.784	15.0
		With Oxide Passivation		
W1	34.6	0.584	0.784	15.9
W2	34.5	0.586	0.794	15.8

PROCESS DEVELOPMENT

Donald B. Bickler, Chairman

Presentations on 10 process development activities were made during this technology session. A 40-minute coffee break was included to allow time to attend a poster session covering four aspects of FSA in-house research efforts.

Solarex Corp. presented the status of the first portion of a study of the hydrogen passivation of polycrystalline silicon cells. This contract was terminated at the request of the contractor.

Westinghouse Electric Corp., Advanced Energy Systems Division, has made progress on the simultaneous diffusion of front and back junctions. However, the use of a belt furnace has been ruled out due to problems with contamination. Very good cell efficiencies have been achieved using sequential diffusion of liquid-dopant-coated dendritic-web cells. Additional experiments will be made to investigate different diffusion techniques. Some early results with laser drive-in have been promising.

M.A. Nicolet of Caltech reported on progress on deposition and characterization of amorphous-metal films. The goal of low diffusivity has been achieved; however, the amorphous films were found to be reactive with adjacent materials such as the substrate and various metallic overlayers. The use of metals that have a low reactivity with silicon is being investigated. Addition of nitrogen by reactive sputtering is one possible solution for reactivity with metal overlayers.

Robert West of Purdue University has been adapting his previous metallo-organic deposition work on ceramics for use on silicon. The choice of solvents during the preparation of silver neodecanoate is important to the quality of the final deposited film. Problems with film adhesion to silicon have been eased by addition of platinum 2-ethylhexanoate. Additional work with other additives is planned, with a bismuth compound being considered. Some Purdue material has been used successfully by JPL and by Westinghouse for direct patterning by lasers.

Westinghouse Electric Corp., R&D Division, has been exploring laser-assisted metallization processes. Laser-assisted gas-phase photolysis has been reviewed but experimental work was not pursued due to toxicity problems. Fortunately, the liquid-phase Purdue metallo-organics were available and were used for laser pyrolysis. Also examined were metal-bearing polymer films. Another successful research area has been in laser-assisted electroplating, where adherent fine-line geometries have been achieved.

The Spectrolab Division of Hughes Aircraft Corp., has completed its research on the molybdenum-tin thick-film ink system. Soldering problems proved to be intractable, but use of a silver ink in a two-step process did provide useable cells.

Microwave energy as a heat source for deposition reactors has been explored by Superwave Technology, Inc. Use of this technique permits the

separation of the plasma reaction from the substrate deposition area, thereby reducing deposition temperature and plasma damage. No depositions have yet been made but are expected soon.

ARCO Solar, Inc., is developing pulsed excimer laser processes for junction formation surface passivation and front metallization. Laser drive-in of liquid dopants and laser annealing of ion-implanted wafers has been accomplished, but there have been uniformity problems with ion-implanted wafers. Laser-beam inhomogeneity is another potential problem area.

Another excimer laser effort is the annealing of ion-implanted wafers at Spire Corp. Both polished and textured wafers are being processed, with results equivalent to diffused-junction cells. Either krypton fluoride (248 nm) or xenon chloride (308 nm) excimer lasers can be used and front junctions as shallow as 0.15 micrometers have been achieved.

Paul Willis of Springborn Laboratories gave a special presentation on his intended study of the yield sensitivity of encapsulation processes. This is not presently a process research contractual effort but is appropriate to FSA's interest in process-yield improvement.

The poster session covered four areas of in-house process research. Ion-cluster beam deposition of silver on silicon and gallium arsenide has been demonstrated using a technology originally developed for ion propulsion in space. A parametric study of a large amorphous-silicon reactor has shown interesting phenomena not normally found. Some work on the effects of PV-cell size scale-up was displayed. Finally, the results of a one-dimensional cell-structure computer modelling program were presented.

Amorphous-silicon film deposition research has defined the region where formation of powdery deposits of silane polymers is reduced. Depositions having a light-to-dark conductivity ratio of 10,000 have been made. Operating voltage of the deposition chamber is not a product of pressure times electrode spacing, as expected; instead, it is a function of pressure only. A strong lateral diffusion mechanism is present in the reaction chamber and is most encouraging for the formation of large-area constant-thickness depositions.

C-5

SOLAREX HYDROGEN PASSIVATION

JET PROPULSION LABORATORY

P. Alexander

CONTRACT OBJECTIVE: INVESTIGATE THE EFFECTS OF HYDROGENATION OF
POLYCRYSTALLINE SILICON MATERIAL. USE CZ
MATERIAL AS CONTROLS.

APPROACH: ° FABRICATE A DC PLASMA HYDROGENATION SYSTEM

° MEASURE CELL CHARACTERISTICS BEFORE AND AFTER HYDRO-
GENATION CELL CHARACTERIZATION TO INCLUDE: LIGHT AND
DARK IV DATA, LBIC GRAPHS, DIFFUSION LENGTH MEASUREMENTS

° ANALYZE DATA, DRAW CONCLUSIONS

PROGRESS: ° DC PLASMA HYDROGENATION SYSTEM COMPLETED

° NO HYDROGENATION DATA WAS GENERATED

° CONTRACT WAS TERMINATED AT THE REQUEST OF THE CONTRACTOR
- AUGUST 1984

Solarex Hydrogenation Equipment for Polycrystalline Cells
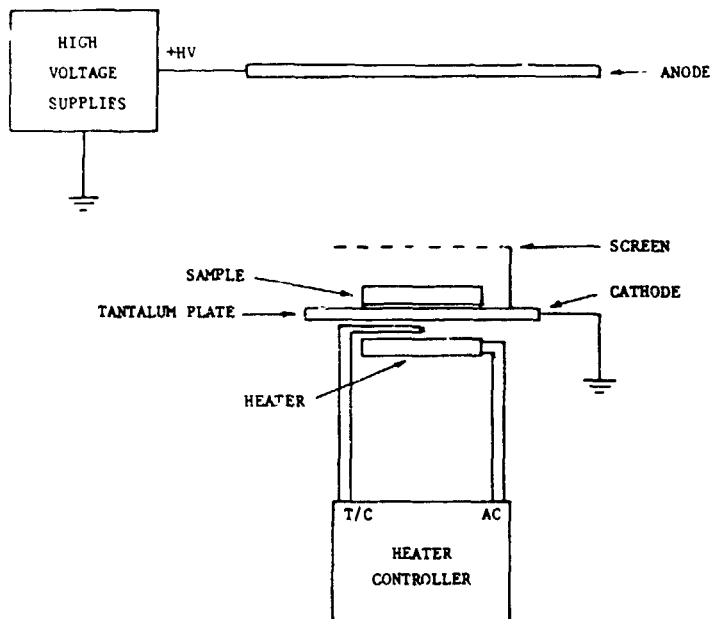
SIMULTANEOUS JUNCTION FORMATION

WESTINGHOUSE ELECTRIC CORP.

R.B. Campbell

Contract Information

OBJECTIVE: INVESTIGATE HIGH-RISK; HIGH-PAYOFF IMPROVEMENTS
TO WESTINGHOUSE BASELINE PROCESS SEQUENCE

TIME PERIOD: MARCH, 1984 - OCTOBER, 1984

Contract Tasks

- EVALUATE FEASIBILITY OF SIMULTANEOUSLY FORMING BACK & FRONT
  JUNCTIONS OF SOLAR CELLS USING LIQUID DOPANTS ON DENDRITIC
  WEB SILICON

- COMPARE SIMULTANEOUS DIFFUSION TO SEQUENTIAL DIFFUSION

- TEST OF BELT FURNACE FOR DIFFUSION PROCESS

WHEN SHOWN FEASIBLE:
- DEVELOP PROCESS CONTROL PARAMETERS AND SENSITIVITIES

- PERFORM COST ANALYSES

Potential Benefits

- FEWER PROCESSING STEPS

- LESS OPPORTUNITY FOR CONTAMINATION AND BREAKAGE DURING PROCESSING
  DUE TO HANDLING

- LESS COSTLY PROCESS

HOWEVER

- PROCESS WILL REQUIRE CAREFUL SELECTION OF DOPANTS, DIFFUSION
  MASKS, AND WEB CONDUCTIVITY TYPE

Approaches

- DIFFUSION

  N-TYPE DENDRITIC WEB

  - PHOSPHORUS O, ARSENIC FOR BACK N^+N JUNCTION
  - BORON OR ALUMINUM FOR FRONT P^+N JUNCTION

  P-TYPE DENDRITIC WEB (LOW RESISTIVITY)

  - PHOSPHORUS FOR FRONT N^+P JUNCTION
  - BORON OR ALUMINUM FOR BACK P^+P JUNCTION
  - BACK SURFACE DAMAGE

- BASELINE PROCESS EXCEPT FOR DIFFUSION

- TEST OF VARIOUS VENDORS' DOPANTS AND DIFFUSION MASKS

- EXCIMER LASER DRIVE IN
  - PHOSPHORUS, BORON, AND ALUMINUM DOPANTS

Results: n-Type Web

- LIQUID SOURCE - SEQUENTIAL DIFFUSION OF B (FRONT) AND P (BACK) PRODUCED CELLS WITH η_{AV} >13%

- LIQUID SOURCE - SIMULTANEOUS DIFFUSION USING B & P PRODUCED JUNCTION DEPTHS OF 0.25 μm (P^+N) AND 0.6 μm (N^+N)

- SUITABLE JUNCTIONS ALSO OBTAINED USING BORON (FRONT) AND ARSENIC (BACK)

- IN ANY EXPERIMENT WHERE TWO DOPANT SPECIES WERE PRESENT, CELL PROPERTIES WERE DEGRADED DUE TO CROSS DOPING OF THE FRONT JUNCTION

- CELL EFFICIENCIES VARIED FROM <1% TO 6-7% WITH A FEW CELLS >10%

- CROSS DOPING ALSO OCCURRED WHEN SIO_2 DIFFUSION MASKS (LIQUID OR THERMAL) WERE USED

- EFFECT ALSO OCCURRED AT LOWER DIFFUSION TEMPERATURES

- PROBLEM DUE TO HIGH MOBILITY OF P AT DIFFUSION TEMPERATURES REQUIRED

- EFFECT STUDIED USING DARK IV AND CONDUCTIVITY MEASUREMENTS

Shorting Paths in Front p^+n Junction Due to Contamination With Back-Surface Dopant
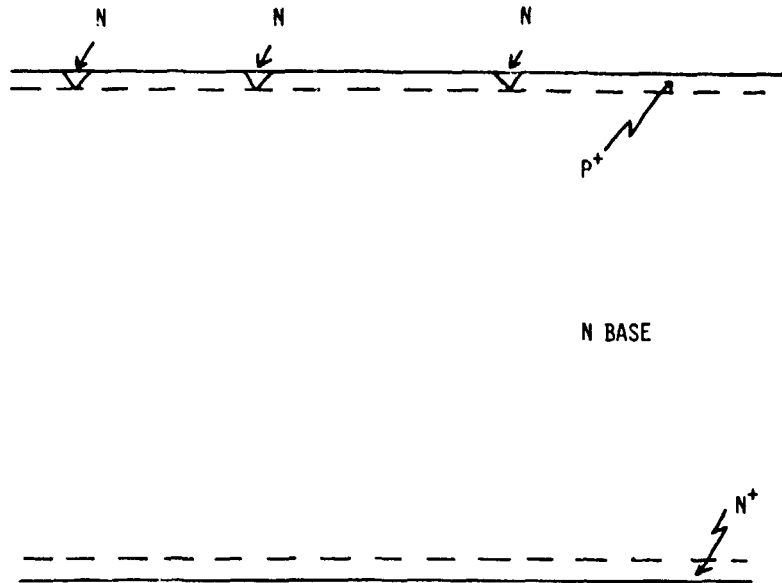
Results: p-Type Web

- SHALLOW B-DOPED BSF DUE TO LOW TEMPERATURE DIFFUSION (REQUIRED FOR FRONT P-DOPED JUNCTION); HIGH RESISTIVE CONTACT PROBABLY SCHOTTKY BARRIER. $r_{max} = 7\%$

- AL BSF ALSO GAVE HIGH RESISTANCE CONTACT WITH $n_{max} = 8\%$

- CELLS OF >12% EFFICIENCY FABRICATED USING PHOSPHORUS FRONT DOPING ONLY WITH THE BACK SURFACE DAMAGED (0.5 ncm - 1.5 ncm)

- NO NOTICEABLE CROSS DOPING IN CELLS

Belt Furnace Test

- TEST CARRIED OUT AT RADIANT TECHNOLOGY CORPORATION

- PROPER TEMPERATURE AND TEMPERATURE GRADIENTS OBTAINED

- SUITABLE JUNCTION DEPTHS OBTAINED

- CELLS SHOWED EFFECT OF CROSS-DOPING

Junction Formation Using an Excimer Laser

APPROACH

HEAT SURFACES OF WEB WITH LASER TO DRIVE IN LIQUID DOPANTS

CONDITIONS

WAVELENGTH - 3080 nM

POWER INPUT TO WEB 1 $\rightarrow$ 2 J/cm^2

EXPERIMENT

DRIVE IN B, P, AND AL INTO BOTH N-TYPE AND P-TYPE WEB

INITIAL STUDY CARRIED OUT AT MATHEMATICAL SCIENCES NORTHWEST, INC.

Sample 17B, p-Base Web, Phosphorus Emitter 1.15 J/cm^2

Sample 17B, p-Base Web, Boron BSF 1.15 J/cm^2
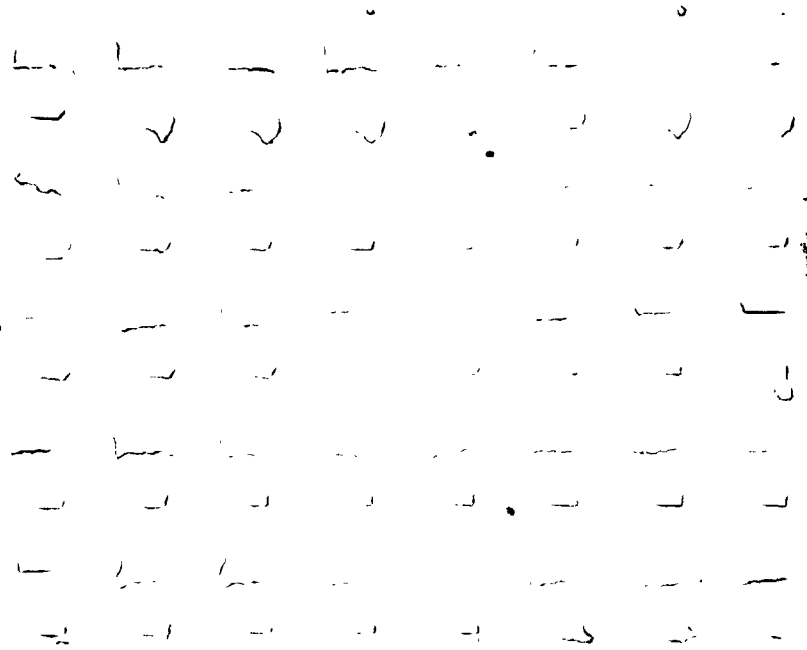
Results: Excimer Laser

- JUNCTION CHARACTERISTICS

  N$^+$N OR N$^+$P (PHOS. DOPED) Co = 10^{19}/cm^2 X$_j$ = 0.2 - 0.25 µm

  P$^+$N OR P$^+$P (B DOPED) ESSENTIALLY NO JUNCTION

  P$^+$P (AL DOPED) SHALLOW JUNCTION

- CELL PROPERTIES

  P TYPE WEB, n_{max} = 9% - DUF TO HIGH RESISTANCE BACK CONTACT (BOTH B & AL BSF)

  N TYPE WEB, n_{max} <1% - POOR B DOPED EMITTER

- LOW DIFFUSION CONSTANT OF BORON WILL REQUIRE HIGHER POWER INPUT

- NO CROSS CONTAMINATION NOTED

- CRYSTAL PAIRS PROCESSED BASELINE SEQUENCE - $\hat{n}$ = 13.7%

n⁺p Front Junction by Laser Drive-in
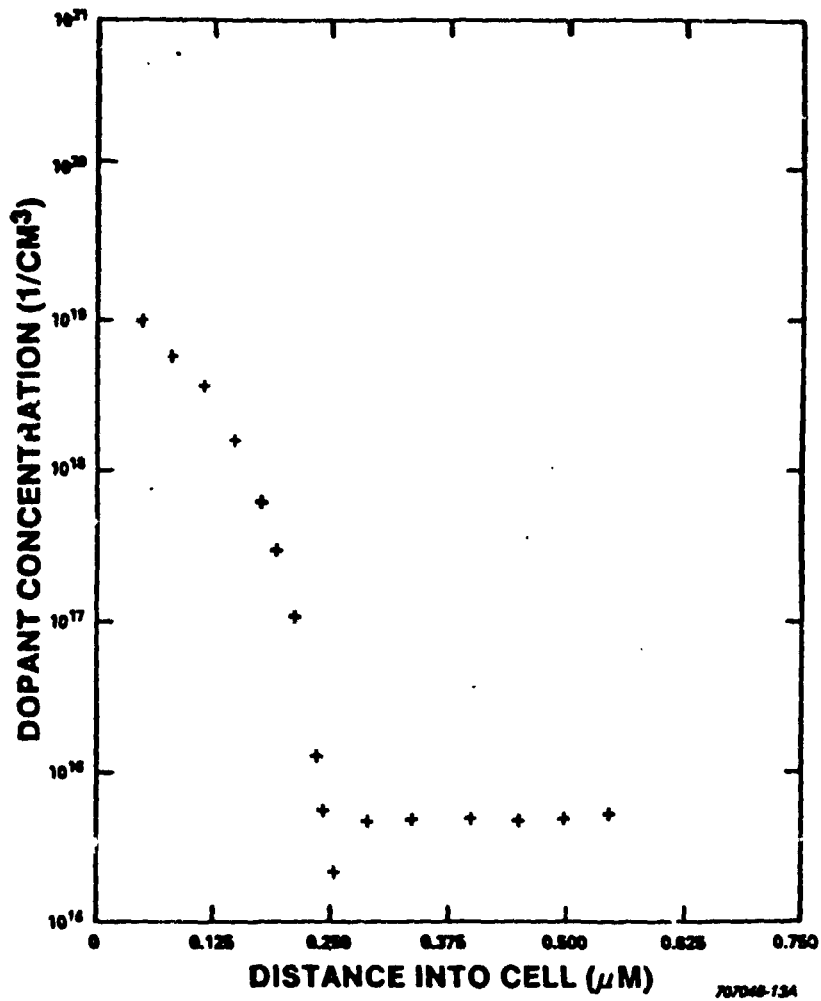
p⁺p Back Junction by Laser Drive-in
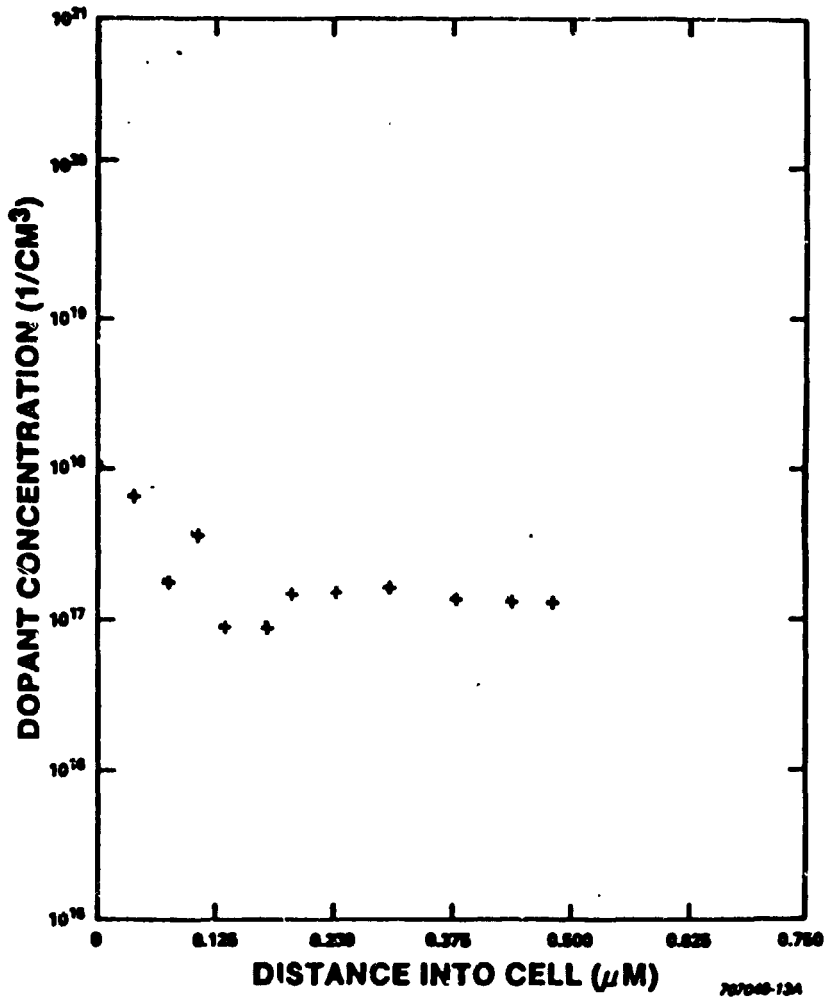
Conclusions

- SEQUENTIAL DIFFUSION OF N-TYPE WEB - USING LIQUID B & P SOURCES, CELLS WITH AVERAGE EFFICIENCIES >13% PRODUCED

- SIMULTANEOUS DIFFUSION - N TYPE WEB - WITH PRESENT DOPANTS AND DIFFUSION MASKS, A SUITABLE PROCESS HAS NOT BEEN DEFINED. PROBLEM DUE TO HIGH MOBILITY OF PHOSPHORUS AT TEMPERATURES REQUIRED FOR BORON DIFFUSION WHICH CAUSES FRONT JUNCTION CONTAMINATION.

- SIMULTANEOUS DIFFUSION - P TYPE WEB - AL BSF WITH PHOSPHORUS DOPED EMITTER GAVE BEST RESULTS. FURTHER STUDY REQUIRED TO OBTAIN LOW RESISTANCE BACK CONTACT AND OPERATIONAL BSF.

- EXCIMER LASER DRIVE IN

  - EXCELLENT PHOSPHORUS DOPED JUNCTIONS FABRICATED BOTH N^+P AND N^+N

  - FURTHER STUDY REQUIRED TO PRODUCE BORON DOPED LAYERS FOR P^+N AND P^+P JUNCTIONS

  - NO CROSS-CONTAMINATION PROBLEM OBSERVED

AMORPHOUS METALLIC FILMS IN SILICON METALLIZATION SYSTEMS

CALIFORNIA INSTITUTE OF TECHNOLOGY

Marc-A. Nicolet
Hannu Kattelus
Frank So

The general objective of this project is to determine the potential of amorphous metallic thin films as a means of improving the stability of metallic contacts to a silicon substrate. The specific objective pursued in the reporting period was to determine the role of nitrogen in the formation and the resulting properties of amorphous thin-film diffusion barriers.

Amorphous metallic films are attractive as diffusion barriers because of the low atomic diffusivity in these materials. Our previous investigations have revealed that in meeting this condition alone, good diffusion barriers are not necessarily obtained, because amorphous films can react with an adjacent medium (e.g., Si, Al) before they recrystallize. In the case of a silicon single-crystalline substrate, correlation exists between the temperature at which an amorphous metallic binary thin film reacts and the temperatures at which the films made of the same two metallic elements react individually. We thus investigated amorphous binary films made of Zr and W, both of which react with Si individually only at elevated temperatures. We confirmed that such films react with Si only above 700°C when annealed in vacuum for 30 min.

When these films are in contact with metallic polycrystalline films (Ag, Al, Au, Ni); however, they react at significantly lower temperatures. The question arises how the reactivity of an amorphous metallic thin-film diffusion barrier can simultaneously be reduced on both sides of the film (substrate and metallization). Conceptual solutions do exist if the reactivity of two amorphous binary metallic thin films is low.

Amorphous W-N films were also investigated. They are more stable as barriers between Al and Si than polycrystalline W. Nitrogen effectively prevents the W-Al reaction that sets in at 500°C with polycrystalline W. In this respect, amorphous W-N films even outperform TiN diffusion barriers.

The study of W-N will continue, and that of Zr-N is planned, to determine deposition conditions that yield amorphous layers and how the properties vary with deposition conditions, using backscattering spectrometry, X-ray diffraction, and sheet resistivity measurements and transmission electron microscopy (TEM) for analysis.

Previous Findings

AMORPHOUS FILMS (MO-NI, NI W):

- REACT WITH SI SUBSTRATE AND AL
  OVERLAYER BELOW CRYSTALLIZATION
  TEMPERATURE T_c (600, 650°C).

- NI DIFFUSES INTO SI SUBSTRATE.
  W DIFFUSES INTO AL OVERLAYER.

- NI-SI REACTION INTERFACIALLY
  CONTROLLED AND LATERALLY CONFINED.

- ADDING N (NI-N-W) LOWERS T_c TO
  $\simeq$ 600°C, SUPPRESSES NI-SI REACTION
  BELOW 725°C AND AL-W REACTION UP TO
  550°C.

Approaches

WAYS TO CIRCUMVENT REACTION:

- AVOID NI (AND CO, PD, PT), E.G. ZR-W.

- TERNARY AMORPHOUS FILMS,
  E.G. NI-N-W.

- USE BUFFER LAYER,
  E.G.

(A) NI-W
NISI
<SI>

- MULTILAYERED AMORPHOUS FILMS.

Results on Amorphous $W_{60}Zr_{40}$ Films

EXPERIMENTAL PROCEDURES:

- ON <100> N-TYPE SI AND SiO_2 SUBSTRATES.

- R.F. SPUTTERING, 10 MTORR AR, 300 W, 5^{h_1},
  60 Å/MIN; (2 x 10^{-6} TORR VACUUM).

- EVAPORATED METAL FILMS (AL, AU, AG, NI)
  (3 x 10^{-7} TORR).

- ANNEALING IN VACUUM $\leq$ 5 x 10^{-7} TORR,
  30 MIN.

- RBS AND X-RAY DIFFRACTION.

Crystallization on SiO_2

INTERACTION WITH <SI> SUBSTRATE.

- STABLE BELOW 700°C.
- UNIFORM REACTION AT 750°C
  ($\rightarrow WSi_2$, ZRSI OR Zr_2SI) SEE FIG. 1
- SAME AS W, ZR FILMS ON <SI> .
- SI IS DIFFUSING SPECIES, NOT W, ZR
  (NO INTERFACIAL PENETRATION OF <SI>)
  REACTION AT T < T_c.

CONCLUSION

AVOIDING NI (CO, PD, PT) IS BENEFICIAL.
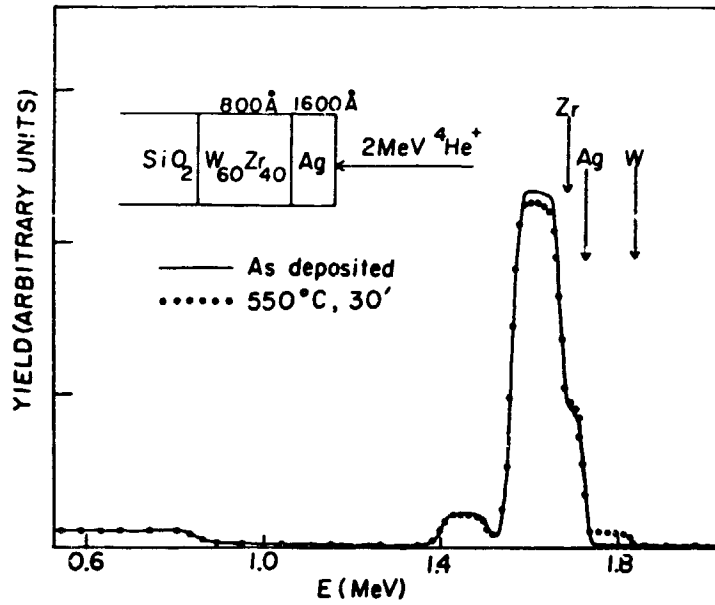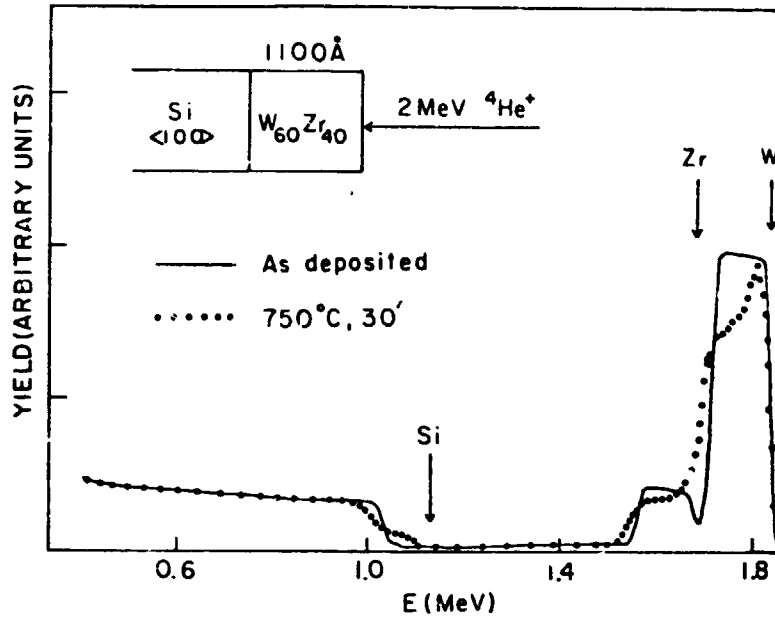
Interaction With Au, Ag, Al and Ni Overlayers: Reactions Below T_C

METAL	Au	Ag	Al	Ni
FILM THICKNESS (Å)	∿ 500	∿ 1600	1200	1300
REACTION TEMPERATURE (°C)	∿ 400	∿ 550	∿ 550	∿ 550
COMPOUND PHASES AT 550°C	AuW $AuZr_2$ $AuZr_3$	AgZr	Al_3Zr $Al_{12}W$	NiZr

- REACTION LATERALLY UNIFORM FOR Ni ONLY.

- PENETRATION OF W INTO Ag GRAIN BOUNDARIES
  SEE FIG. 2.

Schematic of $W_{60}Zr_{40}$-Ag Reaction
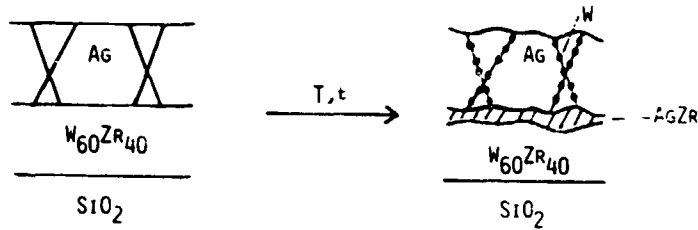
FIG. 3

CONCLUSIONS

AMORPHOUS W-ZR FILMS NOT OPTIMIZED FOR
        STABILITY WITH METAL OVERLAYER.
    - CONCEPTUAL REMEDY: AMORPHOUS BILAYER
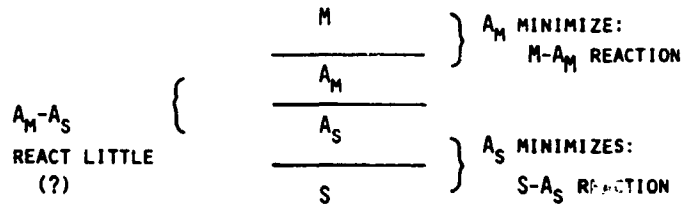
CONCENTRAT' ON MINIMIZING M-A_M REACTIONS.

Results on Amorphous W-N Films

- NI-N-W SUPERIOR TO NI-W WITH AL.
- INVESTIGATE W-N VERSUS W

    W-N VERSUS ZRN

    W-ZR-N.

EXPERIMENTAL PROCEDURES:

- ON <100> N-TYPE SI AND SiO_2 SUBSTRATES.
- R.F. SPUTTERING, 10 MTORR (AR + N_2), N_2
  CONCENTRATION: 0, 5, 10, 20, 40, 80%, 400 W,
  3"φ; (1 · 10^{-6} TORR VACUUM).
- R.F. SPUTTERED AL FILMS IN THE SAME VACUUM.
- ANNEALING IN VACUUM $\leq$ 7 · 10^{-7} TORR,
  30 MIN.
- RBS AND X-RAY DIFFRACTION.

Crystallization

$\%N_2$	CRYSTALLINE CHARACTER	CRYSTALLIZATION TEMPERATURE
0	POLY	-
5	POLY	-
10	AMORPHOUS	$\gtrsim$ 500°C
20	AMORPHOUS	$\gtrsim$ 550°C
40	POLY	-
80	POLY	-

BARRIER BETWEEN SI AND AL FILM.

- AMORPHOUS W-N (20% N_2) MORE STABLE THAN W,
  SEE FIG. 3(A) AND (B).

- AT 550°C, 30 MIN
  SLIGHT W DIFFUSION INTO SI
  UNCHANGED W-N/AL INTERFACE.
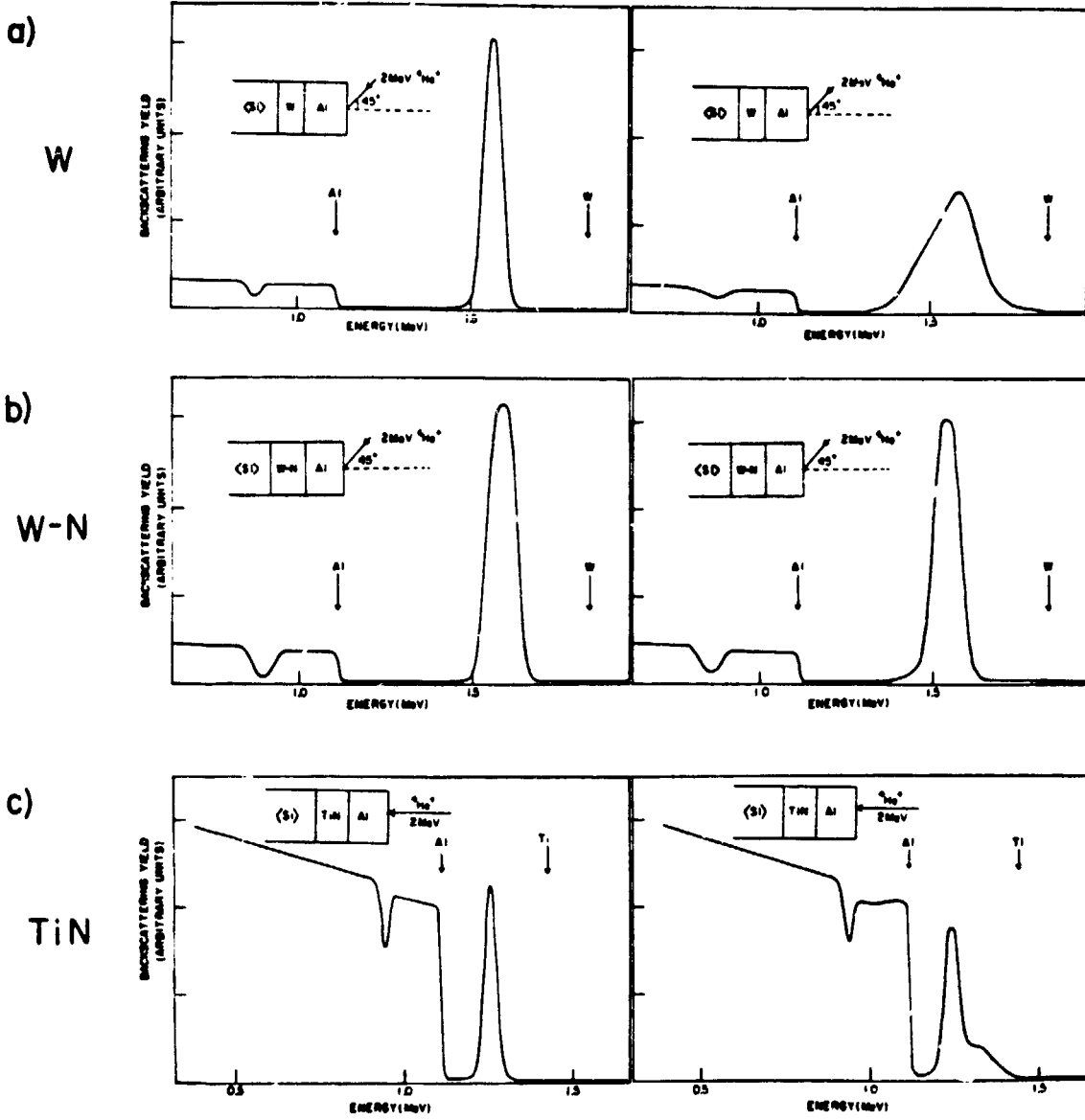
Comparison With TiN

- TiN AND ZrN STABLE BETWEEN Si AND Al BELOW
  ∿ 550°C.
- TiN AND Zr-N FAILURE MAY BE:
  1) REACTION TO FORM COMPOUNDS
     LIKE $TiAl_3$ (Fig. 3(c)) OR $ZrAl_3$.
  2) LOCAL STRESS-INDUCED CRACKING.

CONCLUSION

- W-N MUCH BETTER THAN Zr-W AGAINST Al.

- W-N AT LEAST AS GOOD AS Ni-N-W AGAINST Al.

Outlook

QUESTIONS: WHY DOES N IN Ni-N-W
INHIBIT LOCAL Ni-Si REACTION?

WHY DOES N IN W-N INHIBIT
W-Al REACTION?

STUDY W-N AND W-N/Al
    Zr-N
    Zr-W/W-N BILAYER

387

MOD SILVER METALLIZATION FOR PHOTOVOLTAICS

PURDUE UNIVERSITY

G.M. Vest and R.W. Vest

Approach

1. Identify and characterize suitable metallo-organic (MO) compounds.

2. Develop generic synthesis procedures for the MO compounds.

3. Develop generic fabrication procedures for screen printing inks.

4. Optimize processing parameters for top surface cell metallization.

5. Model the interrelationships between ink chemistry and processing, and film properties and cell performance.

Ag Neodecanoate Synthesis and Characterization

Reaction:

$$R_2 - \overset{\overset{\displaystyle R_1}{|}}{\underset{\underset{\displaystyle R_3}{|}}{C}} - COOH + NH_4OH \xrightarrow[25^{\circ}C]{H_2O} R_2 - \overset{\overset{\displaystyle R_1}{|}}{\underset{\underset{\displaystyle R_3}{|}}{C}} - COONH_4 + H_2O$$

$$R_2 - \overset{\overset{\displaystyle R_1}{|}}{\underset{\underset{\displaystyle R_3}{|}}{C}} - COONH_4 + AgNO_3 \xrightarrow[25^{\circ}C]{H_2O} R_2 - \overset{\overset{\displaystyle R_1}{|}}{\underset{\underset{\displaystyle R_3}{|}}{C}} - COOAg + NH_4OH$$
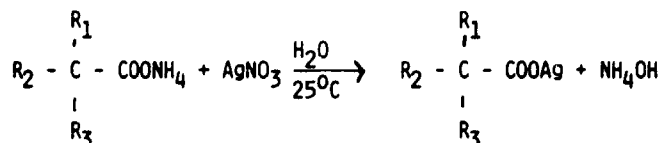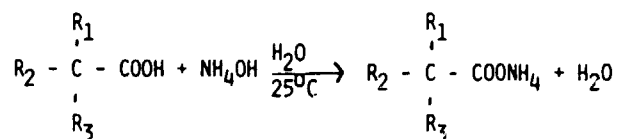
$R_1 + R_2 + R_3 = C_8H_{19}$

w/o Silver: 38.7

Form: white solid

Solubility: aromatic solvents

Thermogram of Ag Neodecanoate in Benzene
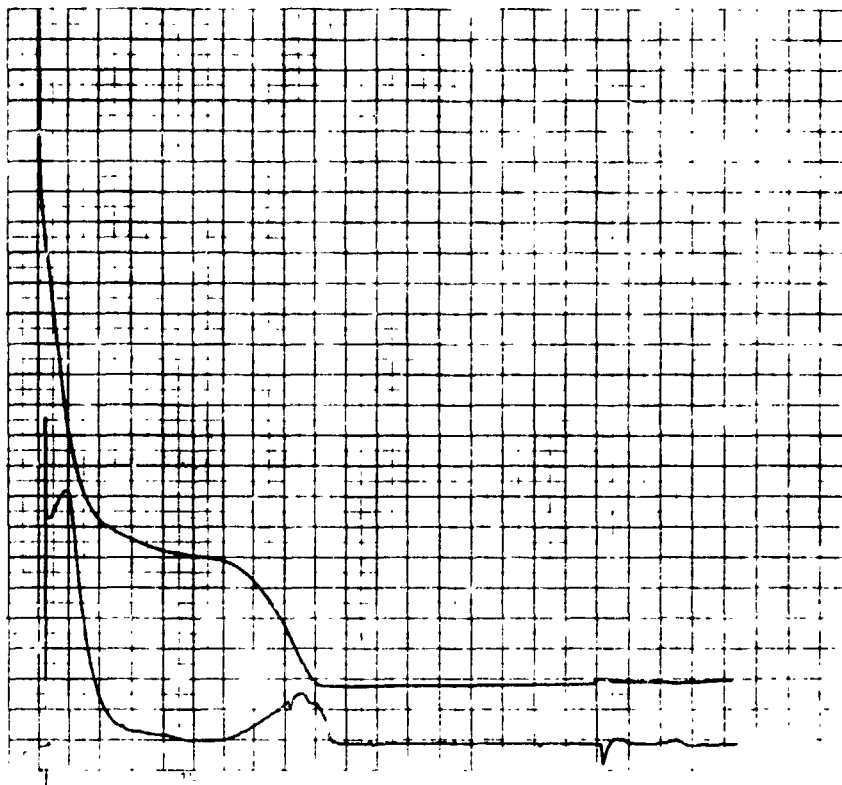
Platinum (II) 2-ethylhexanoate
Synthesis and Characterization

Reaction:

$$C_7H_{15}COOH + (C_2H_5)_3N \xrightarrow[R.T.]{H_2O} C_7H_{15}COO^-(C_2H_5)_3NH^+$$

$$K_2PtCl_4 + 2C_7H_{15}COO^-(C_2H_5)_3NH^+ \xrightarrow[50^0]{H_2O} Pt(C_7H_{15}COO)_2 + 2KCl + 2(C_2H_5)_3NHCl$$
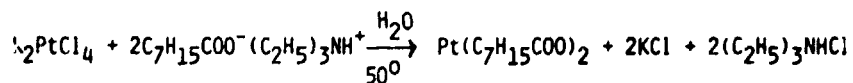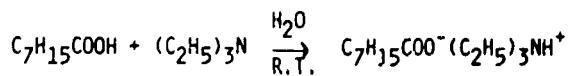
w/o Platinum: 41
Form: block oil
Solubility: aromatic solvents

Thermogram of Pt 2-ethylhexanoate in Benzene
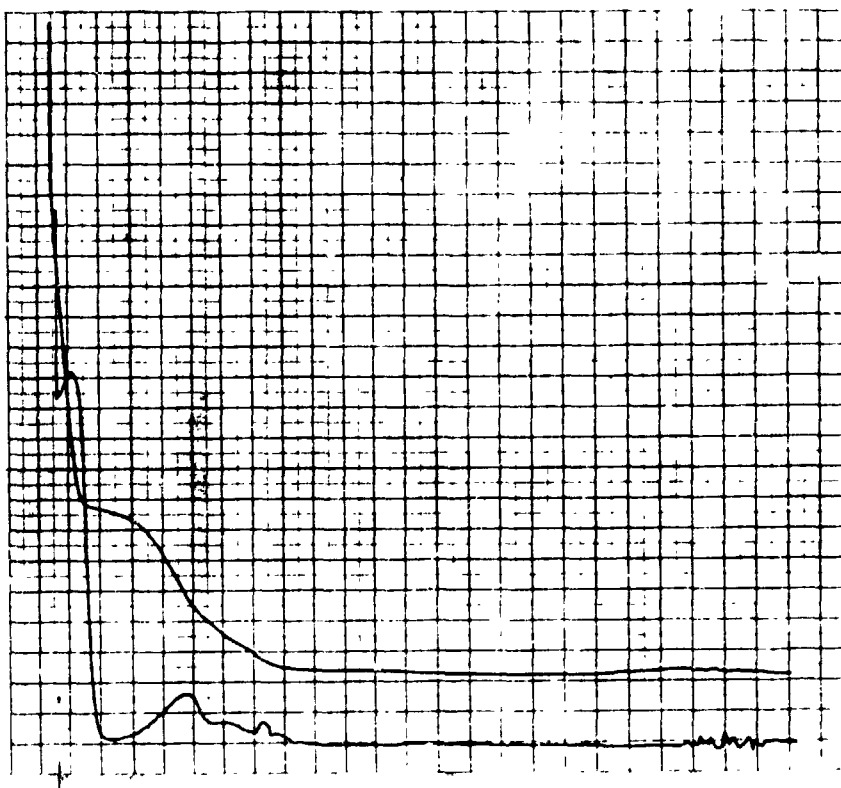
Thermogram of Ag Neodecanoate Plus 2-ethylhexanoate in Benzene
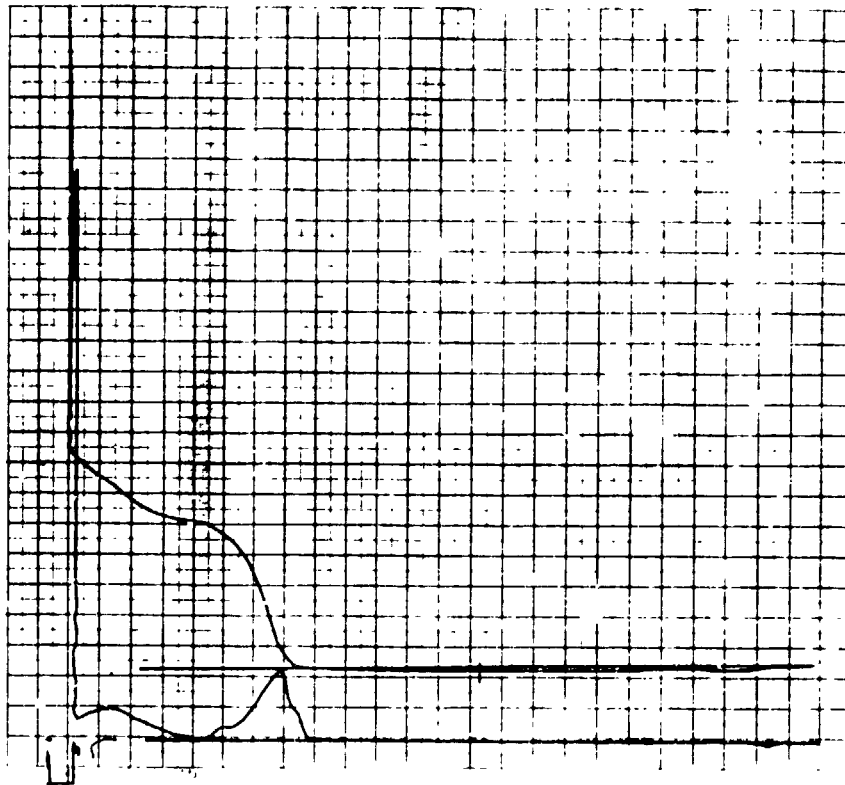
Screen-Printing Ink Fabrication
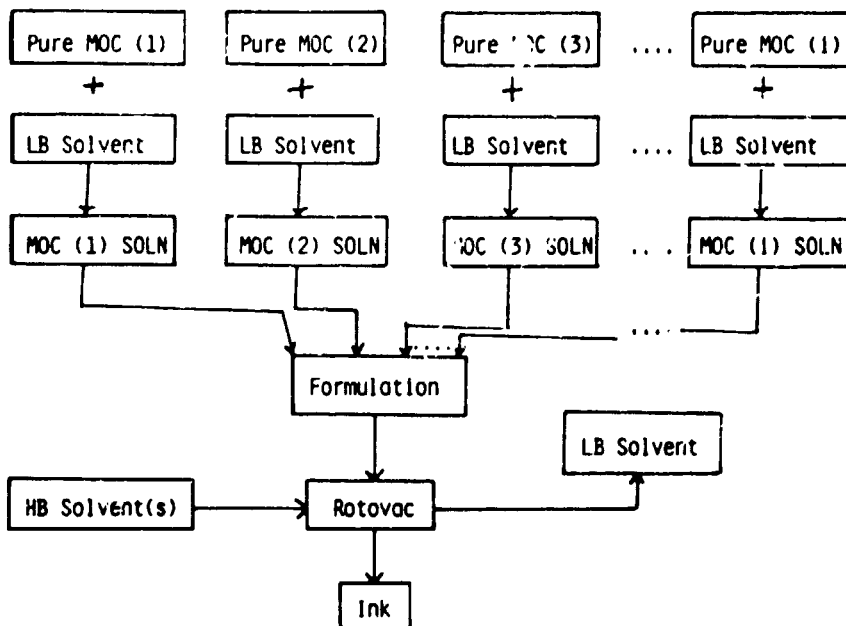
Critical Steps in Ink Fabrication

Metallo-organic compounds
1. Selection
2. Purity

Low Boiling Solvent
1. Selection
2. Purity

High Boiling Solvent(s)
1. Selection
2. Purity
3. Amount

Rotovac
1. Time
2. Temperature
3. Pressure

Low Boiling Solvents Evaluated

	B.P. ($^{\circ}$C)	Comments
xylene	137	incomplete solvent exchange dark films
toluene	111	incomplete solvent exchange dark films
benzene	80	near complete solvent exchange silver films
tetrahydrofuran	66	near complete solvent exchange silver films

High-Boiling Solvents Evaluated

	B.P. ($^\circ$C)
α- terpineol	217-218
butyl carbitol acetate	236-249
phenyl ether	259
dodecane	215-217
neodecanoic acid	250-257
triglyme	216
decalin	˙ϑϑ-195

Ink SPC1-YZ

1. Dissolve x grams of Ag neodecanoate in benzene to give approximately 11 w/o Ag in solution.

2. Add Pt 2-ethylhexanoate in benzene to give fired composition 96 w/o Ag - 4 w/o Pt.

3. Add 0.13x grams of butyl carbitol acetate and 0.26x grams of neodecanoic acid.

4. Mix in the rotovac for 15 minutes at room temperature and pressure.

5. Solvent exchange in the rotovac for 1 hour at 40°C under water pump vacuum.

6. The smooth, black ink screen prints well and produces 24.5 w/o Ag + Pt when fired to 285°C or higher.

Thermogram of Ag-Pt Ink SPC1-1A

TEMPERATURE °C (CHROMEL ALUMEL)
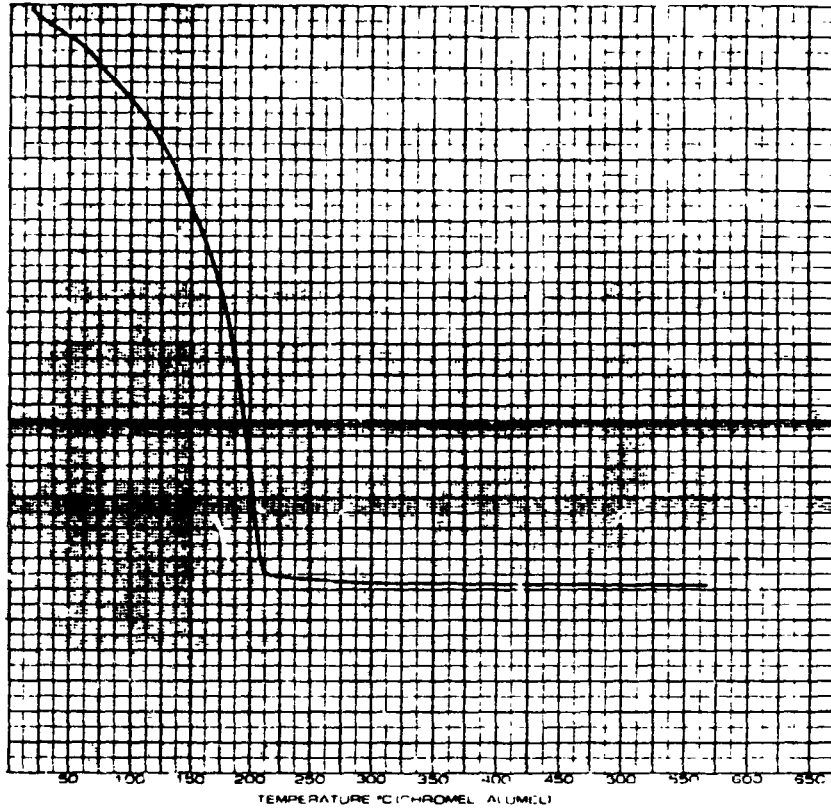
Standard Firing Sequence No. 1 Profile
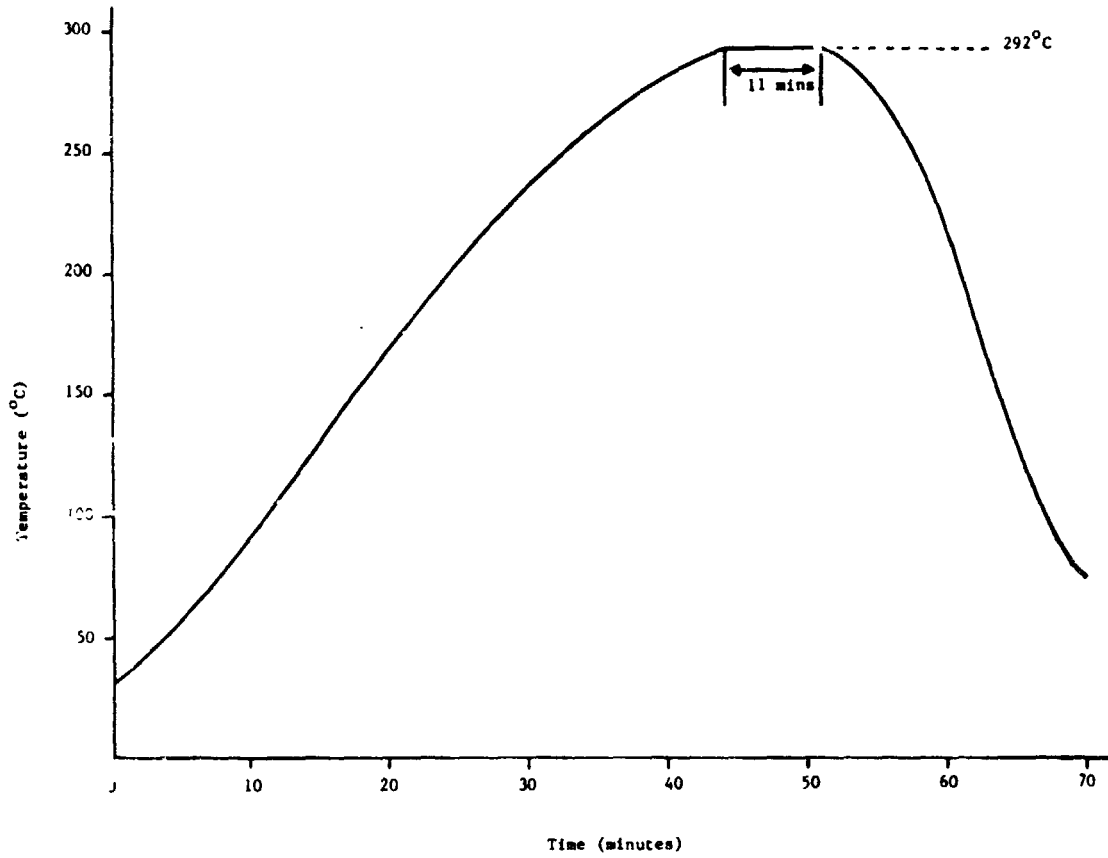
Film Characteristics Evaluated

1. Appearance

2. Sheet Resistance (Density)

3. Line Definition

4. Adehsion

Rating System for Reporting Line Definition of Fired Films Using the JPL Pattern

A. Excellent   B. Acceptable   C. Unacceptable

ORIGINAL PAGL iS
OF POOR QUALITY

Firing Study Results for Ink SPC1-YZ

Test#	Ink#	Firing Sequence Temp (°C)	Firing Sequence Time (min)	Type of Furnace	Substrate*	Surface Appearance	Line Defin.	Sheet Resist. (mΩ/sq)	Adhesion
1	SPC1-1A Age-3.5 hr R.H.=42%	65 200 325	30 30 20	1	Al_2O_3[d]	whitish silver	B	56	excellent (poor on connecting bar)
2	SPC1-1C Age-19 days R.H.=54%	65 200 325	30 30 30	1	cells[d],[i] (batch 172-2)	whitish silver	B(A for narrow lines)	40	poor to fair
3	SPC1-1A Age-3.5 hr R.H.=42%	65 200 325	30 30 20	1	cells[a],[d] (batch 172-2)	whitish silver	A	45	zero
4	SPC1-1A[b] Age-3.5 hr R.H.=42%	65 200 325	30 30 20	1	Al_2O_3[d]	whitish silver	B	26	poor
5	SPC1-1B Age-16 day R.H.=52%	65 200 325	30[c] 30 30	1	Al_2O_3[d]	whitish silver	A	62	zero
6	SPC1-1D Age-25 day R.H.=54%	65 200 325	30 30 30	1	Al_2O_3	whitish silver	B	80	good on narrow lines, poor on connecting bar
7	SPC1-1D Age-25 day R.H.=54%	Std. Firing Sequence #1[e]		4	Al_2O_3	whitish silver	B(A for connecting bar)	72	excellent
8	SPC1-1E Age-27 day R.H.=unknown	Std. Firing Sequence #1		4	cells[i] (batch 341-177)	whitish silver	A	58	good to excellent on narrow lines, fair to poor on wide connecting bar
9	SPC1-2A Age-2 hr R.H.=50%	65 200 325	30 30 30	1	cells[i] (batch 341-177)	whitish silver	B	87	poor (zero)
10	SPC1-2A Age-2 hr R.H.=50%	Std. Firing Sequence #1		4	cells[i] (batch 341-177)	whitish silver	B	54	excellent
11	SPC1-2A Age-2 hr R.H.=50%	2nd layer printed and the firing sequence of Test 10 repeated		4	cells[i] (batch 341-177)	whitish silver	B	23	poor to fair

Test#	Ink#	Firing Sequence Temp (°C) Time (min)	Type of Furnace	Substrate*	Surface Appearance	Line Defin.	Sheet Resist. (mΩ/sq)	Adhesion
12[f]	SPC1-2B Age-8 day R.H.=48%	Std. firing sequence #1		cells[1] (batch 341-177)	whitish silver	C	47	excellent
13	SPC1-2B Age-8day R.H.=48%	Std. Firing Sequence #1		cells[1] (batch 341-177)	whitish silver	B	56	excellent
14	SPC1-2A Age-8 day R.H.=48%	Second layer printed and the firing sequence of test #2 was repeated		cells[1] (batch 341-177)	whitish silver	B	24	excellent
15	SPC1-2B Age-8 day R.H.=48%	Same as test #3 except batch drying step (30 mins at 65°C) is skipped after 2nd layer is printed		cells[1] (batch 341-177)	whitish silver	B	24	excellent
16	SPC1-2C Age-15 day R.H.=54%	Std. Firing Sequence #1		cells[d],[1] (batch 341-177)	whitish silver	B	51	excellent
17	SPC1-2C Age-15 day R.H.=54%	Std. Firing Sequence #1		cells[1] (batch 341-177)	whitish silver	B	53	excellent
18	SPC1-2C Age-15 day R.H.=54%	Second layer printed and the firing sequence of test #6 was repeated		cells[1] (batch 341-177)	whitish silver	B	26	excellent
19	SPC1-2C Age-15 day R.H.=54%	Third layer printed and fired. Unfortunately, firing was insufficient due to mechanical failure).		cells[1] (batch 341-177)	whitish silver	C[g]	16	fair to poor
20	SPC1-2E Age-28 days R.H.=54%	2 layers printed with only a drying step between layers of 30 mins at 70°C. Once 2nd layer was printed the Std. Firing Sequence #1 was used.		cells[1] (batch 341-177)	whitish silver	B	29	excellent
21	SPC1-2E Age-28 days R.H.=54%	Std. Firing Sequence #1		cells[1] (batch 341-177)	whitish silver	B	76	excellent
22	SPC1-2D Age-28 day R.H.=54%	Std. Firing Sequence #1		cells[1] (batch 346-193)	whitish silver	B	72	excellent (initially)
23	SPC1-2F Age-53 day R.H.=60%	Std. Firing Sequence #1		cells[1] (batch 346-193)	whitish silver	B	77.8	excellent

Test#	Ink#	Firing Sequence Temp (°C) Time (min)	Type of Furnace	Substrate*	Surface Appearance	Line Defin.	Sheet Resist. (mΩ/sq)	Adhesion
24	SPC1-2F Age-53 day R.H.=60%	Std. Firing Sequence #1		cells[(1)] (batch 346-193)	whitish silver	B	61.4	excellent
25	SPC1-2F Age-53 day R.H.=60%	Std. Firing Sequence #1		cells[(a)] (batch 346-193)	whitish silver	B[(k)]	60.3	excellent
26	SPC1-3A Age-6 hr R.H.=58%	Std. Firing Sequence #1		cells[(1)] (batch 346-193)	whitish silver	A/B[(1)]	62.0	excellent or narrow line; poor on connecting bar
27	SPC1-3A Age-6 hr R.H.=58%	Std. Firing Sequence #1		cells[(a)] (batch 346-193)	whitish silver	A	57.7	excellent
28	SPC1-3A Age-8 hr R.H.=58%	Second layer printed and Std. Firing Sequence #1 repeated		cells[(1)] (batch 346-193)	whitish silver	A/B	22.9	poor
29	SPC1-3A Age-8 hr R.H.=58%	Second layer printed and Std. Firing Sequence #1 repeated		cells[(a)] (batch 346-193)	whitish silver	A/B	23.5	poor
30	SPC1-3A Age-10 hr R.H.=58%	Third layer printed and Std. Firing Sequence #1 repeated		cells[(1)] (batch 346-193)	whitish silver	B	20.0	poor
31	SPC1-3A Age-10 hr R.H.=58%	Third layer printed and Std. Firing Sequence #1 repeated		cells[(a)] (batch 346-193)	whitish silver	A/B	14.9	poor

*Al_2O_3 = AlSiMag 838 substrates

cells = solar cells supplied by JPL.

(a) cells cleaned in hydrofluoric acid prior to printing by HF cleaning procedure.
(b) 2 layers printed. Sequence = print-dry-fire-print-dry-fire.
(c) the length of time at 65°C was varied from 30 minutes to 120 minutes in increments of 30 minutes but no effect on fired film properties was observed.
(d) cells or other substrates printed as-received. No pre-drying step of at least 30 mins. at 65°C was perform.
(e) Standard Firing Sequence #1 as detailed in section 3.2 is as follows:

Temp.	Time	
65	30 --	batch dry
R.T.-263	6.7°/min	
263-292	4.6°/min	
292	11.3 min	belt fire
292-245	7°/min	
245-62	18.3°/min	
62-R.T.	1.1°/min	

(f) two layers printed with no heat treatment between printings.
(g) poor line definition was due to mechanical problems with screen printer which have subsequently been correc
(h) see Table 4.4 for detailed results of Test NO. 22.
(i) cells not cleaned prior to printing.
(j) cells cleaned by methanol cleaning procedure.
(k) lines sharper but more thready than above two.
(l) A/B rating means some cells showed A rating and others B rating.

Adhesion vs Time Study With Single-Layer
Fired Films of Ink SPC1

Time since printing & firing (days)	Relative humidity at time of test (%)	Adhesion (estimated % of total surface area)	Comments
0	54	100,100	
1	52	100	
2	53.5	100	
4	59.5	68,80	For two samples adhesion loss occurred on connecting bar only.
10	60.5	56,65	Nearly complete loss of adhesion on connecting bar. Adhesion beginning to degrade slightly on narrow lines.
10	60.5	2	Test done on one of the samples from day zero which had shown 100% adhesion after first test.
15	57.5	30,65	Adhesion losses occurring both on connecting bar and narrow lines.
21	55	30,40	Complete adhesion loss on connecting bar and significant loss on narrow lines.
26	53.5	35,45	Same as for day 21 except less loss on narrow lines.
42	55.5	10,30	Considerable adhesion losses. Only small sections of some narrow lines are adhering.

Brief Adhesion/Time Study with Single Layer Fired Films of Ink SP1[a]
on Substrates Which Have Undergone 3 Types of Surface Preparation Prior
to Printing.

Time since printing & firing (days)	Cleaning Method	Relative Humidity at time of test (%)	Adhesion (estimated % of total sur-face area)	Comments
0	None[b]	60%	100	
0	HF[c]	60%	100	
0	MeOH[d]	60%	100	
1	None	56%	100	
1	HF	56%	100	
1	MeOH	56%	100	
3	None	53.5%	100	
3	HF	53.5%	100	
3	MeOH	53.5%	100	
5	None	54.5%	100	
5	HF	54.5%	100	
5	MeOH	54.5%	60	90% of connecting bar lifted. Still excellent adhesion of narrow lines
6½	None	58%	100	
6½	HF	58%	70	Adhesion losses occurred about equally to connecting bar and narrow lines.
6½	MeOH	58%	100	Adhesion restored on this MeOH sample. No apparent visual difference between this and day 5 sample above.
18	None	55.5%	1	shortage of samples caused the delay between these last two sets of tests. Almost total loss of adhesion occurred between day 6½ and day 18
18	HF	55.5%	2	
18	MeOH	55.5%	1	

Summary

1. Bright Ag or Ag/Pt films with near theoretical density can be formed on Si below 300°C provided:

   a. the proper MO compounds are selected (Ag neodecanoate and Pt 2-ethylhexanoate work);

   b. the proper low boiling solvent is used in the formulation (benzene or tetrahydrofuran work);

   c. the proper high boiling solvent is used in the ink (a mixture of butyl carbitol acetate and neodecanoic acid works);

   d. the MO compounds are suitably purified;

   e. a low temperature drying step is used (30 minutes at 65°C works; and

   f. a proper firing profile is used (a 70 minute cycle with 11 minutes at 292°C works).

2. Excellent adhesion can be achieved with the proper ink chemistry and processing conditions, but the adhesion begins to degrade after several days.

3. A binding agent will be required to achieve reproducible, long term adhesion.

LASER-ASSISTED SOLAR-CELL METALLIZATION PROCESSING

WESTINGHOUSE ELECTRIC CORP.

Subhadra Dutta

Milestone Chart

Tasks/Milestones	1983				1984								
	S	O	N	D	J	F	M	A	M	J	J	A	S
1. Conduct Literature Search On Current State-Of-The Art Laser Metallization Schemes													
2. Assemble And Test Each Of The Following Systems:													
2.1 Photolytic metal deposition using a focused CW UV laser													
2.2 Photolytic metal deposition using a mask and UV flood illumination													
2.3 Pyrolytic metal deposition using a focused CW laser													
3. Fabricate Fifty Solar Cells													
4. Characterize The Cells And Determine The Effects Of Transient Heat On Solar Cell Junctions And On Bulk Lifetime													
5. Compare Economics Of Laser Assisted Processing With Competing Technologies Preliminary Report Final Report													
6. Support Meetings			As Directed By JPL										
7. Provide Documentation													

PROCESS DEVELOPMENT

```
┌─────────────────────────────────────┐
│ Photolithographic Pattern Definition │
└─────────────────────────────────────┘
              ┌──────────────────┐
              │  Film Deposition │
              └──────────────────┘
              ┌──────────────────┐
              │ Lift-Off Or Etching │
              └──────────────────┘
```
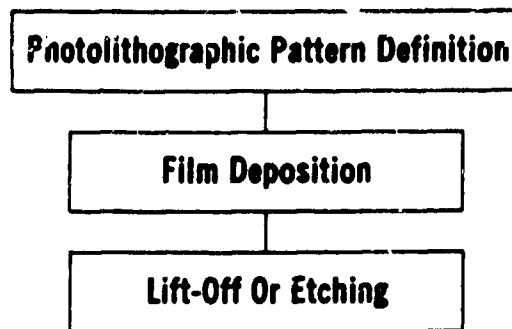
Laser-Assisted Metallization Techniques Are Essentially
One-Step Processes:

```
┌──────────────────────────┐
│  Laser-Surface Interaction │
│        Resulting In         │
│    Localized Film Growth    │
└──────────────────────────┘
```

Potential Advantages of Laser Deposition
Techniques for Photovoltaic Systems

- **High Resolution**

- **No Photolithography**

- **Clean And Contamination - Free**

- **In-Situ Sintering**

- **Low Contact Resistance**

Laser-Assisted Deposition Techniques

Pyrolytic Deposition (Thermal)

- Laser Chemical Vapor Deposition (LCVD)
- Laser Deposition From Solutions

Photolytic Deposition (Non-Thermal)

- Laser Photodissociation Of Vapors
- Laser Photodissociation Of Solutions

Laser Assisted Electroplating

Photolytic Deposition

Laser-Induced Photodecomposition of Gas-Phase Organometallic Compounds:

This Technique is Fundamentally Different from Thermally Based Laser Processes

Gas-Phase
Organometallic
Molecules

Photons

Non-Thermal
Severing of
Bonds

Substrate

Liberated
Metal
Atoms

Photons

Substrate

Metal Condenses
on Illuminated
Regions of Substrate
Forming Patterned Film

Photons

Metal
Film

Substrate
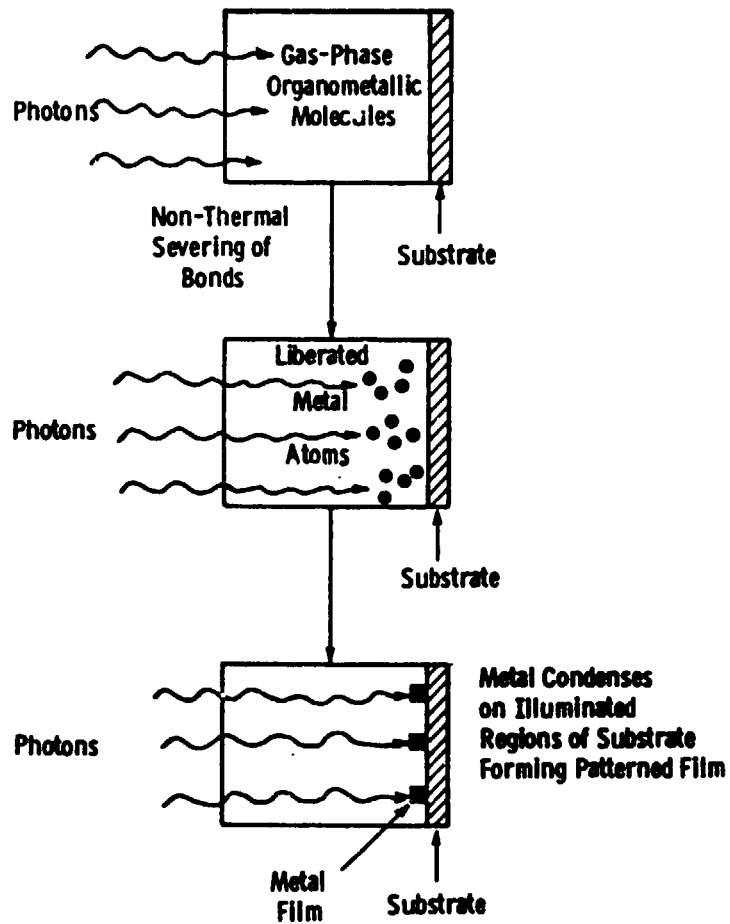
Experimental Setup for Laser-Assisted Electroplating
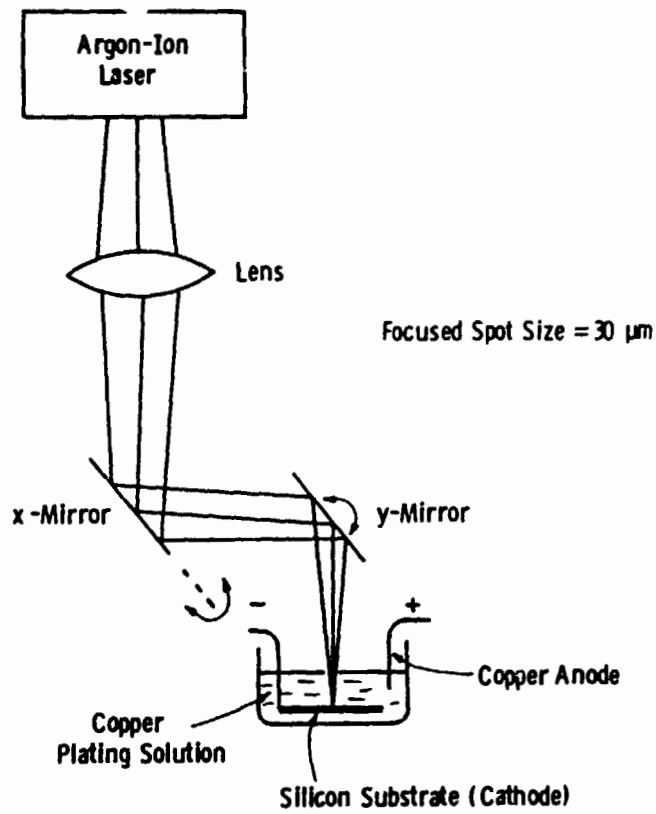
S. Dutta
l. t. -m. z. 3-9-84

Dwg. 9358A48

Laser Power Dependence of Electroplated Spot Size

Plating Current = 1 mA
Dwell Time = 5 sec
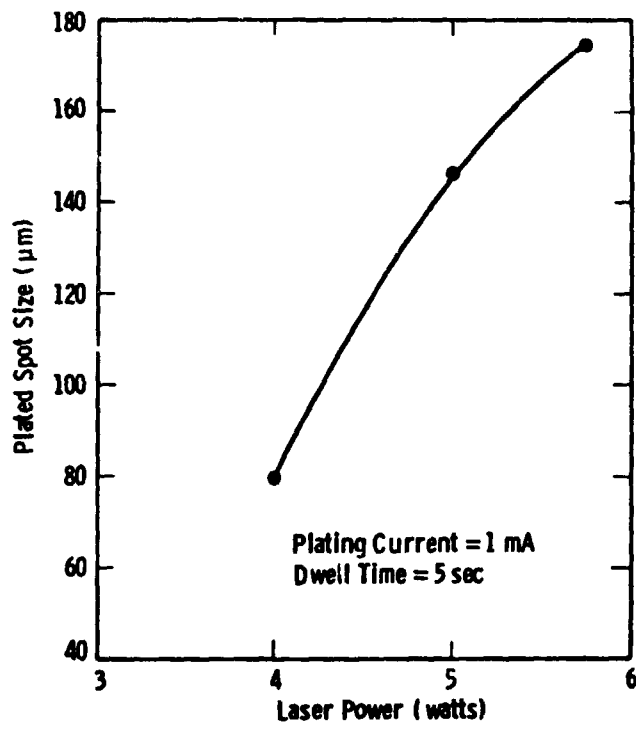
Nomarski Micrograph (200X) of Copper Line
Deposited by Laser-Assisted Electroplating Results

25 μm

Linewidth = 25 μm   Line Thickness = 6000 Å
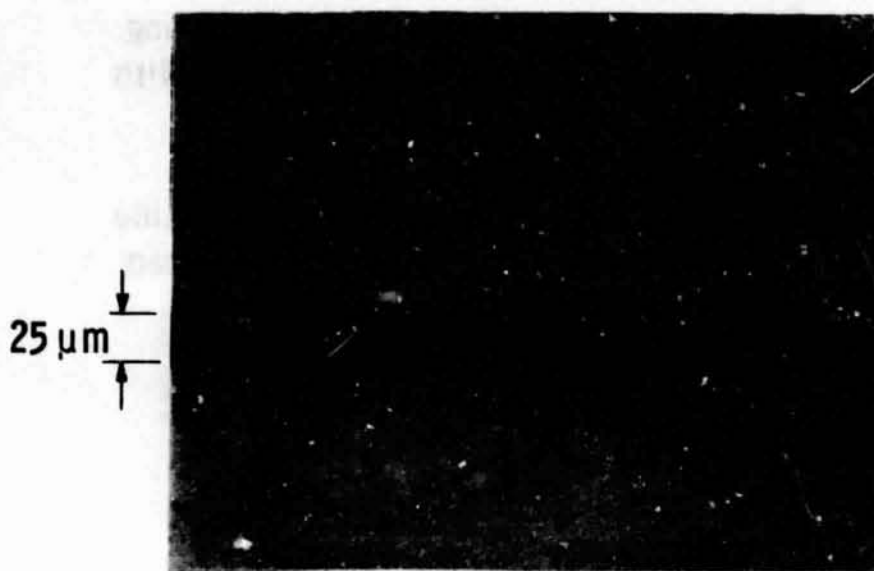
Laser Power = 4 W   Plating Current = 2 mA

Laser Dwell Time = 50 μsec

Summary of Laser-Assisted
Electroplating Results

- **Novel Technique For Greatly Enhancing Local Plating Rates – Yield Fine-Line, Directly-Written Patterns With Excellent Adhesion**

- **Multiple Rapid Laser Scans Yield Finer, More Even Line And Higher Local Plating Rate Than Single Slow Scan (Same Total Exposure Time)**

- **Plated Linewidth Depends On Laser Power, Plating Current, And Electrolyte Level**

Laser Pyrolysis of Spun-on Metallo-Organic Film

Scanning Mirrors

Ar^+ Laser Beam

Lens

Deposited Silver

Spun-On Silver Neodecanoate Film

Silicon Substrate
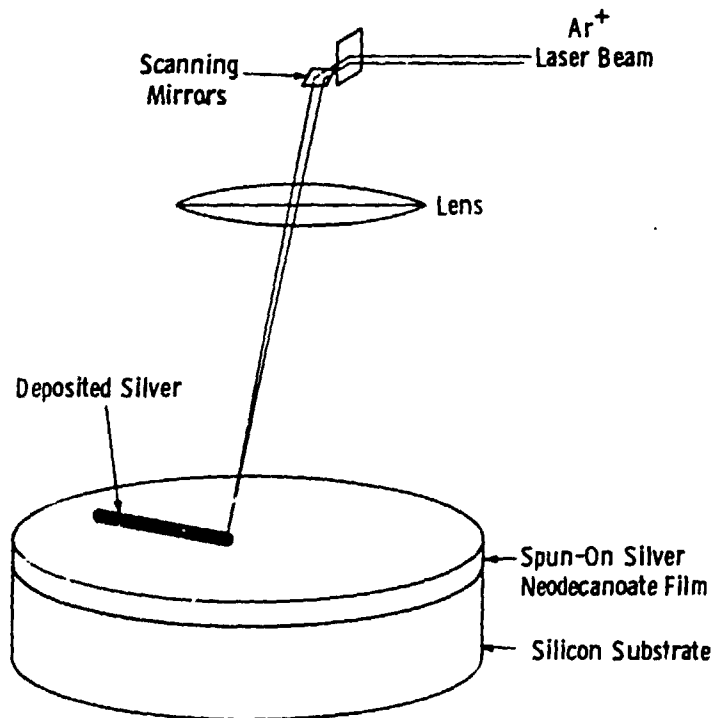
Sample Base Temperature 75°C

Focussed Laser Spot Decomposes Spun-On Film

Silver Metallization Patterns are Formed by Direct-Writing

Line Width vs Laser Power and Substrate Temperature
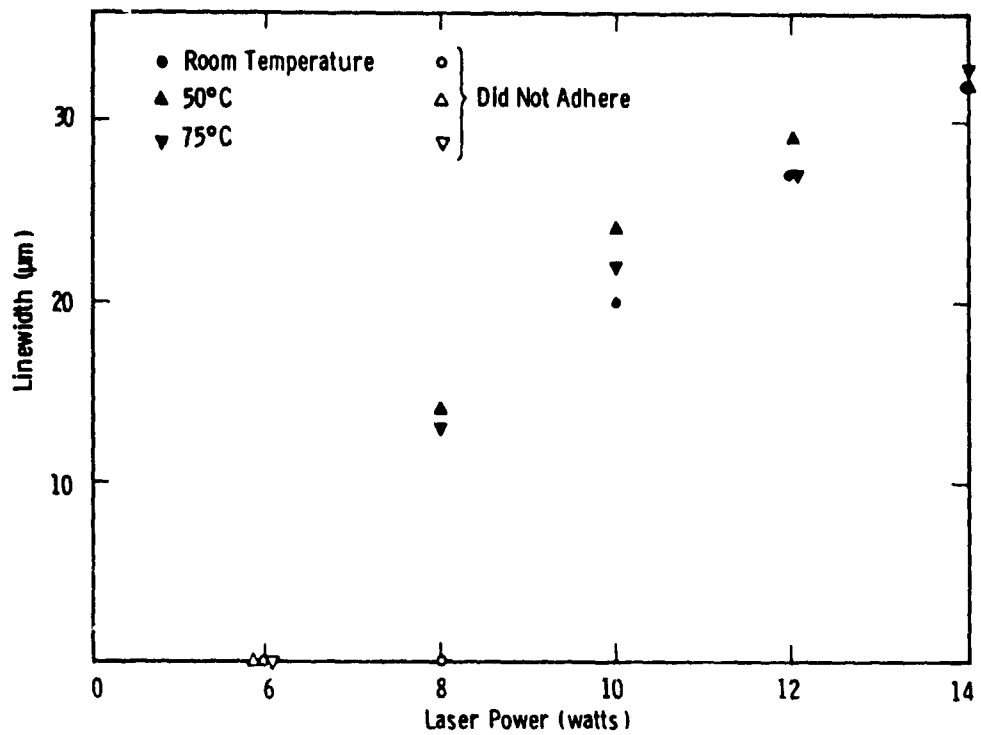
Nomarski Micrographs (200X) of Silver Lines Decomposed
at (a) 4 W, (b) 8 W, (c) 14 W Before & After Tape Test
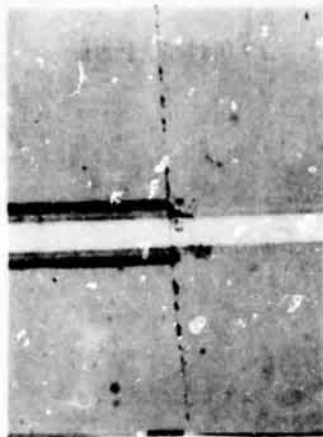
(a) Scotch Tape Tested
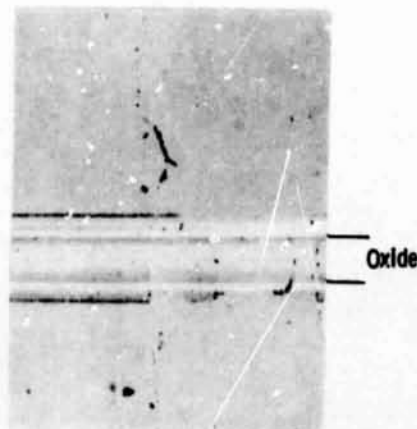
(b) Scotch Tape Tested

Oxide

(c) Scotch Tape Tested

Deposited Line Widths as a Function of Scan Speed and Laser Power
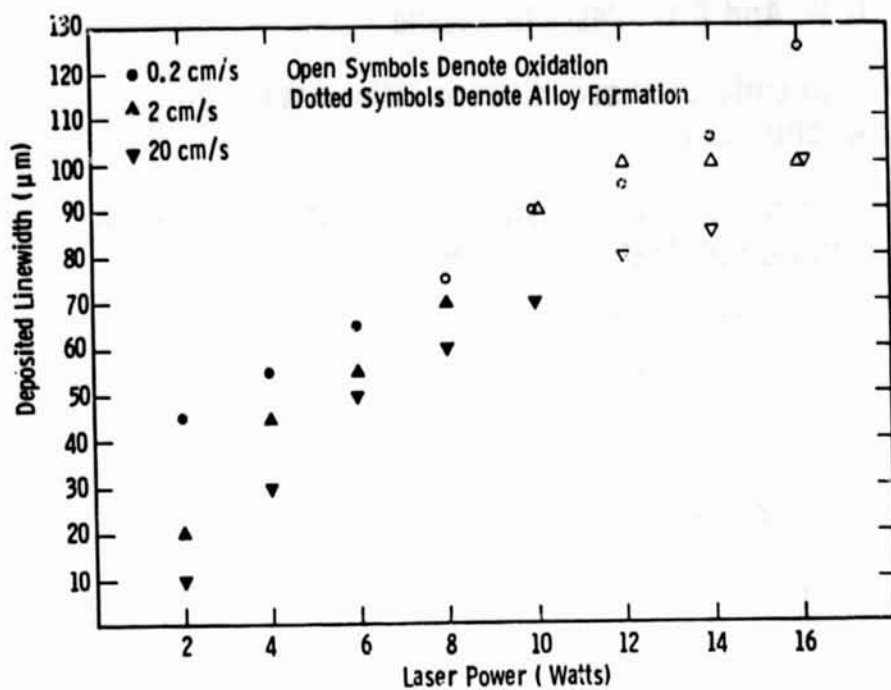
Laser-Written Solar-Cell Metallization Patterns Using Spun-on Silver Neodecanoate
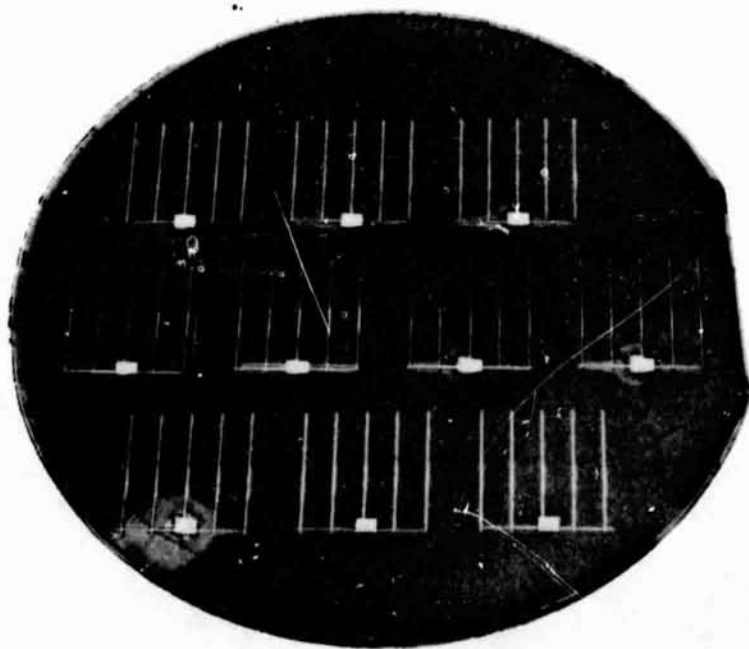
Laser Metallization Process

1. Make Solution Of Silver Neodecanoate (Obtained From G.M. And R.W. Vest) In Xylene

2. Spin Onto Diffused, Coated Silicon Wafers At 1000 rpm

3. Decompose Film Locally With Argon-ion Laser To Form Comb Metallization Patterns
   - Laser Power = 8W
   - Spot Size = 50 μm
   - Scan Speed = 20 cm/s
   - Scan Overlap (Contact Pads) = 60%
   - Deposited Silver Thickness = 400 Å

4. Electroplate Selectvely Onto Patterns
   - Plated Silver Thickness = 8 μm

5. Define Mesas To Isolate Cells And Characterize Cells

Lighted I-V Data for Unsintered Laser-Metallized Cells

Cell I.D.	Short-Circuit Current J_{sc} (mA)	Open-Circuit Voltage V_{OC} (V)	Fill Factor	Efficiency (%)
Laser 1-2	23.1	0.557	0.761	9.8
Laser 1-3	22.8	0.558	0.755	9.6
Laser 1-6	23.7	0.557	0.776	10.3
Laser 1-7	23.7	0.556	0.770	10.1
Laser 1-8	23.7	0.559	0.764	10.1
Laser 1-9	24.2	0.560	0.764	10.3
Laser 1-10	24.2	0.558	0.772	10.4
Laser 1-11	23.8	0.553	0.774	10.2
Laser 1-12	24.2	0.558	0.773	10.4
Laser 1-14	24.6	0.558	0.769	10.5
Laser 1-15	24.5	0.562	0.755	10.4
Laser 5-7	24.3	0.562	0.734	10.0
Laser 5-10	24.7	0.562	0.650	9.0
Laser 5-11	24.7	0.566	0.751	10.5
Laser 5-14	24.6	0.567	0.762	10.6
Laser 5-15	25.1	0.570	0.776	11.1

Lighted I-V Data for Unsintered Baseline Cells

Cell I.D.	Short-Circuit Current J_{sc} (mA)	Open-Circuit Voltage V_{OC} (V)	Fill Factor	Efficiency (%)
RSC 1-2	23.4	0.573	0.772	10.4
RSC 1-3	23.2	0.562	0.681	8.9
RSC 1-5	23.4	0.571	0.762	11.0
RSC 1-6	25.0	0.569	0.746	10.6
RSC 1-7	25.0	0.567	0.718	10.2
RSC 1-8	24.6	0.571	0.734	10.3
RSC 1-9	23.5	0.568	0.751	10.0
RSC 1-10	25.4	0.569	0.768	11.1
RSC 1-11	25.6	0.568	0.734	10.7
RSC 1-12	25.9	0.567	0.710	10.5
RSC 1-14	26.1	0.571	0.716	10.6
RSC 1-15	25.9	0.567	0.608	8.9
RSC 2-2	25.8	0.569	0.764	11.2
RSC 2-3	26.1	0.567	0.746	11.1
RSC 2-5	26.3	0.569	0.719	10.8
RSC 2-6	25.9	0.566	0.759	11.1
RSC 2-7	25.8	0.566	0.753	11.0
RSC 2-8	25.6	0.567	0.735	10.7
RSC 2-9	25.6	0.566	0.722	10.5
RSC 2-10	25.9	0.566	0.749	11.0
RSC 2-14	26.1	0.567	0.702	10.4
RSC 2-15	26.0	0.567	0.636	9.4

Comparison of Laser-Metallized and Baseline Cells Lighted I-V Data

Cell I.D.	Short-Circuit Current J_{sc} (mA/cm^2)	Open-Circuit Voltage V_{OC} (V)	Fill Factor	Non-AR-Coated Cell Efficiency (%)
Laser 1-14	24.6	0.558	0.769	10.5
Baseline 2-9	25.6	0.566	0.722	10.5
Laser 5-11	24.7	0.566	0.751	10.5
Baseline 1-12	25.9	0.567	0.710	10.5
Laser 5-14	24.6	0.567	0.762	10.6
Baseline 1-6	25.0	0.569	0.746	10.6
Laser 5-15	25.1	0.570	0.776	11.1
Baseline 2-3	26.1	0.567	0.746	11.1

Lighted I-V Characteristics of Laser-Metallized Solar Cell
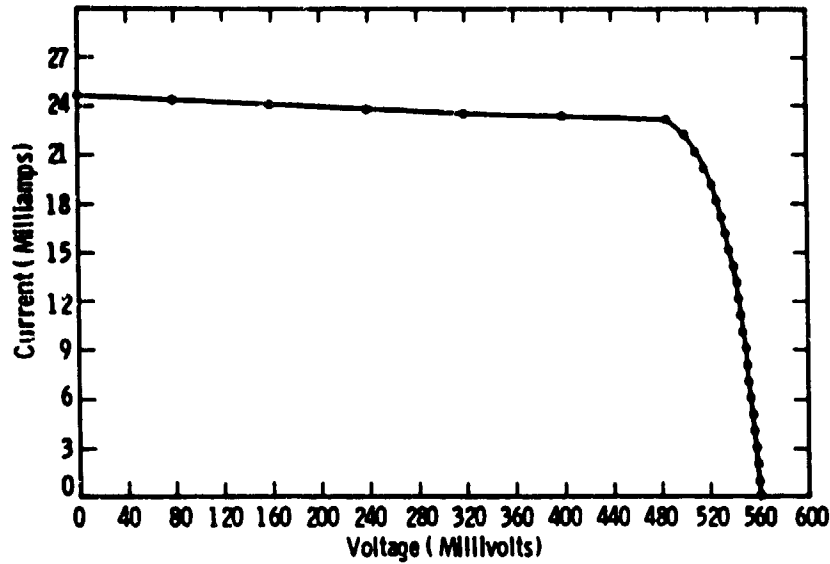
Dark I-V Data for Baseline Cells

Cell I.D.		Normalized Series Resistance (Ω-cm^2)	Normalized Shunt Resistance (KΩ cm^2)	J_{01} (A/cm^2)	J_{02} (A/cm^2)	Efficiency (%)
RSC 1-3	Before Sintering	1.3	0.8	5.1×10^{-12}	2.4×10^{-5}	8.3
	After Sintering	0.9	6.9	4.3×10^{-12}	3.8×10^{-6}	10.1
RSC 1-9	Before Sintering	1.0	4.9	4.2×10^{-12}	8.8×10^{-5}	10.0
	After Sintering	0.8	113.7	4.4×10^{-12}	1.3×10^{-6}	10.9
RSC 1-10	Before Sintering	1.0	$>10^3$	4.5×10^{-12}	1.7×10^{-7}	11.1
	After Sintering	0.8	769.9	4.9×10^{-12}	1.1×10^{-6}	10.9
RSC 1-15	Before Sintering	2.2	2.4	4.0×10^{-12}	4.7×10^{-6}	8.9
	After Sintering	0.8	5.8	4.3×10^{-12}	3.5×10^{-6}	8.9
RSC 2-2	Before Sintering	1.0	$>10^3$	4.2×10^{-12}	8.7×10^{-9}	11.2
	After Sintering	0.7	$>10^3$	4.2×10^{-12}	3.1×10^{-8}	11.3
RSC 2-3	Before Sintering	1.1	0.4	5.0×10^{-12}	3.9×10^{-5}	11.1
	After Sintering	0.8	1.3	4.3×10^{-12}	1.1×10^{-5}	11.1
RSC 2-12	Before Sintering	1.5	$>10^3$	4.3×10^{-12}	1.8×10^{-8}	7.4
	After Sintering	1.0	77.6	3.4×10^{-12}	2.4×10^{-5}	7.0
RSC 2-15	Before Sintering	1.8	$>10^3$	4.1×10^{-12}	9.1×10^{-9}	9.4
	After Sintering	1.3	$>10^3$	3.3×10^{-12}	4.9×10^{-8}	9.3

Conclusions

- **High Quality Solar Cells Obtained By Laser Metallization Technique**
  - **Non-AR-Coated Cell Efficiency = 11.1%**

- **In-Situ Sintering Occurs During Laser Writing Process**
  - **Series Resistance Of Laser-Metallized Cells Lower**

- **Finer Lines Should Yield Higher Efficiencies**
  - **Laser-Written Linewidths = 50 μm**
  - **Baseline Linewidths = 25 μm**
  - **Comparable Efficiencies Despite Greater Cell Shadowing In Laser-Metallized Cells**

A NON-NOBLE FRONT METALLIZATION PROCESS

SPECTROLAB, INC.

Alexander Garcia III

Objectives

- OPTIMIZATION, EVALUATION AND DEMONSTRATION OF A NOVEL METALLIZATION SYSTEM

- Mo/Sn/TiH SYSTEM

- ITO CONDUCTIVE AR SYSTEMS

Approach

- SCREEN PRINTING

- AIR FIRING

- REDUCING ATMOSPHERE

- CONDUCTIVE AR COATING (ITO)

Front Metallization Pattern

Symm About
¢

→||← 0.060

2.040

└─ 0.127
Typ Spacing
of 17 Grid-
lines
.008 wide

Tol non-cum

→|0.240|←

|←———— 2.040 ————→|
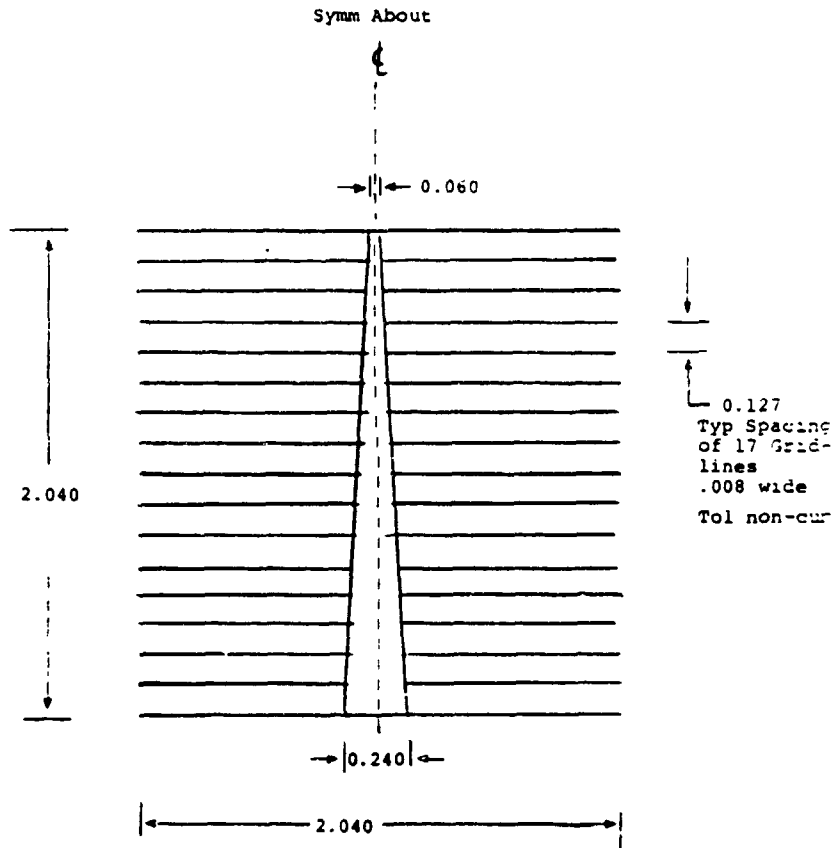
Mo-Sn vs Ag

CELL	V_{OC}	I_{SC}	I_{500}	P_{MAX}	FF	E
1728M-90 (Mo/Sn)	.601	.678	.596	.229	.73	10.5%
1728M-72 (Ag)	.601	.680	.600	.302	.74	10.6%

Standard Ag Cell

SOLAR CONVERTER E I CURVE

SPECTROLAB Q C FORM 3001
SYLMAR, CALIFORNIA   DATE: 4-29-83

PROJECT: METALLIZATION
SERIAL NC 41082-92-2 Stand Ag
☐ CELL ☐ MODULE ☐ PANEL DESIGNATION:

SOURCE: ☐ SUN ☐ TUNGSTEN ☐ XENON
☐ COLLIMATED   ☐ UNCOLLIMATED
TEST TEMP.: _____ °C _____ °F
TEST NO. _____ PROC. NO. _____
Isc = _____ Voc = _____
PMp = _____ SY _____

Typical Mo-Sn Cell

SOLAR CONVERTER E I CURVE

SPECTROLAB Q C FORM 3001

SYLMAR, CALIFORNIA DATE: 4-20-83

PROJECT: METALLIZATION TP F523

SERIAL NO 41082-70

☐ CELL ☐ MODULE ☐ PANEL DESIGNATION:
IR 600 18"   H2 Sint 600 90 Sec

SOURCE: ☐ SUN ☐ TUNGSTEN ☐ XENON
☐ COLLIMATED   ☐ UNCOLLIMATED

TEST TEMP.: _____ °C _____ °F

TEST NO. _____ PROC. NO. _____

Isc = _____ Voc = _____

PMp = _____ BY _____
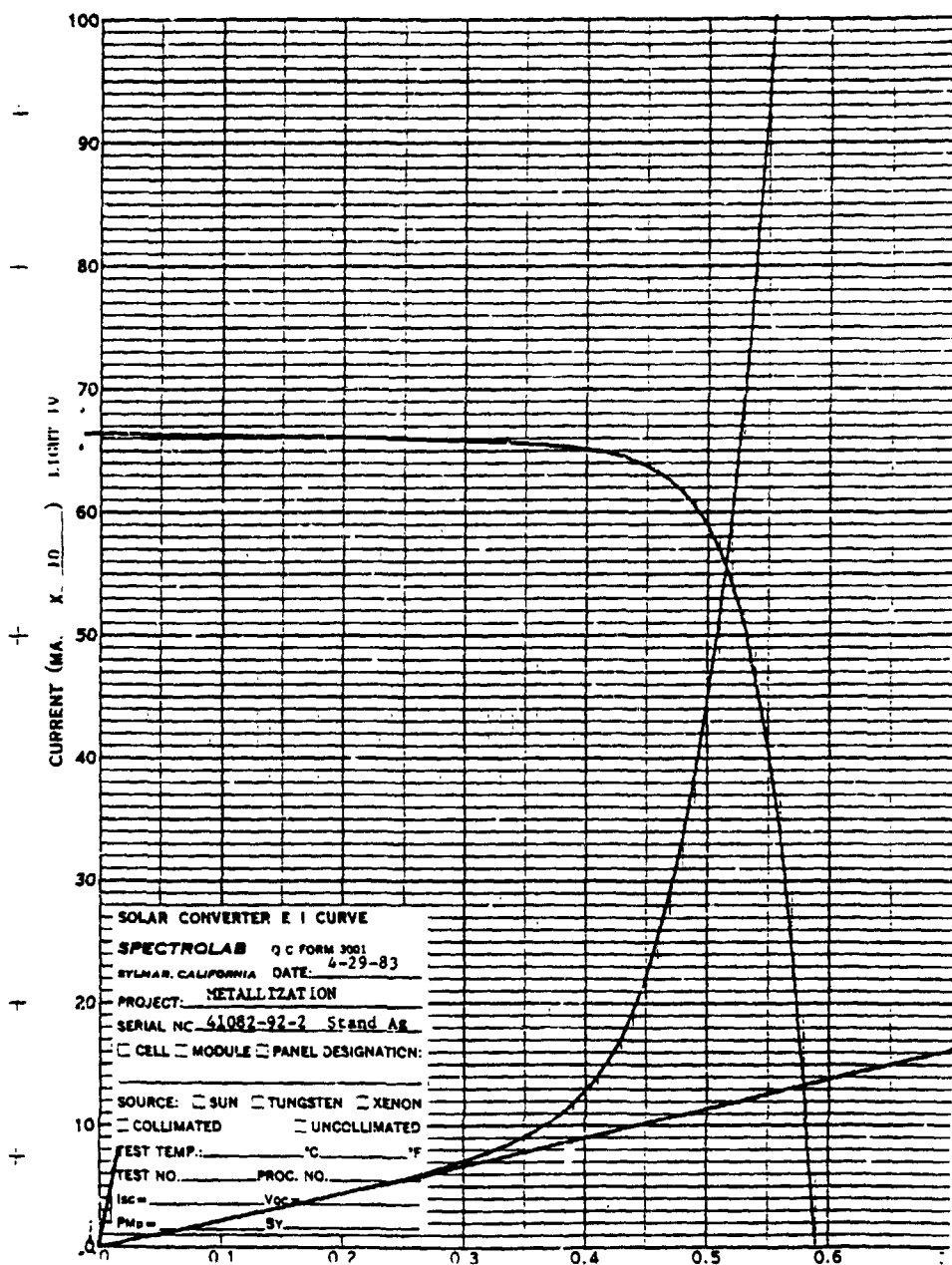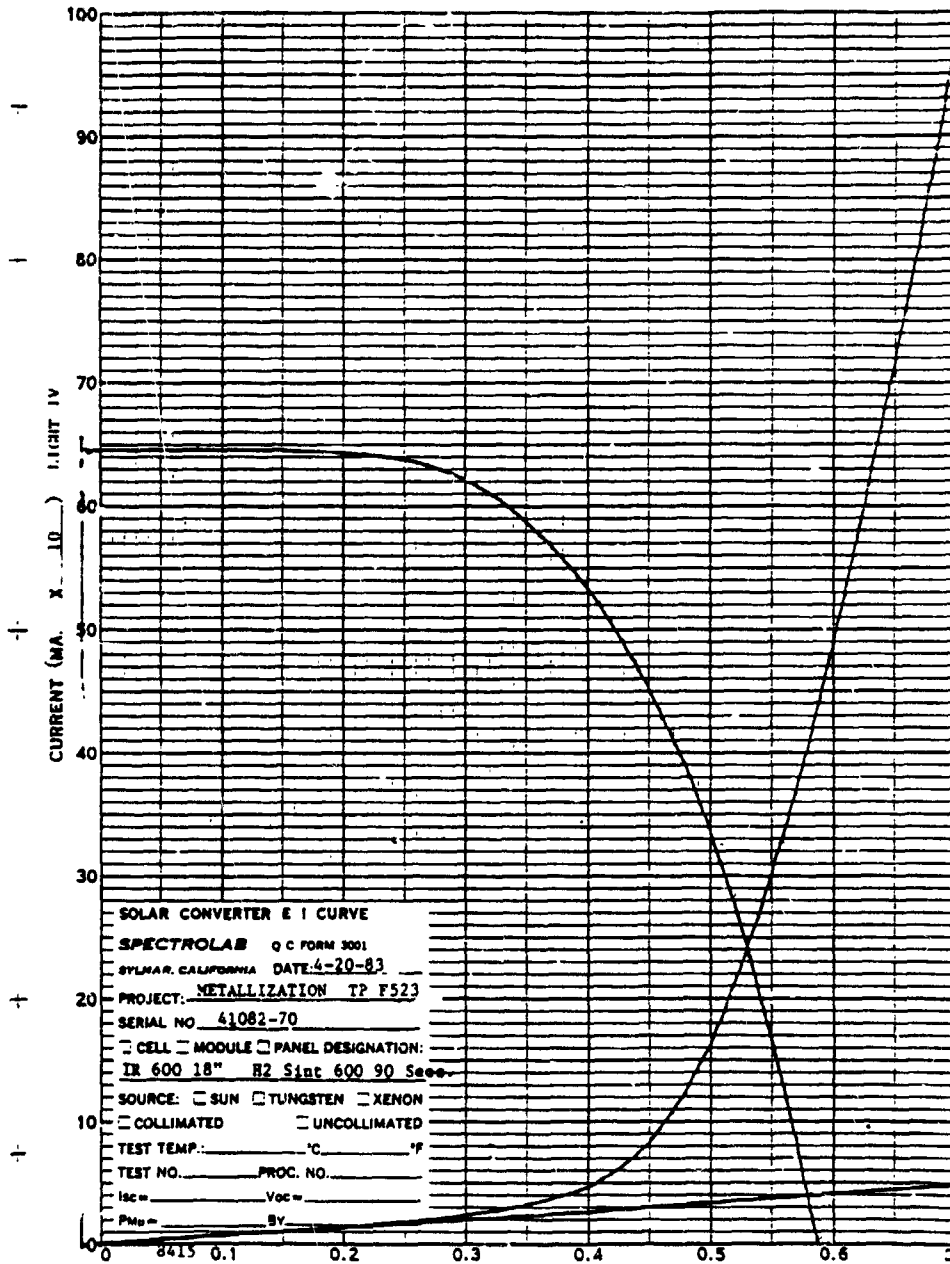
Problems With Hydrogen Reduction

- POOR ADHESION

- FRIT DOES NOT APPRECIABLY WORK

- SI-POWDER BOND A PROBLEM

- SOLDERING A PROBLEM

Paste Additives Investigated

- INDIUM

- LEAD

- CADMIUM

- ANTIMONY

- ZINC

New Pastes Investigated

- MoO_3 PASTE

- BORANE-PYRIDINE

- AG NEODECANATE

- AG RESINATE

- IN RESINATE

SOLAR CONVERTER E I CURVE

SPECTROLAB Q C FORM 3001

SYLMAR, CALIFORNIA DATE:_____

PROJECT: _600-10 H₂ E+ D_

SERIAL NO. _1983-40_

☒ CELL ☐ MODULE ☐ PANEL DESIGNATION:

SOURCE: ☐ SUN ☒ TUNGSTEN ☐ XENON

☐ COLLIMATED ☒ UNCOLLIMATED

TEST TEMP.: _28_ °C _____°F

TEST NO. _____ PROC. NO _____

Isc = _____ Voc = _____

Pmp = _____

CURRENT (MA. X 10)

VOLTAGE (VOLTS X 1)

8415
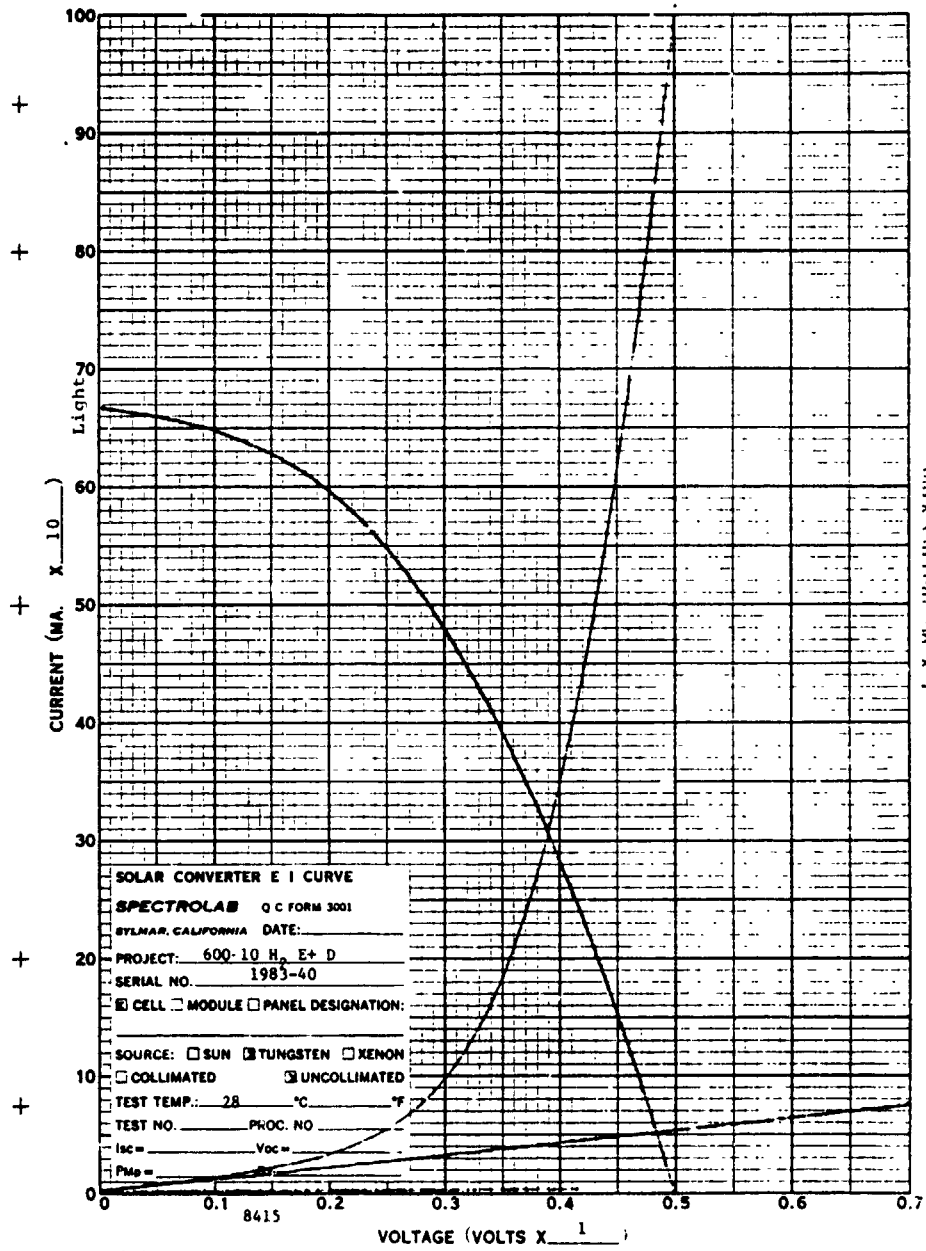
New Analytical Technique

- CONTROLLED ATMOSPHERE SEM

- VIDEO TAPE PICTURE AS SAMPLE IS BEING HEATED

- VARIOUS GASES AVAILABLE @ 5 TORR

Controlled-Atmosphere SEM
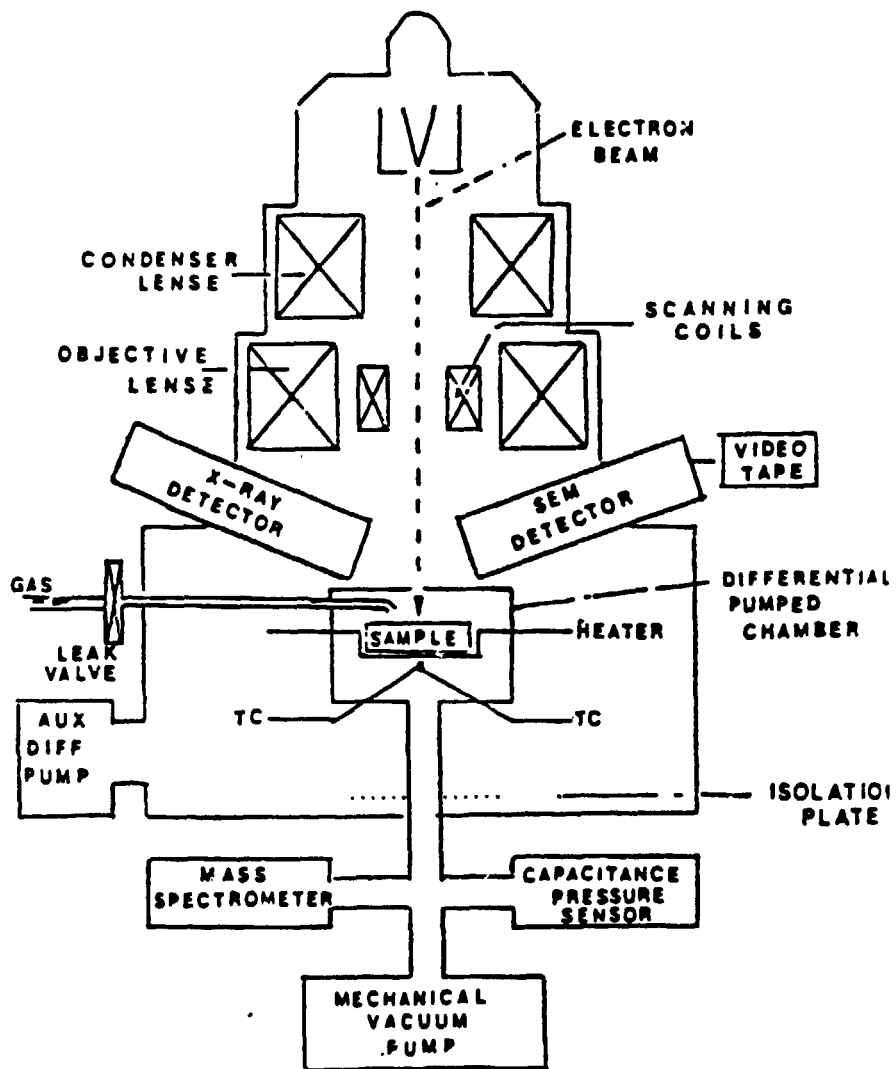
ORIGINAL PAGES
OF POOR QUALITY
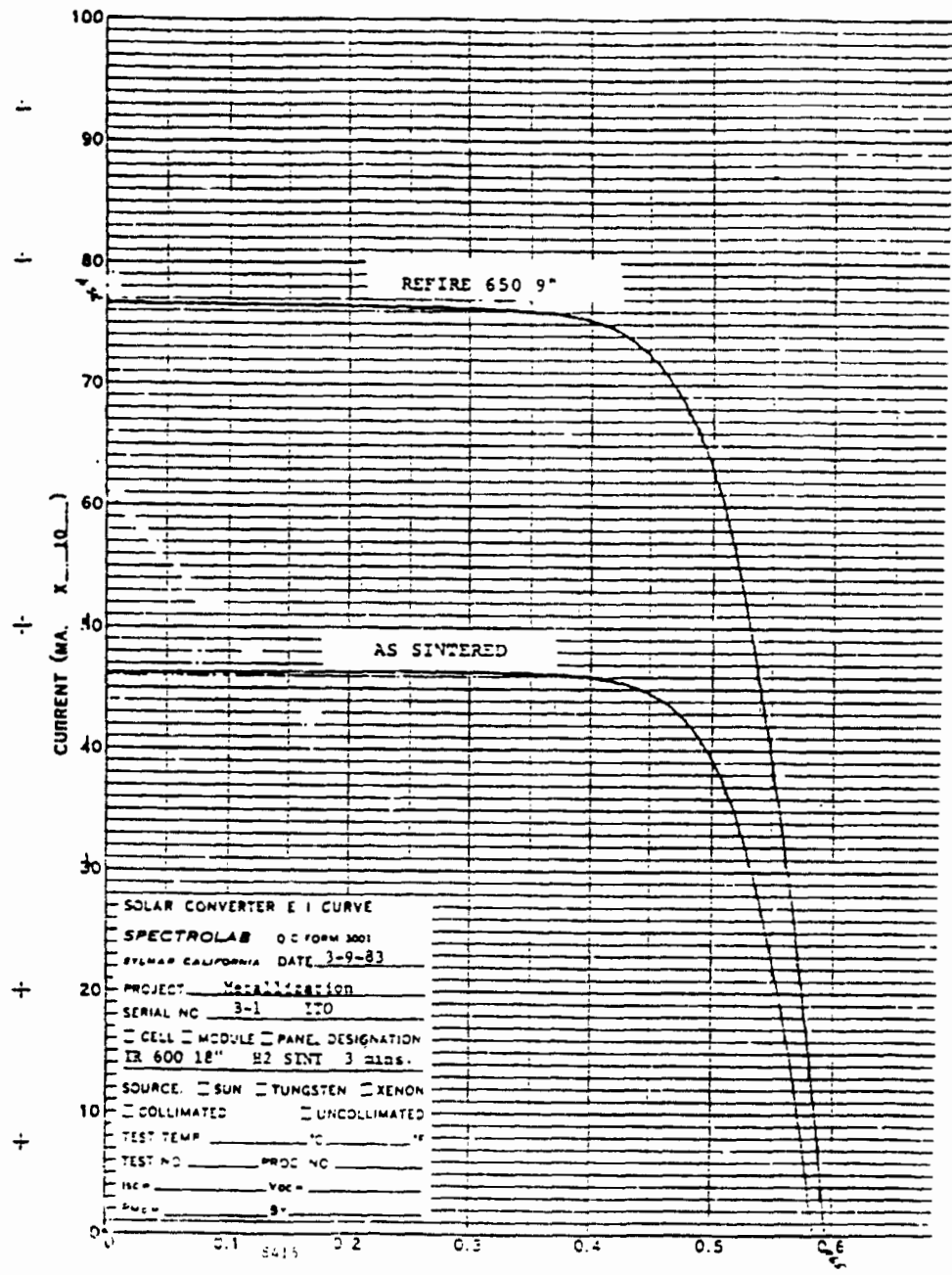
SOLAR CONVERTER E I CURVE

SPECTROLAB O C FORM 3001

SYLMAR CALIFORNIA   DATE 3-9-83

PROJECT ___Metallization___

SERIAL NC ___3-1   ITO___

☐ CELL ☐ MODULE ☐ PANEL DESIGNATION
IR 600 18"   H2 SINT   3 mins.

SOURCE. ☐ SUN ☐ TUNGSTEN ☐ XENON
☐ COLLIMATED   ☐ UNCOLLIMATED

TEST TEMP _____ °C _____ °F

TEST NO _____ PROC NO _____

ISC = _____ Voc = _____

PMAX = _____ gV _____

REFIRE 650 9"

AS SINTERED

ITO Shunted Cell

SPECTROLAB, INC.
a subsidiary of Hughes Aircraft Co.
12500 Gladstone Ave Sylmar CA 91342

SOLAR CELL I-V CURVE

DATE: _____ BY: _____
SIMULATOR: _____ TEST TEMP: _____ °C
☐CELL ☐MODULE PROJECT: _____
LOT NO.: _C_____ SERIAL NO.: _____
I_{sc} = _____ E_{oc} = _____
LOAD = _____ AT _____ ☐MV ☐MA

CURRENT (MA. X____)

VOLTAGE (VOLTS X_____)

8415
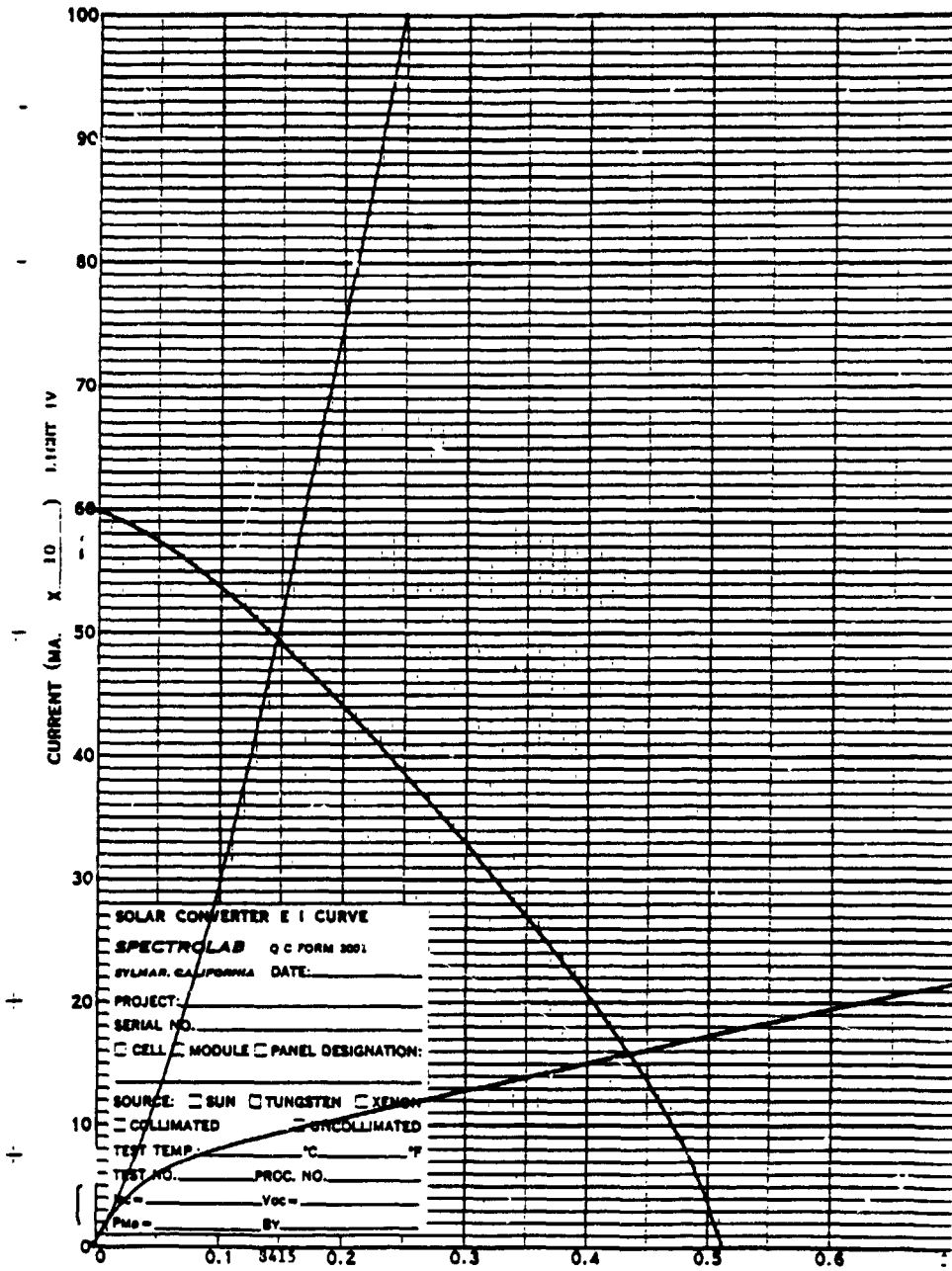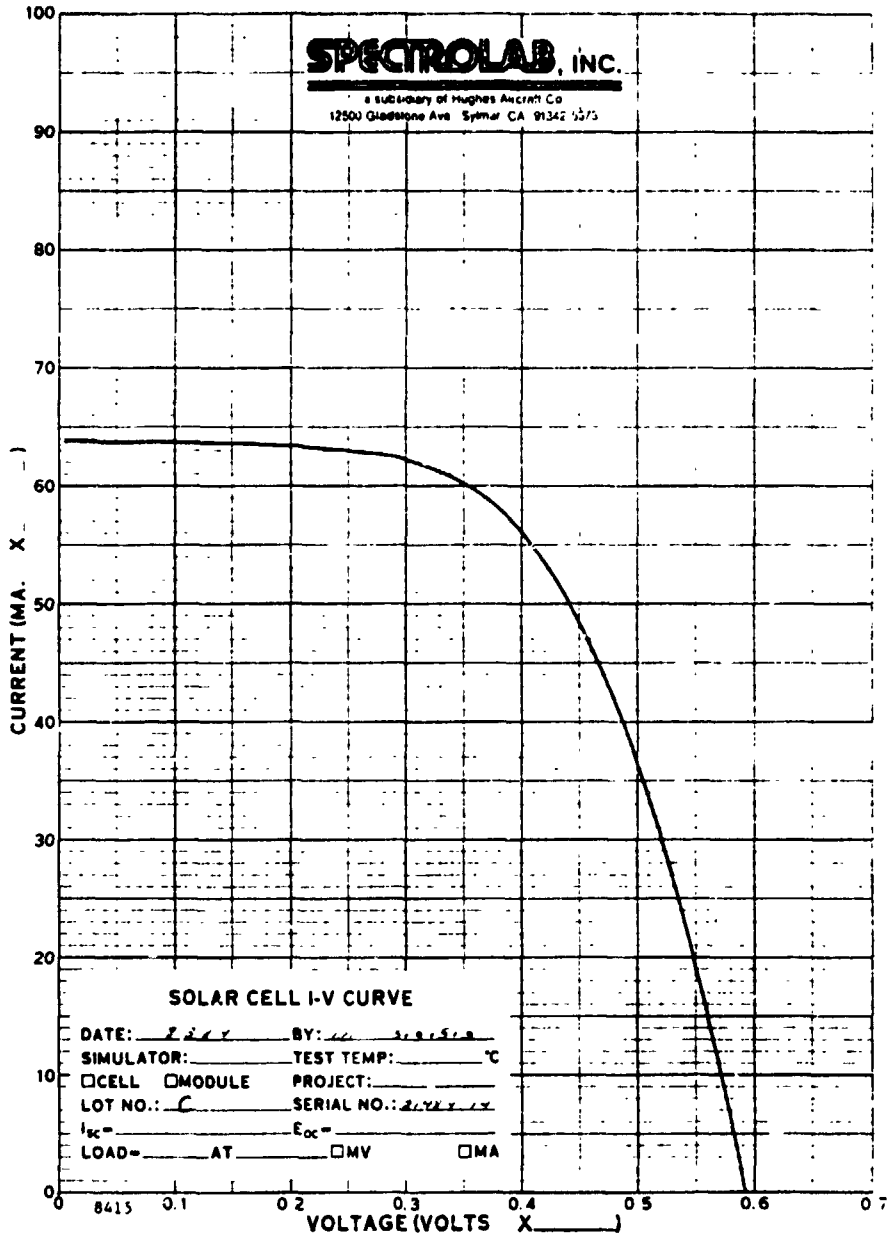
Two-Step Process

1) PRINT MO/SN

2) PRE-FIRE

3) PRINT AG PASTE

4) FIRE SILVER

5) FIRE MO/SN

● MO/SN MUST BE PRINTED FIRST

Results

● VARIOUS ADDITIVES UNSUCCESSFUL ON IMPROVING ADHESIVE

● SEM RESULTS SHOW TIN DOES NOT WET SYSTEM AT LOW TEMPERATURE

● TWO-STEP PROCESS MOST SUCCESSFUL

Conclusions

● MO/SN HAS ADEQUATE CONDUCTIVITY FOR SCREEN PRINTING

● SHUNTING IS NEVER A PROBLEM

● SOLDERABILITY A MAJOR PROBLEM

● MORE WORK NEEDED ON WETTING PHENOMENA

● CELLULOSIC VEHICLE BEST

● TWO-STEP PROCESS MOST SUCCESSFUL

MICROWAVE-ENHANCED THIN-FILM DEPOSITION

SUPERWAVE TECHNOLOGY INC.

S. Chitre

● **OBJECTIVE**

   deposition of semiconducting and insulating thin films at low temperature using microwave technology.

● **BACKGROUND**

1. Microwave plasma research began early 60's.

2. Microwave excitation:

   a. used to promote variety of chemical reactions

   b. offers more dense and longer lived active species (leads to separation of deposition chamber from discharge zone, eliminating harmful influences on samples due to direct exposure to plasma)

   c. Offers good uniformity & reproducibility (substrates kept at low temps.)

   d. endpoint detection & plasma diagnostics done with ease & accuracy

● **APPROACH**

1. Method of plasma formation

2. System consideration

   a. selecting a power source

   b. design of the microwave plasma cavity

   c. microwave circuitry

   d. impedance matching

   e. plasma diagnostics

   f. deposition chamber

   g. vacuum system

Microwave Plasma Cavity and Associated Circuitry
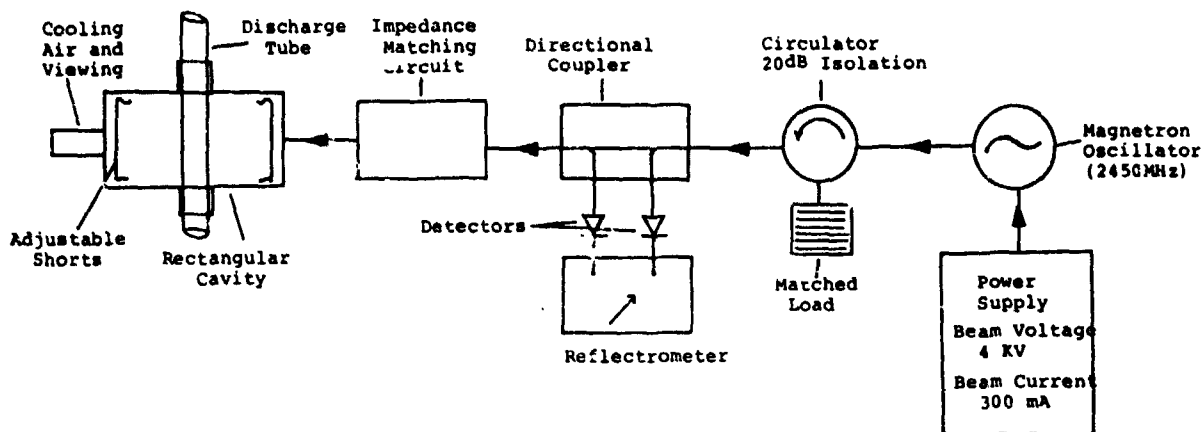
Structure of Magnetron
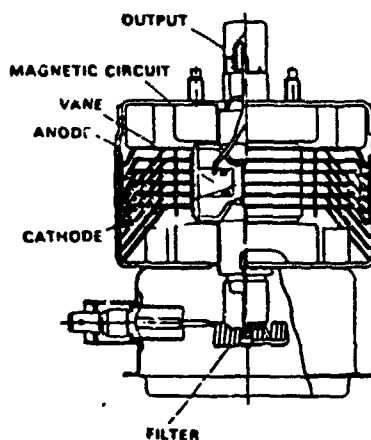
Principle of Magnetron Oscillation
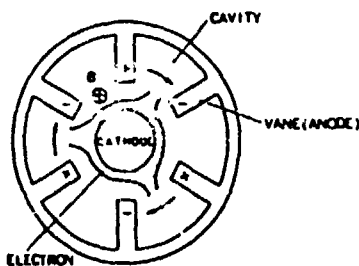
Construction of Microwave Plasma Cavity

INPUT WAVEGUIDE

HIGH Q CAVITY

MICROWAVE CHOKE

PLASMA TUBE

PLASMA REGION

MICROWAVE PLASMA CAVITY

ADJUSTABLE SHORT

MICROWAVE CHOKE

HIGH Q CAVITY

ADJUSTABLE SHORT

INPUT FLANGE

PLASMA REGION
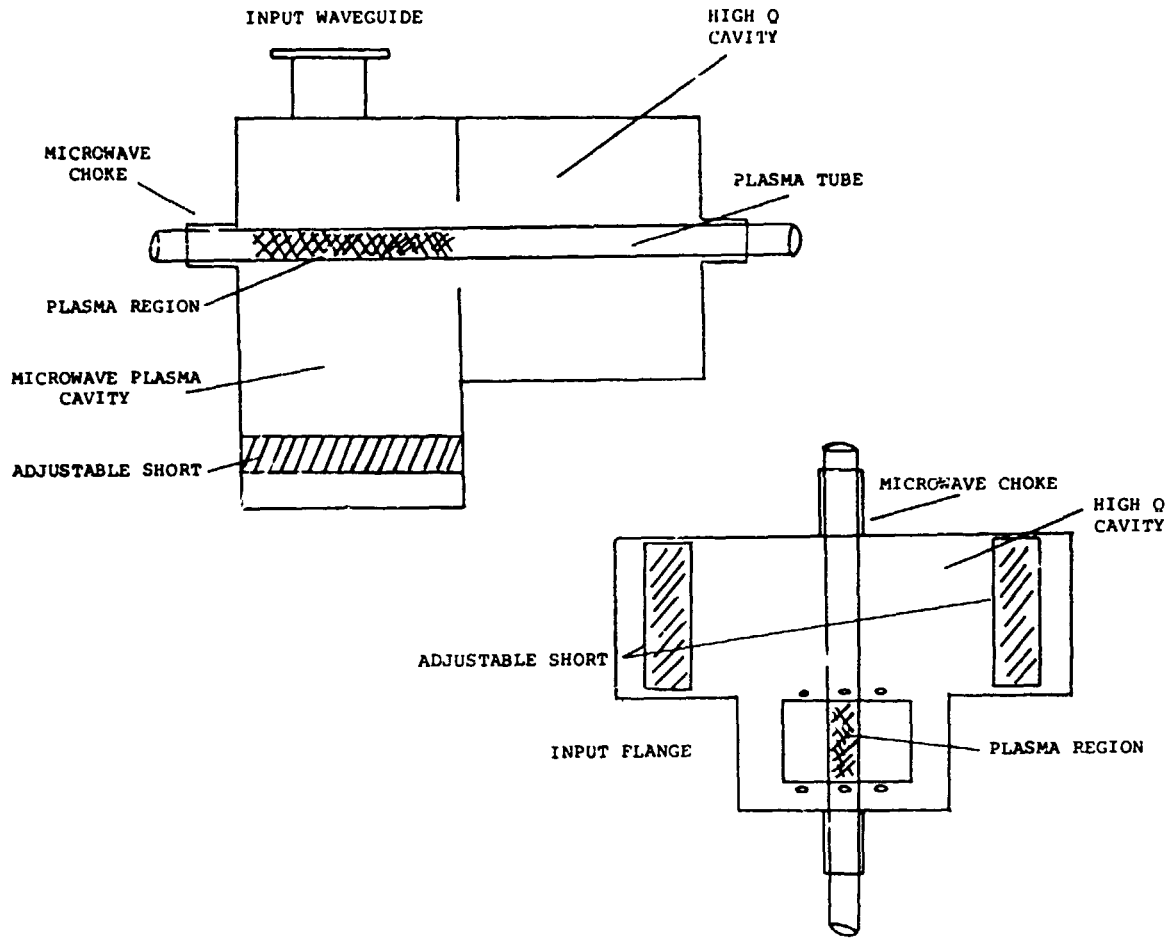
Elements of Microwave Deposition System

Flow Meters

Regulator

Substrate Holder Table

Needle Valve

On/Off Valve

SiH$_4$

Throttle Valve

Sieve Trap

Purge Line

N$_2$

Air Inlet Valve

MW Cavity

Needle Valve

Ar

Mechanical Pump

Convection Guage

Flow Meters
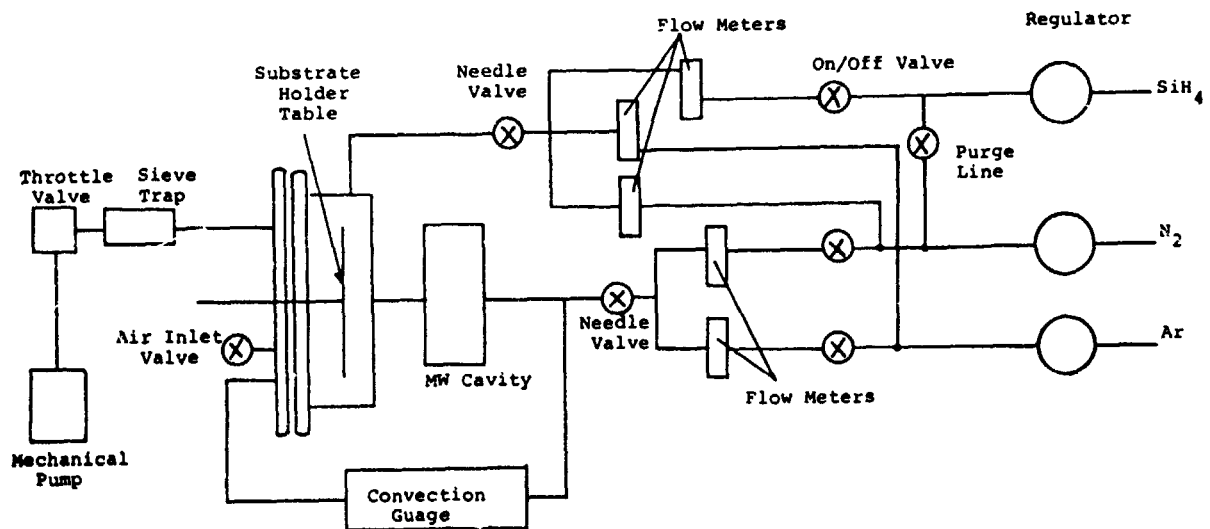
PULSED EXCIMER LASER PROCESSING
FOR COST-EFFECTIVE SOLAR CELLS

ARCO SOLAR, INC.

D. Wong

CONTRACT TITLE: ADAPT PULSED EXCIMER LASER PROCESSING
FOR COST EFFECTIVE SOLAR CELLS

CONTRACT NO: 956831

GOAL: TO DEMONSTRATE THE COST EFFECTIVE FEASIBILITY OF FABRICATING 16%
EFFICIENT SOLAR CELLS ON 125 MM DIAMETER Cz WAFER USING PULSED
EXCIMER LASER FOR JUNCTION FORMATION, SURFACE PASSIVATION, AND
FRONT METALLIZATION.

Texturing

0.4 J/CM^2 (70% OVERLAP) SUFFICIENT TO MELT THE SURFACE.

CELLS WERE SHUNTED. 650°C, 30 MIN. FURNACE ANNEALING MOST OFTEN
IMPROVED THE V_{OC}.

$\langle \eta \rangle$ -6.5%   BEFORE 650°C

$\langle \eta \rangle$ -11%   AFTER 650°C

EXCESSIVE SURFACE MELTING IS BELIEVED TO LIMIT CELL EFFICIENCY.

PRECEDING PAGE BLANK NOT FILMED

SOURCE LAMP: ELC   IV TESTER: #2   SINGLE/POLY
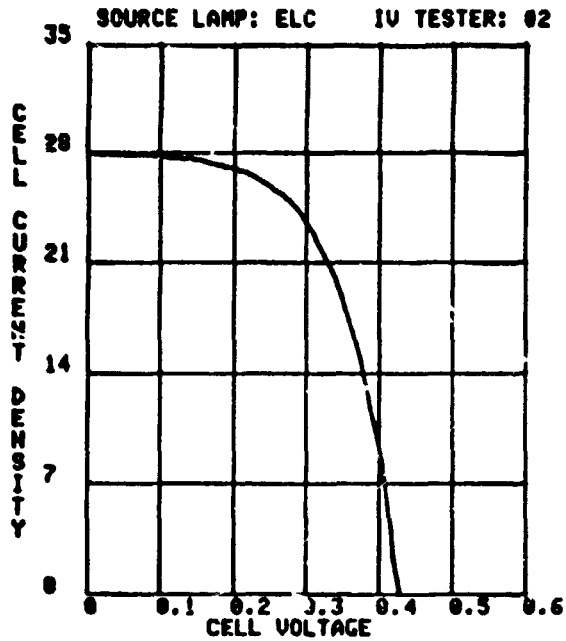
LIGHT IV AT 25C
OPERATOR:DW
CELL:L5B, CONTROL#1
Date/time:09-JUL-84 10:53:07

AREA: 4.00 (sq.cm)

Isc: 0.112 (amps)

Jsc: 28.00 (ma/sq)

Voc: 0.427 (volts)

Ipm: 0.093 (amps)

Jpm: 23.24 (ma/sq)

Vpm: 0.305 (volts)

Pm: 0.028 (watts)

Cff: 59.21 %

Eff: 7.09 %

RUN 5 B, ENERGY/= 0.4J/CM2, OVERLAP 50%
SINTERED

SOURCE LAMP: ELC   IV TESTER: #2   SINGLE/POLY
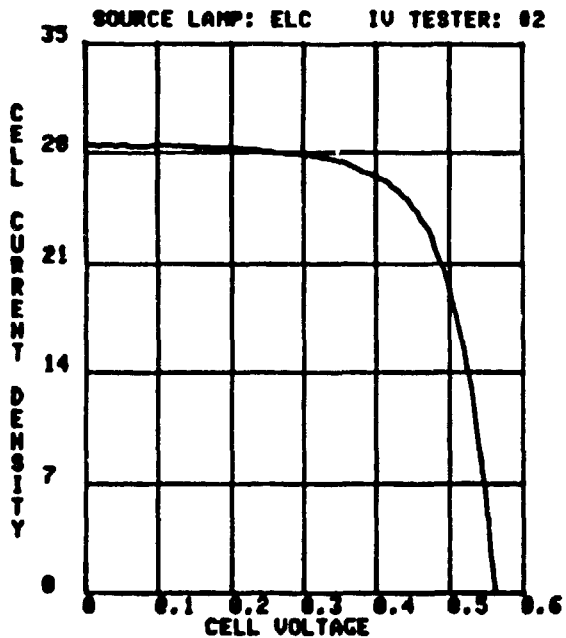
LIGHT IV AT 25C
OPERATOR:DW
CELL:L5B ANNEALED 3
Date/time:27-JUN-84 09:50:20

AREA: 4.00 (sq.cm)

Isc: 0.114 (amps)

Jsc: 28.54 (ma/sq)

Voc: 0.563 (volts)

Ipm: 0.100 (amps)

Jpm: 25.09 (ma/sq)

Vpm: 0.442 (volts)

Pm: 0.044 (watts)

Cff: 69.10 %

Eff: 11.10 %

RUN 5 B, ENERGY =0.J/CM2| OVERLAP 50%
ANNEALED THERMALLY @ 650 C 30 MIN.
NO SINTERED

438

Threshold Energy Density for Textured
Surface to Start Melting
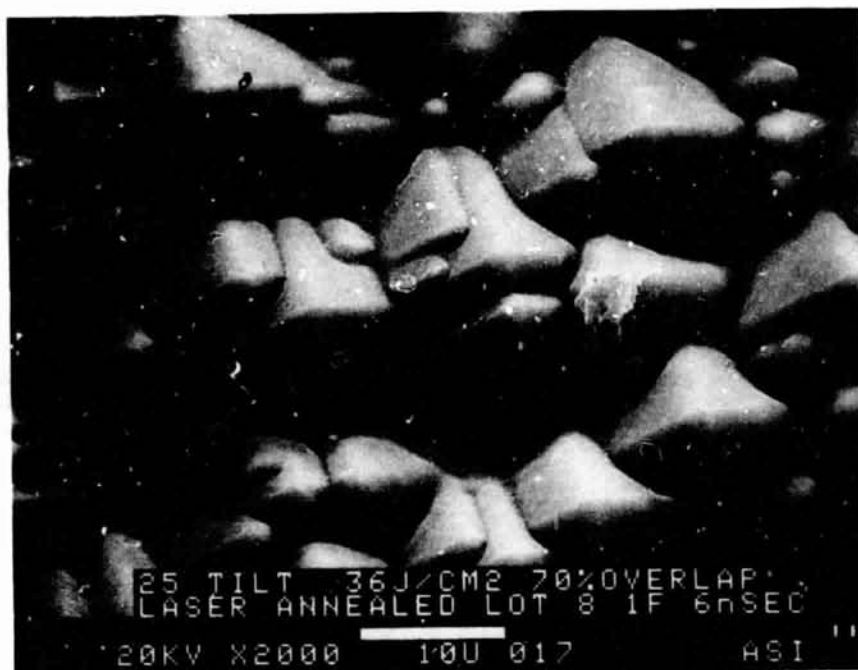
Surface Melting on Textured Surface Due to Laser Annealing at Different Laser Energy
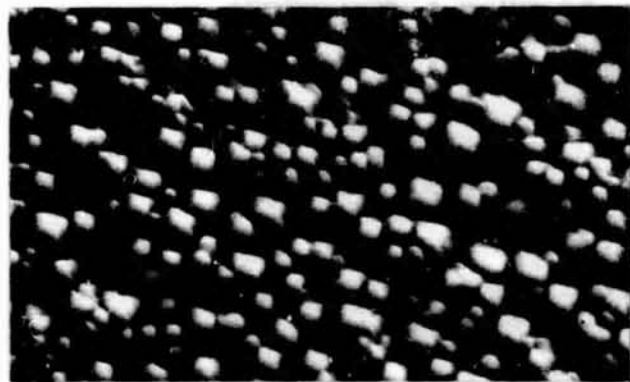
0.4 J/CM^2
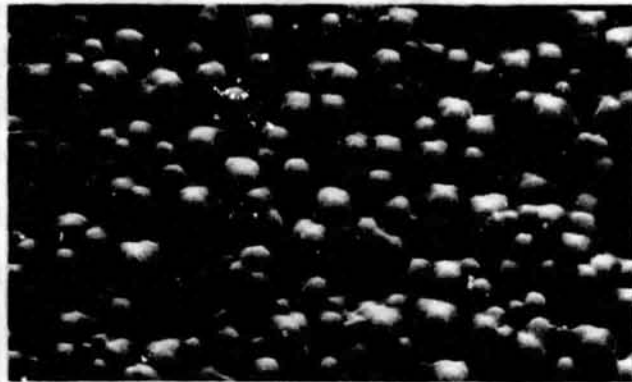
0.7 J/CM^2

0.9-1.2 J/CM^2

2 J/CM^2

Comparison of Baseline Process With
Proposed Excimer Laser Process

BASELINE PROCESS

TEXTURING

```
                          |
 _____      |         _____              _____
| STARTING  |     |        | PHOSPHORUS |            | SCREEN PRINT |
| MATERIAL  |_____>|  THERMAL   |_____>| METALLIZATION|____ η -13%
| P TYPE Cz |              | DIFFUSION  |            |  AND FIRING  |
|_____|             |_____|             |_____|
```

LASER PROCESS

TEXTURING

```
                          |         _____
                          |        | ION IMPLANT |            _____
 _____             '        | AND LASER ANNEAL|        | LASER ASSISTED |
| STARTING  |     |        | => IDEAL JUNCTION |_____>|    SURFACE    |_____>
| MATERIAL  |_____>|  EXCELLENT BLUE   | GAIN 1% |  PASSIVATION  | GAIN 1%
|_____|             |    RESPONSE       |        |_____|
                          |_____|
```

```
                           _____
                          | LASER WRITING |
                          | FINE GRIDLINES|
                          |  => INCREASE   |
          _____> | ACTIVE AREA   |_____> η  -16%
                          | REDUCE I$^2$R | GAIN 1%
                          |    DROP       |
                          |_____|
```

Experimental

```
                        _____
                       I  P SUBSTRATE   I
                       I 0.3 - 0.7 OHM-CM I
                       I_____I
                              |
                   _____/ _____
                  /                       \
SURFACE PREPARATION I TEXTURING I          I POLISHING I
                    I_____I          I_____I
                         |                      |
                   _____|_____          _____|_____
DOPANT SOURCE     I SPIN-ON SOURCE I      I ION IMPLANT I
                  I_____I       I_____I
                         \                      /
                          _____/
                                   |
                          _____
                         I LASER ANNEAL  I
                         I_____I
                               |
                        _____
                       I METALLIZATION I  82% active area
                       I BY EVAPORATION I
                       I_____I
                               |
                          _____
                         I  TEST  I  (JPL STANDARD)
                         I_____I
```

Polished Wafer (p-Type Cz) Ion Implant $^{31}p^+$

(J/cm^2)	BEAM SIZE (MM X MM)	OVERLAP (%)	PULSE (NS)	IMPLANT (KEV)	DOSAGE (1×10^{15})	RHO (OHM/SQ) APPROX	η %
0.7	1.1 X 0.8	40	6	10	5	31	7.3
0.7	1.1 X 0.8	40	6	10	1	90	4.2
1.3	0.95 X 0.95	70	25	5	2.5	50	7.1
1.3	0.75 X 0.6	20	25	5	1	70	8.9
1.3	9.0 X 7.5	20	80	5	2.5	50	8.4
1.45	9.6 X 8.3	12	90	5	1	90 - 100	9.3
1.55	8.9 X 7.5	12	90	5	1	90 - 100	9.3
2.0	7.5 X 6.5	12	90	5	1	90 - 100	9.4

Laser Energy Density

LASER ENERGY DENSITY FROM 1.45 J/CM^2 TO 2 J/CM^2 YIELDED SIMILAR RESULTS IN CELL EFFICIENCY FROM THE SAME IMPLANT. HOWEVER, SURFACE DAMAGE STARTED TO BE OBSERVED AT 2 J/CM^2.

Overlap, %

NECESSARY FOR COMPENSATING BEAM NONUNIFORMITY. HOWEVER, FOR HIGHLY NONUNIFORM BEAM, OVERLAP WOULD PRODUCE SEVERE SURFACE DAMAGES.

MORE UNIFORM LASER WITH LARGER BEAM SIZE REDUCES OVERLAP REQUIREMENT ———> HIGHER CELL EFFICIENCY.

Kaleidoscope Beam Profile (MSNW Inc.)

RELATIVE INTENSITY
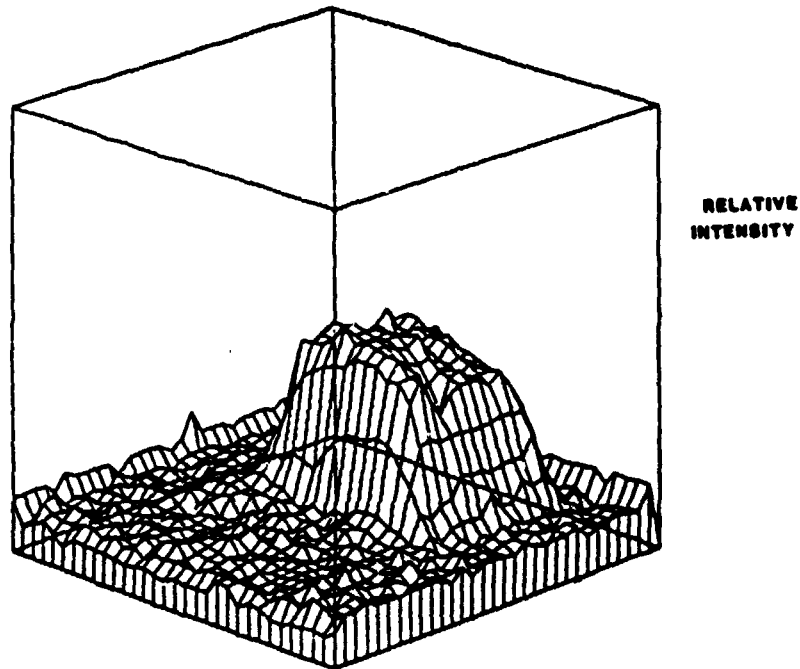
Profile of Excimer Output Beam (MSNW Inc.)
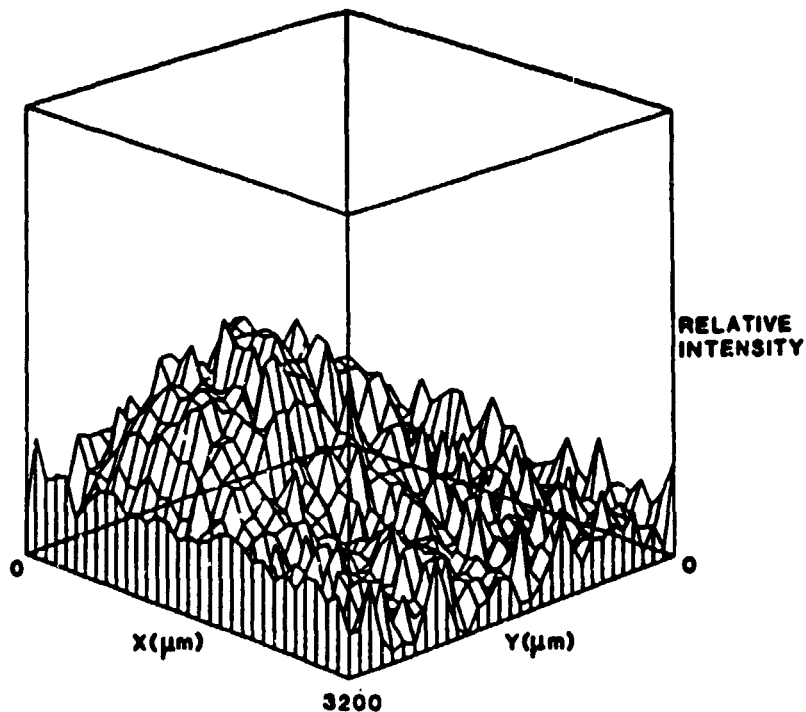
Ion Implant

5 KEV $^{31}P^+$ CHANNELED TO ABOUT 0.16 - 0.22 μM WHICH REQUIRES LASER ENERGY AT LEAST 1.6 J/CM^2 - 1.8 J/CM^2 TO REMOVE LATTICE DAMAGES COMPLETELY.

Indirect Proof

CZ WAFER WITH THERMAL N+ DEPOSITION (830°C 10 MIN) FOLLOWED BY LASER ASSISTED DIFFUSION AT 1.25 J/CM^2 (12% O.L.) YIELDED ALMOST IDENTICAL IN ELECTRICAL PERFORMANCE AS THE THERMALLY DIFFUSED CELL ($\geq$10%).

Depth Profile
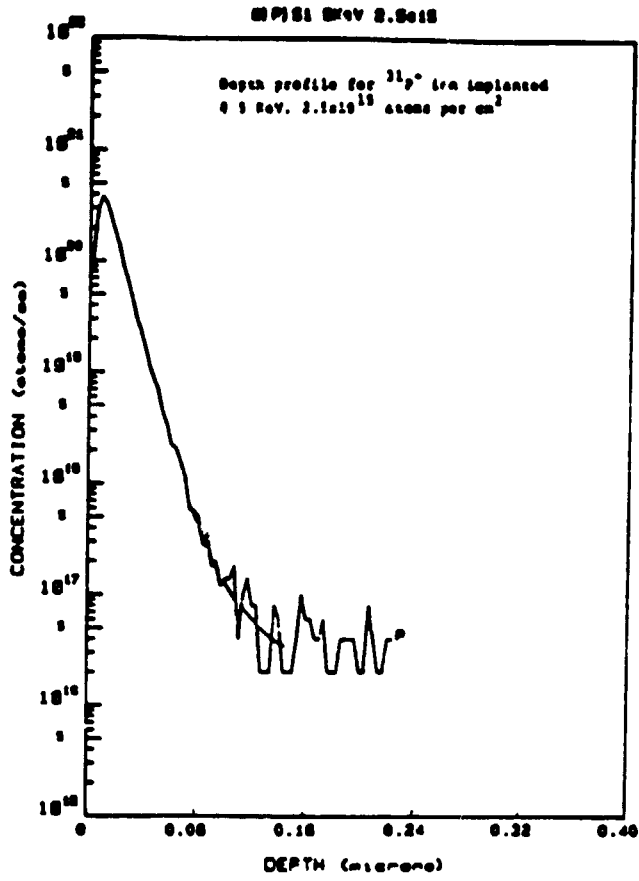
SIMS Depth Profile for $^{31}p^+$ Ion Implanted at 5 keV, 2.5 x 10^{15} Atom per cm^2. Substrate Resistivity -0.3 ohms-cm Boron Doped.

Summary on Junction Formation

IDEAL JUNCTION REQUIRES

(I) SHALLOW ION IMPLANT TO MINIMIZE LASER ENERGY DENSITY FOR COMPLETE LATTICE DAMAGE REMOVAL.

(II) UNIFORM LASER BEAM THAT REQUIRES LESS THAN 5% OVERLAP.

Plans for Next Quarter

(I) IMPROVE LASER UNIFORMITY

(II) INVESTIGATE THE CAPABILITY OF 1 KEV ION IMPLANTATION BY GLOW DISCHARGE TECHNIQUE.

(III) COMPLETE GAS CELL SYSTEM AND INITIATE EXPERIMENT ON LASER ASSISTED SURFACE PASSIVATION AND GRIDLINE WRITING.

EXCIMER LASER ANNEALING FOR FABRICATION OF LOW-COST SOLAR CELLS

SPIRE CORP.

A.C. Greenwald

Program Goal

TO DETERMINE IF PULSED EXCIMER LASER ANNEALING (PELA)
IS COST EFFECTIVE COMPARED TO BASELINE PROCESS.

BASELINE PROCESS	LASER PROCESS
CLEAN	CLEAN
DRY	DRY
DIFFUSE JUNCTION	ION IMPLANT
ALUMINUM BSF	LASER ANNEAL
CLEAN	
PRINT Ag BACK	PRINT Ag BACK
PRINT Ag FRONT	PRINT Ag FRONT
LASER CUT	LASER CUT
TEST AND SORT	TEST AND SORT

PROCESS DEVELOPMENT

Objectives

- BUILD AN EXCIMER LASER PULSED ANNEAL APPARATUS

- DEVELOP ANNEAL PROCESSING FOR HIGH EFFICIENCY CELLS

- FABRICATE 300 SOLAR CELLS

- PERFORM ECONOMIC ANALYSIS

Fluence Measured Across Beam Width (at Lens)
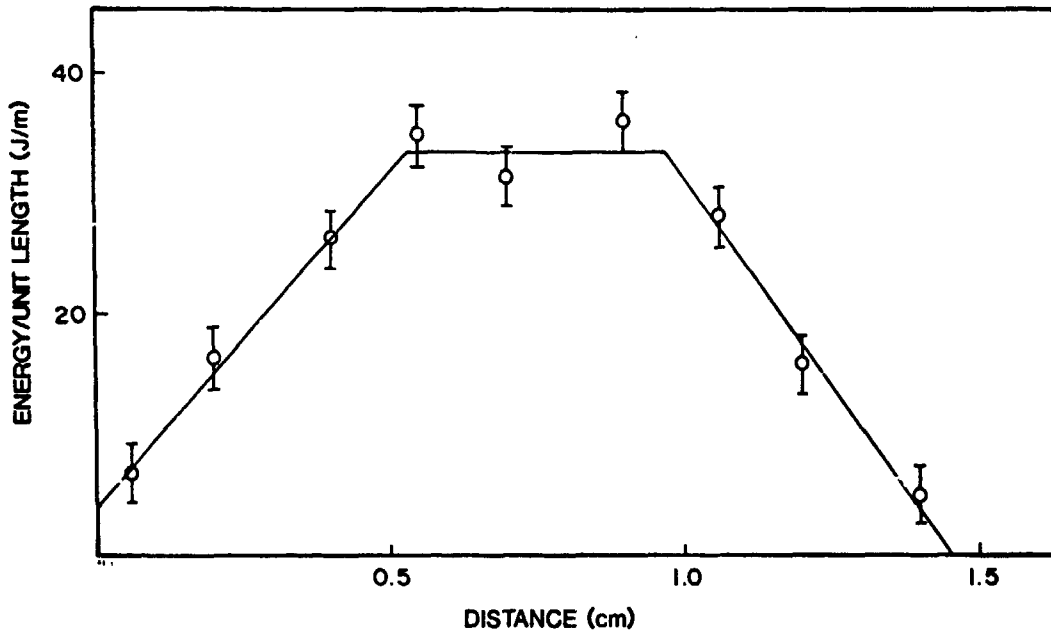
Fluence Measured Across Beam Length (at Lens)
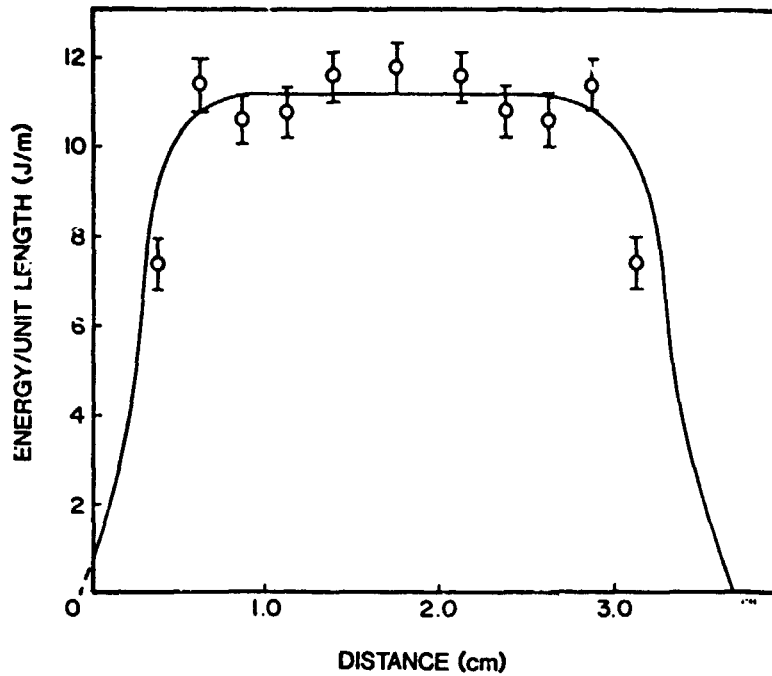
Scanning Pattern for Annealing a 100 cm² Wafer (Total Transit Time at 10 cm/s Is 5.5 Seconds)
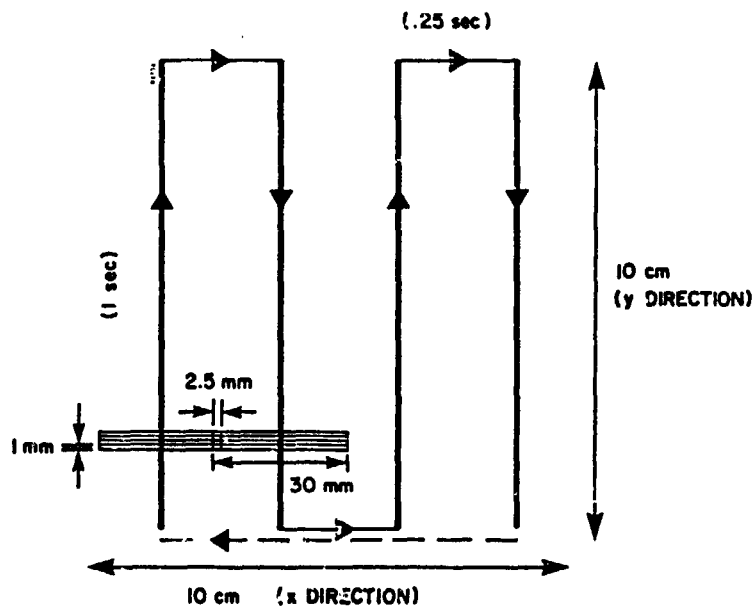
PROCESS DEVELOPMENT

Implantation Parameters

	FRONT (TEXTURED)	FRONT (POLISHED)	BACK (EITHER)
ION	P^+	P^+	B^+
ENERGY	10 keV	10 keV	25 keV
DOSE	$4.3 \times 10^{15} cm^{-2}$	$2.5 \times 10^{15} cm^{-2}$	$5 \times 10^{15} cm^{-2}$

Pulsed Excimer Laser Annealing Polished Surfaces
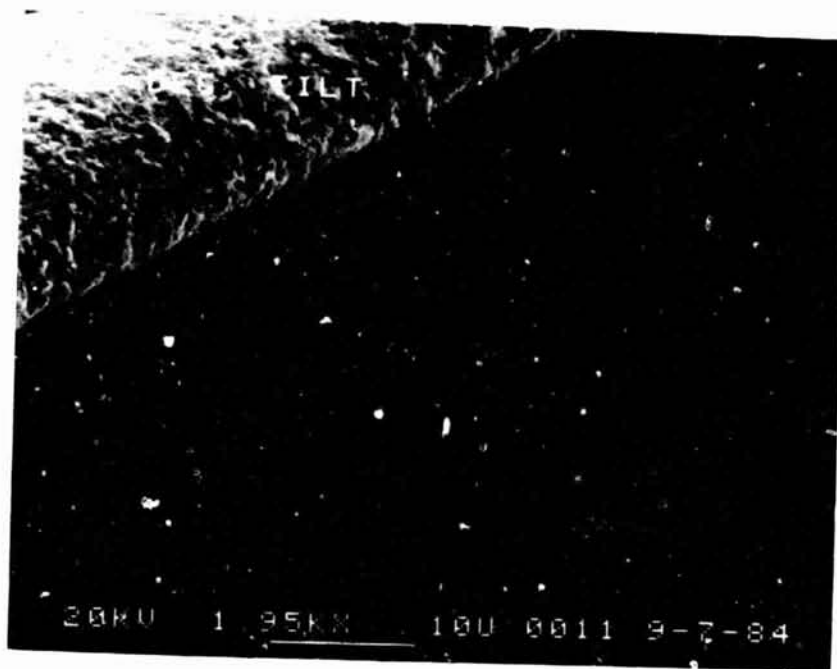
FURNACE
ANNEAL
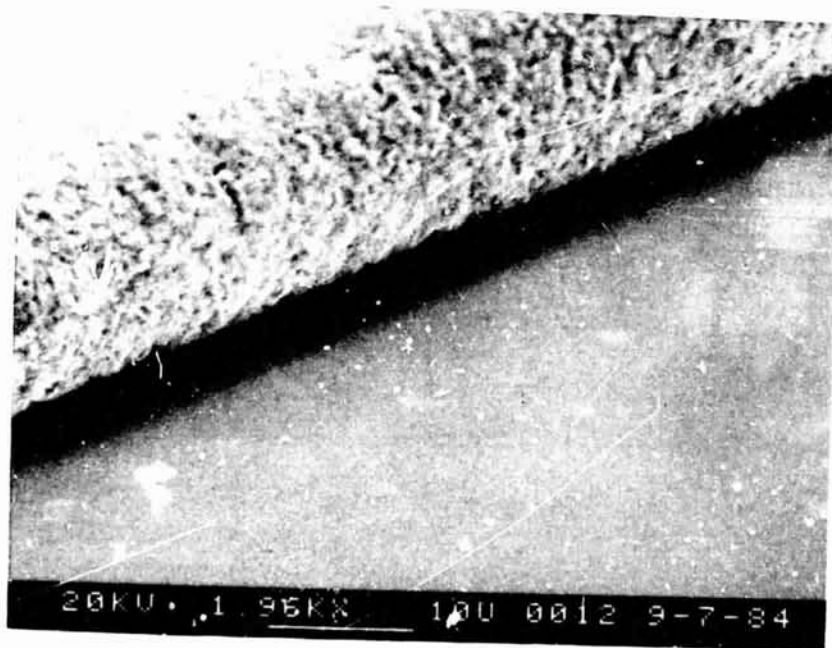
PELA

Sheet Resistance Uniformity of PELA Sample 4520-1b
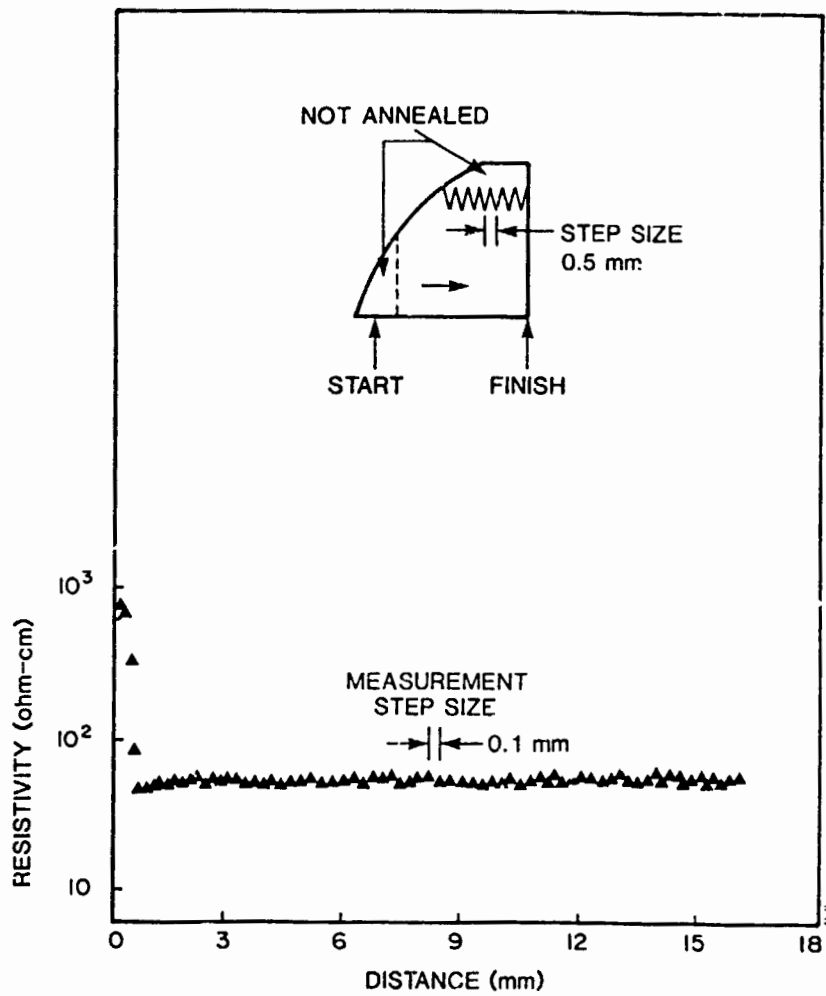
PELA Junction Depth Profile, Sample 4520-16

ION: $^{31}P^+$

DOSE: $2.5 \times 10^{15}/cm^2$

ENERGY: 10 keV

λ: 248 nm

FLUENCE: 2.0 J/cm^2
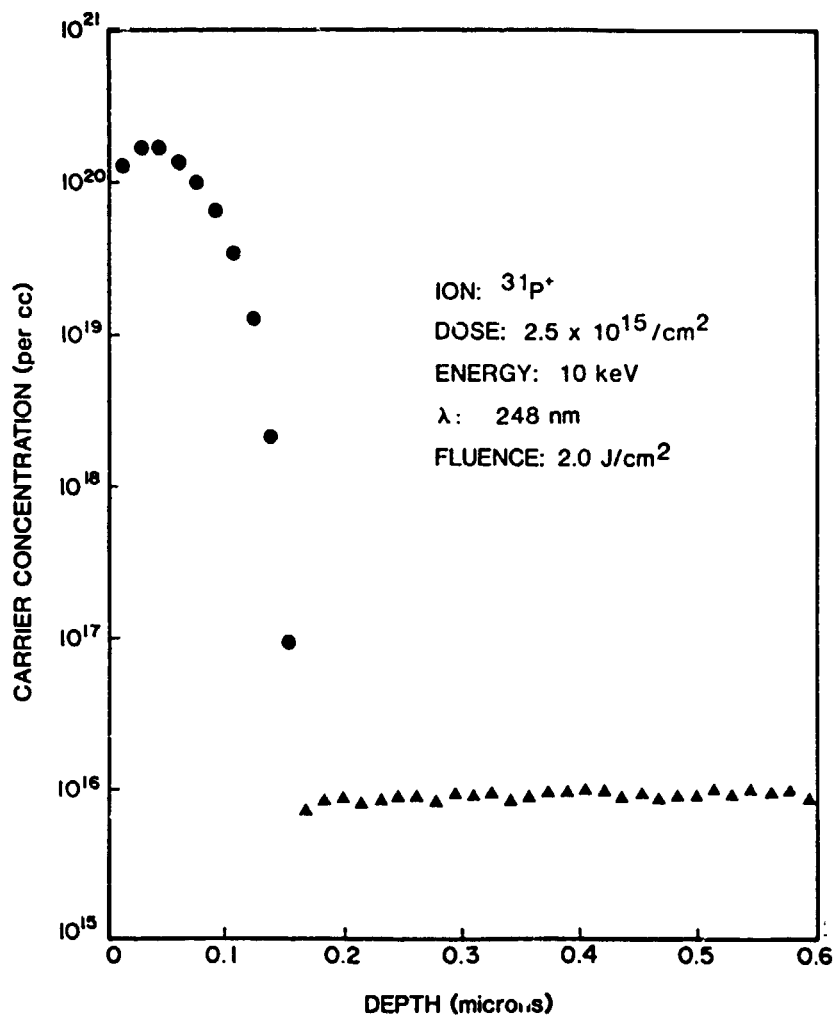
Efficiency vs Laser Fluence: Polished Wafers, No AR Coating

LOT	η (%)	FLUENCE (J/CM^2)	NO. OF PULSES
I	8.9	1.2	1-2
	8.4	1.8	1
$\lambda = 248$ nm	8.9	1.9	2-3
	9.1	2.0	1-2
	9.1	FURNACE CONTROL	
	7.3	0.8	1
II	8.1	1.0	4
	9.7	1.4	1
$\lambda = 308$ nm	10.5	1.8	1
	10.2	1.8	2-3
	7.5	FURNACE CONTROL (?)	

Melting of Texture-Etched Surfaces
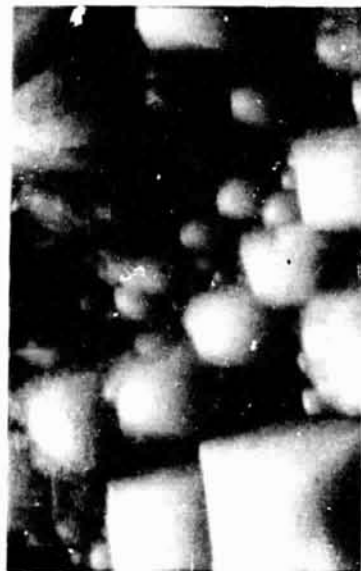
1.4 J/cm² 1 PULSE

>1.8 J/cm² 2 PULSES

NOT PULSED

5 μm
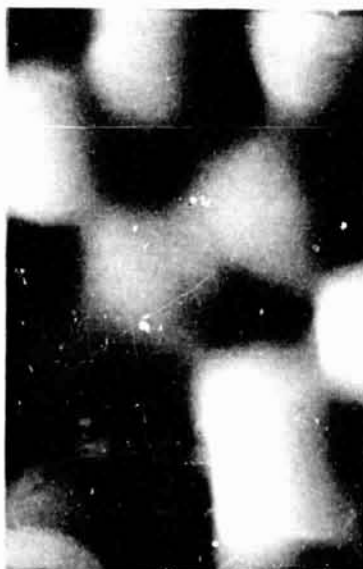
2 PULSES

Efficiency vs Laser Fluence: Texture-Etched Wafers, No AR Coating

LOT	η (%)	FLUENCE (J/CM^2)	NO. OF PULSES
I	10.8	1.2	1-2
	10.5	1.8	1
$\lambda = 248$ nm	8.2	1.8	2
	9.2	2.0	1-2
	12.9	FURNACE CONTROL	
	9.1	0.8	1
II	8.7	0.8	2
	9.1	0.8	4
$\lambda = 308$ nm	11.8	1.0	4
	12.4	1.4	2
	8.8	1.8	2
	8.1	FURNACE CONTROL (?)	

Best Cell to Date

IMPLANT: $^{31}P^+$ 2.5 x 10^{15} ions/cm^2 10 keV

ANNEAL: XeCl LASER, 1.8 J/cm^2 1 pulse
minimum overlap

V_{oc} = J78 mV

J_{sc} = 23.0 mA/cm^2

FF = 78.6%

EFF = 10.5%

WITH AN AR COATING, EFFICIENCY WOULD
BE ABOUT 15%

$V_{OC} = 578$ mV
$J_{sc} = 23.0$ mA/cm^2
FF = 78.6%
Eff = 10.5%

$I_{sc}-V_{oc}$

n = 1.1

I–V

T = 28°C
NO AR COATING

CELL 4520-9B
NO AR COATING
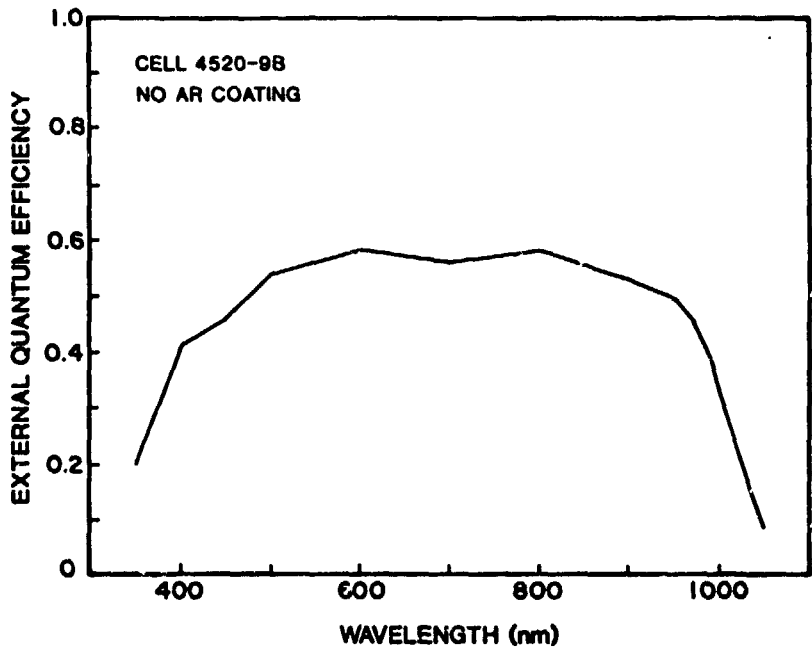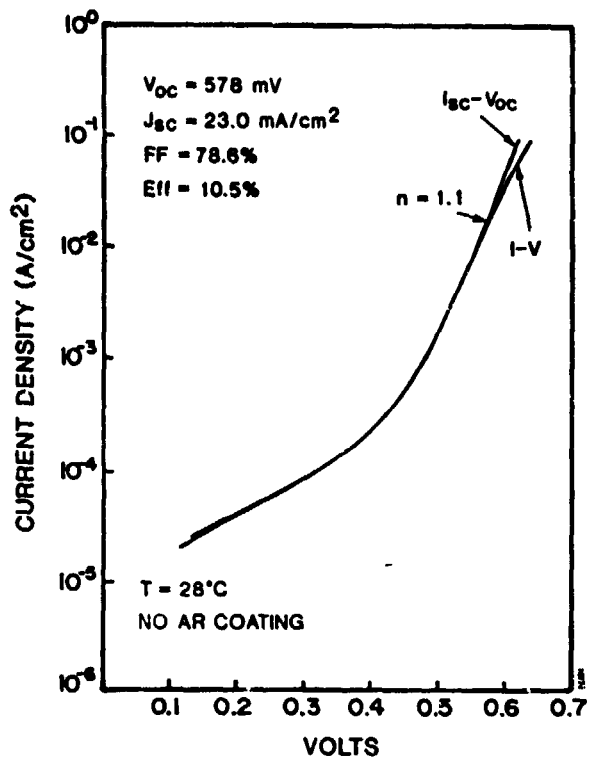
Can the Laser Deliver Enough Power
to Rapidly Anneal a Large Wafer?

THE 50 WATT LASER ANNEALED A 4" ROUND
POLISHED WAFER, A 4" ROUND TEXTURED WAFER,
AND A 10 cm x 10 cm SILSO WAFER, EACH IN
UNDER 10 SEC.

Laser Parameters

GAS	Kr, F$_2$, and Ne
WAVELENGTH	248 nm
POWER	50 watts
REP. RATE	160 Hz
PULSE WIDTH	20 nanoseconds

Anneal Parameters

FLUENCE	~1.4 J/cm^2 at sample
SPOT SIZE	~0.7 mm x 25 mm
TABLE SPEED	10 cm/sec.

Summary of Process Variables

● LASER POWER OF 2 J/cm^2 IS REQUIRED FO'   ⎣⎤
  WAFERS, LESS FOR TEXTURED WAFERS.

● WAVELENGTH (KrF v XeCl) IS NOT IMPORT: ·

● BEAM UNIFORMITY MUST BE BETTER THAN 5%
  BUT NOT NEE J NOT BE BETTER THAN 2%.

● DUST IS NOT TOO IMPORTANT.

● UNANNEALED AREAS REDUCE Jsc BUT DO NOT
  SHUNT JUNCTION.

● OVERLAP IS IMPORTANT FOR TEXTURED WAFERS.

Program Schedule

TASK	1984										1985			
	M	A	M	J	J	A	S	O	N	D	J	F	M	A
TASK 1														
A- SELECT PROCESS														
B- ASSESS SENSITIVITY TO VARIABLES														
● SET-UP ANNEALER														
● ANNEAL ^{31}P$^+$ IMPLANT														
● TEXTURE-ETCH SURFACE														
● BSF PARAMETERS														
● SCREEN PRINTING														
C- DEMONSTRATE LASER POWER														
D- DEMONSTRATE PRODUCT														
● WAFER PREP														
● IMPLANT & PELA														
● FABRICATION & TEST														
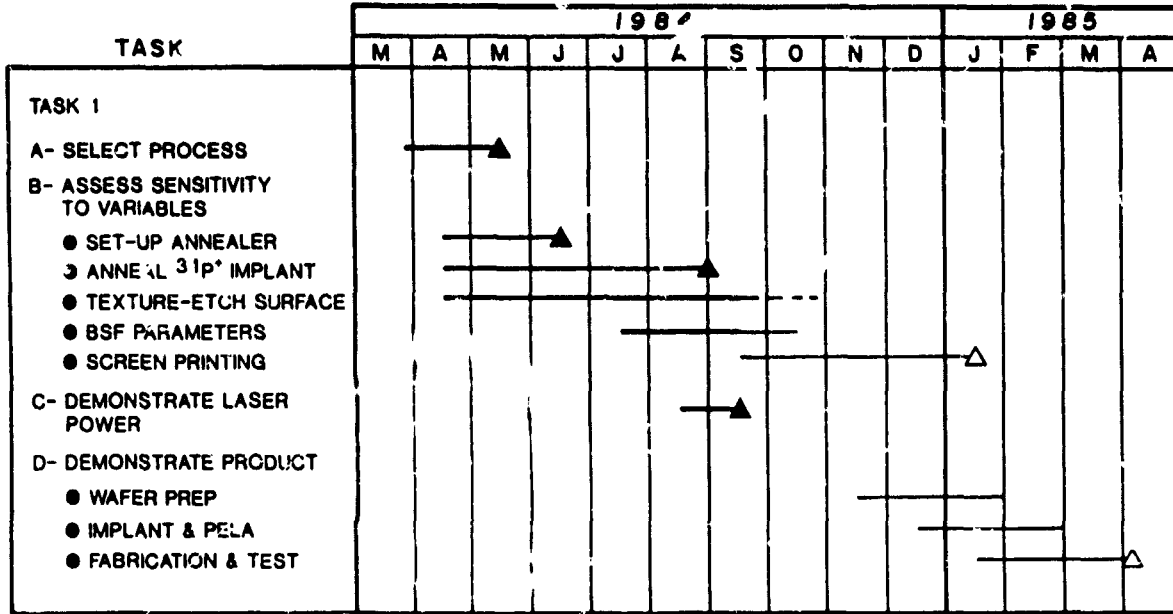
Summary

● AN EXCIMER LASER ANNEALER HAS BEEN BUILT AND TESTED.

● SOLAR CELL EFFICIENCY, WITHOUT AR, OF UP TO 10.5% HAS BEEN ACHIEVED (~15% WITH AR).

● REQUIRED THROUGHPUT FOR ECONOMICAL OPERATION APPEARS FEASIBLE AT THIS TIME.

ENCAPSULATION PROCESSING AND MANUFACTURING YIELD ANALYSIS

SPRINGBORN LABORATORIES, INC.

P. Willis

- ADD - ON ACTIVITY TO BASELINE
  CONTRACT ON DEVELOPMENT OF
  ADVANCED ENCAPSULATION MATERIALS
  (PHASE III)

- NOT YET FUNDED

GOALS:

- UNDERSTAND THE RELATIONSHIPS BETWEEN:

  - FORMULATION VARIABLES

  - PROCESS VARIABLES

- DEFINE CONDITIONS REQUIRED FOR OPTIMUM
      PERFORMANCE

- RELATE TO MODULE RELIABILITY

- PREDICT MANUFACTURING YIELD

- PROVIDE DOCUMENTATION TO INDUSTRY

PRECEDING PAGE BLANK NOT FILMED

C-6

Material Variables

LAMINATION POTTANTS
- ETHYLENE/VINYL ACETATE (EVA)
- ETHYLENE/METHYL ACRYLATE (EMA)

CASTING POTTANTS
- ALIPHATIC POLYURETHANE (PU)

ADHESIVES/PRIMERS
- THREE BASIC PRIMER SYSTEMS

COVER FILMS
- TEDLAR, ACYRLICS, FEP

FORMULATION VARIABLES:
 TYPE AND AMOUNT OF:

- CURING AGENTS (PEROXIDES)
- ANTIOXIDANTS
- ULTRAVIOLET SCREENERS
- ULTRAVIOLET STABILIZERS (HALS)
- SELF PRIMING AGENTS

 STORAGE CONDITIONS:
- TIME, TEMPERATURE, HUMIDITY, LIGHT
        AIR EXPOSURE
 QUALITY CONTROL:
- DETERMINE ANLYTICAL METHODS TO VERIFY
        COMPOSITION
- PUBLISH QC SPECIFICATIONS FOR MATERIAL
        CERTIFICATION

Process Variables

(VACUUM BAG LAMINATiON)

- AMBIENT CONDITIONS:
      TEMPERATURE
      HUMIDITY
      BAROMETRIC PRESSURE

- VACUUM PRESSURE (INITIAL) AND TIME
      OF EVACUATION

- TEMPERATURE - - RATE OF RISE

- TEMPERATURE - - ULTIMATE

- DWELL TIME, AT TEMPERATURE

- RATE OF COOLING

- TIME/TEMPERATURE/PRESSURE INTER-
      RELATIONSHIP

(CASTING LIQUID SYSTEMS)

ABOVE VARIABLES, PLUS:

- 2 COMPONENT MIX TIME

- DEGASSING PRESSURE

- PUMP AND FILL TIMES

- MIX UNIFORMITY

- GEL TIME

Quality and Performance Criteria

METHOD: • PREPARE TEST MODULES AND/OR OTHER TEST
            SPECIMENS WITH CHANGE IN SIGNIFICANT
            VARIABLE(S)

           • DETERMINE THE EFFECT

COMPONENT	CONDITION	TEST
POTTANT	ADEQUATE CURE	PERCENT GEL THERMAL CREEP
	TRAPPED BUBBLES	VISUAL
	DISCOLORATION	VISUAL
CELLS	BREAKAGE	VISUAL, RESISTANCE
	INTERCONNECT	RESISTANCE
	REGISTRATION	VISUAL
COVER FILMS	TEARS/PUNCTURES	VISUAL
	WARPING/SHRINKAGE	VISUAL
GLASS (SUPERSTRATE)	FRACTURE	VISUAL
ADHESION	BOND STRENGTH	PEEL TEST
	ENDURANCE	WATER SOAK (50°C)

- - - - - - - - - -

NEED TO DECIDE ON:

            • STANDARD TEST SPECIMEN(S)
            • STANDARD TEST PROTOCOL
            • UNIFORM DATA SETS

Data Analysis

- STATISTICAL ANALYSIS COMPLICATED BY LACK OF
    UNIFORMITY IN DATA TYPE

- TWO TYPES OF DATA:

DISCRETE (PASS/FAIL)	CONTINUOUS
CELL FRACTURE	GEL CONTENT
INTERCONNECT BREAKAGE	PEEL STRENGTH
TRAPPED BUBBLES	STABILIZER LOSS
THERMAL CREEP	
GLASS FRACTURE	

FOR CONTINUOUS DATA TYPES:

- TWO LEVEL FACTORIAL EXPERIMENTS
    (MOST INFORMATION, FEWEST EXPERIMENTS)

- NO. EXPERIMENTS = 2^K, K = NO. VARIABLES

- DETERMINES EFFECT OF SINGLE VARIABLE AT TWO LEVELS

- DETERMINES FACTOR INTERACTIONS (SEVERAL VARIABLES)

- PERMITS RANKING OF VARIABLES ACCORDING TO MAGNITUDE
    OF EFFORT

- LINEAR ANALYSIS POSSIBLE FOR SUBSEQUENT PREDICTIVE
    CAPABILITY

FOR DISCRETE DATA TYPES:

- PREPARE SCATTER PLOT VS. VARIABLE

- PLOT THE ZERO FAILURE LINE

- USE GRAPHICS TO SPECIFY BOUNDRY CONDITIONS AND
    ACCEPTABLE PROCESSING "WINDOWS"

- DETERMINE FAILURE PROBABILITIES - BINOMIAL DISTRIBUTION

Manufacturing Practice

DISCRETE VARIABLES

- PREPARE GRAPHICAL INTERPRETATION OF DATA
- DETERMINE "ZERO FAILURE" LINE
- DEFINE BOUNDRY CONDITIONS FOR DEFECT-FREE
  MANUFACTURING

EXAMPLE: CELL BREAKAGE

O = PASS
X = FAIL

RESIN
TEMPERATURE
(°C)

BACKFILL RATE
(MM HG/SEC)

ZERO FAILURE
LINE

VACUUM PRESSURE
(MM HG)
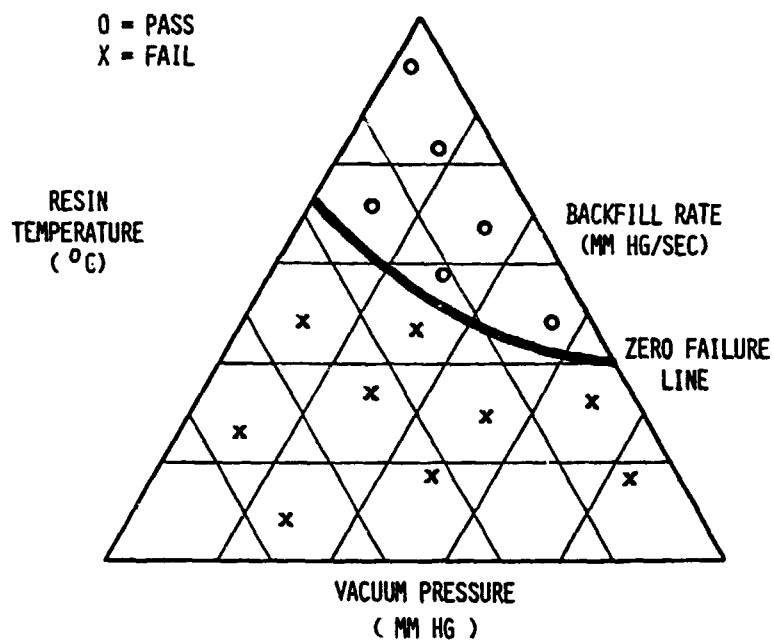
MANUFACTURING PRACTICE

CONTINUOUS VARIABLES

- GRAPHICAL PRESENTATION ALSO GOOD FOR CONTINUOUS VARIABLES

- PROVIDES BOUNDRIES FOR PROCESS/FORMULATION VARIABLES BASED ON CRITERIA OF ACCEPTABILITY

- EASILY USED IN MANUFACTURING PRACTICE

EXAMPLE: PERCENT GEL
(DEGREE OF CURE)

PROPERTY LINES
70%
60%
50%

TEMPERATURE
(°C)

DWELL TIME
(MINUTES)
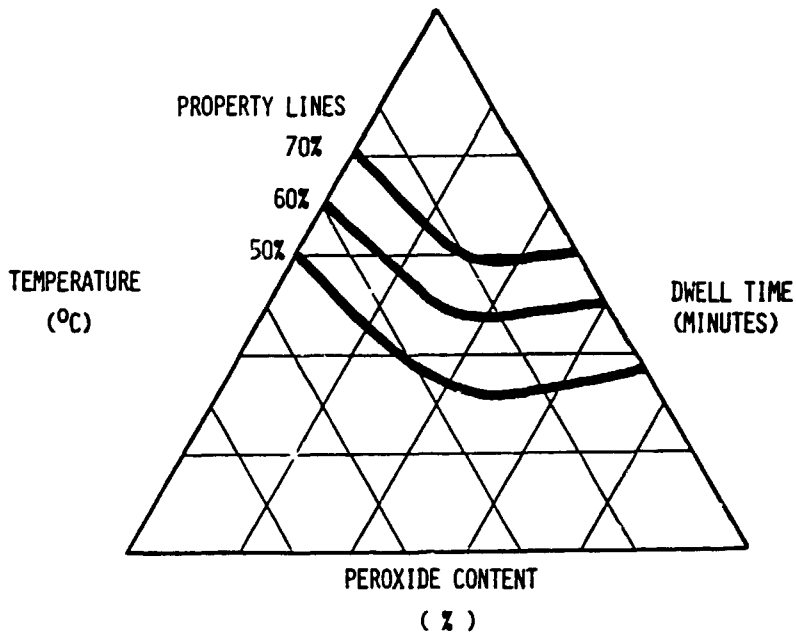
PEROXIDE CONTENT
(%)

Future Work

- IDENTIFY SIGNIFICANT VARIABLES
    - FORMULATION
    - PROCESSING

- DETERMINE MATERIALS SPECIFICATIONS
  AND QUALITY CONTROL METHODS

- ASSESS EFFECT OF VARIABLE(S) AND
  RANK ACCORDING TO IMPORTANCE

- DEFINE FORMULATION AND PROCESSING
  "WINDOWS" (ZERO FAILURE)

- CONVERT DATA TO PRACTICAL ENGINEERING
  FORMAT

- RELATE DATA TO MANUFACTURING YIELD
    - ASSIGN PROBABILITY OF FAILURE
    - NORMAL DISTRIBUTION (?)
    - WEIBUL (?)

- PREPARE TROUBLE-SHOOTING GUIDE:
  "WHAT'S WRONG IF . . . .?"

JPL Process Sensitivity Analysis

```
                    ┌──────────────────┐
                    │ DEFINE VARIABLES │
                    └──────────────────┘
          ┌──────────────┐      ┌──────────────┐
          │  PROCESSING  │      │   MATERIAL   │
          └──────────────┘      └──────────────┘
                    ┌──────────────────┐
                    │    DETERMINE      │
                    │   CRITERIA OF     │
                    │   PERFORMANCE     │
                    └──────────────────┘
                    ┌──────────────────┐
                    │  UNIFORM TEST     │
                    │   SPECIMEN(S)     │
                    └──────────────────┘
                    ┌──────────────────┐
                    │  UNIFORM TEST     │
                    │   PROTOCOL        │
                    └──────────────────┘
                    ┌──────────────────┐
                    │  UNIFORM DATA     │
                    │     SET           │
                    └──────────────────┘
```

DISCRETE DATA — PLOT DATA — RANK VARIABLES AND COFACTORS — BRACKETS AND BOUNDRIES — BERNOULLI PROBABILITY DISTRIBUTION — GRAPHICAL PRESENTATION

CONTINUOUS DATA — FACTORIAL EXPERIMENTATION — RANK VARIABLE(S) AND COFACTORS — BRACKETS AND BOUNDRIES — MULTIVARIATE ANALYSIS — GRAPHICAL PRESENTATION

ASSIGN PROBABILITY VALUES-REQUIRED CRITERIA

DETERMINE MANUFACTURING YIELDS

SILICON SHEET

Andrew D. Morrison, Chairman

Nine presentations were made covering research on Si shaped-sheet technology.

Westinghouse Electric Corp. reported on its work (experimental and modeling) to develop the dendritic-web process for making single-crystal silicon (Si) ribbon. Progress toward attaining the end-of-1984 goal of demonstrating a growth rate of at least 10 cm^2/min for ribbon lengths of at least 10 meters under conditions of constant melt level was described.

The Jet Propulsion Laboratory presented preliminary results of its in-house program on Si ribbon stress/strain modeling and plans for Si properties measurement.

The University of Kentucky reported on its work to analyze stress/strain relationships in Si ribbon. Results of calculations of conditions for onset of buckling were reasonably consistent with experimental observations.

Mobil Solar Energy Corp. described results of stress studies of ribbon produced by the edge-defined film-fed growth (EFG) method, and results of studies on electrical characterization of defects in stressed float-zone, Czochralski, and EFG Si.

The University of Illinois at Chicago reported on its program to measure residual stresses in sheet Si by interferometry and to investigate abrasion and wear mechanisms in Si.

The Massachusetts Institute of Technology described progress in a study of high-speed inclined growth of Si sheet . The formulation of a model for finite-element analysis of inclined-meniscus growth was discussed.

Energy Materials Corp. reported on technology development of a low-angle Si sheet (LASS) growth process. The work addressed achieving controlled melt circulation to suppress natural convection; microstructural and electrical evaluations of LASS material were also performed.

The Solar Energy Research Institute reported on a solid-melt interface study that was completed, and also on a recently started program to study the sheet-material requirements for high-efficiency Si solar cells. Development of lifetime measurement techniques that will be used to evaluate the material is under way.

SILICON DENDRITIC WEB GROWTH

WESTINGHOUSE ELECTRIC CORP.

S. Duncan

Technology	Report Date
Single crystal ribbon growth	10/3/84

Approach	Status
Silicon dendritic web growth **Contractor** Westinghouse Electric Corp. Advanced Energy Systems Division JPL Contract 955843	• 6 ½ meters of uninterruped, continuously melt replenished web growth has been achieved with three different growth configurations • Steady-state web growth of 8 cm²/min has been achieved • Major improvement in web growth reproducibility has been achieved • Concepts for higher growth rate have been developed

Goals	
For 1984 • Demonstrate 10 meter length of continuously melt replenish web crystal growth • Demonstrate 10 square centimeters per minute steady-state web growth	

Principal Activities This Period

- **Grow Long Web Crystals From Continuously Replenished Melt**

- **Develop Temperature Distribution In Web And Melt**

- **Improve Reproducibility Of Growth**

- **Develop Configurations For Increased Growth Rates (Width And Speed)**

- **Develop New Growth System Components As Required For Improved Growth**

- **Evaluate Quality Of Web Grown**

PRECEDING PAGE BLANK NOT FILMED

Continuously Melt-Replenished Web Growth

Three Web Growth Configurations Have Achieved Long Growth (Approx. 6 Meters)

J435   (3.3 cm width)

J460L   (/ ! cm width)

J460LS   (5.1 cm width)

Critical Regions of Temperature Distribution
in Silicon Web Growth

- Between Crucible Compartments
  (Growth And Melt Replenishment Compartments)

- Within The Growth Compartment

- Vertical Profile Within The Growing Web

- Horizontal Profile Within The Growing Web

Melt Temperature Distribution

$T_M + 14$ —
$T_M + 4$ —
T_M —

$\vdash \Delta T \dashv$

Required $\longrightarrow$

$\Delta T = 0.4 \pm 0.2°C$
$\Delta T = 1.2°C$
$\Delta T = 2.5°C$
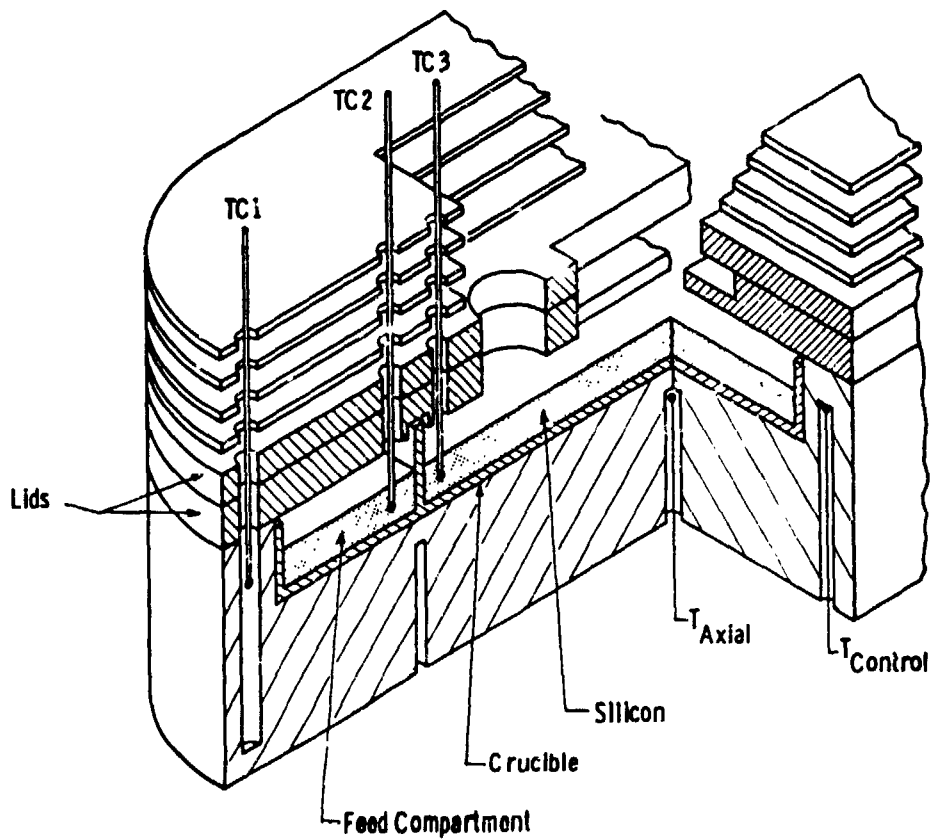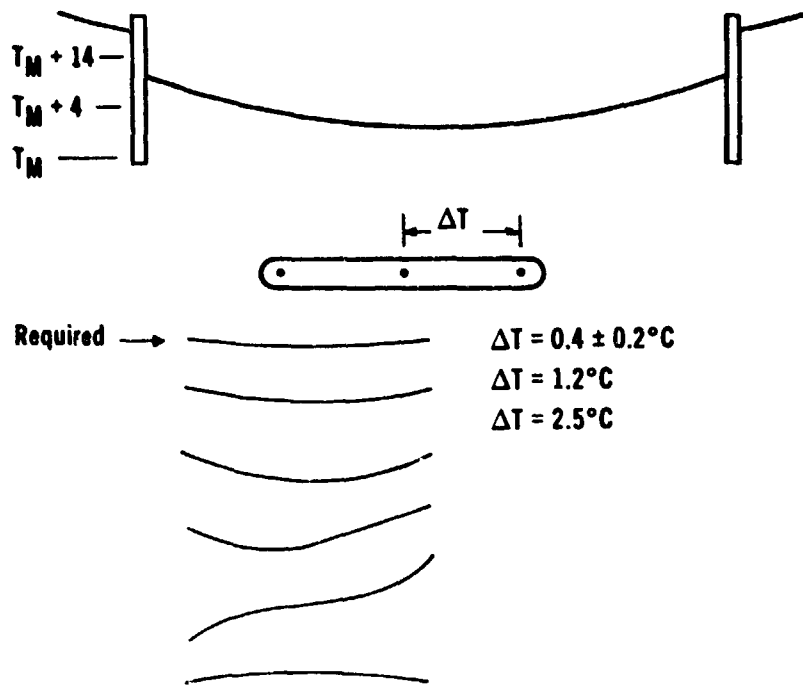
Principal Methods for Control of Melt Temperature Distribution

- Stationary Shield Configuration

- Dynamically Positionable Shield Configuration

- Dynamically Positionable Work Coil

- Design Of The Barrier Which Separates Crucible Compartments

Susceptor Shields

For Control Of Melt Temperature Distribution Includes Both Fixed And Adjustable Shields
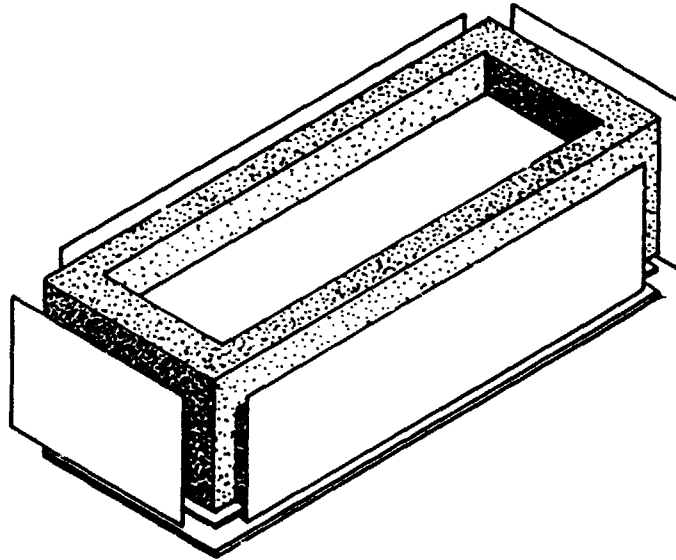
Temperature Distribution Within the Growing Web

- **Determined By Design Of The Susceptor L.ds And Top Shields**

- **Predicted By Computer Model**

- **Lid And Shield Temperatures Measured In Growth System**

Reproducibility of Web Growth

Improvements This Period

- Crucible Re-Designed For Better Susceptor Fit And Improved Thermal Transfer

- Rectangular Work Coil Fabricated With Precision Dimensions

- Perimeter Shields Re-Designed For Reproducible Spacing

- Mated Parts Fitted For Uniform Thermal Transfer

Configurations for Increased Growth Rates
(Width and Speed)

- Concepts Are Generated Through Computer Modeling

- Initial Design Specification Derived From Models

- Design Is Verified Through Experimental Web Growth

- Experimental Web Growth And Measurements Provide Data For Additional Input To Model

Growth System Component Development

Major Examples Of Component Development In This Reporting Period:
New Crucibles
Improved Crucible Barriers
New Induction Heating Work Coils
New Furnace Cover Plate For Higher Growth Rate
Improved Feeder For Polysilicon Pellets
Thermal Elements For New Growth System Designs
Instrumentation For Monitoring Dendrite Thickness
(Incomplete)

Web Quality Evaluation

Sources

From This Program

- Residual Stress Via Web Split Width Measurements
- Dislocation Density Via Etch Pit Counting
- Defect Type, Distribution And Structure Via X-Ray Topography

From Associated Programs

- Impurity Evaluation
- Electrical Properties
- Solar Cell Data

WEB SAMPLES FOR STRUCTURE ANALYSIS
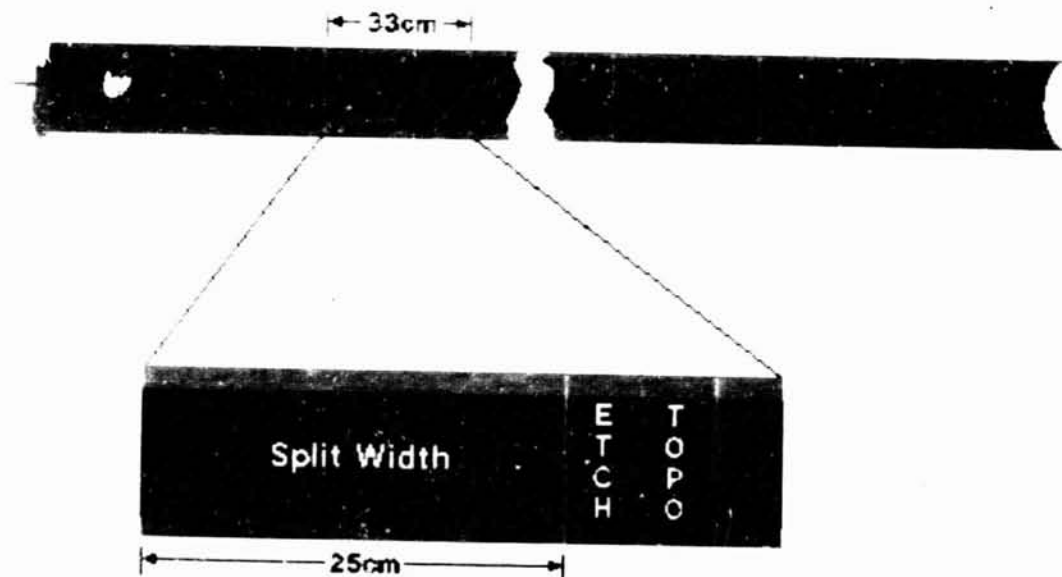
J435 Lid Configuration
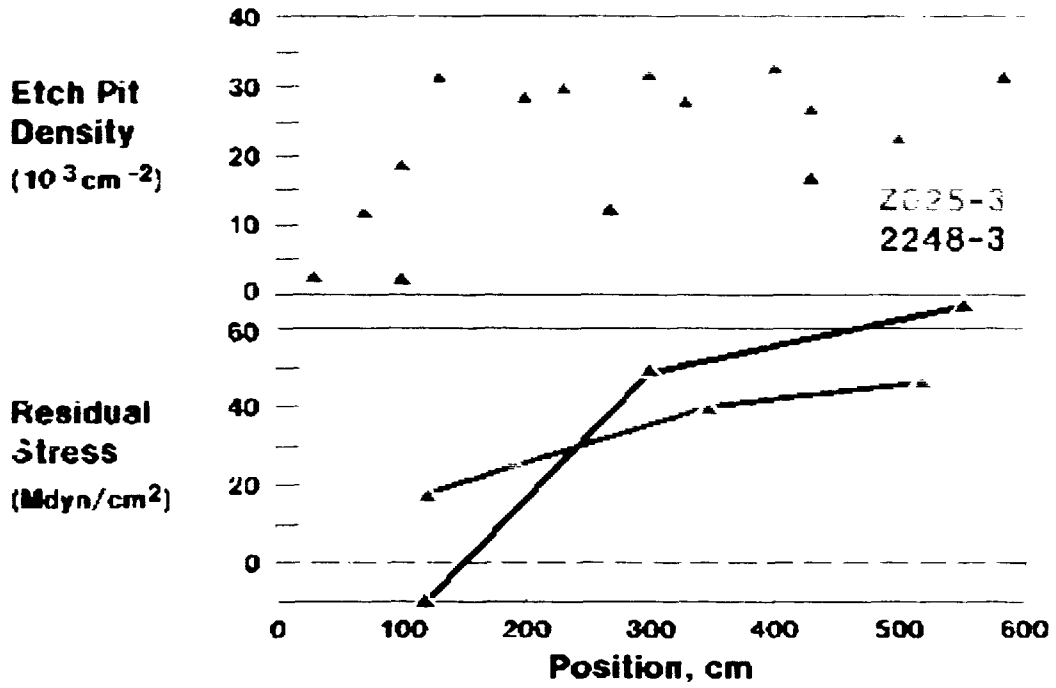
J460 Lid Configuration
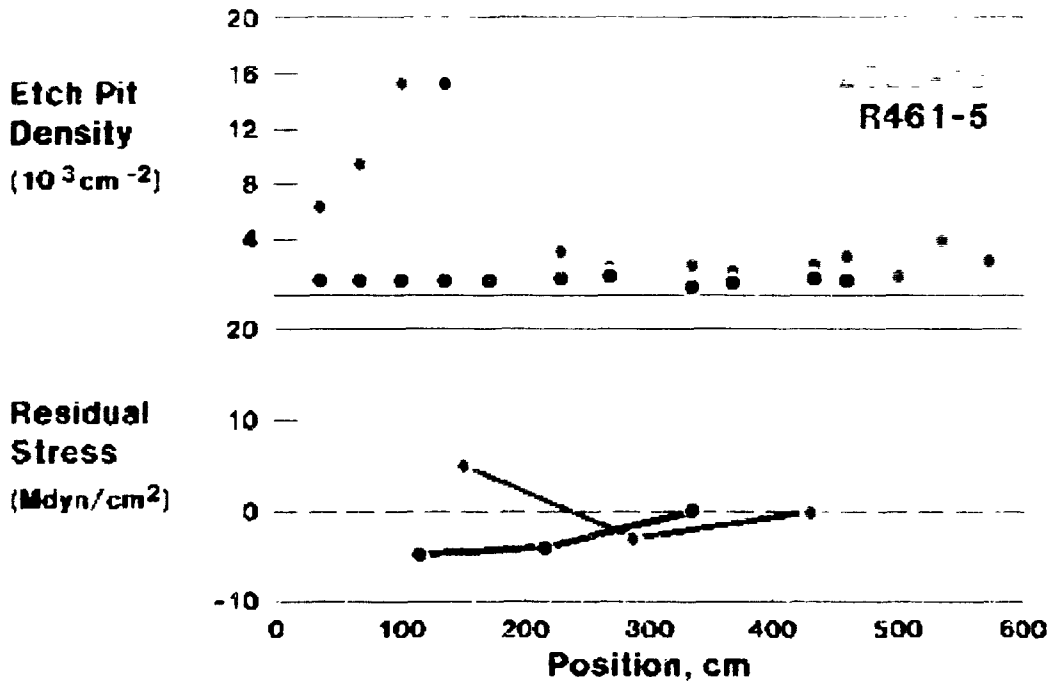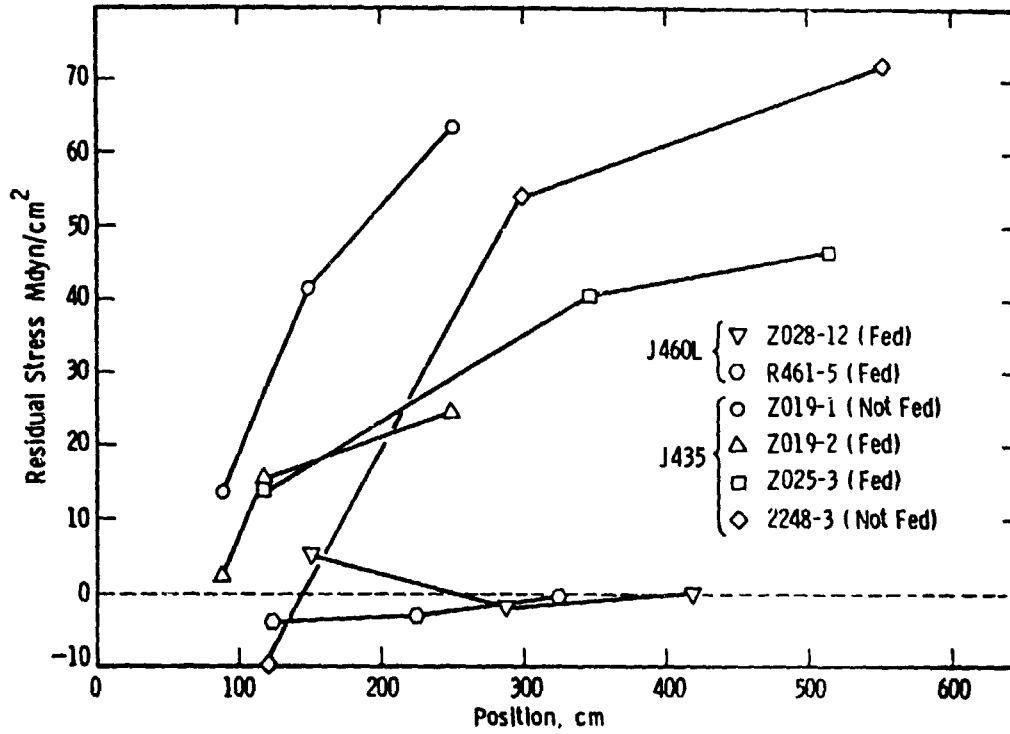
Problems and Concerns

Calendar Schedule Of Goals Is Tight

Summary

- **Technology And Direction Of Development Sufficient To Surpass Goals When Fully Developed**

- **Major Improvement Achieved In Length Of Continuously Melt Replenished Crystal Growth**

TEMPERATURE-STRESS MODELING

WESTINGHOUSE ELECTRIC CORP.

R. Seidensticker

Overall Goals

- Develop Higher Throughput Systems
- Clarify Limitations on Ultimate Throughput

Current Work

- Temperature/Stress Fields near Growth Front
- Effects of Lateral Temperature Gradients
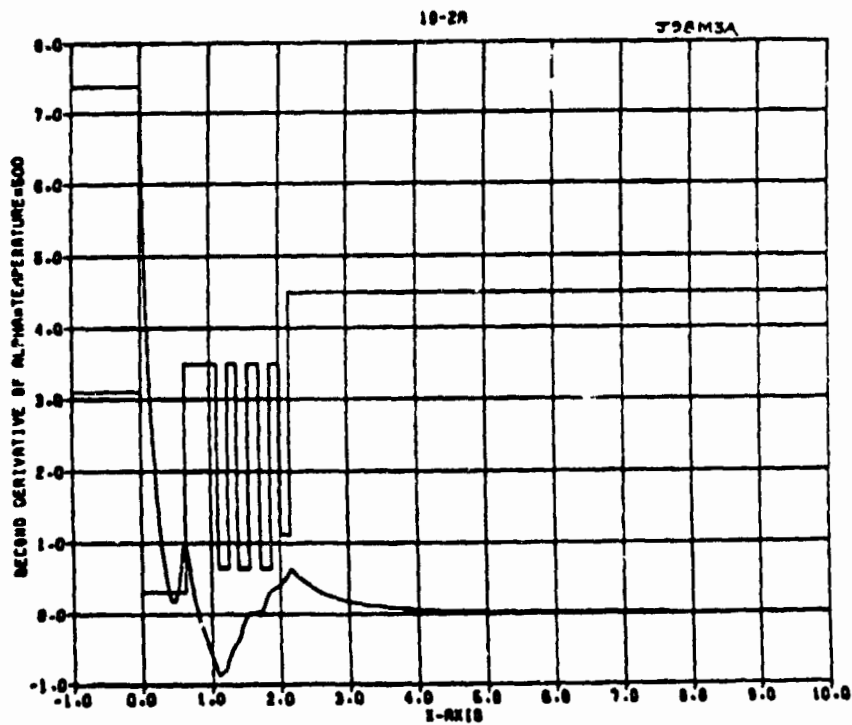
PRECEDING PAGE BLANK NOT FILMED
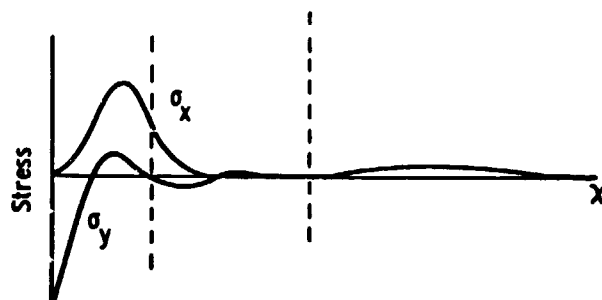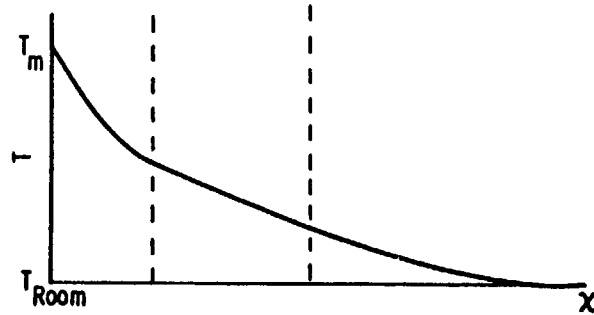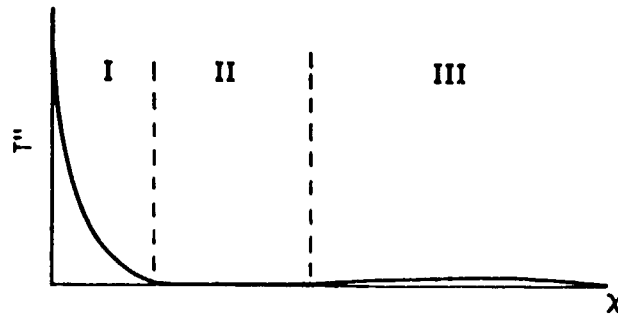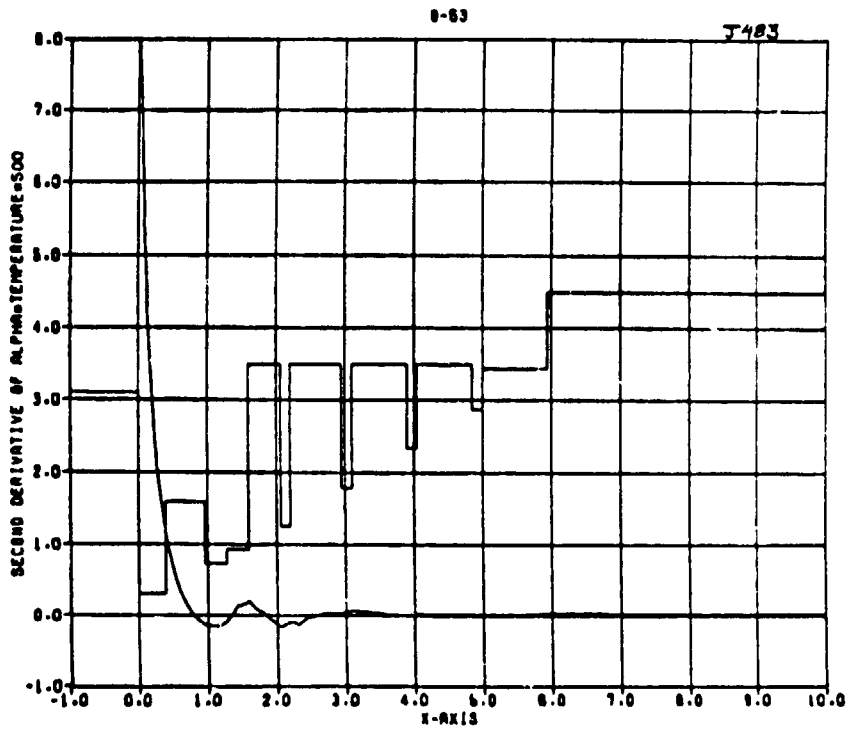
484

Dependence of σ_y at Interface on A/B; w = 1.35 cm
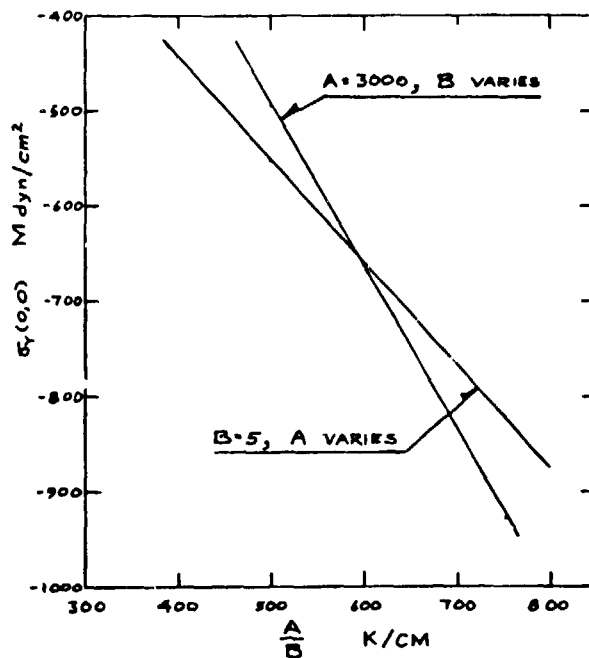
Stress Fields at Growth Front

Model Representation

$$T(x) = \frac{A}{B^2} \exp(-Bx) + Cx + D$$

$$T''(x) = A \exp(-Bx)$$

$$T'(0) = -\frac{A}{B} + C$$

Results:

**Stress fields depend on A and B
but _not_ on C and D**
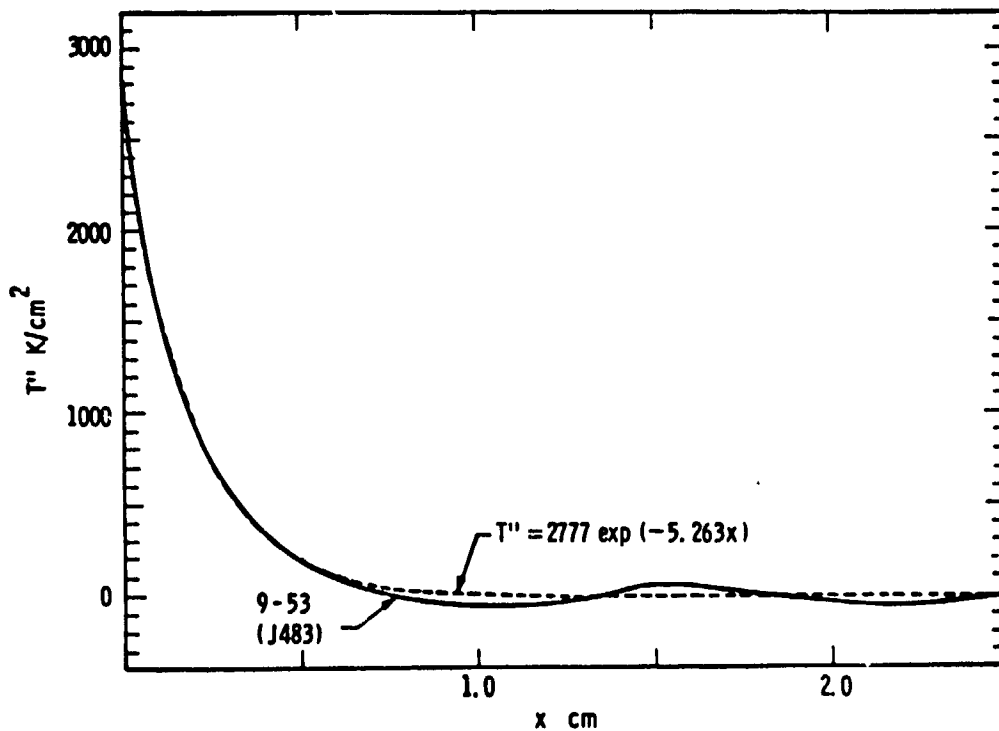
Lateral Temperature Variation

With Dr. R. F. Sekerka

Causes:

1. Variation in thermal environment across width of web
2. Variation in cross section across width of web

Modeling Representation

$$T(x,y) = T(x)\, g(y)$$

where

$$T(x) = \frac{A}{B^2}\exp(-Bx) + Cx + D$$

and

$$g(y) = \frac{1 + c_n(y/w)^n}{1 + c_n/(n + 1)}$$

where w = ribbon half width

$c_n > 0$ concave upward (smiling)

$c_n < 0$ concave downward (frowning)

$n = 2$ quadratic case

$n = 4$ quartic case

486

Temperature Profile at X = 0
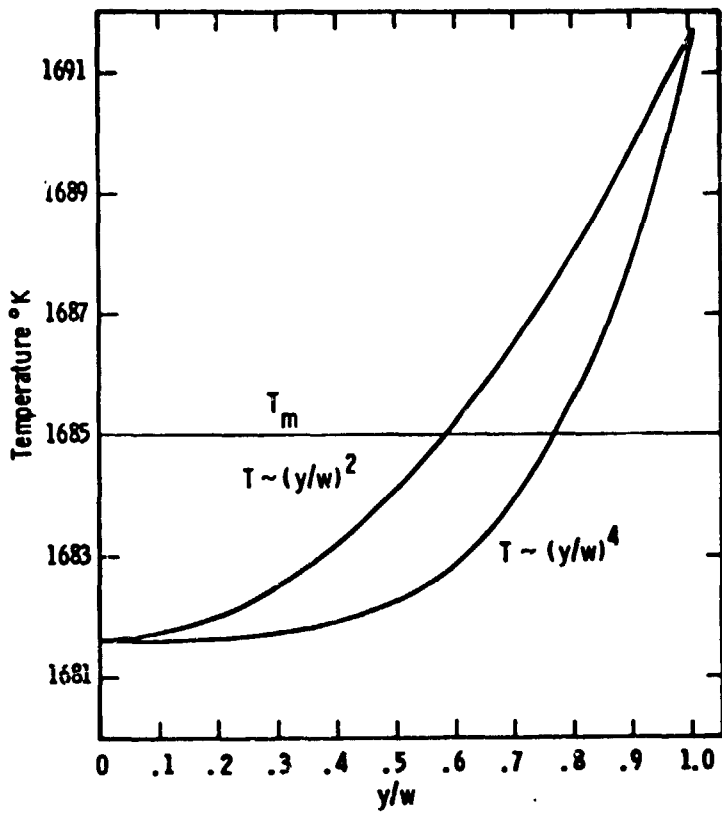
Interface Shape for Curved Isotherms
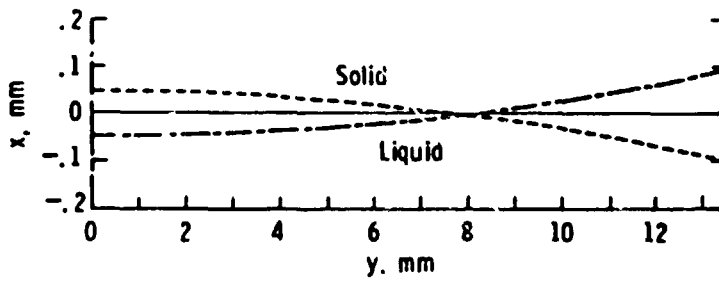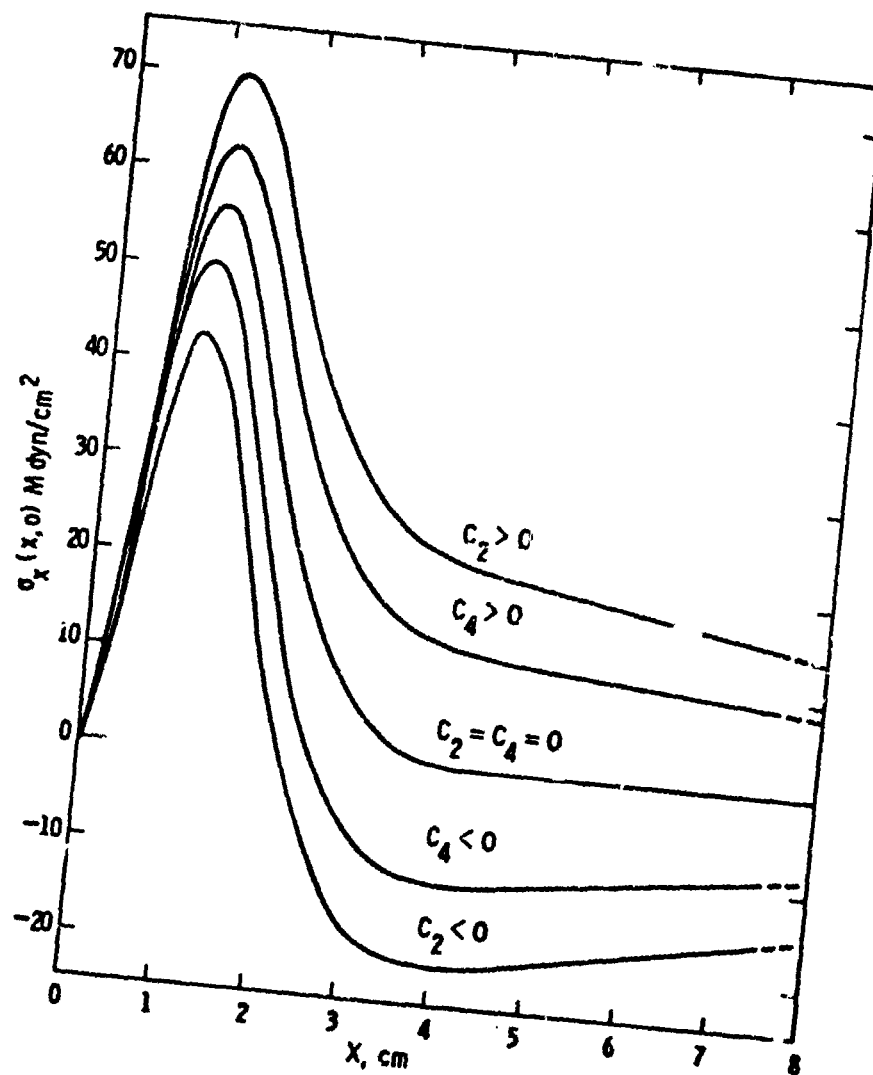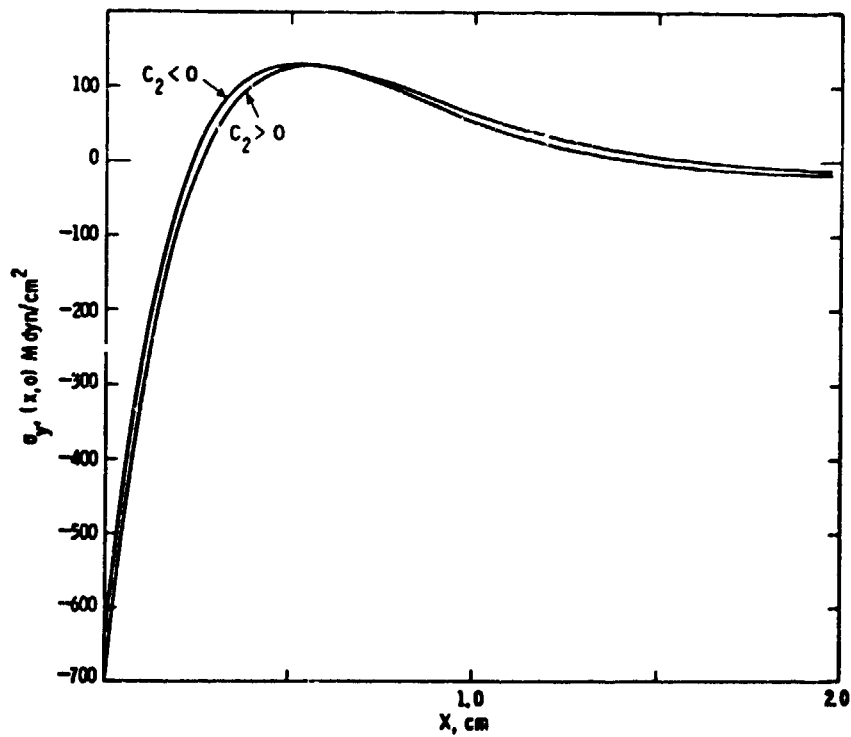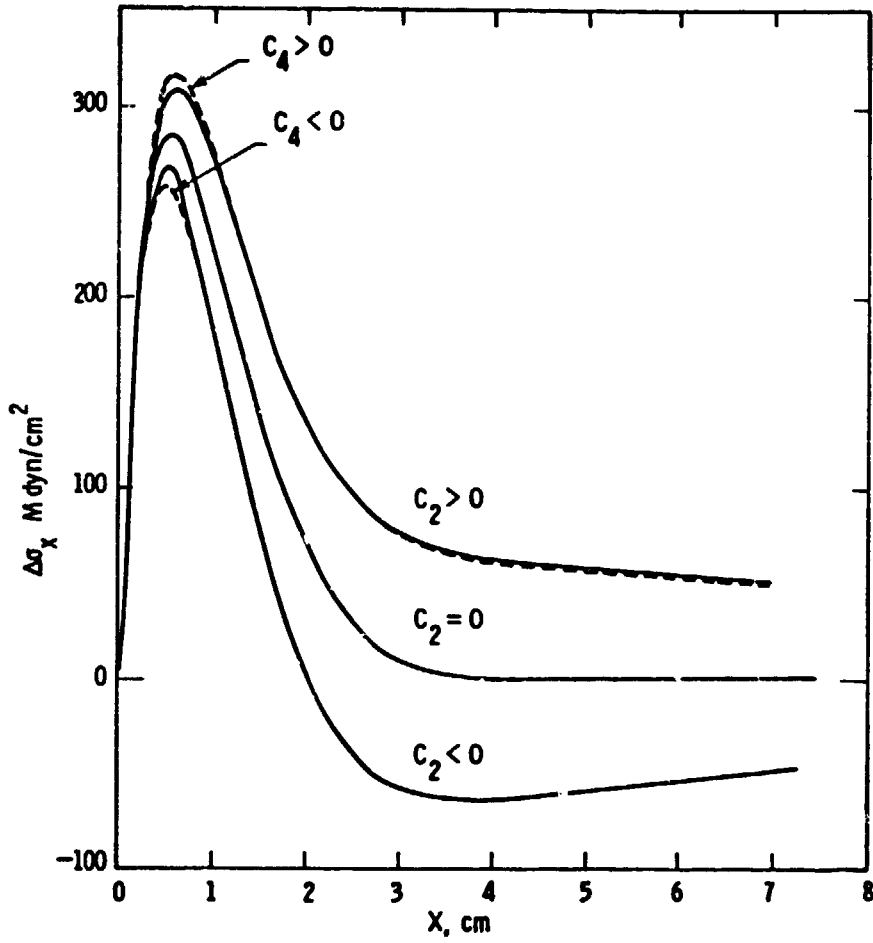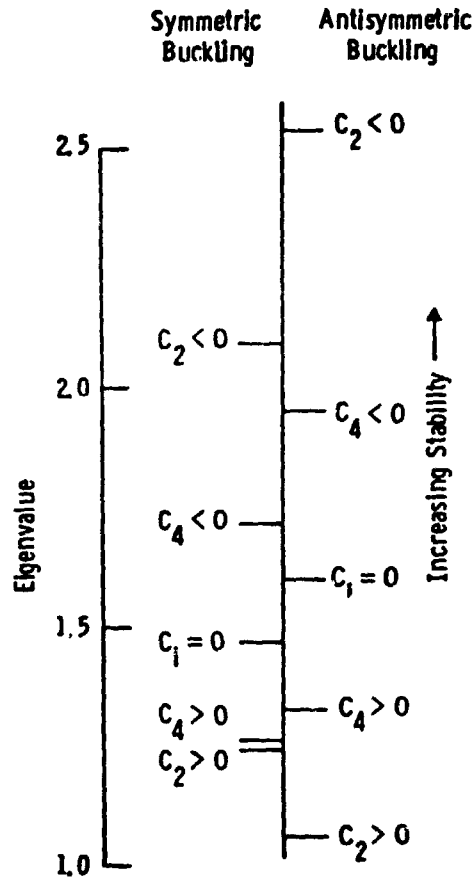
Lateral Temperature Variation: Summary

"Frowning" Isotherms:

- Inhibit buckling

- Should not affect residual stresses

The J460L configuration has been modified to produce more frowning" isotherms in the web

SILICON RIBBON STRESS-STRAIN ACTIVITIES

JET PROPULSION LABORATORY

B.K. Wada
C.F. Shih
C.P.Kuo
W.M. Phillips

Objective

PRESENT PRELIMINARY RESULTS

* STRESS - STRAIN

* MATERIAL PROPERTIES

Ultimate Goal

• ULTIMATE GOAL -ANALYTICAL SIMULATION

INFLUENCE OF
• GEOMETRY, NONAGON, ...
• SPEED, VELOCITY, TRANSIENT
• TEMPERATURE PROFILE, TRANSIENT
• GROWTH METHOD
• FORCES, GRAVITY, SUR. TEN,...
• PRODUCTION

ON

• RESIDUAL STRESS
• DEFORMATION
• EFFICIENCY
$$= \int_A c_{ij}\, dA$$
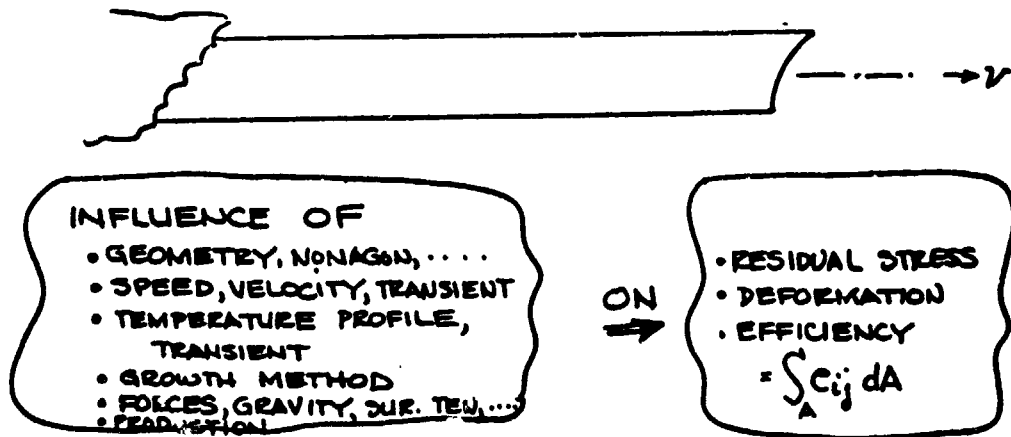
• VALUABLE FOR
   • LOWER COST, LOWER YIELD
   • HIGH EFFICIENT CELLS

JPL Stress-Strain Effort

* USE EXISTING FINITE ELEMENT CODES
    * FLEXIBILITY IN GEOMETRY
* TWO APPROACHES

I. QUASI-STATIC NASTRAN DR. C-F SHIH	II. IN-PROCESS GROWTH ANSYS DR. C. P. KUO

* TOTAL PROBLEM
    * STRESS, BUCKLING, MATERIAL NON-LINEARITY, CREEP, IMPERFECTION -----> WHAT'S CRITICAL?
    * PARAMETRIC STUDY -----> VARY ENGINEERING PARAMETERS
        * -----> SUPPORT PROJECT

Quasi-Static

In-Process Growth

- (1) ▢   (2) ▭ . . . . (n) ▭■

- MATERIAL PROP = $f(T, \sigma_{ij}, \dot{\epsilon}_{ij}, t)$

σ vs t, x

σ_1
σ_2
σ (QUASI - STATIC)
σ_3
σ_i
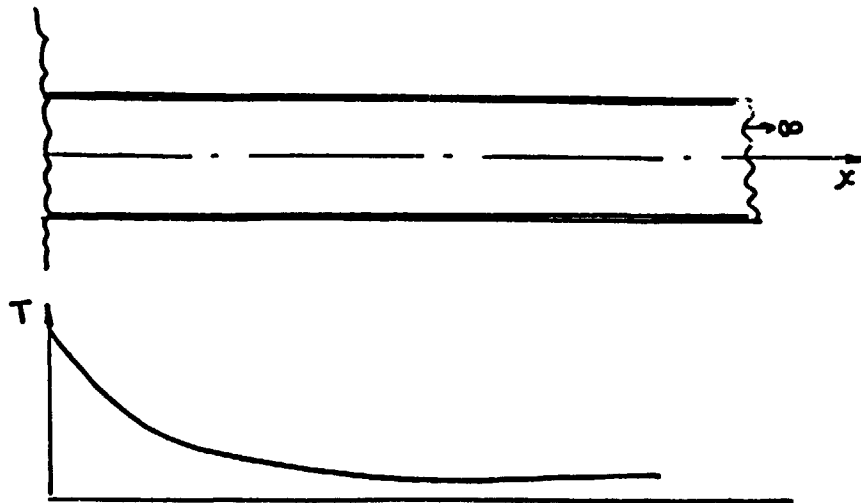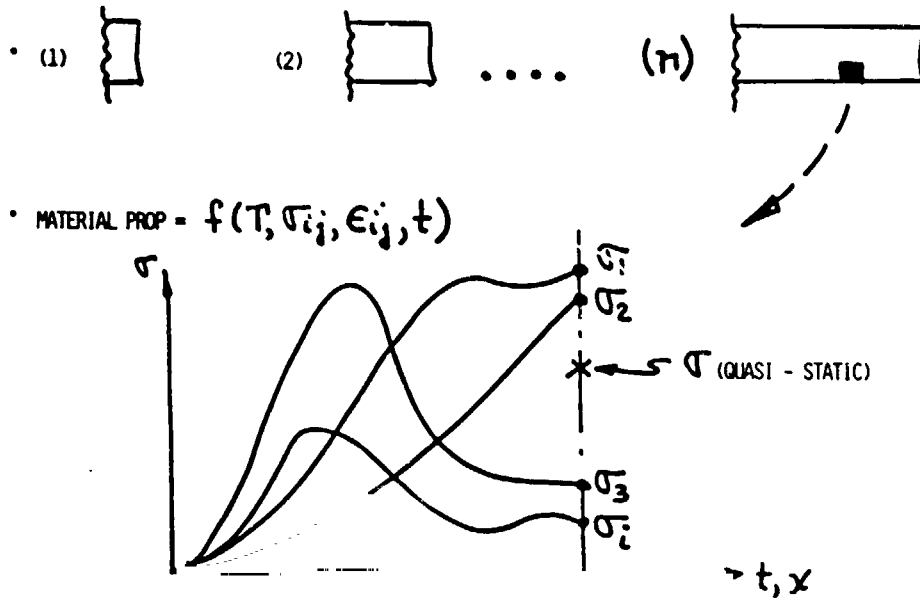
Failure Considerations

- HIGH FINAL RESIDUAL STRESS --------> HANDLING PROBLEMS

- HIGH IN-PROCESS RESIDUAL STRESS --------> DISLOCATIONS ------> LOW EFFICIENCIES

- BUCKLING -------> DEFORMED PRODUCTS --------> INSTALLATION -------> BREAKAGE

Temperature Profile

$$\otimes : T(x) = 1620 - 260x + 10x^2 \quad (x \leq 10)$$
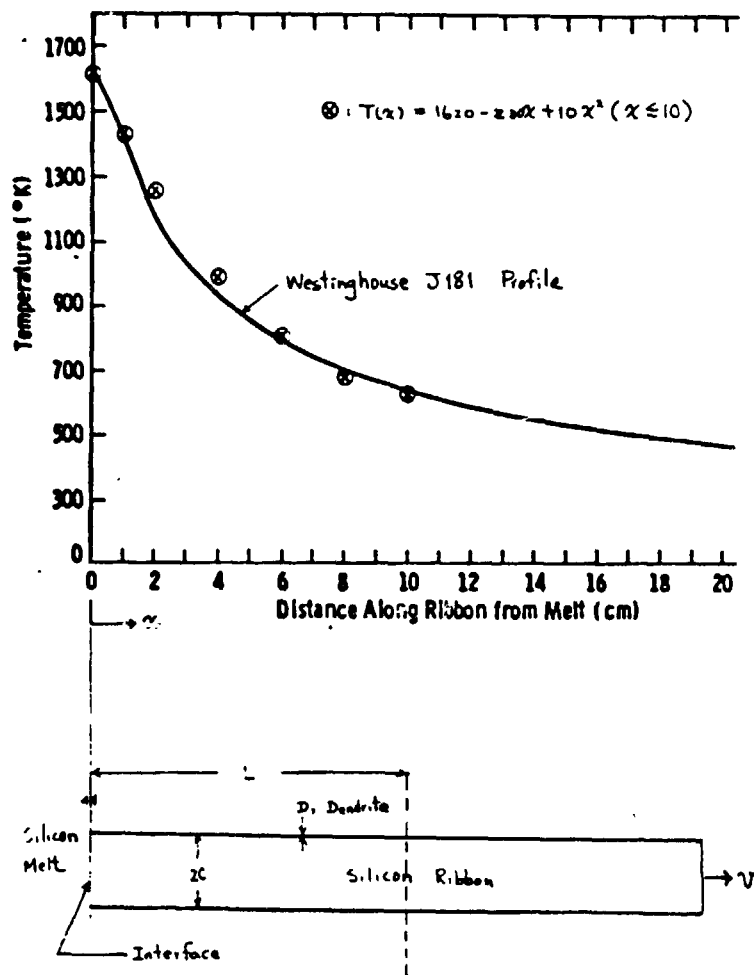
Finite Element Model of 4 × 2 in. Silicon Ribbon

A-A Cross Section
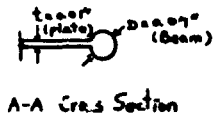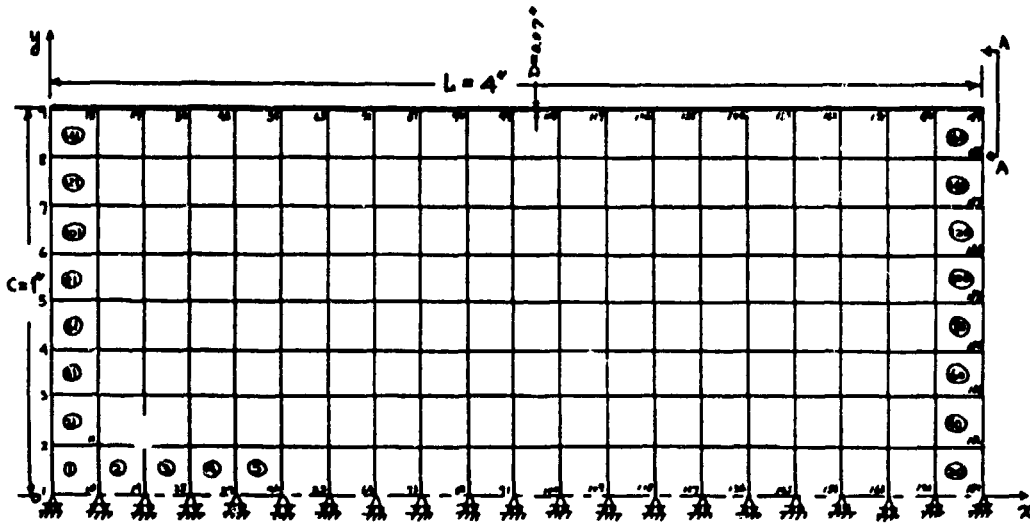
Elastic Constant as a Function of Temperature (Burenkov)

Scatter plot with vertical axis "Elastic Constant, E (10^6 Psi)" ranging from 19 to 23, and horizontal axis "Temperature (°C)" ranging from 200 to 1400.
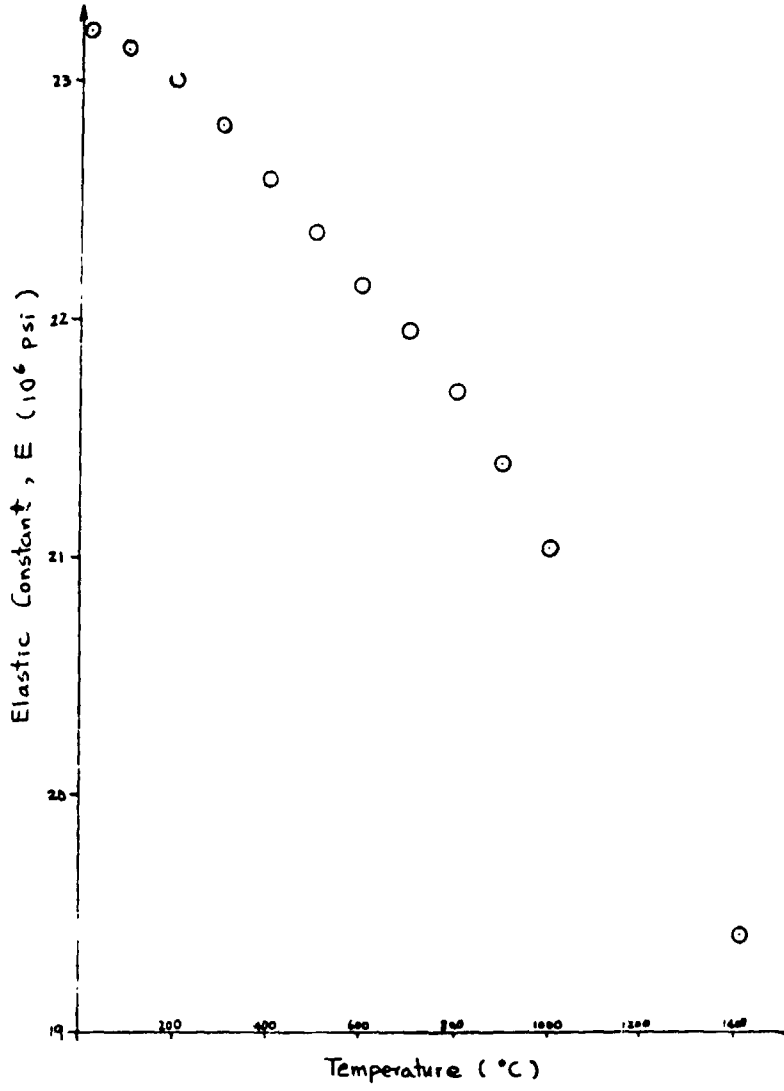
Stress Contours and Their Corresponding Stress Levels
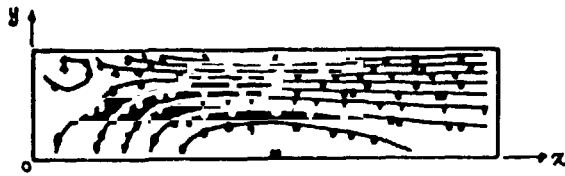
Fig. 3a X-X Normal Stresses

No.	σ_{xx} (Psi)
1	-3.017454E-03
2	-2.202389E+03
3	-1.387321E+03
4	-5.722522E+02
5	2.426183E+02
6	1.057685E+03
7	1.872053E+03
8	2.864322E+03
9	3.503099E+03
10	4.318159E+03

Fig. 3b Y-Y Normal Stresses

No.	σ_{yy} (Psi)
1	-1.064383E+04
2	-9.196611E+03
3	-7.729086E+03
4	-6.273180E+03
5	-4.816466E+03
6	-3.359740E+03
7	-1.903082E+03
8	-4.463157E+02
9	1.010403E+03
10	2.467187E+03
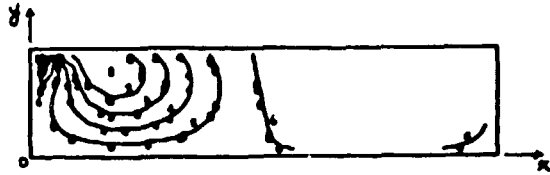
Fig. 3c X-Y Shear Stresses

No.	σ_{xy} (Psi)
1	-2.400780E+03
2	-1.914588E+03
3	-1.428297E+03
4	-9.420589E+02
5	-4.558147E+02
6	3.042651E+01
7	5.164677E+02
8	1.032989E+03
9	1.469135E+03
10	1.975391E+03

L = 4 in., c = 1 in., t = 0.01 in., D = 0.07 in.
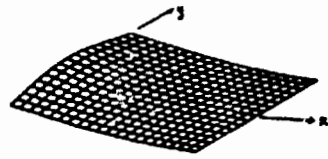
1st Mode
$\lambda_1 = 0.2126$
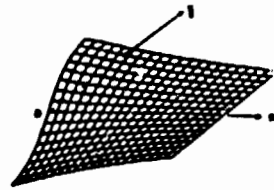
2nd Mode
$\lambda_2 = 0.2281$

Multiplier factors
stress used for
buckling. To obtain
buckling stress, change
1 until $\lambda = 1.0$.
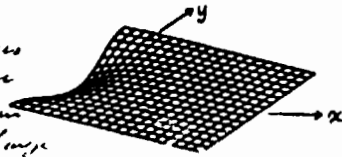
3rd Mode
$\lambda_3 = 0.3987$

4th Mode
$\lambda_4 = 0.7289$

5th Mode
$\lambda_5 = 1.1649$

First Five Buckling Modes of EFG Ribbon (D = 0.0 in.)
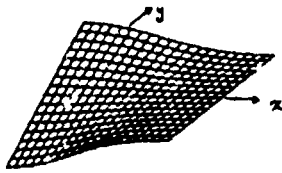
1st Mode
$\lambda_1 = 0.3632$
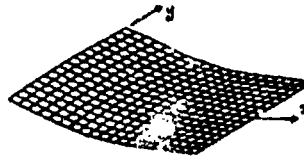
2nd Mode
$\lambda_2 = 0.3786$
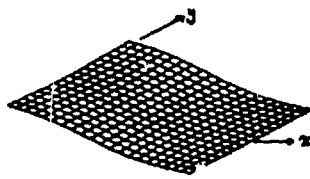
3rd Mode
$\lambda_3 = 0.5142$

4th Mode
$\lambda_4 = 0.5479$
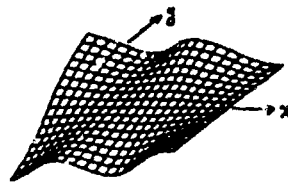
5th Mode
$\lambda_5 = 0.7762$

Buckling Mode (D = 0.035 in.)
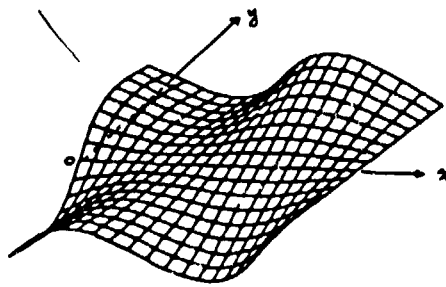
Buckling Mode Shapes at Melt Interface (x = 0) and Their Corresponding Eigenvalues
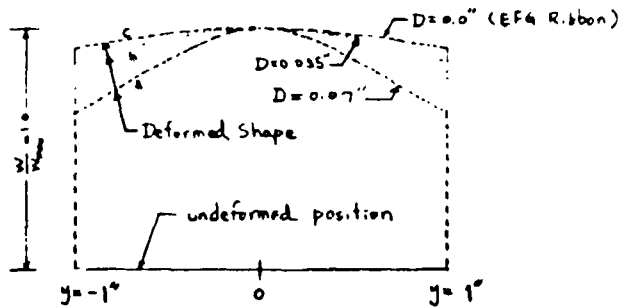
a. $\lambda_1 = 0.2126$ (1st mode)
b. $\lambda_1 = 0.3289$ (1st mode)
c. $\lambda_1 = 0.3786$ (2nd mode)
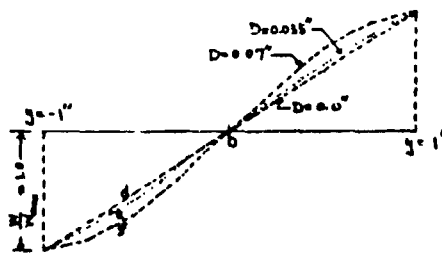
d. $\lambda_1 = 0.3632$ (1st mode)
e. $\lambda_2 = 0.3964$ (2nd mode)
f. $\lambda_2 = 0.2281$ (2nd mode)

Dendrites Effect

	D = 0.07"	D = 0.035"	D = 0.0"
σ_x	−3017 psi	−5011 psi	−6043 psi
	+4318 psi	+3792 psi	+3396 psi
$\Delta\sigma_x$	7335 psi	8803 psi	9439 psi
σ_j	−10643 psi	−5990 psi	−4997 psi
	+2467 psi	+1648 psi	+1450 psi
$\Delta\sigma_j$	13110 psi	7638 psi	6447 psi
λ_1	0.213	0.329	0.363
λ_2	0.228	0.396	0.379

λ increases as σ_j (compression) decrease

SILICON SHEET

Influence of Young's Modulus (Sylwestrowica)
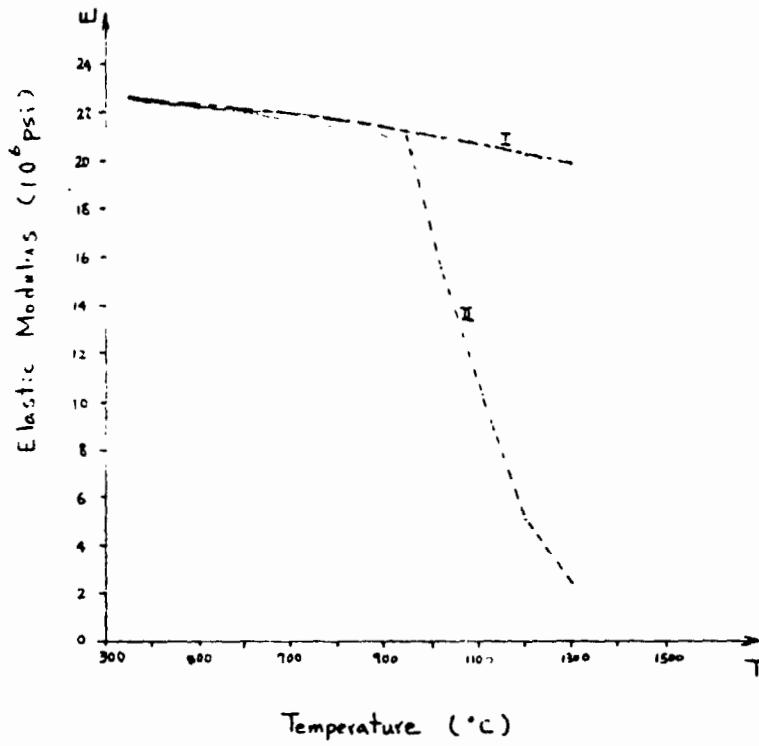
Temperature (°C)

	E_I	E_{II}
σ_{xx}	-3017 psi	-2666 psi
	$+4318$ psi	$+3805$ psi
σ_{yy}	-10643 psi	-3828 psi
	$+2467$ psi	$+1818$ psi
λ_1	0.213	0.085
λ_2	0.228	0.109

502

Buckling Mode Shapes at Melt interface (x = 0) and Their Corresponding Eigenvalues
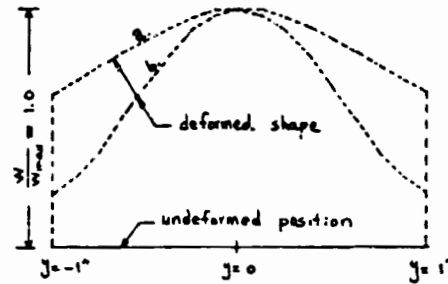
a. $\lambda_1 = 0.2126$ (model in ref. 1) E_I

b. $\lambda_1 = 0.0849$ (Current Model) E_{II}

Finite Element Model of 8 in. × 2 in. Silicon Ribbon

Temperature Profile

$\odot$: $T(x) = 1630 - 20x + 10x^2$ $(x \leq 10)$

$\square$: Linear Interpolation between $x = 10$ cm. and $x = 20$ cm.

Westinghouse J181 Profile

Temperature (°K) — vertical axis: 1700, 1500, 1300, 1100, 900, 700, 500, 300, 0

Distance Along Ribbon from Melt (cm) — horizontal axis: 0, 2, 4, 6, 8, 10, 12, 14, 16, 18, 20

$\longrightarrow x$
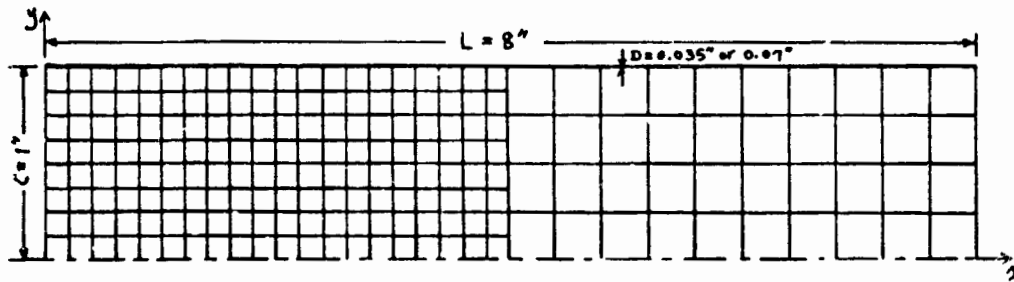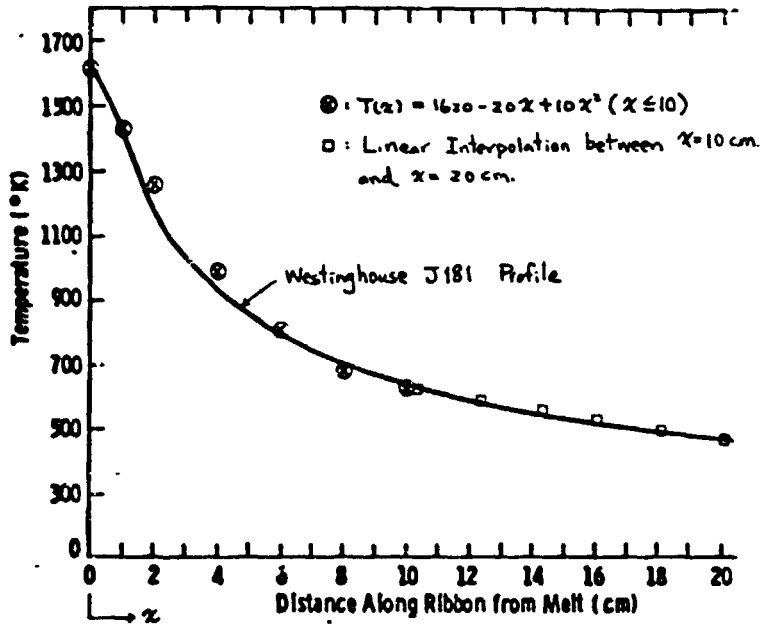
	D = 0.07"	D = 0.035"	D = 0.0"
σ_x	−3017 psi (−2967 psi) +4318 psi (+4245 psi)	−5011 psi (−5315 psi) +3792 psi (+3787 psi)	−6043 psi +3396 psi
$\Delta\sigma_x$	7335 psi	8803 psi	9439 psi
σ_y	−10643 psi (−10644 psi) +2467 psi (+2505 psi)	−5990 psi (−5994 psi) +1648 psi (+1650 psi)	−4997 psi +1450 psi
$\Delta\sigma_y$	13110 psi	7638 psi	6447 psi
λ_1	0.213 (0.147)	0.329 (0.311)	0.363
λ_2	0.228 (0.249)	0.396 (0.393)	0.379
λ_3	0.399 (0.420)	0.730 (0.707)	

λ increases as σ_y (compression) decrease

504

Temperature Profiles Across the Ribbon Width
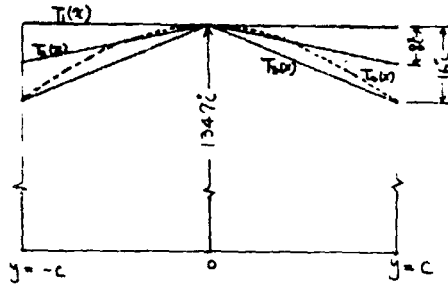
Eigenvalues for Corresponding Temperature Profile Acting on a Dendritic Web (D = 0.07 in)

Mode No.	$T_1(x)$	$T_2(x,y)$	$T_3(x,y)$	$T_4(x,y)$
1st	0.2126	0.2150	0.2174	
2nd	0.2281	0.2644	0.2695	0.2705
3rd	0.3987	0.4645	0.4751	0.4751
4th	0.7289	0.7685	0.7853	

Eigenvalues of EFG Ribbon (D = 0.0 in.) Subjected to Two Temperature Profiles

Mode No.	$T_1(x)$	$T_3(x,y)$
1st	0.3632	0.4116
2nd	0.3786	
3rd	0.5142	0.5868

Eigenvalues of EFG Ribbon With Constant Material Properties

Mode No.	$T_1(x)$	$T_2(x,y)$	$T_3(x,y)$
1st	0.632	0.714	0.821
2nd	0.664	0.759	1.112

505

Temperature Profiles Along the Ribbon Length
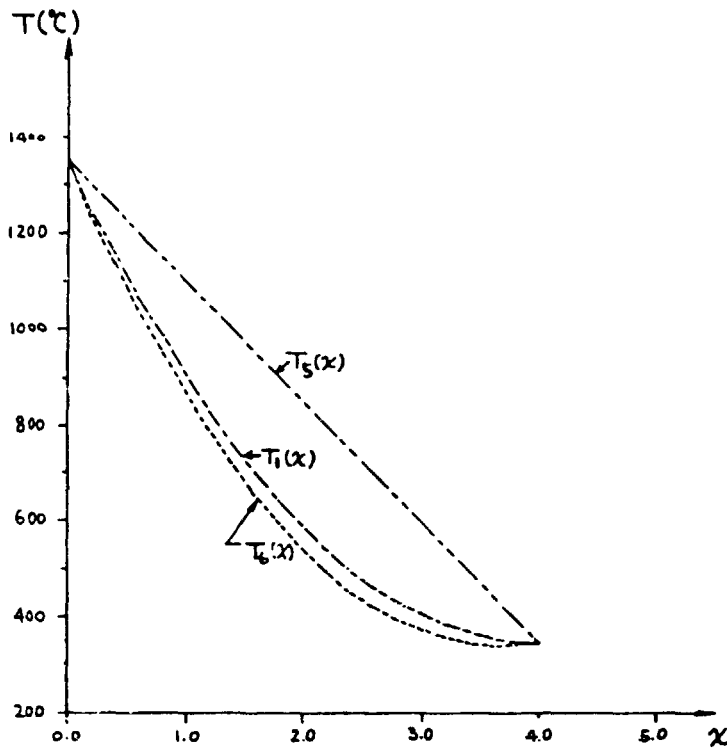
Eigenvalues of a Dendritic Web (D = 0.07 in.) Subjected to Two 1-D Temperature Profiles

Mode No.	$T_1(x)$	$T_5(x)$	$T_6(x)$
1st	0.2126	0.295	0.204
2nd	0.2281	0.466	0.244
3rd	0.3987	0.929	0.429
4th	0.7289		

Eigenvalues of Ribbons Subjected
to Linear Temperature Profile

Mode No.	Dendritic Web $D=0.07$; $\alpha(T); E(T)$	Dendritic Web α, E are uniform	EFG Ribbon $D=0.0$; $\alpha(T), E(T)$
1	0.295	0.406	0.566
2	0.466	0.753	0.581
3	0.929		1.087

Summary: Linear Buckling Analysis

1. σ_y PLAY AN IMPORTANT PART IN THE RIBBON BUCKLING PROBLEM.

2. $\Delta\sigma_x$ IS NOT AN ADEQUATE DESIGN PARAMETER.

3. BUCKLING MODE INCLUDES BOTH BEAM TYPE AND PLATE TYPE.

4. DENDRITES AFFECT THE THERMAL STRESSES AS WELL AS THE BUCKLING ANALYSIS.

5. $L = 4''$ MODEL PROVIDES SUFFICIENTLY GOOD RESULTS.

6. NEED MORE RELIABLE DATA OF $E(T)$ FOR $1000°C < T < 1400°C$.

7. EFFECT OF TEMPERATURE VARIATION ACROSS THE RIBBON WIDTH IS MORE SIGNIFICANT IN THE EFG RIBBON.

8. LINEAR TEMPERATURE PROFILE PROVIDES A SLIGHTLY HIGHER CRITICAL TEMPERATURE MULTIPLIER. A BETTER TEMPERATURE PROFILE SHOULD BE INVESTIGATED TO ACHIEVE ZERO STRESS (IF POSSIBLE).

Elastic-Plastic Stress-Strain Relationship
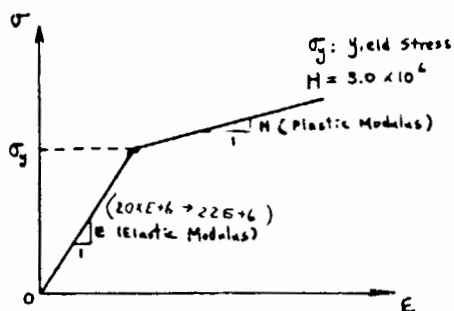
Yield Stress vs Distance From Interface

Effective Stresses of a Dendritic Web at T(x)

4795	1897	1523	1328	1170	1164	1178	1133	1050	1001	933									
4692	1283	1807	1231	893	654	620	574	518	532	482									
4611	1090	1627	1290	821	529	429	378	346	364	336									
4576	1140	1363	1250	916	722	673	646	622	588	553									
4565	1283	1073	1158	1022	968	965	954	924	859	808									
4566	1430	795	1045	1102	1164	1198	1196	1164	1078	1013									
4570	1539	541	945	1153	1299	1336	1361	1312	1227	1153									
4575	1599	862	586	1176	1359	1434	1443	1403	1502	1273	1131	1068	972	908	849	797	754	722	720

$\lambda_{min} = 1.02$ (Elastic Buckling)

$\lambda = 0.8$ $\sigma_{e\,max} = 4244$ psi   No Yield

$\lambda = 0.85$ $\sigma_{e(141)} = 4502$ psi   Yield on element #141

$\lambda = 0.90$ $\begin{cases} \sigma_{e(121)} = 4514 \text{ psi} \\ \sigma_{e(141)} = 4590 \text{ psi} \end{cases}$ Yield on elements #121, #141

$\lambda = 0.95$ $\sigma_{e(1)} = 4516$ psi ; $\sigma_{e(11)} = 4605$ psi

        $\sigma_{e(11)} = 4511$ psi ; $\sigma_{e(141)} = 4697$ psi

        $\sigma_{e(61)} = 4506$ psi   element no.

        $\sigma_{e(41)} = 4503$ psi

        $\sigma_{e(91)} = 4509$ psi

        $\sigma_{(101)} = 1536$ psi

Residual Stresses on a Dendritic Web at Room Temperature (20°C)

σ_{xR} : Residual Stresses of σ_{xx} (x-x Normal Stress)

(σ_{yR}) : Residual Stresses of σ_{yy} (Y-Y Normal Stress)

$D = 0.07''$

$t = 0.015''$

$C = 0.5''$

$\lambda_{min} = 1.02$

ORIG... OF POOR QUALITY

Geometrical Nonlinearity and Imperfection (5.0×10^{-4} in.)

TABLE 1. Thermal Stresses (PSI) at Each Increment ($\xi = 5.0 \times 10^{-4}$ in.)

λ	Case I $\Delta\lambda = 0.05$ "SEMI.QN" Method	Case II $\Delta\lambda = 0.025$ "SEMIQN" Method	Case III $\Delta\lambda = 0.025$ "ITER" Method
0.10	-515.5 -483.7	-515.5 -483.7	-515.0 -484.2
0.125		-644.5 -604.5	-644.2 -604.9
0.15	-773.6 -725.0	Numerical Unstable	-773.2 -7255
0.175			Diverging
0.20	Negative Diagonal Numerical Unstable		
0.225			

Creep Analysis

- CREEP LAW

$$\varepsilon^c = a \, \sigma^b \, c^{(T_o/T - 1)} \, t$$

- RESULTS

SILICON SHEET

$$\xi^c = 2\sigma^{-b}C^{(\gamma_0 - 1)}$$
$$f(T) = (1.0 \times 10^{-5})^{(T/T_0 - 1)}$$

Time (hr.)
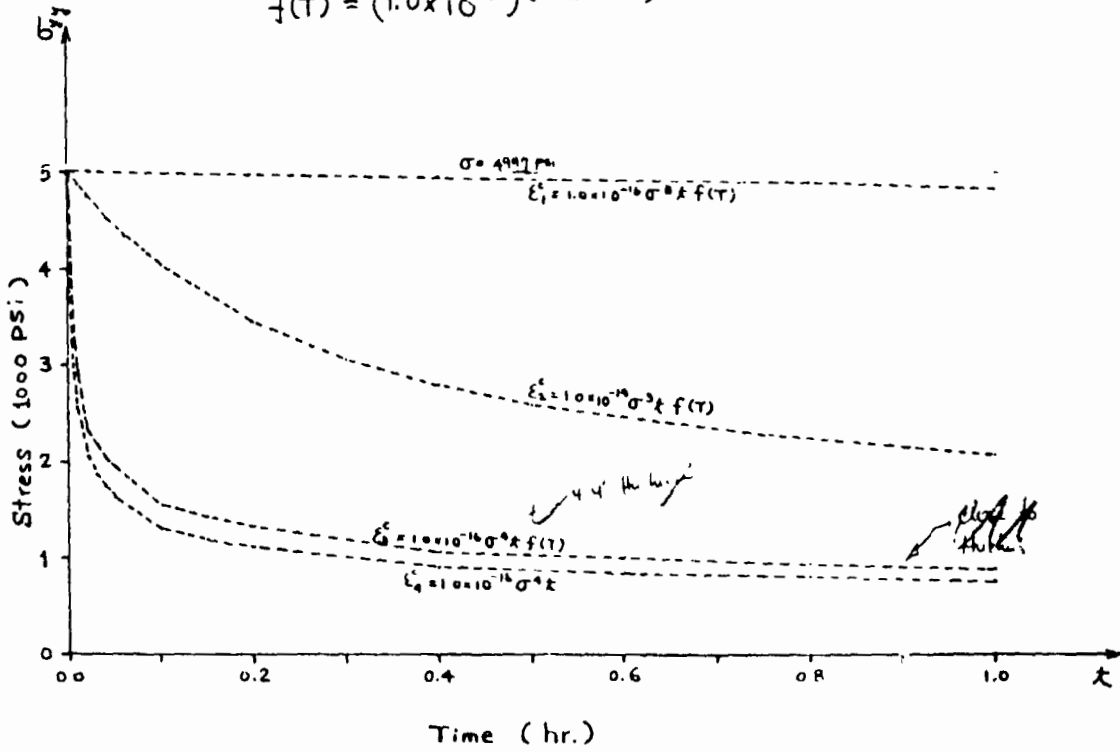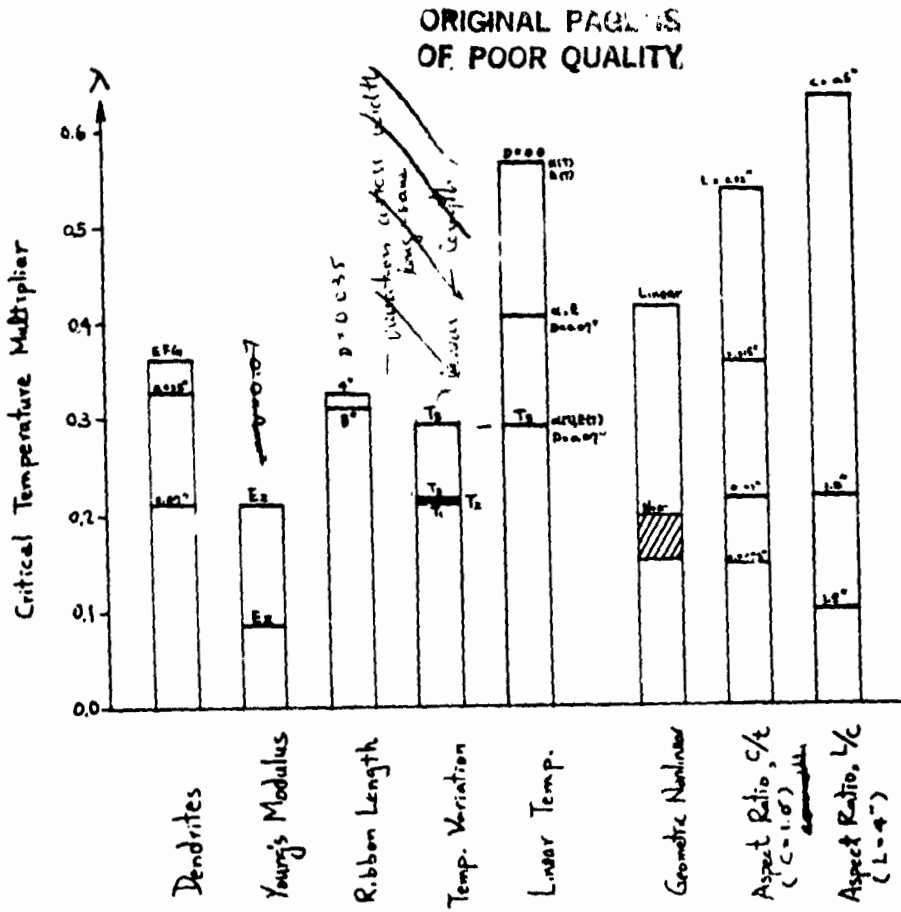
SILICON SHEET
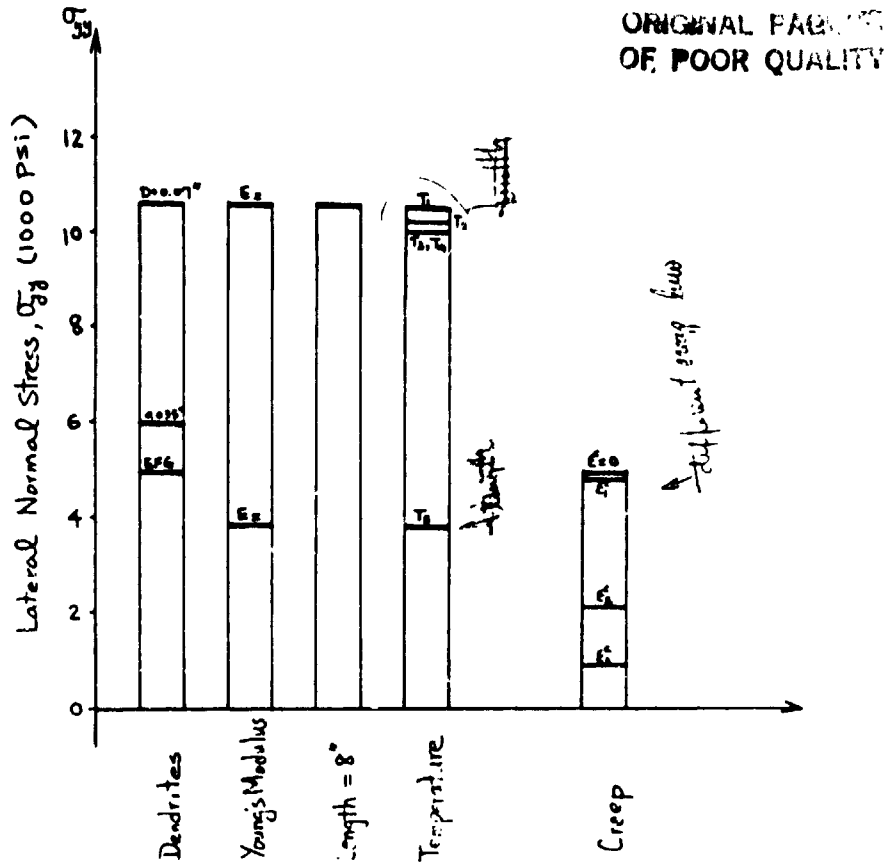
What Is the Pull-Up Process?
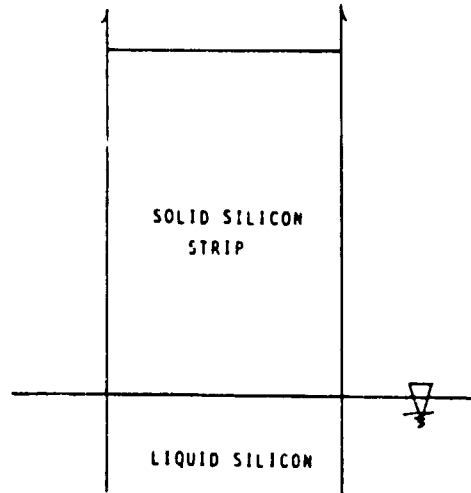
MATERIAL PROPERTIES ARE:

(1) HOMOGENEOUS AND ISOTROPIC (NO CRACKING, DISLOCATIONS, ETC.)

(2) MECHANICAL PROPERTIES OF SILICON BEING A FUNCTION OF TEMPERATURE ONLY (NOT A FUNCTION OF STRESS OR STRAIN)

(3) HAVING A BI-LINEAR STRESS-STRAIN CURVE (TRUE STRESS-STRAIN CAN BE USED)

(4) HAVING A PRIMARY AND A SECONDARY CREEP FUNCTION

$$\frac{d\,\varepsilon_{cr}}{dt} = c_1\,\sigma^{c_2}\varepsilon^{c_3}\,e^{-\frac{c_4}{T}} + c_7\,\sigma^{c_8}\,e^{-\frac{c_{10}}{T}}$$

$c_1, c_2, c_3, c_4, c_7, c_8, c_{10}$ = CONSTANTS

ε = EQUIVALENT STRAIN

σ = EQUIVALENT STRESS

T = TEMPERATURE (ABSOLUTE)

Methods, Criteria and Model Used in the Analysis

(1) FINITE ELEMENT METHOD

(2) ANSYS (GENERAL PURPOSE STRUCTURAL ANALYSIS PROGRAM)
2-DIMENSIONAL ISOPARAMETRIC PLANE STRESS ELEMENT
3-DIMENSIONAL ELEMENT
CAPABILITIES: PLASTICITY, CREEP, LARGE DEFORMATION, STRESS STIFFNESS, ETC.

(3) MODEL:
2" WIDE AND 4" LONG STRIP
294 D.O.F., 100 2-D PLANE STRESS QUADRALTERAL ELEMENTS
20 3-D BEAM ELEMENTS (FOR DENDRITE)

(4) CRITERIA:
TEMPERATURE IS CONSTANT LATERALLY (ACROSS THE WIDTH)

ANALYSIS OF STRESS-STRAIN RELATIONSHIPS IN SILICON RIBBON

UNIVERSITY OF KENTUCKY

O. Dillon

Stress vs Strain for Si (Temperatures in °C)

$1 MN/M = 145.033 psi$

$\dot{\varepsilon} = 1.2 \times 10^{-4} sec^{-1}$

$N_0 = 2 \times 10^4 cm^{-2}$

$C_{0_2} = 1 \times 10^{14} cm^{-3}$

$2.45 = 315.33 psi$

$E = 31,414$

$\dfrac{2.52 - 2.43}{5.0} = 0.018$

Ref. 1000°C

$1.0 = 145.03$

$E\ E = 32,230$

$\dfrac{1.15 - 0.98}{5} = 0.034$ 1350°C

1200°C

$e\ b = 87 psi$

$E = 34,80 psi$

$\dfrac{0.25 - 0.595}{5} = 0.031$

LEGEND: TEMP ●—● 1000 ◆—◆ 1200 ✕—✕ 1350
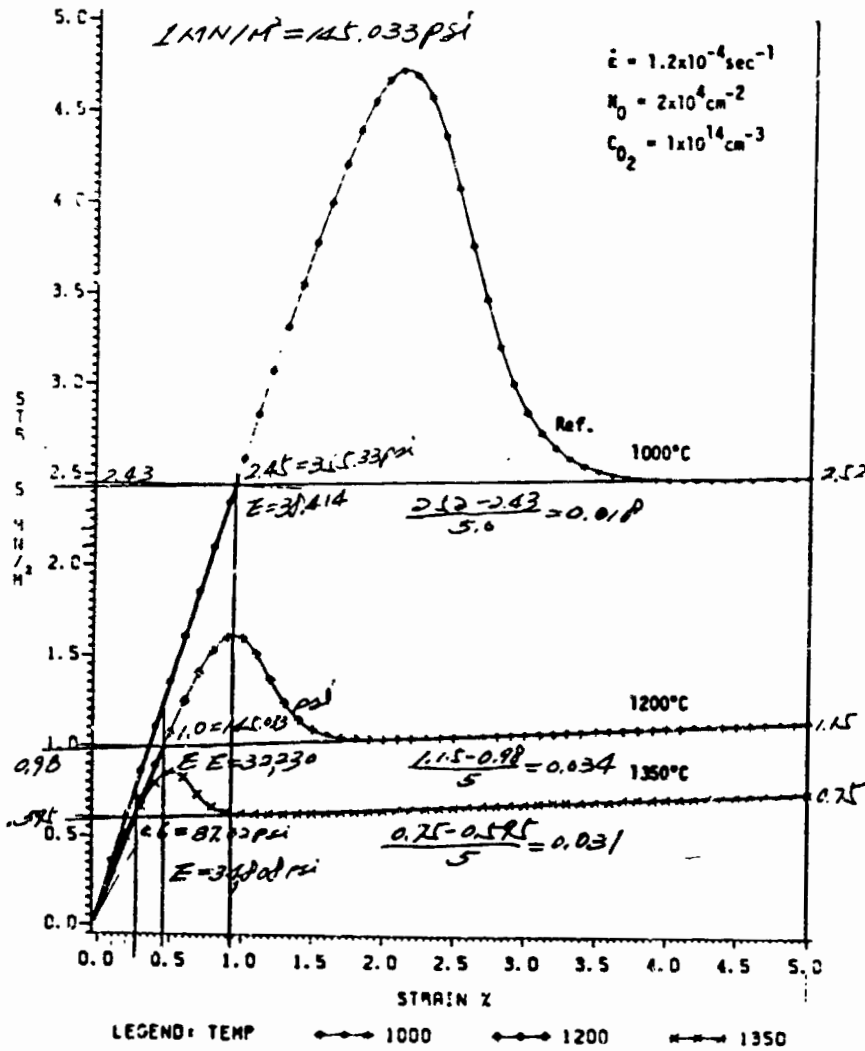
SILICON SHEET
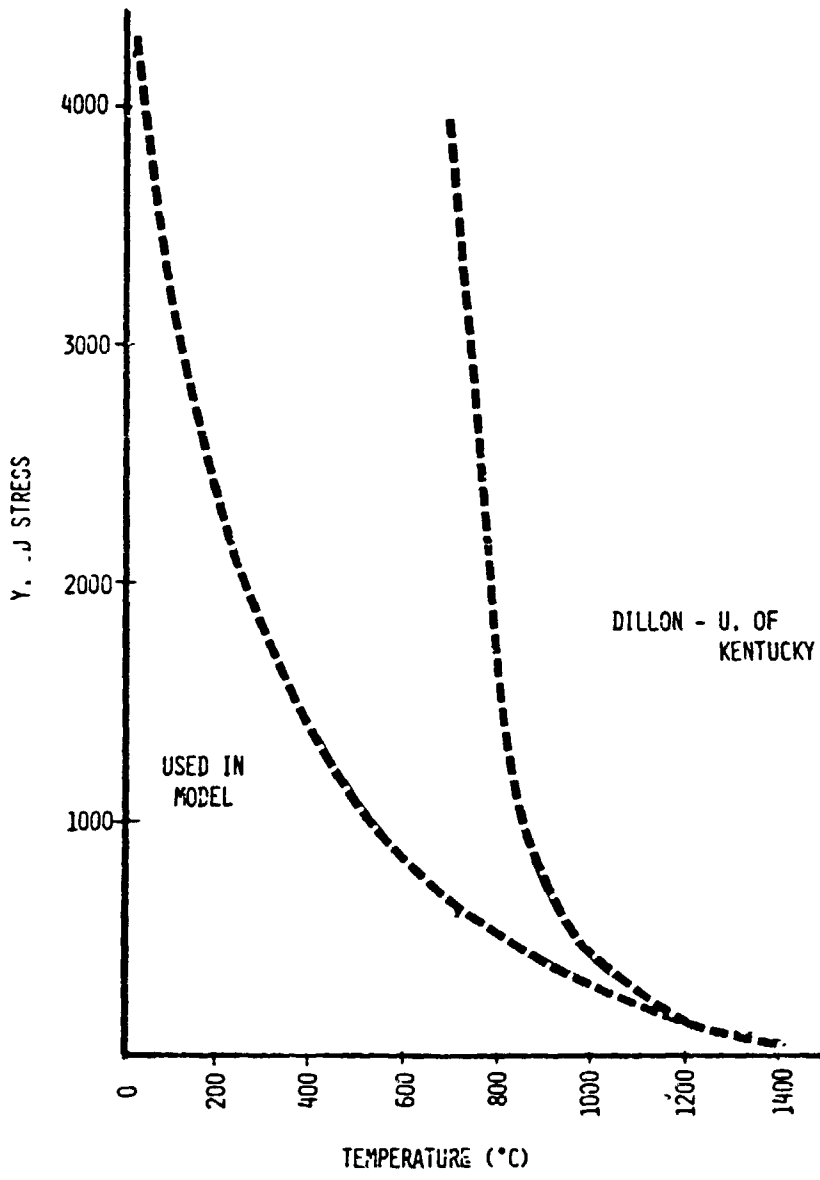
Approaches

(1) CONVENTIONAL APPROACH

A SERIES OF MODELS TO PRESENT EACH INTERMEDIATE STAGE
(QUASI-STATIC ANALYSIS)
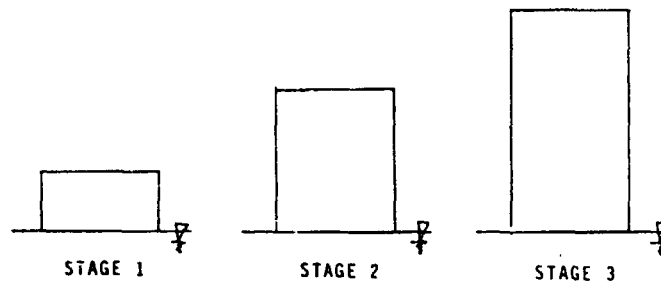
ADVANTAGE: SMALL MODEL IN EARLY STAGES

DISADVANTAGE: 1. A SERIES OF MODELS (LABOR INTENSIVE)

2. POST-STRESS HISTORY IGNORED

(2) RECOMMENDED APROACH

A MODEL TO PRESENT ENTIRE PROCESS (DYNAMICAL TRANSIT ANALYSIS)
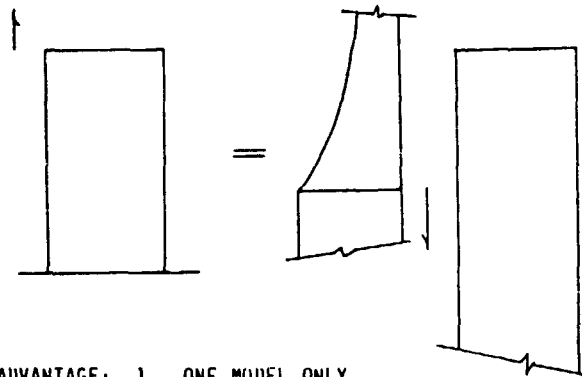
ADVANTAGE: 1. ONE MODEL ONLY

2. ALL PAST-DEFORMATION INCLUDED

DISADVANTAGE: COSTLY AT EARLY STAGE ANALYSIS

SILICON SHEET

Model
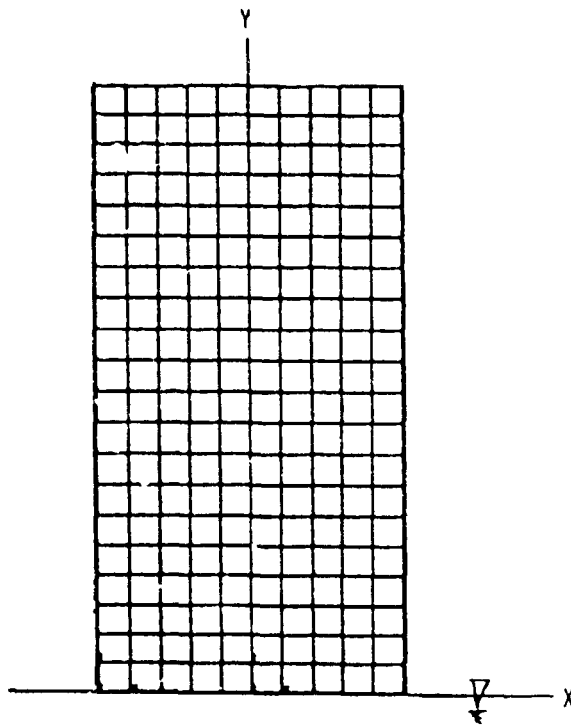
Deformed Shapes by Steps

STEP 1	STEP 5	STEP 10	STEP 15	STEP 20
Δy @ 1 = .1271-2	.1129-2	.5279-3	.2150-3	.9347-4
Δx @ 6 = -.5085-3	-.2301-2	-.2979-2	-.3134-2	-.3202-2

(INCHES)

521
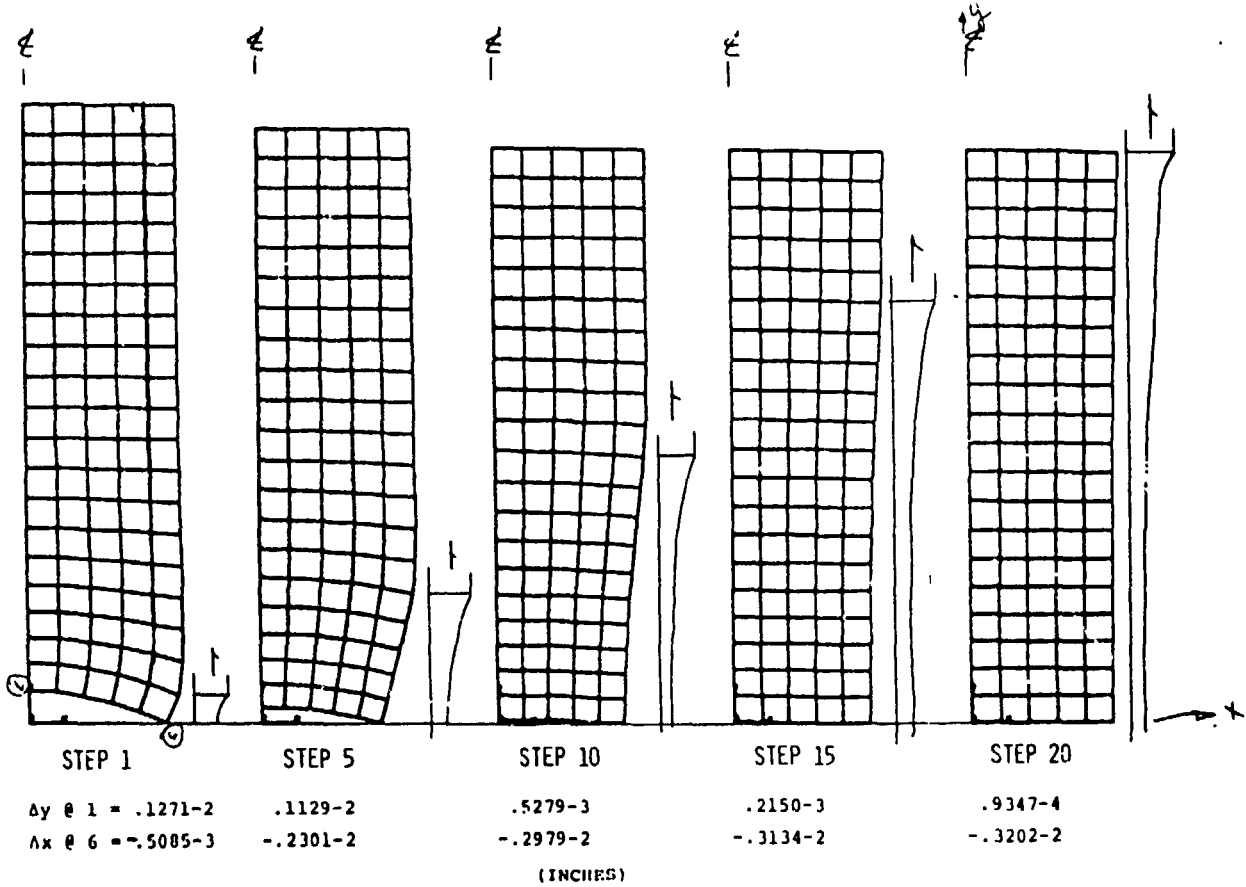
SILICON SHEET

Stress Contours of σ_y by Steps
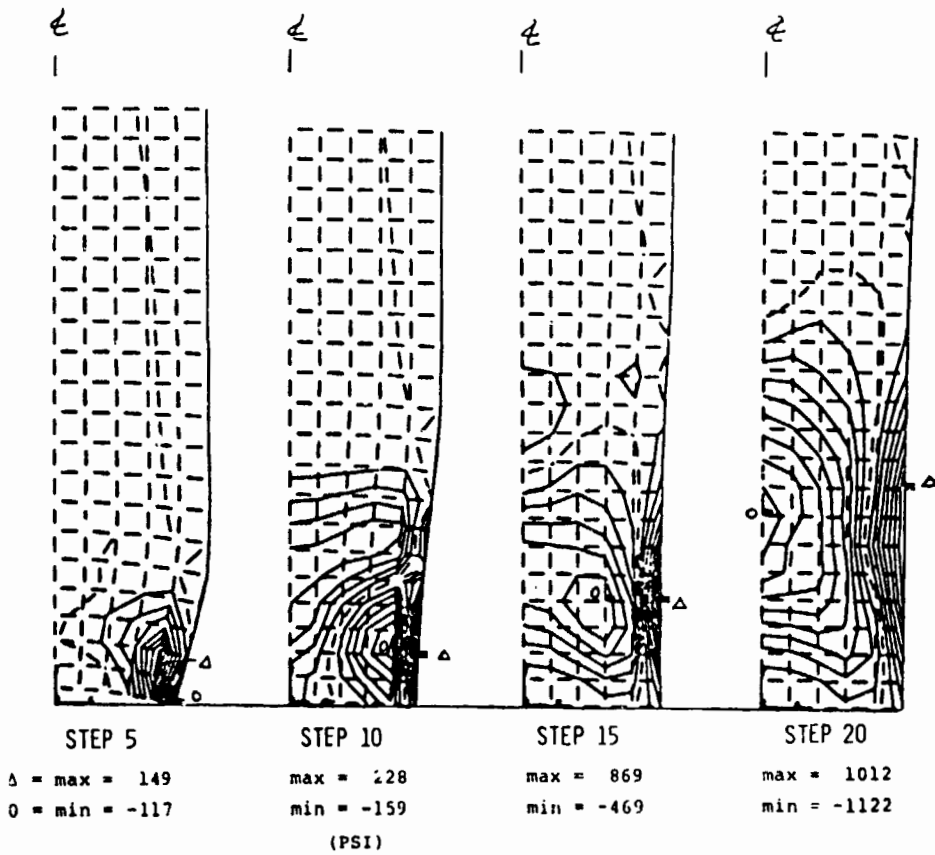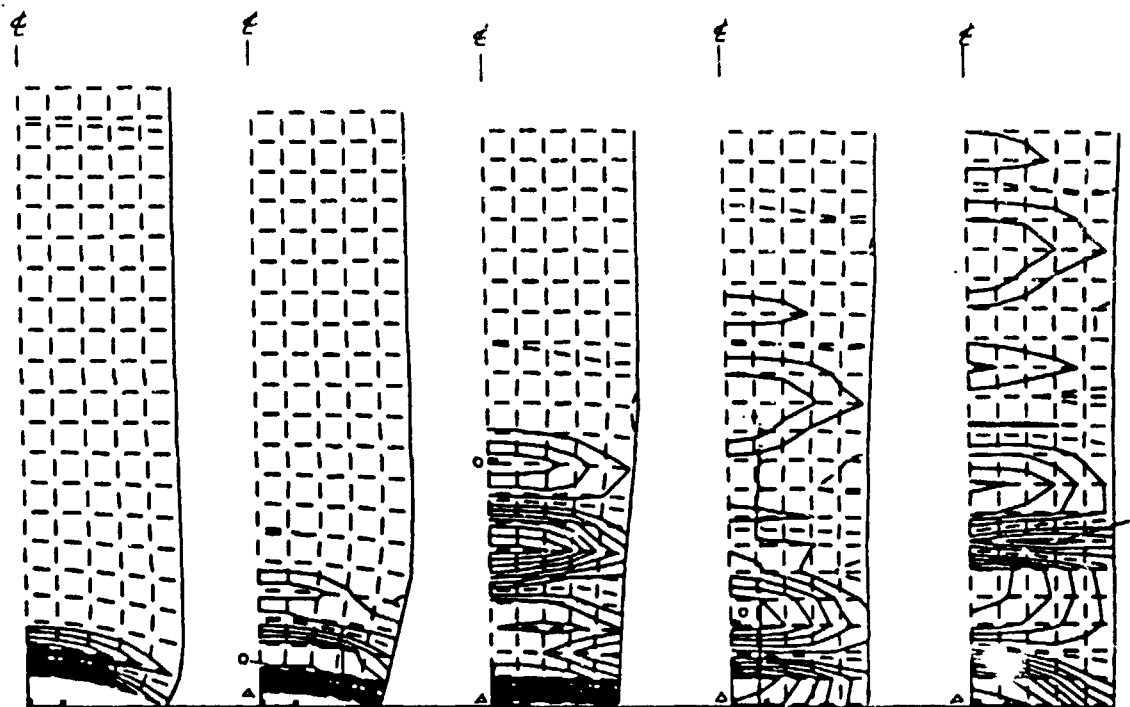
STEP 5	STEP 10	STEP 15	STEP 20
Δ = max = 149	max = 228	max = 869	max = 1012
0 = min = -117	min = -159	min = -469	min = -1122
	(PSI)		

Stress Contours of σ_x by Steps

STEP 1	STEP 5	STEP 10	STEP 15	STEP 20
Δ = max = .05	max = 374	max = 782	max = 1293	max = 1885
0 = min = -.02	min = -657	min = -314	min = -1159	min = -858
		(PSI)		

Stress Contours of τ_{xy} by Steps

STEP 5	STEP 10	STEP 15	STEP 20
Δ = max = 91	max = 180	max = 556	τ_{xy} max = 712
0 = min = -167	min = -209	min = -337	τ_{xy} min = -416
	(PSI)		
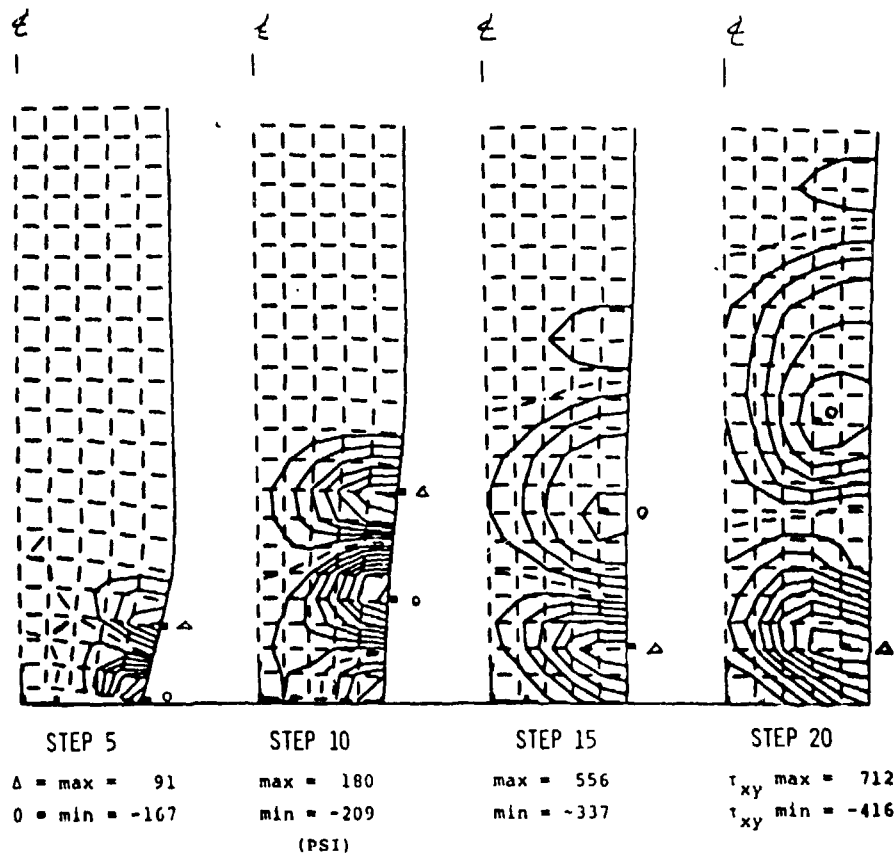
Conclusion

- DYNAMICAL TRANSIT APPROACH WORKS

- PAST-STRAIN HISTORY IS SIGNIFICANT

STRESS AND BUCKLING ANALYSIS

UNIVERSITY OF KENTUCKY

O. Dillon

TECHNOLOGY	REPORT DATE
STRESS AND BUCKLING ANALYSIS	10/3/84

APPROACH	STATUS
MODEL MATERIAL BEHAVIOR MODEL BUCKLING DUE TO THERMAL STRESSES **CONTRACTOR** UNIVERSITY OF KENTUCKY	• ELASTIC STRESS AND BUCKLING ANALYSIS COMPLETED FOR CONSTANT MATERIAL PROPERTIES. • CRITICAL SHEET THICKNESS VS. SHEET WIDE COMPARED FOR FOUR THERMAL PROFILES.
GOALS • PROVIDE GUIDANCE BASED ON ANALYSIS FOR THERMAL PROFILES FOR REDUCING STRESSES AND IMPROVING FLATNESS IN WIDE RIBBON. • HAVE RESULTS BE APPLICABLE TO ALL SHEET GROWTH SYSTEMS.	• RESULTS ARE REASONABLY CONSISTENT WITH EXPERIMENT. SURVEY OF THE MECHANICAL PROPERTIES OF SILICON PRE-BUCKLED STRESSES IN PLASTIC RANGE

SILICON SHEET
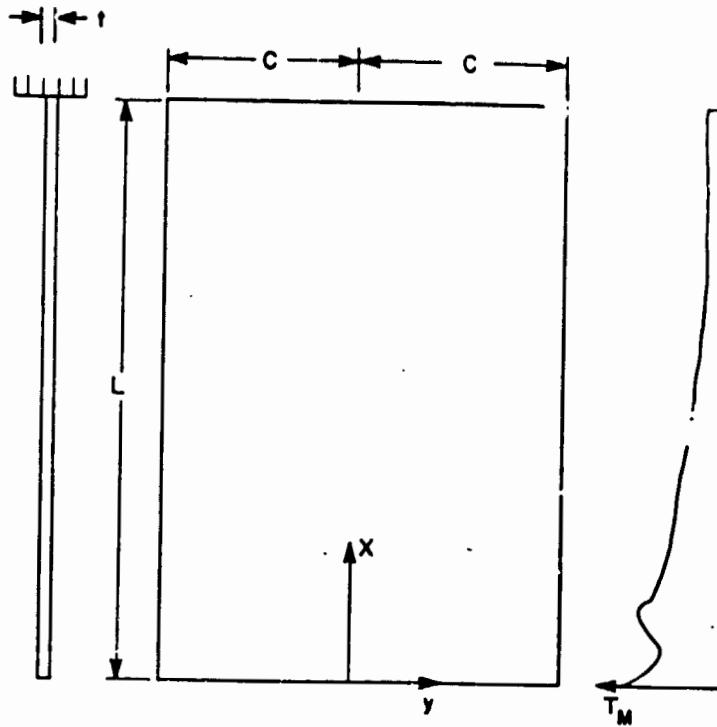
@ FLORIDA (1983)

ASSUME: $F = (c^2 - y^2) f(x)$ (pre buckled)

ELASTIC
BUCKLING

WAS ZERO ⟶   ⟵ NEW

$$w = W_0(x) + y W_1(x) + y^2 W_2(x)$$

TWIST   "curling"

COMBINE
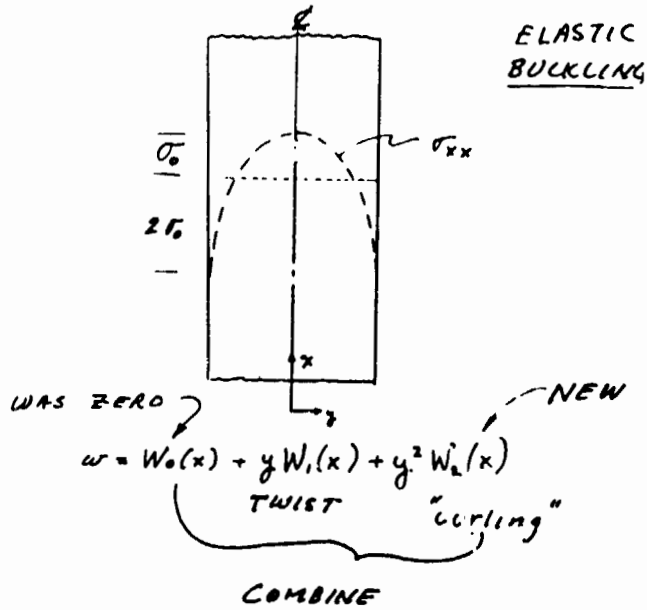
USE ANALYTICAL METHODS
TO OBTAIN _CRITICAL_
THICKNESS

$T_c'' = 24$

BENDING + CURLING

FLAT

TWISTING

BUCKLED

THICKNESS, μm

½ WIDTH C (cm)
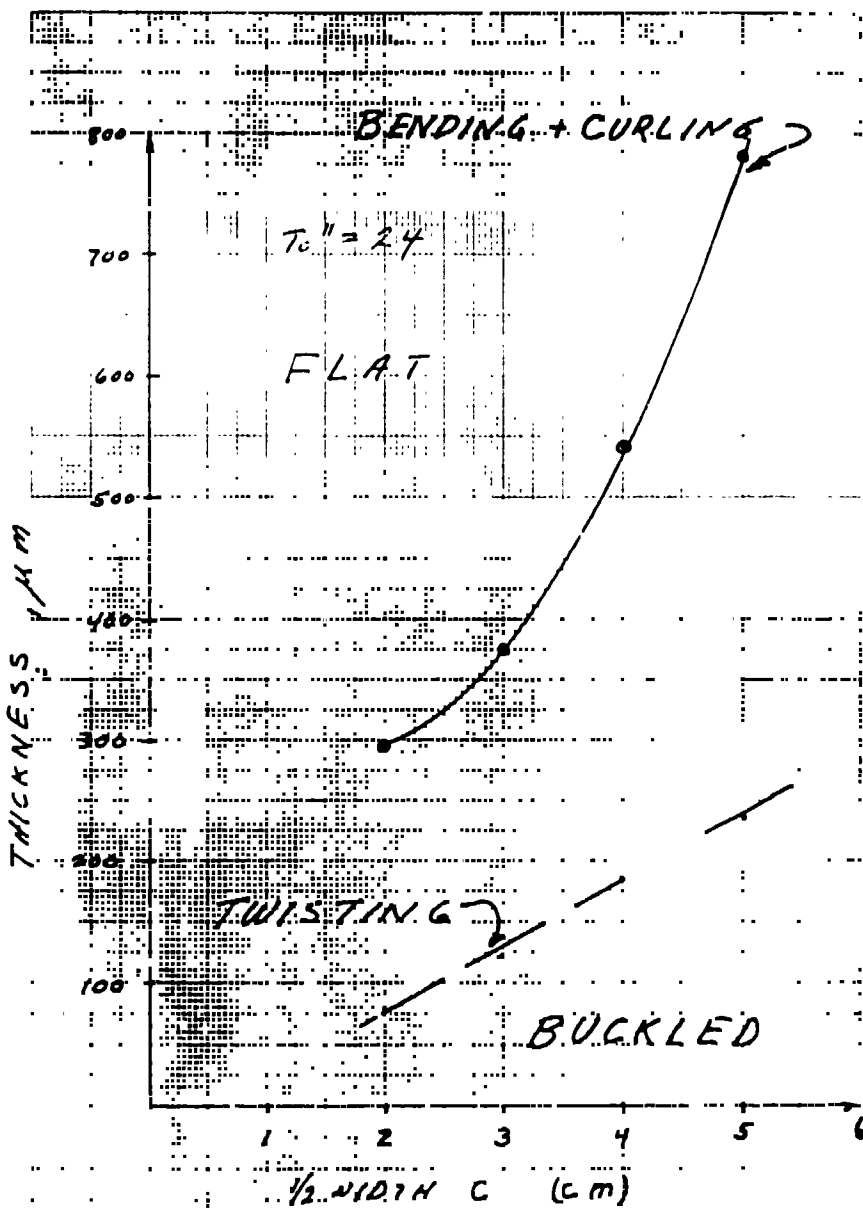
Calculated Buckled Web Shape
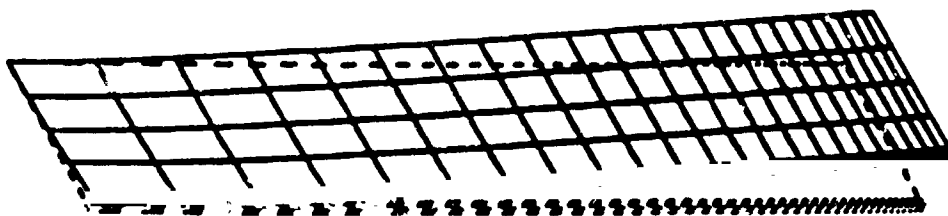
Sumino

$$\dot{\epsilon}^{PL} = \frac{bB}{\tau_0^m} N_m (\tau - D/R_m)^m e^{-Q/RT}$$

MOBILE DISLOCATION DENSITY   BACK STRESS

$$\dot{N}_0 = K_1 N_m (\tau - D/R_m)^{\lambda+m} e^{-1/RT}$$

DENSITY CHANGES

Stress vs Strain for Si (Temperature in °C)

$\dot{\epsilon} = 1.2 \times 10^{-4} sec^{-1}$

$N_0 = 2 \times 10^4 cm^{-2}$

$C_{O_2} = 1 \times 10^{14} cm^{-3}$

Ref. 1000°C

← NOT "ELASTIC"

1200°C

1350°C

STRESS MN/m²

STRAIN %

LEGEND. TEMP   ←→ 1000   •—•—• 1200   •—•—• 1350
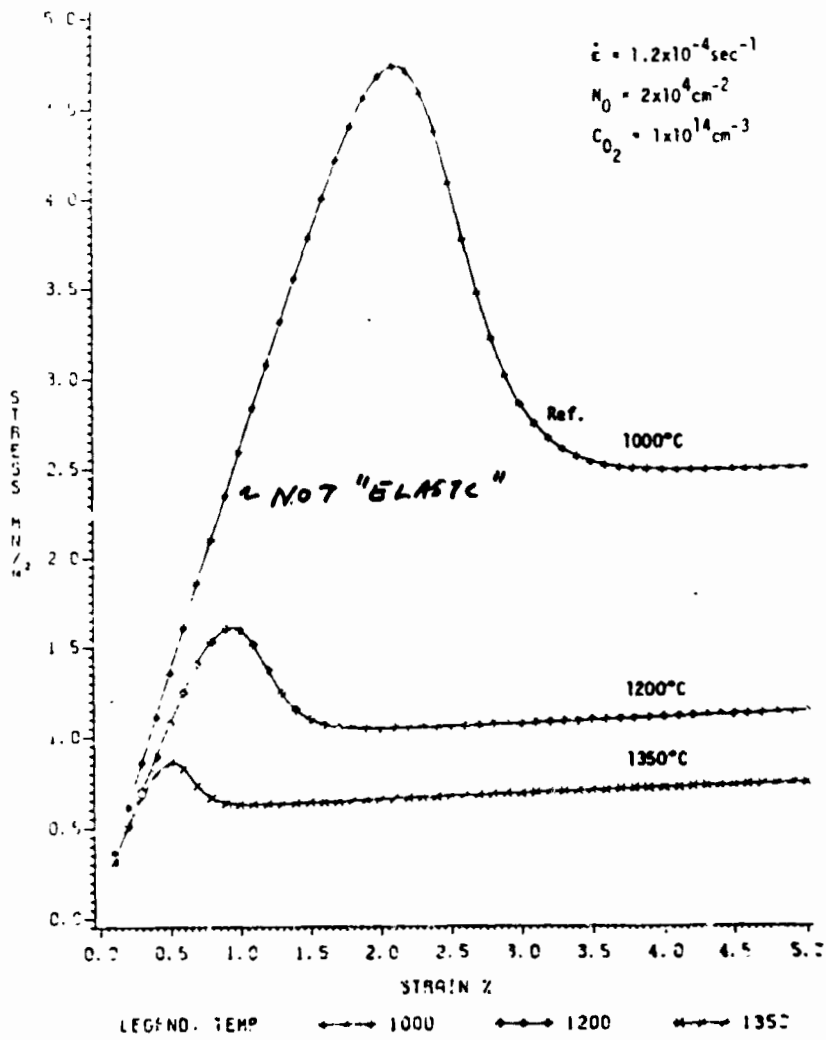
Stress vs Strain for Si (Strain Rate 1/sec)

$N_0 = 2 \times 10^8 cm^{-2}$
$T = 1000°C$
$C_{O_2} = 1 \times 10^4 cm^{-3}$

$1.2 \times 10^{-3} sec^{-1}$

NOT ELASTIC

Ref.

$1.2 \times 10^{-4} sec^{-1}$

$1.2 \times 10^{-5} sec^{-1}$

Y.P.

STRESS MN/m^2

STRAIN %

LEGEND: SRATE $\longrightarrow$ 0.000012 $\longrightarrow$ 0.00012 $\times\!\!-\!\!\times$ 0.0012
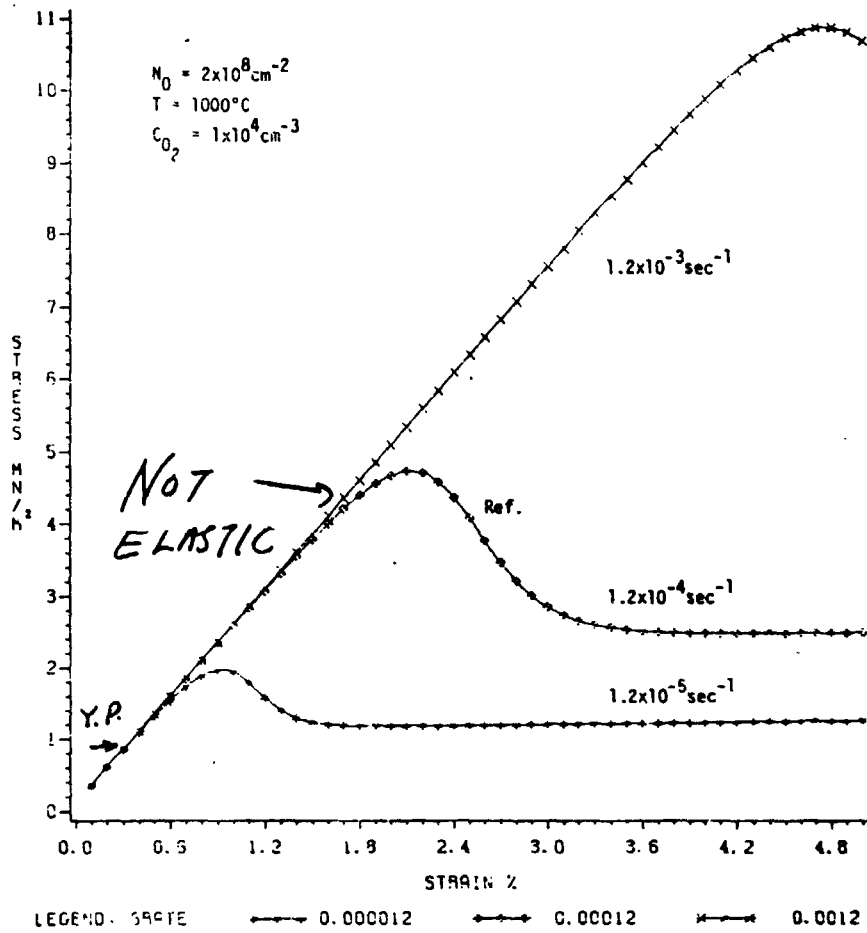
TEMPERATURE=1000 C

$\dot{N} = .1N$ etc.

TEMPERATURE = 1350 C   OXYGEN CONTENT = 1.00E14
STRAIN RATE = 2.00E-2   INITIAL DISL. DENS. = 1.00E0

UNIVERSITY OF KENTUCKY

$\dot{N} = 1.N$ etc.

TEMPERATURE = 1350 C   OXYGEN CONTENT = 1.00E14
STRAIN RATE = 2.00E-2   INITIAL DISL. DENS. = 1.00E0

UNIVERSITY OF KENTUCKY

530

$\dot{N}$ = .1N etc.

TEMPERATURE = 1350 C   OXYGEN CONTENT = 1.00E14
STRAIN RATE = 2.00E-2   INITIAL DISL. DENS. = 1.00E0

UNIVERSITY OF KENTUCKY
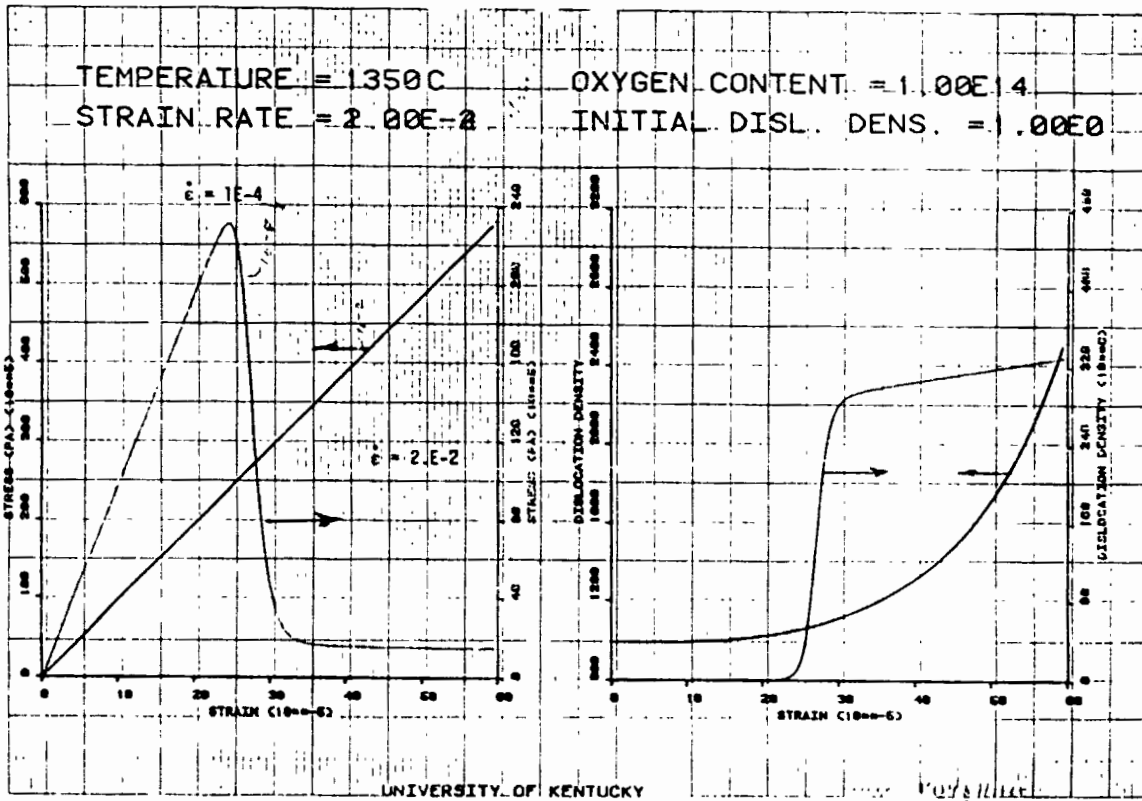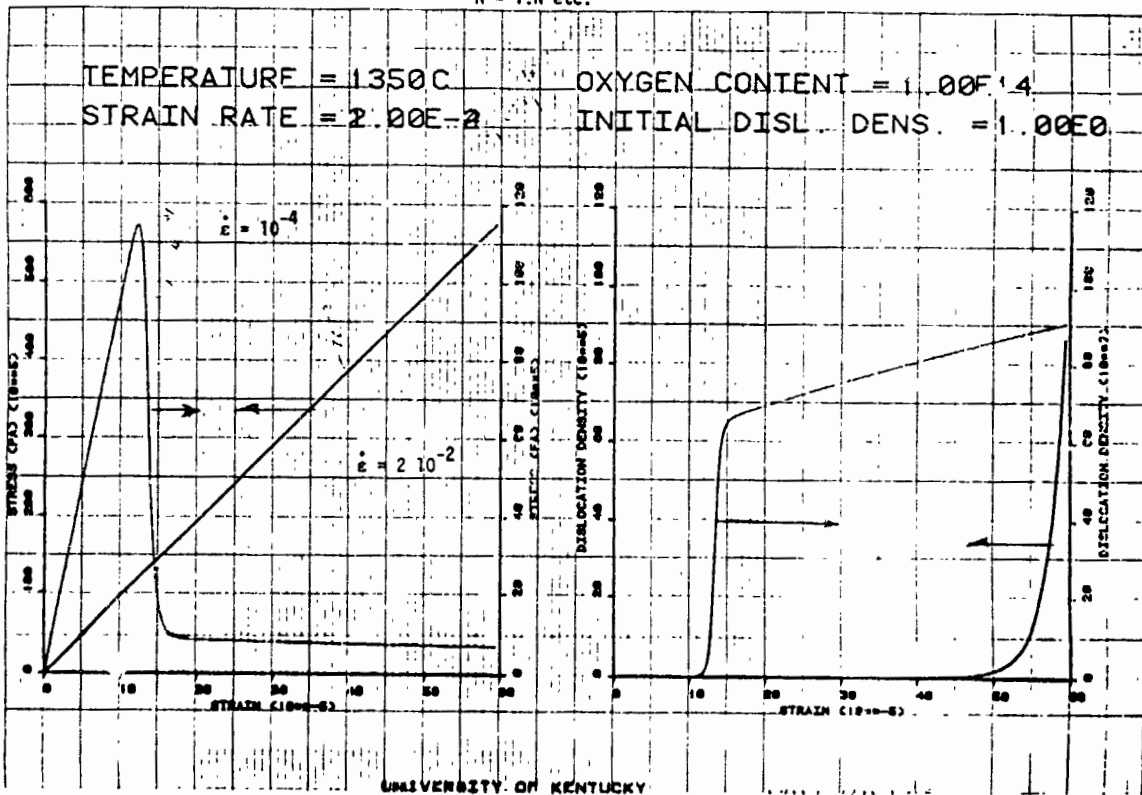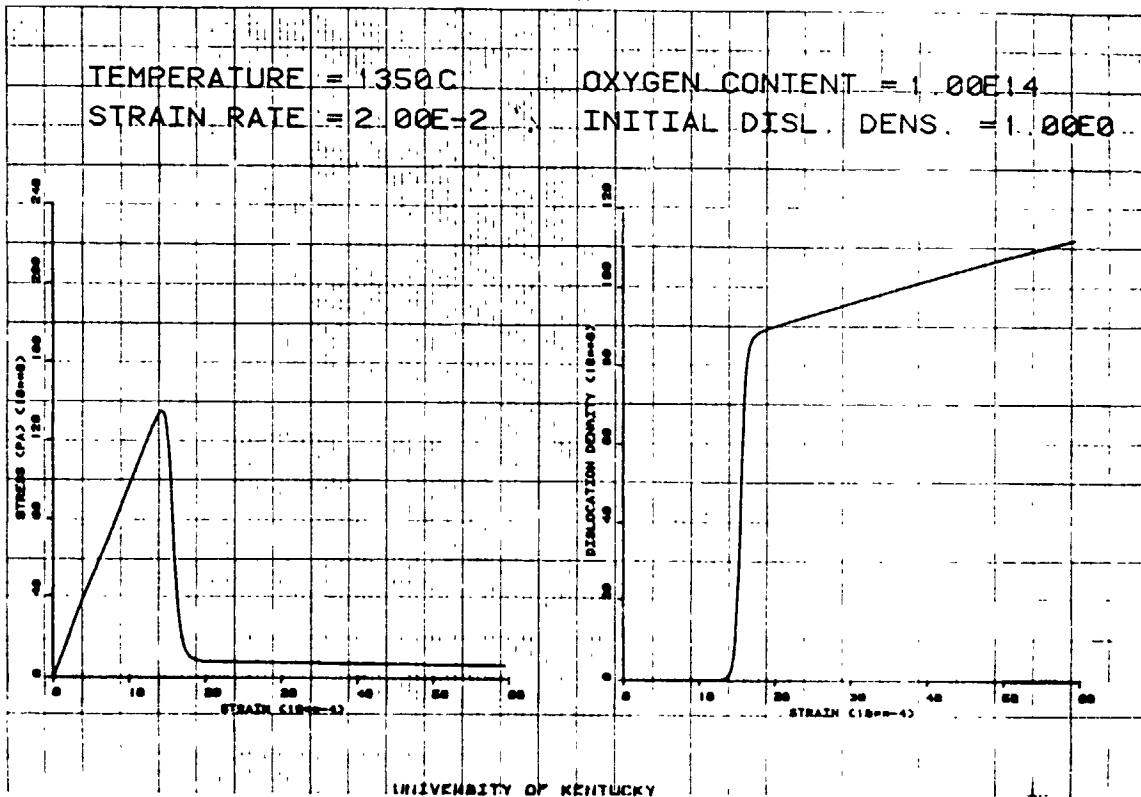
Pre-Buckled Stresses

Elastic

APPENDIX A

The equations governing the stress in a ribbon consist of those which reflect that the material is in equilibrium, that the deformations are compatable and that there is a material constitutive relation. Assuming that (a) one can neglect the three stresses σ_{iz}, (b) that the material is elastic and that Young's modulus and Poissons ratio are constant, the governing equations are

Equilibrium

$$\frac{\partial \sigma_{xx}}{\partial x} + \frac{\partial \sigma_{xy}}{\partial y} = 0 .$$

$$\frac{\partial \sigma_{xy}}{\partial x} + \frac{\partial \sigma_{yy}}{\partial y} = 0 .$$

(A-1)

Compatability

$$\frac{\partial^2 \epsilon_{xx}}{\partial y^2} + \frac{\partial^2 \epsilon_{yy}}{\partial x^2} = 2 \frac{\partial^2 \epsilon_{xy}}{\partial x \partial y}$$

(A-2)

Constitutive relations

$$\epsilon_{xx} = \frac{\sigma_{xx}}{E} - \frac{v}{E} \sigma_{yy} + \alpha T$$

(A-3)

$$\epsilon_{yy} = \frac{\sigma_{yy}}{E} - \frac{v}{E} \sigma_{xx} + \alpha T$$

$$\epsilon_{xy} = \frac{(1+v) \sigma_{xy}}{E}$$

(A-4)

Equations (A-1) combine to yield

$$\frac{\partial^2 \sigma_{xx}}{\partial x^2} = \frac{\partial^2 \sigma_{yy}}{\partial y^2}$$

(A-5)

While Eqs. (A-2) through (A-4) yield

$$\frac{\partial^2 \sigma_{yy}}{\partial x^2} = - \frac{\partial^2 \sigma_{xx}}{\partial x^2} - \frac{\partial^2 \sigma_{yy}}{\partial y^2} - \frac{\partial^2 \sigma_{xx}}{\partial y^2} - \frac{\alpha E \partial^2 T}{\partial x^2}$$

(A-6)

Second order central differences equivalents of these equations are:

$$\sigma_{xx}(I+1,J) = 2\sigma_{xx}(I,J) - \sigma_{xx}(I-1,J)$$

$$+ [\sigma_{yy}(I,J+1) - 2\sigma_{yy}(I,J)$$

$$+ \sigma_{yy}(I,J-1)] \; \Delta x^2/\Delta y^2 \qquad \text{A-5a}$$

and

$$\sigma_{yy}(I+1,J) = 2\sigma_{xx}(I,J) - \sigma_{yy}(I-1,J)$$

$$- \sigma_{xx}(I+1,J) + 2\sigma_{xx}(I,J)$$

$$- \sigma_{yx}(I-1,J) - \frac{\alpha E \partial^2 T}{\partial x^2} \Delta x^2$$

$$- \left(\frac{\Delta x}{\Delta y}\right)^2 [\sigma_{xx}(I,J+1) - 2\sigma_{xx}(I,J)$$

$$+ \sigma_{xx}(I,J-1) + \sigma_{yy}(I,J+1) - 2\sigma_{yy}(I,J)$$

$$+ \sigma_{yy}(I,J-1)] \qquad \text{(A-6a)}$$

$$\sigma_{xx}=0$$
$$\sigma_{xy}=0$$

$$\sigma_{xy}=0 \qquad\qquad \sigma_{yy}=0$$
$$\sigma_{yy}=0 \qquad\qquad \sigma_{xy}=0$$

x

c   c

Note
$\sigma_{yy}\neq0$ $\sigma_{xx}=0$ $\sigma_{xy}=0$

y

MELT

Assumes $t > t_r$

(NO BUCKLING)

Temp
(°C)

$$T_1 = 1157 \, e^{-.066x} + 437 \, e^{-1.36x} \cos \pi x$$
$$- 317 \, e^{-.7x} \sin\left(\frac{\pi x}{2} + \frac{\pi}{6}\right)$$

$$T_2 = 1600 \, e^{-.0827x} + 85 \, e^{-.5x} \cos \pi x$$
$$4 > x > 0. \quad + 75 \sin \frac{\pi x}{4} - 273$$
$$= 1600 \, e^{-.0827x}$$
$$- 35 \sin\left(\pi \frac{[x-4]}{6}\right)$$
$$10 > x > 4.$$
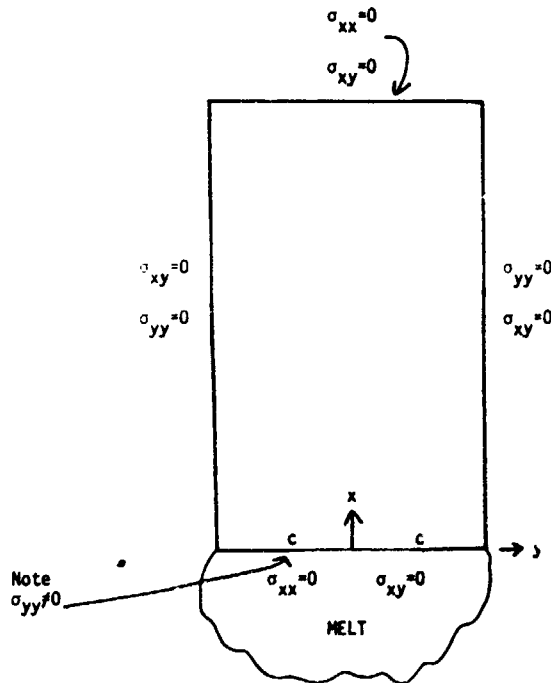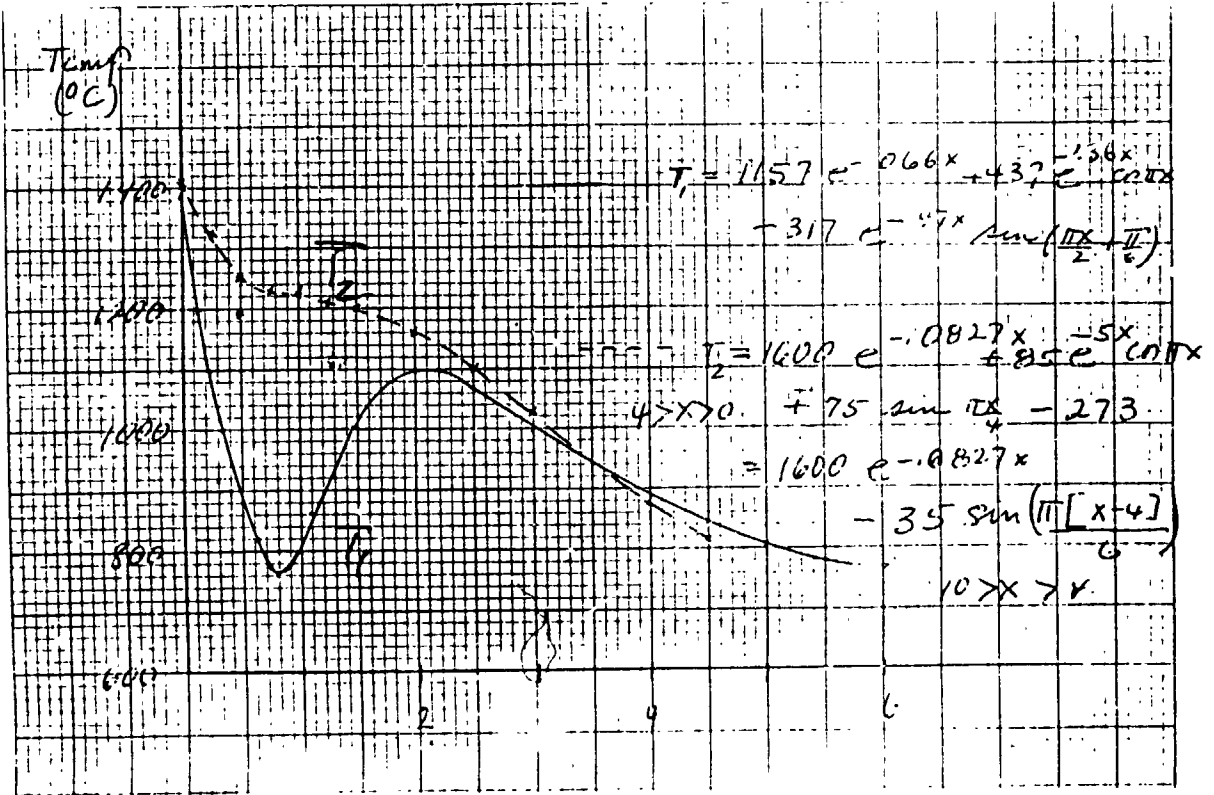
ⓐ Run V-0807 12 Sept 84   ⓞ Run V-0100 15 Sept
$$l = 10 \, cm$$
FLAT PLATE
$$T = T_W$$

AXIAL STRESS
$$T_{xx}(c_1, x) \times 10^{-7} \ (pascals)$$

$$2c = 6 \, cm$$
$$2c = 10 \, cm$$
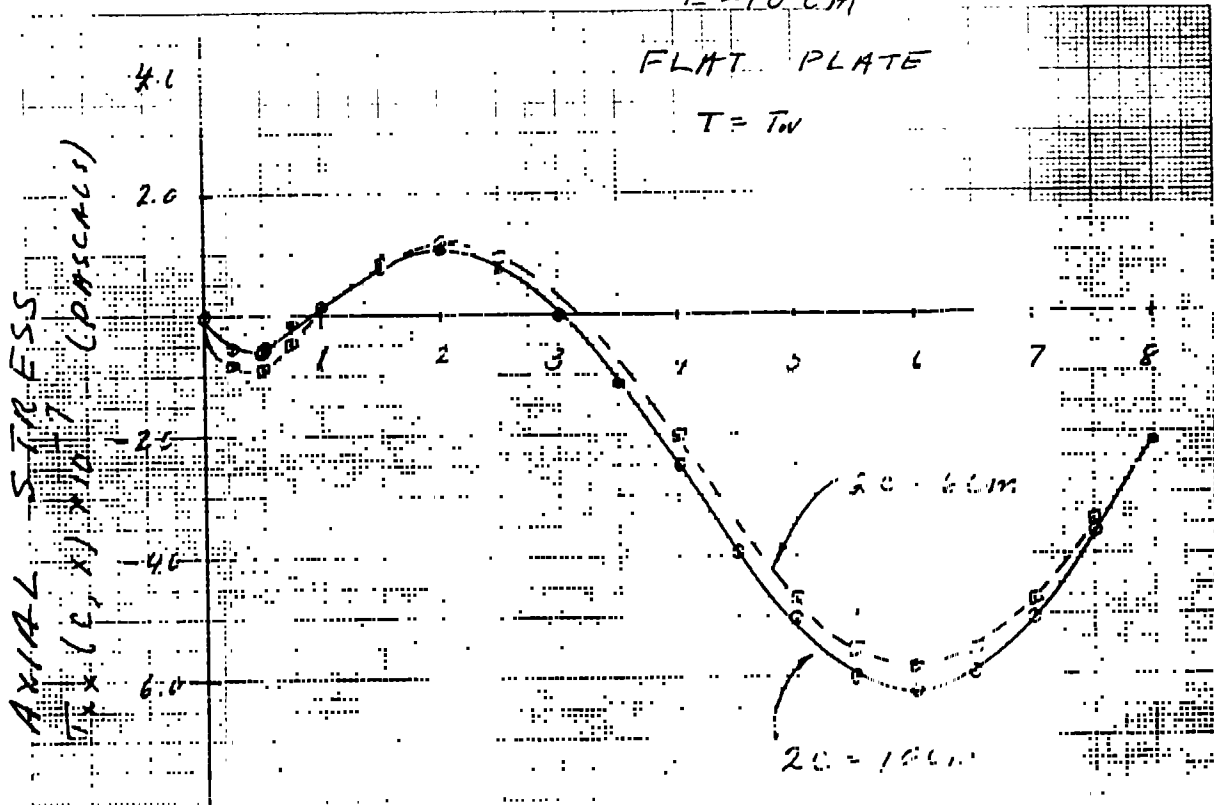
We assume the Sumino model of viscoplastic behavior, i.e.

$$\dot{\epsilon}_{ij}^{PL} = \frac{bB}{\tau_0^m} \frac{N_m(\sqrt{J_2} - D/N_m)^m e^{-Q/kT}(\sigma_{ij} - \sigma_{KK}\delta_{ij}/3)}{\sqrt{J_2}}$$

$$\sqrt{J_2} > D/N_m$$

DISLOCATION DENSITY CHANGES!!

$$\dot{N}_m = K_1 N_m(\tau - D/\bar{N}_m)^{\lambda+m} e^{-Q/k_1}$$

MOBILE

<u>NEW:</u>   SOME BASIS FOR A "SHAPE" FACTOR

VS.
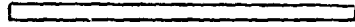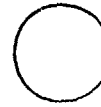
$$K_1 \rightarrow \frac{K_1}{10}$$

$$\left.\begin{array}{l} \lambda \\ b \\ B \\ \tau_0 \\ m \\ D \\ K_1 \\ Q \end{array}\right\} \text{MATERIAL "CONSTANTS"}$$

SILICON SHEET

$$\frac{\partial^2 \dot{\sigma}_{xx}}{\partial x^2} = \frac{\partial^2 \dot{\sigma}_{yy}}{\partial y^2} \tag{1}$$

The compatibility equation is

$$\frac{\partial^2 \dot{\varepsilon}_{xx}}{\partial y^2} + \frac{\partial^2 \dot{\varepsilon}_{yy}}{\partial x^2} = 2 \frac{\partial^2 \dot{\varepsilon}_{xy}}{\partial x \partial y} \tag{2}$$

$$\dot{\varepsilon}_{ij} = \frac{1+\nu}{E} \dot{\sigma}_{ij} - \frac{\nu}{E} \dot{\sigma}_{KK} \delta_{ij} + \alpha \dot{T} \delta_{ij} + \dot{\varepsilon}_{ij}^{PL} \tag{3}$$

Eqs (2) and (3), to yield

$$\frac{\partial^2 (\dot{\sigma}_{xx} + \dot{\sigma}_{yy})}{\partial x^2} + \frac{\partial^2}{\partial y^2} (\dot{\sigma}_{xx} + \dot{\sigma}_{yy}) \tag{4}$$

$$= - E\alpha \left(\frac{\partial^2}{\partial x^2} + \frac{\partial^2}{\partial y^2} \right) \dot{T}$$

$$+ \left(\frac{\partial^2 \dot{\varepsilon}_{xx}^{PL}}{\partial y^2} + \frac{\partial^2 \dot{\varepsilon}_{yy}^{PL}}{\partial x^2} - 2 \frac{\partial^2 \dot{\varepsilon}_{xy}^{PL}}{\partial x \partial y} \right) E$$

PLASTIC

$$\frac{\partial^2(\sigma_{xx}+\sigma_{yy})}{\partial x^2} + \frac{\partial^2(\sigma_{xx}+\sigma_{yy})}{\partial y^2} = -\alpha E \frac{\partial^2 T}{\partial x^2} -$$

$$+ \int_0^x \frac{E}{v} \left(\frac{\partial^2 \dot{\varepsilon}^{PL}_{xx}}{\partial y^2} + \frac{\partial^2 \dot{\varepsilon}^{PL}_{yy}}{\partial x^2} - 2 \frac{\partial^2 \dot{\varepsilon}^{PL}_{xy}}{\partial x \partial y} \right) dx$$

PULL RATE

$$\frac{\partial^2 \sigma_{xx}}{\partial x^2} = \frac{\partial^2 \sigma_{yy}}{\partial y^2}$$

_____ _____ _____ _____

$\dot{\varepsilon}^{PL}_{ij}$ = function of stresses and N_m

$\dot{N}_m = K_1 N_m (\tau - D\sqrt{N_m})^{\lambda+m} e^{-Q/RT}$

_____ _____ _____

$\therefore$ SOLVE VIA INTERATION!!!!

"0" = ELASTIC
:
:
"20"

OUTPUT   STRESSES (x,y)
         STRAIN RATES (x,y)
VERY NEW $\longrightarrow$ DISLOCATION DENSITY (x,y)

$$L = 1 \text{ cm} \qquad \dot{\varepsilon} \doteq 10^{-2} \text{ sec}^{-1}$$

$$C = 2 \text{ cm}$$

$$T = Tw \qquad \dot{\varepsilon}^{PL} \doteq 10^{-7} \text{ sec}^{-1}$$

$$\sigma^{el}_{xx_{max}} = .1147 \times 10^8 \text{ pascals}$$
$$\left.\vphantom{\sigma^{el}_{xx_{max}}}\right\} \text{ Typical}$$
$$\sigma^{PL}_{xx_{max}} = .1086 \times 10^8 \text{ pascals}$$

$$N_{init} = 1.0/\text{cm}^2$$

$$N_{final} = 12/\text{cm}^2 \text{ at outer edge}$$
$$6/\text{cm}^2 \text{ at center}$$

EVERY PROBLEM DIFFERENT

$$\dot{\varepsilon} \doteq 10^{-3} \rightarrow 10^{-2} \text{ sec}^{-1}$$

$$\dot{\varepsilon}^{PL} \doteq 10^{-9} \rightarrow 10^{-4} \text{ sec}^{-1}$$

$$\rightarrow 10^{-3} \text{ sec}^{-1} \text{ once in awhile}$$

ORIGINAL PAGE
OF POOR QUALITY

$L = 10$
$2C = 10$
$T = T_W$

$N_0 = .001/cm^2$

Graph: DISLOCATION DENSITY $(10^3/cm^2)$ vs $X (cm)$

Temp.
$N_0 = .001 /cm^2$
$C = 2. cm$
$L = .65 cm.$

$N_0 = .001 /cm^2$

NOTE:
$L = .70$ BLOWS UP
$N = 10^{50}/cm^2$
at $.0035 cm$

Run V-0595 21 Sept

$N_o = .01/cm^2$
$T = 16 r_o$
$L = 65 cm$
$e = 3.5 /0.86$

$\dot{a} \left(10^{-4} \, cm/m/sec \right)$

$\dot{e}^{PL} \left(10^{-6} \, sec^{-1} \right)$
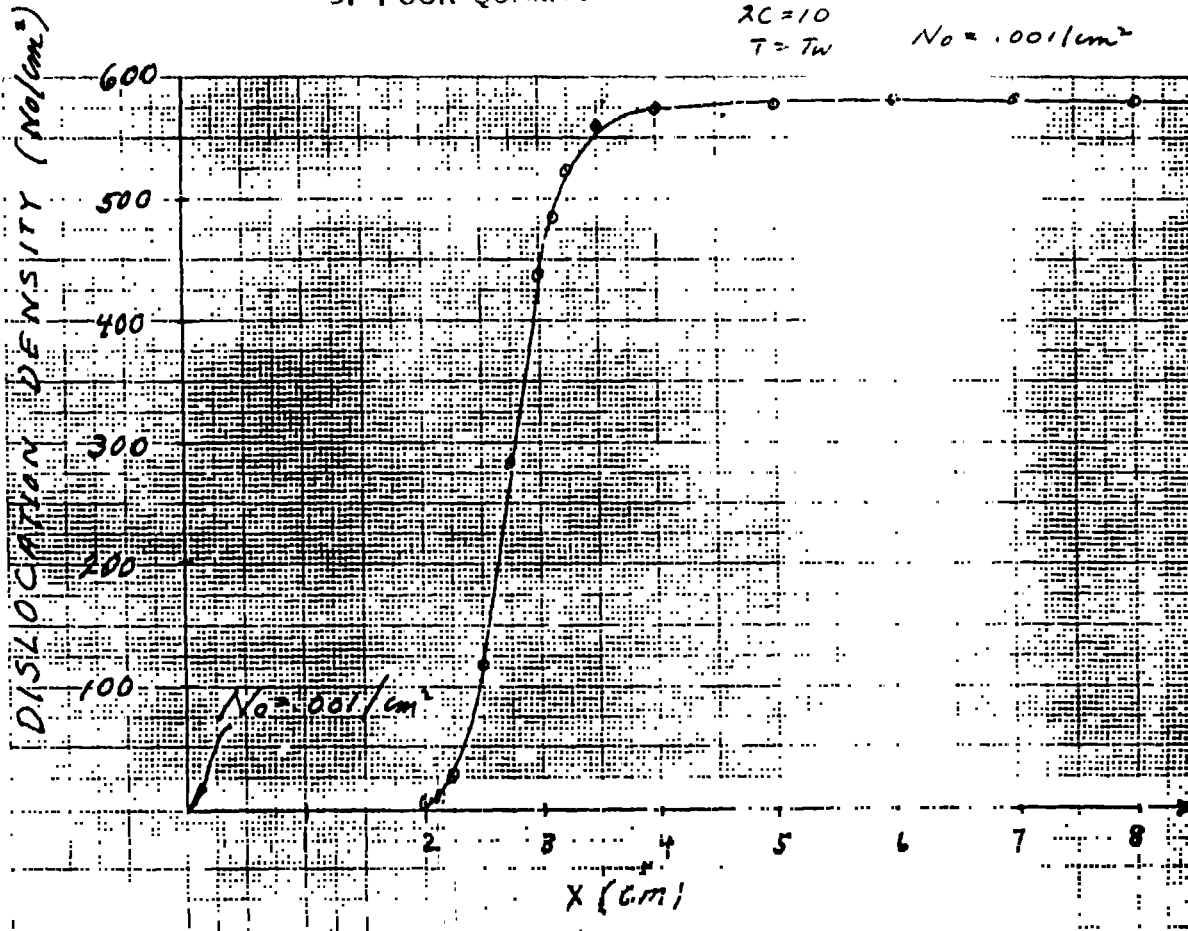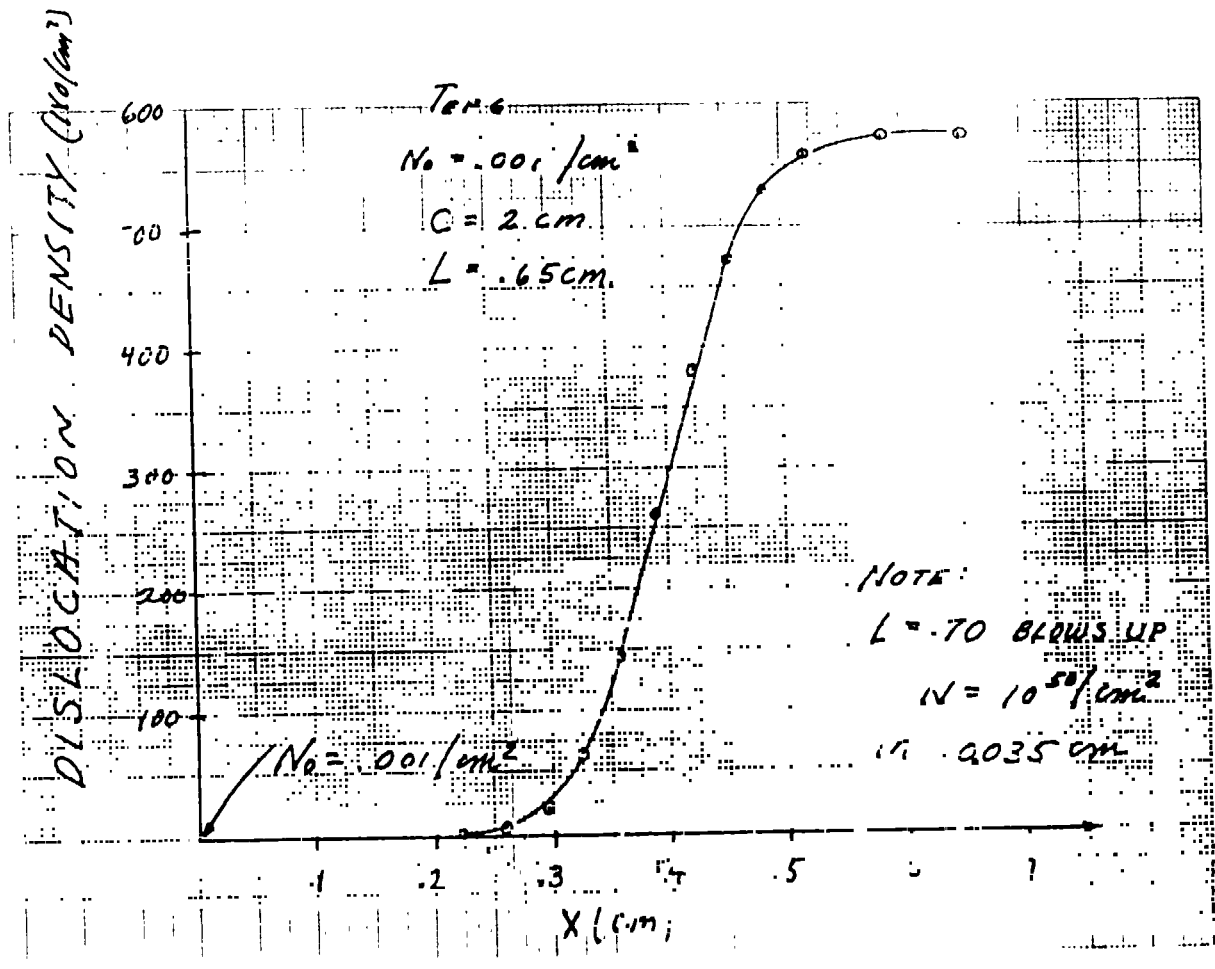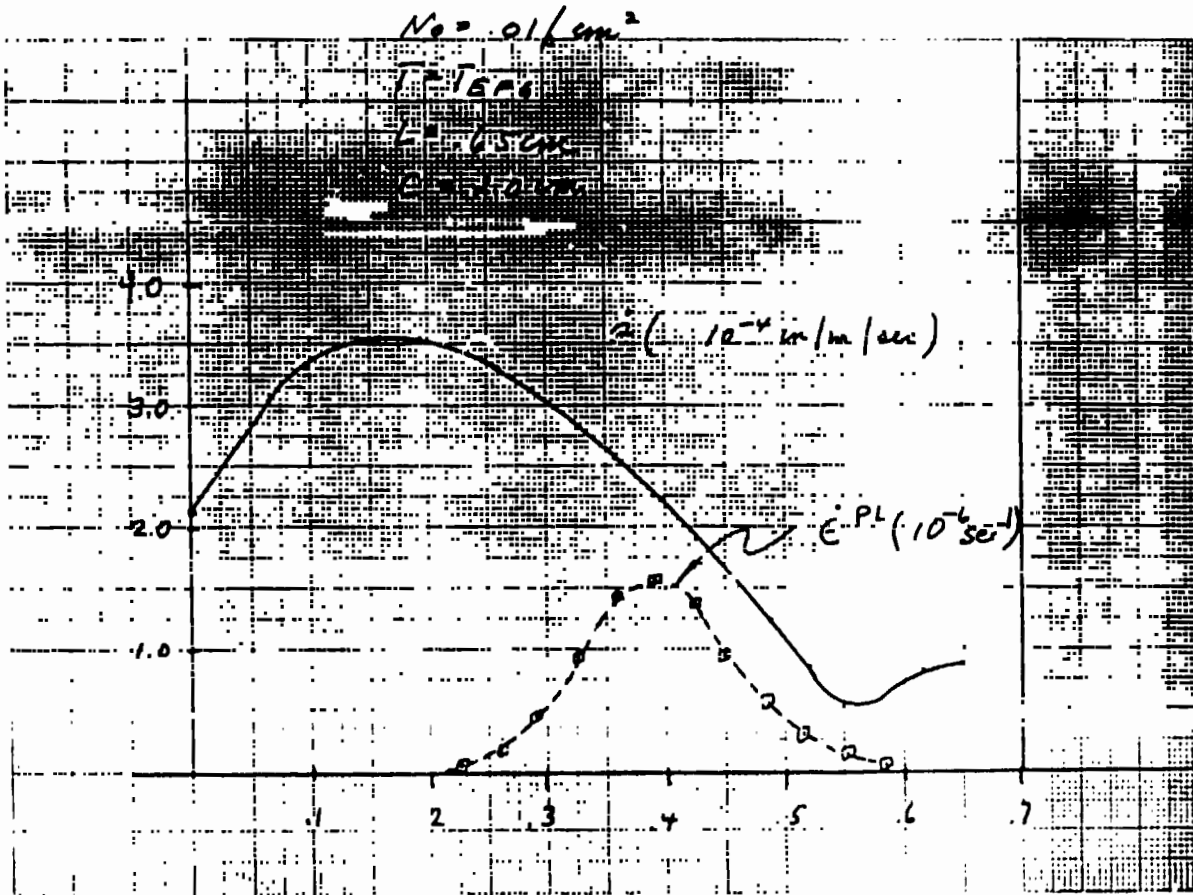
SILICON SHEET

NUMERICAL
PROCEDURE
$\Big\{$

CONVERGES RAPIDLY
change in σ is $\approx 10^{-4}\sigma$

DOES NOT CONVERGE

NOTE 1: ELASTIC REGION NO PROBLEM

NOTE 2: DOES NOT CONVERGE

MEANS $\dot{\varepsilon}^{PL} = 10^3 \sec^{-1}$

$N_m = 10^{50}/cm^2$

NOTE 3:

MAJOR OBSERVATION $\Big\{$

$L = .65$ cm CONVERGES

$L = .70$ cm DOES NOT

$L = 0.5 \div 10.$ CONVERGES WITH $[...]$ TEMP PROFILE

FOR STRESSES USE ELASTIC

FOR RESIDUAL STRESSES

PLASTICITY

$$\dot{\varepsilon}^{PL}_{ij}(x,y)$$

$\uparrow$ THIS IS PROBLEM.

PLASTICITY IS SMALL BUT IS JUST AS BAD AS A LOT.

$\dot{\varepsilon}$ is HIGH σ_{ij} ARE HIGH

$T \approx 750°$ x + .75 cm

MODEL INADEQUATE

Re: DEFORMATION MODE CHANGES (twins)

Problems and Concerns

1. N_0 at MELT INTERFACE (x=0)

2. VALIDITY OF CONSTRANTS FOR SUMINO MODEL FOR RI^BON

3. SHOULD WE THINK "TWINS"?

4. SHOULD WE WORK OTHER PROFILES?

5. ROLE OF CHANGING "L"

STRESS AND EFFICIENCY STUDIES IN EFG

MOBIL SOLAR ENERGY CORP.

J. Kalejs

TECHNOLOGY	REPORT DATE
ADVANCED MATERIALS RESEARCH TASK	OCTOBER 2, 1984

APPROACH	STATUS
STRESS AND EFFICIENCY STUDIES IN EFG	● DEVELOPMENT OF INTEGRATED STRESS AND THERMAL MODELS FOR EFG GROWTH PROCESS IS COMPLETED
	- EFG TEST SYSTEM OPERATIVE.
CONTRACTOR MOBIL SOLAR ENERGY CORPORATION, CONTRACT NUMBER 956312	- NEW CREEP DATA FOR STRESS ANALYSIS AVAILABLE.

GOALS	
● TO DEFINE MINIMUM STRESS CONFIGURATION FOR SILICON SHEET GROWTH. ● TO QUANTIFY DISLOCATION ELECTRICAL ACTIVITY AND LIMITS ON CELL EFFICIENCY. ● TO STUDY BULK LIFETIME DEGRADATION DUE TO INCREASE IN DOPING LEVELS.	● EBIC ANALYSIS IS UNDERWAY TO QUANTIFY RELATIONSHIPS BETWEEN ELECTRICAL ACTIVITY AT DISLOCATIONS AND BULK L_N. ● LOW RESISTIVITY SHEET DEFECTS CHARACTERIZATION HAS BEEN STARTED.

Work in Progress

- DEFINITION OF MINIMUM STRESS SHEET GROWTH CONFIGURATIONS:

  - MODELING OF NEW EFG TEST SYSTEM GROWTH AND STRESS/DEFECT
    CHARACTERIZATION OF RIBBON.

  - EVALUATION OF NEW CREEP DATA FOR PREDICTING STRESS
    RELIEF.

- EBIC CHARACTERIZATION OF DEFECTS:

  - DEVELOPMENT OF HIGH RESOLUTION QUANTITATIVE MEASUREMENTS
    OF LOCAL L_N VARIATIONS.

  - ROOM AND LOW TEMPERATURE COMPARISON OF DISLOCATIONS.

- OPTICAL AND HREM STUDY OF DEFECTS IN HIGHLY DOPED ($\leq$ 1
  Ω-CM) SHEET:

  - EFG RIBBON COMPARISON OF B, P GA DOPING EFFECTS.

Combined Thermal-Stress Analysis

- THERMAL ANALYSIS DEFINES OPERATING SPACE FOR GIVEN
  SYSTEM BOUNDARY CONDITIONS.

- SHEET TEMPERATURE PROFILES ARE GENERATED FOR GROWTH
  CONDITIONS.

- SHEET STRESS STATE IS RELATED TO OPERATING POINT;
  FIND:

  - STRESS LEVEL CHANGE WITH T, V_S DEPENDENT ON
    OPERATING POINT LOCATION.

θ

INSULATION

CRUCIBLE

HEATER

DIE
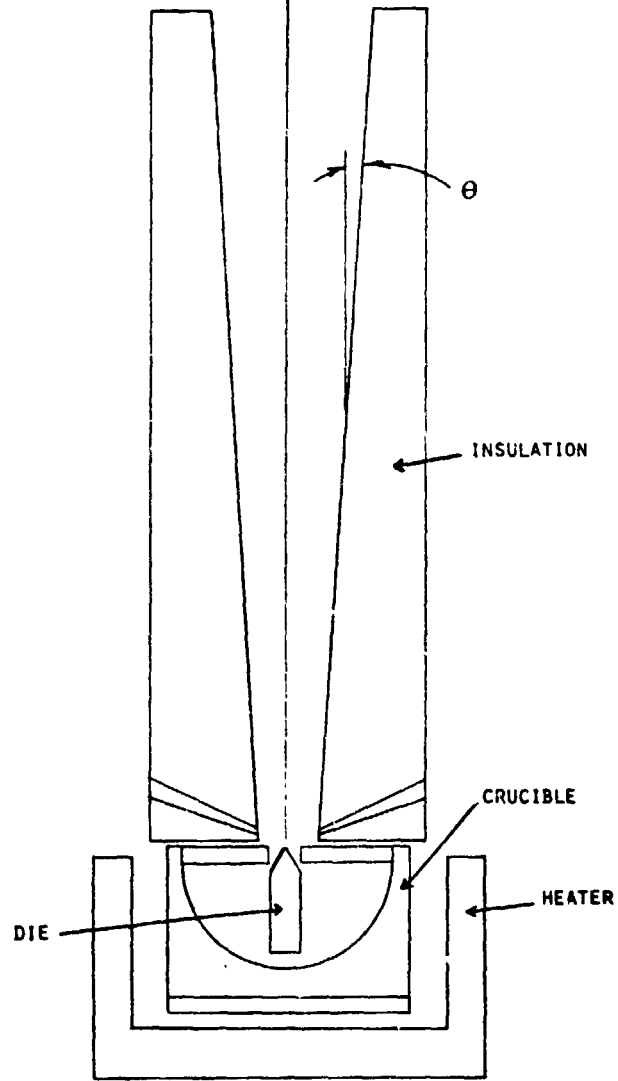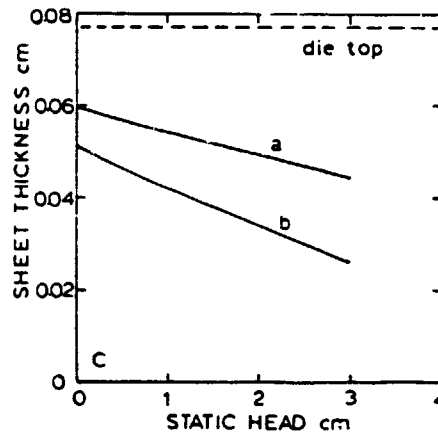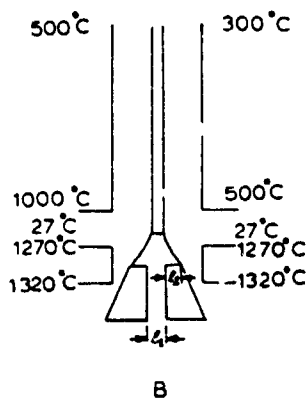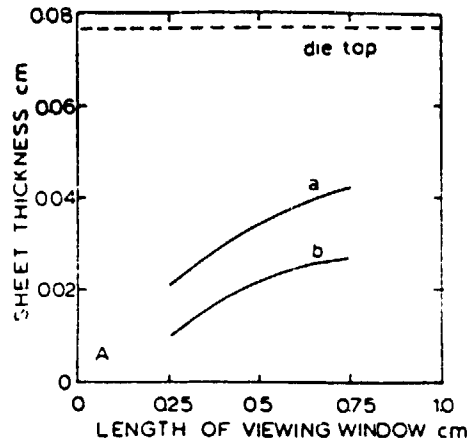
(A) Effect of dimensions of the capillary spacing and die flats and length of the viewing slot on the sheet thickness for new system at capillary spacing (ℓ_1) of: (a) 0.0254 cm and (b) 0.0662 cm. (B) Asymmetric environment temperature distribution. (C) Dependence of the sheet thickness on the static head for (a) symmetric and (b) asymmetric heat transfer surroundings.
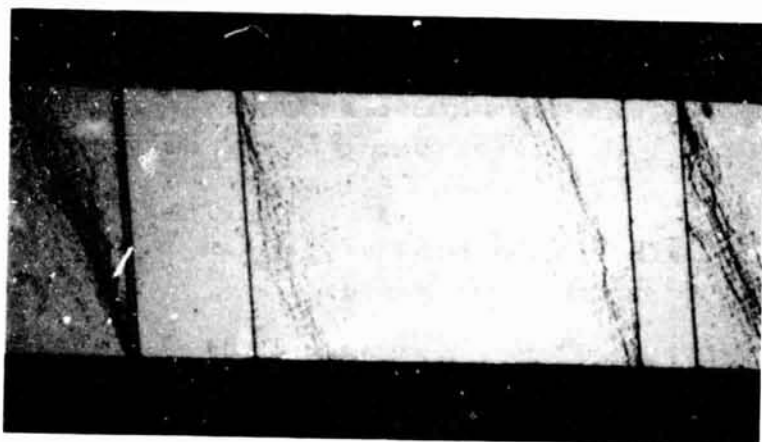
(a)
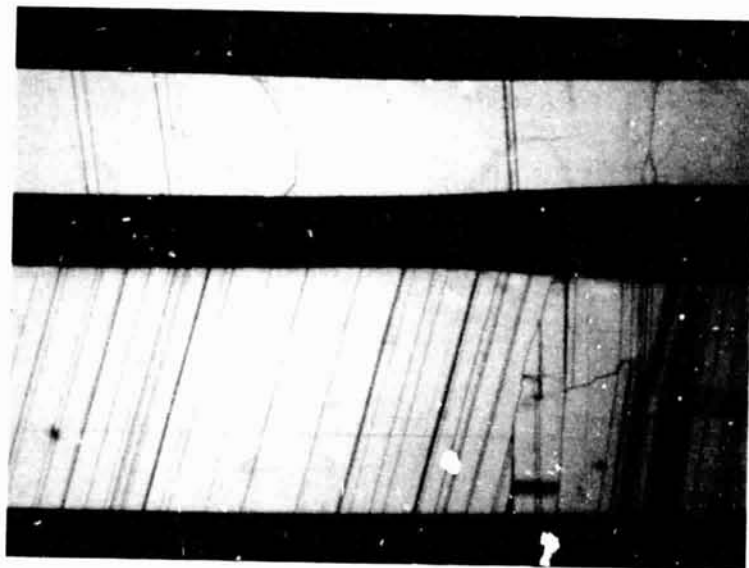
(b)

Fig. 2. EFG ribbon grown at 0.8-0.9 cm/min: (a) high
magnification dislocated region of Lüders
bands (thickness 0.23 mm); (b) low magnifica-
tion dislocation-free regions of thin (0.36
mm) and thick (0.75 mm) ribbon.

New Creep Law Formulation

- SILICON SHEET RESPONDS AS A PLASTIC SOLID DURING STRESS TRANSIENTS TYPICAL OF EFG SHEET GROWTH ABOVE 1200°C.

- LIMITATIONS AT LOW STRESS ($\leq$ 5 MPA) ARE IMPOSED BY DISLOCATION/DEFECT DENSITIES:

  - CREEP RATE IS REDUCED ESSENTIALLY TO ZERO WITH N_D APPROACHING 1 x 10^7/CM^2.

  - TWIN BOUNDARIES, IMPURITIES PROVIDE ADDITIONAL CONSTRAINTS.

- AT HIGH STRESS LEVELS ($\geq$ 10 MPA) STRESS RELIEF IN EFG SHEET OCCURS BY LÜDERS OR SHEAR BAND FORMATION.
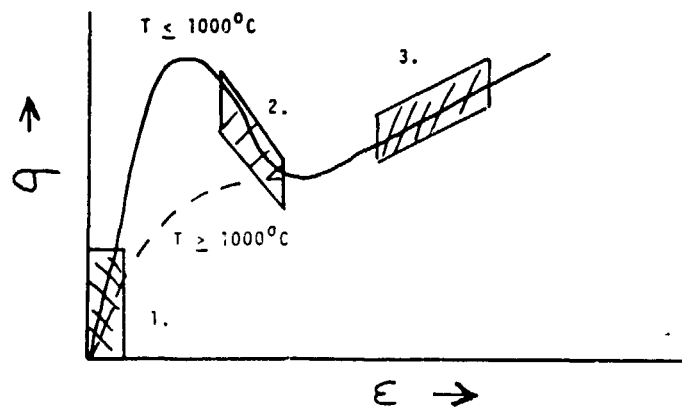
1. **Primary Creep - Present Work**

$$0 \leq \varepsilon \leq 10^{-2} \qquad , \ 0 \leq \dot{\varepsilon} \leq 10^{-3} \ s^{-1}$$

$$N_D \leq 5 \times 10^7/cm^2$$

2. **Lüders Bands (Mahajan et al., Acta Met. 27(1979) 1165.)**
   Observed for T $\leq$ 1000°C

3. **Secondary Creep - Steady-State**

$$\varepsilon \geq 1 - 10\% \qquad , \ N_D \geq 10^8/cm^2$$

Comparison of Secondary and Primary
Creep Laws for Silicon Above 1200°C

Secondary (Steady-State) $\dot{\epsilon}_{ij} = C[\exp(-\beta/T)/T]\,(\tau/\mu)^{n-1}\,S_{ij}$

Reference	C (°K/GPa-s)	β (°K)	n	$\dot{\epsilon}(s^{-1})$*
"High Creep" Condition	1.05×10^{31}	59,760	5	1×10^{-4}
Siethoff and Schröter (1983)	5.85×10^{22}	41,800	3.6	41×10^{-4}

Primary (Transient) $\dot{\epsilon}_{ij} = C\,(\sigma_o/\mu)^{n-1}\,S_{ij}$

Reference	C (GPa-s)$^{-1}$		n	$\dot{\epsilon}(s^{-1})$**
Present Work (111) FZ	7.45×10^{31}		10	4.7×10^{3}

---

*Calculated strain rate for $\tau/\mu = 10^{-3}$ and $T = 1300°K$.

**Calculated strain rate for $\sigma_o/\mu = 10^{-3}$

$\sigma_o = \sqrt{(3/2)\,S_{ij}\,S_{ij}}$

$S_{ij} = \sigma_{ij} - 1/3\,\sigma_{kk}\,\delta_{ij}$

Stress Analysis

● Incorporation of <u>very</u> high creep relaxation above 1200°C:

    - $\sigma \simeq 0$ down to some $T_O < T_M$.

● New thermal expansion coefficient (Y. Okada and Y. Tokumara, J. Appl. Phys., 56, 314 (1984)):

$\alpha = 3.725 \times 10^{-6} \left\{ 1 - \exp[-5.88 \times 10^{-3}\,(T - 124)] \right\} + 5.548 \times 10^{-10}\,T \; (K^{-1}).$

New Creep Presentation

$$\dot{\epsilon} \sim \infty, \ \sigma_{YY}, \ \sigma_{XX} \simeq 0 \qquad T_M > T > T_0$$

$$\dot{\epsilon} = (C/T) \ [\text{EXP}(-\beta/T)] \ \sigma^5 \qquad T_0 > T > 300^0 K$$

MODEL CASES

$T_0 = 1200^0 C, \ 1000^0 C$

WIDTH = 8 CM, 4 CM

GROWTH SPEED = 3 CM/MIN

HIGH CREEP CONDITION

DISTANCE FROM INTERFACE (cm)

SILICON SHEET

DISTANCE FROM INTERFACE (cm)

1. Elastic solution, $2W = 8$ cm
2. $T_o = 1200^\circ C$, $2W = 8$ cm
3. $T_o = 1200^\circ C$, $2W = 4$ cm
4. $T_o = 1000^\circ C$, $2W = 8$ cm
5. $T_o = 1000^\circ C$, $2W = 4$ cm
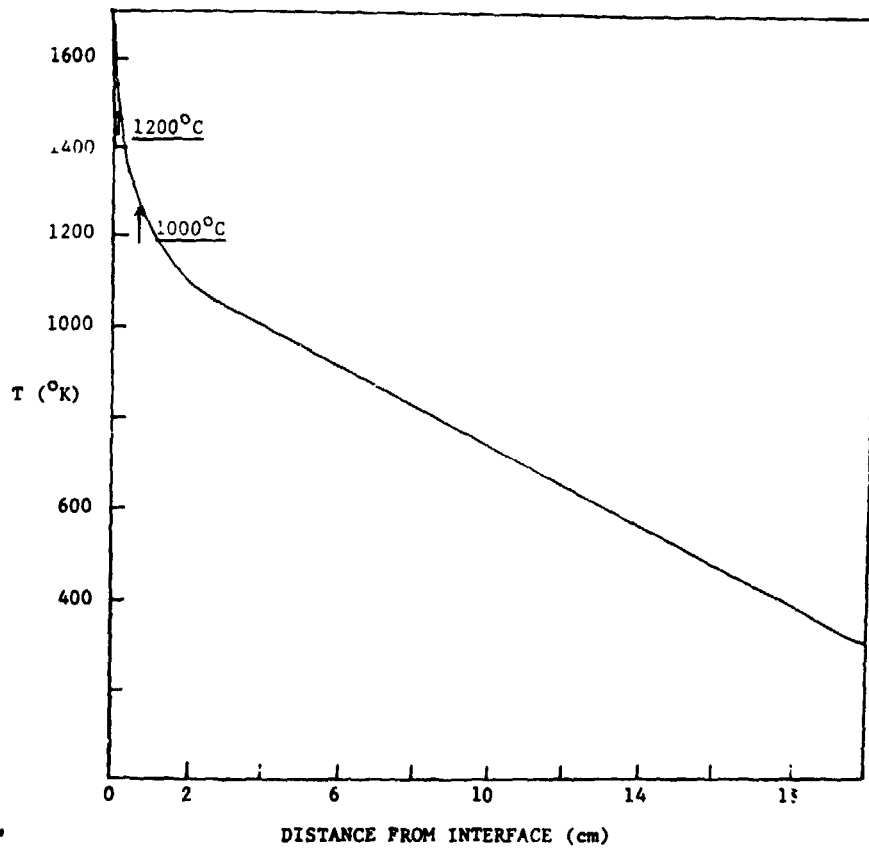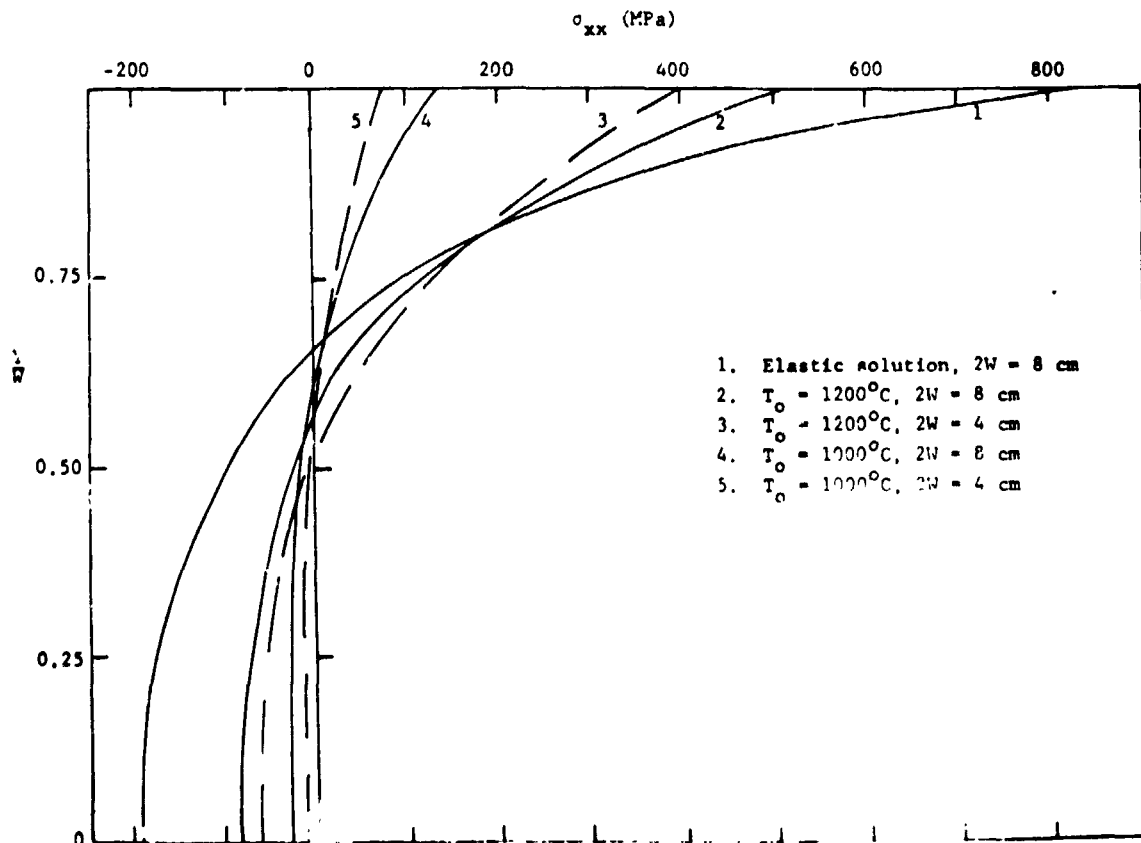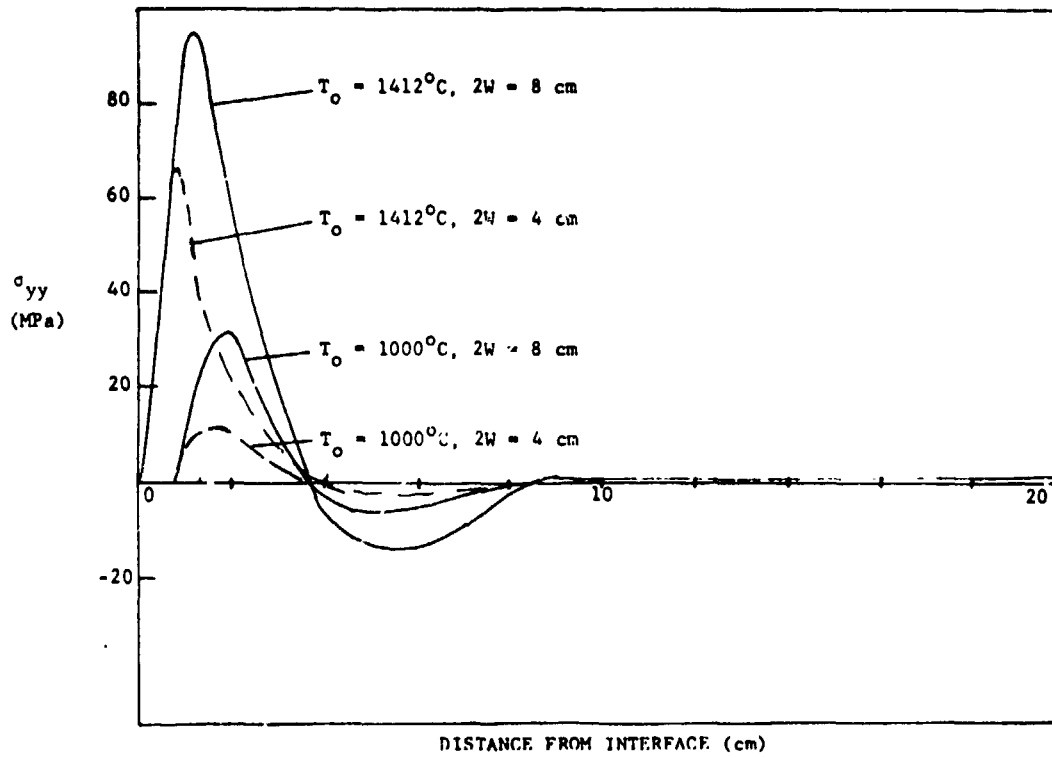
Dislocation-Efficiency Studies

- DEVELOP METHODS TO QUANTIFY INFLUENCE OF DISLOCATION ELECTRICAL ACTIVITY ON BULK LIFETIME WITH ROOM AND LOW TEMPERATURE EBIC.

- STUDY EFFECTS OF DISLOCATION DENSITY, STRESS LEVEL AND TEMPERATURE OF GENERATION OF DISLOCATIONS ON BULK LIFETIME.

WORK IN PROGRESS - COMPARISON OF STRESSED FZ, CZ AND EFG RIBBON.
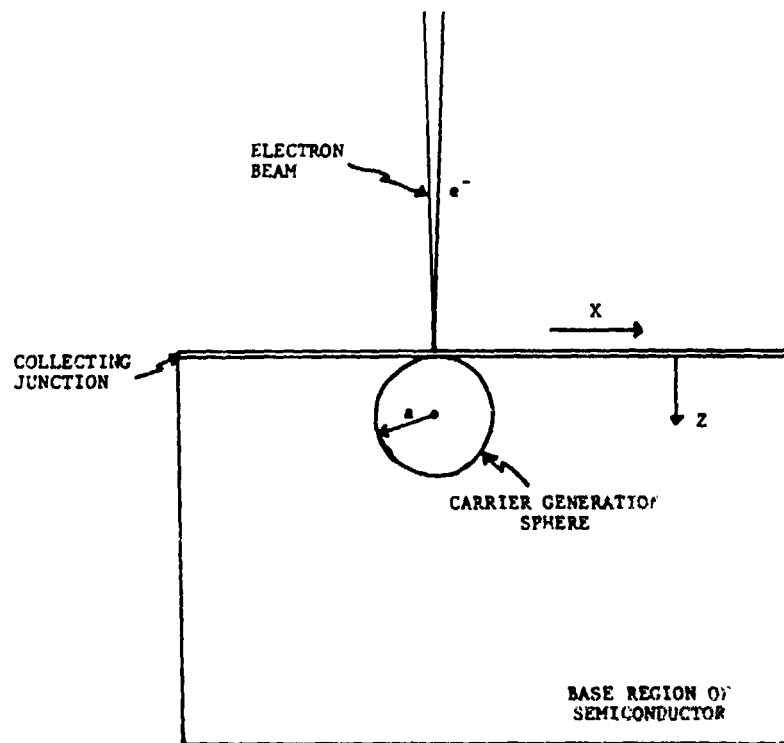
$$I = 3q\aleph_0 (L/a)^3 e^{-a/L} [a/L \cosh a/L - \sinh a/L]$$

C. Donolato, Optik, 52 19 (1979)

FRACTION OF CHARGE COLLECTED ($I/I\aleph_0$)

- EXPERIMENT (...)
- THEORY

REFERENCE CELL

L = DIFFUSION LENGTH
a = RADIUS OF THE GENERATION SPHERE

L (μm)
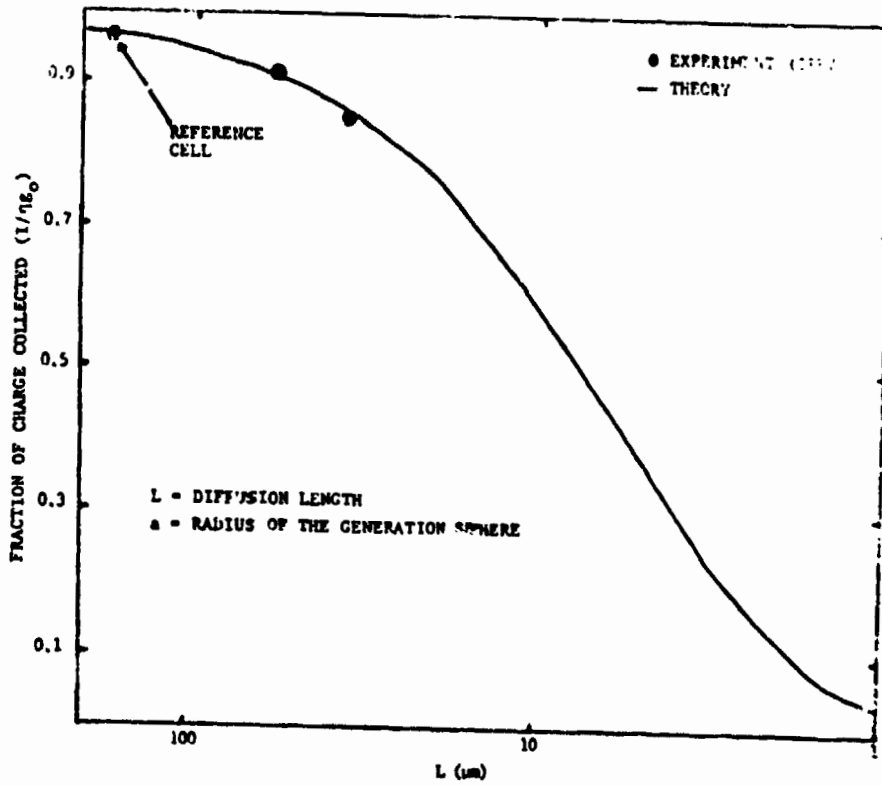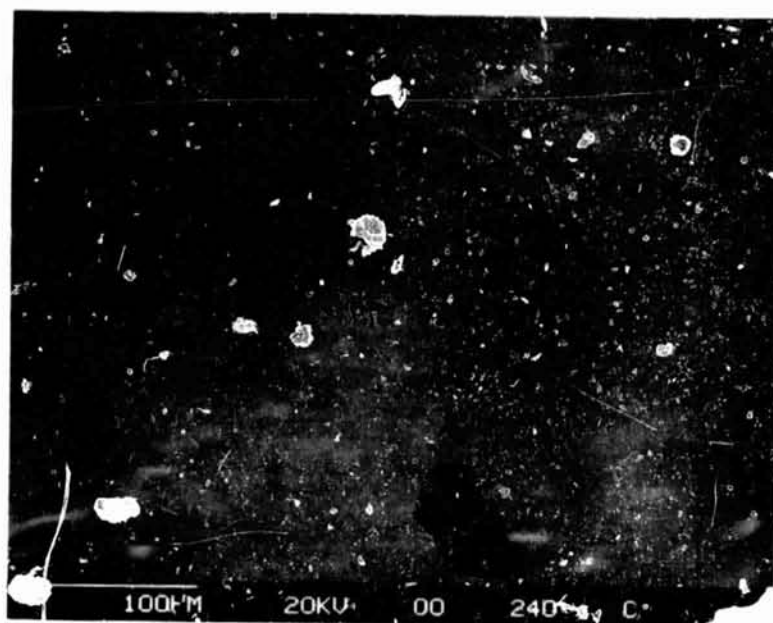
(a)
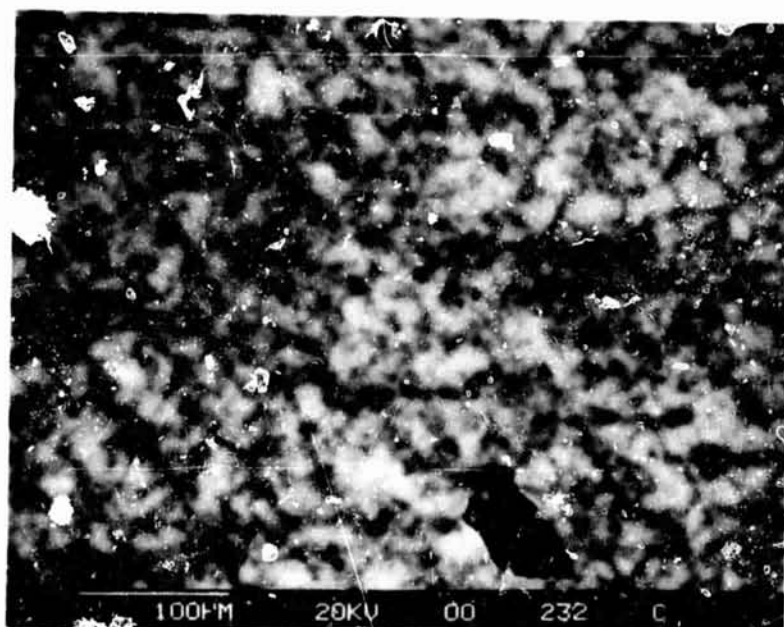
(b)

Fig. 12. (a) Room temperature, and (b) low temperature EBIC
of same region for stressed carbon-rich CZ.
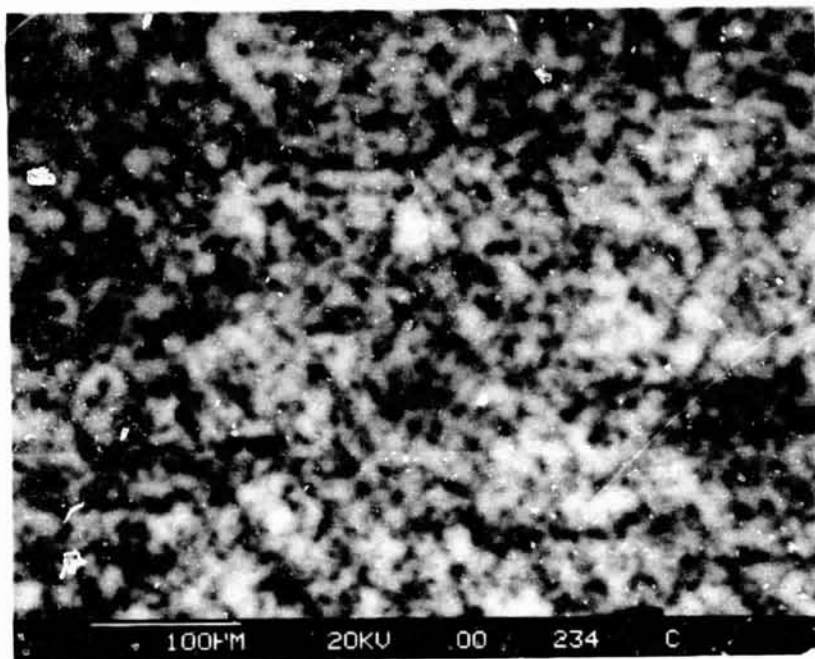
(a)
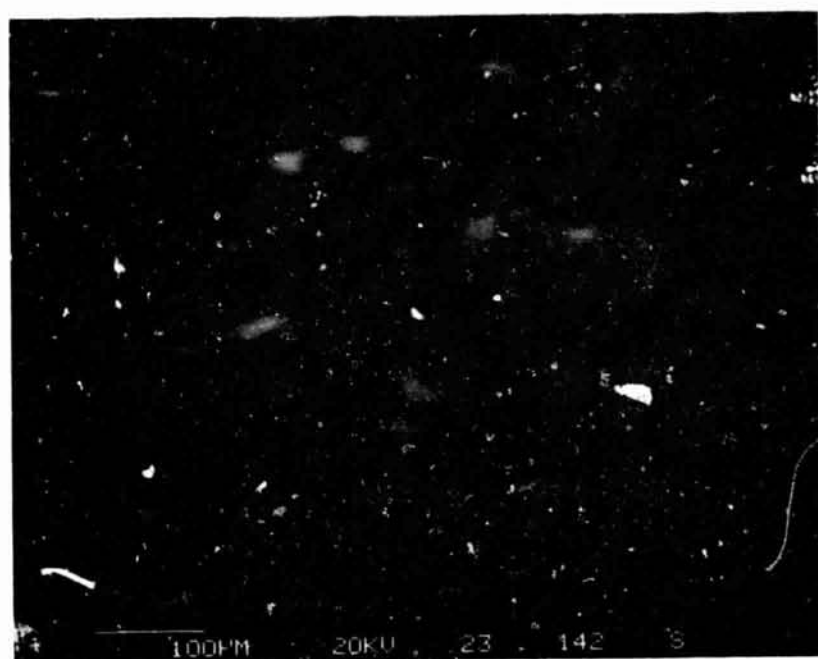
(b)

Fig. 11. Low temperature EBIC micrographs of (a) center and
(b) edge of stressed carbon-doped CZ wafer.

C-7
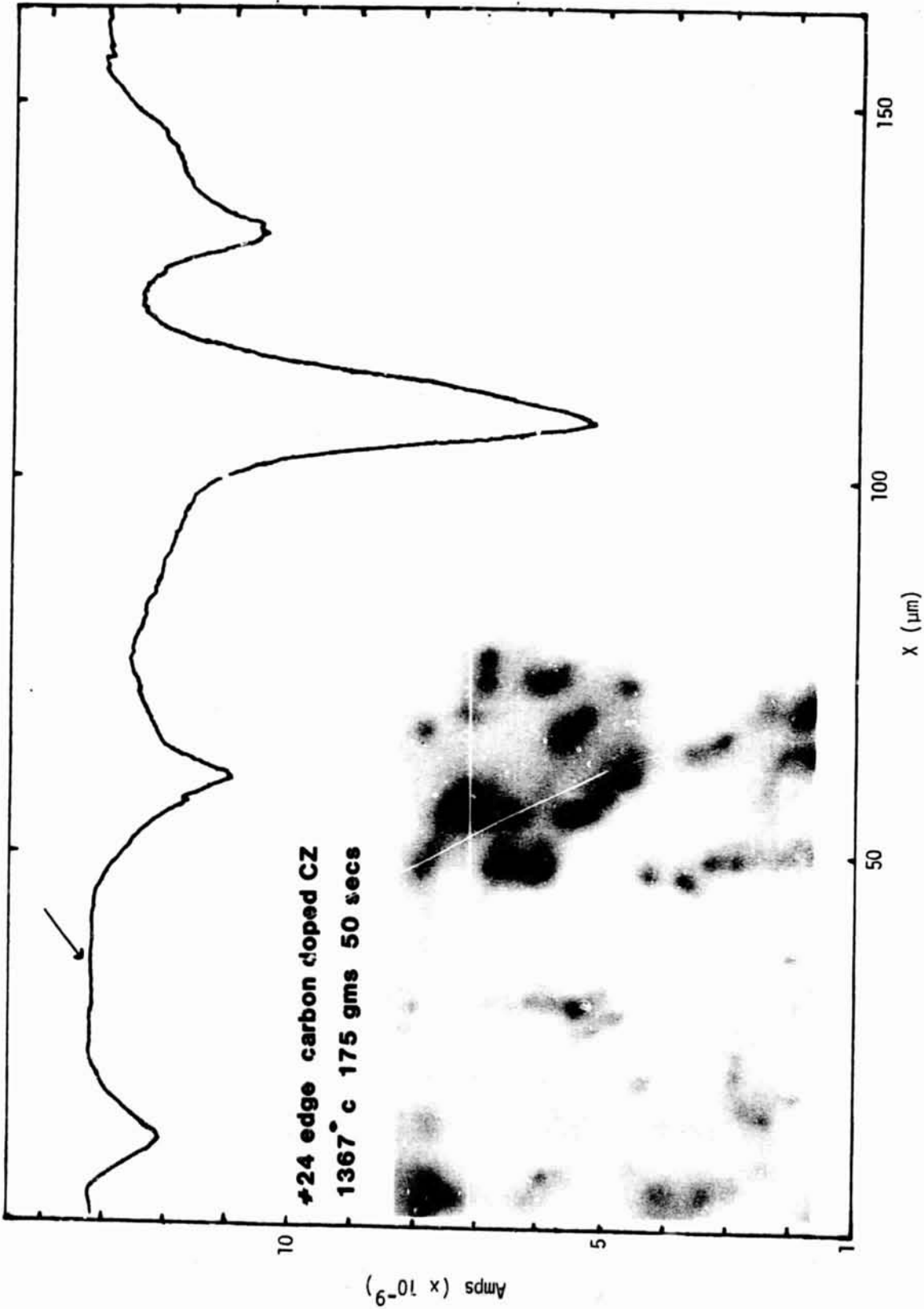
Fig. 8. High magnification (500X) low temperature EBIC line scan of stressed carbon-doped CZ.

#24 edge carbon doped CZ
1367°C 175 gms 50 secs

X (μm)

Amps (x 10⁻⁹)

Low Resistivity Studies

- POWER OUTPUT OF SILICON SOLAR CELLS MAXIMIZED BELOW 1 Ω-CM, BUT SEVERE DEGRADATION OF I_{SC}, V_{OC} OCCURS IN MORE DEFECTED SILICON BELOW 1 Ω-CM.

- BORON-IMPURITY-DEFECT INTERACTIONS LEADING TO DEFECTS RESPONSIBLE FOR DEGRADATION HAVE NOT BEEN STUDIED.

- PURPOSE IS TO CHARACTERIZE LOW RESISTIVITY MATERIAL DEFECT STRUCTURE AND ATTEMPT TO RELATE IT TO DEGRADATION.
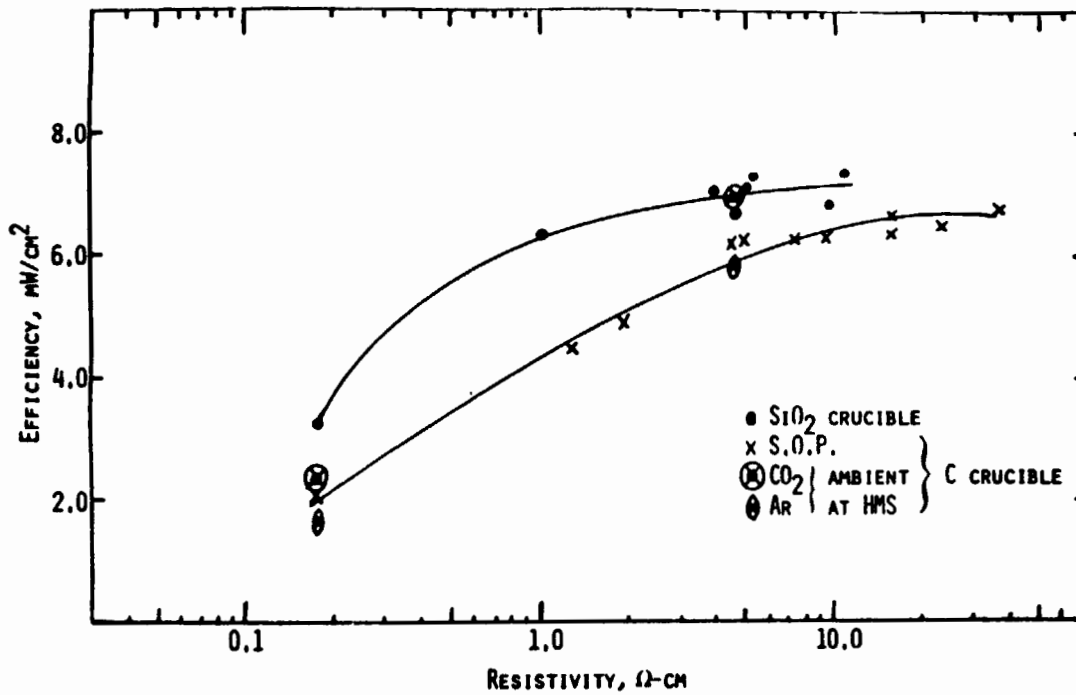
EFFICIENCY AS A FUNCTION OF RESISTIVITY IN EFG MATERIAL, B-DOPING, GROWTH FROM FUSED SILICA AND GRAPHITE CRUCIBLES. AMBIENT EFFECTS WITH GRAPHITE CRUCIBLE GROWTH ARE NOTED IN THE FIGURE.

Problems and Concerns

● RESIDUAL STRESS MEASUREMENTS NEED TO BE RELATED TO GROWTH VARIABLES.

● DISLOCATION ELECTRICAL ACTIVITY DEPENDENCE ON:

  − TEMPERATURE AT WHICH THEY WERE FORMED.

  − CARBON, OXYGEN IMPURITY AVAILABILITY.

  − CELL PROCESSING VARIABLES.

● LOW RESISTIVITY DEGRADATION MECHANISMS IN MORE HIGHLY DEFECTED SILICON MUST BE AVOIDED.

Future Work

● ANALYSIS TO DEFINE MINIMUM STRESS CONFIGURATIONS:

  − STUDY EFFECTS OF NEW CREEP LAW AND PREDICTIONS FOR EFG TEST SYSTEM.

  − TEMPERATURE FIELD CHARACTERIZATION.

  − RESIDUAL STRESS-DEFECT EVALUATION OF RIBBON (U. OF ILLINOIS).

● ROOM AND LOW TEMPERATURE EBIC CORRELATION OF DISLOCATION STRUCTURE AND ELECTRICAL ACTIVITY WITH BULK L_N.

● CHARACTERIZE LOW RESISTIVITY SILICON MATERIAL:

  − DISLOCATION STRUCTURE WITH VARYING LEVELS OF DOPING, (B, B-GA).

  − HREM (CORNELL) STUDY OF MICRODEFECTS.

N85-32441

SILICON SHEET SURFACE STUDIES

UNIVERSITY OF ILLINOIS AT CHICAGO

S. Danyluk

Relative Magnitudes of Residual Stresses
in Web and Mobil Silicon Sheet

TECHNOLOGY	REPORT DATE October 2, 1984
APPROACH Residual stresses in sheet silicon by interfero-metry. Simulation of abrasion of silicon by diamond by scratching and indentation tests. **CONTRACTOR**	**STATUS** Developed an interferometry technique for measuring residual stresses in short, thin silicon sheet. Measured the residual stresses in WEB and Mobil sheet. Correlated experimental wear rate with a wear model. Determined the residual stresses due to scratching.
GOALS Develop non-destructive residual stress measurement technique. Determine wear mechanism in silicon.	Showed that dislocations are associated with scratching and indentations performed at room temperature.
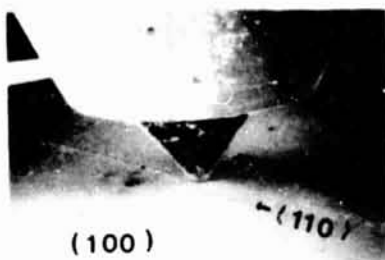
SILICON SHEET

(100)   ~(110)   1 Scratch   10 Scratches

Air
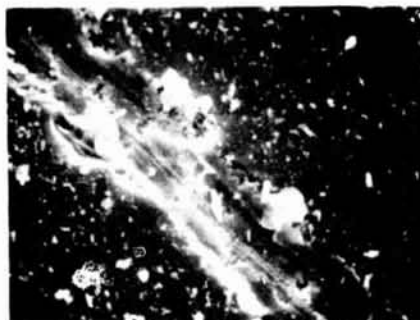
DI H$_2$O

Acetone

Ethanol

10 um
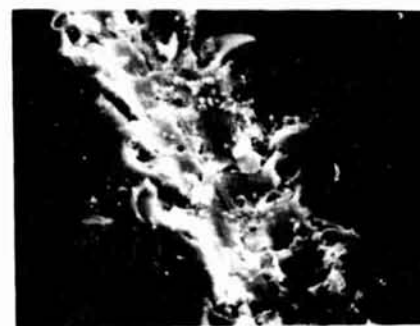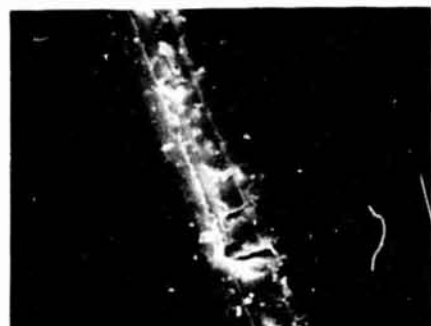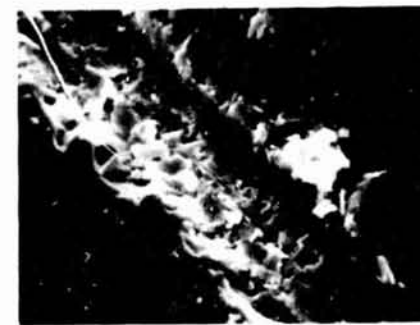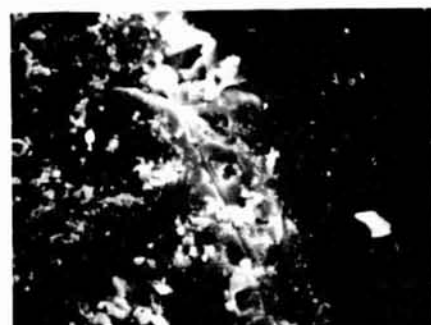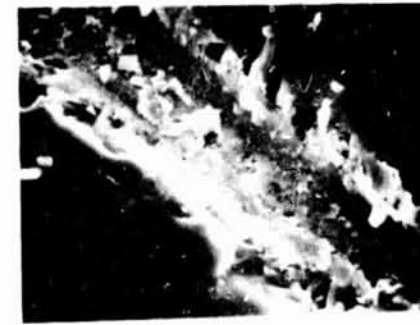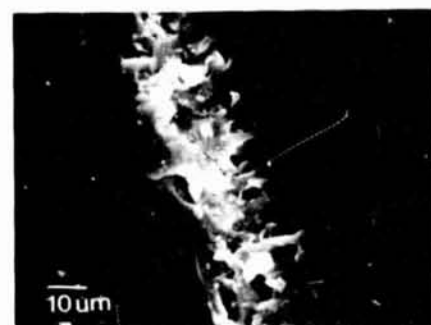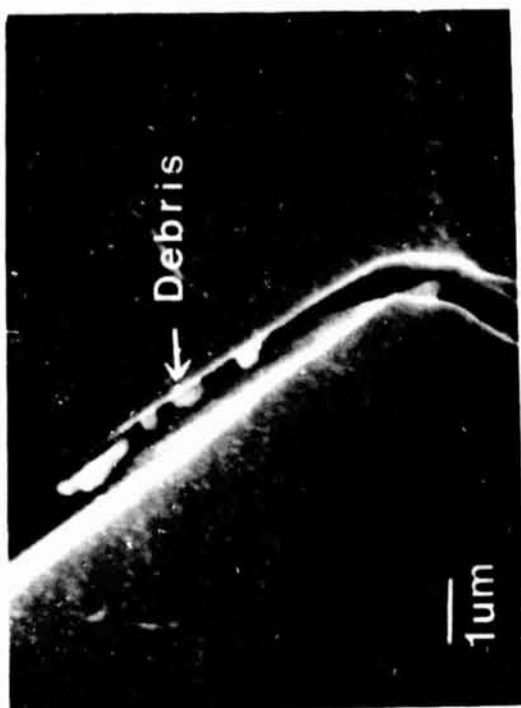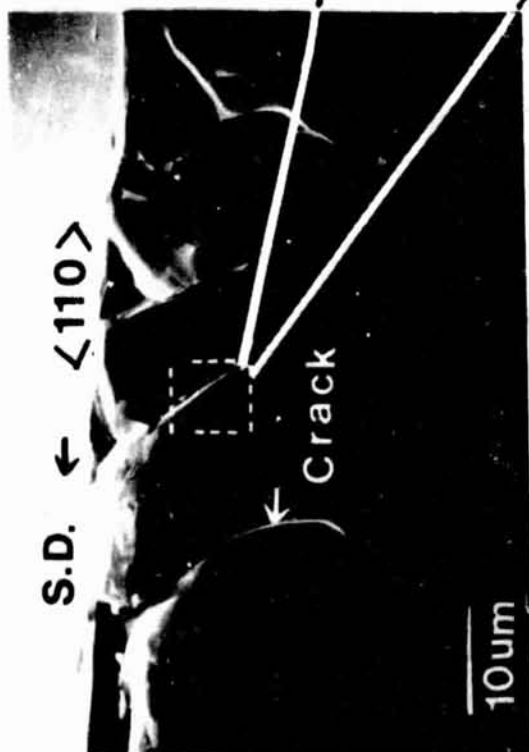
Plastic Deformation

Crack

1 um

Debris

10 um

10 um
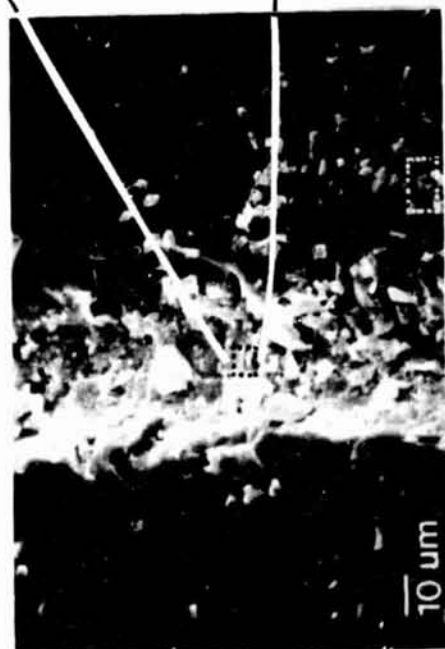
SEM MICROGRAPH OF (III) P-TYPE SILICON INDENTED UNDER A LOAD OF 0.49N IN 10^{-3} M/L NaI; ANNEALED AT 1373 K-2HRS AND ETCHED IN DILUTE SIRTL SOLUTION.

SILICON SHEET

- Indentation of ₐp-type silicon at RT in 10^3 M/ℓ NaI; annealed at 1373°K-2HRS. (present work)
- Indentation at RT & annealed at 1220°K-30min. (PaTu data)
- Indented at 873°K (S.M. Hu data)

P(N), INDENTATION LOAD

INDENTATION ROSETTE LENGTH x(10^{-6} m)

SILICON SHEET

Optical flat (or master grid)

fringes

M

M

Relative deflection

σ_{xx} profiles

b

h

t

residual stresses are uniform

residual stresses decrease to zero near the ends

L
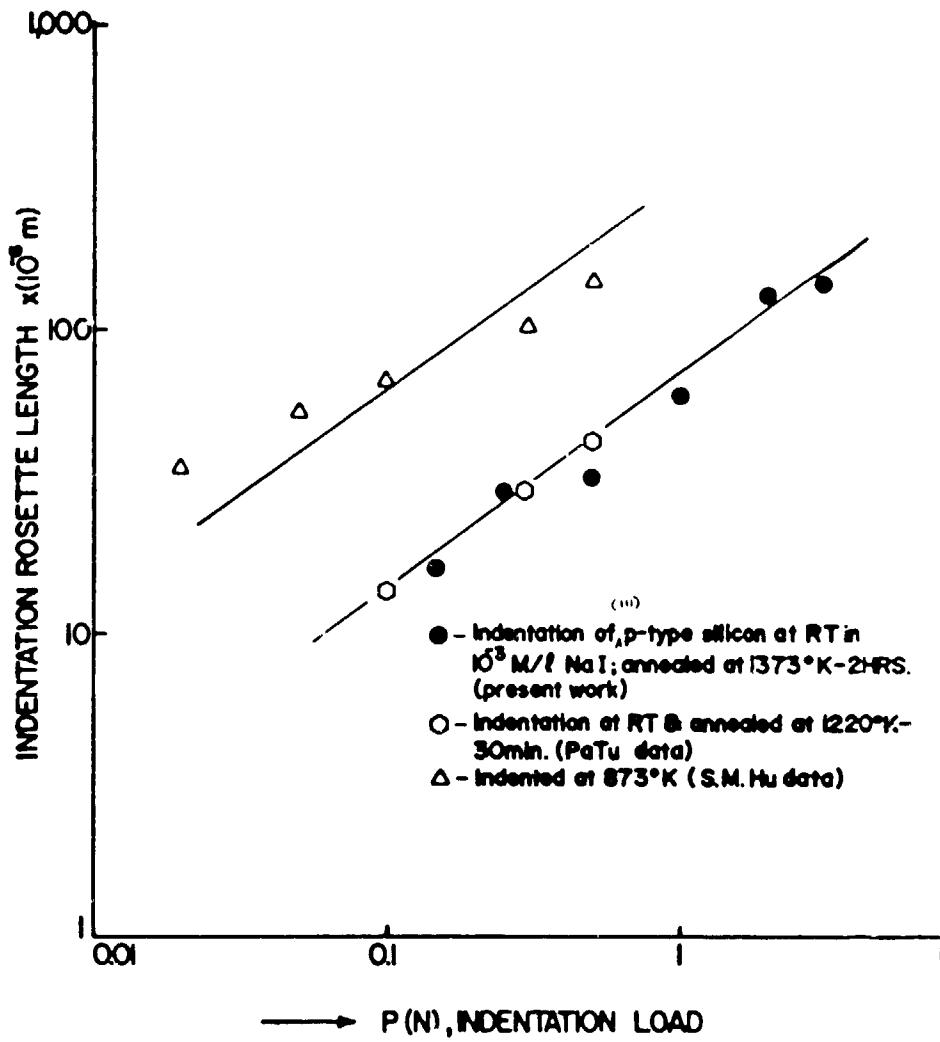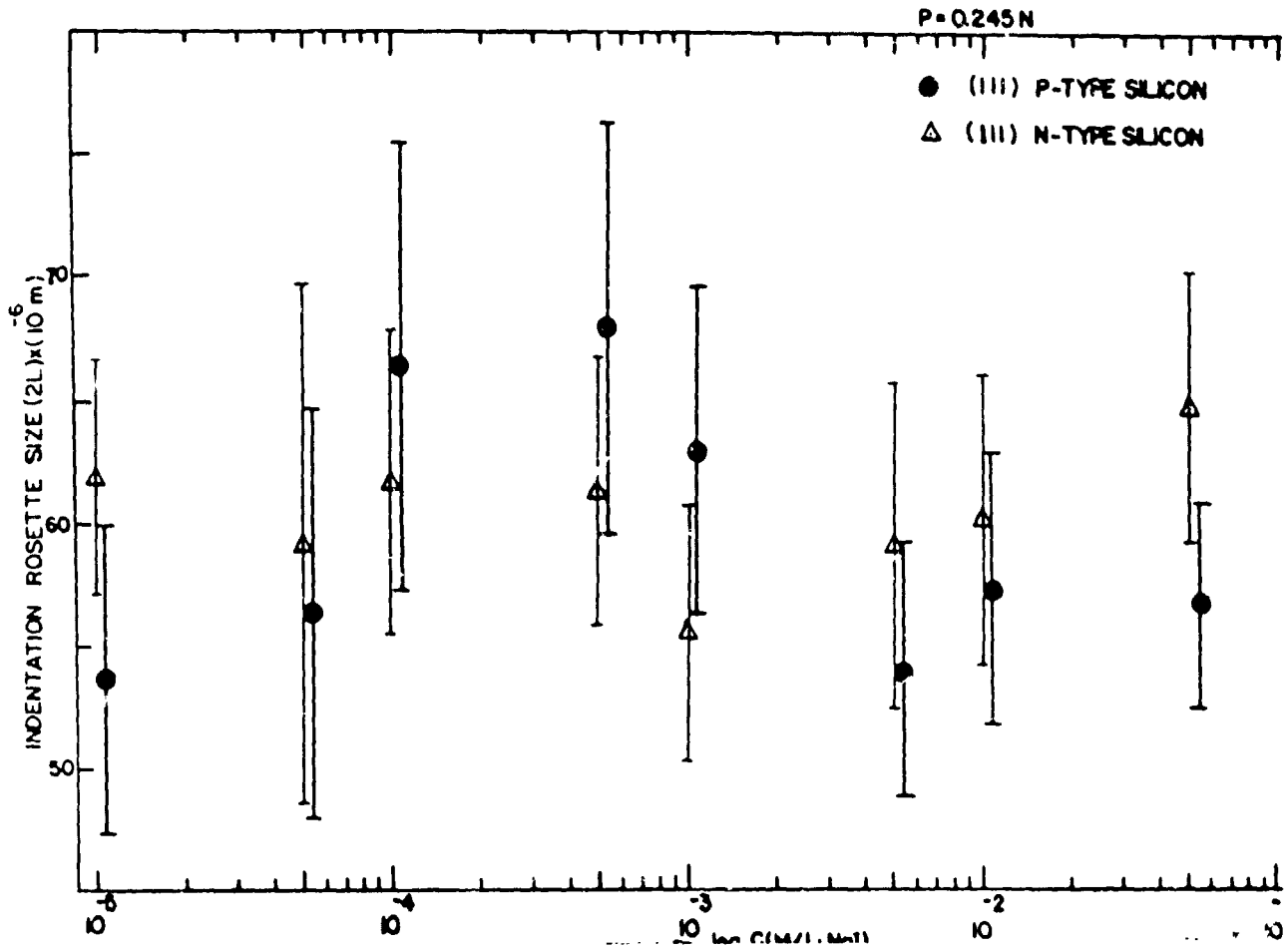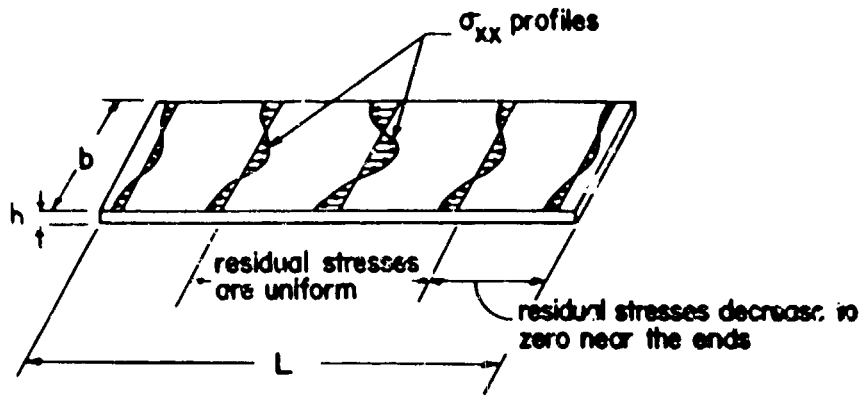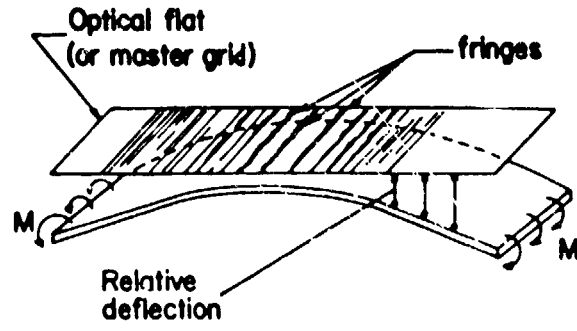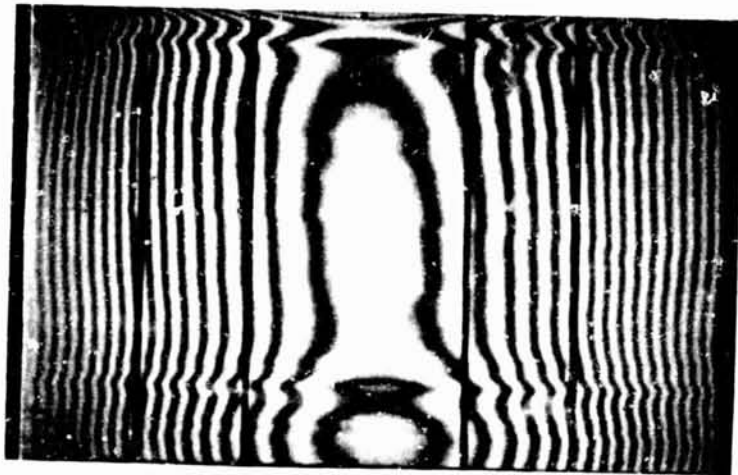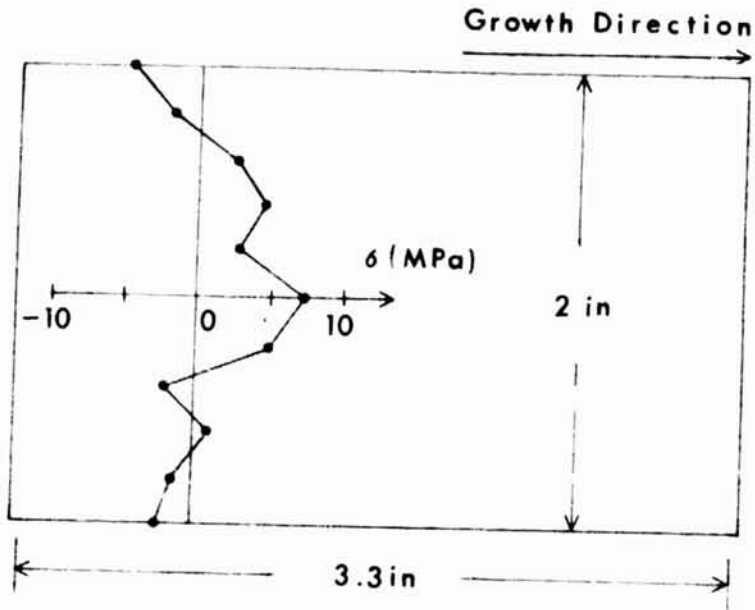
Outer Support
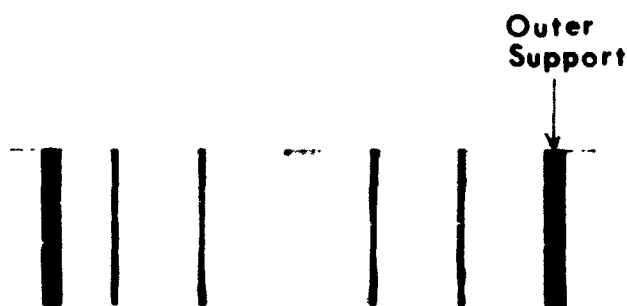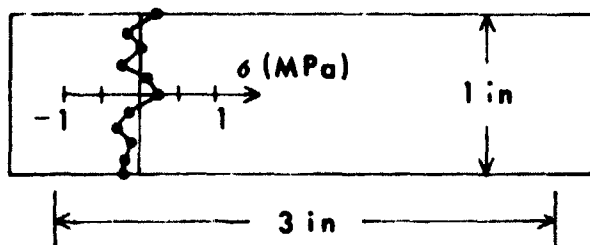
	Sample No.	Magnitude of Maximum Residual Stress (MPa)	Growth Speed (cm/min)
WEB	JS15-2.3a	2.5	
	J460-2.5a	0.4	
Mobil	47R1-1	9.0	2.00
	-2	5.0	2.00
	-3	7.3	1.75
	-4	6.5	2.25

Problems and Concerns

1. Do the residual stress measurements correlate with strain gauge measurements or dislocation distributions?

2. Is the fluid chemistry changed as a result of microcrack or dislocation generation?

3. Does the abrasion mechanism change when abrasion speeds are high? What is the contact temperature.

ANALYSIS OF INCLINED GROWTH OF SILICON SHEET

MASSACHUSETTS INSTITUTE OF TECHNOLOGY

Robert A. Brown

Program Goals

- DEVELOP A GENERAL-PURPOSE FINITE ELEMENT PROGRAM FOR ANALYSIS OF SILICON SHEET GROWTH IN INCLINED CONFIGURATIONS. VERIFY ANALYSIS WITH EXPERIMENTAL DATA OF OTHERS.

- USE PROGRAM TO STUDY PARAMETRIC SENSITIVITY OF VARIOUS GROWTH GEOMETRIES WITH RESPECT TO:

    - THERMAL CONTROL AND GROWTH RATE

    - DOPANT SEGREGATION

    - THERMAL STRESS

    - INTERFACE MORPHOLOGY AND INSTABILITY

- UNDETERSTAND TRANSITIONS IN INTERFACE MORPHOLOGY AND RELATIONSHIP TO DOPANT SEGREGATION.

Outline

1. THERMAL-CAPILLARY MODELING OF MENISCUS-DEFINED RIBBON-GROWTH
2. PREVIOUS RESULTS FOR EDGE-DEFINED FILM-FED GROWTH
3. PROTOTYPE MODEL FOR INCLINED RIBBON GROWTH
4. CALCULATIONS OF NONLINEAR MORPHOLOGICAL STRUCTURE

Prototype of Inclined Ribbon Growth
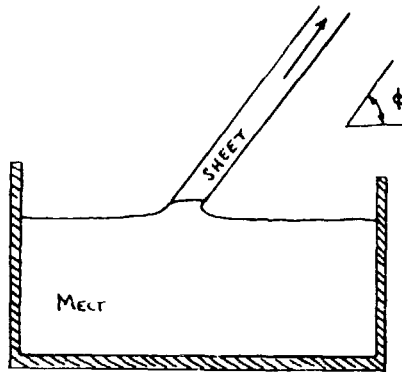
SOLUTION INVOLVES DETERMINING

1. TEMPERATURE FIELD IN MELT
2. MELT/CRYSTAL INTERFACE SHAPE
3. MELT/GAS INTERFACE SHAPE
4. CRYSTAL THICKNESS

Complete Analysis of Meniscus-Defined Growth System Required

1. SOLUTION OF ENERGY EQUATIONS IN ALL PHASES (MELT, CRYSTAL, DIE) AND ACCURATE ACCOUNT OF RADIATIVE HEAT TRANSPORT TO SURROUNDINGS

2. DETERMINATION OF MELT/SOLID INTERFACE SHAPE

3. CALCULATION OF MELT/GAS INTERFACE SHAPE TO SATISFY EQUATION OF HYDROSTATICS.

4. CALCULATION OF SHEET THICKNESS TO SATISFY EQUILIBRIUM GROWTH ANGLE.

• DEFINES A VERY COMPLEX NONLINEAR FREE-BOUNDARY PROBLEM. ALGORITHM FOR SOLUTION HAS ALREADY BEEN DEVELOPED.

Strategy for Development of Analysis

- COMPUTER-AIDED CALCULATIONS ARE BASED ON FINITE ELEMENT METHODS DEVELOPED FOR EFG SYSTEM IN COLLABORATION WITH RESEARCHERS AT MOBIL SOLAR ENERGY COMPANY.

- THERMAL STRESS ANALYSIS ALSO BASED ON FINITE ELEMENT SOLUTION OF NONLINEAR EQUATIONS FOR ELASTOPLASTIC DEFORMATION COUPLED WITH THERMAL-CAPILLARY HEAT TRANSFER ANALYSIS.

- COMPARISON WITH EXPERIMENTS WILL INTEGRATE HEAT TRANSFER BOUNDARY CONDITIONS APPROPRIATE FOR PARTICULAR GROWTH CONFIGURATION DIRECTLY INTO THE FINITE ELEMENT ANALYSIS.

EDGE-DEFINED FILM-FED GROWTH
OF THIN SILICON SHEETS

MOBIL SOLAR ENERGY CORP.

H.M. Ettouney and J.P. Kalejs
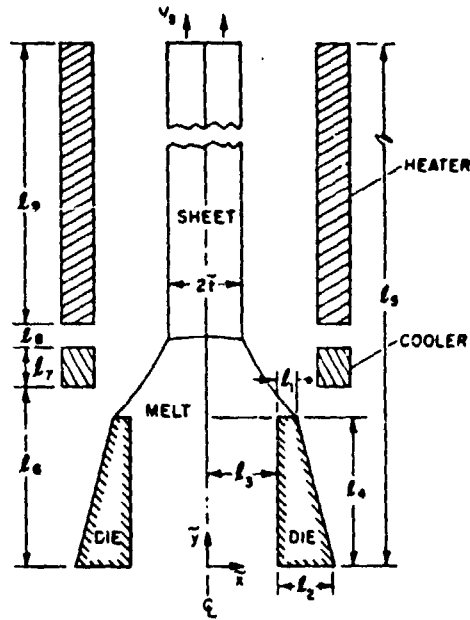
Thermal-Capillary Model

- TEMPERATURE FIELD DETERMINED
  CONDUCTION DOMINATED HEAT TRANSFER
  IN MELT AND CRYSTAL.

- MELT/SOLID INTERFACE SHAPE DETERMINED AS
  .. MELTING POINT ISOTHERM.

- MENISCUS SHAPE DETERMINED BY BALANCE OF SURFACE
  TENSION AND HYDROSTATIC FORCES.

- THICKNESS OF SHEET DETERMINED BY CONDITION
  FOR EQUILIBRIUM GROWTH ANGLE.

- DISTANCE FROM DIE TIP TO HEIGHT OF MELT POOL
  SETS REFERENCE PRESSURE IN MENISCUS REGION.
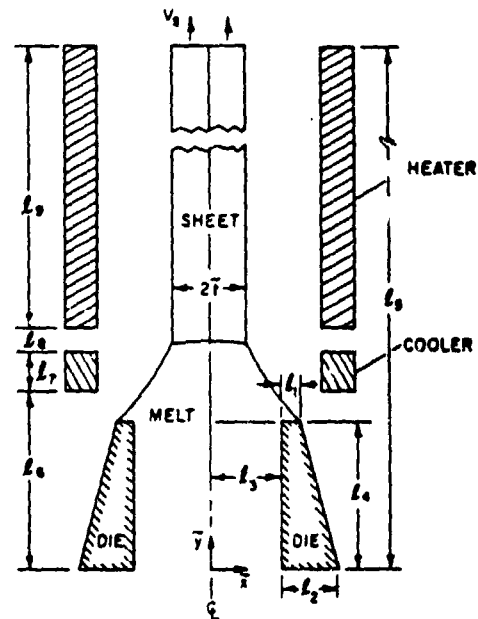
PRECEDING PAGE BLANK NOT FILMED

Model Description

- **Finite Element Analysis to Provide:**
  - **Coupled Solutions for Heat Transfer and Capillarity in Three-Phase Domain of EFG Die/Melt/Crystal.**
  - **Three Unknown Boundaries for Crystal Thickness, Melt/Solid, Melt/Gas Interfaces.**

- **Two-Dimensional Navier-Stokes Flow Field in Die Top and Meniscus (Interface) Melts**

- **Diffusion Equation Solutions for Segregated Aluminum Dopant**

Physics Is Best Explained for Growth Into Ambient at Uniform Surrounding Temperature

(CRYSTAL THICKNESS)

t

SPECIFIED

H_e

T_∞

Die Geometry

P_e (GROWTH RATE)

d=0.005 cm
b = 0.125 cm
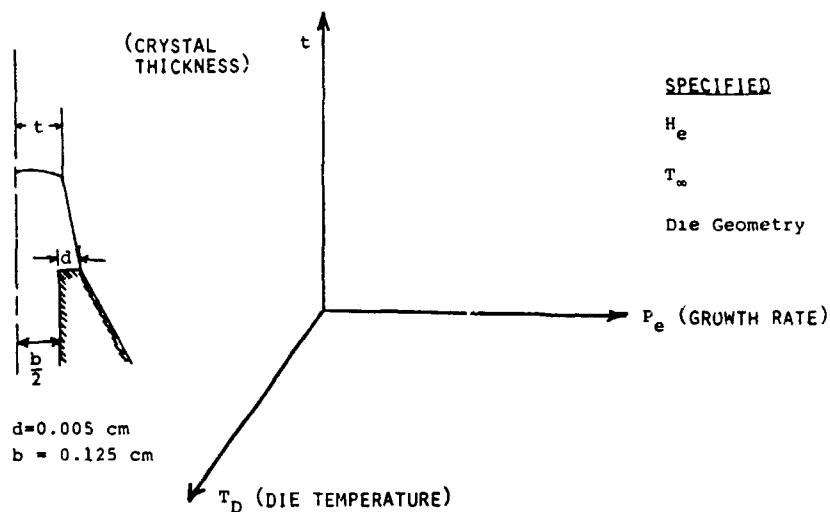
T_D (DIE TEMPERATURE)

Operating Diagram for EFG
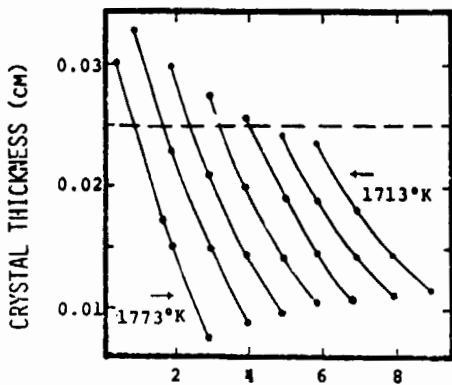
GROWTH RATE (CM/MIN)

CONTROL SCHEME FOR MAINTAINING CONSTANT THICKNESS
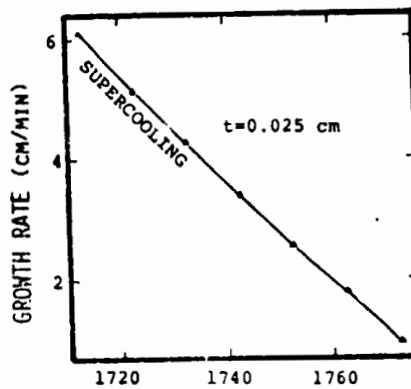
INLET MELT TEMPERATURE, T_D

- MELT BECOMES SUPERCOOLED FOR LOW DIE TEMPERATURES

Crystal Thickness Is Maintained Constant by Simultaneously Changing v and T_D
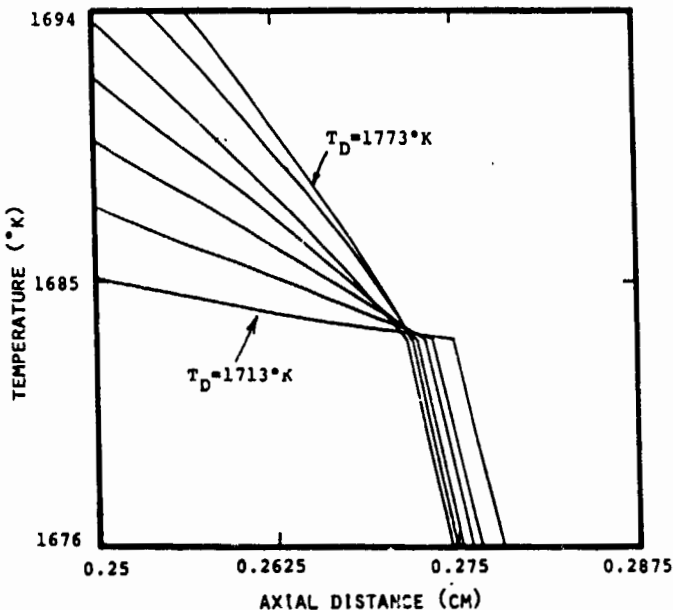
$T_D(°K)$	V(cm/min)	$\frac{dT_L}{dy}(\frac{°C}{cm})$
1773	0.96	875
1763	1.81	743
1753	2.57	612
1743	3.41	475
17..	4.28	333
1723	5.15	186
1713	6.11	31

- A MAXIMUM GROWTH RATE EXISTS WHERE TEMPERATURE GRADIENT AT INTERFACE DROPS TO ZERO, ONSET OF SUPERCOOLING.

Ambient Temperature Distribution Used
for Comparison With Experiments
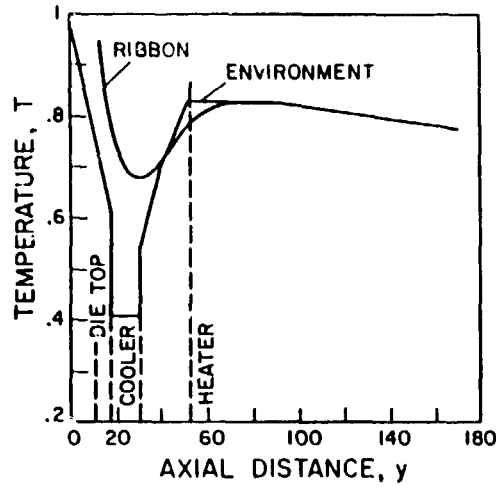
Comparison of Calculations and Measurements for
Prediction of Thickness Variation With Pull Rate
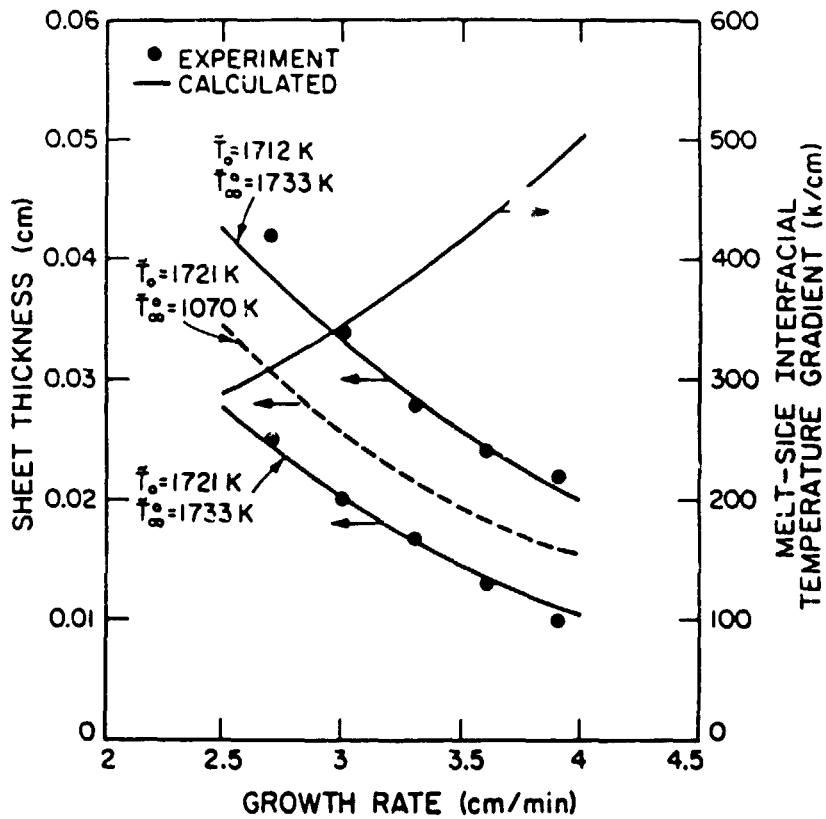
Operating Region Predicted by Finite Element Analysis
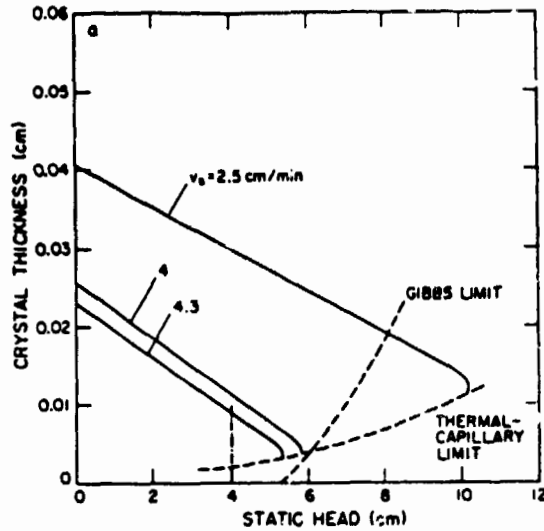
Dopant Segregation Effects

Distribution of Dopant Through Ribbon Thickness Depends on:

(1) Interface Shape – Heat Transfer Solution

(2) Solidification Flow Field - Navier Stokes Solutions

Parameterized by Die Geometry, Meniscus Configuration

(3) Surface Tension–Driven Flow

Accurate Calculation of Dopant Segregation

- FINITE ELEMENT ANALYSIS OF THERMAL-CAPILLARY MODEL SETS SHAPE OF MELT.

- VELOCITY FIELD IN MELT COMPUTED BY FINITE ELEMENT SOLUTION FULL NAVIER-STOKES EQUATIONS IN MELT.

- DOPANT CONCENTRATION FIELD CALCULATED BY SOLVING SPECIES CONSERVATION EQUATION

$$\nabla^2 c - Pe_B \nabla \cdot (c\, v) = 0$$

$$Pe_B = 2l_3 V^o / D$$

- NO ADJUSTABLE PARAMETERS IN CALCULATION !
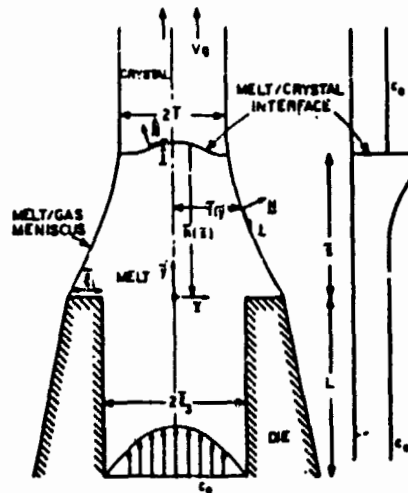
Lateral Dopant Segregation
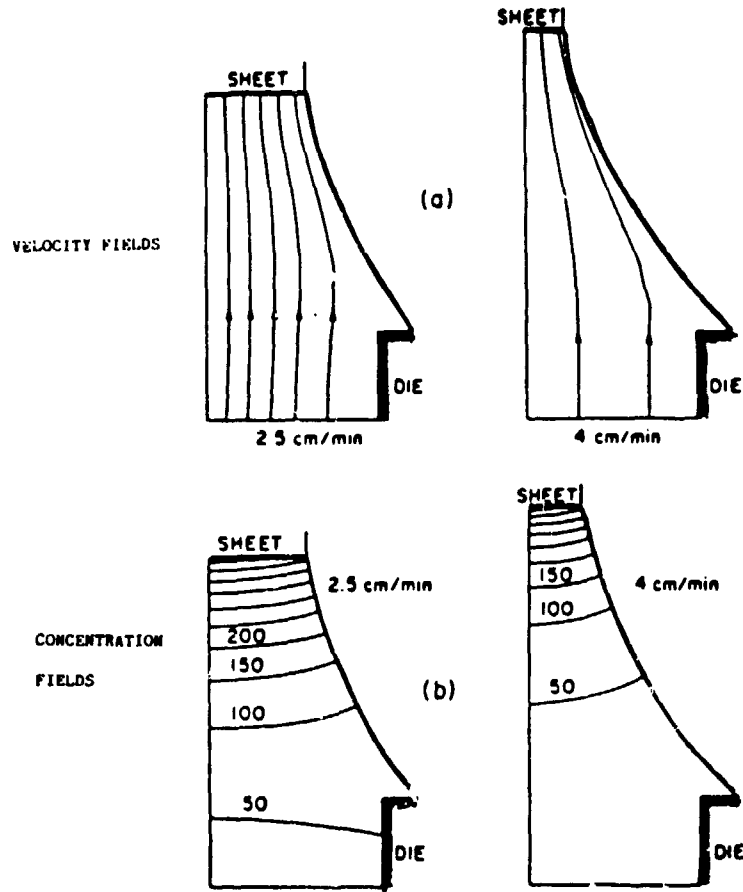
LATERAL DOPANT SEGREGATION PREDICTED BY CALCULATION OF DETAILED VELOCITY
AND CONCENTRATION FIELDS IN THE MELT USING HEAT TRANSFER ANALYSIS.

Aluminum Distribution Across Thickness of Si Sheet
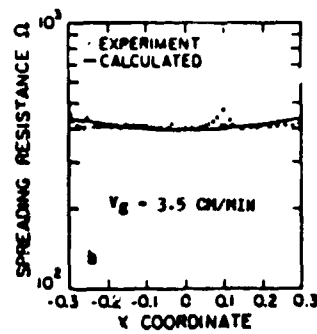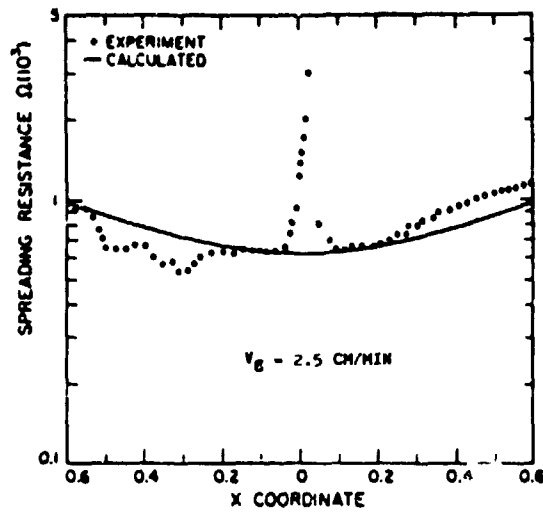
Surface-Tension-Driven Flow

$$V = \frac{d\sigma}{d\widetilde{T}} \frac{\Delta T^{\circ}}{\mu}$$

For silicon sheet EFG:

$\Delta T^{\circ} \sim 5\text{-}20^{\circ}K$ (model)

$\frac{d\sigma}{d\widetilde{T}} = -0.2$ dynes/cm-K (Hardy)

$\mu = 0.0088$ poise

$V = 120$ cm/sec $\gg V_s$ (0.04 cm/sec)

SILICON SHEET

Summary

● Fit of Finite Element Model Predictions to Experimental Data Achieved For:

- t-V_s Relationship
- Growth Rate Limits
- Aluminum Dopant Segregation Dependence on t, V_s

With One Adjustable Parameter τ_0.

● Comprehensive Nature of Finite Element Model Demonstrated
  for Predicting Process Variable Relationships,
  Interface Configuration and Dopant Segregation

NONLINEAR ANALYSIS OF MORPHOLOGICAL TRANSITIONS DURING DIRECTIONAL SOLIDIFICATION TRACES EVOLUTION OF PLANAR INTERFACE INTO HIGHLY STRUCTURED CELLULAR AND DENDRITIC FORMS.

INCREASING VELOCITY

CRYSTAL | MELT

PLANE   CELLS   DENDRITES

- ANALYSIS COMBINED FINITE-ELEMENT-METHODS FOR SOLVING EQUATION-SET FOR TRANSPORT AND MORPHOLOGY WITH NEW METHODS IN NONLINEAR ANALYSIS

- FIRST TO PREDICT TRANSITION TO DEEP CELLS

- SHOW FUNDAMENTAL MODE FOR REDUCTION OF CELL WAVELENGTH

- FIRST TO EXPLAIN ROLE OF GRAIN BOUNDARIES IN ONSET OF CELLULAR STRUCTURE

- ANALYSIS CAPABLE OF PREDICTION OF ONSET OF DENDRITIC GROWTH

Two-Dimensional Model of Interface Morphology

$$\nabla^2 C + Pe \frac{\partial C}{\partial y} = 0$$

$$\nabla^2 T + Pe_{Th} \frac{\partial T}{\partial y} = 0$$

Melt

Interface

$$T = 1 + mC + \Gamma \mathcal{H}$$

$$\underline{n} \cdot \nabla T + R \underline{n} \cdot \nabla T_s = Pe_{Th} St$$

$$\underline{n} \cdot \nabla C + R_m \underline{n} \cdot \nabla C_s = \underline{n} \cdot \underline{e}_y Pe (k-1)C$$

Solid

$$R_m \nabla^2 C_s + Pe \frac{\partial C_s}{\partial y} = 0$$

$$R \nabla^2 T_s + Pe_{Th} \frac{\partial T_s}{\partial y} = 0$$

$$R = \kappa_s / \kappa$$

$$R_m = D_s / D$$

$$Pe = \lambda v / D$$

$$Pe_{Th} = \lambda v / \kappa$$

$$St = L / \rho C_p T_m$$
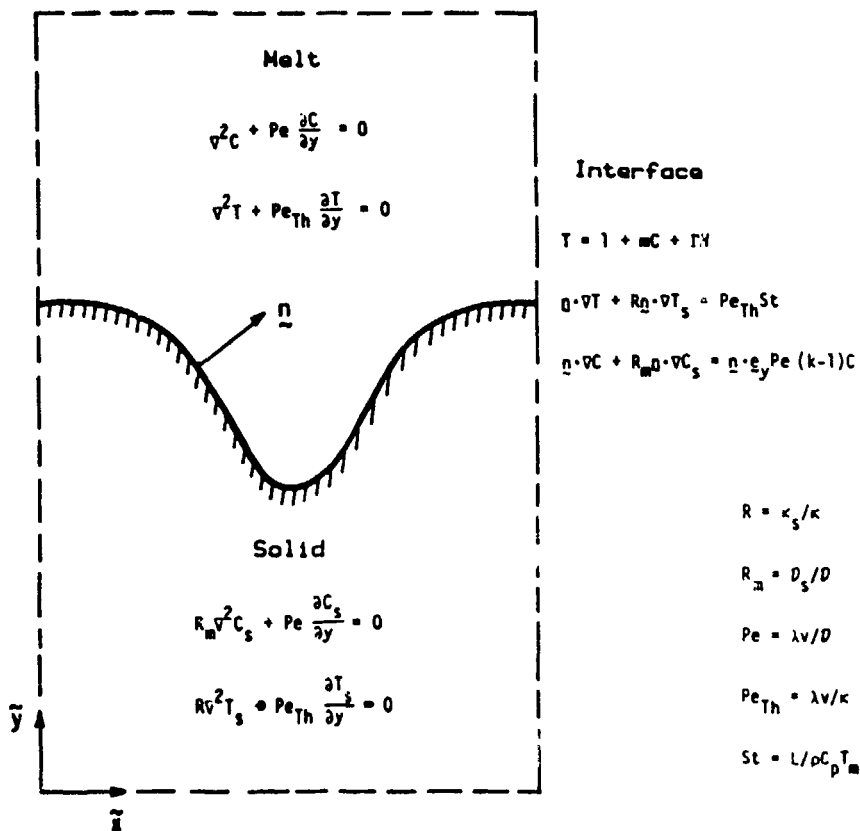
Models for Studying Morphological Structure

MODEL	LATENT HEAT	THERMAL CONDUCTIVITIES	CONVECTIVE HEAT TRANSPORT	SOLID DIFFUSION	REFERENCE
THERMAL-SOLUTAL (TSM)	YES	NOT EQUAL	YES	YES	UNGAR ET AL. (1984)
ONE-SIDED TSM	YES	NOT EQUAL	YES	NO	MULLINS AND SEKERKA J. Appl. Phys. 34 323 (1963)
EQUAL CONDUCTIVITY	YES	EQUAL	YES	NO	MC FADDEN AND CORIELL Physica D in press (1984)
SOLUTAL MODEL (SM)	NO	EQUAL	NO	YES	UNGAR AND BROWN, Phys. Rev. B. (1984)
SYMMETRIC SM	NO	EQUAL	NO	YES $(B_L = B_s)$	LANGER, Rev. Mod. Phys. 52, 1 (1980)
ONE-SIDED SM	NO	EQUAL	NO	NO	UNGAR AND BROWN Phys. Rev. B. 29, 1367 (1984)

SILICON SHEET
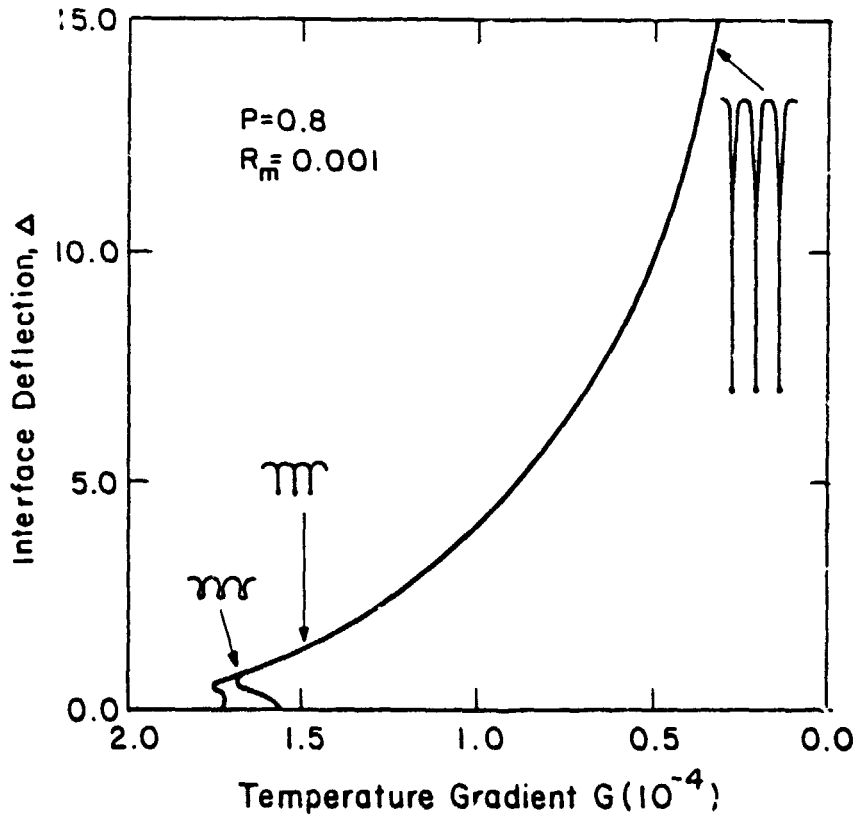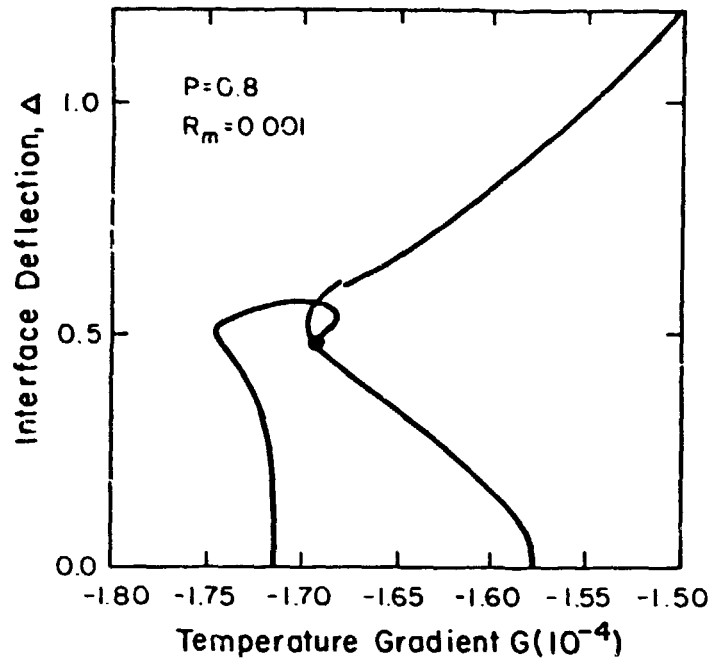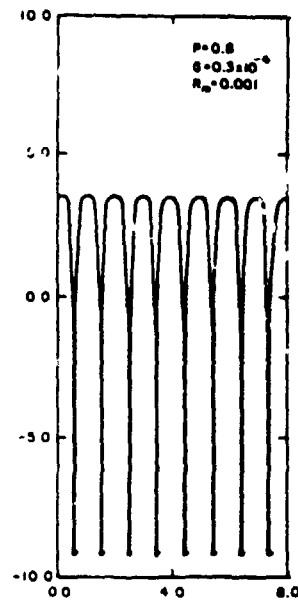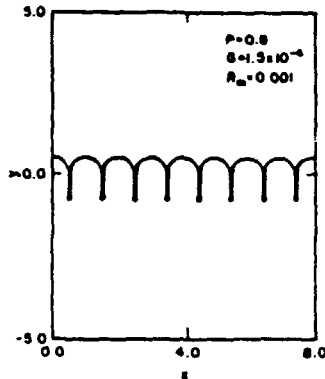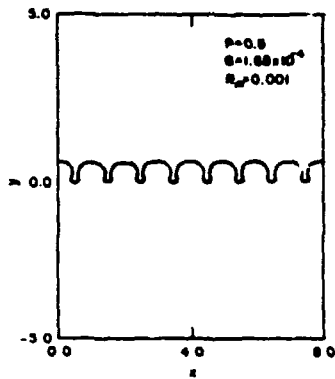
Progress Report

1. FINITE ELEMENT PROGRAM FOR IDEALIZED GROWTH INCLINED GROWTH SYSTEM HAS JUST BEEN COMPLETED. RADIATIVE COUPLING BETWEEN MELT AND CRYSTAL SURFACES IN UNDERWAY.

2. PROGRAM WILL BE READY FOR COMPARISON WITH EXPERIMENTS BY 01/01/1985.

3. COUPLING OF THERMAL STRESS ANALYSIS TO THERMAL-CAPILLARY MODEL WILL BEGIN THIS FALL AND BE COMPLETED IN LATE SPRING.

4. FINITE ELEMENT ANALYSIS OF MICROSCOPIC INTERFACE MORPHOLOGY BEYOND THE POINT OF LINEAR INSTABILITY HAS BEEN DEVELOPED. CALCULATIONS FOR SILICON UNDER SHEET GROWTH CONDITIONS WILL BE COMPLETED BY EARLY SPRING.

Summary

Finite element analysis is being used on two length scales to understand crystal growth of thin silicon sheets.

1. Thermal-capillary models of entire ribbon-growth systems. Demonstrated for EFG; model presented for inclined-meniscus system.

2. Microscopic modeling of morphological structure of melt/solid interfaces beyond the point of linear instability. The formation of deep cells and dendrites. Application to silicon system is underway.

HIGH-PURITY SILICON CRYSTAL GROWTH

SOLAR ENERGY RESEARCH INSTITUTE

T. Ciszek

TECHNOLOGY	REPORT DATE
HIGH PURITY SILICON CRYSTAL GROWTH INVESTIGATIONS	9/21/84

APPROACH	STATUS
INVESTIGATE CRYSTAL GROWTH PARAMETER EFFECTS ON MINORITY CARRIER LIFETIME AND SOLAR CELL EFFICIENCIES USING HIGH PURITY TECHNIQUES SUCH AS FLOAT ZONING (FZ).	• CONCLUSION OF SOLID/MELT IN-TERFACE STUDIES.

CONTRACTOR

SOLAR ENERGY RESEARCH INSTITUTE

GOALS

- OPTIMIZE DOPANTS AND MINORITY CAR-RIER LIFETIME IN FZ MATERIAL FOR HIGH EFFICIENCY SILICON SOLAR CELL APPLICATIONS.

- IMPROVE THE UNDERSTANDING OF LIFE-TIME DEGRADATION MECHANISMS (POINT DEFECTS, IMPURITIES, THERMAL HIS-TORY, SURFACE EFFECTS, ETC.

- CRYSTALLOGRAPHIC DEFECT CHARACTER-IZATION OF FLOAT-ZONED AND RIBBON CRYSTALS VIA X-RAY TOPOGRAPHY.

STATUS

- CONCLUSION OF SOLID/MELT IN-TERFACE STUDIES.

- FEASIBILITY DEMONSTRATION OF A CRUCIBLE-FREE HORIZONTAL RIBBON GROWTH METHOD.

- GROWTH OF SILICON SHEETS BY ESP FROM A COLD CRUCIBLE

- SOLAR CELL DATA OBTAINED ON COLD CRUCIBLE AND HORIZONTAL CRUCIBLE-FREE RIBBONS.

- X-RAY TOPOGRAPHY USED TO EX-AMINE DENDRITIC WEBS AND WEB CELLS, COLD CRUCIBLE CZ, AND FZ CRYSTALS.

- MINORITY CARRIER LIFETIME MEASUREMENT TECHNIQUES UNDER WAY.

- INITIATION OF HEAVILY DOPED, DISLOCATION-FREE, FZ CRYSTAL GROWTH STUDIES.

Growth form of a (110)-surface silicon sheet
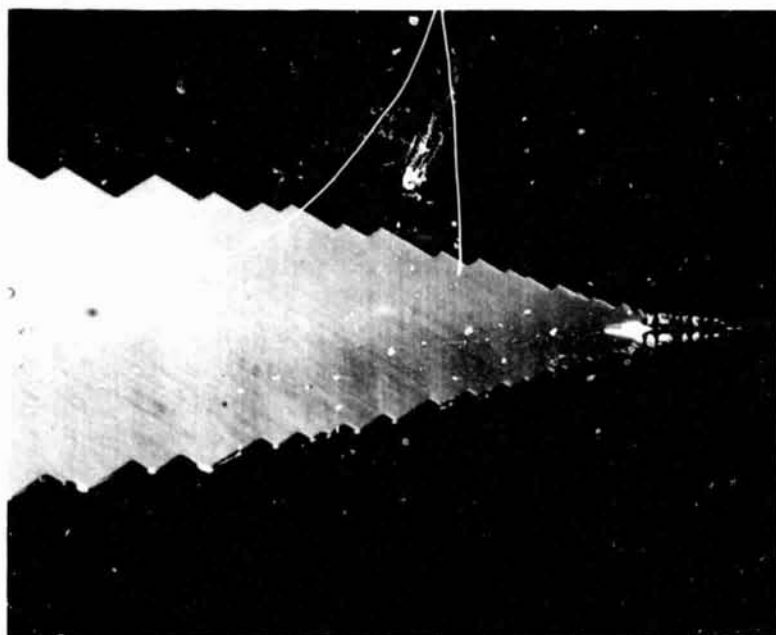
Growth form of a (111)-surface silicon dendrite

Size vs. time for a (100)-surface silicon sheet in <001> and <110> directions
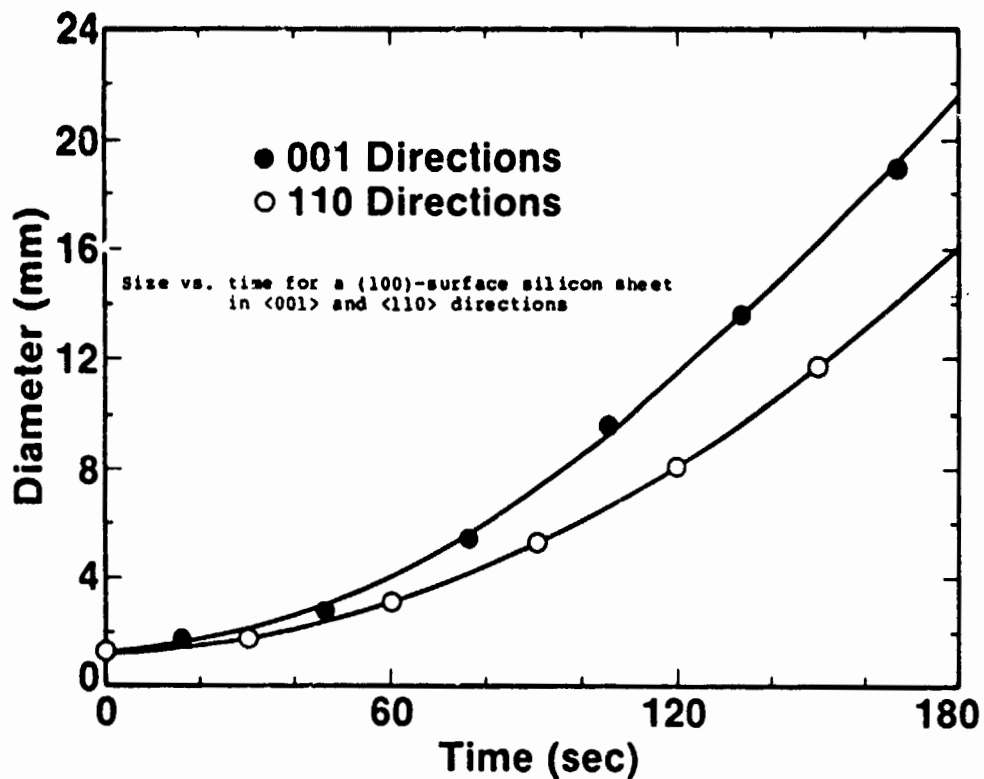
Growth rate anisotrophy ratios for a (111)-surface silicon sheet in <112>/<011̄> directions and for a (100)-surface Si sheet in <011>/<001> directions
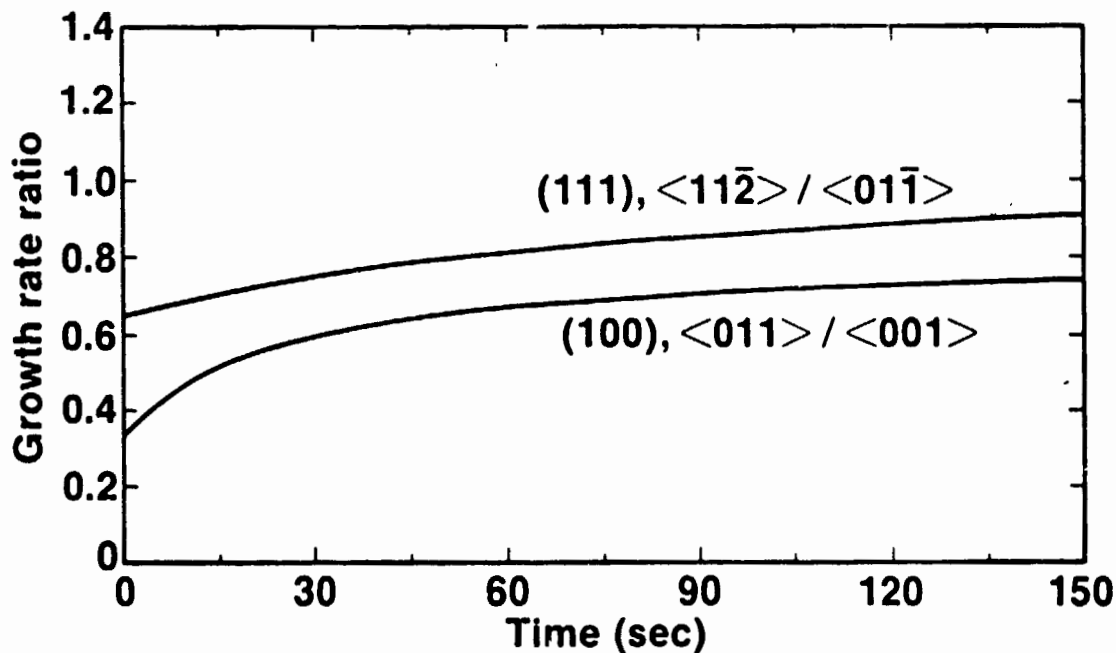
Crucible-Free Horizontal (CFH)
Silicon-Ribbon Growth Method

$$v_f = \frac{4 W t \, v_s}{\pi D^2}$$
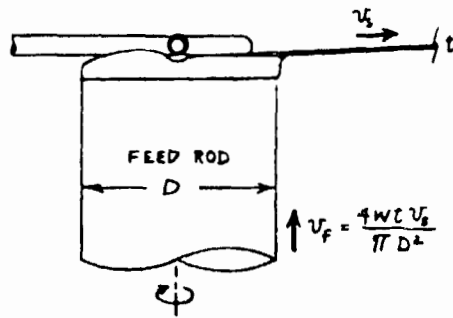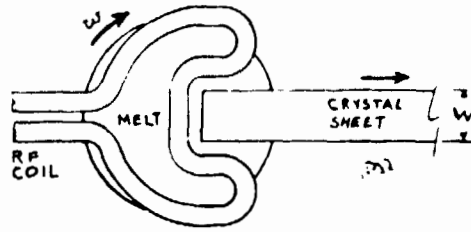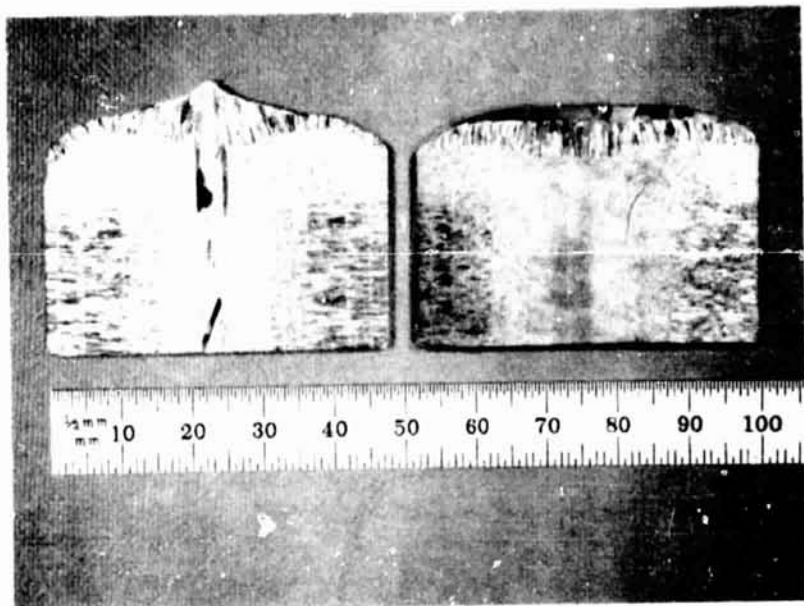
Cross sections of feed rods for CFH silicon
ribbon growth. Flattening of interface due
to shorting ring is seen at right.
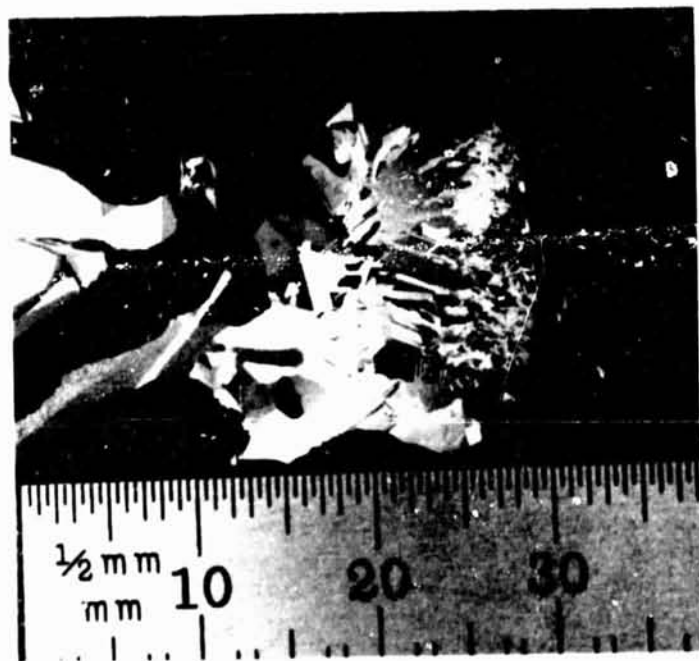
Lapped and etched cross section of a short
CFH silicon sheet

SILICON SHEET

	5/12/84 CONTROL 1 NO ARC	5/12/84 CONTROL 1-2 MESA DEFINED	5/12/84 CONTROL 1-3	5/12/84 CONTROL 2-1	5/12/84 CONTROL 2-2	5/12/84 CONTROL 2-3
Voc	.573 v	.573 v	.567 v	.566 v	.565 v	.566 v
Isc	2.4 mA	2.3 mA	2.3 mA	2.3 mA	2.3 mA	2.3 mA
Jsc	23.5 mA/cm²	23.3 mA/cm²	23.0 mA/cm²	23.1 mA/cm²	23.3 mA/cm²	23.2 mA/cm²
Vmp	.486 v	.488 v	.485 v	.496 v	.486 v	.495 v
Imp	2.2 mA	2.2 mA	2.1 mA	2.1 mA	2.2 mA	2.2 mA
Pmax	1.1 mW	1.1 mW	1.0 mW	1.1 mW	1.2 mW	1.2 mW
FF	.81	.81	.78	.81	.82	.82
Eff	10.9 %	10.8 %	10.2 %	12.6 %	12.5 %	12.5 %
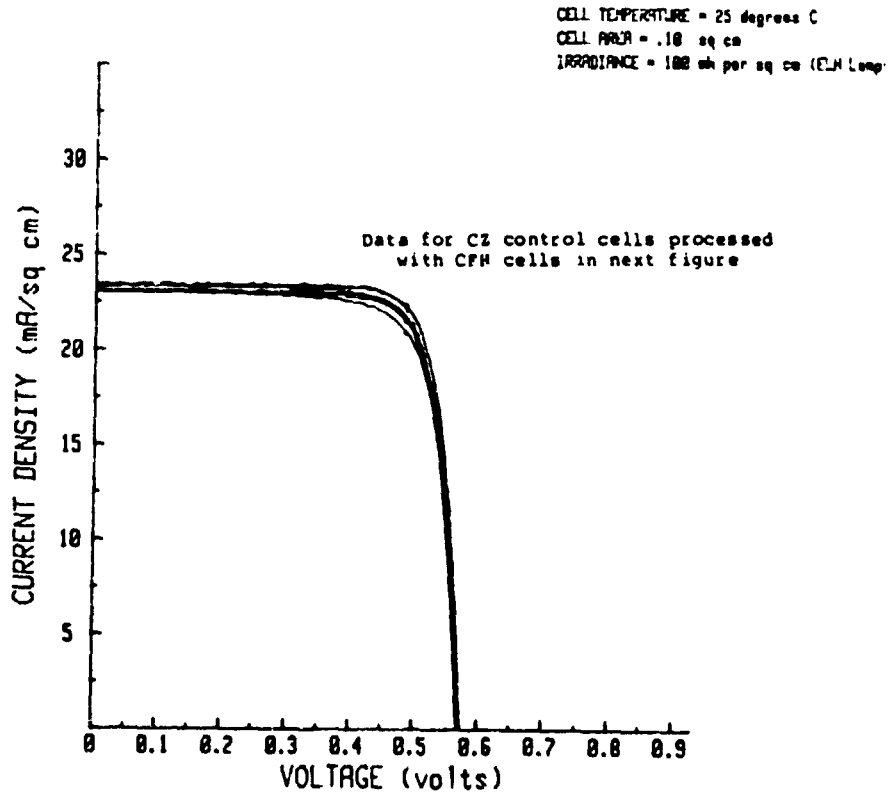
CELL TEMPERATURE = 25 degrees C
CELL AREA = .10 sq cm
IRRADIANCE = 100 mW per sq cm (ELH Lamp)

SERI SSR DEVICE GROUP

Data for CZ control cells processed
with CFH cells in next figure

CURRENT DENSITY (mA/sq cm) vs VOLTAGE (volts)

	5/12/84 HORIZONTAL RIBBON LARGE -1	5/12/84 NO ARC Lg-2	5/12/84 Lg-3	5/12/84 Lg-4	5/12/84 Lg-5	5/12/84 Lg-6
Voc	.562 v	.573 v	.573 v	.565 v	.553 v	.565 v
Isc	2.4 mA	2.4 mA	2.3 mA	2.2 mA	2.4 mA	2.4 mA
Jsc	24.4 mA/cm²	23.6 mA/cm²	23.2 mA/cm²	22.3 mA/cm²	23.5 mA/cm²	23.6 mA/cm²
Vmp	.433 v	.496 v	.486 v	.475 v	.453 v	.475 v
Imp	1.9 mA	2.2 mA	2.2 mA	2.1 mA	1.9 mA	2.1 mA
Pmax	.8 mW	1.1 mW	1.1 mW	1.0 mW	.9 mW	1.0 mW
FF	.60	.79	.79	.79	.67	.76
Eff	8.2 %	10.7 %	10.5 %	10.0 %	8.7 %	10.1 %

CELL TEMPERATURE = 25 degrees C
CELL AREA = .10 sq cm
IRRADIANCE = 100 mW per sq cm (ELH Lamps)

Data for CPH cells fabricated in
large-grained region (left side)
of sheet shown in previous photo
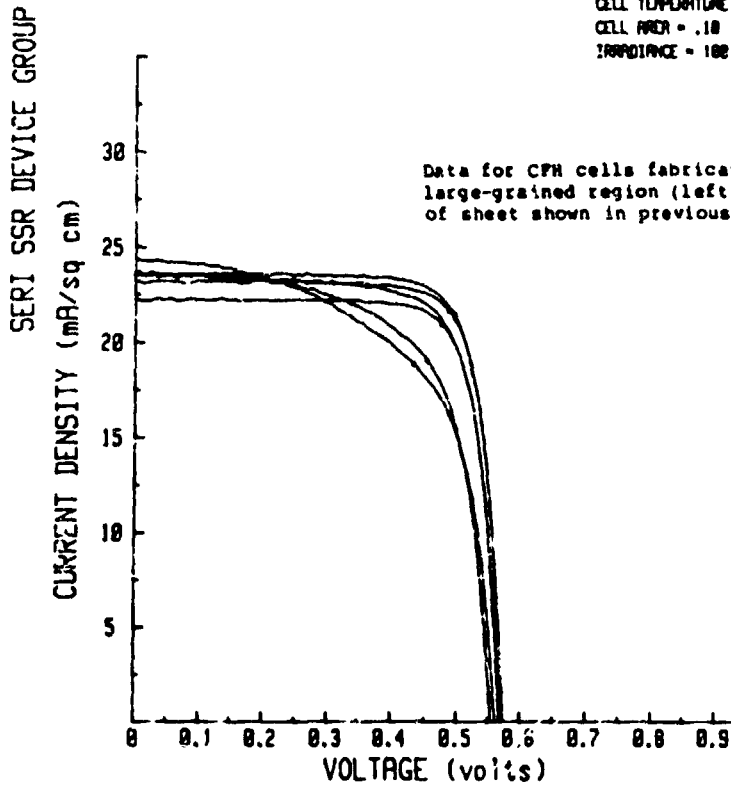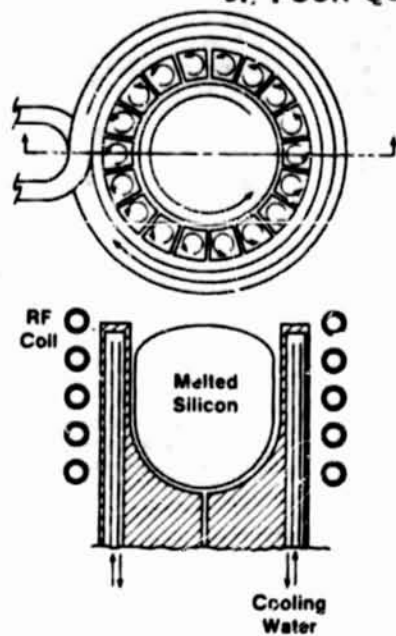
Principle of cold crucible melt confinement
showing instantaneous current directions
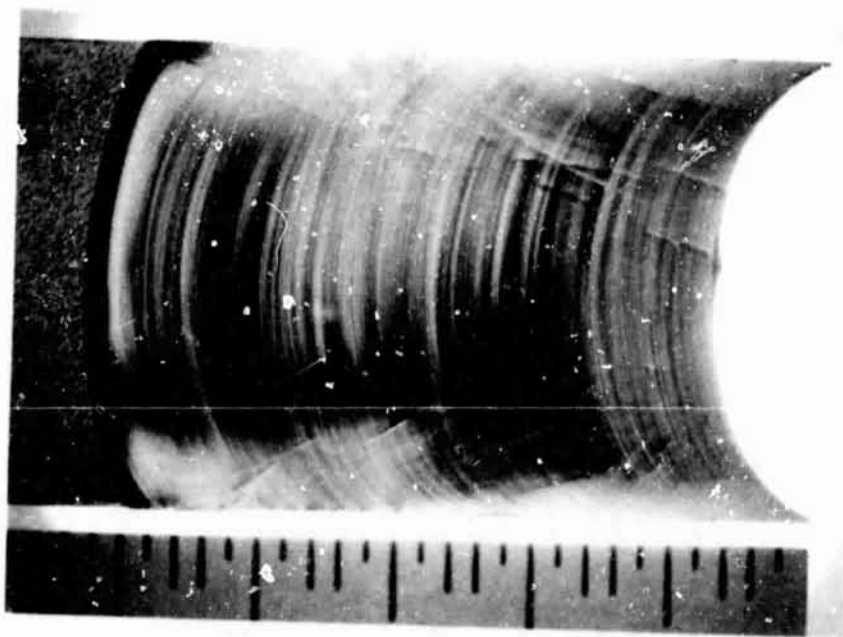
17-mm-wide ESP silicon sheet grown using
quartz capillary filaments
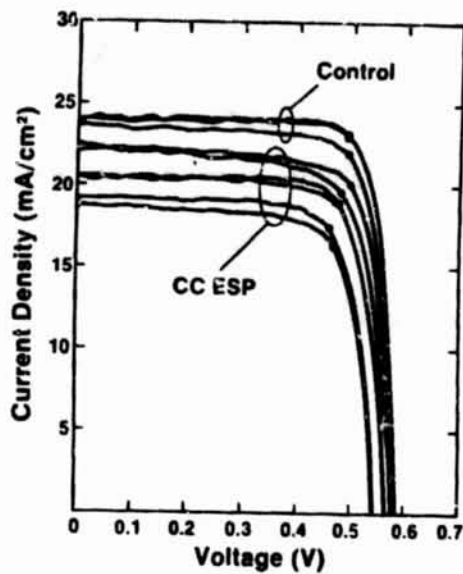
Solar cell I/V curves for cold crucible ESP
and conventional CZ control material

Dislocation-free silicon crystal being
pulled from a cold crucible

595

Properties of Cz Cold Crucible Crystals

* MINORITY CARRIER LIFETIME: 195 microsec.
  (<111>, P, ~150 OHM-CM, DF)

* HALL MOBILITY: 295 cm ^{2}/V-sec
  (<100>, P, 2.6 OHM-CM, DF)

* OXYGEN/CARBON: similar to FZ

* GOLD CONTENT (NAA):   0.14 ppbw

* COPPER CONTENT (NAA):   15 ppbw
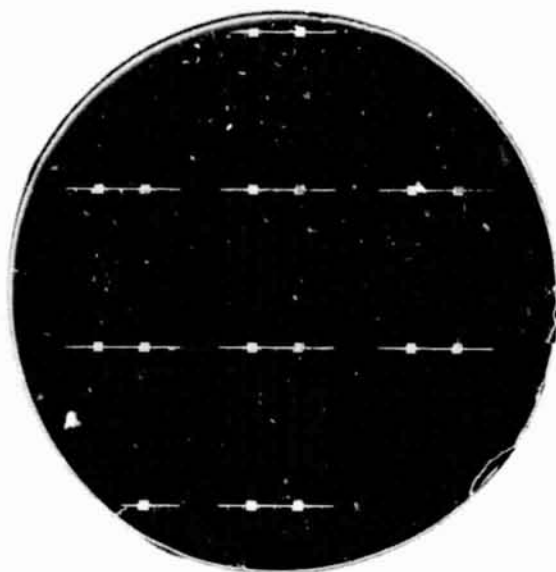
Solar cells on a (100) dislocation-free
wafer from a cold crucible CZ crystal

Cell Measurement Conditions	Cell Description	No. of Cells	V_{oc} (mV)	J_{sc} (mA/cm²)	FF (%)	Eff. (%)
100 mW/cm², ELH lamps, 25°C, no AR coating, 0.1 cm² cell area	Cz Control	3	573(±1)	23.8(±.2)	80(±1)	10.9(±.3)
	Cold Crucible	8	579(±3)	24.9(±.4)	81(±1)	11.7(±.2)
100 mW/cm² SERI filtered Xenon simulator 28°C, no AR coating, 0.1-cm² cell area	Cz Control	3	561(±.4)	22.9(±.1)	79.4(±.3)	10.2(±.1)
	Cold Crucible	4	568(±.7)	23.5(±.4)	78.9(±.2)	10.6(±.2)

Cell data comparing cold crucible CZ and
conventional control CZ PV performance
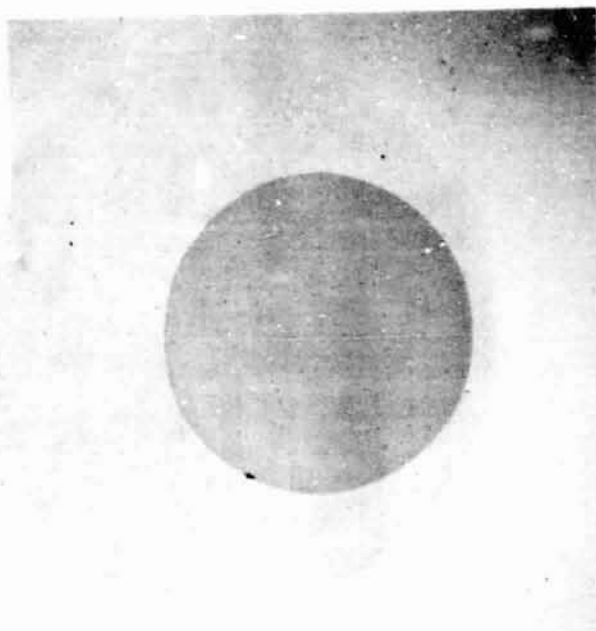
(220) transmission x-ray topograph of a (111)
dislocation-free cold crucible CZ wafer
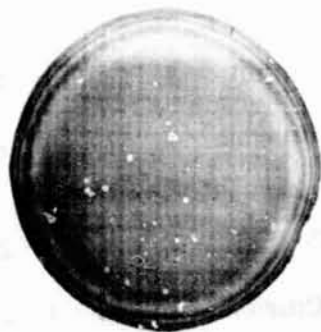
(220) transmission x-ray topograph of a (100)
dislocation-free cold crucible CZ wafer
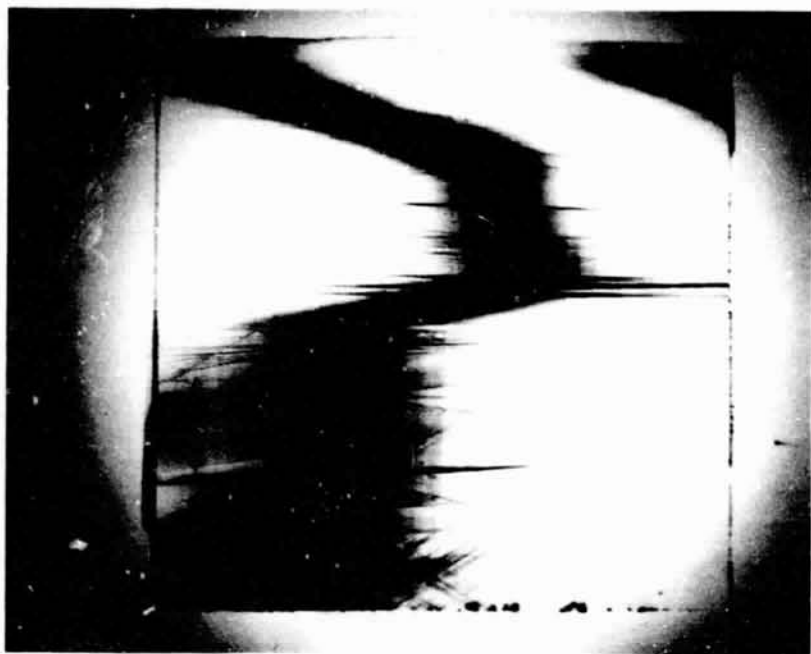
(220) transmission x-ray topograph of a moderately stres-
sed Si dendritic web crystal showing lattice bending
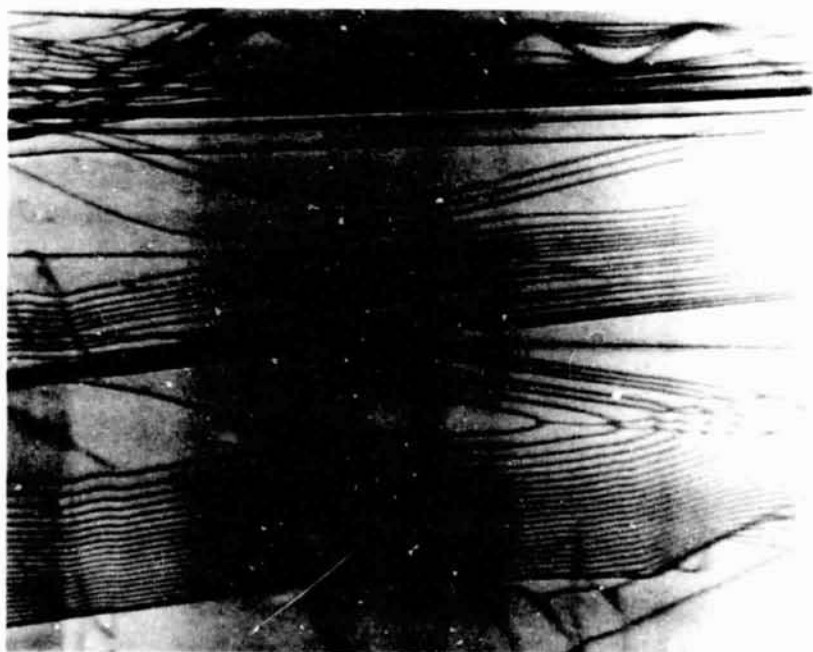
Enlarged detail of same topograph
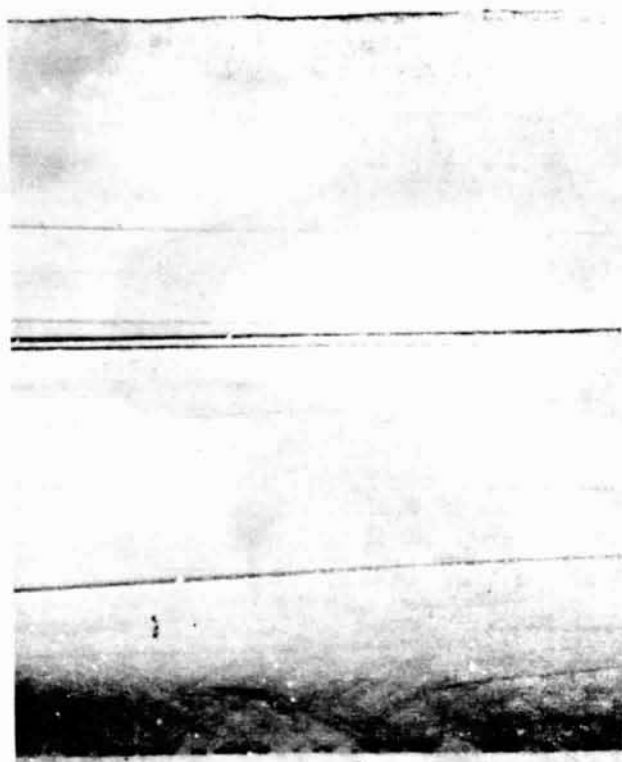
(220) transmission x-ray topograph of
same dendritic web, with oscillation
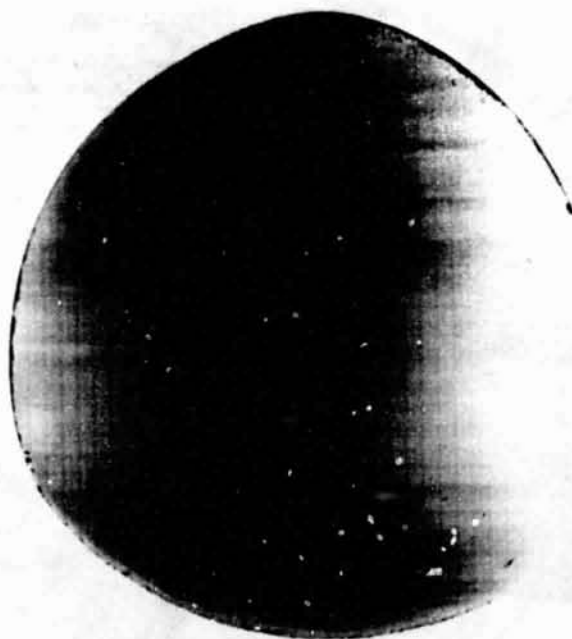
(220) transmission x-ray topograph of a
dislocation-free 0.1 ohm-cm Ga-doped
float-zoned silicon crystal wafer
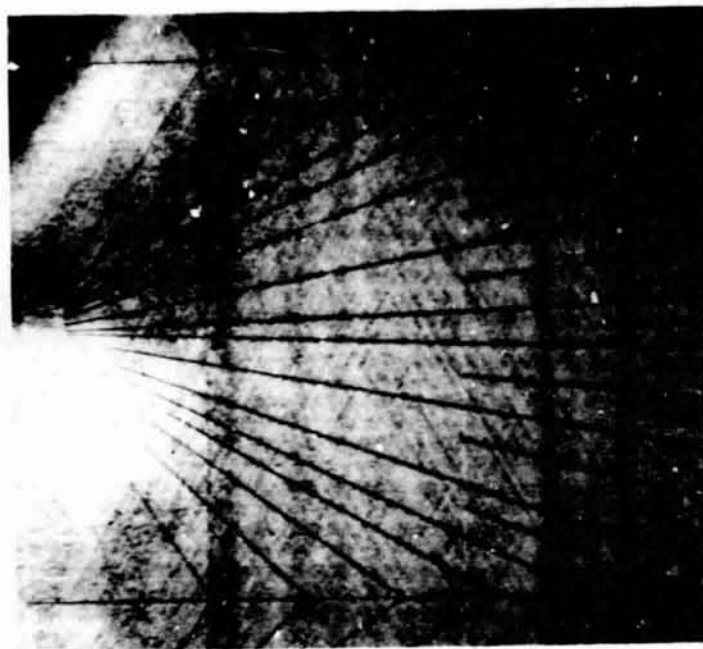
($\bar{1}$11) transmission x-ray topograph of a <8% efficient (111) dendritic web solar cell
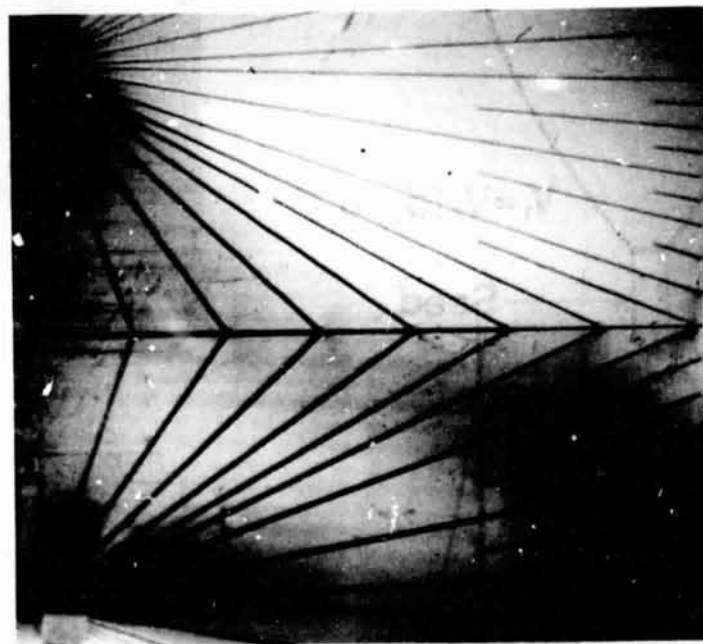
($\bar{1}$11) transmission x-ray topograph of a >13% efficient (111) dendritic web solar cell
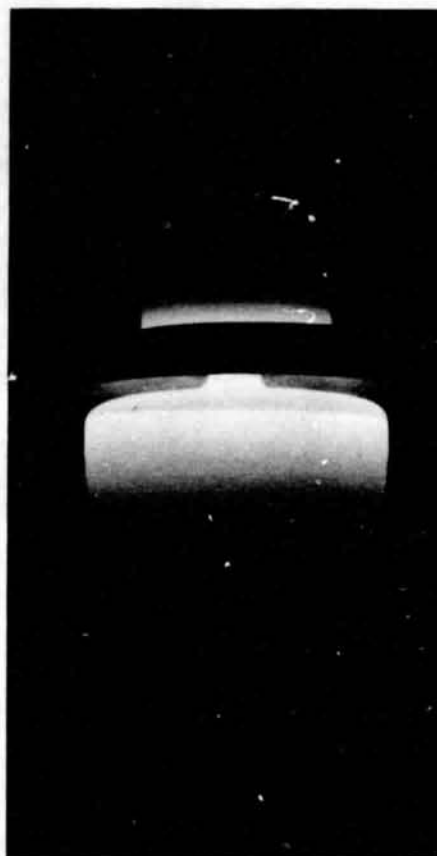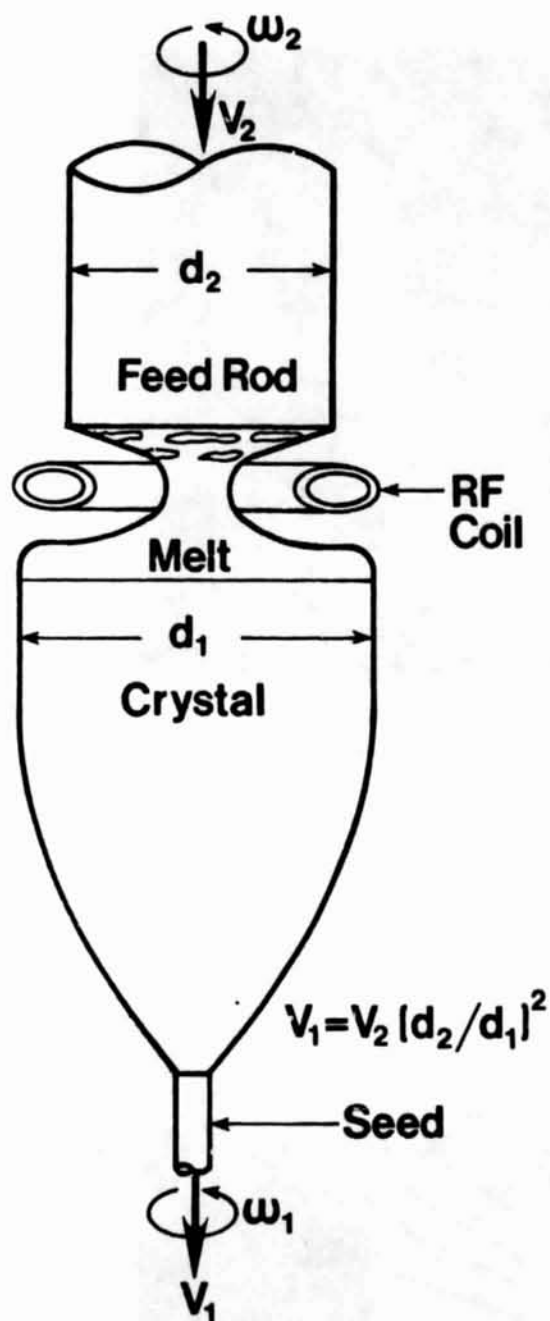
Schematic diagram of the float-
zoning crystal growth process
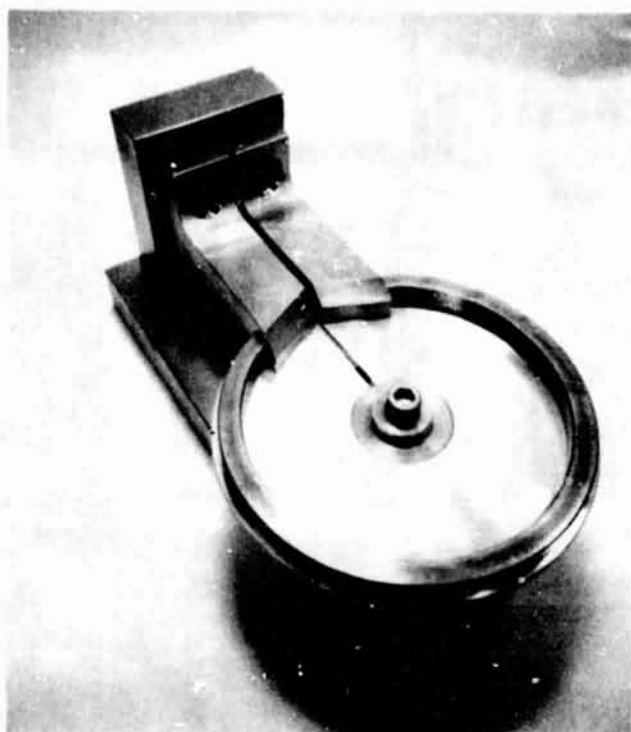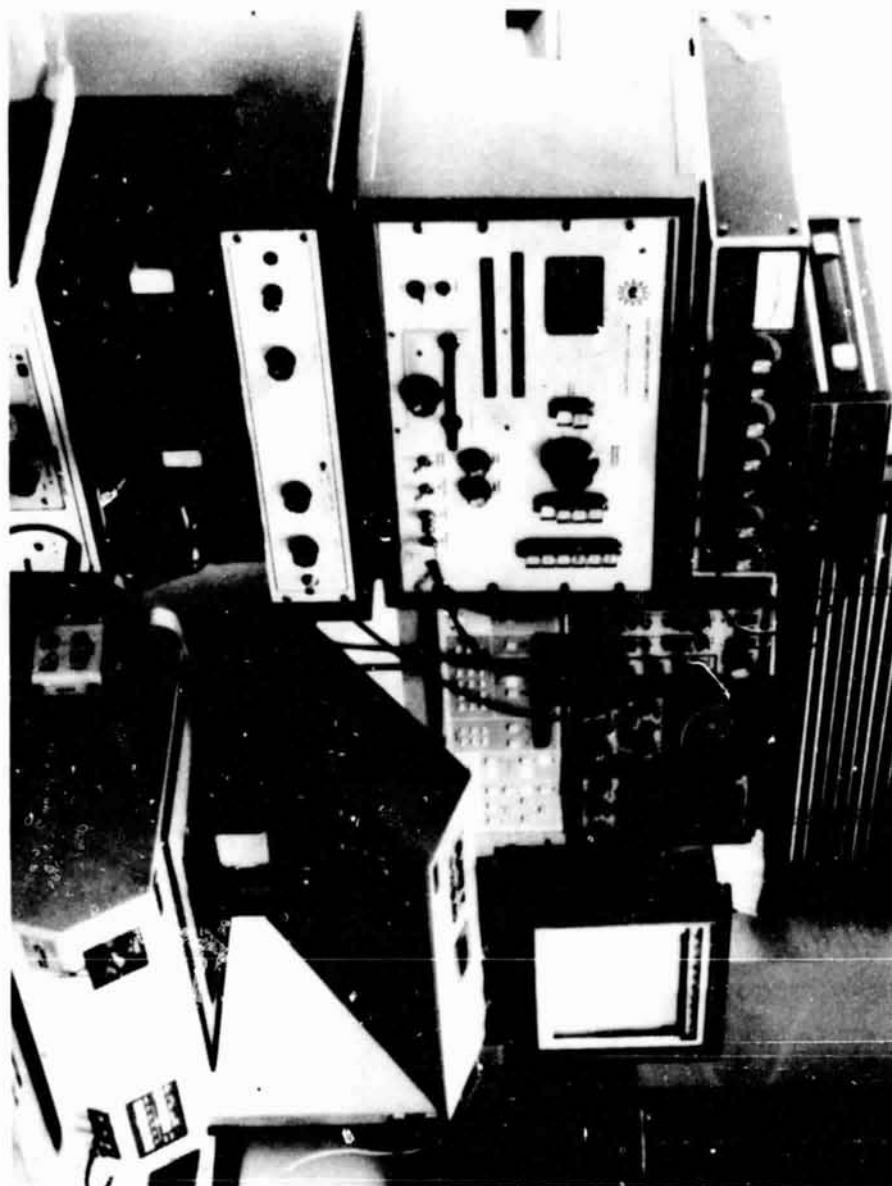
Float-zoning RF coil assembly
and jig for silver soldering
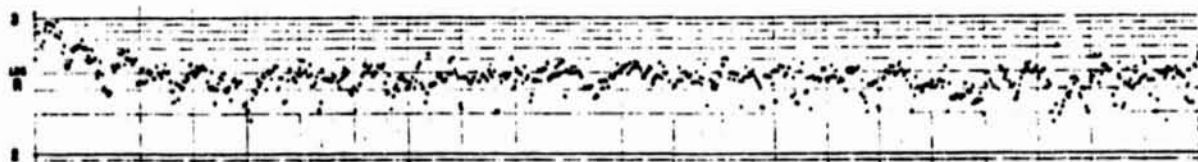
Spreading resistance along a diameter
of a (111), Ga doped, 0.1 ohm-cm silicon wafer.

Apparatus for diffusion length, minority carrier ingot life-
time, and minority carrier wafer lifetime measurements

Minority carrier bulk lifetimes in the range 900–
1300 microseconds have been measured for the
5 ohm–cm Ga–doped FZ crystals using the ASTM
photoconductive attenuation method on 1x1x2 cm
samples.   We have not yet been able to measure
0.1 ohm–cm samples.

Problems and Concerns

● AVAILABILITY OF HIGH PURITY POLYCRYSTALLINE SILICON FEED RODS

● SCAN AND SLIT IRREGULARITIES OF X-RAY TOPOGRAPHY CAMERA

● MINORITY CARRIER LIFETIME MEASUREMENTS IN HEAVILY DOPED Si

● CHANGE OF FLOAT-ZONING TECHNICIANS AND DELAY DUE TO TRAINING

MODULE DEVELOPMENT AND ENGINEERING SCIENCES

Melvin I. Smokler
and Ronald G. Ross, Jr., Chairmen

M.I. Smokler of JPL discussed the status of the Advanced Module Development task, which consists of high-efficiency, low-cost module design in support of the DOE Five-Year Research Plan module cost and efficiency goals.

M.B. Spitzer of Spire Corp. described Spire progress on the extrapolation of high-efficiency cell-processing techniques used in the demonstration of an 18%-efficient 4 cm^2 cell to the manufacture of 53.3 cm^2 cells for use in high-efficiency modules.

J.S. Griffith of JPL reviewed the history of Block V hipot and ground continuity tests on modules, with details of failure modes encountered.

R.S. Sugimura and D.H. Otth of JPL reported on the results of flammability tests of modules. A list was given of back-surface materials available for fire-ratable modules, and work necessary to pass the Class A burning-brand test was outlined.

L. Wen and D.M. Berns of JPL described an improved procedure for measuring the Nominal Operating Cell Temperature (NOCT) of modules. By measuring module temperature relative to the temperature of a temperature-calibrated reference plate, NOCT can be determined within a relatively short period of time because of greatly reduced test-condition requirements.

R.G. Ross, Jr., of JPL gave an overview of thin-film reliability and engineering, describing the work necessary to achieve reliable design guidelines for amorphous-silicon modules.

J. Lathrop of Clemson University discussed exploratory tests on the reliability of amorphous-silicon cells as part of a program to identify failure mechanisms of thin-film cells.

Q. Kim of JPL presented a status report on the development of techniques for performing failure analysis on amorphous-silicon modules, with emphasis on the use of multiple laser bandwidths in the Solar Cell Laser Scanner for detecting cell anomalies.

R.G. Mueller of JPL reviewed reference-cell calibration activities, providing an update on the secondary calibration method, description of two international round robins of reference cell measurements, and a plan for measurement system modifications to accommodate amorphous-silicon devices.

ADVANCED MODULE DEVELOPMENT OVERVIEW

JET PROPULSION LABORATORY

M.I. Smokler

Objective

Development of advanced module designs supporting achievement of DOE Five-Year Research Plan module cost and efficiency goals

DOE Milestones: Crystalline-Silicon Modules

Year	Module Parameters	For Energy Cost of
1985	12%, $100/m^2	21¢/kWh
1988	15%, $90/m^2	15¢/kWh

APPROACH

- **Perform module efficiency vs cost tradeoff based on energy cost criteria**

- **Choose specific silicon technology**

- **Prepare preliminary module design**

- **Award module contracts**

- **Conduct module reliability investigation**

- **Specify final module design**

- **Develop prototype module**

PRECEDING PAGE BLANK NOT FILMED

Efficiency-Cost Tradeoff: Initial Results

**21 ¢/kWh goal more likely to be achieved by
exceeding 12% module efficiency, based on:**

Sensitivity of efficiency/cost tradeoff

Module efficiency predictions

Module cost models:

Float-zone ingot

Dendritic-web ribbon

Completed Activities

- **Decision made: focus on both float-zone and dendritic-web silicon**

- **Preliminary module packaging configuration selected:
  glass/EVA/plastic film**

- **Contract issued to Spire for high-efficiency modules**

- **Procurement plan initiated for dendritic-web modules**

Spire Corp. Contract

- **Deliverables:**

    53-cm^2 float-zone cells for evaluation

    84-cell modules for evaluation

    12-cell modules for reliability investigation

- **Module efficiency goals:**

    At 25°C: 12.6%

    At NOCT: 11.5%

- **Major problem:**

    Supply of float-zone wafers

FY85 Schedule

- Delivery of sample FZ 84-cell module   10/84
- Delivery of FZ 84-cell modules for qualification test 5/85
- Delivery of FZ 12-cell modules for reliability tests 6/85
- Initiate reliability tests on FZ modules   7/85
- Delivery of dendritic-web modules for reliability tests 8/85
- Initiate reliability tests on dendritic-web modules 9/85

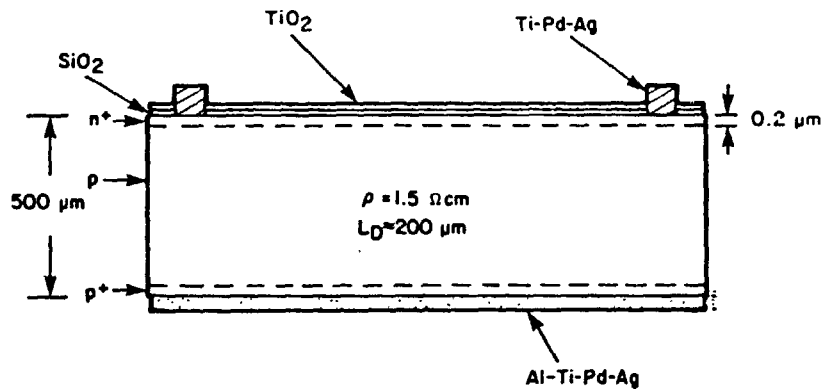# STATUS OF HIGH-EFFICIENCY MODULE DESIGN AND FABRICATION

SPIRE CORP.

M.B. Spitzer

Objective

FABRICATION OF HIGH EFFICIENCY MODULES (η>13% at NOCT) WITH EMPHASIS ON REDUCED OPERATING TEMPERATURE.

REDUCTION OF NOCT IMPROVES BOTH EFFICIENCY AND MODULE LIFETIME.

Cell Design

- Al USED FOR BSR
- SiO_2 USED TO PASSIVATE SURFACE
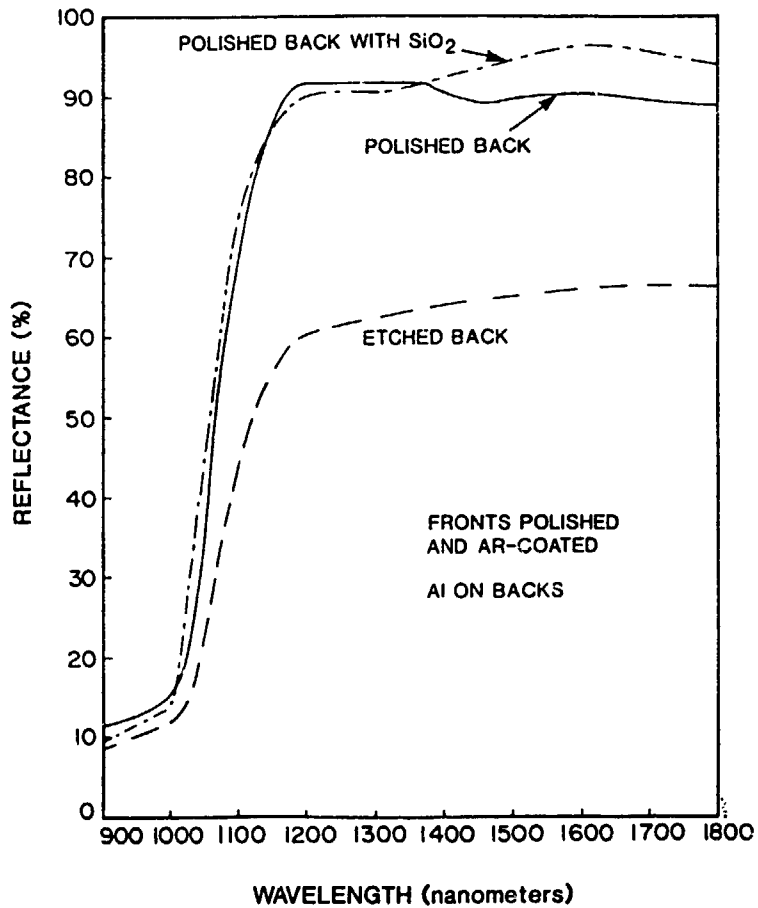- p^+ SIMPLE OHMIC CONTACT (NOT BSF)
- NO EDGE PASSIVATION USED

PRECEDING PAGE BLANK NOT FILMED

Illustration of the Cell Design
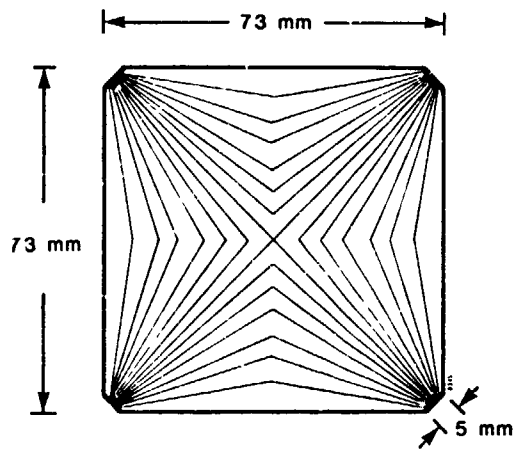
CELL AREA: 53.04 cm^2

SHADOW LOSS: 5%

LINE WIDTH: 20 um

FRONTS TEXTURED
AND AR-COATED

AI ON BACKS
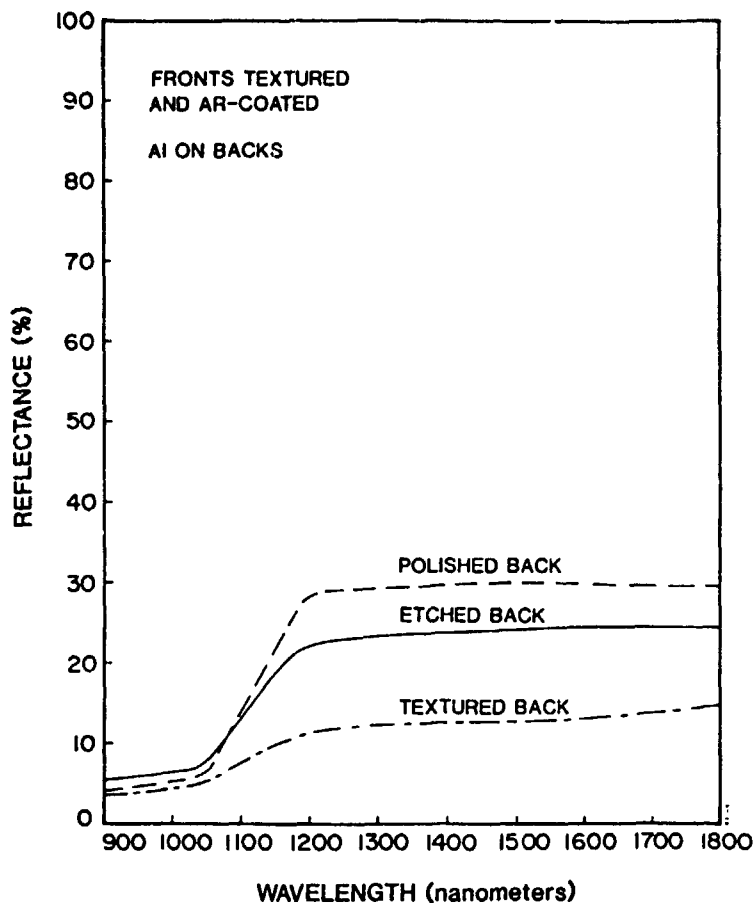
Summary of Reflectance Data

| SURFACES | | BACK | | R | R |
FRONT	BACK	METAL	DIELECTRIC	(1200 nm)	(1400 nm)
POL	POL	AI	SILOX	0.90	0.94
POL	POL	AI	NONE	0.92	0.90
POL	POL	Ti	SILOX	0.55	0.28
POL	POL	Ti	NONE	0.30	0.02
TEX	POL	AI	SILOX	0.41	0.39
TEX	POL	AI	NONE	0.22	0.24
TEX	TEX	AI	SILOX	0.36	0.34
TEX	TEX	AI	NONE	0.12	0.13
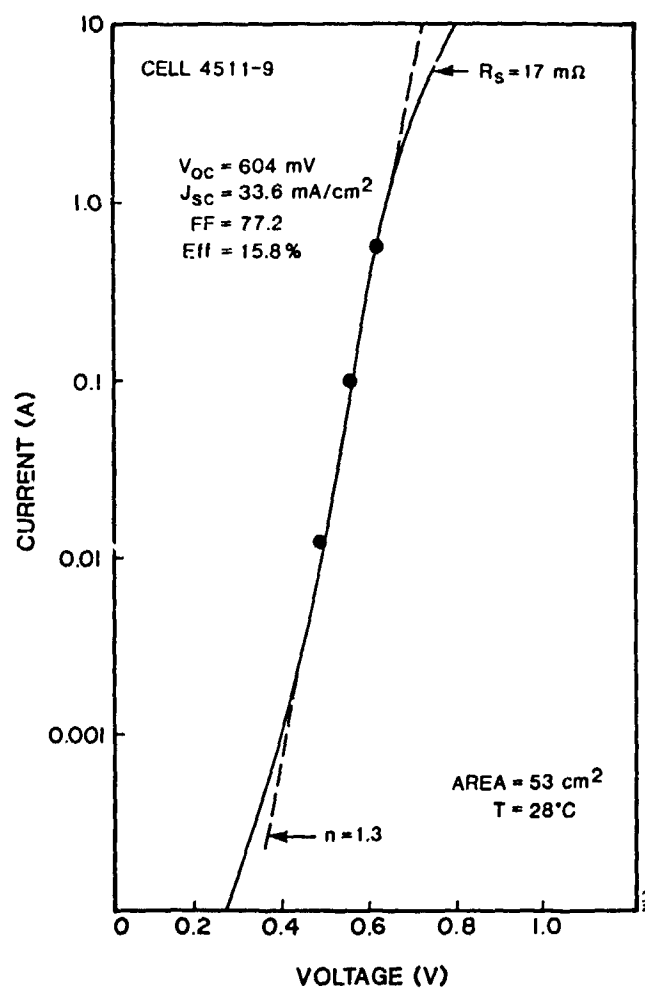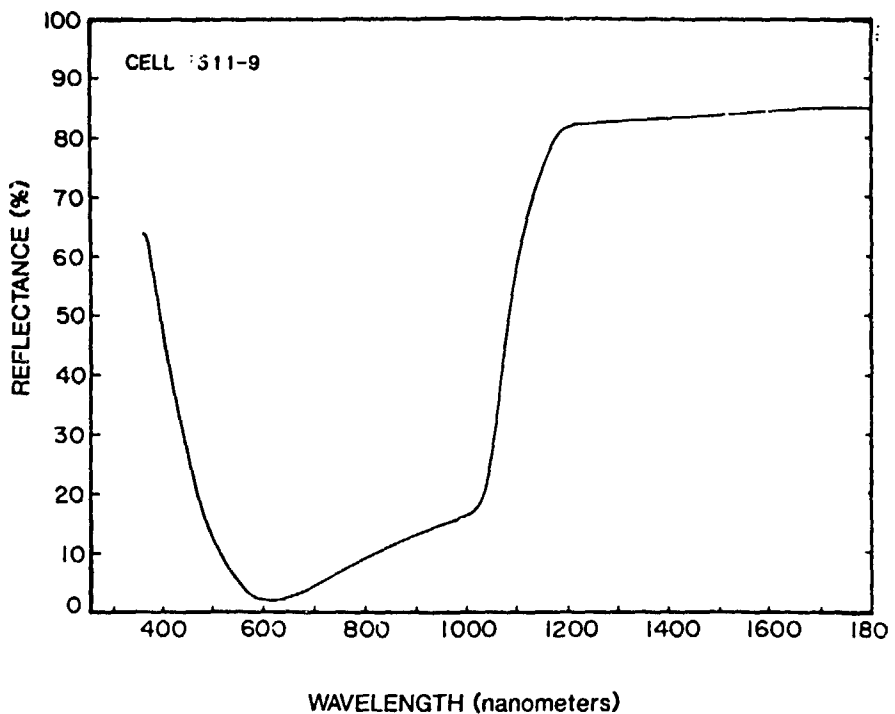
Performance Data for 10 Deliverable Cells

CELL	V_{OC} (mV)	J_{SC} (mA/cm^2)	FF (%)	EFF (%)
1	607	33.5	74.8	15.2
2	604	33.3	76.8	15.4
3	604	33.4	74.4	15.0
4	607	33.2	77.6	15.6
5	604	33.3	78.2	15.7
6	604	33.0	77.3	15.4
7	607	33.4	76.8	15.6
8	609	33.5	77.3	15.8
9	609	33.6	77.2	15.8
10	601	33.7	76.9	15.6

NOTES: INSOLATION WAS AM1.5, 100 mW/cm^2. T=28°C.
AREA=53 cm^2.

Possible Efficiency-Improving Features

● TEXTURE SURFACES – INCREASES J_{SC} BUT ALSO RAISES NOCT.

● THINNER WAFER – REDUCES J_{OB} BUT ALSO REDUCES YIELD.

● REDUCE RESISTIVITY – REDUCES J_{OB} BUT ALSO J_{SC}.

SOLDER
JOINTS

CORRUGATED
FOR STRESS
RELIEF

SOLDER
JOINTS

EPDM GASKET

BUTYL EDGE
SEALANT

INTERCONNECT
RIBBON

GLASS

STAINLESS
STEEL
FRAME

EVA POTTANT

SOLAR CELL

BUS RIBBON

FIBERGLASS SPACER
EMBEDDED IN EVA

PVF/ALUMINUM/PVF
BACK COVER

618
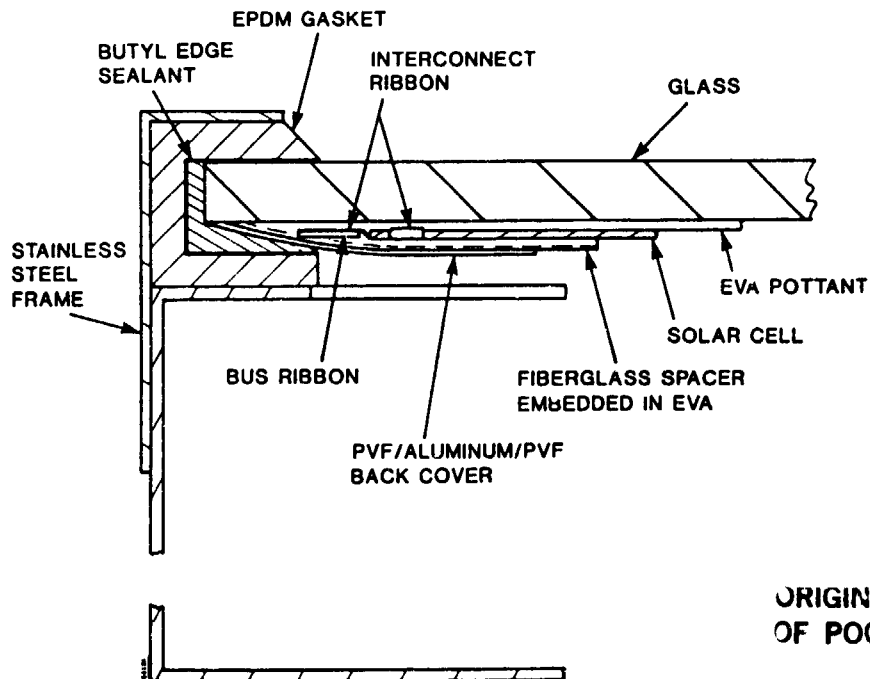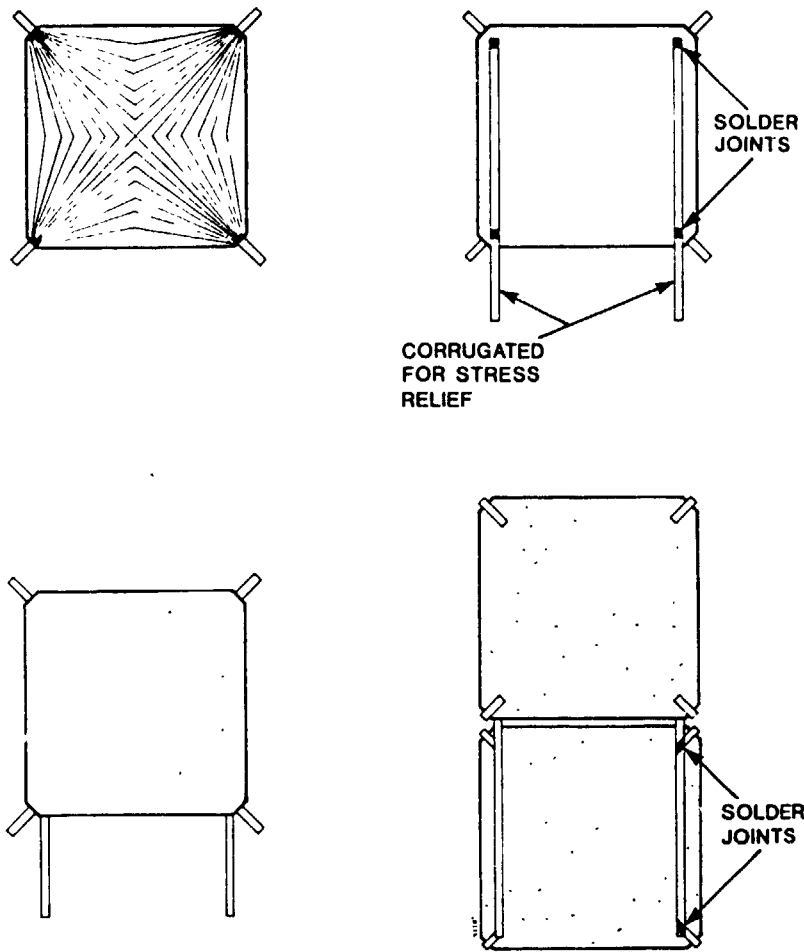
MODULE HIPOT AND GROUND CONTINUITY TEST RESULTS

JET PROPULSION LABORATORY

John S. Griffith

Hipot (high voltage potential) and module frame continuity tests are important parts of determining the suitability of solar modules for deployment into large arrays for electric power production. Since field arrays operate at hundreds of volts above (or below) ground potential at some point in the field, it is necessary to ensure adequate voltage isolation of the solar cell circuits. This subject is discussed in this presentation as outlined in Figure 1. The discussion is based on test procedures used at the Jet Propulsion Laboratory and as given in JPL Internal Documents Nos. 5101-161 and 5101-162.

The purpose of hipot and continuity testing (Figure 2) is to reveal potentially hazardous voltage conditions of modules before field installation. It also reveals leakage currents that potentially may result in significant loss of power or cause ground-fault system problems. The tests reveal first the current leakage potential and second how the leakage or hazardous voltages will be distributed. Notice the word "potentially" is used in all cases. If the hipot current leakage is a few microamperes too high or the frame continuity a few milliohms too high, one can't say that the module would be an immediate catastrophe if mounted in an array. However, the tests generally do indicate any weaknesses in the design that are potentially hazardous and need to be corrected. In the last few years, hipot and continuity tests have resulted in the highest failure rates of any measurements we make.

The hipot test procedure described in Figure 3 will be discussed first. Figure 4 shows typical equipment used. The Hipotronics HD115 tester supplies the needed voltage and measures the current leakage. The polyurethane boards shown in Figure 4 help isolate the lead wires and reduce any spurious current leakage external to the module.

The next several figures show some of the problems that arise in hipot and continuity testing.

The zinc-based feedthrough connector shown in Figure 5 and at the left side of Figure 6 had very low current leakage (0.6 µA) but corroded badly in the Block V humidity-freeze test. The module manufacturer substituted the stainless feedthrough shown at the right in Figure 6, containing what appeared to be the same internal rubber pottant. However, the latter passed 60 µA of current, resulting in hipot test failure in the connector alone. A minor change in the additives in the rubber caused the excessive leakage.

Figure 7 shows the back side of a simulated roof section holding a module laminate. The galvanized drip troughs around the glass laminate shown in Figure 7 and 8 were unconnected and required bonding wires (Figure 7). The module failed hipot because the black rubber gasket around the laminate was slightly conductive.

Polyvinyl butyral is a popular encapsulant and generally has adequate
dielectric strength at room temperature to pass the hipot test. However,
leakage increases by about 400 times at hot-day field temperatures
(Figure 9). If high ground-fault currents might be a problem in a particular
large array, modules should undergo leakage tests at elevated temperatures.

The continuity test used at JPL is discussed next, with illustrations in
Figures 10 through 15. As shown in Figure 10, the JPL Block IV tests required
a continuity test between metal components of the module frame with a
50-milliohm upper limit. Block V required a continuity test but without a
stated limit. At first the same value was used as had been used for Block
IV: 50 milliohms. Recently, a high-current continuity test was adopted.
Current is passed through the module frame at a level of twice the
short-circuit current. Maximum voltage drop permissible is 1 volt from the
beginning of the test through a two-minute hold period. This high-current
test was based on an interim report of a JPL-Underwriters Lab study. The
final report, UL 1703, is the same test except that it calls for only a 1/2
volt drop.

Figure 11 shows the relationship between these tests. The module
milliohm resistance is plotted against module short-circuit current. The
milliohmmeter test used in Block IV and early Block V was independent of
module current. The more recent tests appear as slanting straight lines on
log paper. At high module currents the old test was easier to pass and vice
versa for low module currents. This comparison assumes that high current will
not burn out or weld together point contacts at the joints and that the basic
frame resistance remains unchanged.

Figure 12 shows a continuity test setup using a Simpson Model 1699
milliohmmeter. Sometimes the resistance is greater than the instrument's
50-ohm full scale limit. A Fluke 8060AS multimeter shown at the left is used
for resistance levels above 50 ohms. Most of the testing done in the past was
done using the milliohmmeter and the data presented here was all obtained that
way. In the photograph this module shows good continuity with approximately
zero resistance. However, in Figure 13, modest forces are being applied to
the corner, resulting in a reading on the next meter scale of more than
100 milliohms, a continuity test failure. At JPL the test is ordinarily run
with and without "handling forces" applied.

Figure 14 shows the test setup for the newer high-current continuity
test. The power supply provides current to the module, generally through the
precision shunt shown here. The dial gauges are only coarse indicators but
now, at low voltage and high current, digital voltmeters are used to give
precise values.

Notice the heavy battery clamps and lead wires. The photo shows the
small voltage leads attached improperly. The contact resistance of the
battery clamps are frequently 10-15 milliohms. A module with high
short-circuit current through this contact resistance will produce a false
high voltage and apparent failure. The proper way to attach the leads is to
the polished metal frame close to the large clamps.

Figure 15 shows a portion of a two-piece, U-shaped metal frame joined by a riveted joint at each end of the module. The rivets seemed to be well installed and tight. Behind the flange is an ordinary inspection mirror showing the small metal clip that serves to hold the two pieces together. Unbelievably, these two parallel joints showed a combined resistance of over 200 megohms.

The results of the testing are shown in Figures 16-19. For the approximately 250 individual modules in Figure 16, initially 10% and 12% failed hipot and continuity, respectively. All of these didn't complete environmental tests, so there is a smaller population for final tests. 16% and 31% failed final tests, respectively. For the data on sets of modules, in Figure 17, one failure per set is considered a failure of the whole set.

For the sets there was initially a 26% failure in hipot and 9% in continuity. After environmental testing, these failures went to 36%. The last two columns take the most critical viewpoint. If we use the criterion that any failure of hipot or continuity, either before or after environmental exposure, causes the set to fail, there was a 69% failure rate. In spite of these gloomy statistics, most of these problems could be fixed easily. A little more care in fabrication, keeping the bus bars and other conductors a little farther from the frames, better metal joining, etc., would lower the failure rates significantly.

Figure 18 shows the voltages at failure of individual modules. Initially, the clear bars show that relatively few modules failed until the 1000-2000 V range was reached. More than half of all modules that failed did so in this range below 2000 V. After environmental tests the voltage at failure rises, with one failing below 500 V but a considerable number getting to 3000 V only to fail in less than one minute.

Figure 19 shows the resistance in ohms at failure. Initially, there were more failures at more than one ohm than at less than one ohm. After environmental testing the situation was reversed. The right side of Figure 19 is distorted. Initially, high resistance was read simply as "greater than 50 ohms." Later, the digital ohmmeter was used showing that most of these "greater than 50 ohms" were probably "greater than 10 megohms." Therefore, these two bars should be considered in the same group. Notice there are no readings between 10 and 50 ohms and, probably, nothing between 10 ohms and several megohms.

Figure 1. Contents

- PURPOSE OF HIPOT AND CONTINUITY TESTING

- HIPOT TESTING - EQUIPMENT, PROCEDURES, PROBLEMS

- CONTINUITY TESTING - EQUIPMENT, PROCEDURES, PROBLEMS

    - OLD AND NEW PROCEDURES - MILLIOHMMETER VS HIGH CURRENT

- RESULTS OF RECENT TESTS

Figure 2. Purpose of Hipot and Continuity Testing

- REVEAL POTENTIALLY HAZARDOUS VOLTAGE CONDITIONS OF INSTALLED MODULES

- REVEAL LEAKAGE CURRENTS THAT POTENTIALLY MAY RESULT IN SIGNIFICANT ' _ᵣ
  OF POWER OR CAUSE GROUND FAULT SYSTEM PROBLEMS

- REVEAL BY THESE TWO TESTS FIRST, THE CURRENT LEAKAGE POTENTIAL AND SECOND,
  HOW THE LEAKAGE OR VOLTAGES WILL BE DISTRIBUTED.

Figure 3. Hipot Test

- APPLY DC VOLTAGE AT A RATE NOT TO EXCEED 500 V/SEC TO 3000V, BOTH
  POLARITIES, BETWEEN THE MODULE CELL STRING AND THE METAL FRAME
  AND HOLD FOR ONE MINUTE.

- LEAKAGE IS LIMITED TO 50 μA WITH NO SIGNS OF ARCING OR FLASHOVER.

Figure 4. Hipot Test Setup
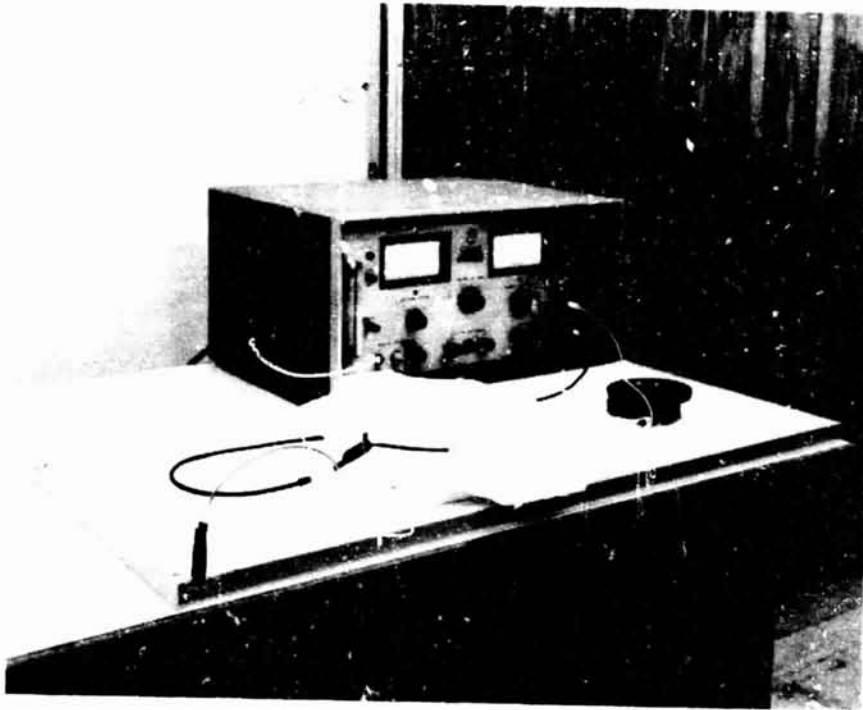
Figure 5. J-Box With Zinc-Based Connector Feedthrough

Figure 6. Zinc Alloy and Stainless Feedthroughs
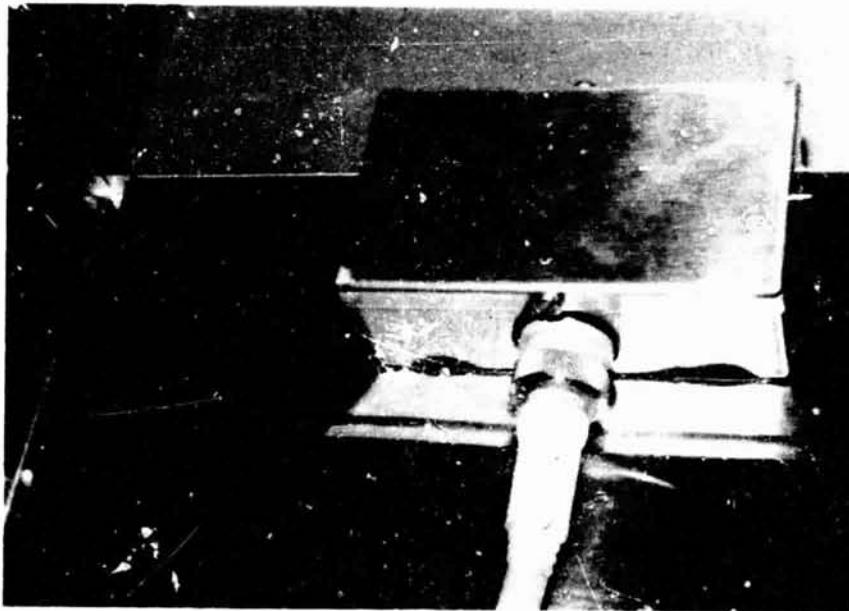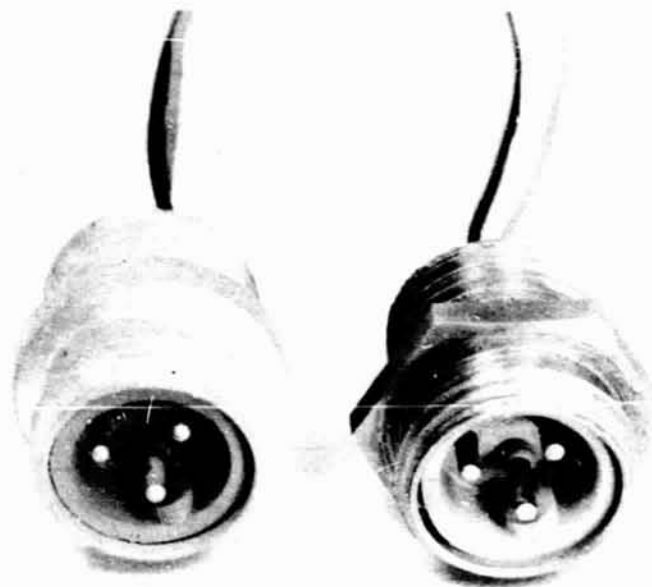
Figure 7. Module in Simulated Roof Section

Figure 8. Roof Drip Troughs and Module Gasket
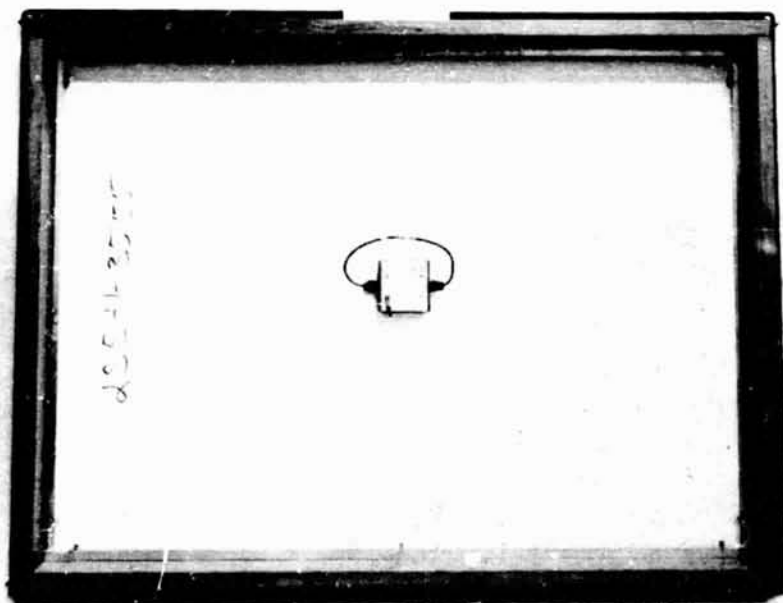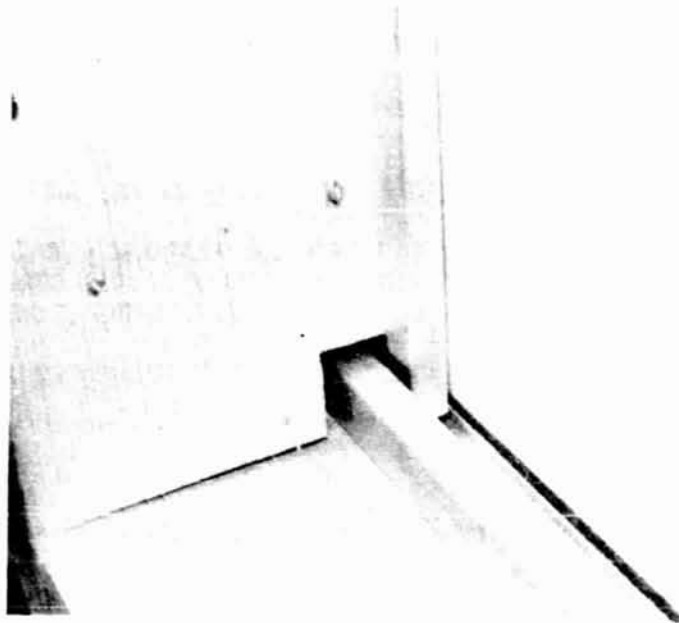
Figure 9. Dc Leakage Current vs Temperature and Voltage
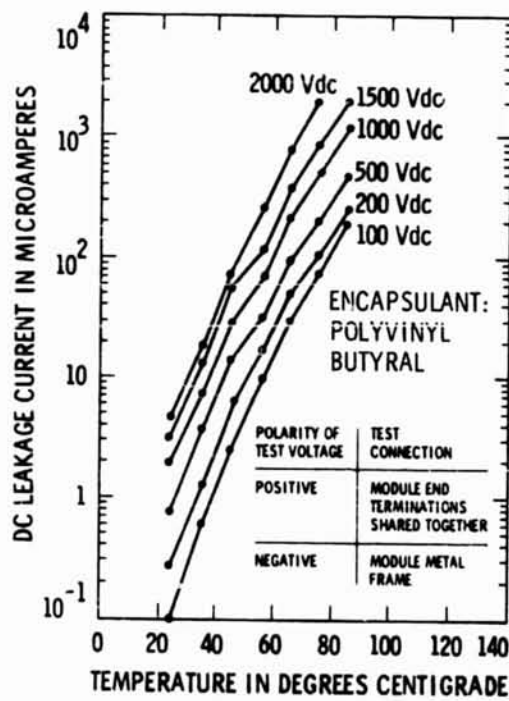
Figure 10. Continuity Test

- BLOCK IV: 50 MILLIOHMS MAX RESISTANCE BETWEEN METAL COMPONENTS OF THE MODULE FRAME.

- BLOCK V: CONTINUITY TEST WAS REQUIRED BUT THE TEST VALUES WERE UNDEFINED UNTIL RECENTLY.

   - EARLY ON – SAME LIMITS WERE USED AS FOR BLOCK IV: 50 MILLIOHMS.

   - LATELY – APPLY CURRENT FROM ZERO TO TWICE THE SHORT CIRCUIT CURRENT IN FIVE SECONDS BETWEEN GROUND AND THE OTHER METAL COMPONENTS AND HOLD FOR TWO MINUTES. MAXIMUM VOLTAGE DROP IS ONE VOLT.

   - UL 1703 – ALSO TWICE THE SHORT CIRCUIT CURRENT BUT MAXIMUM VOLTAGE DROP ALLOWED IS 1/2 VOLT.

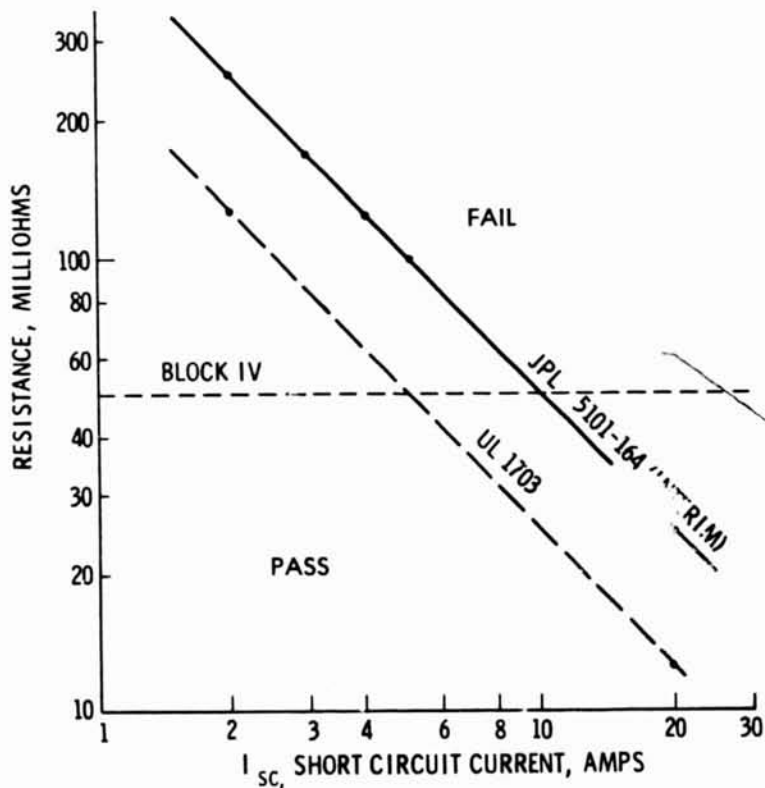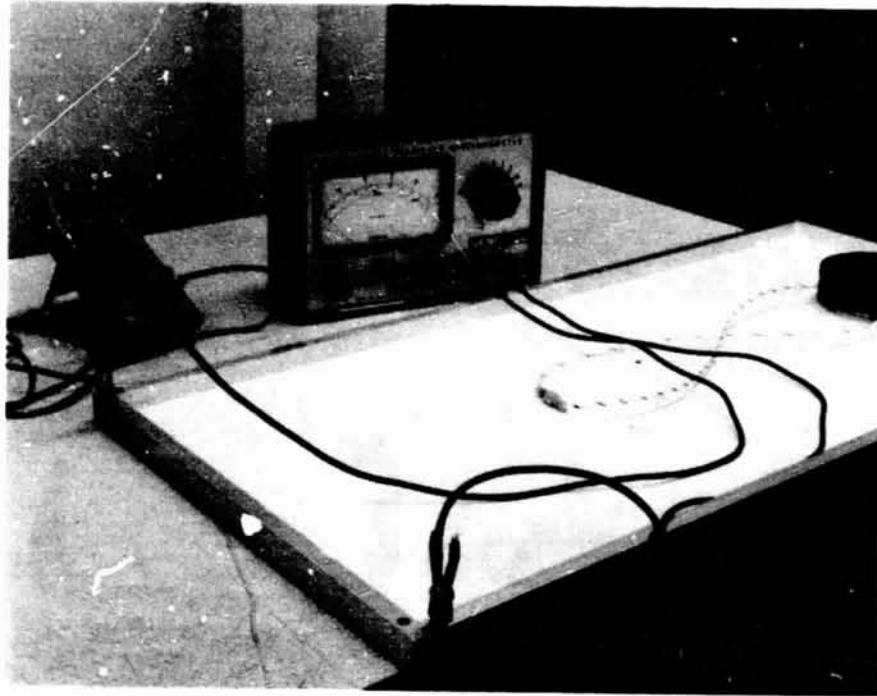## Figure 11. Continuity Test: Various Test Limits

Figure 12. Continuity Test Setup

Figure 13. Applying Moderate Forces to Corner Joint

Figure 14. High-Current Continuity Test
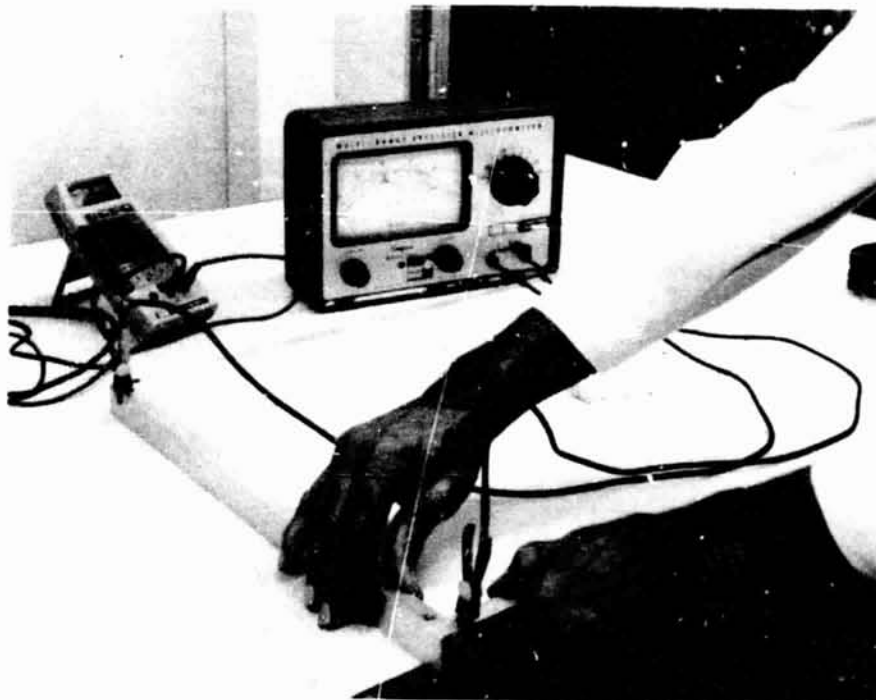

Figure 15. High-Resistance Riveted Joint
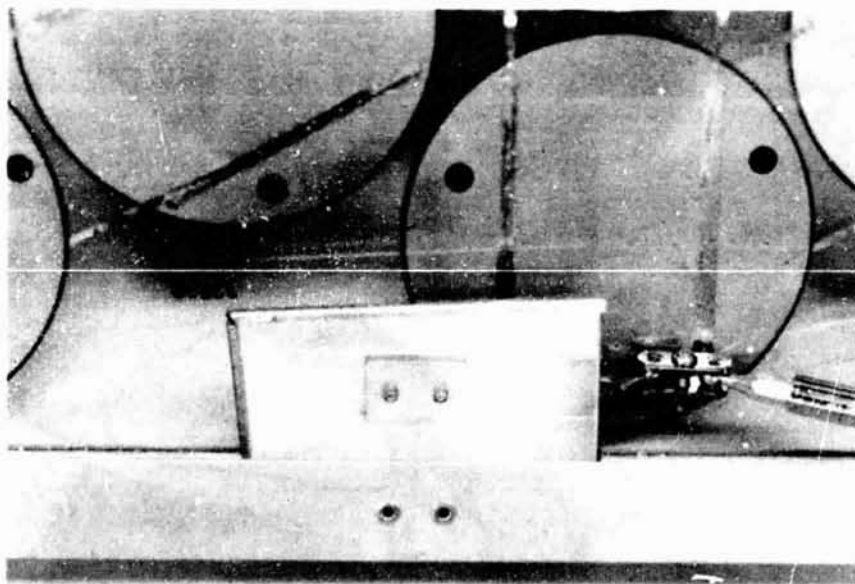
Figure 16. Results of Hipot and Continuity Tests for Individual Modules

	INITIAL TESTS		FINAL TESTS	
	NUMBER TESTED	PERCENT FAILED	NUMBER TESTED	PERCENT FAILED
HIPOT	280	10	192	16
CONTINUITY	238	12	149	31

Figure 17. Results of Hipot and Continuity Tests for Sets of Modules

	INITIAL TESTS		FINAL TESTS		SETS THAT FAILED ONE OF THE FOUR TESTS	
	NUMBER TESTED	PERCENT FAILED	NUMBER TESTED	PERCENT FAILED	NUMBER OF SETS	PERCENT FAILED
HIPOT	35	26	36	36	29	69
CONTINUITY	33	9	28	43		

*A SET OF MODULES IS A GROUP OF MODULES OF THE SAME TYPE FROM A MANUFACTURER AND AVERAGES EIGHT IN NUMBER

Figure 18. Voltage at Failure: Hipot Test
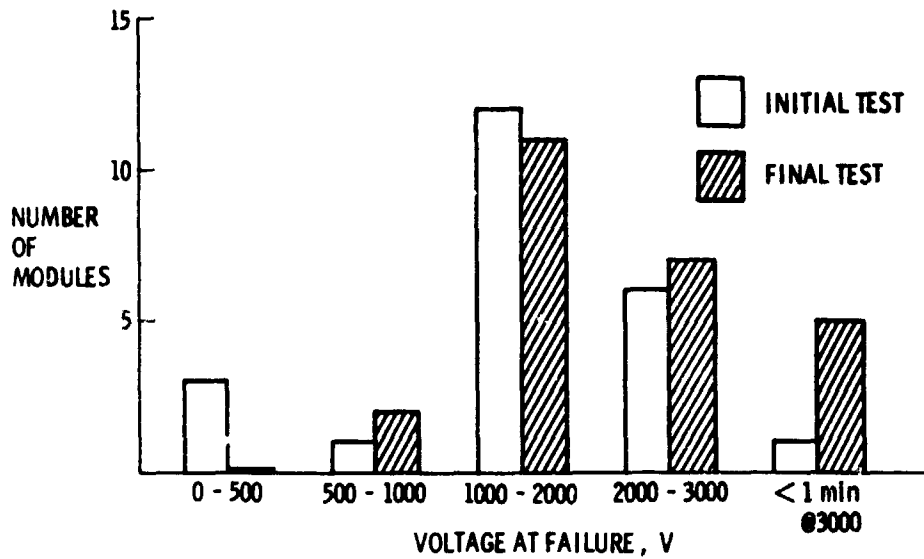
Figure 19. Resistance at Failure: Continuity Test
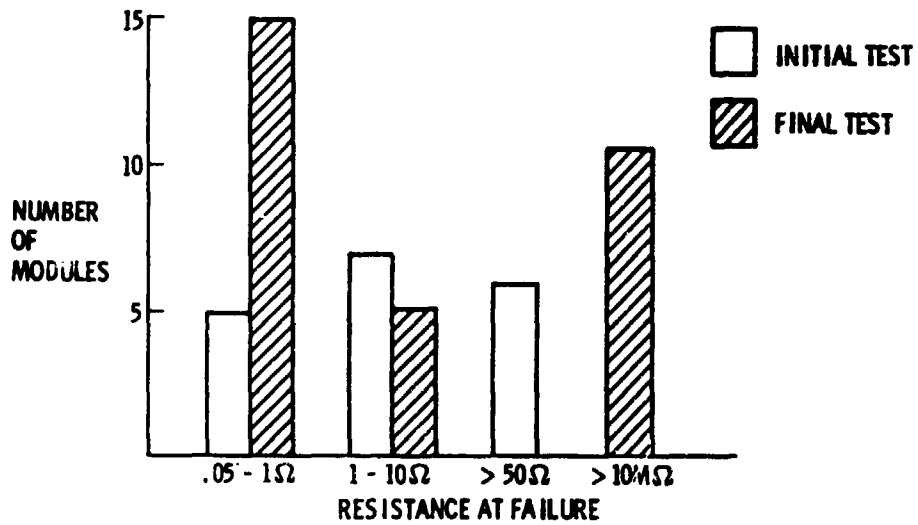
Figure 20. Summary

- HIPOT AND CONTINUITY TESTS HAVE CLEARLY DEFINED LIMITS FOR PASS-FAIL IN JPL PROCEDURES

  - CONTINUITY LIMITS FOR BLOCK V TESTS ARE DERIVED FROM UNDERWRITERS LABORATORY STUDIES

- THESE TESTS RESULT IN MANY FAILED MODULES. A MAJORITY OF THE MODULE DESIGNS FAIL IF THE CRITERION OF ONE FAILURE PER SET OF EIGHT IS USED

- A MAJORITY OF THE FAILURES CAN BE PREVENTED BY SIMPLE CHANGES IN DESIGN OR MODULE PROCESSING

631

Figure 20. Summary

PHOTOVOLTAIC MODULE SPREAD-OF-FLAME TESTING

JET PROPULSION LABORATORY

R.S. Sugimura
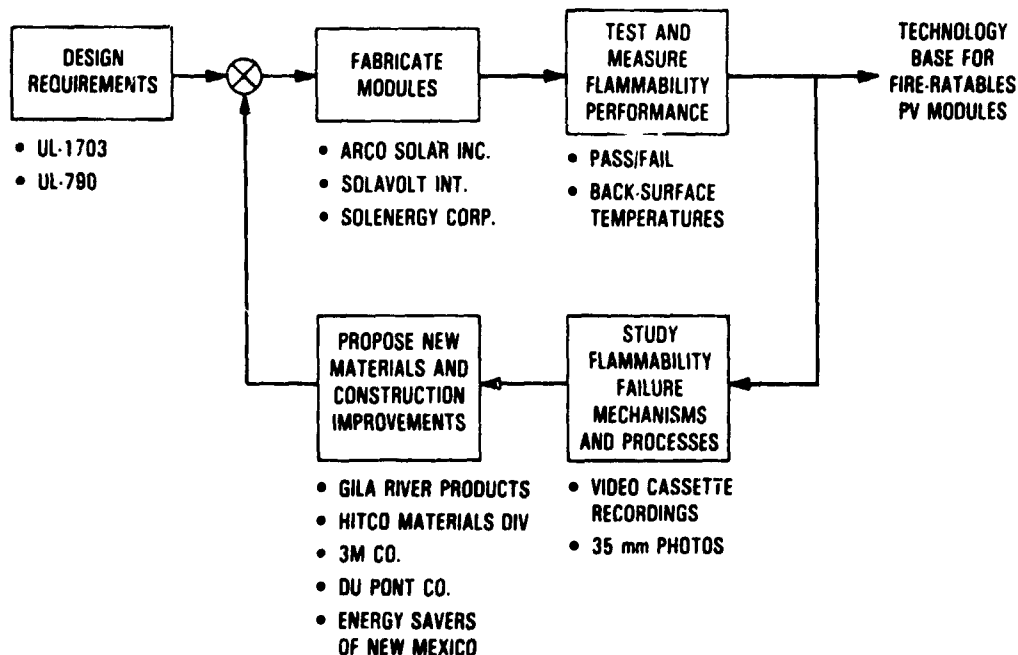D.H. Otth

ARCO SOLAR, INC.

J.C. Arnett

Objective

Develop the technology base required to construct fire-ratable modules

- Evaluate the flammability of existing module designs

- Identify module design features that control flammability

- Identify improved construction concepts and materials that achieve Class A fire-resistance characteristics

Approach

DESIGN REQUIREMENTS	⊗	FABRICATE MODULES	TEST AND MEASURE FLAMMABILITY PERFORMANCE	TECHNOLOGY BASE FOR FIRE-RATABLES PV MODULES
• UL-1703		• ARCO SOLAR INC.	• PASS/FAIL	
• UL-790		• SOLAVOLT INT.	• BACK-SURFACE	
		• SOLENERGY CORP.	TEMPERATURES	

PROPOSE NEW MATERIALS AND CONSTRUCTION IMPROVEMENTS	STUDY FLAMMABILITY FAILURE MECHANISMS AND PROCESSES
• GILA RIVER PRODUCTS	• VIDEO CASSETTE RECORDINGS
• HITCO MATERIALS DIV	• 35 mm PHOTOS
• 3M CO.	
• DU PONT CO.	
• ENERGY SAVERS OF NEW MEXICO	

Lessons Learned From Class B Burning-Brand Tests

- Module integrity is difficult to maintain
  - Glass shatters due to thermal stress
  - Hydrocarbon encapsulants are highly flammable
  - Test failures result from penetration of back-surface material;
    key failure mechanisms of the back surface include:
    - Melting (Tedlar)
    - Ripping (Kapton)
    - Porosity (fiberglass cloth)

- Most promising approach is to improve back-surface integrity

- Synergisms exist between back-surface materials and module configuration

New Back-Surface Constructions Being Assessed

Material Description	Adhesive*	Configuration**	Cost, $/ft²
Kapton (2 mils)	PS	Add-on	1.05
Kapton (2 mils)	–	Alternative	1.05
Kapton (3 mils)	PS	Add-on	1.81
Kapton (3 mils)	–	Alternative	1.81
Thermoseal mica plate (15 mils)	–	Add-on	0.37
Fiberglass · silicone rubber (one side)	–	Alternative	0.95
Fiberglass · neoprene rubber (one side)	–	Alternative	0.63
Fiberglass · neoprene rubber (two sides)	–	Alternative	0.52
T (1½ mils) - P (5 mils) · black EVA (4%)	–	Alternative	0.60

*PS - pressure sensitive

**Add-on · material added to T-P-T; alternative · material replaces T-P-T

Tests for Fire Resistance of Roof-Covering
Materials UL-790

Fire Rating	Spread-of-Flame Test			Burning-Brand Test		
	Flame Temperature, °F	Flame Application Time, min	Allowable Flame Spread Distance, ft	Brand Size, in.	Brand Ignition Temperature, °F	Approximate Peak Module Temperature, °F
Class A	1400	10	< 6	12 x 12 x 2¼	1830	1900
Class B	1400	10	< 8	6 x 6 x 2¼	1830	1400
Class C	1300	4	< 13	1½ x 1½ x 25/32	–	–

Module Back-Surface Temperature History:
Spread-of-Flame and Burning-Brand Tests
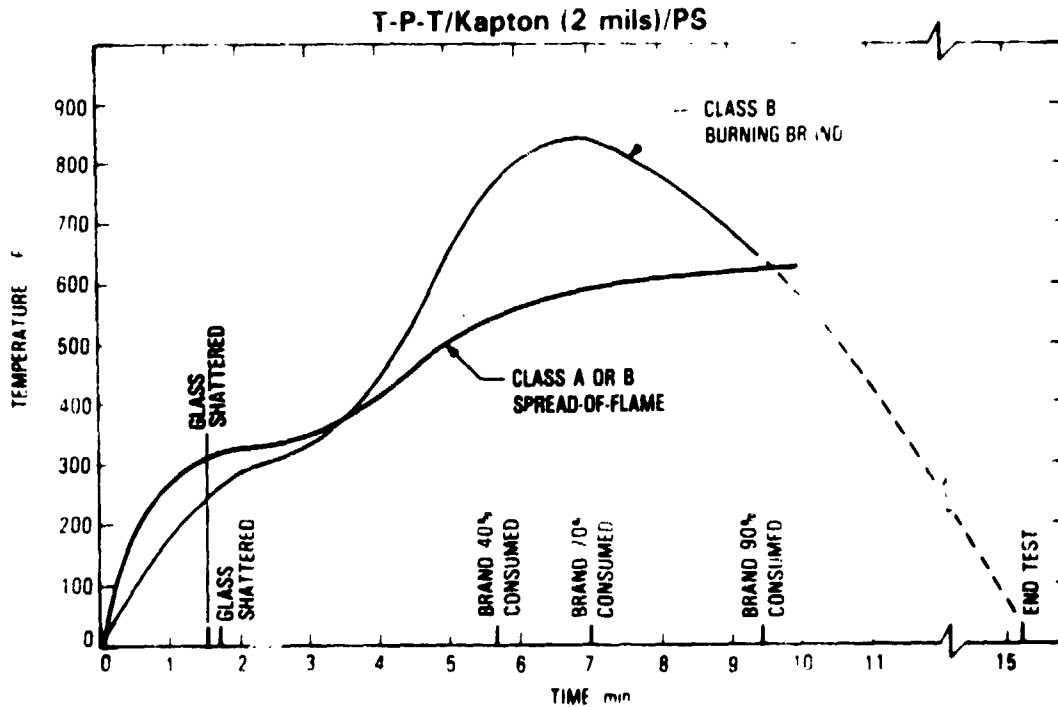
T-P-T/Kapton (2 mils)/PS

Flammability Test Summary

Module Back-Cover Configuration	Test Results*		
	Flame	B Brand	A Brand
T-P-T/Kapton (2 mils); PS**	●	●	○
K-P-T/Kapton (2 mils); TS**		○	
T-P-T/Kapton (3 mils); PS	●		○
Kapton (2 mils)	●	●	
Kapton (3 mils)	●		○
T-P-T/fiberglass - fine-woven (stabilized); TS		●	
T-P-T/fiberglass - fine-woven (stabilized); PS		○	
Fiberglass - fine-woven (stabilized)		○	
Fiberglass - silicon rubber (one-side)	●	●	
Fiberglass - neoprene rubber (one-side)	●	●	
Fiberglass - neoprene rubber (two-sides)	○		
T-P-T/thermoseal mica plate (15 mils)	○		
T (1½ mils) - P (5 mils) - black EVA (4%)	○	○	
Aluminum foil (3 mils) in four-layer laminate		●	○
T-P-T/stainless steel foil (2 mils); PS		●	●

*● - Pass; ○ - Fail
**PS - pressure sensitive adhesive; TS - thermoset adhesive

Module Back-Surface Temperature History:
Class A and Class B Burning-Brand Tests
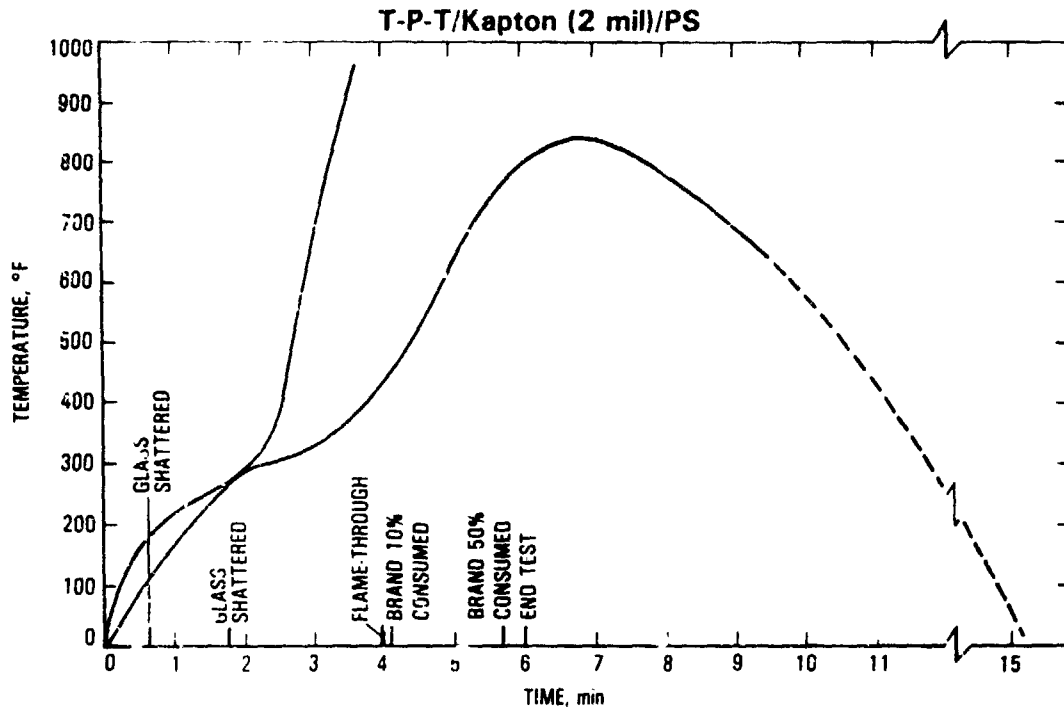
T-P-T/Kapton (2 mil)/PS

Summary

- Candidate back-surface materials are available for Class B
  fire-ratable modules
  - T-P-T/Kapton (2 mils)/PS
  - Fiberglass-silicone (one side)
  - Fiberglass-neoprene (one side)
  - Aluminum foil (3 mils) in four-layer laminate
  - Stainless steel foil (2 mils)

- Class A burning-brand test is much more severe than the
  Class B burning-brand test

- Additional innovative materials needed to pass Class A burning-brand
  test

MODULE DEVELOPMENT AND ENGINEERING SCIENCES

Future Work

- Characterize temperature-time history of Class A burning-brand and conduct exploratory tests of candidate Class A module constructions
  - Gila River Products - proprietary material
  - HITCO Materials Division - Refrasil, proprietary material

- Assess fire-test impact on module edges and array joints

- Assess applicability of UL-790 to other rooftop installation methods

IMPROVED NOMINAL OPERATING CELL TEMPERATURE (NOCT) TEST PROCEDURE

JET PROPULSION LABORATORY

L. Wen

D. Berns

Objective

- Understand causes of data scatter in currently used NOCT evaluation proceaures

- Develop procedure modifications as required to reduce scatter and NOCT test costs

Nominal Operating Cell Temperature

- Significance

    - A direct measure of module thermal design

    - Representative temperature for average environmental conditions in the United States

- Applications

    - Prediction of array energy production

    - Lifetime assessment

- Definition

    - Open circuit

    - Open-back rack mount

    - Nominal thermal environment (NTE)

        - Effective insolation = 80 mW/cm^2

        - Ambient temperature = 20°C

        - Average wind speed = 1 m/s

- Principle

    - Temperature difference is largely a function of insolation

$$(T_c - T_a) = m \cdot S$$

Current NOCT Test Procedure

- Adjustable tilt angle

- Detailed instrumentation

- High sampling rate
  (two to four measurements/minute)

Current NOCT Evaluation Procedures

- Conventional evaluation

  - Run tests for one or two days with suitable weather

  - Select data points that satisfy wind-level screening criteria

  - Determine average value using all valid data points

  - Apply correction factors for wind and air temperature

- Alternative evaluation

  - Run daily tests over extended period (months)

  - Select data from days with suitable 10-minute (calm-air) periods

  - Determine one NOCT for each day (10-minute period)

  - Determine NOCT as average for selected test days

Discussion

- Both evaluation procedures contain significant scatter

- Scatter attributed to two factors

  - Secondary test environments are not controlled

    - Sky radiation

    - Ground reflection

    - Ground emission

    - Tilt angle

  - Steady-state analysis ignores transient thermal effects

Proposed NOCT Refinements

- **Define NOCT for particular secondary NTE conditions**

    - **Atmospheric radiation: clear sky**

    - **Ground reflection: 10% of insolation level**

    - **Ground emission: from 30°C ground temperature, effective emittance of 0.8**

    - **Effective wind direction: 135° from north**

    - **Module tilt angle: 30° from the horizon**

- **Measure module temperature relative to calibrated reference plate**

    - **Painted aluminum plate (front-black, back-white), Bostic paint**

    - **Plate temperature calibrated under refined NTE is 48.3°C**

    - **Level of ΔT, (T cell-T plate) is approximately constant**

    - **NOCT = 48.3°C + ΔT**

Proposed Test Setup and Conditions

- **Test set-up**
    - **Module and reference plates subjected to the same test environments**

    - **Two reference plates; refinished surface coating at staggered 6-month intervals**

- **Test conditions**

    - **Minimal constraints on wind**

    - **Minimal constraints on air temperature**

    - **Minimal constraints on secondary test environment conditions**

    - **Insolation level higher than 60 mW/cm^2**

    - **3 to 4 hours test duration around solar noon**

    - **30° tilt**

Proposed Test and Evaluation Procedure

- Data collection
  - Module and test plate temperatures
  - Relative temperature accuracy: 0.5°C
  - Measurement frequency approximately one per minute
  - Approximate insolation level

- Data processing
  - Average cell-plate ΔT over selected time interval
    - Interval to have initial and final temperatures within 0.2°C (for all thermocouples)
    - Interval length to be longer than 40 minutes
  - NOCT = 48.3°C + average ΔT

Conclusions

- Proposed procedure offers improved
  - Simplicity
    - Does not require long-term testing
    - Does not require sophisticated wind and irradiance instrumentation
    - No data screening judgment or tedious corrections
    - Broader test window
  - Accuracy
    - Excellent repeatability (accuracy depends on temperature error)
    - Some discoloration of reference plate over one-year field exposure, but no measurable change in calibration temperature
- Requires additional demonstrations

THIN-FILM RELIABILITY AND ENGINEERING OVERVIEW

JET PROPULSION LABORATORY

R.G. Ross, Jr.

Scope

- Development of the reliability and engineering technology base required for thin-film modules
    - Emphasis on amorphous-silicon
    - Emphasis on module and array-level issues
    - De-emphasis of cell-intrinsic reliability issues such as light-induced effects

- Closely coordinated with SERI's thin-film cell research activities as a part of DOE's Amorphous Silicon Program, managed by Ed Sabisky

Thin-Film Differences Requiring New or Expanded Research

- New cell environmental durability (temperature/humidity/UV) failure modes

- Altered hot-spot heating failure mechanisms

- Short-circuit cell failure modes and effect on cell size and series/parallel redundancy

- New cell electrical interconnect failure modes

- Altered glass breaking strength

- Flexible substrate technology demands

- High cell stresses due to glass bending

- Non-linear electrical response and effect on module measurement

- Cell-to-cell electrical variability and effect on electrical mismatch and circuit design

R&ES Crystalline-Si Research Applicability to Thin-Film Modules

- Circuit reliability model development   ◑
- Interconnect mechanical fatigue   ○
- Electrical insulation breakdown research   ●
- Glass-fracture mechanics   ◑
- Cell-fracture mechanics   ○
- Cell temperature/humidity endurance (Clemson)   ◑
- Module temperature/humidity endurance (Wyle)   ◑
- Module hail-impact resistance   ◑
- Optical-surface soiling   ●
- Electrochemical corrosion   ◑
- Encapsulant photo-thermal degradation   ●
- Encapsulant debonding   ●
- Hot-spot heating   ◑
- Bypass diode integration studies (GE)   ●
- Module flammability and arcing research (UL)   ●

● = generally applicable,   ○ = significant changes

FY85 R&ES Thin-Film Research Thrusts

- Temperature-humidity reliability research

- Glass breaking strength research

- Point defect system analysis

- Hot-spot heating assessment

- Electrical measurements technology development

Temperature-Humidity Reliability Research

- Objective
  - Assess stability of α-Si cells in T/H environments
  - Assess requirements for encapsulation

- Status
  - Initial α-Si cell samples acquired (ARCO, Sanyo, Chronar)
  - Additional samples procurements underway (Hughes and Chronar)
  - Exploratory tests initiated at Clemson

Glass Breaking-Strength Research

- Objective
  - Determine breaking strength versus α-Si processing
  - Assess need for glass strength enhancement
  - Develop glass strength enhancement techniques
  - Develop glass support techniques

- Status
  - FY 1985 start, building on extensive experience with glass on crystalline-Si modules
  - Tin-oxide-coated glass samples acquired from Chronar for test

Point-Defect System Analysis

- Objective
  - Assess present areal density levels of defects
  - Assess economic penalty/allowable levels for defects
  - Determine optimum cell interconnection/geometry to minimize impact

- Status
  - Computer program operational for computing system power loss due to orted cells
  - Laser scanner being modified to allow defect mapping

Hot-Spot Heating Assessment

- Objective
  - Establish susceptability of a-Si cells to hot-spot phenomena
  - Establish bypass diode recommendations for modules

- Status
  - Just initiated

Electrical Measurements Technology Development

- Objective
  - Establish means for accurate repeatable measurement of electrical I-V performance of a-Si cells and modules

- Status
  - LAPSS verified as appropriate light source
  - Filters identified to convert LAPSS to AM 1.5 global spectrum
  - Filters identified to alter crystalline-Si spectral response to provide reference cells for a-Si

Research Forum on Reliability and Engineering of Thin-Film Modules (San Diego, Feb. 18-20, 1985)

Focus: Reliability and performance issues relate.
integrating a-Si cells into power modules, inclu- ....
review of current status, ider tfication of proble .... as, a
definition of needed research.

Tentative Agenda
- Cell performance overview
- Module reliability considerations
- Module performance considerations
- Electrical performance measurement

ACCELERATED STRESS FACTORS AND FAILURE/DEGRADATION MECHANISMS IN TERRESTRIAL SOLAR CELLS

CLEMSON UNIVERSITY

Jay W. Lathrop

REPEATABILITY
ERROR 1%

ELECTRICAL
MEASUREMENT

ELECTRICAL
MEASUREMENT

STRESS

VISUAL
INSPEC N

VISUAL
INSPECTION
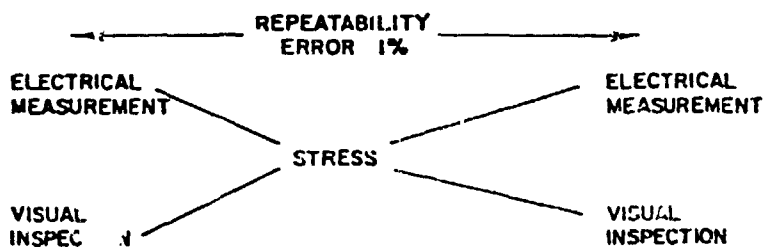
ELECTRICAL PARAMETERS

V_{oc} I_{sc} R_s V_m I_m P_m

INSPECTION
LOW POWER MAGNIFICATION
PHOTOGRAPHY

## Planned Development of Amorphous-Cell Accelerated Test Measurement Instrumentation

|	PHASE 1	PHASE 2	PHASE 3
LIGHT SOURCE	4-LAMP ELH 4-INCH DIAM D SHUTTERED	11-LAMP ELH 12-INCH SQR AC SHUTTERED DIFFUSER	ADDED UV 11-LAMP ELH 12-INCH SQR AC SHUTTERED CONTINUOUS DIFFUSER
REFERENCE CELL	CONVENTIONAL SILICON CELL	SIMULATED AMORPHOUS	SIMULATED AMORPHOUS
ELECTRICAL CONNECTION	KELVIN METAL PROBE	KELVIN LINEAR ELASTIC	KELVIN LINEAR ELASTIC
TEMPERATURE CONTROL	CONTROLLED AIR FLOW	CONTROLLED AIR FLOW	CONTROLLED AIR FLOW SOFTWARE CORRECTION
CHARACTERISTIC	POWER QUAD	POWER QUAD FAR-FORWARD	POWER QUAD FAR-FORWARD REVERSE

11-Lamp ELH Solar Simulator

C - 8
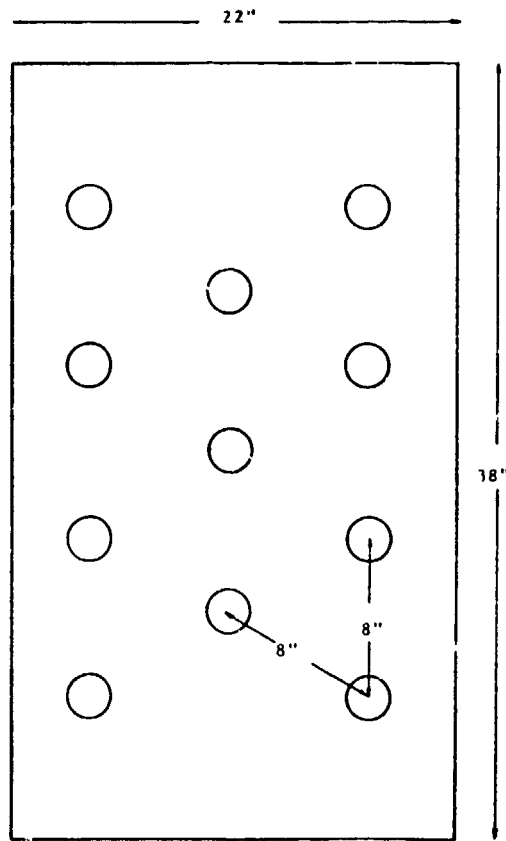
Ac Light-Source Instrumentation
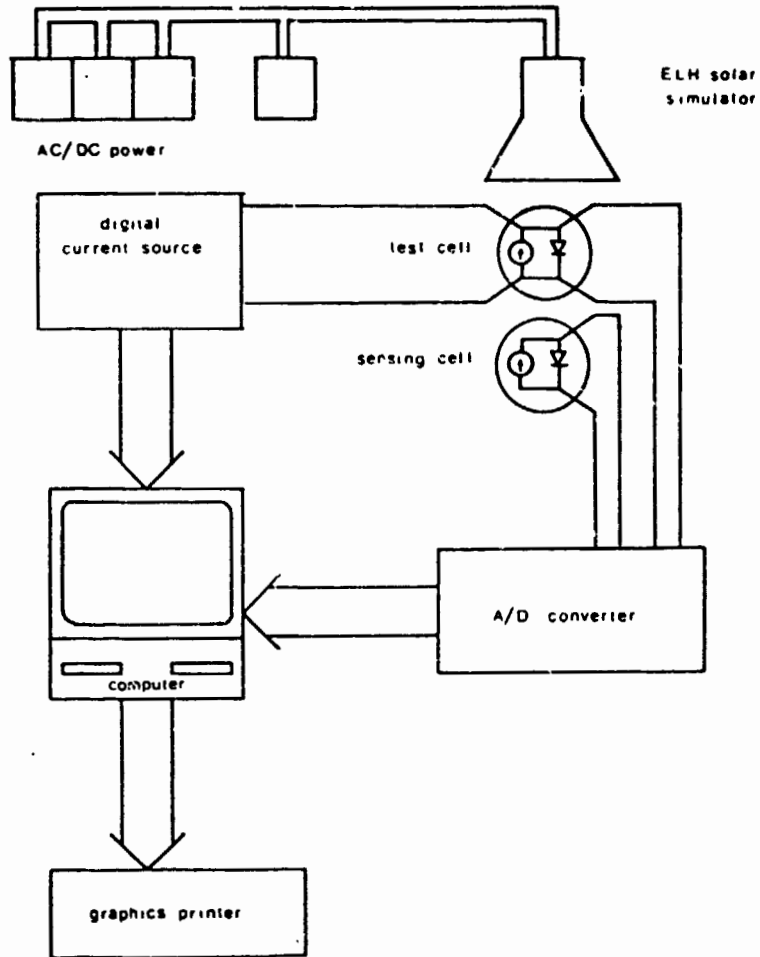
Timing of Measurements When Ac Light Source Is Used
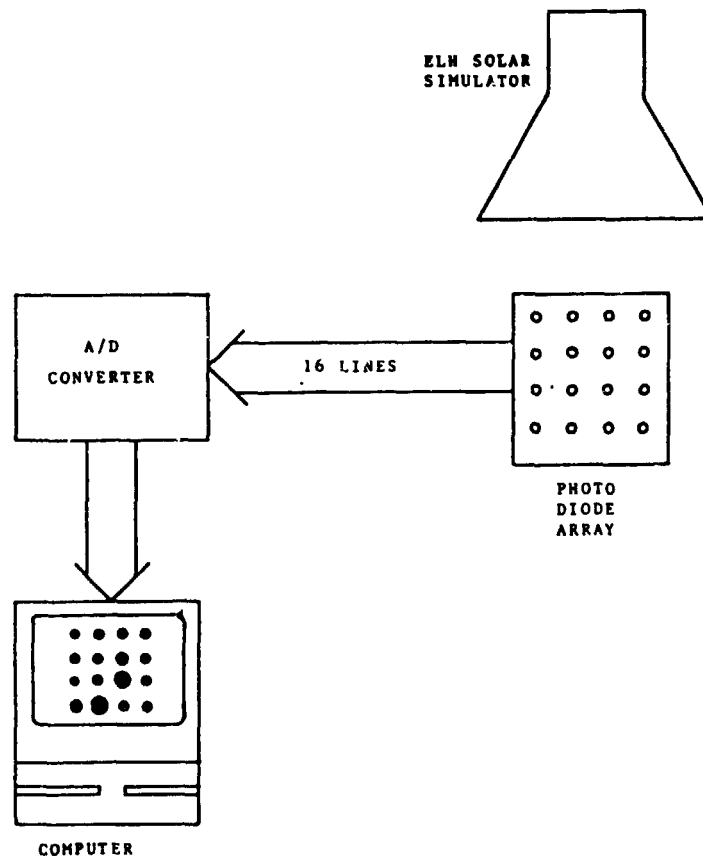

t_m = time a measurement is taken
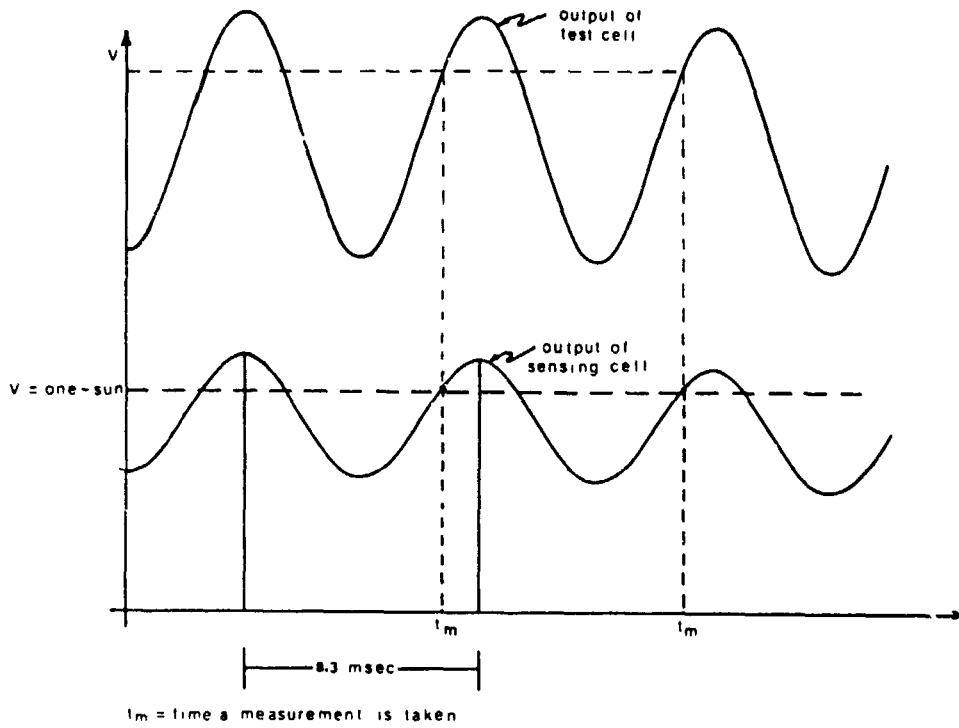
Crystalline Silicon Cell: Dc Analysis
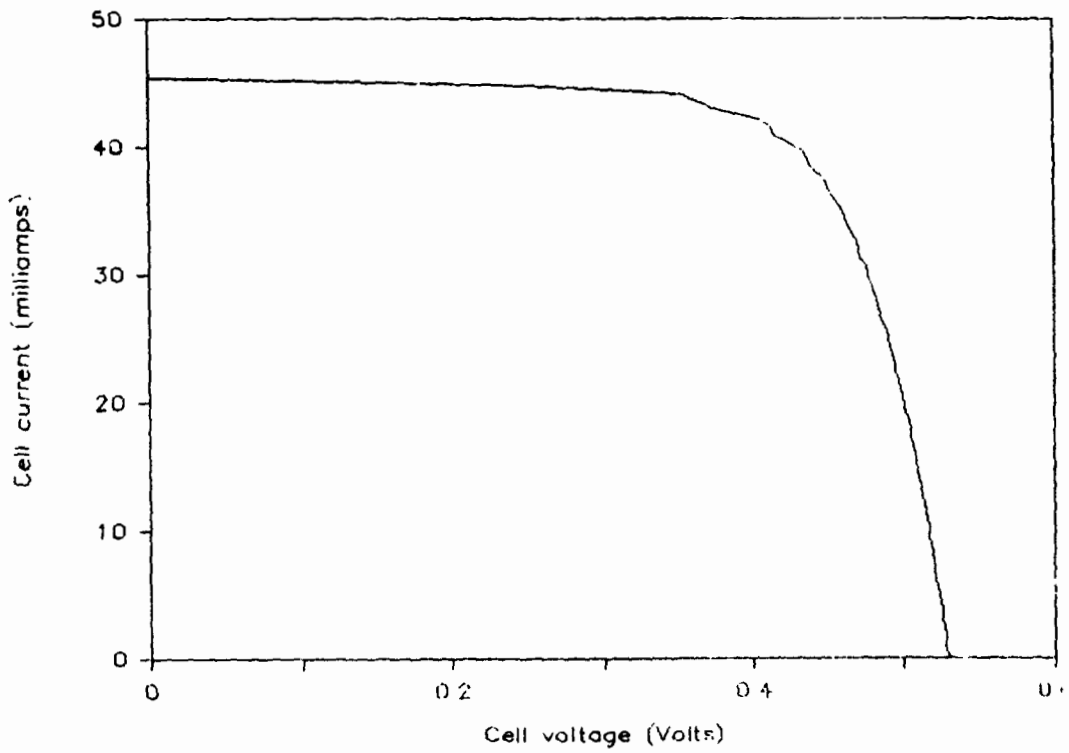
Crystalline Silicon Cell: Ac Analysis
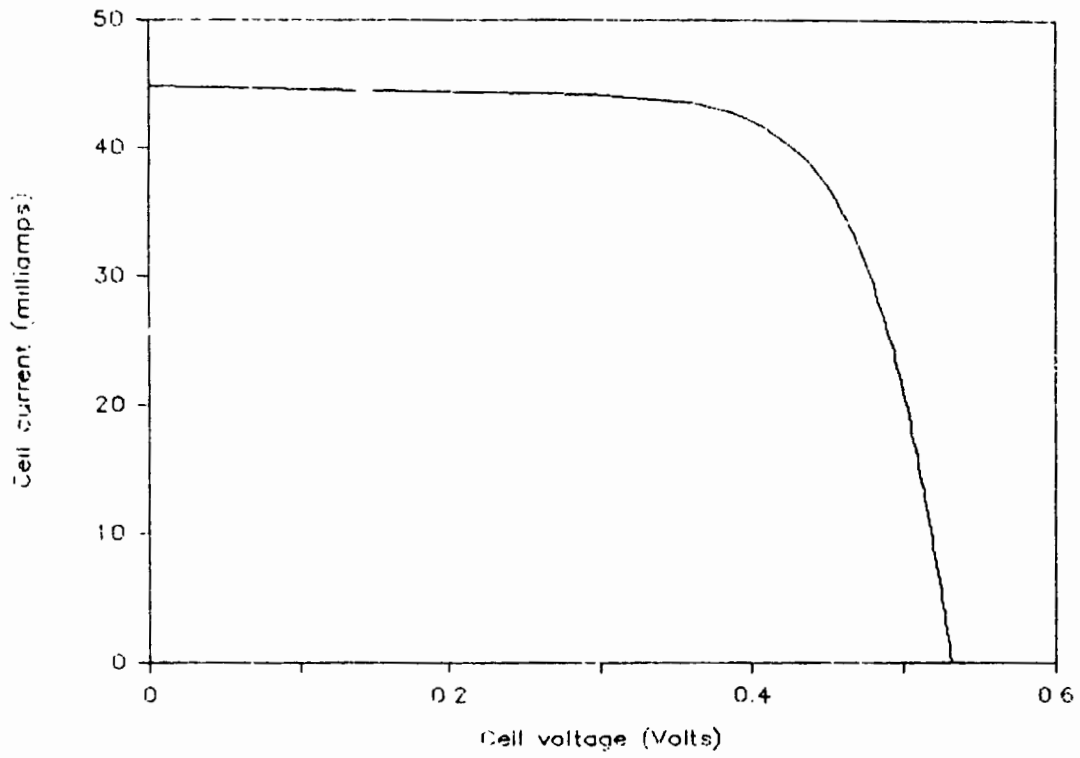
Intensity Monitoring and Adjustment

ELH SOLAR
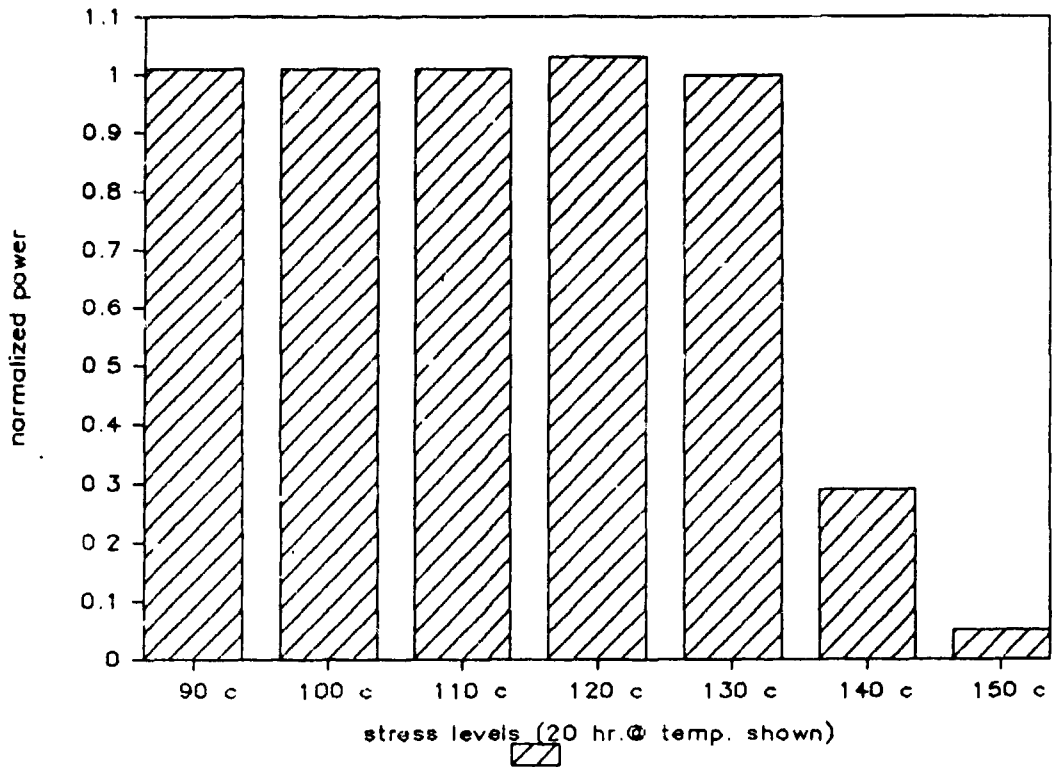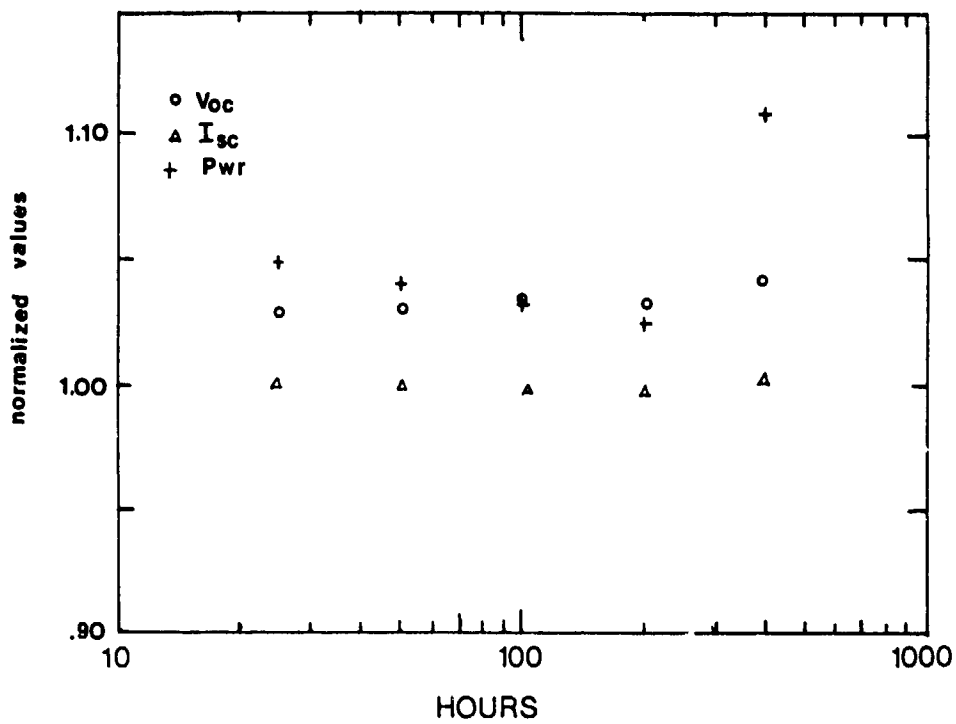SIMULATOR

A/D
CONVERTER

16 LINES

PHOTO
DIODE
ARRAY

COMPUTER

Simulated Amorphous Reference Cell
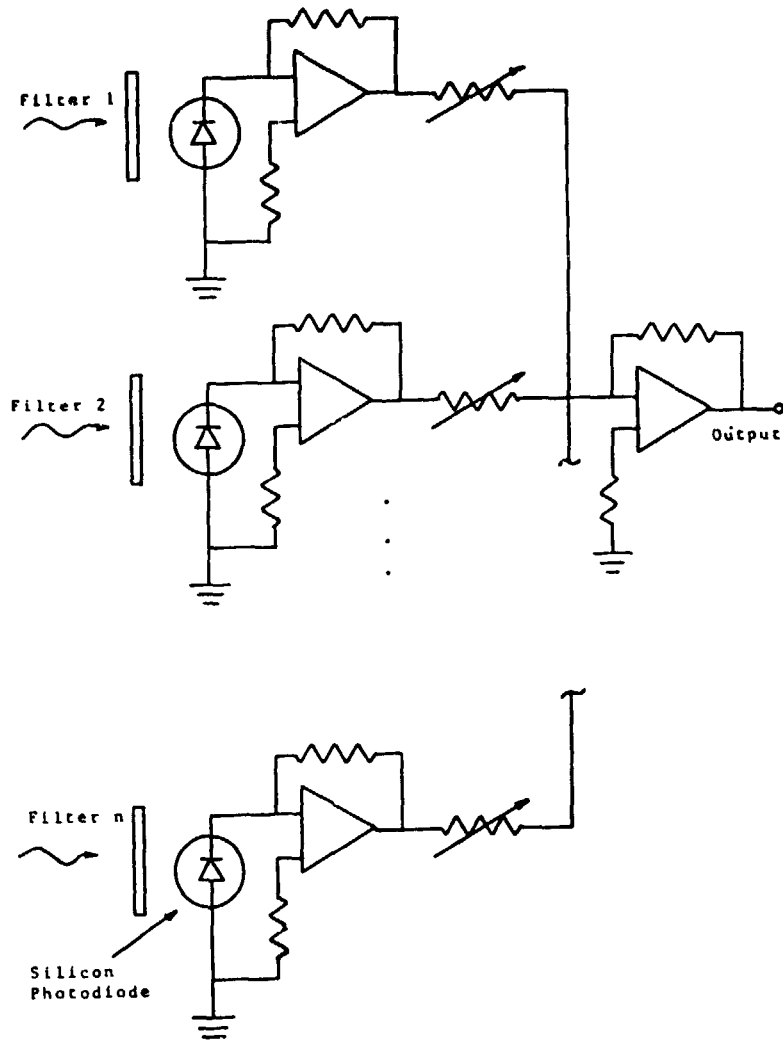
Temperature Step Stress

a-Si at 75°C

FAILURE ANALYSIS OF THIN-FILM AMORPHOUS-SILICON SOLAR-CELL MODULES

JET PROPULSION LABORATORY

Q. Kim

Failure Analysis

PURPOSE:

o PROVIDE INFORMATION AND DATA FOR APPROPRIATE CORRECTIVE ACTION THAT CAN RESULT IN IMPROVEMENTS IN PRODUCT QUALITY AND RELIABILITY.

APPROACHES:

o EXPAND EXISTING TECHNIQUES AND CAPABILITY IN ORDER TO EVALUATE AND CHARACTERIZE DEGRADATIONAL PERFORMANCE OF A-SI SOLAR CELLS.

o INVESTIGATE IN DEPTH MICROSCOPIC AND MACROSCOPIC DEFECTS AND FLAWS THAT SIGNIFICANTLY CONTRIBUTE TO PERFORMANCE DEGRADATION.

o DEVELOP NEW ANALYTICAL TECHNIQUES.

State of the Art of α-Si Solar Cells

TABLE 1. PERFORMANCE OF BEST REPORTED SINGLE JUNCTION p-i-n
AMORPHOUS SILICON SOLAR CELLS

STRUCTURE	V_{oc} mV	J_{sc} mA/cm^2	FF %	EFF. %	AREA cm^2	
GLASS /TCO /p (a-SiC:H) - i - n (a-Si:H) /Me				10.1	1.09	RCA
p-i-n	836	16.7	66.0	9.2	0.05	ECD
GLASS /TCO /p (a-SiC:H) - i - n (a-Si:H) / Me	845	13.03	74.0	8.15	0.04	SANYO
GLASS /TCO /p (a-SiC:H) - i - n (a-Si:H) /Me	880	15.21	60.0	8.04	0.033	OSAKA
GLASS /TCO /p (a-SiC:H) - i - n (a-Si:H) /Me	932	14.00	67.6	7.87	1.09	RCA
TCO /n (mC-Si) - i - p (a-Si:H) /SS	860	13.90	65.2	7.80	1.20	FUJI
GLASS /TCO /p (a-SiC:H) - i - n (a-Si:H) /Me	900	14.60	58.0	7.62	0.09	SUMITOMO
TCO /n (mC-Si) - i - p (a-Si:H) /SS	889	13.80	60.0	7.36	0.09	TEIJIN
TCO /n - i - p (a-Si:H) /Me	839	13.80	64.0	7.40	0.06	SIEMENS
BEST INDIVIDUAL PARAMETERS	950	16.70	74.0	(11.70)		

- HIGH CONVERSION EFFICIENCY: 7.4 - 11.7%
- DIFFERENT DEVICE STRUCTURES: p - i - n
  n - i - p
- DIFFERENT FABRICATION PROCESS: GLOW DISCHARGE
  REACTIVE SPUTTERING
  CHEMICAL VAPOR DEPOSITION

Solar Battery Charger (NC-AM1), Sanyo Electric Co. Lt
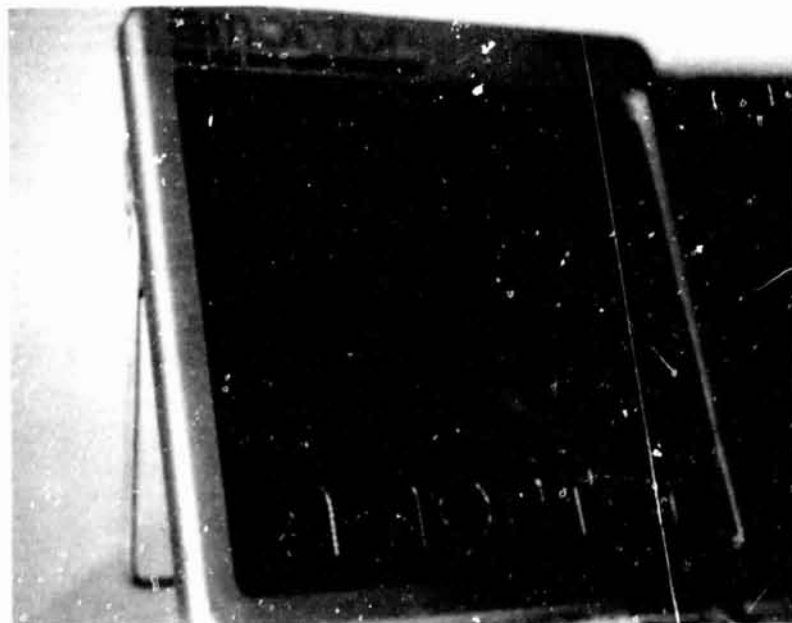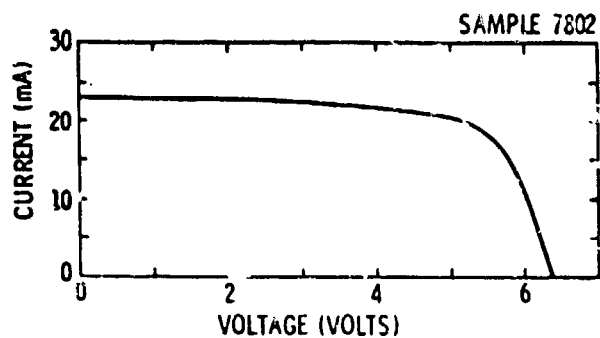
Some Test Results

FIGURE 1. IV CHARACTERISTICS

AFTER ANNEALING (160°C FOR 1/2 HR IN AIR)

J_{SC}	$\cdot 2.973$ m A/cm^2	$\eta \cdot 1.68\%$	
V_{oc}	$\cdot 0.798$ V	SHUNT RESISTANCE:	1.495 KΩ
P_{max}	$\cdot 1.58$ mw/cm^2	SERIES RESISTANCE:	4.163 Ω
FF	$\cdot 0.709$	THERMAL ACTIVA ENERGY:	0.14 eV
CELL AREA	$\cdot 7.738$ x 8 cm^2		

PRACTICAL CONSIDERATIONS

- LARGE DIFFERENCES IN η SUGGESTS A NEED FOR AN IN-DEPTH EVALUATION OF DEGRADATIONAL MECHANISMS
- MANY OF THE MECHANISMS ARE LIKELY TO BE PROCESS PARAMETER SENSITIVE ON WHICH THERE IS SOME LIMITED INFORMATION
- EFFECT OF ENVIRONMENTAL STRESS ON OTHER MECHANISMS APPEAR TO BE LESS UNDERSTOOD

Amorphous-Silicon Solar Cell

- VERY SHORT DIFFUSION LENGTH (< 1 / 1000 X C-Si)
- VERY HIGH ABSORPTION COEFFICIENT (> 10 x C-Si)
- CARRIER TRANSPORT BY DRIFT

p   i   n
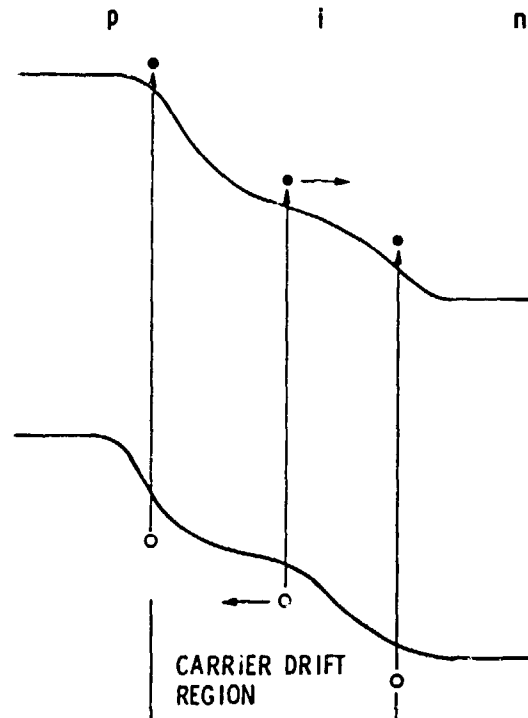
CARRIER DRIFT
REGION

FIGURE 2.   ENERGY BAND DIAGRAM OF p-i-n JUNCTION

- OPTIMIZF ABSORPTION AND I-LAYER INTERNAL ELECTRIC
  FIELD BY ADJUSTING THE THICKNESSES AND FILM
  CHARACTERISTICS

Current Activity

o INVESTIGATING DEGRADATIONAL MECHANISMS ON COMMERCIAL
   A-SI SOLAR CELL PRODUCTS.

   o THESE CELLS ARE TYPICALLY LOW EFFICIENCY BUT PROVIDE
      AN OPPORTUNITY FOR CONTRIBUTING DIRECTLY TO THE
      IMPROVEMENT OF COMMERCIAL TECHNOLOGY.

o EXAMINING DEVICE STRUCTURES, AND OPTICAL AND ELECTRICAL
   CHARACTERISTICS.

   o POLARIZING MICROSCOPE, SEM, CURVE TRACER, SUN-U-LATOR,
      SCLS, FTIR, CAPACITOR BRIDGE, HIGH PRECISION ELECTRO-
      METER, ELLIPSOMETRY, ETC.

Solar-Cell Laser Scanner
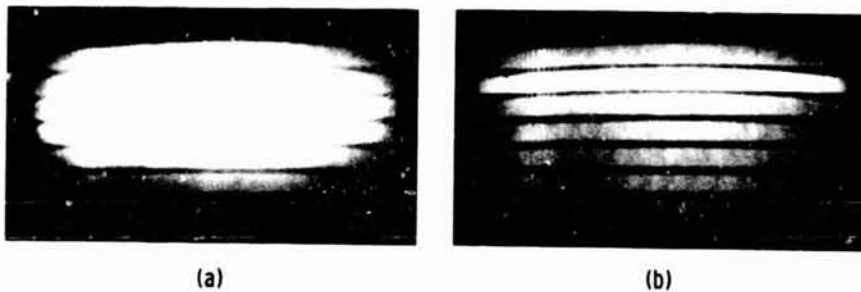

(a)   (b)
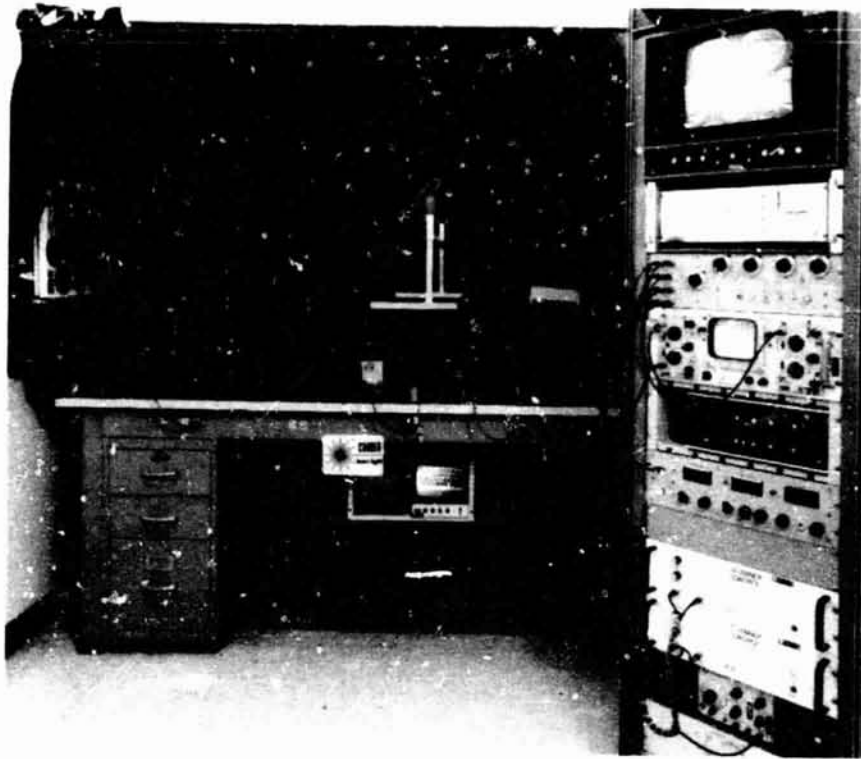
FIGURE 3. SCLS IMAGE OF SAMPLE 7703-1 BY TWO DIFFERENT
MONOCHROMATIC LIGHTS (4880Å (a) AND 5145Å (b))

- IT ALLOWS FOR NON-DESTRUCTIVE EVALUATION AND FAILURE ANALYSIS OF ENTIRE SOLAR MODULE   AS WELL AS INDIVIDUAL CELL

- IT MAKES IT POSSIBLE TO DISCRIMINATE BETWEEN ACTIVE AND PASSIVE (COSMETIC) DEFECTS

- IT MAY PROVIDE MEANS FOR ABSTRACTING INFORMATION ON DIFFERENT LAYERS OF THE THIN-FILM SOLAR CELL

MODULE DEVELOPMENT AND ENGINEERING SCIENCES

Future Plans for α-Si Solar Cells

o UPGRADE SCLS CAPABILITY TO PROBE PHOTOCURRENT RESPONSE IN
   DIFFERENT LAYERS OF THE DEVICE.

o EVALUATE AND CHARACTERIZE MODULE DEGRADATIONAL PHENOMENA IN
   THIN-FILM AMORPHOUS SILICON SOLAR CELLS WITH PARTICULAR
   EMPHASIS ON MICRO AND MACROSCOPIC DEFECTS/FLAWS.

o DEVELOP METHODS TO ANALYZE FAILURE MODES RESULTING FROM
   DEGRADATION DUE TO ENVIRONMENTAL EFFECTS SUCH AS OPTICAL,
   THERMAL, MECHANICAL AND MOISTURE.

REFERENCE-CELL CALIBRATION ACTIVITIES

JET PROPULSION LABORATORY

R. Mueller

Reference-Cell Calibration Method

1. TYPE II (SECONDARY) CALIBRATION USING ASTM 130

2. LIGHT SOURCE IS THE JPL AM 1.5 FILTERED LAPSS

3. PRIMARY REFERENCE CELLS CALIBRATED IN SUNLIGHT BY COMPARISON WITH A PYRHELIOMETER USING ASTM 130

4. TEMPERATURE OF DEVICE AND REFERENCE CONTROLLED

Spectral Irradiance (AM1.5 Direct)
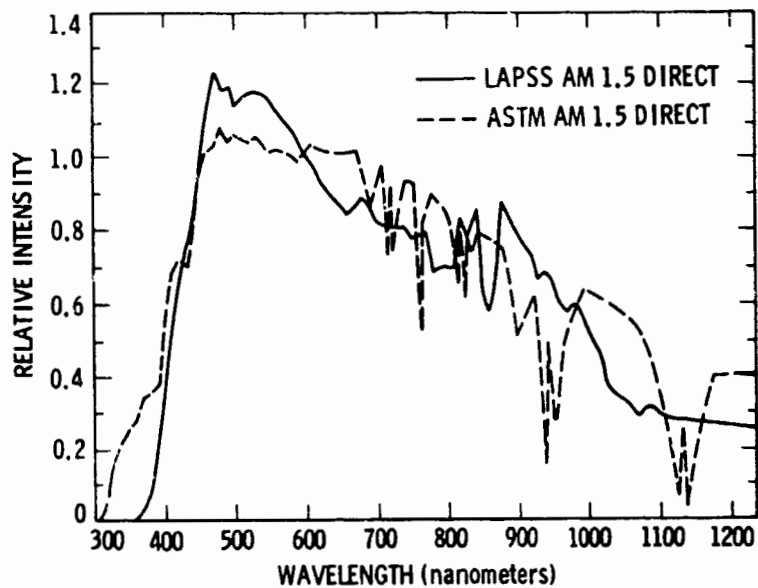
Why Use Secondary Calibration in LAPSS?

1. PRIMARY CALIBRATION IN SUNLIGHT IS TIME CONSUMING

2. ONLY A LIMITED SUN CALIBRATION OF A SET OF PRIMARY REFERENCE CELLS IS REQUIRED

3. THE LAPSS LIGHT SOURCE IS FILTERED TO CLOSELY MATCH THE AM1.5 DIRECT SPECTRUM

4. TEMPORAL STABILITY OF THE FILTERED LAPSS IS EXCELLENT

5. PRIMARY REFERENCE CELL NEED NOT BE SPECTRALLY MATCHED TO DEVICE UNDER CALIBRATION

6. LOWER COST AND TIMELY METHOD OF PROVIDING REFERENCE CELLS

7. POSSIBLY LOWER ERROR THAN USING A SPECTRALLY MATCHED, SUN CALIBRATED REF CELL WITH UNFILTERED LAPSS.

List of Organizations Provided Secondary Calibration of Reference Cells

ARCO SOLAR
BRITISH PETROLEUM
CLEMSON UNIVERSITY
COMMISSION OF THE EUROPEAN COMMUNITIES
JET PROPULSION LABORATORY
KYOCERA INTERNATIONAL
MASSACHUSETTS INST. OF TECHNOLOGY
ONTARIO RESEARCH FOUNDATION, CANADA
SANYO
SOLAR ENERGY RESEARCH INSTITUTE
SOLAREX CORP.
SOLAR POWER CORP.
SOLAVOLT
SOLEC INTERNATIONAL
SOLENERGY CORP.
SPIRE
TIDELAND CO.
YALE UNIVERSITY

MODULE DEVELOPMENT AND ENGINEERING SCIENCES

CEC Round Robin

MANAGED BY: COMMISSION OF THE EUROPEAN COMMUNITIES
JOINT RESEARCH CENTRE
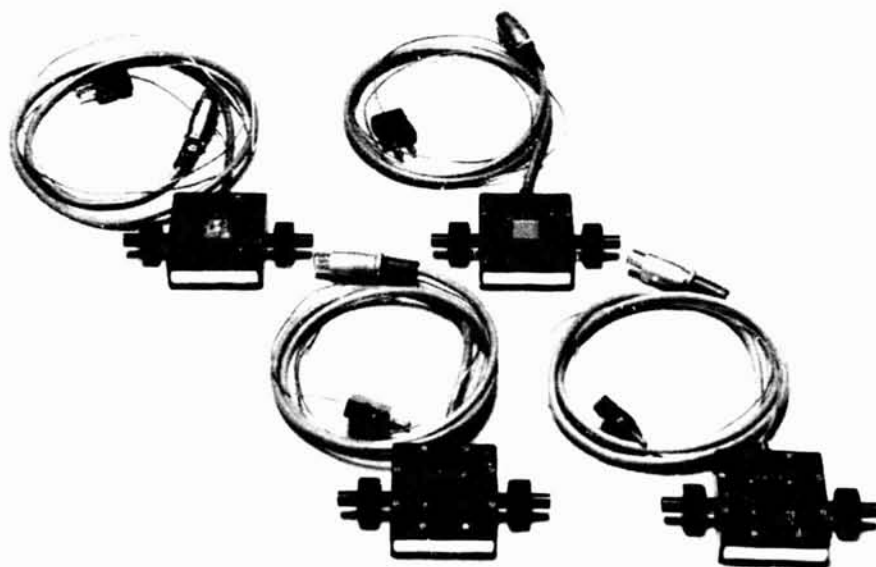ISPRA ESTABLISHMENT
21020 ISPRA (VARESE) ITALY

OBJECT: TO RESOLVE DISAGREEMENT IN MEASURFMENTS

REFERENCE CELLS PROVIDED BY:

4 CELLS	AMORPHOUS SILICON	JMI (JAPAN MACHINERY & METALS INSPECTION INSTITUTE)
5 CELLS	MONO & POLYCRYSTALLINE	ENEA (NUCLEAR & ALTERNATIVE ENERGY AGENCY), ITALY
2 CELLS	POLYCRYSTALLINE SILICON	AEG (TELEFUNKEN) GERMANY
3 CELLS	MONOCRYSTALLINE SILICON	PW (PHOTOWATT ORGANIZATION), FRANCE
4 CELLS	MONO & POLYCRYSTALLINE	JPL (JET PROPULSION LABORATORY), USA

18 CELLS TOTAL

665

MODULE DEVELOPMENT AND ENGINEERING SCIENCES
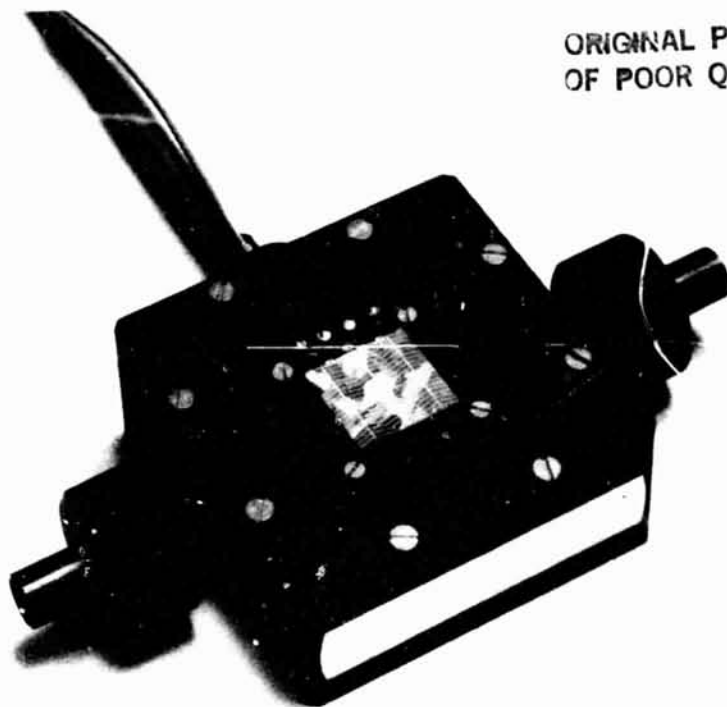
CEC Round Robin Measurements Time Table

UNTIL AUG 7, 1984	JRC (JOINT RESEARCH CENTRE) ISPRA, ITALY
AUG 15 - SEPT 15, 1984	RAE (ROYAL AIRCRAFT ESTABLISHMENT), UNITED KINGDOM
SEPT 15 - OCT 15, 1984	CNES (NATIONAL CENTRE FOR SOLAR ENERGY), FRANCE
OCT 15 - NOV 15, 1984	ENEA (NUCLEAR AND ALTERNATIVE ENERGY AGENCY), ITALY
NOV 15 - DEC 15, 1984	DFVLR (RESEARCH & EXPERIMENT INSTITUTE FOR AIR & SPACE TRAVEL), GERMANY
JANUARY 1985	NRC (NATIONAL RESEARCH CENTRE), CANADA
FEBRUARY 1985	JPL (JET PROPULSION LABORATORY), USA
MARCH 1985	JMI (JAPAN MACHINERY & METALS INSPECTION INSTITUTE), JAPAN
APRIL 1985	JRC (JOINT RESEARCH CENTRE) ISPRA, ITALY

MODULE DEVELOPMENT AND ENGINEERING SCIENCES

BPC Round Robin

MANAGED BY: BRITISH PETROLEUM COMPANY P.L.C.
                      BP RESEARCH CENTRE
                      MIDDLESEX, ENGLAND

OBJECT: TO RESOLVE DISAGREEMENT IN MEASUREMENT

6 MODULES AND 1 REFERENCE CELL PROVIDED BY:

                      PHOTOWATT
                      PHOTON TECHNOLOGY
   TIDELAND
                      ARCO SOLAR
                      HELIOS
                      KYOCERA INTERNATIONAL

MEASUREMENTS TIMETABLE:

≈ AUGUST 1984	RAE (ROYAL AIRCRAFT ESTABLISHMENT), U.K.
SEPT - OCT 1984	JPL (JET PROPULSION LABORATORY), USA
OCT - NOV 1984	JRC (JOINT RESEARCH CENTRE), ISPRA, ITALY

Amorphous Silicon Activities

1. DEFINED A LAPSS MODIFICATION TO PROVIDE AM 1.5
   GLOBAL SIMULATION

2. DEFINED A REFERENCE CELL FOR USE WITH AMORPHOUS
   SILICON MODULES

Spectral Irradiance (AM1.5 Global)
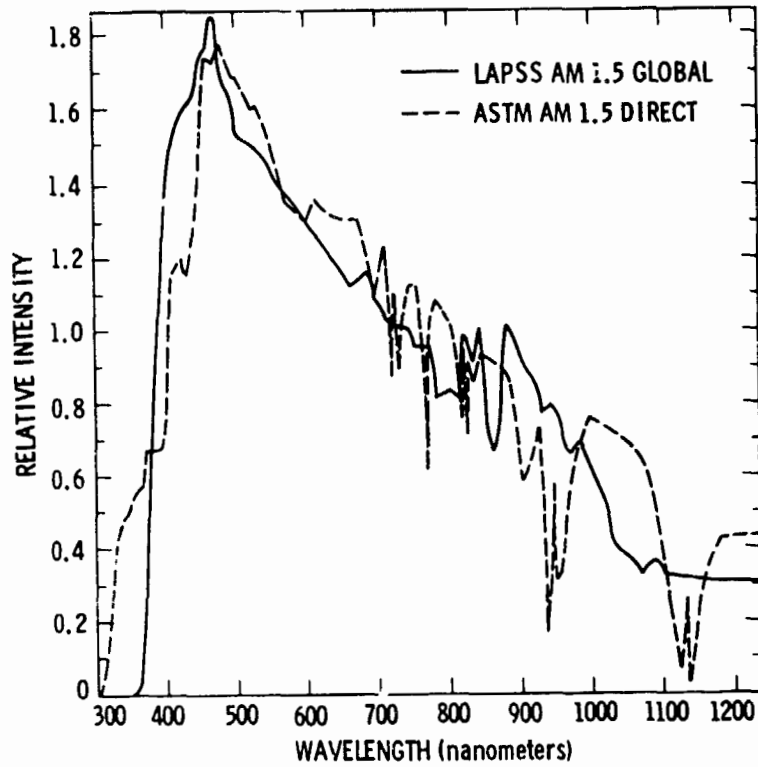
Spectral Response (Amorphous Silicon)